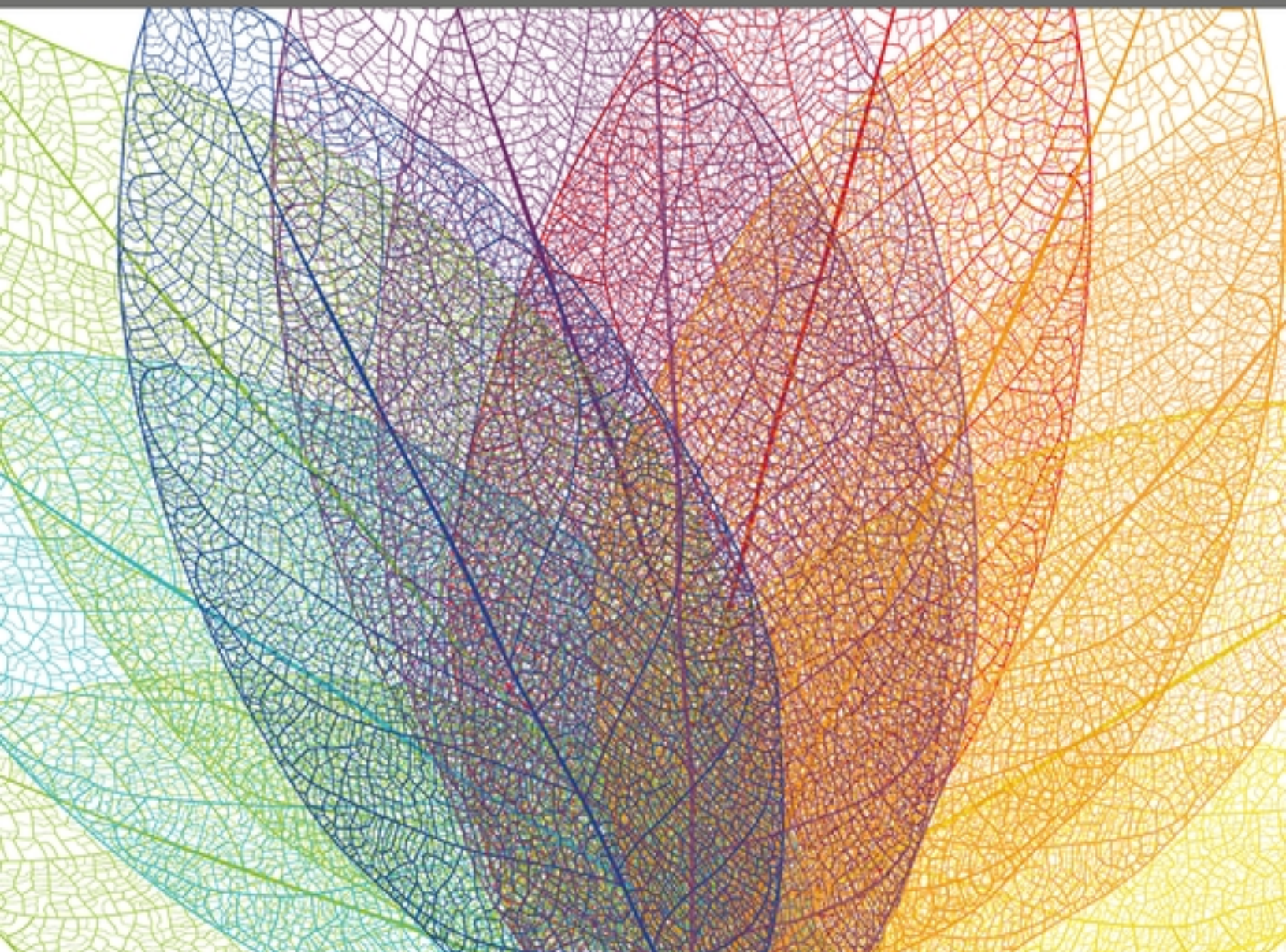


# GLOBAL OCCURRENCE OF PINE WILT DISEASE: BIOLOGICAL INTERACTIONS AND INTEGRATED MANAGEMENT

EDITED BY: Margarida Espada, Ryoji Shinya, Hong Mei Li, Anna Filipiak and  
Claudia S. L. Vicente

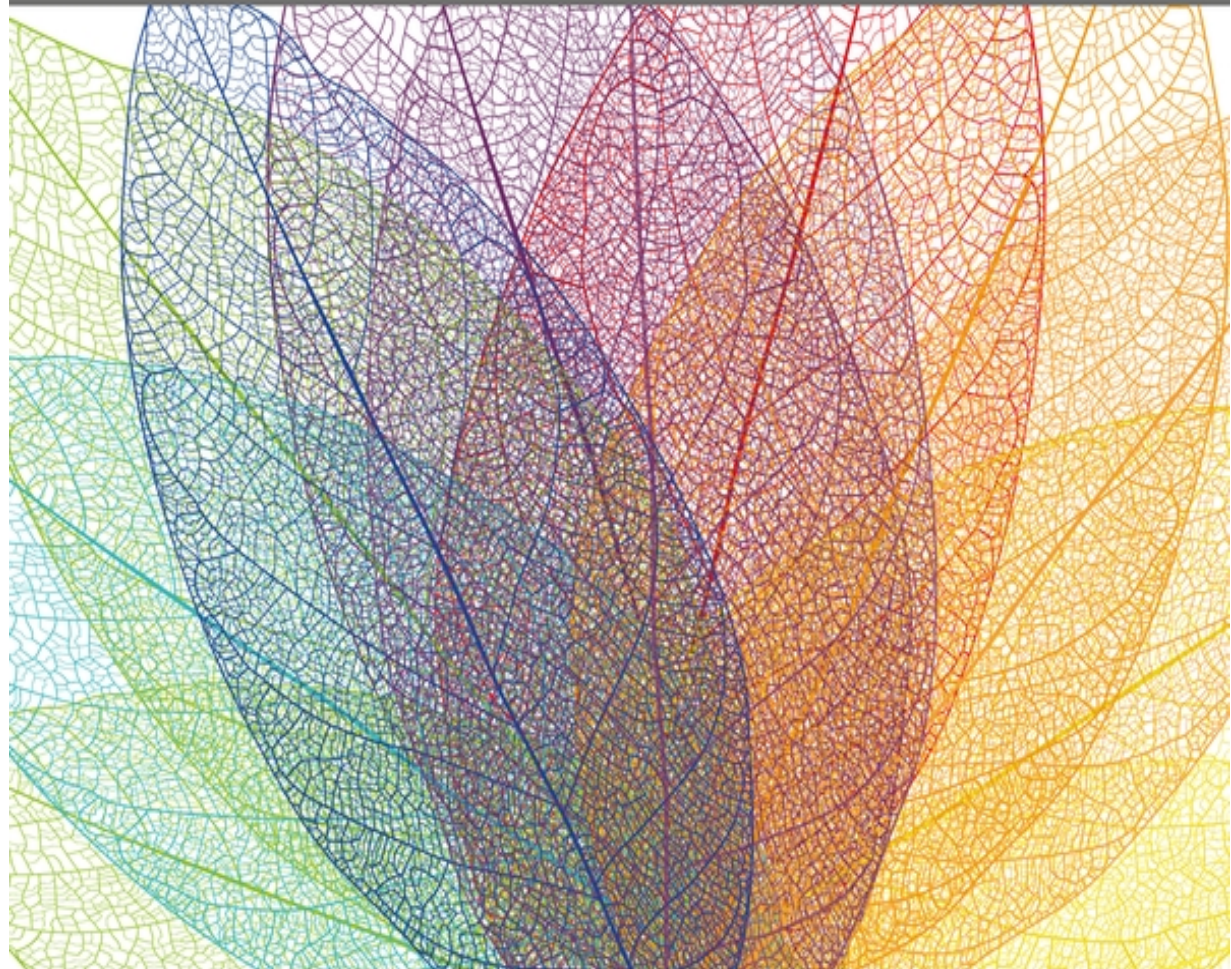
PUBLISHED IN: *Frontiers in Plant Science*



# GLOBAL OCCURRENCE OF PINE WILT DISEASE: BIOLOGICAL INTERACTIONS AND INTEGRATED MANAGEMENT

EDITED BY: Margarida Espada, Ryoji Shinya, Hong Mei Li, Anna Filipiak and  
Claudia S. L. Vicente

PUBLISHED IN: *Frontiers in Plant Science*



## **Frontiers eBook Copyright Statement**

The copyright in the text of individual articles in this eBook is the property of their respective authors or their respective institutions or funders. The copyright in graphics and images within each article may be subject to copyright of other parties. In both cases this is subject to a license granted to Frontiers.

The compilation of articles constituting this eBook is the property of Frontiers.

Each article within this eBook, and the eBook itself, are published under the most recent version of the Creative Commons CC-BY licence. The version current at the date of publication of this eBook is CC-BY 4.0. If the CC-BY licence is updated, the licence granted by Frontiers is automatically updated to the new version.

When exercising any right under the CC-BY licence, Frontiers must be attributed as the original publisher of the article or eBook, as applicable.

Authors have the responsibility of ensuring that any graphics or other materials which are the property of others may be included in the CC-BY licence, but this should be checked before relying on the CC-BY licence to reproduce those materials. Any copyright notices relating to those materials must be complied with.

Copyright and source acknowledgement notices may not be removed and must be displayed in any copy, derivative work or partial copy which includes the elements in question.

All copyright, and all rights therein, are protected by national and international copyright laws. The above represents a summary only. For further information please read Frontiers' Conditions for Website Use and Copyright Statement, and the applicable CC-BY licence.

ISSN 1664-8714

ISBN 978-2-88976-867-7

DOI 10.3389/978-2-88976-867-7

## **About Frontiers**

Frontiers is more than just an open-access publisher of scholarly articles: it is a pioneering approach to the world of academia, radically improving the way scholarly research is managed. The grand vision of Frontiers is a world where all people have an equal opportunity to seek, share and generate knowledge. Frontiers provides immediate and permanent online open access to all its publications, but this alone is not enough to realize our grand goals.

## **Frontiers Journal Series**

The Frontiers Journal Series is a multi-tier and interdisciplinary set of open-access, online journals, promising a paradigm shift from the current review, selection and dissemination processes in academic publishing. All Frontiers journals are driven by researchers for researchers; therefore, they constitute a service to the scholarly community. At the same time, the Frontiers Journal Series operates on a revolutionary invention, the tiered publishing system, initially addressing specific communities of scholars, and gradually climbing up to broader public understanding, thus serving the interests of the lay society, too.

## **Dedication to Quality**

Each Frontiers article is a landmark of the highest quality, thanks to genuinely collaborative interactions between authors and review editors, who include some of the world's best academicians. Research must be certified by peers before entering a stream of knowledge that may eventually reach the public - and shape society; therefore, Frontiers only applies the most rigorous and unbiased reviews.

Frontiers revolutionizes research publishing by freely delivering the most outstanding research, evaluated with no bias from both the academic and social point of view.

By applying the most advanced information technologies, Frontiers is catapulting scholarly publishing into a new generation.

## **What are Frontiers Research Topics?**

Frontiers Research Topics are very popular trademarks of the Frontiers Journals Series: they are collections of at least ten articles, all centered on a particular subject. With their unique mix of varied contributions from Original Research to Review Articles, Frontiers Research Topics unify the most influential researchers, the latest key findings and historical advances in a hot research area! Find out more on how to host your own Frontiers Research Topic or contribute to one as an author by contacting the Frontiers Editorial Office: [frontiersin.org/about/contact](http://frontiersin.org/about/contact)

# GLOBAL OCCURRENCE OF PINE WILT DISEASE: BIOLOGICAL INTERACTIONS AND INTEGRATED MANAGEMENT

Topic Editors:

**Margarida Espada**, University of Évora, Portugal

**Ryoji Shinya**, Meiji University, Japan

**Hong Mei Li**, Nanjing Agricultural University Nanjing, China

**Anna Filipiak**, Institute of Plant Protection – National Research Institute, Department of Biological Pest Control, Poland

**Claudia S. L. Vicente**, University of Évora, Portugal

**Citation:** Espada, M., Shinya, R., Li, H. M., Filipiak, A., Vicente, C. S. L., eds. (2022). Global Occurrence of Pine Wilt Disease: Biological Interactions and Integrated Management. Lausanne: Frontiers Media SA. doi: 10.3389/978-2-88976-867-7

## Table of Contents

### ***Editorial: Global occurrence of pine wilt disease: Biological interactions and integrated management***

**Margarida Espada, Anna Filipiak, Hongmei Li, Ryoji Shinya and Claudia S. L. Vicente**

### ***Primary Metabolite Adjustments Associated With Pinewood Nematode Resistance in Pinus pinaster***

**Ana M. Rodrigues, Isabel Carrasquinho and Carla António**

### ***Systemic Acquired Resistance-Mediated Control of Pine Wilt Disease by Foliar Application With Methyl Salicylate***

**Hee Won Jeon, Ae Ran Park, Minjeong Sung, Namgyu Kim, Mohamed Manna, Gil Han, Junheon Kim, Yeonjong Koo, Young-Su Seo and Jin-Cheol Kim**

### ***Virulence Biomarkers of Bursaphelengus xylophilus: A Proteomic Approach***

**Joana M. S. Cardoso, Sandra I. Anjo, Bruno Manadas, Hugo Silva, Isabel Abrantes, Katsunori Nakamura and Luís Fonseca**

### ***Differential Impact of the Pinewood Nematode on Pinus Species Under Drought Conditions***

**Mariana Estorninho, Sergio Chozas, Angela Mendes, Filipe Colwell, Isabel Abrantes, Luís Fonseca, Patrícia Fernandes, Catarina Costa, Cristina Mágua, Otília Correia and Cristina Antunes**

***Rapid On-Site Detection of the Bursaphelenchus xylophilus Using Recombinase Polymerase Amplification Combined With Lateral Flow Dipstick That Eliminates Interference From Primer-Dependent Artifacts***

**Qinzheng Zhou, Ya Liu, Zheng Wang, Huimin Wang, Xingyao Zhang and Quan Lu**

***Quantitative Trait Loci Analysis Based on High-Density Mapping of Single-Nucleotide Polymorphisms by Genotyping-by-Sequencing Against Pine Wilt Disease in Japanese Black Pine (Pinus thunbergii)***

**Tomonori Hirao, Koji Matsunaga and Kenta Shirasawa**

***Novel Functional Analysis for Pathogenic Proteins of Bursaphelenchus xylophilus in Pine Seed Embryos Using a Virus Vector***

**Haru Kirino, Ken-ichi Konagaya and Ryoji Shinya**

***Parallel Evolution of C-Type Lectin Domain Gene Family Sizes in Insect-Vectored Nematodes***

**Jing Ning, Jiao Zhou, Haixiang Wang, Yaning Liu, Faheem Ahmad, Xiaohui Feng, Yu Fu, Xiaoting Gu and Lilin Zhao**

***Genes Encoding Potential Molecular Mimicry Proteins as the Specific Targets for Detecting Bursaphelenchus xylophilus in PCR and Loop-Mediated Isothermal Amplification Assays***

**Fanli Meng, Zhenkai Liu, Yongxia Li and Xingyao Zhang**

***Invasion History of the Pinewood Nematode Bursaphelenchus xylophilus Influences the Abundance of Serratia sp. in Pupal Chambers and Tracheae of Insect-Vector Monochamus alternatus***

Haokai Tian, Tuuli-Marjaana Koski, Lilin Zhao, Ziying Liu and Jianghua Sun

***Simulating Pine Wilt Disease Dispersal With an Individual-Based Model Incorporating Individual Movement Patterns of Vector Beetles***

Chunlei Xia, Tae-Soo Chon, Fugo Takasu, Won Il Choi and Young-Seuk Park

***UGT440A1 Is Associated With Motility, Reproduction, and Pathogenicity of the Plant-Parasitic Nematode Bursaphelenchus xylophilus***

Min Wang, Guicai Du, Junna Fang, Linsong Wang, Qunqun Guo, Tingting Zhang and Ronggui Li

***Fungal Communities of the Pine Wilt Disease Complex: Studying the Interaction of Ophiostomatales With Bursaphelenchus xylophilus***

Cláudia S. L. Vicente, Miguel Soares, Jorge M. S. Faria, Margarida Espada, Manuel Mota, Filomena Nóbrega, Ana P. Ramos and Maria L. Inácio

# Editorial: Global occurrence of pine wilt disease: Biological interactions and integrated management

Margarida Espada<sup>1\*</sup>, Anna Filipiak<sup>2</sup>, Hongmei Li<sup>3</sup>, Ryoji Shinya<sup>4</sup> and Claudia S. L. Vicente<sup>1</sup>

<sup>1</sup> MED—Mediterranean Institute for Agriculture, Environment and Development & CHANGE—Global Change and Sustainability Institute, Institute for Advanced Studies and Research, Universidade de Évora, Pólo da Mitra, Évora, Portugal

<sup>2</sup> Institute of Plant Protection—National Research Institute, Poznań, Poland

<sup>3</sup> Department of Plant Pathology, Nanjing Agricultural University, Nanjing, China

<sup>4</sup> School of Agriculture, Meiji University, Kawasaki, Japan



Check for updates

## OPEN ACCESS

### EDITED AND REVIEWED BY

Eustachio Tarasco, University of Bari Aldo Moro, Italy

### \*CORRESPONDENCE

Margarida Espada, [mespada@uevora.pt](mailto:mespada@uevora.pt)

### SPECIALTY SECTION

This article was submitted to Plant Pathogen Interactions, a section of the journal *Frontiers in Plant Science*

RECEIVED 13 July 2022

ACCEPTED 14 July 2022

PUBLISHED 26 July 2022.

**CITATION**

Espada M, Filipiak A, Li H, Shinya R and Vicente CSL (2022) Editorial: Global occurrence of pine wilt disease: Biological interactions and integrated management. *Front. Plant Sci.* 13:993482. doi: 10.3389/fpls.2022.993482

**COPYRIGHT**

© 2022 Espada, Filipiak, Li, Shinya and Vicente. This is an open-access article distributed under the terms of the [Creative Commons Attribution License \(CC BY\)](#). The use, distribution or reproduction in other forums is permitted, provided the original author(s) and the copyright owner(s) are credited and that the original publication in this journal is cited, in accordance with accepted academic practice. No use, distribution or reproduction is permitted which does not comply with these terms.

**KEYWORDS**

tree pathogen, control, plant-parasitic nematode, pinewood nematode, plant nematode interaction, forestry sustainable management

## Editorial on the Research Topic

### **Global occurrence of pine wilt disease: Biological interactions and integrated management**

Plant pathogens cause severe losses in a wide range of crops and forestry plant species worldwide, being a major obstacle toward achieving sustainable agriculture and forestry. In forests, pathogens can affect sustainable management by affecting economic trade and serious ecological losses can occur, such as the ability to store carbon, reduce flood risk or purify water (Boyd et al., 2013). Ranking in the top ten of the most damaging plant-parasitic nematodes worldwide, the migratory endoparasitic nematode *Bursaphelenchus xylophilus* (pinewood nematode, PWN) is the causal agent of Pine wilt disease (PWD) being responsible for the tremendous decline of conifers species in Eurasian conifer forests (Mota and Vieira, 2008; Futai, 2013; Jones et al., 2013). This complex disease results from a tripartite species interaction (plant-nematode-insect), where each participant involved may be a target for research and understanding at a molecular, evolutionary, chemical, and biological levels. In the present climate change and global warming scenarios, the dispersal of this pathogen has negative impact in forestry practices. The PWN pathogenicity is more severe at high

temperatures and drought will likely emphasize PWN-associated issues, increasing its adaptability and incidence on conifers forest worldwide (Ohsawa and Akiba, 2014; Hirata et al., 2017). Currently, the strategies used for PWN control are preventive and new durable and greener solutions are needed. This Research Topic gathered work on several aspects of this disease aiming for a better understanding not only on the molecular mechanisms by which PWN interacts with all partners in the disease, but also in the development of new control targets and methods that could be potentially used in plant science diagnostic and research. Here, we compiled eleven original research articles and two theoretical issues that focus on different aspects of the complex PWD. An overview of the scientific content is summarized below.

Pest management strategies relies on efficient detection methods (Barzman et al., 2015). The close morphological similarity of *B. xylophilus* to a number of other tree-inhabiting species from the *xylophilus* group makes the problem particularly important, as any misidentification of nematodes extracted from the material subjected to phytosanitary inspection may lead to disturbances in the international wood trade and serious economic consequences (Braasch et al., 2001). For the development of new PWN detection strategies, two new molecular alternatives were proposed. Zhou et al. developed a rapid detection system for *B. xylophilus* that allow non-nematology researchers to detect the presence of PWN, as well as other nematodes, by RPA-LFD (recombinase polymerase amplification combined with lateral flow dipstick) in biological material. Based in previous studies (Meng et al., 2018), Meng et al. proposed a new LAMP methodology for detection and identification of pine wood nematode targeting the possibly pathogenicity-related gene. This technique can be used as a routine and/or combined with traditional PCR.

The complexity of this disease is also a result of the biological interactions co-occurring between plant-nematode-microbe. Tian et al. studied the temporal variation of bacteria to fungi ratio in PWD sites with different PWN invasion histories and evaluated the insecticidal/nematicidal activities of the most abundant bacteria (genus *Serratia*) extensively found in the pupal chambers and the tracheae of the *Monochamus alternatus*. The authors found that microbial communities changed with the duration of PWN invasion, and that *Serratia* were more expressive in sites with the longest PWN presence. In the same line of thought, Vicente et al. showed that fungal

communities also changed along sites with different PWD history, emphasizing the effect of a prolong exposure to PWN has a tremendous effect on these co-occurring multi-species interactions.

Understanding the molecular mechanisms underpinning the parasitism of the PWN are pivotal for the development of novel control strategies. Since the release of genomic and transcriptomic data there has been an effort to study potential parasitism-related genes and understand their evolutionary and functional role in plant-parasitic nematodes. Ning et al. presented a study on comparison of C-type lectin (CTL) family genes in insect-vectored and self-dispersing nematodes, and demonstrated that this gene family contributed to this evolutionary transition. In the phoretic nematode *B. xylophilus*, the similarity in the CTL gene family sizes, that clustered into separate phylogenetic *sister* clades, is due to parallel evolution, when similar phenotypes occur in closely related taxa, that are produced by orthologous genes. In a functional study, Wang et al. showed that PWN UGTs (uridine diphosphate-glycosyltransferases), specifically the UGT440A1, may be involved in the pathogenic process of the PWN in the disease. Knocking down UGT440A1 suppressed PWN core metabolism (motility, feeding and reproduction) which *in planta* slowed down their infectiveness. In a different approach, Cardoso et al. presented a comparative proteomic study in two PWN isolates with different virulence and geographical location. Thirteen proteins were found significantly increased in the proteome of the virulent isolate as compared with the less virulent one and were selected as potential virulence biomarkers. One of the main research challenges to study tree pathogens is the lack of genetic tools to functionally analyze nematode parasitism candidate genes. Kirino et al. described a new powerful tool for transient overexpression of nematode genes using an exogenous gene expression system applied in pine seed embryos with ALSV vector (virus vector). These authors showed that the use of natural host pine embryos is more reliable for functional analysis than using *Nicotiana benthamiana*-based methods.

The basis of the pine host genetic traits for resistance to PWD will be relevant to the future pine breeding programmes. Hirao et al. focused on the genetic mapping of resistance to PWD with the goal of improving resistance in Japanese Black Pine (*Pinus thunbergii*). The authors provided a high-density linkage map and quantitative trait loci (QTL) mapping of PWD resistance for *P. thunbergii*. This study also validates the GBS technology

and UNEAK pipeline as tools for use in QTL mapping in the species without a reference genome sequence. The results demonstrated that the locus linked to PWD resistance was identified on LG-3. This locus will be a good candidate to develop molecular markers associated with the phenotype. In Europe, maritime pine (*Pinus pinaster*) is the one of most susceptible hosts to PWN and genetic variability has been found in natural populations associated to heritable PWD resistance. Rodrigues *et al.* presented a physiologic and primary metabolite responses of susceptible and resistance *P. pinaster* seedlings to PWN. The authors showed that specific traits are associated with pine resistance to PWD, such as GABA shunt-related metabolites, and the plant defense response was regulated and able to reduce the ability of the nematode migration. Jeon *et al.* tested previously known 12 SAR (systemic acquired resistance) elicitors to manage PWD by SAR in pine trees. Methyl salicylate (MeSA) was found to induce resistance against PWD in *Pinus densiflora* seedlings. Moreover, qRT-PCR analysis confirmed that MeSA induced the expression of defense-related genes, and can inhibit and delay the migration and reproduction of PWN in pine seedlings by modulating gene expression.

Forest mortality due to PWN infection, and the fast spread of PWD might be exacerbated by climate (more drought events and higher temperatures), topography, and human activities (i.e., infected timber exports). The study conducted by Estorinho *et al.* analyzed the symptom development of the PWD in three pine species inoculated with PWN under controlled temperature and water availability. The authors showed that the impact of PWN is species-dependent, being infected *P. pinaster* and *P. radiata* more prone to physiological and morphological damage than *P. pinea*. Moreover, they suggested a synergistic impact of PWN infection and drought triggering disease symptoms and mortality of these species. The spread of PWD in pine forests of the Mediterranean regions may be possibly facilitated by predicted drought conditions (i.e., high temperatures and low water availability). Xia *et al.* demonstrated a theoretical method based on the individual dispersal of the insect vector—pine sawyer beetle (*Monochamus* spp.)—to elucidate the dispersal of PWD and evaluated the control strategies applied for the eradication of the disease in Korea.

In summary, this Research Topic with thirteen scientific contributions consolidates and expands our knowledge regarding recent advances in pine wilt disease.

## Author contributions

All authors listed have made a substantial, direct, and intellectual contribution to the work and approved it for publication.

## Conflict of interest

The authors declare that the research was conducted in the absence of any commercial or financial relationships that could be construed as a potential conflict of interest.

## Publisher's note

All claims expressed in this article are solely those of the authors and do not necessarily represent those of their affiliated organizations, or those of the publisher, the editors and the reviewers. Any product that may be evaluated in this article, or claim that may be made by its manufacturer, is not guaranteed or endorsed by the publisher.

## References

Barzman, M., Barberi, P., Birch, A. N. E., Boonekamp, P., Dachbrodt-Saaydeh, S., Graf, B., et al (2015). Eight principles of integrated pest management. *Agron. Sustain. Dev.* 35, 1195–1215. doi: 10.1007/s13593-015-0327-9

Boyd, I. L., Freer-Smith, P. H., Gilligan, C. A., and Godfray, H. C. J. (2013). The consequence of tree pests and diseases for ecosystem services. *Science* 342, 1235773. doi: 10.1126/science.1235773

Braasch, H., Tomiczek, C., Metge, K., Hoyer, U., Burgermeister, W., Wulfert, I., et al. (2001). Records of *Bursaphelenchus* spp. (*Nematoda, Parasitaphelenchidae*) in coniferous timber imported from the Asian part of Russia. *For. Pathol.* 31, 129–140. doi: 10.1046/j.1439-0329.2001.00233.x

Futai, K. (2013). Pine wood nematode, *Bursaphelenchus xylophilus*. *Annu. Rev. Phytopathol.* 51, 5.1–5.23. doi: 10.1146/annurev-phyto-081211-172910

Hirata, A., Nakamura, K., Nakao, K., Kominami, Y., Tanaka, N., Ohashi, H., et al. (2017). Potential distribution of pine wilt disease under future climate change scenarios. *PLoS ONE* 12, e0182837. doi: 10.1371/journal.pone.0182837

Jones, J. T., Haegeman, A., Danchin, E. G. J., Gaur, H. S., Helder, J., Jones, M. G. K., et al. (2013). Top 10 plant-parasitic nematodes in molecular plant pathology. *Mol. Plant Pathol.* 14, 946–961. doi: 10.1111/mpp.12057

Meng, F., Wang, X., Wang, L., Gou, D., Liu, H., Wang, Y., et al. (2018). A loop-mediated isothermal amplification-based method for detecting *Bursaphelenchus xylophilus* from *Monochamus alternatus*. *For. Pathol.* 48, e12404. doi: 10.1111/efp.12404

Mota, M., and Vieira, P, (eds.). (2008). *Pine Wilt Disease: A Worldwide Threat to Forest Ecosystems*. Dordrecht: Springer Science+Business Media B.V. doi: 10.1007/978-1-4020-8455-3

Ohsawa, M., and Akiba, M. (2014). Possible altitude and temperature limits on pine wilt disease: the reproduction of vector sawyer beetles (*Monochamus alternatus*), survival of causal nematode (*Bursaphelenchus xylophilus*), and occurrence of damage caused by the disease. *Eur. J. For. Res.* 133, 225–233. doi: 10.1007/s10342-013-0742-x

ORIGINAL RESEARCH

published: 24 November 2021

doi: 10.3389/fpls.2021.777681



# Primary Metabolite Adjustments Associated With Pinewood Nematode Resistance in *Pinus pinaster*

**Ana M. Rodrigues<sup>1†</sup>, Isabel Carrasquinho<sup>2,3</sup> and Carla António<sup>1\*†</sup>**

<sup>1</sup>*Plant Metabolomics Laboratory, Instituto de Tecnologia Química e Biológica António Xavier, Universidade Nova de Lisboa, Oeiras, Portugal*

<sup>2</sup>*Instituto Nacional Investigação Agrária e Veterinária I.P., Oeiras, Portugal*

<sup>3</sup>*Linking Landscape, Environment, Agriculture and Food, Instituto Superior de Agronomia, Universidade de Lisboa, Lisbon, Portugal*

**Edited by:**

Carolina Escobar, University of Castilla-La Mancha, Spain

**Reviewed by:**

Margarida Espada, University of Évora, Portugal

Rafael Zas, Misión Biológica de Galicia, Consejo Superior de Investigaciones Científicas (CSIC), Spain

**\*Correspondence:** Carla António, [plantmetabolomicslabpt@gmail.com](mailto:plantmetabolomicslabpt@gmail.com)

**†Present address:** Ana M. Rodrigues, Carla António, Plant Metabolomics Lab Portugal, Centro de Estudos Florestais, Instituto Superior de Agronomia, Universidade de Lisboa, Lisbon, Portugal

**Specialty section:** This article was submitted to Plant Pathogen Interactions, a section of the journal *Frontiers in Plant Science*

**Received:** 15 September 2021

**Accepted:** 01 November 2021

**Published:** 24 November 2021

**Citation:** Rodrigues AM, Carrasquinho I and António C (2021) Primary Metabolite Adjustments Associated With Pinewood Nematode Resistance in *Pinus pinaster*. *Front. Plant Sci.*

The pinewood nematode (PWN) *Bursaphelenchus xylophilus* is the causal agent of the pine wilt disease (PWD) and represents one of the major threats to conifer forests. The detection of the PWN in Portugal, associated with *Pinus pinaster*, increased the concern of its spread to European forests. Despite its susceptibility to PWD, genetic variability found among *P. pinaster* populations has been associated with heritable PWD resistance. Understanding the mechanisms underlying tree resistance constitutes a valuable resource for breeding programs toward more resilient forest plantations. This study investigated changes in anatomy, chlorophyll *a* fluorescence (ChlF), and primary metabolism in susceptible and resistant *P. pinaster* half-sib plants, after PWN inoculation. Susceptible plants showed a general shutdown of central metabolism, osmolyte accumulation, photosynthetic inhibition, and a decrease in the plant water status. The ChlF transient rise (OJIP curve) revealed the appearance of L- and K-bands, indicators of environmental stress. In contrast, resistant plants revealed a regulated defense response and were able to restrict PWN migration and cellular damage. Furthermore, the accumulation of  $\gamma$ -aminobutyric acid (GABA) and succinate suggested a role of these metabolites in PWD resistance and the possible activation of the GABA shunt. Altogether, these results provide new insights to the role of primary metabolism in PWD resistance and in the selection of resistant phenotypes for disease mitigation.

**Keywords:** pinewood nematode (*Bursaphelenchus xylophilus*), maritime pine (*Pinus pinaster*), forest tree metabolomics, pine wilt disease (PWD), primary metabolism, chlorophyll *a* fluorescence (OJIP), plant resistance

## INTRODUCTION

The pinewood nematode (PWN) *Bursaphelenchus xylophilus* is the causal agent of the pine wilt disease (PWD), and represents a major threat to worldwide conifer forests, especially *Pinus* spp., with significant ecological

and economical losses. The PWN is vectored by long-horned beetles (*Monochamus* spp.) and spread into healthy trees during maturation feeding or into decaying trees through oviposition (Evans et al., 1996, 2008). In general, PWD symptoms include needle chlorosis and wilting that reflect the blockage of the water-conducting system caused by cavitation and embolism of the tracheids in the xylem, leading to rapid tree desiccation and death (Myers, 1988; Fukuda, 1997; Futai, 2013).

The PWN is native to North America and was introduced in Japan in 1905 where the PWD was first reported in Japanese red pine (*Pinus densiflora*) (Futai, 2008). It then spread to other East Asian countries devastating other native pine species, such as *Pinus thunbergii* and *Pinus massoniana* (Nose and Shiraishi, 2008). Human activities (e.g., international wood trade) promoted the geographic expansion of the PWN, and in 1999 it was detected in Portugal associated with maritime pine (*Pinus pinaster*) (Mota et al., 1999). Since then, the PWN has reached Spanish border territories, thereby increasing the concern of its spread to European forests (Abelleira et al., 2011).

The PWN is classified by the European and Mediterranean Plant Protection Organization as a A2 quarantine pest. As a consequence, the open trade of wood products derived from geographic areas where its occurrence is documented is highly regulated (EPPO, 2018). To control the presence of the PWN and prevent its spread to other European territories, current phytosanitary safety measures mainly include the identification and elimination of symptomatic trees, the creation of a buffer zone across the Portugal-Spain border, and the control of the insect vector population (Rodrigues, 2008; ICNF, 2019). However, the expansion of the PWD to European forests is projected to be aggravated in the current global climate change scenario, due to the intensity and frequency of adverse environmental-stress factors, such as increased temperatures and drought events (Hirata et al., 2017; de la Fuente and Beck, 2018; de la Fuente et al., 2018; Ikegami and Jenkins, 2018; Gruffudd et al., 2019).

Breeding for resistance is one relevant forest management strategy to control pest and disease outbreaks and promote the health of forest ecosystems that are under increasing environmental stress. The implementation of mass selection breeding programs is crucial to generate populations with quantitative resistance and accelerate the widespread dissemination of resistant genotypes (Ennos, 2015). Intraspecific variation in PWD resistance

within susceptible species prompted the launch of breeding programs in Asian countries affected by the disease; namely, Japan in 1978 for the selection of resistant *P. densiflora* and *P. thunbergii* trees, and China in 2001 for resistant *P. massoniana* (Nose and Shiraishi, 2008). In 2009, a similar resistance breeding program for *P. pinaster* was initiated in Portugal (Ribeiro, 2012). From a reference population of 457 *P. pinaster* plus trees, 96 half-sib families were tested for genetic survival variability to PWN infection and the 15 top-ranked families were selected for clonal seed orchard establishment (Carrasquinho et al., 2018). However, resistance to PWN infection is a quantitative trait, and within a half-sib family, only a small fraction of the individuals may prove resistant while the majority are susceptible. For the selected 96 *P. pinaster* half-sib families, predicted survival means at 157 days after inoculation ranged from 7 to 23% (Carrasquinho et al., 2018). *Pinus pinaster* is a native species from the western Mediterranean basin, but its distribution is greatly fragmented. Studies on molecular markers and quantitative traits have shown high genetic variability in morphological and adaptative traits among populations from different provenances (González-Martínez et al., 2002). This genetic variability has been further correlated with significant differences in susceptibility to PWN infection among different *P. pinaster* populations from the Iberian Peninsula and France (Zas et al., 2015; Menéndez-Gutiérrez et al., 2017).

Despite the numerous studies on PWN and PWD, the current knowledge on the molecular mechanisms underlying tree resistance to PWD is still very limited. In addition, only few studies have focused on the comparison of transcriptional responses between resistant and susceptible plants, within susceptible species, namely in *P. thunbergii* (Hirao et al., 2012), *P. massoniana* (Liu et al., 2017) and more recently *P. pinaster* (Modesto et al., 2021). These studies showed that resistance and susceptibility to PWD do not rely only on qualitative differences in gene expression, but also on variations in the timing and magnitude of their expression. In general, the transcriptome profiling of *Pinus* spp. after PWN infection has revealed differentially expressed genes mostly related to secondary metabolism (e.g., phytohormone, phenylpropanoid, and terpenoid biosynthesis), ROS detoxification, and also to primary metabolism, namely carbohydrate metabolism (Gaspar et al., 2017, 2020; Liu et al., 2017; Lee et al., 2018, 2019; Modesto et al., 2021). Alterations in secondary metabolism in response PWN infection include an increase in defense-related phytohormones involved in jasmonic acid (JA) and salicylic acid (SA) pathways in PWN-susceptible *P. pinaster*, but not in

resistant phenotypes (Modesto et al., 2021; Rodrigues et al., 2021). On the other hand, transcriptomic profiling of *P. pinaster* plants revealed an enrichment in amino sugar and nucleotide sugar metabolic pathways only in resistant plants (Modesto et al., 2021). The regulation of primary metabolism in biotic stress responses has gained increasing interest, mainly due to its key role in fulfilling the energetic demands for plant defense mechanisms and as a source of signaling molecules (Berger et al., 2007; Bolton, 2009; Steinbrenner et al., 2011; Rojas et al., 2014). Thus, following the recent advances in transcriptomic analysis, a metabolomics approach would provide comprehensive information on the metabolite profiling of pine tree tissues in response to PWN infection, as it is considered the molecular phenotype of a living organism, reflecting the interaction between the genetic traits and environmental factors (Fiehn, 2002; Fernie et al., 2004).

In this study, a gas chromatography coupled to time-of-flight mass spectrometry (GC-TOF-MS) platform was used to characterize the primary metabolome of a *P. pinaster* half-sib family, after PWN inoculation. This family has been previously genetically evaluated for PWD resistance in a mass selection program using Empirical Best Linear Unbiased Prediction (EBLUP) and estimated Breeding Values (Carrasquinho et al., 2018). Primary metabolite profiling of susceptible and resistant plants was further integrated with morphological, physiological and anatomical parameters for a comprehensive characterization of *P. pinaster* differential response to PWN infection. This integrative approach can allow the identification of potential primary metabolism-related resistance traits that can be further used in future studies for PWD management.

## MATERIALS AND METHODS

### Plant Material

*Pinus pinaster* Aiton seeds were obtained from a plus tree (half-sib family 440) belonging to a breeding population for PWD resistance at “Herdade da Comporta” (38°21'28.52"N; 8°45'49.89"W) in southern Portugal (Ribeiro, 2012). This half-sib family was classified as one of the 15 top-ranked half-sib families (out of 96) regarding the resistance to PWD (Carrasquinho et al., 2018). After cold-wet stratification (three weeks in the dark at 4°C), stratified seeds were germinated in forestry trays (54-universal, Sinorplásticos,

Espinho, Portugal) in greenhouse conditions. Plants were grown for 22 months under natural daylight in a greenhouse equipped with a cooling system and an automatic sprinkler irrigation system set for 5 min/48 h during the winter and 3 min/24 h during the summer.

### **Pinewood Nematode Inoculum**

*Bursaphelenchus xylophilus* (Steiner and Buhrer) Nickle isolate Bx013.003 used in this study was obtained from an infected field tree exhibiting PWD symptoms in central Portugal (39°43'33.8"N, 9°01'55.7"W) and was included in the nematode collection of the Nematology Laboratory at INIAV (Oeiras, Portugal). The sequence of the internal transcribed spacer (ITS) region is available at GenBank database (NCBI) under the accession number MF611984.1. Nematodes were extracted using the “tray” method (Whitehead and Hemming, 1965) and maintained in cultures of a non-sporulating *Botrytis cinerea* strain grown on steam-sterilized hydrated barley (*Hordeum vulgare*) grains, at 25 ± 1°C. Prior to inoculation, nematodes were allowed to grow on sterilized wood. Nematodes were isolated from the culture media using the tray method (Whitehead and Hemming, 1965) and suspended in water in a concentration of 1000 PWN/mL.

### **Experimental Design**

The experimental design layout consisted of a completely randomized design, with two factors: inoculation and time after inoculation, with three and four levels, respectively (Figure 1). For inoculation levels were: (i) non-inoculated, (ii) mock-inoculated, and (iii) PWN-inoculated plants; and for time after inoculation levels were: (i) 14, (ii) 21, (iii) 28, and (iv) 35 days after inoculation (DAI), respectively. For a total of 633 plants, the height and basal stem diameter were measured before inoculation, using a marked scale and a digital caliper (Mitutoyo CD-15DCX, Mitutoyo Corp., Kawasaki, Japan).

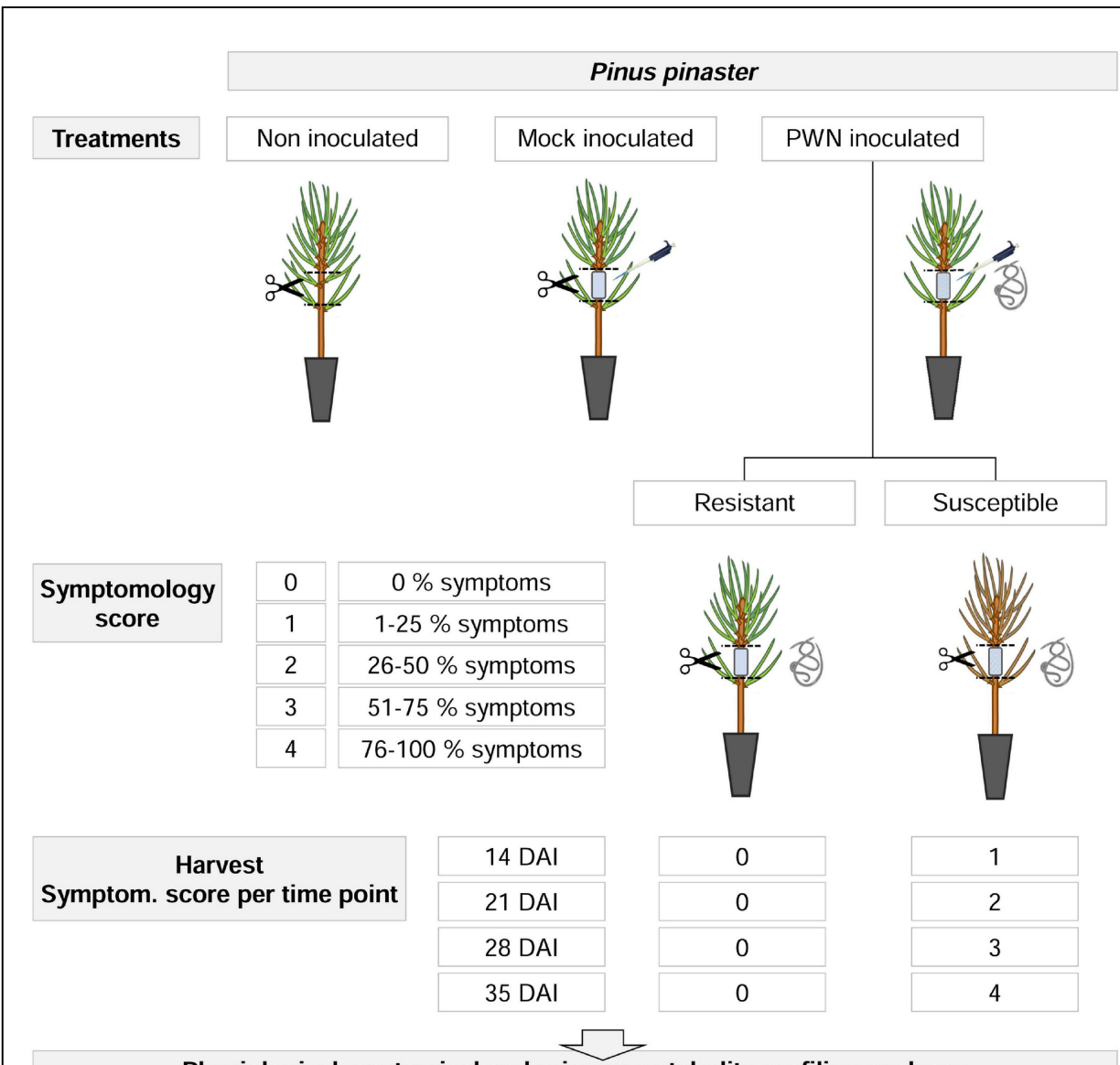


**FIGURE 1.** Experimental design for physiological, anatomical and primary metabolite profiling analyses in 22-month-old *Pinus pinaster* half-sib plants, up to 35 days after inoculation (DAI) with the pinewood nematode (PWN) *Bursaphelenchus xylophilus*. First, three manipulative treatments were applied (i.e., non-inoculated, mock-inoculated and PWN-inoculated). For PWN-inoculated plants, a symptomology score was established based on external symptoms development, ranging from 0 (no external symptoms, i.e., resistant plants) to 4 (76–100% external symptoms). At each sampling time point (14, 21, 28, and 35 DAI), PWN-inoculated plants were characterized as resistant or susceptible, according to the symptomology score and harvested as indicated.

## Inoculation and Sampling Procedure

For the inoculation process (Supplementary Figure 1), needles were manually removed from an area of ca. 5 cm in the upper part of the stem of each plant. In this area, superficial longitudinal incisions were performed with a sterile razor blade, and a sterilized piece of cotton was placed and fixed with Parafilm®. A suspension with an estimated number of 500 PWNs (at various stages of development) was applied with a micropipette, and the cotton was gently covered with Parafilm® to prevent the inoculum from drying. A mock inoculation was performed by replacing the PWN suspension with sterile water.

For PWN-inoculated plants, a symptomology score ranging from 0 to 4 was established based on the percentage of discolored and wilted needles; namely, 0 (i.e., no external symptoms), 1 (1–25 %), 2 (26–50 %), 3 (51–75 %), and 4 (76–100 %). At each sampling time point (14, 21, 28, and 35 DAI), PWN-inoculated plants were classified as resistant or susceptible according to the symptomology score, and harvested according to PWD symptom progression as indicated in Figures 1, 2. To assure that metabolomics analysis reflected the PWD symptom progression only plants with score 1 were harvested at 14 DAI; score 2 harvested at 21 DAI; score 3 harvested at 28 DAI; and finally score 4 at 35 DAI. In this study, resistance to PWN infection was considered when inoculated plants showed no external symptoms (i.e., no discolored and/or wilted needles), and were able to limit nematode multiplication and infection (Kover and Schaal, 2002; Pagán and García-Arenal, 2018).

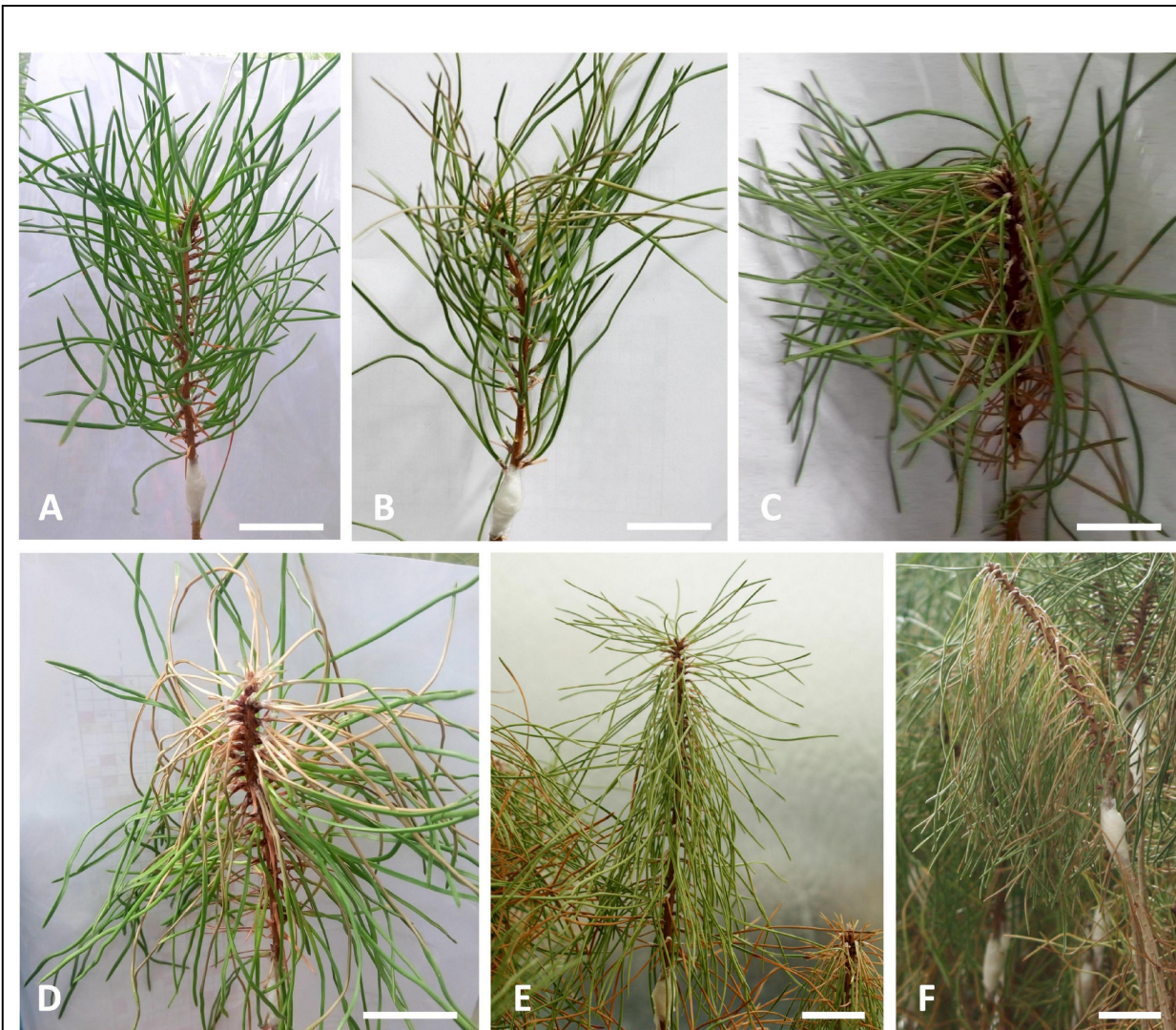


**FIGURE 2.** Visual evaluation of external symptoms in 22-month-old *Pinus pinaster* half-sib plants after inoculation with the pinewood nematode (PWN) *Bursaphelenchus xylophilus*, up to 35 days after inoculation (DAI) and according to a symptomatology score defined by the percentage of discolored and/or wilting needles, namely **(A)** 0 % (35 DAI), **(B)** 1–25 % (14 DAI), **(C)** 26–50 % (21 DAI), **(D)** 51–75 % (28 DAI), **(E,F)** 76–100 % (35 DAI). Scale bars = 5 cm.

The inoculation area of 15 biological replicates, as well as the corresponding stem portion in non-inoculated plants, were collected, immediately placed in liquid nitrogen, and stored at  $-80^{\circ}\text{C}$  until sample processing for GC-TOF-MS analysis. Needles from each biological replicate were also collected for plant water status characterization. Stem segment samples, from three biological replicates, were immediately placed in buffered glutaraldehyde for microscopy analysis.

During the course of the experiment, the average day/night air temperature and relative humidity was 27/21°C and 63/76 %, respectively.

## Plant Physiological Characterization

### Plant Water Status

Plant water status was estimated *via* relative water content (RWC) as previously described in Amaral et al. (2019). From each 15 biological replicates, fresh weight (FW) of six needles was measured immediately after collection. Needles were transferred to tubes with distilled water and incubated overnight at 4°C. The excess water was then carefully removed and turgid weight (TW) was registered. Needles were oven-dried at 60 °C for one week and reweighted for dry weight (DW) determination. RWC was calculated as:

$$RWC (\%) = \frac{FW - DW}{TW - DW} \times 100$$

### Chlorophyll a Fluorescence

Chlorophyll *a* fluorescence (ChlF) kinetic measurements were made *in vivo* at 10 am using a Handy Plant Efficiency Analyzer (PEA) – Chlorophyll Fluorimeter (Hansatech Instruments, Kings Lynn, United Kingdom). The needles to be measured (green, non-detached) were arranged in parallel completely covering the 4 mm<sup>2</sup> test hole, and were dark adapted with light-withholding leaf clips (Hansatech Instruments, Kings Lynn, United Kingdom) for 15 min. Samples were then exposed to a saturating light pulse (3500 µmol m<sup>-2</sup> s<sup>-1</sup>) for 1 s in order to ensure closure of all PSII reaction centers (RC) and obtain the ChlF transient rise (OJIP curve) (Strasser et al., 2004, 2010; Stirbet and Govindjee, 2011; Goltsev et al., 2016). ChlF intensity at 20 µs was considered as the minimum fluorescence F<sub>0</sub> (Strasser et al., 2004). Each OJIP curve represents the mean values obtained from 15 biological replicates.

For a better visualization of the effect of PWN inoculation on the transient dynamics, the OJIP curves were plotted as (i) fluorescence intensity; (ii) relative variable fluorescence (V<sub>t</sub>) double normalized to F<sub>0</sub> and maximum fluorescence F<sub>m</sub>; and (iii) differences in relative fluorescence rise kinetics

$(\Delta V_t)$  by subtracting the  $V_t$  values recorded for non-inoculated control plants from those recorded for mock-inoculated and PWN-inoculated plants.

ChlF transients were analyzed using data extracted from the OJIP-test parameters; namely, (i) normalized derived data; (ii) energy fluxes per active RC and per leaf cross section at fully closed RC ( $CS_m$ ) or fully open RC ( $CS_0$ ); (iii) quantum yields; (iv) density of RC, and (v) rates and performance indexes (PI). Definitions and derivations of all OJIP-test transients (Strasser et al., 2004, 2010; Stirbet and Govindjee, 2011; Goltsev et al., 2016) are summarized in Supplementary Table 1.

### **Gas Chromatography Coupled to Time-of-Flight Mass Spectrometry Primary Metabolite Profiling**

Primary metabolites were extracted from 100 mg fresh weight (FW) of finely homogenized stem material per biological replicate (previously macerated under liquid nitrogen), in 1400  $\mu$ L ice-cold methanol with 60  $\mu$ L of ribitol (0.2 mg  $mL^{-1}$  ribitol in water) as internal standard, as previously described in Lisec et al. (2006). The mixtures were vortex-mixed and incubated in a shaker (ThermoMixer, Eppendorf, Hamburg, Germany) for 15 min at 70°C and 950 rpm. After centrifugation at room temperature and 12000 g for 10 min, the supernatant was collected, mixed with 750  $\mu$ L chloroform and 1500  $\mu$ L water, and vortex-mixed. The mixtures were centrifuged again at 2200 g for 15 min, and 150  $\mu$ L of the polar (upper) aqueous/methanol phase were evaporated to dryness using a centrifugal concentrator for a minimum of 3 h at 30°C (Vacufuge Plus, Eppendorf, Hamburg, Germany), and stored at -80°C.

Primary metabolites were derivatized using methoxyamination and trimethylsilylating reagents and analyzed as in Lisec et al. (2006). Briefly, dried samples were dissolved in 40  $\mu$ L of methoxyamine hydrochloride (20 mg  $mL^{-1}$  in pyridine), and incubated in a shaker for 2 h at 37°C. Next, 70  $\mu$ L of *N*-methyl-*N*-(trimethylsilyl)trifluoroacetamide (MSTFA) and 20  $\mu$ L of a mixture of fatty acid methyl esters (FAMEs) were added and shaken for 30 min at 37°C.

Primary metabolite profiling analysis of the derivatized samples (1  $\mu$ L aliquots) was performed on an Agilent 6890N gas chromatograph (Agilent Technologies, Böblingen, Germany), and a LECO Pegasus III TOF-MS running in electron ionization (EI) mode (LECO Instrumente, Mönchengladbach, Germany). The chromatographic separation was performed

on a VF-5MS column (Varian Inc., 30 m length, 0.25 mm inner diameter, and 0.25  $\mu\text{m}$  film thickness). The temperature program was set as follows: isothermal for 2 min at 85°C, followed by a 15°C  $\text{min}^{-1}$  ramp to 360°C, and hold at this temperature for 6 min. The injector and transfer line temperatures were set to 230°C and 250°C, respectively, and the injection was performed both in the splitless and split (1:5) mode with helium carrier gas flow set to 2  $\text{mL min}^{-1}$ . After a solvent delay of 180 s, mass spectra were scanned from  $m/z$  70–600 with acquisition rate of 20 spectra  $\text{s}^{-1}$  and a detector voltage between 1700 and 1850 V.

Biological variations were controlled by analyzing FAMEs as retention time index internal standard markers, and a quality control standard solution of 41 pure reference compounds (i.e., the most detected and abundant metabolites) throughout the analysis. GC-TOF-MS data were evaluated using AMDIS (Automated Mass Spectral Deconvolution and Identification System) software (v. 2.71). Primary metabolites were annotated using the TagFinder 4.0 software (Luedemann et al., 2008) and a reference library of ambient mass spectra and retention indices from the Golm Metabolome Database<sup>1</sup> (Kopka et al., 2005; Schauer et al., 2005). Metadata information of this experiment following minimum reporting standard guidelines of the Metabolomics Standard Initiative (Lisec et al., 2006; Fiehn et al., 2007; Sumner et al., 2007; Fernie et al., 2011; Alseekh et al., 2021) can be found in Supplementary Table 2.

## Histological Characterization

*Pinus pinaster* stem samples were fixed with glutaraldehyde 2.5 % (v/v) in 0.1 M sodium phosphate buffer, pH 7.2. Samples were kept in the fixative under vacuum at room temperature for 30 min, followed by three days at 4°C. The material was then washed in the fixative buffer and dehydrated in a graded series of ethanol before being infiltrated and embedded in Technovit® 7100 resin (Heraeus Kulzer, Wehrheim, Germany), according to the manufacturer's instructions. Transversal cross sections (2  $\mu\text{m}$  thick) were cut using a Leica RM 2155 microtome (Leica Microsystems, Nussloch, Germany) and heat-fixed to slides. To highlight the contrast between the plant tissues and PWNs, sections were stained with a periodic acid-Schiff (PAS) staining system (Sigma Aldrich), following manufacturer standard procedure for polysaccharides detection and counter-stained with Coomassie blue stain for proteins (Fisher, 1968). Stained sections were examined under a Leica DM6

B Upright microscope, coupled to a Leica DFC7000 T camera and using the LAS X system of image capture software (Leica Microsystems GmbH, Wetzlar, Germany).

## Statistical Analysis

Statistical analyses were performed in R and R Studio software (RStudio Team, 2018; R Core Team, 2019). R Packages used to perform statistical analysis include “agricolae” (Mendiburu, 2020), “car” (Fox and Weisberg, 2019), “gplots” (Warnes et al., 2020), “ggplot2” (Wickham, 2016), “mixOmics” (Rohart et al., 2017), “olsrr” (Hebbali, 2020), “scales” (Wickham and Seidel, 2020), and “stats” (R Core Team, 2019). Plant height, diameter, physiological and metabolite data were used as response variables. Each time point was analyzed independently as a single factor with four inoculation levels (i.e., non-inoculated, mock inoculated, susceptible PWN-inoculated, and resistant PWN-inoculated plants). The wound effect was assessed by comparing mock-inoculated with non-inoculated controls. PWN infection was evaluated comparing PWN-inoculated with mock-inoculated plants.

To analyze plant survival, a logistic regression, i.e., a generalized linear model with logit link function and binomial error distribution, was fitted. The model considered the effects of plant height and plant diameter as predictors in the survival outcome. Binned residual plot was used to confirm the fit of the regression model.

Physiological data was analyzed using the Kruskal-Wallis non-parametric test, with a False Discovery Rate (FDR) correction on the *p*-values.

For the metabolomics data, the relative abundance of primary metabolite levels was normalized to the internal standard (ribitol) and the fresh weight of the samples. Metabolomics data were log-transformed before statistical analysis to fit the normality and homoscedasticity assumptions of the ANOVA using Shapiro-Wilk and Levene’s test, respectively. For each time point of data collection, one-way ANOVA at a 95 % confidence level was used to assess differences between treatments, with an FDR correction on the *p*-values for multiple comparisons. In addition, multiple comparison analysis was performed using Tukey’s HSD test.

Supervised Partial Least Squares – Discriminant Analysis (PLS-DA) was performed using the leave-one-out cross-validation embedded in the “mixOmics” package. Sparse PLS (sPLS) was used to integrate physiological

and metabolomics data. Specifically, metabolite data were used as predictors for physiological data. The regression models were tuned based on total Q2 for component selection and Mean Square Error for variable selection for each component (Lê Cao et al., 2008).

## RESULTS

### Pine Wilt Disease Progression

After inoculation with the PWN, PWD external symptoms were assessed weekly (Figure 2). At 14 DAI, needles of susceptible plants started to fade to a grayish color (needle discoloration). Symptoms progressed rapidly during the following days as needles wilted and turned to a yellowish and brown colors. At 28 DAI, more than half of the plants scored level 3 or 4; that is, plants exhibited at least 50 % of needle discoloration and/or wilting. At 35 and 42 DAI, 77 % and 92 % of the plants, respectively, showed more than 75 % of needles being desiccated and brown (score level 4). Resistant plants showed no external symptoms of disease progression. Results from the logistic regression model, showed that the effect of plant height and plant diameter on plant survival were not statistically significant ( $p > 0.05$ ), and thus, were not considered as covariates in the subsequent metabolomics and physiological analysis.

### Histological Characterization of Pinewood Nematode-Inoculated *Pinus pinaster* Plants

Pine wilt disease (PWD) progression and the presence of the PWN in inoculated *P. pinaster* plants was characterized by light microscopy in comparison to controls (Figure 3). The typical anatomy of a pine stem was observed in control plants; namely, several axial resin ducts distributed in the cortex and in the xylem as well as radial resin ducts along the xylem rays extending from the secondary xylem to the cortex with no signs of cell degradation (Figures 3A,B). Resistant plants (i.e., no external symptoms at 35 DAI) showed destroyed epithelial cells in some cortical and axial resin ducts and the formation of cavities in the cortex (Figures 3C–F). Nematodes were observed within these cavities, and in the lumen of the destroyed resin ducts. However, cell degradation in resistant plants was limited to a small area of the stem, most likely the inoculation area. The occlusion of the cortical resin

canals by a gel-like resin was also observed in resistant plants (Figure 3F). In susceptible plants with ca. 50 % external symptoms, cortical and axial resin ducts were completely destroyed, and cavities were formed due to the degradation of cells in the cambial zone as well as in the cortical resin ducts and surrounding parenchyma cells (Figure 3G). Nematodes were found within these cavities in the cambial region, cavities in the cortex, and in the degraded axial resin ducts (Figures 3H–J). As the disease progressed in susceptible plants, severe degradation of all stem tissues was visible. Cells in the cortex were completely degraded, the cavities in the cambium and phloem enlarged and fused, and as a result of the migration of the nematodes to the inner tissues, the pith tissue was severely destroyed. Nematodes were found in the pith area, cavities in the cambium, and in the lumen of the axial resin ducts (Figures 3K–M).

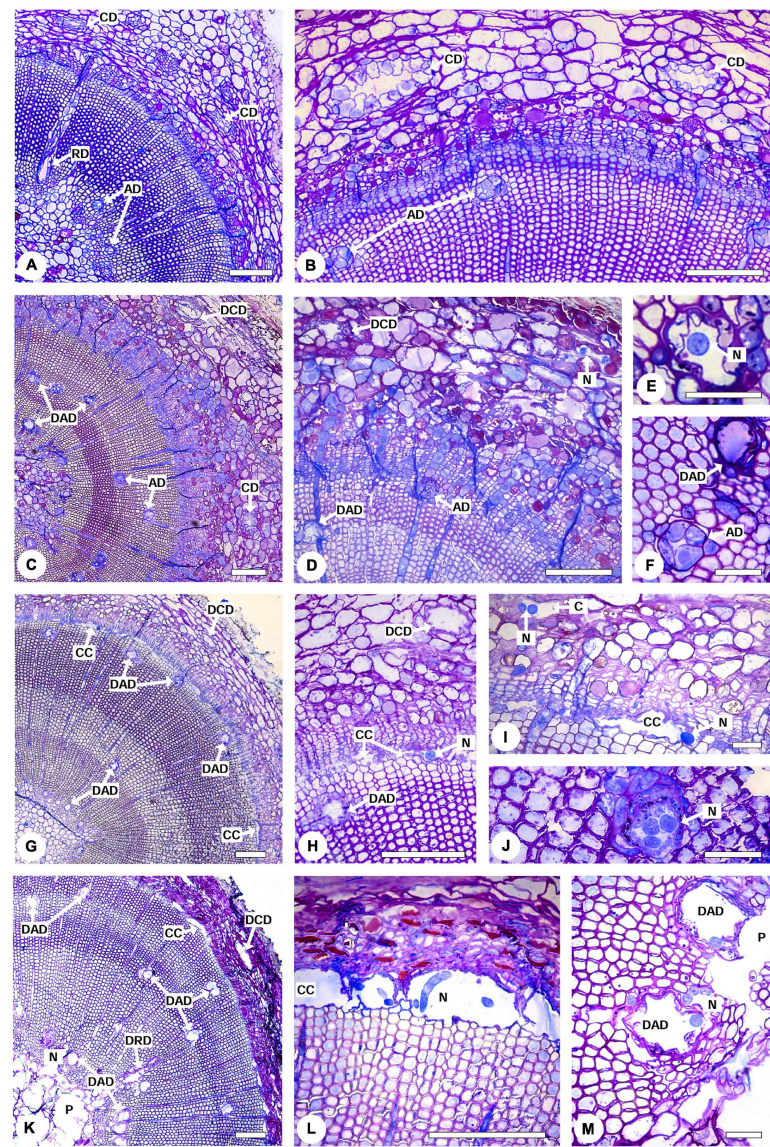


**FIGURE 3.** Light micrographs of stem cross-sections from 22-month-old *Pinus pinaster* plants non-inoculated and 39 days after inoculation with the pinewood nematode (PWN) *Bursaphelengus xylophilus*. **(A,B)** Non-inoculated control plant showing the characteristic anatomy of a pine stem with no signs of cell degradation, namely cortical resin ducts (CD), radial (RD) and axial resin ducts (AD) surrounded by intact epithelial cells. **(C–F)** PWN-inoculated resistant plant showing destruction of the epithelial cells of some cortical and axial resin ducts (DCD and DAD, respectively). Nematodes (N) were observed within cavities in the cortex **(D)** and the lumen of the axial resin ducts **(E)**. **(F)** Detail of an intact (AD) and destroyed (DAD) axial resin duct. **(G–J)** PWN inoculated susceptible plant with 50 % external symptoms showing cavities formed by the degradation of cells in the cambial zone (CC) and destruction of the epithelial cells of the cortical (DCD) and axial (DAD) resin ducts. Nematodes (N) can be observed within cavities in the cambial region **(H)**, cortex **(I)**, and within the axial resin ducts **(J)**. **(K–M)** PWN-inoculated susceptible plant with 100 % external symptoms. The pith tissue was completely destroyed (P), cavities in the cambium enlarged (CC) and nematodes (N) were observed in the pith area **(K)**, cavities in the cambium **(L)** and axial resin ducts **(M)**. Scale bars = 200 µm **(A–D,G,H,K–M)**, 50 µm **(E,F,I,J)**.

## Plant Water Status

Pinewood nematode (PWN) inoculation caused a decrease in the RWC of susceptible plants, in relation to non-inoculated and mock-inoculated control groups (Figure 4). This decrease was more pronounced at 35 DAI, with RWC values reduced to 50 %. Resistant plants showed a significant decrease in the RWC at 21 and 28 DAI. Nevertheless, at 35 DAI, the RWC was restored to levels similar to those of control plants.

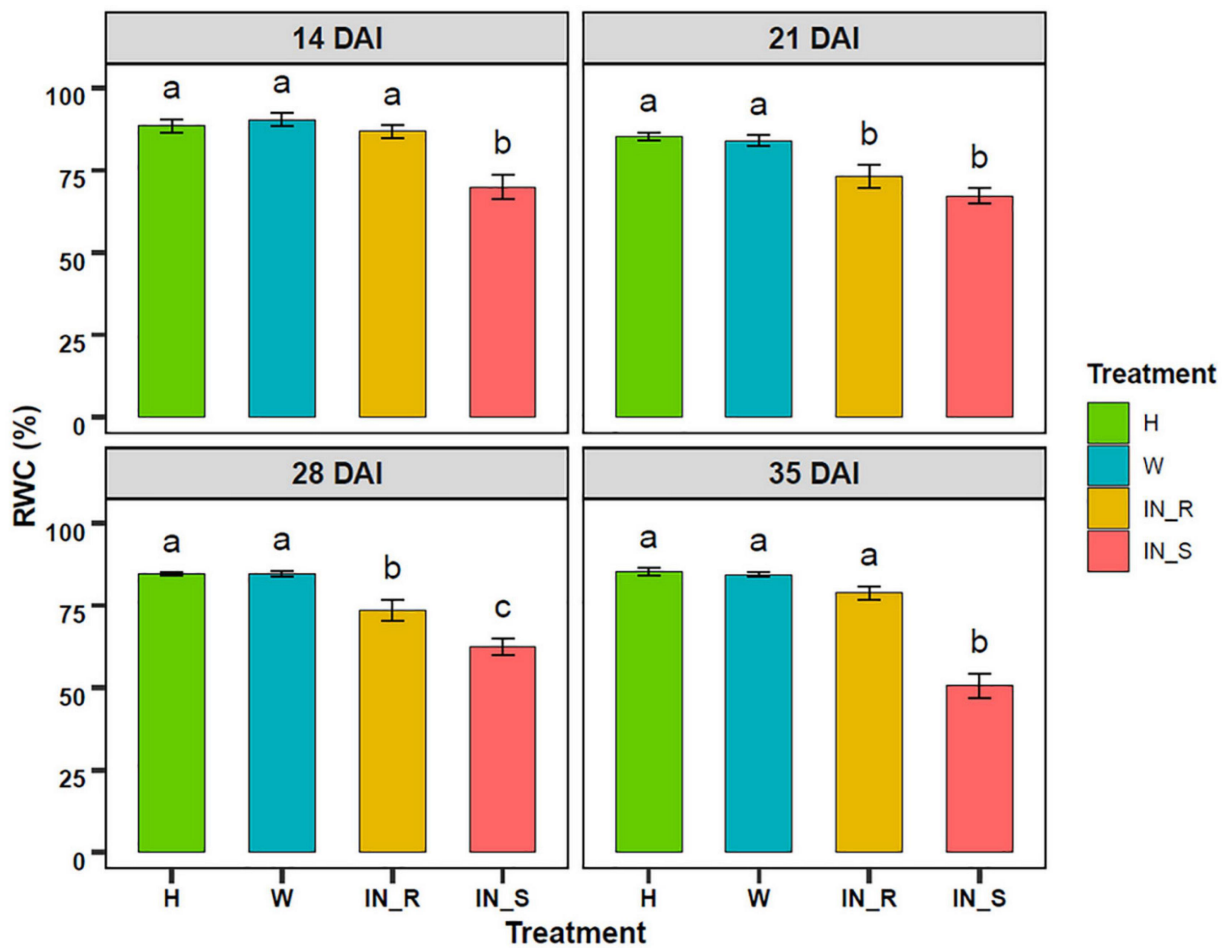


**FIGURE 4.** Variation of the relative water content (RWC, %) in needles of 22-month-old *Pinus pinaster* plants 14, 21, 28, and 35 days after inoculation (DAI) with the pinewood nematode *Bursaphelenchus xylophilus*. Bars represent the mean values  $\pm$  SE from 15 independent measurements. One-way ANOVA ( $p < 0.05$ ) followed by Tukey's HSD test was performed for means comparison and different letters express significant differences between treatments: non-inoculated (healthy, H), mock-inoculated (wounded, W), resistant PWN-inoculated (IN\_R), susceptible PWN-inoculated (IN\_S).

## OJIP Curves

The OJIP curves described the ChlF rise from O ( $F_0$ ) to P ( $F_m$ ), with two intermediate steps; namely, J ( $F_J$  at ca. 3 ms) and I ( $F_I$  at ca. 30 ms). In general, the OJIP curves of non-inoculated and mock-inoculated control plants presented the typical three phase kinetics (O-J, J-I, and I-P) (Figures 5A,B). In comparison, OJIP curves of PWN inoculated plants showed a significant increase in  $F_0$  in susceptible plants and a significant decrease in  $F_m$  in

susceptible and resistant plants, with exception of susceptible plants at 14 DAI and resistant plants at 28 DAI (Figure 5A and Supplementary Tables 3–5). The severe decrease in ChlF in susceptible plants strongly affected the shape of the OJIP curves (Figure 5A). In addition, double normalized OJIP curves showed that the largest deviations in relative fluorescence occurred in susceptible plants at the J step ( $V_J$ ), with a progressive increase starting at 21 DAI (Figure 5B). Further analysis of the  $\Delta V_t$  curves revealed positive bands for susceptible plants at 21, 28 and 35 DAI, from O to the I-P phase, indicating differences in electron transport rates when compared to resistant and control plants (Figure 5C). A closer analysis of the differential curves for the O-J phase confirmed the existence of an intermediate K-band between  $F_0$  and  $F_J$  (ca. 0.3 ms) and a L-band between  $F_0$  and  $F_K$  (ca. 0.15 ms) in susceptible plants at 21, 28 and 35 DAI (Figures 5D,E).

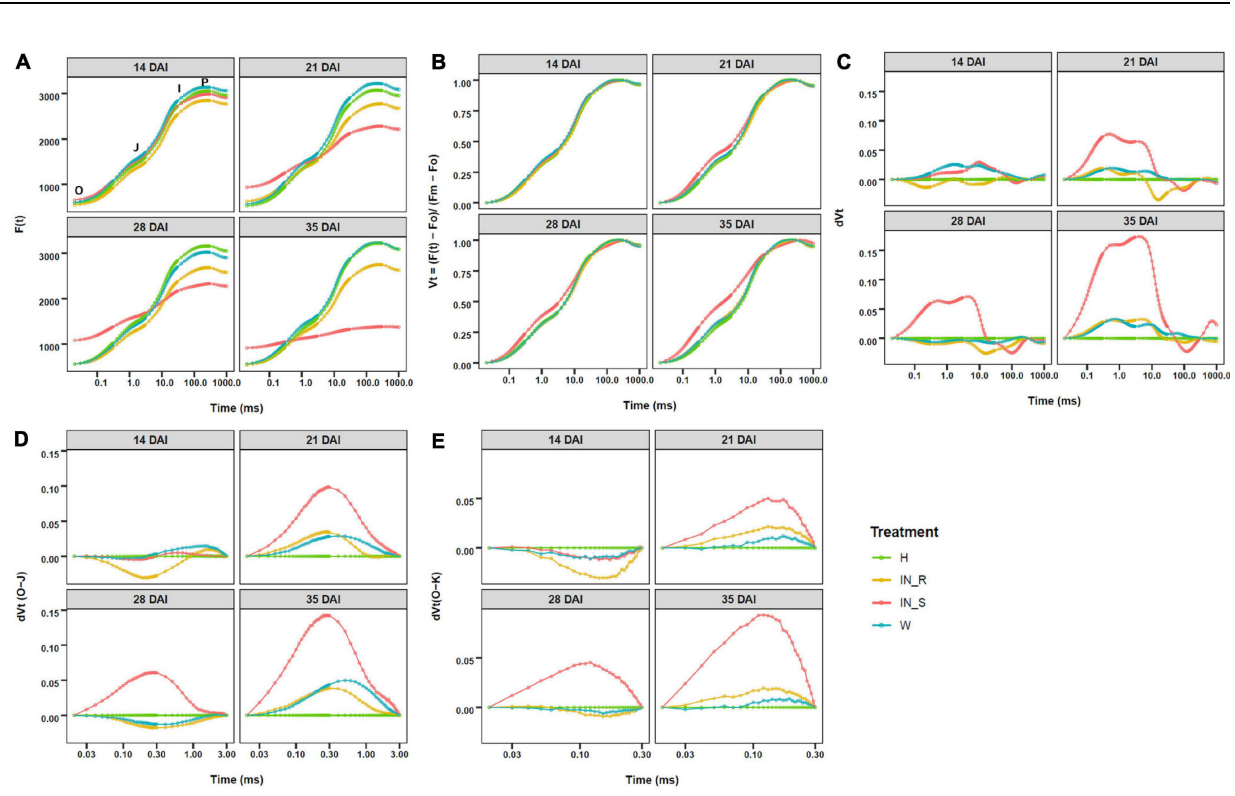


**FIGURE 5.** Fast chlorophyll a fluorescence (ChlF) OJIP curves (log time scale) recorded in dark-adapted needles of 22-month-old *Pinus pinaster* plants at 14, 21, 28, and 35 days after inoculation (DAI) with the pinewood nematode *Bursaphelenchus xylophilus*. Fluorescence values are expressed as: **(A)** raw ChlF transient curves; **(B)** relative variable fluorescence double normalized between  $F_0$  and maximum fluorescence ( $F_m$ ); **(C)** changes in O-P phase relative variable fluorescence intensity; **(D)** detail on changes in O-K phase relative variable fluorescence intensity; **(E)** detail on changes in O-K phase relative variable fluorescence intensity. Treatments were grouped in non-inoculated (healthy, H) mock-inoculated (wounded, W), susceptible PWN-inoculated plants (IN\_S) and resistant PWN-inoculated plants (IN\_R).

## OJIP-Test Parameters

The effect of PWN inoculation on the photosynthetic apparatus of *P. pinaster* plants caused significant variations in several OJIP-test parameters (Figure 6A and Supplementary Tables 3, 4). No significant differences were found when comparing mock-inoculated and non-inoculated controls (Supplementary Table 5). Most significant changes were observed in susceptible plants at 21, 28 and 35 DAI. In these plants, and according to the OJIP curves, the complementary area between  $F_0$  and  $F_m$  (Area) which represents the electron transport from PSII RC to the quinone pool, significantly decreased. The time needed to reach  $F_m$  ( $t_{Fm}$ ) significantly increased and the time needed to

obtain total RC closure ( $S_m/tF_m$ ) significantly decreased.  $F_v/F_0$ , considered as an indicator of the number and size of active photosynthetic RCs, significantly decreased from 14 DAI. The total number of electrons transferred to the electron transport chain (N) significantly increased at 21 and 28 DAI. A significant reduction in the number of active RCs (RC/ABS and RC/CS<sub>m</sub>) was supported by a significant increase in the rate of RCs closure ( $dV/dt_0$ ), absorbed energy per active RC (ABS/RC) and trapping per active RC (TR<sub>0</sub>/RC). Electron transport per CS<sub>0</sub> (ET<sub>0</sub>/CS<sub>0</sub>) significantly decreased at 35 DAI. A strong significant increase in heat dissipation DI<sub>0</sub>/RC, DI<sub>0</sub>/CS<sub>0</sub> and DI<sub>0</sub>/CS<sub>m</sub> (up to 18-fold) and in maximum quantum yield of non-photochemical de-excitation ( $F_0/F_m$ ) were observed at 35 DAI. Accordingly, the photochemical de-excitation rate constant (kP/ABS.kF) significantly decreased, whereas the non-photochemical de-excitation rate (kN/ABS.kF) significantly increased. The quantum efficiencies of electron transfer process ( $\phi_{Eo}$ ,  $\psi_{Eo}$ , and  $\phi_{Ro}$ ) significantly decreased as well as the energy fluxes per CS<sub>m</sub> (ABS/CS<sub>m</sub>, TR<sub>0</sub>/CS<sub>m</sub>, ET<sub>0</sub>/CS<sub>m</sub>, and RE<sub>0</sub>/CS<sub>m</sub>). The maximum photochemical efficiency ( $F_v/F_m$  or  $\phi_{P0}$ ) significantly decreased but the strongest significant reduction was observed in PI<sub>TOTAL</sub> and PI<sub>ABS</sub> at 35 DAI.

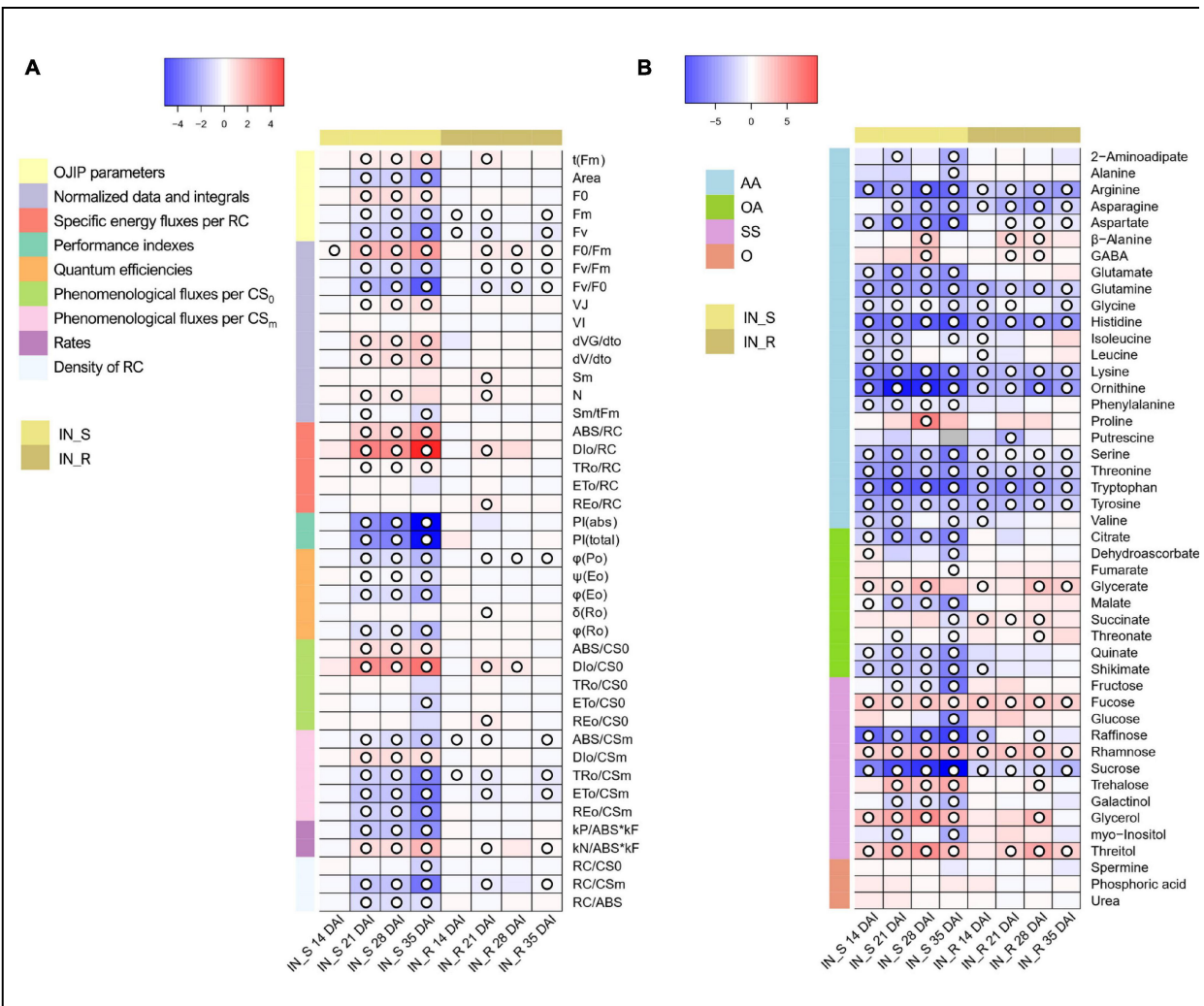


**FIGURE 6. (A)** Heatmap representing the changes in OJIP transients in dark-adapted needles of 22-month-old *Pinus pinaster* plants at 14, 21, 28, and 35 days after inoculation (DAI) with the pinewood nematode (PWN) *Bursaphelenchus xylophilus*. False color imaging was performed on  $\log_{10}$ -transformed data. Fold changes for PWN-inoculated plants (susceptible, IN\_S, and resistant, IN\_R) were calculated in relation to the mock-inoculated control for each time point ( $n = 15$ ). Significant changes using Kruskal-Wallis test are indicated as  $\circ$   $p < 0.05$ , with a false discovery rate (FDR) correction. **(B)** Heatmap representing the changes in relative levels of primary metabolites in stem tissues of 22-month-old *Pinus pinaster* plants 14, 21, 28, and 35 days after inoculation (DAI) with the pinewood nematode *Bursaphelenchus xylophilus*. Relative values (as means of 15 independent measurements) were normalized to the internal standard and fresh weight of the samples; false color imaging was performed on  $\log_{10}$ -transformed data. Fold changes for PWN-inoculated plants (susceptible, IN\_S, and resistant, IN\_R) were calculated in relation to the mock-inoculated control. Significant changes using one-way ANOVA are indicated as  $\circ$   $p < 0.05$ , with a false discovery rate (FDR) correction. Gray-color squares represent not detected (n.d.) values. Metabolites grouped in amino acids & derivatives (AA), organic acids (OA), sugars & sugar alcohols (SS), and others (O).

In resistant plants,  $F_m$  significantly decreased, except at 28 DAI. The normalized area above the OJIP curve which indicates the energy needed to close all RCs ( $S_m$ ) and the electron flux leading to the reduction of PSI ( $RE_0/RC$ ,  $RE_0/CS_0$  and  $\delta_{R0}$ ) significantly increased at 21 DAI. As observed for susceptible plants,  $tF_m$  and  $N$  also significantly increased at 21 DAI. A significant reduction in  $RC/CS_m$  was observed in resistant plants at 21 and 35 DAI. Heat dissipation ( $DI_0/RC$  and  $DI_0/CS_0$ ) significantly increased at 21 and 21-28 DAI, and  $F_0/F_m$  significantly increased at 21, 28 and 35 DAI. Accordingly, the non-photochemical de-excitation rate significantly increased. Energy fluxes per  $CS_m$  significantly decreased ( $ABS/CS_m$  and  $TR_0/CS_m$ , at 14, 21 and 35 DAI, and  $ET_0/CS_m$  and  $RE_0/CS_m$  at 21 and 35 DAI). The  $F_v/F_m$  and  $F_v/F_0$  significantly decreased at 21, 28 and 35 DAI.

### **Gas Chromatography Coupled to Time-of-Flight Mass Spectrometry Primary Metabolite Profiling**

Gas chromatography coupled to time-of-flight mass spectrometry (GC-TOF-MS) analysis allowed the identification of 46 primary metabolites in stem tissues of *P. pinaster*; namely, 22 amino acids, 11 sugars and sugar alcohols, nine organic acids, and four other primary metabolites (Figure 6B and Supplementary Tables 6, 7).

When compared to non-inoculated controls, no significant changes were observed in the levels of primary metabolites of plants subjected to a mock inoculation (Supplementary Table 7). This indicates that the wound caused by the inoculation process had no significant impact in the primary metabolism of *P. pinaster* plants.

Overall, PWN-inoculated susceptible plants showed a significant decrease in the levels of most amino acids, including the branched-chained amino acids (BCAA) leucine, isoleucine and valine, and a significant increase in proline (up to 21-fold at 28 DAI),  $\gamma$ -aminobutyric acid (GABA) and  $\beta$ -alanine (up to 4-fold at 28 DAI) (Figure 6B and Supplementary Table 6). A general significant increase was observed for most sugars; namely, glycerol (up to 15-fold at 28 DAI), fucose (up to 4-fold 28 DAI), rhamnose (up to 6-fold 28 DAI), trehalose (up to 9-fold at 35 DAI), and threitol (up to 13-fold at 28 DAI). However, a significant decrease was observed in the levels of raffinose and sucrose after PWN inoculation. Organic acids also showed an

overall significant decrease; namely, dehydroascorbate, quinate, shikimate and the tricarboxylic acid (TCA)-cycle intermediates citrate, malate and succinate.

The primary metabolite profile of resistant plants differed from that of susceptible plants, with less significant changes observed in the levels of several primary metabolites; namely, alanine, citrate, fructose, galactinol, glucose, glutamate, malate, *myo*-inositol, phenylalanine, and quinate (Figure 6B and Supplementary Table 6). However, similarly to susceptible plants, arginine, asparagine, aspartate, glutamine, glycine, histidine, lysine, ornithine, serine, threonine, tryptophan and tyrosine showed a significant decrease, whereas fucose, rhamnose, and threitol showed a significant increase (up to 8-fold at 28 DAI). A significant increase in the TCA-cycle intermediate succinate (up to 3-fold) was also observed at 14, 21 and 28 DAI. Other commonly known osmolytes also significantly increased in resistance plants, such as GABA (up to 2-fold at 21 and 28 DAI), glycerol and trehalose (up to 6-fold at 28 DAI).

Supervised PLS-DA was applied to GC-TOF-MS primary metabolite data to identify major sources of variation in the data. The PLS-DA score plot of the first two components (PC1 and PC2) showed control groups (non-inoculated and mock-inoculated) clustered together and clearly separated from susceptible samples, particularly by the PC1 which explained 41 % of the total variance (Figure 7A). Resistant samples are scattered between the cluster formed by the control groups and the susceptible samples, overlapping mostly with susceptible samples collected 14 DAI and control samples. For all treatments, no separation between time points could be observed. The contribution plots (Figure 7B) further highlighted the importance of every metabolite for each component, based on the maximum mean relative abundance and respective group category. In general, the metabolites that showed a significant variation ( $p < 0.05$ ) were those that mostly contributed to cluster separation. Control groups (non-inoculated and mock-inoculated plants) presented higher levels of most amino acids that significantly decreased in susceptible samples. In addition,  $\beta$ -alanine, GABA, glycerate, glycerol, proline, rhamnose, and threitol contributed the most for the clustering and separation of susceptible samples 28 DAI from the remaining treatments, while trehalose contributed the most for the separation of susceptible plants 35 DAI. On the other hand, fumarate, malate, succinate, threonate, fructose and fucose were the metabolites that most promoted the clustering of resistant

samples (particularly succinate). The remaining metabolites (mostly amino acids) contributed for the clustering of control groups.

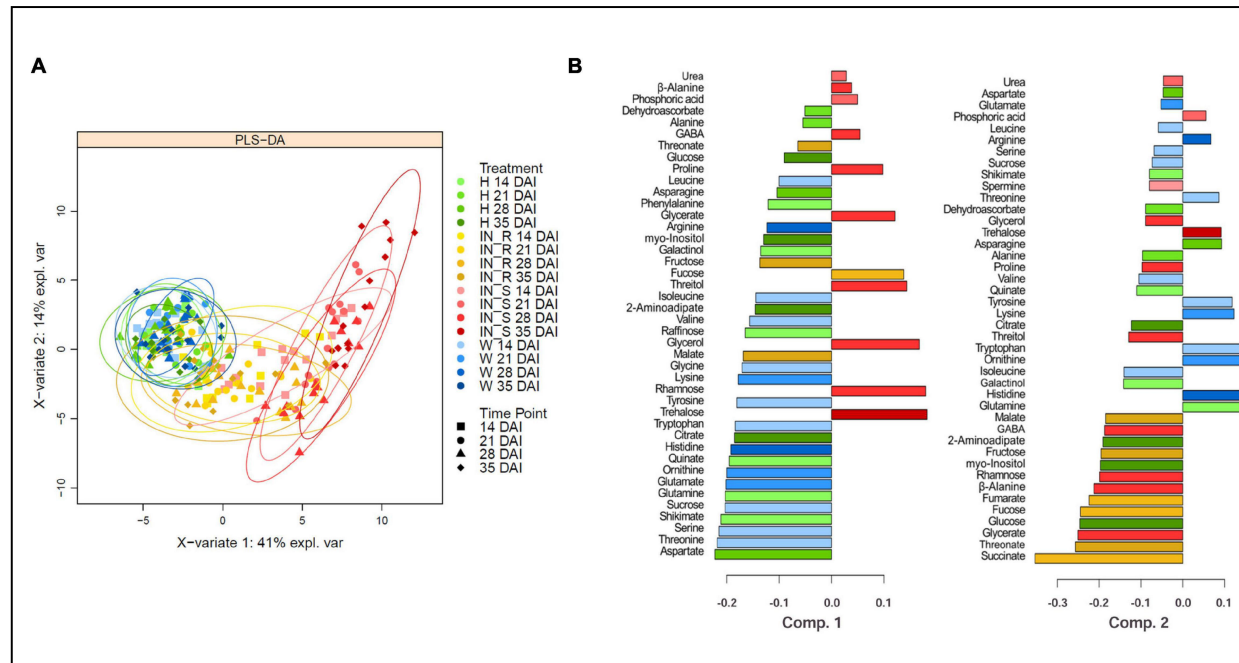


**FIGURE 7.** Partial least square discriminant analysis (PLS-DA) score (**A**), and contribution plots (**B**) of the primary metabolite profile of stems of 22-month-old *Pinus pinaster* plants after inoculation with the pinewood nematode *Bursaphelenchus xylophilus*. Treatments were grouped in non-inoculated (healthy, H) mock-inoculated (wounded, W), susceptible PWN-inoculated plants (IN\_S) and resistant PWN-inoculated plants (IN\_R). DAI indicate days after inoculation. The bar length in the contribution plots represents the loading weights of each metabolite in component 1 and 2, respectively. The color indicates the sample group in which the metabolite has a maximal importance (based on the mean).

## Integration of Metabolomics and Physiological Data

Sparse PLS (sPLS) analysis highlighted the differences between the *P. pinaster* response profiles after PWN inoculation (Figure 8A). A clear separation between susceptible and control plants (i.e., non-inoculated and mock inoculated) was observed on the horizontal axis (x-axis). Sparse PLS analysis further highlighted the separation of the susceptible plants at 35 DAI from all the other clusters. Resistant plants were clustered between susceptible and control plants. The cluster of resistant plants at 35 DAI overlapped with the control plants, revealing a high correlation between these sample groups.

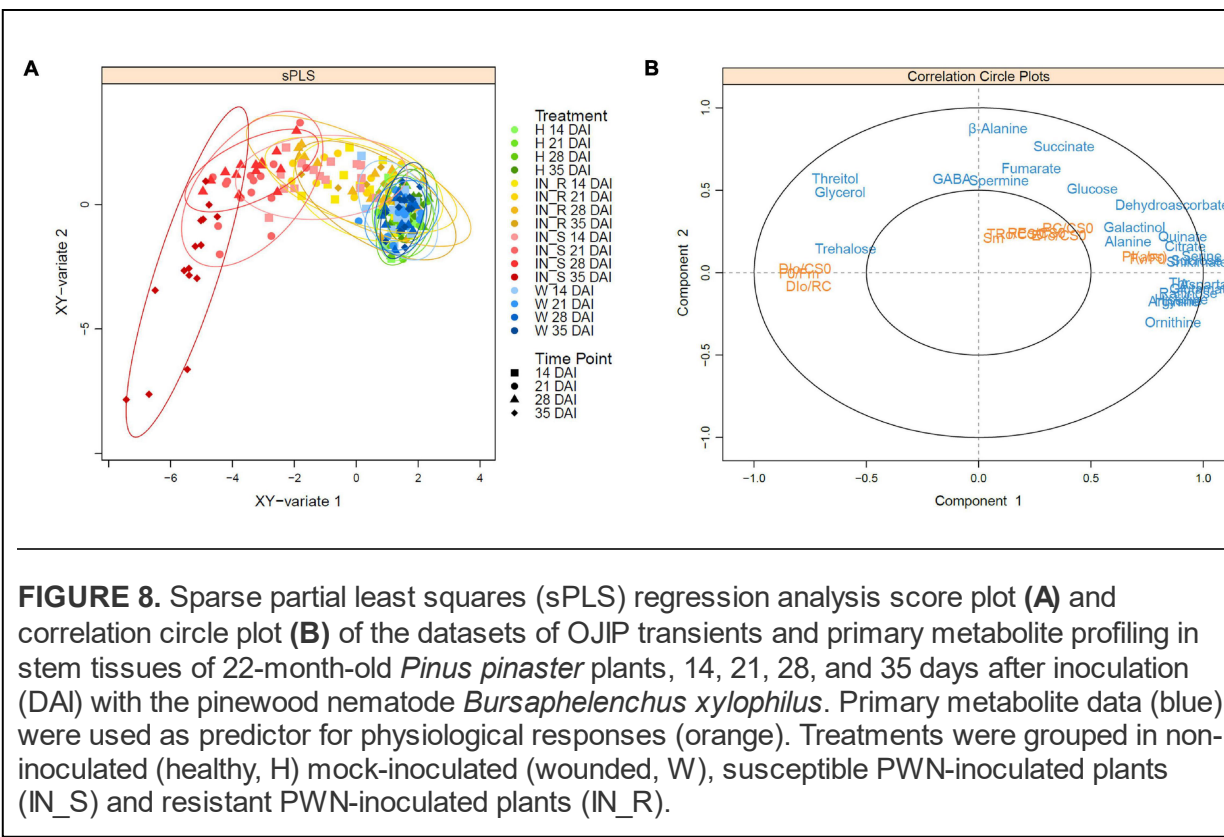


**FIGURE 8.** Sparse partial least squares (sPLS) regression analysis score plot (A) and correlation circle plot (B) of the datasets of OJIP transients and primary metabolite profiling in stem tissues of 22-month-old *Pinus pinaster* plants, 14, 21, 28, and 35 days after inoculation (DAI) with the pinewood nematode *Bursaphelenchus xylophilus*. Primary metabolite data (blue) were used as predictor for physiological responses (orange). Treatments were grouped in non-inoculated (healthy, H) mock-inoculated (wounded, W), susceptible PWN-inoculated plants (IN\_S) and resistant PWN-inoculated plants (IN\_R).

The sPLS correlation circle plot revealed a high number of highly correlated metabolites on the positive side of the x-axis, and together with the physiological parameters  $\text{PI}_{\text{ABS}}$  and  $\text{F}_v/\text{F}_0$ , were responsible for the cluster of control and resistant samples at 35 DAI groups (Figure 8B). On the negative part of the x-axis, sugars glycerol, threitol, and trehalose, and the physiological parameters  $\text{DI}_0/\text{CS}_0$ ,  $\text{DI}_0/\text{RC}$  and  $\text{F}_0/\text{F}_m$ , whose levels significantly increased with PWN infection, were responsible for the separation of the susceptible plants at 35 DAI. On the positive side of the y-axis,  $\beta$ -alanine, GABA, and spermine were responsible for the cluster of the remaining susceptible plants (up to 28 DAI) whereas TCA-intermediates fumarate and succinate were the metabolites most responsible for the cluster of resistant plants.

## DISCUSSION

### Intraspecific Variation of Anatomical Defenses in *Pinus pinaster* Affects Susceptibility to Pine Wilt Disease

The anatomical observations of PWN-inoculated susceptible *P. pinaster* plants are in agreement with previous reports for other susceptible species of the Pinaceae family (Mamiya and Shoji, 2009; Nunes da Silva et al., 2013, 2015). Once inside the plant, the nematodes disperse to the cortex, cortical resin ducts, cambium, xylem axial and radial resin ducts, finally reaching the pith at an advanced PWD stage. The nematodes use the resin ducts to migrate vertically, reproduce, and feed on the epithelial cells lining the ducts (Son et al., 2010). These anatomical modifications lead to PWD symptoms, mainly due to disruption of water transport (Fukuda, 1997). However, in resistant *P. pinaster* plants tissue damage was restricted, presumably to the inoculation site. The observed PWN distribution in compartmentalized areas in resistant plants is likely related with highly lignified cell walls surrounding cambial cavities and resin ducts (Kusumoto et al., 2014). In agreement, gene expression analysis, using the same *P. pinaster* half-sib family, revealed an over-expression of genes involved in lignin synthesis in resistant plants 72 h after infection, which translated to an increase in lignin content and cell wall lignification in stem tissues around the inoculation zone in these plants (Modesto et al., 2021). This modification hinders the PWN horizontal migration and delays damage expansion in the cortex and xylem.

Despite the increase in cell wall lignification in resistant *P. pinaster* plants, primary metabolite profiling did not show an accumulation of phenylalanine, up to 35 DAI. Phenylalanine is the first precursor of the phenylpropanoid pathway which is involved in the production of lignin, among other important secondary metabolites involved in plant defense (e.g., flavonoids, lignans) (Dixon et al., 2002; Bhuiyan et al., 2009; Tohge et al., 2013). No significant increase in phenylalanine levels suggests that the increase in lignin biosynthesis and cell wall lignification in resistant plants occurred in the early hours/days after PWN infection. These results are in agreement with the previous reports of lignin accumulation occurring mainly in the first days after PWN infection in resistant Pinaceae species such as *Picea abies* (Nunes da Silva et al., 2013), and resistant *P. pinaster* plants (Modesto et al., 2021). In *P. abies* by 14 DAI lignin content had already significantly decreased and for resistant *P. pinaster* plants no data was collected at later days after infection.

The observed occlusion of resin ducts with a gel-like resin in resistant plants has also been reported in *P. thunbergii* as an additional resistance mechanism to prevent the vertical migration of the nematodes (Kusumoto et

al., 2014). The reduction in PWN migration and multiplication ultimately allows host plants to survive PWN infection (Fukuda, 1997; Nunes da Silva et al., 2013).

In addition to the intrinsic differences between the PWN-inoculated plants, it should be highlighted that the differential susceptibility to PWN observed in this study could also be due to failures of the inoculation process. Despite the large number of PWN often used in inoculation experiments (up to 10000), only ca. 10 % of the inoculum is estimated to successfully invade the plant tissue (Kuroda, 2008). In susceptible species, the number of nematodes inside the plant rapidly increase resulting in larger numbers than those initially inoculated (Nunes da Silva et al., 2014, 2015; Menéndez-Gutiérrez et al., 2018); for initial concentrations of at least 50 PWN/plant, the success of the inoculation procedure and plant mortality has been reported to be over 92 % (Abelleira et al., 2013).

In this study, because the classification of plant resistance was based solely on external symptoms after PWN-inoculation, microscopy analysis of randomly selected susceptible and resistant plants allowed to confirm the presence of the PWN and/or cellular damage caused by the nematode migration. These observations showed that the nematodes successfully entered the plants through the wounds, thus validating the success of the inoculation process.

## **Pinewood Nematode Infection Impairs Photosynthesis in Susceptible *Pinus pinaster***

The OJIP curve represent the efficiency of electron transfer in the intersystem chain, from the reduction of the primary acceptor of PSII to the end electron acceptors at the PSI acceptor side. Any deviation from its typical shape is an indication of photosystem malfunction (Strasser et al., 2004; Goltsev et al., 2016; Kalaji et al., 2016; Baghbani et al., 2019). In this study, the evaluation of the OJIP curves observed in susceptible plants suggested that susceptible plants are more prone to damage to the photosynthetic apparatus upon PWN infection, in comparison with resistant plants. These changes include the appearance of L- and K- bands, well-known indicators of environmental stress (Kalaji et al., 2016). The K-band is related to damage in the oxygen evolving complex (OEC) due to an imbalance between the electron flow from the OEC to the RC at acceptor site of PSII, leading to a progressive decrease in the rates of photochemical processes (Strasser et al., 2004; Kalaji et al.,

2016; Baghbani et al., 2019). The enhanced L-band is related with a decrease in the excitation energy transfer between PSII units (i.e., PSII connectivity) (Yusuf et al., 2010). The OJIP transients were used to evaluate the electron transport flux from PSII RCs to PSI. Changes in OJIP transients (e.g., Area,  $F_0$ ,  $V_J$ ) in susceptible plants, indicated a blockage in electron transfer from the RC to the quinone pool. When primary quinone  $Q_A$  is unable to accept electrons from PSII, most likely due to inactivation of OEC, the RCs are converted to inactive. In addition, the observed increase in ABS/RC, and  $TR_0/RC$  (i.e., enhanced efficiency per RC), did not result in the increase of electron transport energy  $ET_0/RC$ , but in a sharp increase in  $DI_0/RC$ , implying that most energy was dissipated as heat (Maxwell and Johnson, 2000). The inactivation of RCs is considered a down-regulation mechanism to dissipate the excess of absorbed light and confer protection against photo-oxidative stress (Stirbet and Govindjee, 2011; Monneveux et al., 2013; Kalaji et al., 2014; Meng et al., 2016). In susceptible plants, the reduction in the flux ratio of PSI and PSII was increasingly severe in response to disease progression, whereas the enhanced energy flux of PSI ( $\delta_{R_0}$ ) in resistant plants suggested an increased tolerance of PSI to stress (Gupta, 2019).

The PSII functional status is commonly evaluated by the  $F_v/F_m$  ratio. However, because  $F_v/F_m$  is considered mostly unresponsive to drought stress,  $F_v/F_0$  has been suggested to be a preferable alternative to assess photosynthetic capacity (Maxwell and Johnson, 2000; Mohammed et al., 2003; Oukarroum et al., 2007). In PWN-inoculated plants, both parameters, particularly  $F_v/F_0$ , confirmed the down-regulation of PSII and impairment in the water-splitting efficiency in PWN-inoculated plants, as previously reported for other environmental stress responses (Goltsev et al., 2016; Kumar et al., 2020).

The PI is a widely used parameter to quantitatively assess plant vitality. The three  $PI_{ABS}$ -dependent parameters were drastically decreased in susceptible plants; namely, (i) RC density (RC/ABS), (ii) quantum yield of primary photochemistry ( $\phi_{P0}$ ), and (iii) electron transport beyond  $Q_A$  in PSII ( $\psi_{E0}$ ) (Strasser et al., 2004, 2010; Stirbet and Govindjee, 2011; Banks, 2017).  $PI_{TOTAL}$  further includes information of the reduction of the end electron acceptors at the PSI acceptor side ( $\delta_{R_0}$ ), and therefore, allows to quantitatively assess the integral functional activity of PSII, PSI, and

intersystem electron transport chain. Because  $\delta_{R0}$  remained mostly unchanged in susceptible plants, PI<sub>TOTAL</sub> was influenced by PI<sub>ABS</sub> parameters, indicating a general down-regulation of PSII function (Silvestre et al., 2014; Ceusters et al., 2019).

The decrease in photosynthetic activity was most likely induced by a water deficiency in the leaves, as confirmed by the decrease in the RWC in susceptible plants. Previous physiological studies in PWN-inoculated *Pinus* spp. reported that the disruption of the water conductance, caused by xylem embolism, led to a decrease in leaf water potential, inactivation of the water-splitting complex of PSII, and ultimately, to the cessation of photosynthetic activity (Melakeberhan et al., 1991; Fukuda, 1997; Gao et al., 2017; Menéndez-Gutiérrez et al., 2017). The decrease in energy production, crucial to drive carbon fixation, negatively affects energy demanding processes related to growth and plant defense, thus contributing to plant susceptibility to PWN (Melakeberhan and Webster, 1990). On the other hand, this study showed that, by restricting PWN infection, resistant plants were able to maintain photosynthetic function without major significant changes in OJIP transients, and recover from a decrease in RWC to levels close to control plants at 35 DAI.

### **Primary Metabolite Adjustments Influence *Pinus pinaster* Resistance to Pinewood Nematode**

Pinewood nematode (PWN) infection caused local changes in the primary metabolite levels of *P. pinaster*. The significant decrease in sucrose in PWN-inoculated plants is consistent with reports of enhanced activity of the cell wall invertase that cleaves sucrose into glucose and fructose at the infection site. The accumulation of these metabolites is further associated with induced expression of pathogenesis-related genes (Proels and Hückelhoven, 2014; Rojas et al., 2014). However, as PWD progressed, the levels of glucose and fructose decreased in susceptible plants. Sugar accumulation is highly affected by changes in photosynthetic activity and metabolite uptake (e.g., hexoses) by the pathogen, e.g., during the phytophagous stage of the PWN (Berger et al., 2007; Kanwar and Jha, 2019).

The levels of most amino acids were also significantly reduced, including BCAAs which are usually accumulated in response to osmotic stress (Persson et al., 2016). In the absence of photosynthesis, energy demand under stress conditions can promote the degradation of BCAAs to generate additional

energy from protein degradation (Caldana et al., 2011; Less et al., 2011). Photosynthetic impairments could also explain the decrease in phenylalanine in susceptible plants up to 35 DAI. In trees, a large amount of the fixed carbon is channeled through phenylalanine for the activation of the shikimate pathway and the biosynthesis of phenylpropanoids, including flavonoids, stilbenes, coumarins, SA, tannins, and lignin (Pascual et al., 2016; Abreu et al., 2020). In contrast, studies on *P. pinaster* responses in the first hours after PWN infection showed an over-expression of genes involved in phenylpropanoid biosynthesis, including defense-related flavonoid and lignin biosynthesis (Modesto et al., 2021). The observed decrease in phenylalanine at an advanced stage of PWN infection suggests a decrease in the production of these defense-related secondary metabolites in susceptible plants, and a consequent lack of enhanced cell wall lignification as an inducible physical defense strategy.

The observed accumulation of osmolytes (e.g., fucose, GABA, proline, rhamnose, threitol, and trehalose) contributes to the maintenance of cell turgor through a decrease in the osmotic potential and protection against oxidative damage by restoring cellular redox balance (Krasensky and Jonak, 2012; Arbona et al., 2013; Jorge et al., 2016). In addition to its role as osmolyte, the accumulation of GABA has been suggested to play a role in signaling and regulatory mechanisms of stress responses (Michaeli and Fromm, 2015; Carillo, 2018; Ramos-Ruiz et al., 2019). The observed accumulation of alanine, GABA and succinate, particularly in resistant plants at 21 and 28 DAI, suggests the activation of alanine metabolism and the GABA shunt (i.e., a bypass pathway of the TCA cycle from 2-oxoglutarate via succinyl-CoA to succinate) (Fait et al., 2008). sPLS and PLS-DA analysis further confirmed the strong contribution of succinate to the clustering and separation of resistant plants from the remaining treatments. Alanine metabolism and the GABA shunt are activated at the expense of the production of other amino acids (e.g., asparagine, aspartate, glutamate, glutamine, glycine, serine), thus presumably explaining the observed general decrease in amino acids. Increased GABA-shunt activity has been associated with plant resistance due to the regulation of C:N metabolism and hypersensitive responses (HR), to ultimately delay infection-induced senescence (Seifi et al., 2013; Michaeli and Fromm, 2015; Ramos-Ruiz et al., 2019). A comparison of transcriptional changes associated with PWN infection in *P. thunbergii* revealed that tree resistance likely relies on a moderated and regulated HR and cell wall fortification to restrict PWN migration. On the contrary, fast-induced transcripts in susceptible plants led to

a HR response that ultimately caused tree death (Hirao et al., 2012). A similar observation has been reported for defense-related phytohormones showing a significant increase only in susceptible *P. pinaster* plants as part of an ineffective trigger of the HR (Rodrigues et al., 2021). Immuno-localization of GABA in vascular tissues of pine seedlings (e.g., differentiating xylem, ray parenchyma, and epithelial resin duct cells) further highlights the role of this metabolite not only in vascular processes but also in inducible defense mechanisms, including cell wall lignification (Molina-Rueda et al., 2015).

Defense responses in plants require a large supply of energy, mainly from primary metabolism (e.g., TCA-cycle intermediates) (Berger et al., 2007; Bolton, 2009). In parallel with the downregulation of processes associated with plant growth (e.g., photosynthesis), this energy can be diverted and used for defense responses or for further energy production (Rojas et al., 2014; Kanwar and Jha, 2019). During the host-pathogen interaction, the GABA-shunt activation might help to support the costly defense-related metabolic pathways through the up-regulation of the TCA cycle for energy production, feeding succinate and NADH to maintain respiration (Bolton, 2009; Michaeli and Fromm, 2015). Gao et al. (2017) has reported an increase in the respiration rate in *P. massoniana* upon PWN infection, after the first external symptoms, probably to meet the higher energy demand to support defense responses. In this study, the observed accumulation of succinate in resistant plants might also be explained by its use as electron donor to the respiratory system.

One early symptom of PWD is the cavitation and embolism of the xylem, ultimately leading to a blockage of the water-conducting system (Futai, 2013). Thus, it is possible that oxygen transport *via* the xylem sap is also hindered, leading to a hypoxic environment in stem tissues (Gansert, 2003; Wittmann and Pfanz, 2014). This would also explain the observed accumulation of alanine, GABA and succinate, which are well-known products of hypoxic metabolism in oxygen-deprived plant tissues (van Dongen et al., 2009; Rocha et al., 2010; Zabalza et al., 2011; António et al., 2016). The extent of oxygen deprivation in stem tissues of *Pinus* spp. after PWN infection is still unknown and would be relevant to investigate. The use of stable isotope labeling experiments ( $^{13}\text{C}$  and  $^{15}\text{N}$ ) would provide further evidence for the possible activation of hypoxia-related metabolic pathways (António et al., 2016). Hypoxia mechanisms in plants have been comprehensively described in response to waterlogging, but during the last decade, these studies have been extended to the involvement of hypoxia in plant development (Weits et al., 2020) and plant-pathogen

interactions (Loreti and Perata, 2020; Valeri et al., 2020). In response to pathogen infection, local hypoxia might be required to activate specific oxygen-sensitive resistance pathways, or it might affect the production of elicitor molecules (Loreti and Perata, 2020).

## CONCLUDING REMARKS

Overall, this work provides new insights into the physiological changes associated with *P. pinaster* differential responses to PWN infection. The integration of photosynthetic and metabolic data allowed to identify specific traits possibly associated with *P. pinaster* resistance to PWN, as a valuable resource for future studies. In general, susceptible plants were characterized by an increase in osmolytes (e.g., trehalose and threitol) and in heat dissipation as a protection mechanism against photo-oxidative stress. On the other hand, resistant plants did not show major significant changes in ChlF parameters revealing no photosynthetic impairments after PWN infection. The significant increase in GABA shunt-related metabolites suggests a possible role of these metabolites in *P. pinaster* resistance to PWN and should be further explored. Additional stable isotope labeling experiments coupled to GC-TOF-MS analysis would allow to derive a comprehensive and quantitative overview of the central carbon and nitrogen metabolic network during the time course of PWN infection. Altogether, results from this study provide interesting opportunities for future research on PWD and resistance traits in *Pinus* spp. with particular relevance in modern plant breeding programs and PWD management strategies. Indeed, metabolomics provides a key link between the genotype and phenotype, and is particularly useful for the prediction of complex traits (Fernie and Schauer, 2009; Alseekh and Fernie, 2021; Fernandez et al., 2021). Furthermore, the integration of metabolomics with other omics data can greatly accelerate candidate gene identification and comprehensive metabolic pathway elucidation, ultimately leading to biomarker discovery and plant improvement.

## DATA AVAILABILITY STATEMENT

The raw data supporting the conclusions of this article will be made available by the authors, without undue reservation.

## AUTHOR CONTRIBUTIONS

AR, CA, and IC conceptualized and designed the study. AR performed all experiments, statistical analysis, and wrote the first draft of the manuscript. IC defined the experimental design, provided greenhouse resources, and assisted in PWN inoculation assay and statistical analysis. CA secured funding and supervised the research. All authors reviewed and approved the submitted version of the manuscript.

## FUNDING

This work was supported by national funds from Fundação para a Ciência e a Tecnologia, I.P. (FCT), through the FCT Investigator Program (contract IF/00376/2012/CP0165/CT0003, CA), the R&D units GREEN-IT (UIDB/04551/2020), and LEAF (UIDP/04129/2020). AR gratefully acknowledges FCT and the ITQB NOVA International Ph.D. Program Plants for Life (PD/00035/2013) for the Ph.D. fellowship (PD/BD/114417/2016). IC acknowledges the FCT-funded project Lisboa-01-0145-FEDER-028379.

## ACKNOWLEDGMENTS

We gratefully acknowledge Célia Miguel, Inês Modesto, and Ana Milhinhos (ForGen Lab, FCUL, Portugal) for support in the inoculation experiment and sample preparation for microscopy analysis, Lurdes Inácio (Nematology Laboratory, INIAV, Portugal) for the virulent *B. xylophilus* inoculum, Hugo Matias (ITQB NOVA, Portugal) for greenhouse support, and Instituto de Hortofruticultura Subtropical y Mediterránea “La Mayora” – University of Malaga – Consejo Superior de Investigaciones Científicas (IHSM-UMA-CSIC) for the GC-TOF-MS metabolite profiling platform.

# SUPPLEMENTARY MATERIAL

The Supplementary Material for this article can be found online at: <https://www.frontiersin.org/articles/10.3389/fpls.2021.777681/full#supplementary-material>

## FOOTNOTES

<sup>1</sup><http://gmd.mpimp-golm.mpg.de/>

## REFERENCES

Abelleira, A., Picoaga, A., Mansilla, J. P., and Aguin, O. (2011). Detection of *Bursaphelenchus xylophilus*, causal agent of pine wilt disease on *Pinus pinaster* in northwestern Spain. *Plant Dis.* 95:776. doi: 10.1094/PDIS-12-10-0902

Abelleira, A., Picoaga, A., Mansilla, J. P., Mosquera, P., Díaz, R., and Toval, G. (2013). “Ensayo de inoculación de distintas concentraciones de *Bursaphelenchus xylophilus* aislado en Galicia sobre *Pinus pinaster*,” in *6º Congreso Forestal Español*, eds G. Montero González, M. Guijarro Guzmán, and E. Al (Spain: Sociedad Española de Ciencias Forestales).

Abreu, I. N., Johansson, A. I., Sokołowska, K., Niittylä, T., Sundberg, B., Hvidsten, T. R., et al. (2021). A metabolite roadmap of the wood-forming tissue in *populus tremula*. *New Phytol.* 228, 1559–1572. doi: 10.1111/nph.16799

Alseekh, S., Aharoni, A., Brotman, Y., Contrepois, K., D’Auria, J., Ewald, J., et al. (2021). Mass spectrometry-based metabolomics: a guide for annotation, quantification and best reporting practices. *Nat. Methods* 18, 747–756. doi: 10.1038/s41592-021-01197-1

Alseekh, S., and Fernie, A. R. (2021). “Using metabolomics to assist plant breeding,” in *Crop Breeding. Methods in Molecular Biology*, ed. P. Tripodi (New York, NY: Humana), 33–46. doi: 10.1007/978-1-0716-1201-9\_3

Amaral, J., Correia, B., António, C., Rodrigues, A. M., Gómez-Cadenas, A., Valledor, L., et al. (2019). *Pinus* susceptibility to pitch canker triggers specific physiological responses in symptomatic plants: an integrated approach. *Front. Plant Sci.* 10:509. doi: 10.3389/fpls.2019.00509

António, C., Päpke, C., Rocha, M., Diab, H., Limami, A. M., Obata, T., et al. (2016). Regulation of primary metabolism in response to low oxygen availability as revealed by carbon and nitrogen isotope redistribution. *Plant Physiol.* 170, 43–56. doi: 10.1104/pp.15.00266

Arbona, V., Manzi, M. de Ollas, C., and Gómez-Cadenas, A. (2013). Metabolomics as a tool to investigate abiotic stress tolerance in plants. *Int. J. Mol. Sci.* 14, 4885–4911.

Baghbani, F., Lotfi, R., Moharramnejad, S., Bandehagh, A., Roostaei, M., Rastogi, A., et al. (2019). Impact of fusarium verticillioides on chlorophyll fluorescence parameters of two maize lines. *Eur. J. Plant Pathol.* 154, 337–346.

Banks, J. M. (2017). Continuous excitation chlorophyll fluorescence parameters: a review for practitioners. *Tree Physiol.* 37, 1128–1136. doi: 10.1093/treephys/tpx059

Berger, S., Sinha, A. K., and Roitsch, T. (2007). Plant physiology meets phytopathology: plant primary metabolism and plant–pathogen interactions. *J. Exp. Bot.* 58, 4019–4026. doi: 10.1093/jxb/erm298

Bhuiyan, N. H., Selvaraj, G., Wei, Y., and King, J. (2009). Role of lignification in plant defense. *Plant Signal. Behav.* 4, 158–159.

Bolton, M. D. (2009). Primary metabolism and plant defense fuel for the fire. *Mol. Plant Microbe Interac.* 22, 487–497. doi: 10.1094/MPMI-22-5-0487

Caldana, C., Degenkolbe, T., Cuadros-Inostroza, A., Klie, S., Sulpice, R., Leisse, A., et al. (2011). High-density kinetic analysis of the metabolomic and transcriptomic response of *Arabidopsis* to eight environmental conditions. *Plant J.* 67, 869–884. doi: 10.1111/j.1365-313X.2011.04640.x

Carillo, P. (2018). GABA shunt in durum wheat. *Front. Plant Sci.* 9:100. doi: 10.3389/fpls.2018.00100

Carrasquinho, I., Lisboa, A., Inácio, M. L., and Gonçalves, E. (2018). Genetic variation in susceptibility to pine wilt disease of maritime pine (*Pinus pinaster* aiton) half-sib families. *Ann. For. Sci.* 75:85. doi: 10.1007/s13595-018-0759-x

Ceusters, N., Valcke, R., Frans, M., Claes, J. E., Van den Ende, W., and Ceusters, J. (2019). Performance index and PSII connectivity under drought and contrasting light regimes in the CAM Orchid *Phalaenopsis*. *Front. Plant Sci.* 10:1012. doi: 10.3389/fpls.2019.01012

de la Fuente, B., and Beck, P. S. A. (2018). Invasive species may disrupt protected area networks: insights from the pine wood nematode spread in portugal. *Forests* 9:282. doi: 10.3390/f9050282

de la Fuente, B., Saura, S., and Beck, P. S. A. (2018). Predicting the spread of an invasive tree pest: the pine wood nematode in Southern Europe. *J. Appl. Ecol.* 55, 2374–2385. doi: 10.1111/1365-2664.13177

Dixon, R. A., Achmire, L., Kota, P., Liu, C. J., Reddy, M. S. S., and Wang, L. (2002). The phenylpropanoid pathway and plant defence—a genomics perspective. *Mol. Plant Pathol.* 3, 371–390. doi: 10.1046/j.1364-3703.2002.00131.x

Ennos, R. A. (2015). Resilience of forest to pathogens: an evolutionary ecology perspective. *Forestry* 88, 41–52.

EPPO (2018). PM 9/1 (6) *Bursaphelenchus xylophilus* and its vectors: procedures for official control. *EPPO Bull.* 48, 503–505.

Evans, H. F., McNamara, D. G., Braasch, H., Chadoeuf, J., and Magnusson, C. (1996). Pest risk analysis (PRA) for the territories of the European Union (as PRA area) on *Bursaphelenchus xylophilus* and its vectors in the genus *Monochamus*. *EPPO Bull.* 26, 199–249. doi: 10.1111/j.1365-2338.1996.tb00594.x

Evans, S., Evans, H., and Ikegami, M. (2008). “Modeling PWN-induced wilt expression: a mechanistic approach,” in *Pine Wilt Disease: A Worldwide Threat to Forest Ecosystems*, eds M. M. Mota and P. Vieira (Dordrecht: Springer), 259–278.

Fait, A., Fromm, H., Walter, D., Galili, G., and Fernie, A. R. (2008). Highway or byway: the metabolic role of the GABA shunt in plants. *Trends Plant Sci.* 13, 14–19.

Fernandez, O., Millet, E. J., Rincent, R., Prigent, S., Pétriacq, P., and Gibon, Y. (2021). Plant metabolomics and breeding. *Adv. Bot. Res.* 98, 73–105.

Fernie, A. R., Aharoni, A., Willmitzer, L., Stitt, M., Tohge, T., Kopka, J., et al. (2011). Recommendations for reporting metabolite data. *Plant Cell* 2, 2477–2482.

Fernie, A. R., and Schauer, N. (2009). Metabolomics-assisted breeding: a viable option for crop improvement? *Trends Genet.* 25, 39–48. doi: 10.1016/j.tig.2008.10.010

Fernie, A. R., Trethewey, R. N., Krotzky, A. J., and Willmitzer, L. (2004). Metabolite profiling: from diagnostics to systems biology. *Nat. Rev. Mol. Cell Biol.* 5, 763–769.

Fiehn, O. (2002). Metabolomicsthe link between genotypes and phenotypes. *Plant Mol. Biol.* 48, 155–171. doi: 10.1007/978-94-010-0448-0\_11

Fiehn, O., Sumner, L. W., Rhee, S. Y., Ward, J., Dickerson, J., Lange, B. M., et al. (2007). Minimum reporting standards for plant biology context in metabolomics studies. *Metabolomics* 3, 195–201. doi: 10.1007/s11306-007-0068-0

Fisher, D. B. (1968). Protein staining of ribboned Epon sections for light microscopy. *Histochemie* 16, 92–96. doi: 10.1007/BF00306214

Fox, J., and Weisberg, S. (2019). *An R Companion to Applied Regression*, 3ed Edn. Thousand Oaks CA: Sage.

Fukuda, K. (1997). Physiological process of the symptom development and resistance mechanism in pine wilt disease. *J. For. Res.* 2, 171–181. doi: 10.1007/bf02348216

Futai, K. (2008). “Pine wilt in Japan: from first incidence to the present,” in *Pine Wilt Disease*, eds B. G. Zhao, K. Futai, J. R. Sutherland, and Y. Takeuchi (Tokyo: Springer), 5–12.

Futai, K. (2013). Pine wood nematode, *Bursaphelenchus xylophilus*. *Annu. Rev. Phytopathol.* 51, 61–83.

Gansert, D. (2003). Xylem sap flow as a major pathway for oxygen supply to the sapwood of birch (*Betula pubescens* Ehr.). *Plant Cell Environ.* 26, 1803–1814. doi: 10.1046/j.1365-3040.2003.01097.x

Gao, R., Wang, Z., Shi, J., and Luo, Y. (2017). Effect of *Bursaphelenchus xylophilus* infection on leaf photosynthetic characteristics and resource-use efficiency of *Pinus massoniana*. *Ecol. Evol.* 7, 3455–3463. doi: 10.1002/ece3.2642

Gaspar, D., Trindade, C., Usié, A., Meireles, B., Barbosa, P., Fortes, A. M., et al. (2017). Expression profiling in *pinus pinaster* in response to infection with the pinewood nematode *Bursaphelenchus xylophilus*. *Forests* 8:279. doi: 10.3390/f8080279

Gaspar, D., Trindade, C., Usié, A., Meireles, B., Fortes, A. M., Guimarães, J. B., et al. (2020). Comparative transcriptomic response of two *pinus* species to infection with the pine wood nematode *Bursaphelenchus xylophilus*. *Forests* 11:204. doi: 10.3390/f11020204

Goltsev, V. N., Kalaji, H. M., Paunov, M., Baba, W., Horaczek, T., Mojski, J., et al. (2016). Variable chlorophyll fluorescence and its use for assessing physiological condition of plant photosynthetic apparatus. *Russ. J. Plant Physiol.* 63, 869–893.

González-Martínez, S., Alía, R., and Gil, L. (2002). Population genetic structure in a mediterranean pine (*pinus pinaster* ait.): a comparison of allozyme markers and quantitative traits. *Heredity* 89, 199–206. doi: 10.1038/sj.hdy.6800114

Gruffudd, H. R., Schröder, T., Jenkins, T. A. R., and Evans, H. F. (2019). Modelling pine wilt disease (PWD) for current and future climate scenarios as part of a pest risk analysis for pine wood nematode *Bursaphelenchus xylophilus* (Steiner and Buhrer) Nickle in Germany. *J. Plant Dis. Prot.* 126, 129–144. doi: 10.1007/s41348-018-0197-x

Gupta, R. (2019). Tissue specific disruption of photosynthetic electron transport rate in pigeonpea (cajanus cajan L.) under elevated temperature. *Plant Signal. Behav.* 14:1601952. doi: 10.1080/15592324.2019.1601952

Hebbali, A. (2020). *olsrr: Tools for Building Ols Regression Models*. R Package Version 0.5.3.

Hirao, T., Fukatsu, E., and Watanabe, A. (2012). Characterization of resistance to pine wood nematode infection in *pinus thunbergii* using suppression subtractive hybridization. *BMC Plant Biol.* 12:13. doi: 10.1186/1471-2229-12-13

Hirata, A., Nakamura, K., Nakao, K., Kominami, Y., Tanaka, N., Ohashi, H., et al. (2017). Potential distribution of pine wilt disease under future climate change scenarios. *PLoS One* 12:e0182837. doi: 10.1371/journal.pone.0182837

ICNF (2019). *Plano De Ação Nacional Para Controlo do Nemátodo Da Madeira Do Pinheiro 2018-2022*. Available online at: <http://www2.icnf.pt/portal/florestas/prag-doe/ag-bn/nmp/resource/doc/pancnmp/PANCNMP2018-2022-31out2018.pdf>. (accessed April 06, 2020)

Ikegami, M., and Jenkins, T. A. R. (2018). Estimate global risks of a forest disease under current and future climates using species distribution model and simple thermal model pine Wilt disease as a model case. *For. Ecol. Manag.* 409, 343–352.

Jorge, T. F., Rodrigues, J. A., Caldana, C., Schmidt, R. van Dongen, J. T. Thomas-Oates, J., et al. (2016). Mass spectrometry-based plant metabolomics: metabolite responses to abiotic stress. *Mass Spectrom. Rev.* 35, 620–649.

Kalaji, H. M., Jajoo, A., Oukarroum, A., Brestic, M., Zivcak, M., Samborska, I. A., et al. (2016). Chlorophyll a fluorescence as a tool to monitor physiological status of plants under abiotic stress conditions. *Acta Physiol. Plant.* 38:102. doi: 10.1007/s11738-016-2113-y

Kalaji, H. M., Oukarroum, A., Alexandrov, V., Kouzmanova, M., Brestic, M., Živčák, M., et al. (2014). Identification of nutrient deficiency in maize and tomato plants by *in vivo* chlorophyll a fluorescence measurements. *Plant Physiol. Biochem.* 81, 16–25. doi: 10.1016/j.plaphy.2014.03.029

Kanwar, P., and Jha, G. (2019). Alterations in plant sugar metabolism: signatory of pathogen attack. *Planta* 249, 305–318. doi: 10.1007/s00425-018-3018-3

Kopka, J., Schauer, N., Krueger, S., Birkemeyer, C., Usadel, B., Bergmüller, E., et al. (2005). GMD@CSB.DB: the golm metabolome database. *Bioinformatics* 21, 1635–1638. doi: 10.1093/bioinformatics/bti236

Kover, P. X., and Schaal, B. A. (2002). Genetic variation for disease resistance and tolerance among *Arabidopsis thaliana* accessions. *PNAS* 99, 11270–11274. doi: 10.1073/pnas.102288999

Krasensky, J., and Jonak, C. (2012). Drought, salt, and temperature stress-induced metabolic rearrangements and regulatory networks. *J. Exp. Bot.* 63, 1593–1608.

Kumar, D., Singh, H., Raj, S., and Soni, V. (2020). Chlorophyll a fluorescence kinetics of mung bean (*Vigna radiata* L.) grown under artificial continuous light. *Biochem. Biophys. Rep.* 24:100813. doi: 10.1016/j.bbrep.2020.100813

Kuroda, K. (2008). “Physiological incidences related to symptom development and wilting mechanism,” in *Pine Wilt Disease*, eds B. G. Zhao, K. Futai, J. R. Sutherland, and Y. Takeuchi (Tokyo: Springer), 204–222.

Kusumoto, D., Yonemichi, T., Inoue, H., Hirao, T., Watanabe, A., and Yamada, T. (2014). Comparison of histological responses and tissue damage expansion between resistant and susceptible *Pinus thunbergii* infected with pine wood nematode *Bursaphelenchus xylophilus*. *J. For. Res.* 19, 285–294. doi: 10.1007/s10310-013-0417-y

Lê Cao, K. A., Rossow, D., Robert-Granié, C., and Besse, P. (2008). A sparse PLS for variable selection when integrating omics data. *Stat. Appl. Genet. Mol. Biol.* 7:35. doi: 10.2202/1544-6115.1390

Lee, I. H., Han, H., Koh, Y. H., Koh, Y. H., Kim, I. S., Lee, S. W., et al. (2019). Comparative transcriptome analysis of *Pinus densiflora* following inoculation with pathogenic (*Bursaphelenchus xylophilus*) or non-pathogenic nematodes (*B. thailandae*). *Sci. Rep.* 9:12180. doi: 10.1038/s41598-019-48660-w

Lee, I. H., Kim, J., Woo, K. S., Jang, K. H., Kim, Y. H., and Shim, D. (2018). *De novo* assembly and transcriptome analysis of the *Pinus densiflora* response to pine wilt disease in nature. *Plant Biotechnol. Rep.* 12, 229–236. doi: 10.1007/s11816-018-0488-5

Less, H., Angelovici, R., Tzin, V., and Galili, G. (2011). Coordinated gene networks regulating *Arabidopsis* plant metabolism in response to various stresses and nutritional cues. *Plant Cell* 23, 1264–1271. doi: 10.1105/tpc.110.082867

Lisec, J., Schauer, N., Kopka, J., Willmitzer, L., and Fernie, A. R. (2006). Gas chromatography mass spectrometry-based metabolite profiling in plants. *Nat. Protoc.* 1, 387–396.

Liu, Q., Wei, Y., Xu, L., Hao, Y., Chen, X., and Zhou, Z. (2017). Transcriptomic profiling reveals differentially expressed genes associated with pine wood nematode resistance in masson pine (*Pinus massoniana* Lamb.). *Sci. Rep.* 7:4693. doi: 10.1038/s41598-017-04944-7

Loreti, E., and Perata, P. (2020). The many facets of hypoxia in plants. *Plants* 9:745. doi: 10.3390/plants9060745

Luedemann, A., Strassburg, K., Erban, A., and Kopka, J. (2008). Tag finder for the quantitative analysis of gas chromatography-mass spectrometry (GC-MS)-based metabolite profiling experiments. *Bioinformatics* 24, 732–737.

Mamiya, Y., and Shoji, T. (2009). Pathogenicity of the pinewood nematode, *Bursaphelenchus xylophilus*, to Japanese larch, *Larix kaempferi*, seedlings. *J. Nematol.* 41, 157–162.

Maxwell, K., and Johnson, G. N. (2000). Chlorophyll fluorescence practical guide. *J. Exp. Bot.* 51, 659–668. doi: 10.1093/jxb/51.345.659

Melakeberhan, H., Toivonen, P. M. A., Vidaver, W. E., Webster, J. M., and Dube, S. L. (1991). Effect of *Bursaphelenchus xylophilus* on the water potential and water-splitting complex of photosystem II of *pinus sylvestris* seedlings. *Physiol. Mol. Plant Path.* 38, 83–91. doi: 10.1016/s0885-5765(05)80127-4

Melakeberhan, H., and Webster, J. M. (1990). Effect of *Bursaphelenchus xylophilus* on the assimilation and translocation of <sup>14</sup>C in *pinus sylvestris*. *J. Nematol.* 22, 506–512.

Mendiburu, F. (2020). *agricolae: Statistical Procedures for Agricultural Research. R Package Version 1.3-3*.

Menéndez-Gutiérrez, M., Alonso, M., Jiménez, E., Toval, G., Mansilla, P., Abelleira, A., et al. (2018). Interspecific variation of constitutive chemical compounds in *pinus* spp. xylem and susceptibility to pinewood nematode (*Bursaphelenchus xylophilus*). *Eur. J. Plant Pathol.* 150, 939–953.

Menéndez-Gutiérrez, M., Alonso, M., Toval, G., and Díaz, R. (2017). Variation in pinewood nematode susceptibility among *pinus pinaster* ait. provenances from the Iberian peninsula and France. *Ann. For. Sci.* 74:76. doi: 10.1007/s13595-017-0677-3

Meng, L. L., Song, J. F., Wen, J., Zhang, J., and Wei, J. H. (2016). Effects of drought stress on fluorescence characteristics of photosystem II in leaves of *Plectranthus scutellarioides*. *Photosynthetica* 54, 414–421.

Michaeli, S., and Fromm, H. (2015). Closing the loop on the GABA shunt in plants: are GABA metabolism and signaling entwined? *Front. Plant Sci.* 6:419. doi: 10.3389/fpls.2015.00419

Modesto, I., Sterck, L., Arbona, V., Gómez-Cadenas, A., Carrasquinho, I., Van de Peer, Y., et al. (2021). Insights into the mechanisms implicated in *pinus pinaster* resistance to pinewood nematode. *Front. Plant Sci.* 12:690857. doi: 10.3389/fpls.2021.690857

Mohammed, G. H., Zarco-Tejada, P., and Miller, J. R. (2003). “Applications of chlorophyll fluorescence in forestry and ecophysiology,” in *Practical Applications of Chlorophyll Fluorescence in Plant Biology*, eds J. R. DeEll and P. M. A. Toivonen (Boston: Springer), 79–124. doi: 10.1038/s41477-021-00980-4

Molina-Rueda, J. J., Pascual, M. B., Pissarra, J., and Gallardo, F. (2015). A putative role for  $\gamma$ -aminobutyric acid (GABA) in vascular development in pine seedlings. *Planta* 241, 257–267. doi: 10.1007/s00425-014-2157-4

Monneveux, P., Pastenes, C., and Reynoldsc, M. P. (2013). Limitations to photosynthesis under light and heat stress in three high-yielding wheat genotypes. *J. Plant Physiol.* 160, 657–666. doi: 10.1078/0176-1617-00772

Mota, M., Braasch, H., Bravo, M. A., Penas, A. C., Burgermeister, W., Metge, K., et al. (1999). First report of *Bursaphelenchus xylophilus* in portugal and in Europe. *Nematology* 1, 727–734.

Myers, R. F. (1988). Pathogenesis in pine wilt caused by pinewood nematode, *Bursaphelenchus xylophilus*. *J. Nematol.* 20, 236–244.

Nose, M., and Shiraishi, S. (2008). “Breeding for resistance to pine wilt disease,” in *Pine Wilt Disease*, eds B. G. Zhao, K. Futai, J. R. Sutherland, and Y. Takeuchi (Tokyo: Springer), 334–350. doi: 10.1007/978-4-431-75655-2\_34

Nunes da Silva, M., Cardoso, A. R., Ferreira, D., Brito, M., Pintado, M. E., and Vasconcelos, M. W. (2014). Chitosan as a biocontrol agent against the pinewood nematode (*Bursaphelenchus xylophilus*). *For. Pathol.* 44, 420–423.

Nunes da Silva, M. N., Lima, M. R. M., and Vasconcelos, M. W. (2013). Susceptibility evaluation of *picea abies* and *Cupressus lusitanica* to the pine wood nematode (*Bursaphelenchus xylophilus*). *Plant Pathol.* 62, 1398–1406.

Nunes da Silva, M. N., Solla, A., Sampedro, L., Zas, R., and Vasconcelos, M. W. (2015). Susceptibility to the pinewood nematode (PWN) of four pine species involved in potential range expansion across Europe. *Tree Physiol.* 35, 987–999. doi: 10.1093/treephys/tpv046

Oukarroum, A., Madidi, S. E., Schansker, G., and Strasser, R. J. (2007). Probing the responses of barley cultivars (*hordeum vulgare* L.) by chlorophyll a fluorescence OLKJIP under drought stress and re-watering. *Environ. Exp. Bot.* 60, 438–446. doi: 10.1016/j.envexpbot.2007.01.002

Pagán, I., and García-Arenal, F. (2018). Tolerance to plant pathogens: theory and experimental evidence. *Int. J. Mol. Sci.* 19:810. doi: 10.3390/ijms19030810

Pascual, M. B., El-Azaz, J., de la Torre, F. N., Cañas, R. A., Avila, C., and Cánovas, F. M. (2016). Biosynthesis and metabolic fate of phenylalanine in conifers. *Front. Plant Sci.* 7:1030. doi: 10.3389/fpls.2016.01030

Persson, T., Van Nguyen, T., Alloisio, N., Pujic, P., Berry, A. M., Normand, P., et al. (2016). The N-metabolites of roots and actinorhizal nodules from *alnus glutinosa* and *Datisca glomerata*: can *D. glomerata* change N-transport forms when nodulated? *Symbiosis* 70, 149–157. doi: 10.1007/s13199-016-0407-x

Proels, R. K., and Hückelhoven, R. (2014). Cell-wall invertases, key enzymes in the modulation of plant metabolism during defence responses. *Mol. Plant Pathol.* 15, 858–864. doi: 10.1111/mpp.12139

R Core Team. (2019). *R: A Language and Environment for Statistical Computing*. Vienna: R Foundation for Statistical Computing.

Ramos-Ruiz, R., Martinez, F., and Knauf-Beiter, G. (2019). The effects of GABA in plants. *Cogent Food Agric.* 5:1670553. doi: 10.1080/23311932.2019.1670553

Ribeiro, B. (2012). *Variabilidade de Resposta ao Nemátoide da Madeira do Pinheiro, Bursaphelenchus xylophilus, de Plantas Jovens de Pinheiro Bravo, Pinus Pinaster, Provenientes de Uma População de Melhoramento*. Ph. D. Thesis. Lisboa, PT: Universidade de Lisboa.

Rocha, M., Licausi, F., Araújo, W. L., Nunes-Nesi, A., Sodek, L., Fernie, A. R., et al. (2010). Glycolysis and the tricarboxylic acid cycle are linked by alanine aminotransferase during hypoxia induced by waterlogging of *Lotus japonicus*. *Plant Physiol.* 152, 1501–1513. doi: 10.1104/pp.109.150045

Rodrigues, A. M., Langer, S., Carrasquinho, I., Bergström, E., Larson, T., Thomas-Oates, J., et al. (2021). *Pinus pinaster* early hormonal defence responses to pinewood nematode (*Bursaphelenchus xylophilus*) infection. *Metabolites* 11:227. doi: 10.3390/metabo11040227

Rodrigues, J. M. (2008). “National eradication programme for the pinewood nematode,” in *Pine Wilt Disease: A Worldwide Threat to Forest Ecosystems*, eds M. M. Mota and P. Vieira (Dordrecht: Springer), 5–14. doi: 10.1007/978-1-4020-8455-3\_1

Rohart, F., Gautier, B., Singh, A., and Lê Cao, K.-A. (2017). mixOmics: an R package for 'omics' feature selection and multiple data integration. *PLoS Comput. Biol.* 13:e1005752. doi: 10.1371/journal.pcbi.1005752

Rojas, C. M., Senthil-Kumar, M., Tzin, V., and Mysore, K. S. (2014). Regulation of primary plant metabolism during plant-pathogen interactions and its contribution to plant defense. *Front. Plant Sci.* 5:17. doi: 10.3389/fpls.2014.00017

RStudio Team. (2018). *RStudio: Integrated Development for R*. Boston, MA: RStudio, Inc.

Schauer, N., Steinhauser, D., Strelkov, S., Schomburg, D., Allison, G., Moritz, T., et al. (2005). GC-MS libraries for the rapid identification of metabolites in complex biological samples. *FEBS Lett.* 579, 1332–1337. doi: 10.1016/j.febslet.2005.01.029

Seifi, H. S., Curvers, K., De Vleesschauwer, D., Delaere, I., Aziz, A., and Höfte, M. (2013). Concurrent overactivation of the cytosolic glutamine synthetase and the GABA shunt in the ABA-deficient *sitiens* mutant of tomato leads to resistance against *Botrytis cinerea*. *New Phytol.* 199, 490–504. doi: 10.1111/nph.12283

Silvestre, S., Araújo, S. S., Patto, M. C. V., and da Silva, J. M. (2014). Performance index: an expeditious tool to screen for improved drought resistance in the *lathyrus* genus. *J. Integr. Plant Biol.* 56, 610–621. doi: 10.1111/jipb.12186

Son, J. A., Komatsu, M., Matsushita, N., and Hogetsu, T. (2010). Migration of pine wood nematodes in the tissues of *pinus thunbergii*. *J. For. Res.* 15, 186–193. doi: 10.1007/s10310-009-0171-3

Steinbrenner, A. D., Gómez, S., Osorio, S., Fernie, A. R., and Orians, C. M. (2011). Herbivore-induced changes in tomato (*solanum lycopersicum*) primary metabolism: a whole plant perspective. *J. Chem. Ecol.* 37, 1294–1303. doi: 10.1007/s10886-011-0042-1

Stirbet, A., and Govindjee, G. (2011). On the relation between the kautsky effect (chlorophyll a fluorescence induction) and photosystem II: basics and applications of the OJIP fluorescence transient. *J. Photochem. Photobiol. B*. 104, 236–257. doi: 10.1016/j.jphotobiol.2010.12.010

Strasser, R. J., Srivastava, A., and Tsimilli-Michael, M. (2010). “The fluorescence transient as a tool to characterize and screen photosynthetic samples,” in *Probing Photosynthesis: Mechanism, Regulation and Adaptation*, eds M. Yunus, U. Pathre, and P. Mohanty (London: Taylor and Francis), 443–480. doi: 10.1016/s0269-7491(03)00094-0

Strasser, R. J., Tsimilli-Michael, M., and Srivastava, A. (2004). “Analysis of the chlorophyll fluorescence transient,” in *Chlorophyll Fluorescence: A Signature of Photosynthesis, Advances in Photosynthesis and Respiration*, ed. G. C. Papageorgiou (Dordrecht: Springer), 321–362. doi: 10.1007/978-1-4020-3218-9\_12

Sumner, L. W., Amberg, A., Barrett, D., Beale, M. H., Beger, R., Daykin, C. A., et al. (2007). Proposed minimum reporting standards for chemical analysis. *Metabolomics* 3, 211–221.

Tohge, T., Watanabe, M., Hoefgen, R., and Fernie, A. R. (2013). Shikimate and phenylalanine biosynthesis in the green lineage. *Front. Plant Sci.* 4:62. doi: 10.3389/fpls.2013.00062

Valeri, M. C., Novi, G., Weits, D. A., Mensuali, A., Perata, P., and Loreti, E. (2020). *Botrytis cinerea* induces local hypoxia in *Arabidopsis* leaves. *New Phytol.* 229, 173–185. doi: 10.1111/nph.16513

van Dongen, J. T., Fröhlich, A., Ramírez-Aguilar, S. J., Schauer, N., Fernie, A. R., Erban, A., et al. (2009). Transcript and metabolite profiling of the adaptive response to mild decreases in oxygen concentration in the roots of *Arabidopsis* plants. *Ann. Bot.* 103, 269–280. doi: 10.1093/aob/mcn126

Warnes, G. R., Bolker, B., Bonebakker, L., Gentleman, R., Huber, W., Liaw, A., et al. (2020). *gplots: Various R Programming Tools for Plotting Data. R Package Version 3.0.3*.

Weits, D. A., van Dongen, J. T., and Licausi, F. (2020). Molecular oxygen as a signaling component in plant development. *New Phytol.* 229, 24–35. doi: 10.1111/nph.16424

Whitehead, A. G., and Hemming, J. R. (1965). A comparison of some quantitative methods of extracting small vermiform nematodes from soil. *Ann. Appl. Biol.* 55, 25–38. doi: 10.1111/j.1744-7348.1965.tb07864.x

Wickham, H. (2016). *ggplot2: Elegant Graphics for Data Analysis*. New York: Springer-Verlag.

Wickham, H., and Seidel, D. (2020). *scales: Scale Functions for Visualization. R Package Version 1.1.1.*

Wittmann, C., and Pfanz, H. (2014). Bark and woody tissue photosynthesis: a means to avoid hypoxia or anoxia in developing stem tissues. *Funct. Plant Biol.* 41, 940–953. doi: 10.1071/fp14046

Yusuf, M. A., Kumar, D., Rajwanshi, R., Strasser, R. J., Tsimilli-Michael, M., Govindjee, et al. (2010). Overexpression of  $\gamma$ -tocopherol methyl transferase gene in transgenic brassica juncea plants alleviates abiotic stress: physiological and chlorophyll a fluorescence measurements. *Biochim. Biophys. Acta Bioenerg.* 1797, 1428–1438. doi: 10.1016/j.bbabi.2010.02.002

Zabalza, A., Orcaray, L., Igual, M., Schauer, N., Fernie, A. R., Geigenberger, P., et al. (2011). Unraveling the role of fermentation in the mode of action of acetolactate synthase inhibitors by metabolic profiling. *J. Plant Physiol.* 168, 1568–1575. doi: 10.1016/j.jplph.2011.02.015

Zas, R., Moreira, X., Ramos, M., Lima, M. R. M., Nunes da Silva, M., Solla, A., et al. (2015). Intraspecific variation of anatomical and chemical defensive traits in maritime pine (*Pinus pinaster*) as factors in susceptibility to the pinewood nematode (*Bursaphelenchus xylophilus*). *Trees* 29, 663–673. doi: 10.1007/s00468-014-1143-6

**Conflict of Interest:** The authors declare that the research was conducted in the absence of any commercial or financial relationships that could be construed as a potential conflict of interest.

**Publisher's Note:** All claims expressed in this article are solely those of the authors and do not necessarily represent those of their affiliated organizations, or those of the publisher, the editors and the reviewers. Any product that may be evaluated in this article, or claim that may be made by its manufacturer, is not guaranteed or endorsed by the publisher.

*Copyright © 2021 Rodrigues, Carrasquinho and António. This is an open-access article distributed under the terms of the Creative Commons Attribution License (CC BY). The use, distribution or reproduction in other forums is permitted, provided the original author(s) and the copyright owner(s) are credited and that the original publication in this journal is cited, in accordance with accepted academic practice. No use, distribution or reproduction is permitted which does not comply with these terms.*

ORIGINAL RESEARCH

published: 05 January 2022

doi: 10.3389/fpls.2021.812414



# Systemic Acquired Resistance-Mediated Control of Pine Wilt Disease by Foliar Application With Methyl Salicylate

**Hee Won Jeon<sup>1</sup>, Ae Ran Park<sup>1</sup>, Minjeong Sung<sup>1</sup>, Namgyu Kim<sup>2</sup>, Mohamed Manna<sup>2</sup>, Gil Han<sup>2</sup>, Junheon Kim<sup>3</sup>, Yeonjong Koo<sup>1</sup>, Young-Su Seo<sup>2</sup> and Jin-Cheol Kim<sup>1\*</sup>**

<sup>1</sup>Department of Agricultural Chemistry, College of Agriculture and Life Sciences, Institute of Environmentally Friendly Agriculture, Chonnam National University, Gwangju, South Korea

<sup>2</sup>Department of Integrated Biological Science, College of Natural Science, Pusan National University, Busan, South Korea

<sup>3</sup>Forest Insect Pests and Diseases Division, National Institute of Forest Science, Seoul, South Korea

**Edited by:**

Anna Filipiak, Institute of Plant Protection – National Research Institute, Poland

**Reviewed by:**

Mitsuteru Akiba, Forestry and Forest Products Research Institute, Japan

Ling Ma, Northeast Forestry University, China

**\*Correspondence:** Jin-Cheol Kim, [kjinc@jnu.ac.kr](mailto:kjinc@jnu.ac.kr)

**Specialty section:** This article was submitted to *Plant Pathogen Interactions*, a section of the journal *Frontiers in Plant Science*

**Received:** 10 November 2021

**Accepted:** 13 December 2021

**Published:** 05 January 2022

**Citation:** Jeon HW, Park AR, Sung M, Kim N, Manna M, Han G, Kim J, Koo Y, Seo Y-S and Kim J-C (2022) Systemic Acquired Resistance-Mediated Control of Pine Wilt Disease by Foliar Application With Methyl Salicylate. *Front. Plant Sci.* 12:812414. doi: 10.3389/fpls.2021.812414

Pine wilt disease (PWD), caused by the pinewood nematode, is the most destructive disease in pine forest ecosystems worldwide. Extensive research has been done on PWD, but effective disease management is yet to be devised. Generally, plants can resist pathogen attack via a combination of constitutive and inducible defenses. Systemic acquired resistance (SAR) is an inducible defense that occurs by the localized infection of pathogens or treatment with elicitors. To manage PWD by SAR in pine trees, we tested previously known 12 SAR elicitors. Among them, methyl salicylate (MeSA) was found to induce resistance against PWD in *Pinus densiflora* seedlings. In addition, the foliar applications of the dispersible concentrate-type formulation of MeSA (MeSA 20 DC) and the emulsifiable concentrate-type formulation of MeSA (MeSA 20 EC) resulted in significantly reduced PWD in pine seedlings. In the field test using 10-year-old *P. densiflora* trees, MeSA 20 DC showed a 60% decrease in the development of PWD. Also, MeSA 20 EC gave the best results when applied at 0.1 mM concentration 2 and 1 weeks before pinewood nematode (PWN) inoculation in pine seedlings. qRT-PCR analysis confirmed that MeSA induced the expression of defense-related genes, indicating that MeSA can inhibit and delay the migration and reproduction of PWN in pine seedlings by modulating gene expression. These results suggest that foliar application of MeSA could reduce PWD incidence by inducing resistance and provide an economically feasible alternative to trunk-injection agents for PWD management.

**Keywords:** pine wilt disease, methyl salicylate, systemic acquired resistance, foliar application, qRT-PCR

## INTRODUCTION

Pine wilt disease (PWD), caused by the pinewood nematode (PWN), *Bursaphelenchus xylophilus*, is the most destructive disease in pine forest ecosystems worldwide. PWN can easily migrate within infected trees, but because they cannot move between hosts, they are transmitted through the vector *Monochamus* spp. (Mamiya, 1988; Kim et al., 2021). PWN is fatal to

healthy susceptible pine trees, such as *Pinus densiflora*, *P. thunbergii*, and *P. koraiensis* and new susceptible species are being discovered (Yang and Wang, 1989; Li et al., 2020). PWD-infected pine trees initially turn their needles yellowish to reddish-brown, and then subsequently wilt and die within a few months. PWD was first reported in Japan in 1905 (Yano, 1913), after which it gradually reached Europe (Portugal and Spain) as well as East Asian countries such as China, Taiwan, and Korea (Cheng et al., 1983; Tzean and Jan, 1985; Yi et al., 1989; Mota et al., 1999; Abelleira et al., 2011).

The serious threat posed by PWN has led to considerable efforts to control the disease. Disease control mostly relies on use of chemicals such as metam sodium for fumigation of infected trees, aerial spraying of pesticides to control pine sawyer, and trunk injection of abamectin and emamectin benzoate (Kwon et al., 2005; Lee et al., 2009; Korea Forest Service, 2013). However, with the growing awareness regarding environmental conservation, there is now a demand for environmental-friendly control measures. In line with this, research on elucidating resistance mechanisms related to the relationship between pathogens and host pines is being emphasized upon.

Plants can resist pathogen attack through a combination of constitutive and inducible defense mechanisms, which suppress pathogen reproduction and spread (Spoel and Dong, 2012; Vlot et al., 2021). Induced resistance has two forms: systemic acquired resistance (SAR) and induced systemic resistance (ISR). Specifically, SAR is known as long-lasting and broad-spectrum resistance that sets in following a localized infection by a variety of pathogens or treatment with SAR elicitors. The activation of SAR requires transfer of signals from the primarily infected tissue to systemic tissue. Various substances that activate SAR, such as  $\beta$ -aminobutyric acid (BABA), methyl salicylate (MeSA), and azelaic acid (AZA) have recently been reported (Park et al., 2007; Jung et al., 2009; Ji et al., 2015).

MeSA is a naturally occurring compound that is widely distributed in many plants and is classified into a group of plant hormones that play various regulatory roles in plant metabolism (Hayat and Ahmad, 2007). MeSA, a long-distance signaling compound of SAR, is volatilized and transported to the air. Airborne MeSA is absorbed by uninfected distal tissues, converted into SA, after which it eventually activates SAR (Dempsey and Klessig, 2012). Recently, upon application of MeSA, development of disease resistance was reported against bacterial blight caused by *Xanthomonas oryzae* pv. *oryzae* in

rice and gray mold caused by *Botrytis cinerea* in grape (Kalaivani et al., 2016; García-Pastor et al., 2020).

It has been demonstrated that MeSA can effectively control PWD by inducing flavonoid biosynthesis through comparative *in vivo* transcriptomics on pine seedlings (Park et al., 2020). However, the establishment of optimal treatment conditions for high efficiency of MeSA and application to the field have not been reported. The purpose of this study was to establish the optimal formulation and processing conditions of MeSA for effectively controlling PWD through *in vivo* assays and field experiments, and to elucidate the mechanisms underlying the effects of MeSA against PWD based on qRT-PCR analysis.

## MATERIALS AND METHODS

### Chemicals and Formulations

AZA (>98%), azoxystrobin (98.4%), BABA (>98%),  $\gamma$ -aminobutyric acid (GABA, > 99%), glucan (from black yeast), isotianil (ITL, 98.2%), methyl jasmonate (>90%), MeSA (>99%), probenazole (PBZ, 98.5%), salicylic acid (SA, > 99.5%), tiadinil (TDL, 98.9%), and validamycin A (VMA, 64.24%) were purchased from Tokyo Chemical Industry Co., Ltd. (Tokyo, Japan). The four elicitors selected following screening tests (GABA, MeSA, PBZ, and SA) were formulated by Yoosung Chemical R&T Co., Ltd. (Daejeon, South Korea). A soluble concentrate-type formulation of GABA (GABA 20 SL) was prepared by mixing 20% (w/w) GABA, 10% (w/w) polyethylene glycol-400, 5.0% (w/w) sodium lignin sulfonate, 3.0% (w/w) monotridecyl ether (POE9), and 62.0% (w/w) water. A dispersible concentrate-type formulation of MeSA (MeSA 20 DC) was prepared by mixing 20% (w/w) MeSA, 30% (w/w) propylene glycol monomethyl ether, 20% (w/w) propylene glycol, and 20% (w/w) CR-FL3PG (the mixture of triethanolamine, and polyoxyethylene tristyrylphenyl ether phosphate). An emulsifiable concentrate-type formulation of MeSA (MeSA 20 EC) was prepared by mixing 20% (w/w) MeSA, 20% (w/w) propylene glycol monomethyl ether, 20% (w/w) CR-MOC25 (the mixture of ethoxylated castor oil, calcium dodecylbenzenesulfonate, and tristyrylphenol ethoxylates) as an emulsifier, and 40% (w/w) methylated soybean oil (MOS2). A suspension concentrate-type formulation of PBZ (PBZ 20 SC) was prepared by mixing 20% (w/w) PBZ, 8.0% (w/w) propylene

glycol, 5.0% (w/w) CR-FL3PG, 0.12% (w/w) xanthan gum, 0.1% (w/w) silicon defoamer, and 66.78% (w/w) water. A soluble concentrate-type formulation of SA (SA 20 SL) was prepared by mixing 20% (w/w) SA, 11.6% (w/w) NaOH (50%), 10% (w/w) polyethylene glycol-400, 5.0% (w/w) sodium lignin sulfonate, 3.0% (w/w) monotridecyl ether (POE9), and 50.4% (w/w) water.

## Nematodes and Plants

The PWN *Bursaphelengus xylophilus*, which causes PWD, was isolated from infected pine trees and obtained from the National Institute of Forest Research (NIFoS; Seoul, South Korea). PWN was cultured on the mycelia of *Botrytis cinerea* on potato dextrose agar (Difco; Becton, Dickinson and Company, Sparks, MD, United States) at 25°C for 1 week in dark (Maehara and Futai, 2000). PWNs were harvested from the medium using the Baermann funnel method (Baermann, 1917). For the *in vivo* experiment, 3-year-old *Pinus densiflora* and *P. thunbergii* seedlings of 40–50 cm height and 0.5–1.0 cm diameter were obtained from Daelim seedling farm (Okcheon, South Korea) and transplanted into 15-cm diameter pots containing sterilized nursery soil in the greenhouse, which was maintained at an average temperature of 25°C with the relative humidity of 70%.

## Screening of Various Elicitors Against Pine Wilt Disease by Means of Trunk Injection

Ten chemicals (except glucan and ITL) were dissolved in an aqueous solution containing 10% methanol, while glucan and ITL were dissolved in an aqueous solution containing 10% dimethylformamide, at concentrations of 200 and 20 µg/mL. Three-year-old *P. densiflora* seedlings were treated with 100 µL of each solution via trunk injection. A hole was drilled using a 1.8 mm drill bit at a 45° angle in the trunk of a pine seedling, 5 cm above the ground. A 200 µL pipette tip (Axygen Scientific Inc., Union, CA, United States) was inserted into the hole. One hundred microliters of each chemical solution was injected into the pipette tip. The pipette tip was covered with Parafilm® M (Heathrow Scientific, Vernon Hills, IL, United States) to prevent drying, following which a small hole was made in it using a pin. One week later, the treated pine seedlings were inoculated with PWN, as described below. After making a small slit with a surface-sterilized knife, a small piece of absorbent cotton was inserted into the slit, and a water suspension of nematodes (2,000

nematodes in 100  $\mu$ L) was pipetted onto the absorbent cotton. The slits were then covered with Parafilm® to prevent drying (Kwon et al., 2010). Distilled water containing 10% methanol was used as an untreated control. Three replicates were included in each treatment, and each experiment was performed twice.

### **Effects of Four Selected Elicitors Formulations Against Pine Wilt Disease Upon Foliar Application**

Formulations of GABA 20 SL, MeSA 20 DC, PBZ 20 SC, and SA 20 SL were dissolved in distilled water at a concentration of 10 mM each, and then 5 mL of each solution was foliar sprayed onto 3-year-old *P. densiflora* seedlings. The treatment was conducted twice at an interval of 1 week. One week after the second treatment, the treated 3-year-old pine seedlings were inoculated with 2,000 PWNs. Distilled water containing 250  $\mu$ g/mL Tween® 20 was used as an untreated control and five replicates were used. The severity of PWD was assessed according to the wilting and the ration of the brown leaves of the whole plant leaves (Proença et al., 2010; Kim et al., 2019). To evaluate the control value of treatment against *B. xylophilus*, control value was measured using below formula (Kwon et al., 2010), control value (%) = (1-disaease severity of treatment/disease severity of untreated control)  $\times$  100.

### ***In vitro* Nematicidal Activity of Methyl Salicylate**

To confirm whether the effect of MeSA against PWD was caused by direct nematicidal activity, the nematicidal activity of MeSA was evaluated on *B. xylophilus*. After the suspension containing approximately 50 nematodes was added to each well of a 96-well microplate (Becton Dickinson, Franklin Lakes, NJ, United States), treatments with three concentrations of MeSA, 1,000, 333, and 111  $\mu$ g/mL, were carried out. Sterilized distilled water was used as the negative control. The plates were gently shaken and incubated in a dark plastic box with 100% humidity at an average temperature of 25°C. All experiments were conducted in triplicates and repeated twice. Nematicidal activity was evaluated at 3 days post-treatment, under an optical microscope (Leica DM IL LED; Leica Microsystems CMS GmbH, Wetzlar, Germany). To analyze the nematicidal activity of MeSA against *B. xylophilus*, mortality was converted to percentage mortality and corrected using Abbott's formula (Abbott, 1925), Mortality (%) = [(Mortality percentage in treatment –

Mortality percentage in the negative control)/(100 – Mortality percentage in the negative control)] × 100.

## **Evaluation of Disease Control Efficacy of Methyl Salicylate 20 DC Against Pine Wilt Disease Under Field Conditions**

The field experiment was performed in a pine forest located in Seongbang-ri, Gonmyeong-myeon, Sacheon-si, Gyeongsangnam-do province, Republic of Korea, in 2017. Ten-year-old *P. densiflora* trees, 3–5 m in height and 8–10 cm in diameter at chest height, were used for the experiment. MeSA 20 DC formulation was prepared in distilled water at a concentration of 10 mM and 500–800 mL for a tree. This solution was foliar sprayed onto 10-year-old *P. densiflora* trees through Sprayer Clover (Model TH-33; Taehwan Co., South Korea). The treatment was conducted twice at an interval of 1 month. One month after the second treatment, the treated pine trees were inoculated with PWN via trunk injection. A hole was drilled using a 10 mm drill bit at a 45° angle into the trunk of a pine tree, 30 cm above the ground. One milliliter of water suspension of nematodes (10,000 nematodes) was pipetted into the hole. Inoculation of PWN was performed on June 2, 2017, and the average temperature was 20°C. After inoculation with PWN, the hole was closed using a cork stopper. Distilled water containing 250 µg/mL Tween® 20 was foliar sprayed as a negative control, while emamectin benzoate 2.15 EC (Affirm, Syngenta Co., Seoul, Korea) was administered via trunk injection as a positive control. Sixteen trees were used in each treatment. The incidence of PWD was assessed in terms of the trees being either alive or dead.

## **Selection of Optimal Formulation of Methyl Salicylate Against Pine Wilt Disease in 3-Year-Old *Pinus densiflora* and *Pinus thunbergii* Seedlings**

MeSA 20 DC and MeSA 20 EC were formulated by Yoosung Chemical R&T Co., Ltd. To select the optimal formulation of MeSA, *in vivo* assays were performed on *P. densiflora* and *P. thunbergii* seedlings. Each sample was dissolved in distilled water at a concentration of 10 mM, and then 5 mL of these solutions were foliar sprayed onto 3-year-old *P. densiflora* and *P. thunbergii* seedlings. The treatment was conducted twice at an interval of 1 week. One week after the second treatment, the treated seedlings were inoculated with 2,000 PWNs. Distilled water containing 250 µg/mL Tween® 20 was used as a negative control, and emamectin benzoate 20 mg/mL was

used as a positive control. Five replicates were included in each treatment group. The severity of PWD was assessed according to the wilting and discolored area of the needles.

### **Determination of Optimal Concentration and Application Time of Methyl Salicylate 20 EC Against Pine Wilt Disease in 3-Year-Old *Pinus densiflora* and *Pinus thunbergii* Seedlings**

To determine the optimal concentration of MeSA 20 EC, *in vivo* assays were performed at various concentrations of MeSA 20 EC to select the optimal formulation for MeSA. MeSA 20 EC was dissolved in distilled water at concentrations of 10, 0.1, and 0.01 mM and then 5 mL of these solutions were foliar sprayed onto 3-year-old *P. densiflora* and *P. thunbergii* seedlings. The treatment was conducted twice at an interval of 1 week.

For determination of optimal application time for MeSA 20 EC, it was dissolved in distilled water at a concentration of 0.1 mM, which was selected as the optimal concentration, and then foliar sprayed as follows: 1 week before inoculation (WBI) with PWN; 2 and 1 WBI with PWN; 3 and 1 WBI with PWN; 4 and 1 WBI with PWN. In both the experiments aimed at optimization of concentration and application time, the treated seedlings were inoculated with 2,000 PWNs 1 week after the second treatment. Distilled water containing 250 µg/mL Tween® 20 was used as a negative control. Five replicates were included in each treatment group. The severity of PWD was assessed according to the wilting and discolored area of the needles.

### **Assessment of the Effect of Methyl Salicylate on the Expression of Defense-Related Genes Using qRT-PCR**

Three-year-old *P. densiflora* seedlings were used to analyze the effect of MeSA on expression of defense-related genes. The seedlings were foliar sprayed with MeSA 20 EC (0.1 mM) at an interval of 1 week. For the untreated controls, distilled water containing Tween® 20 (250 mg/L) was used. One week after the second treatment, the treated pine seedlings were inoculated with PWN (2,000 nematodes/100 µL). Three replicates were included in each treatment.

Total RNA was extracted from the pine needles using a hexadecyltrimethylammonium bromide (CTAB)-based extraction buffer (Azevedo et al., 2003). Sampling was performed at 1, 3, and 7 days post-first treatment; 1, 3, and 7 days post-second treatment; and 1, 3, and 7 days post-

inoculation with PWN, to confirm the change over time. First, the samples were coarsely ground in liquid nitrogen using a mortar and pestle. The coarsely ground sample (0.5 g) was put into a 2 mL e-tube and completely ground using a tissuelyser (Qiagen Inc., Valencia, CA, United States). The ground sample was mixed with 1 mL extraction buffer containing 0.1 M Tris-HCl (pH 8.0), 30 mM ethylenediaminetetraacetic acid, 2 M NaCl, 2% CTAB, 0.05% spermidine, 2% polyvinylpolypyrrolidone, 2% 2-mercaptoethanol, and 1.5 mg/mL proteinase K. The suspension was incubated at 42°C for 90 min and then extracted with 15 mL chloroform-isoamyl alcohol (24:1). Total RNA was precipitated using 2 M LiCl. Total RNA was further purified using the IQeasy Plus Plant RNA Extraction Mini Kit (iNtRON, Seongnam, South Korea). RNA quality was assessed using a NanoDrop ND-1000 spectrophotometer (NanoDrop Technologies, Wilmington, DE, United States). The cDNA library was synthesized using oligo (Ji et al., 2015) primers and SuperScript IV reverse transcriptase (Invitrogen Inc., Carlsbad, CA, United States), following the manufacturer's guidelines. The PCR primers used in this study (Table 1; Hirao et al., 2012; Lee et al., 2019) were synthesized by Genotech (Daejeon, South Korea).

---

**TABLE 1.** Primers used in this study.

Gene	Sequence (5'→3')	References
PR-1 For	TGCCCCCTTCAGGTAAATCGT	Hirao et al., 2012
PR-1 Rev	GCGGGTCGTAGTTGCAGATAA	
PR-2 For	CGACAACATTGCCCTTCT	
PR-2 Rev	CTGCAGCGCGGTTGAATAT	
PR-5 For	GAACCAGTGCCCATAACACAGTCT	
PR-5 Rev	CCTGCAGCAACGTTAAAGTC	
PR-9 For	ACACCACCGTGCTGGACATT	
PR-9 Rev	GTGCGGGAGTCGGTAGAG	
ETS For	CGAATGTAATTCCGAAGTTGCA	
ETS Rev	CCATCCCAAACCACCAAGTCT	
XET For	TCTGCGCCCCTACTTTCC	
XET Rev	AGCTGGCGATTGATCATGT	
PdEIF4A-2 For	AATGCTTGTCCCACCAACAC	Lee et al., 2019
PdEIF4A-2 Rev	AGTGTCAAGGCGCTAGTTTG	

qRT-PCR was performed using iQ™ SYBR Green supermix with a CFX96 Touch™ Real-Time PCR Detection System (Bio-Rad, Hercules, CA, United States). Relative expression levels were calculated using the comparative  $2^{-\Delta\Delta CT}$  method, with *EIF4A-2* as an internal control (Livak and Schmittgen, 2001).

## Statistical Analysis

Statistical analysis was performed to determine significant differences between the groups. All statistical analyses were performed using SPSS statistical analysis software (version 21.0 for Windows; SPSS, IBM Corp., Armonk, NY, United States). Data were evaluated using one-way analysis of variance, and the means of the treatments were determined using the Tukey's HSD test. Results with  $p < 0.05$  were considered statistically significant.

# RESULTS

## Screening of Various Elicitors Against Pine Wilt Disease by Means of Trunk Injection

Twelve elicitors known to induce resistance in various plants were used for *in vivo* screening of PWD in *P. densiflora* seedlings (Table 2). Treatment with the elicitors was carried out via trunk injection to ascertain their effects. Among the 12 candidates, four elicitors (GABA, MeSA, PBZ, and SA) showed more than 75% control values at both the concentrations of 200 and 20  $\mu\text{g/mL}$  (Table 2). Glucan, TDL, and VMA showed control effects at specific concentrations but their effects at the other concentration were not significant.

**TABLE 2.** screening of various elicitors against pine wilt disease by trunk injection into 3-year-old *Pinus densiflora* seedlings.

<b>Treatment</b>	<b>Concentration (μg/mL)</b>	
	<b>200</b>	<b>20</b>
Azelaic acid	+	+
Azoxystrobin	+	+
β-aminobutyric acid	+	—
γ-aminobutyric acid	+++	++
Glucan	+	++
Isotianil	++	+
Methyl jasmonate	+	+
Methyl salicylate	+++	+++
Probenazole	++	+++
Salicylic acid	+++	++
Tiadinil	++	+
Validamycin A	++	+
Control	—	—

++, high activity, more than 75% of control value; ++, moderate activity, 74–50% of control value; +, low activity, 49–25% of control value; —, no activity, 24–0% of control value.

### **Control Effect of the Four Selected Elicitor Formulations Against Pine Wilt Disease Upon Foliar Application Onto 3-Year-Old *Pinus densiflora* Seedlings**

The four selected elicitors were formulated for stability according to the properties of each chemical. Foliar application was used to control PWD more effectively. Among the four selected formulations, only MeSA 20 DC significantly reduced the severity of PWD in *P. densiflora* seedlings. Disease severity in *P. densiflora* seedlings foliar sprayed with MeSA 20 DC was significantly reduced compared to that in the untreated control. The MeSA 20 DC-treated and -untreated groups showed disease severity of 20 and 84%,

respectively, at 43 days post-inoculation with PWN, while the MeSA 20 DC-treated group showed 76.2% control value (Figure 1). GABA 20 SL, PBZ 20 SC, and SA 20 SL did not affect PWD when foliar sprayed. Additionally, when tested against the PWN, *B. xylophilus*, no nematicidal activity of MeSA was observed. MeSA led to 3.5, 1.9, and 0.8% mortality at concentrations of 1,000, 333, and 111  $\mu$ g/mL, respectively, and showed results comparable to distilled water (mortality: 2.1%) used as a negative control (Supplementary Table 1). On the contrary, emamectin benzoate, which used as a positive control, showed a high mortality of 98.8% even at a very low concentration of 0.11  $\mu$ g/mL. MeSA leads to approximately 95% mortality at a concentration of 2,000  $\mu$ g/mL (Kim et al., 2011), but no such activity was observed when it was used at a concentration of 200  $\mu$ g/mL in the screening test. Therefore, it indirectly suggested that the control effect of MeSA against PWD was due to inducing resistance, not direct nematicidal activity.

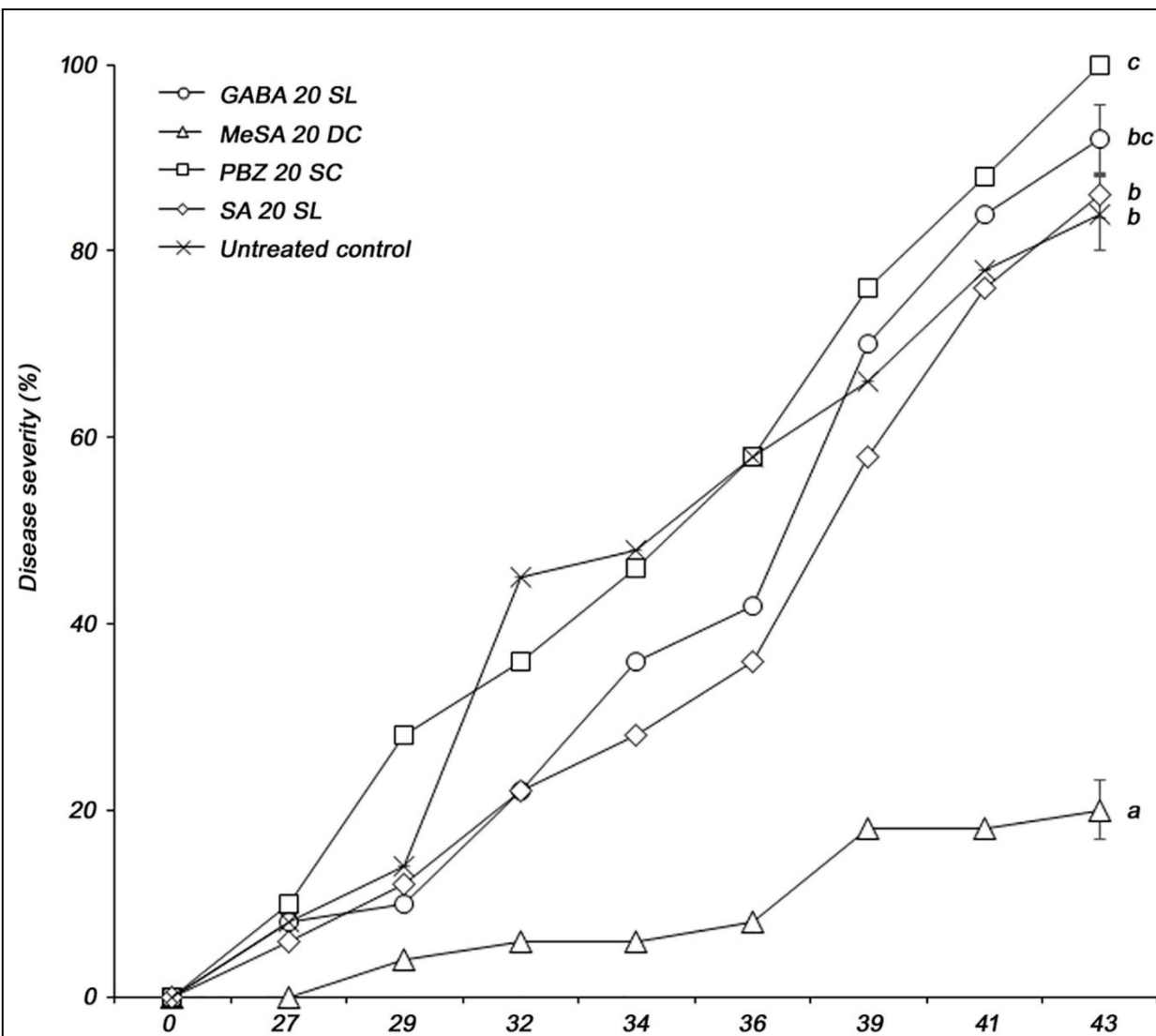


**FIGURE 1.** Pine wilt disease severity in 3-year-old *Pinus densiflora* seedlings treated by foliar application with formulations of four elicitors (GABA,  $\gamma$ -aminobutyric acid; MeSA, methyl salicylate; PBZ, probenazole; and SA, salicylic acid). Each value represents the mean  $\pm$  standard error of five replicates. The different letters indicate significant differences with  $p < 0.05$ , as calculated using the Tukey's HSD test.

### Determination of Optimal Formulation, Concentration, and Application Time of Methyl Salicylate Against Pine Wilt Disease in 3-Year-Old *Pinus densiflora* and *Pinus thunbergii* Seedlings

Two formulations of MeSA were evaluated for their ability to control PWD in *P. densiflora* and *P. thunbergii* seedlings, which are susceptible to PWD. In *P. densiflora*, the MeSA 20 DC and MeSA 20 EC formulations showed 47.7 and

52.3% control values, respectively, compared to the untreated group; moreover, there was no significant difference between the two formulations (Figure 2). In contrast, against *P. thunbergii*, the MeSA 20 DC and MeSA 20 EC formulations showed 6.7 and 57.8% control values, respectively, compared to the untreated group. Furthermore, it was confirmed that the activity of the MeSA 20 DC formulation was significantly reduced. Emamectin benzoate, which was used as a positive control in *P. densiflora* and *P. thunbergii*, showed excellent control values of 95.5 and 100%, respectively. Therefore, MeSA 20 EC was selected as the optimal formulation, and was used for the subsequent experiments.

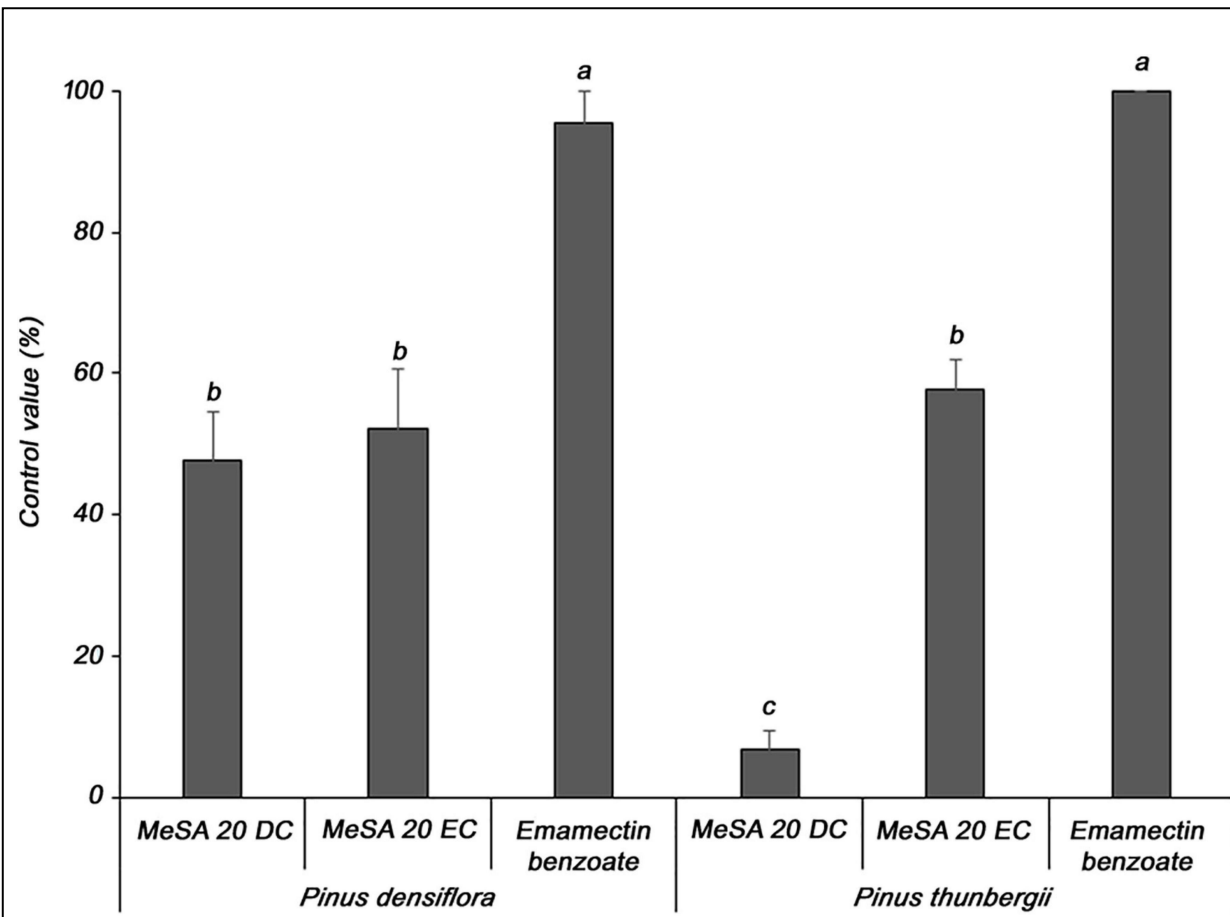


**FIGURE 2.** Determination of the optimal formulation of methyl salicylate against pine wilt disease in 3-year-old *Pinus densiflora* and *Pinus thunbergii* seedlings. The formulations of methyl salicylate were treated with 10 mM, and emamectin benzoate was treated with 20 mg/mL. Each value represents the mean  $\pm$  standard error of five replicates. Different letters indicate significant differences with  $p < 0.05$ , as calculated using the Tukey's HSD test.

Subsequently, the optimal concentration of MeSA 20 EC formulation was determined for the effective control of PWD. In *P. densiflora*, the control value was higher (54.8%) at 0.1 mM MeSA 20 EC, a concentration 100-fold lower than the other tested concentration, which was 10 mM (33.3%) (Figures 3A,C). However, 0.01 mM did not control PWD. The results in *P. thunbergii* showed a higher control value at 0.1 mM (56.3%) than at 10 mM (45.8%), similar to the results in *P. densiflora*. Therefore, 0.1 mM was selected as the optimal concentration of the MeSA 20 EC formulation for effectively controlling PWD.

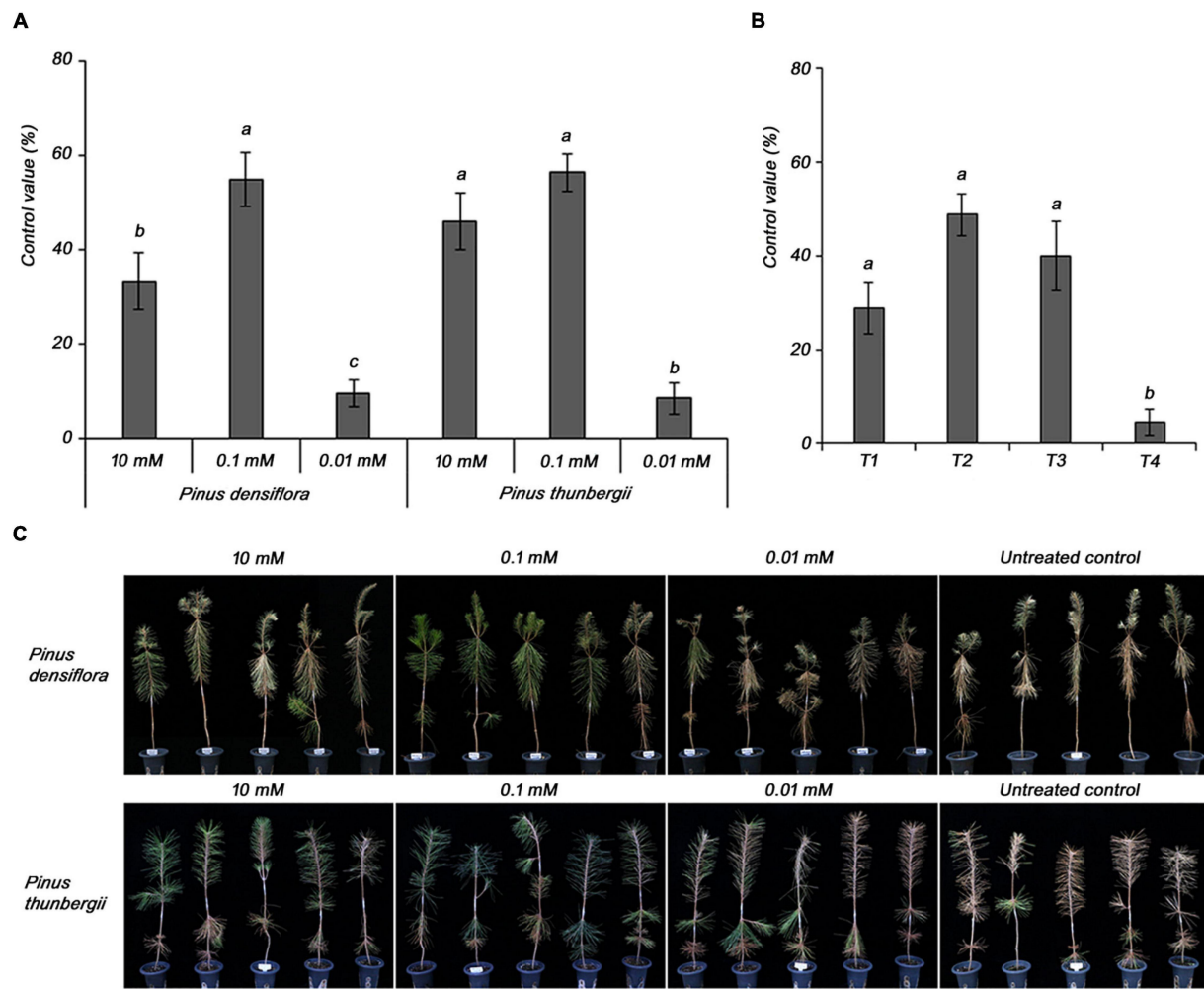


**FIGURE 3.** Determination of **(A)** optimal concentration of methyl salicylate 20 EC in 3-year-old *Pinus densiflora* and *Pinus thunbergii* seedlings, and **(B)** application time of 0.1 mM methyl salicylate 20 EC in 3-year-old *Pinus densiflora* seedlings against pine wilt disease. T1, treatment at 1 week before inoculation with pine wood nematode; T2, treatment at 2 and 1 weeks before inoculation with pine wood nematode; T3, treatment at 3 and 1 weeks before inoculation with pine wood nematode; T4, treatment at 4 and 1 week before inoculation with pine wood nematode. Each value represents the mean  $\pm$  standard error of five replicates. Different letters indicate significant differences with  $p < 0.05$ , as calculated using the Tukey's HSD test. **(C)** The representing pictures of *P. densiflora* and *P. thunbergii* after inoculation with PWN with or without MeSA. From 10 to 0.01 mM of MeSA was treated 2 and 1 weeks before PWN inoculation with indicated concentrations.

The optimal treatment time was determined using 0.1 mM MeSA 20 EC as the optimal concentration. The control values were 48.9 and 40.0% for T2 and T3, respectively. There was no significant difference between T2 and T3, but considering T4 (4.4%), we inferred that longer treatment interval worsened

the efficacy. Therefore, the optimal treatment time was selected as T2 (Figure 3B).

### **Evaluation of Disease Control Efficacy of Methyl Salicylate 20 DC Against Pine Wilt Disease Under Field Conditions**

The disease control efficacy of MeSA 20 DC formulation was evaluated under field conditions using 10-year-old *P. densiflora*. The disease incidences in response to treatment with MeSA 20 DC and control were 25 and 62.5%, respectively, at 4 months post-inoculation (Figure 4A). In addition, MeSA 20 DC and emamectin benzoate 2.15 EC, which was used as positive controls, showed control values of 60 and 46.7%, respectively, compared to the untreated control. There was no significant difference between MeSA and emamectin benzoate (Figure 4B). The pictures taken using drone showed distinct wilting brownish between MeSA treatment and untreated control (Figure 4C). Therefore, based on the results of the field tests, we confirmed that MeSA can effectively control PWD in adult trees as well as 3-year-old seedlings.

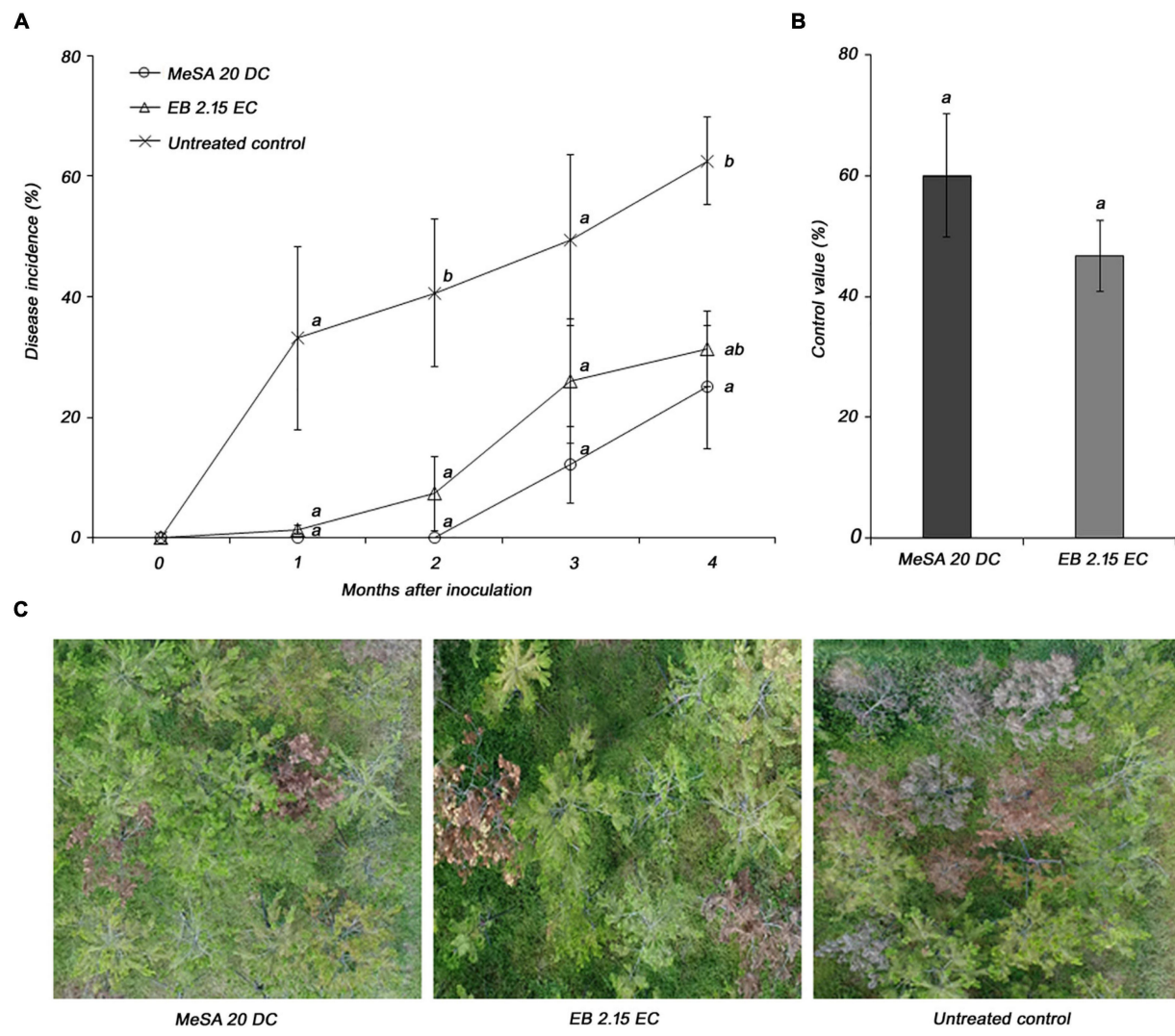


**FIGURE 4.** Evaluation of disease control efficacy of methyl salicylate 20 DC (MeSA 20 DC) against pine wilt disease upon foliar application onto 10-year-old *Pinus densiflora* under field conditions. Emamectin benzoate 2.15 EC (EB 2.15 EC) was used as positive control and applied via trunk injection. Each pine tree was inoculated with 10,000 juveniles of pine wood nematode. **(A)** Disease severity after inoculation of pine wood nematode. Each value represents the mean  $\pm$  standard error of four replicates with each replicate consist of four trees. The different letters indicate significant differences with  $p < 0.05$ , as calculated using the Tukey's HSD test. **(B)** Disease control efficacy at 4 months post-inoculation with pinewood nematode. **(C)** The pictures of pine trees treated with MeSA 20 DC, EB 2.15 EC, and Tween<sup>®</sup> 20 (untreated control).

## Assessment of the Effect of Methyl Salicylate on the Expression of Defense-Related Genes Using qRT-PCR

The expression of defense-related genes was analyzed using qRT-PCR following treatment with PWN, MeSA, and both PWN and MeSA (Figure 5A). Expressions of *PR-1*, *PR-2*, *PR-5*, and *ETS* were modulated upon PWN inoculation or MeSA spraying. The relative expression level of the *PR-1* was similar to or slightly higher in the MeSA-treated group than in the untreated group; however, the MeSA-treated group showed a 2.2-fold higher expression level than the untreated group at 7 days post-inoculation with PWN (I7) (Figure 5B). The relative expression level of the *PR-2* was 6.2- and 5.7-fold higher than that of the untreated control group at 7 days post-first treatment (1T7) and 3 days post-second treatment with MeSA (2T3), respectively. Post-inoculation with PWN, the expression of *PR-2* was consistently higher than that of the untreated group. The expression levels of *PR-2* in the untreated group also increased over time, but the MeSA-treated group showed a much greater increase; in particular, it displayed 4.4- and 4.5-fold higher upregulation than the untreated group at 3 and 7 days post-inoculation with PWN (I3 and I7), respectively (Figure 5C). The relative expression levels of *PR-5* was 3.1- and 6-fold higher in the MeSA-treated group than in the untreated group at 7 days post-first and -second treatment with MeSA (1T7 and 2T7), and 1.8- and 2.2-fold higher, respectively, at 3 and 7 days post-inoculation with PWN (Figure 5D). *PR-1*, *PR-2*, and *PR-5*, which are the markers of salicylic acid-dependent SAR, showed similar patterns of upregulation as the untreated groups, post-treatment with MeSA and -PWN inoculation. Upon treatment with PWN or MeSA, *PR-9* expression was induced 5- or 2-fold, respectively, as compared to the untreated condition, at all the time points monitored. Upon treatment with both PWN and MeSA, however, *PR-9* expression was induced up to 15-fold as compared to that in the normal condition, and 2–3-fold that in the PWN inoculation only condition (Figure 5E). These results demonstrated the boosting effect of MeSA treatment, presenting a strong evidence that MeSA treatment and PWN target the same plant defense system.

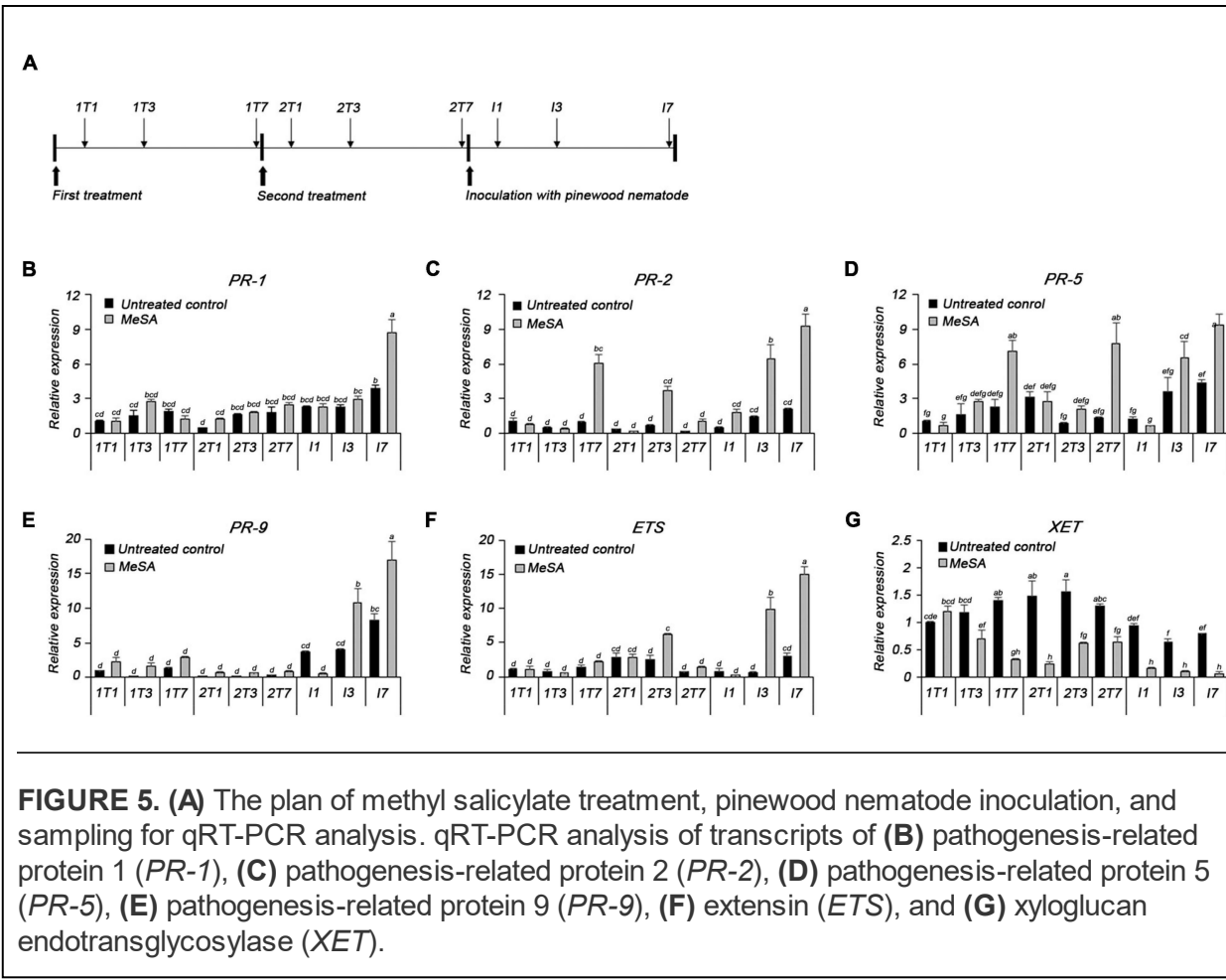


**FIGURE 5. (A)** The plan of methyl salicylate treatment, pinewood nematode inoculation, and sampling for qRT-PCR analysis. qRT-PCR analysis of transcripts of **(B)** pathogenesis-related protein 1 (*PR-1*), **(C)** pathogenesis-related protein 2 (*PR-2*), **(D)** pathogenesis-related protein 5 (*PR-5*), **(E)** pathogenesis-related protein 9 (*PR-9*), **(F)** extensin (*ETS*), and **(G)** xyloglucan endotransglycosylase (*XET*).

The MeSA-treated group displayed 2.5-fold higher expression of *ETS*, a cell wall-related gene, than the untreated group, at 3 days post-second treatment with MeSA (2T3). The expression level of *ETS* markedly increased 17.1- and 5.1-fold, respectively, compared to the untreated group, at 3 and 7 days post-inoculation with PWN (I3 and I7) (Figure 5F). Similarly, the *PR-9* expression was also induced at I3 and I7, as compared to the untreated group (2.7- and 2.1-fold, respectively). On the contrary, expression of *XET*, which loosens the cell wall, was downregulated as compared to the untreated group, except at 1 day post-first treatment with MeSA, and was expressed at a very low level post-inoculation with PWN (Figure 5G).

Based on the results of the gene expression test, we concluded that treatment with MeSA via foliar spraying induced SAR in pine trees, including the PWN-related defense system. In addition, MeSA application strengthened the cell wall structure by upregulating *ETS* or downregulating *XET* expression, thereby increasing pine tree defense against PWN.

## DISCUSSION

The control of PWD is a challenging process particularly in large scale forests where trunk injection with nematicides is hardly applicable and would require rigorous effort. In addition, spraying insecticides against the *Monochamus* vector, that is among the main methods used for conventional PWD management, was shown to have a limited effect in hindering PWD spread and might result in emergence of insect resistance along with encompassing a great deal of environmental burden and adverse effects on human and other non-target species (Ikenaka et al., 2019; Jung et al., 2021). Induction of resistance using chemical elicitors represent a promising alternative that is sustainable and eco-friendly as there is no direct nematicidal activity or effect on other non-target species (Oka et al., 2000). However, utilization of induced resistance elicitors require evaluation and accurate setting up of the effective formulation, concentration, and time of foliar spray application. In this study, four SAR elicitors, including MeSA, were selected among 12 candidates known to induce resistance in various plants, based on *in vivo* screening via trunk injection into 3-year-old *P. densiflora* seedlings. The stability and effectiveness of the four selected resistance elicitors were assessed and MeSA was selected post-*in vivo* testing of its potency upon application as a foliar spray. MeSA is a volatile long-range signaling compound produced by many plants for induction of SAR and may activate resistance in neighboring plants or in the healthy tissues of the infected plant. MeSA in the air is absorbed by the uninfected distal tissue and converted to SA for the establishment of acquired resistance (Shulaev et al., 1997). Signaling in plants by volatile compounds such as MeSA can overcome the spatial and temporal limitations of the vascular system (Heil and Ton, 2008). The timing of defense responses is crucial and can mark the difference between whether the plant overcomes or succumbs to the pathogen infection.

Two types of MeSA formulations (MeSA 20 DC and MeSA 20 EC) were tested for foliar spray application in this study. Unlike *P. densiflora*, treatment with MeSA 20 DC was ineffective in controlling PWD when tested on *P. thunbergii* seedlings. Although both *P. densiflora* and *P. thunbergii* belong to the same genus *Pinus*, their leaves are histologically different, as *P. thunbergii* has a thicker epidermis and stronger subcutaneous tissue than *P. densiflora* (Shaw, 1914). To overcome this difference, a new formulation, MeSA 20 EC, was prepared. Upon comparing the two formulations, MeSA 20 EC showed

better control efficiency in both *P. densiflora* and *P. thunbergii* seedlings (52.3 and 57.8%, respectively), while MeSA 20 DC showed a similar effect (47.7%) to MeSA 20 EC in *P. densiflora*, but not in *P. thunbergii* (6.7%). Unlike DC, EC uses methylated soy bean oil (MSO2) as the solvent with a high flash point, thus resulting in a lower volatility of MeSA, allowing for prolonged exposure on the leaves, thus improving its efficiency on *P. thunbergii*. Therefore, the MeSA 20 EC formulation was selected as the optimal formulation.

Resistance inducing elicitors generally show maximum efficiency at specific concentrations, depending on the plant, unlike chemicals that have direct concentration-dependent antimicrobial activity. For example, SA showed the highest effect at a concentration of 1.5 mM against *Fusarium oxysporum* in tomato and at a concentration of 0.5 mM against *Ralstonia solanacearum* in pepper (Ojha and Chatterjee, 2012; Chandrasekhar et al., 2017). We tested several concentrations of MeSA 20 EC formulation to determine the optimal concentration, which was eventually selected as the optimal formulation for treating PWD. The highest control efficiency was observed at MeSA concentration of 0.1 mM in both *P. densiflora* and *P. thunbergii* (54.8 and 56.3%, respectively). Using this optimum concentration of MeSA 20 EC, the optimal treatment time was tested and confirmed the control values of 48.9 and 40.0% at T2 and T3, respectively. There was no significant difference between T2 and T3, but considering the effect at T4 (4.4%), we inferred that the longer treatment interval worsened the efficacy; thus, T2 was selected as the optimal treatment time. Based on these results, it was established that treatment with MeSA 20 EC formulation at a concentration of 0.1 mM at 2 and 1 week before inoculation of PWN (T2) were the optimal formulation and processing conditions for MeSA, respectively, to achieve effective control against PWD.

Field experiments on 10-year-old *P. densiflora* have also confirmed the efficiency of MeSA foliar treatment against PWD as the disease incidence of treated trees were significantly reduced to levels comparable to those achieved with trunk injection with Emamectin benzoate. However, since we have established that 0.1 mM of MeSA EC is the optimal treatment condition through the optimized greenhouse test of MeSA, additional field tests according to the optimal treatment conditions are required, and a better effect can be expected.

Our previous studies reported genome-wide analyses of pine trees treated with MeSA against the nematode *B. xylophilus* (Park et al., 2020). The application of the MeSA, effective in terms of reducing PWD severity, mainly induce genes involved in systems for protection from ROS damage as well as genes encoding flavonoid biosynthesis. Flavonoids not only contribute to a neutralizing ROS (Agati et al., 2012), but affect the fitness of nematodes at different life stages (Chin et al., 2018) based on network and gene ontology (GO) analyze. In this study, we focused on expression analyze of defense-related genes. It has been reported that the transcript levels of defense-related gene expression are different between susceptible and resistance pine trees and the inoculation with PWN further increase such difference in gene expression levels (Hirao et al., 2012). To elucidate the mechanism underlying the observed control value of MeSA against PWD, qRT-PCR analysis was performed in this study using *P. densiflora* leaves. When MeSA was applied to pine leaves, *PR-1*, *PR-2*, and *PR-5* expressions were significantly upregulated compared to the untreated group, before and after inoculation with PWN. *PR-1*, *PR-2*, and *PR-5* are commonly used as marker genes for SAR induction (Molinari et al., 2014). Recent studies have reported that upregulation of *PR-1*, *PR-2*, and *PR-5* expression significantly inhibits infection of beet-cyst (*Heterodera schachtii*) and root-knot (*Meloidogyne incognita*) nematodes in *Arabidopsis thaliana* and tomato (Uehara et al., 2010; Hamamouch et al., 2011). Furthermore, it has been reported that the difference between whether a plant is susceptible or resistant depends on the differences in the timing and magnitude of defense response (Tao et al., 2003). Therefore, the optimum timing and high expression of the *PR* may contribute to the effective inhibition of PWD development.

Upon MeSA treatment, expressions of cell wall-related genes, *PR-9* and *ETS*, were upregulated, while that of *XET* was downregulated. Extensin, encoded by the *ETS*, is believed to play an important part in cell wall biosynthesis in plants (Cannon et al., 2008). Extensin plays an essential role in biotic and abiotic stress responses by being involved in maintaining the strength of the cell wall (Deepak et al., 2010). In addition, peroxidase encoded by the *PR-9* strengthens the cell wall by catalyzing lignification and enhancing resistance against various pathogens (Van Loon et al., 2006). The *XET* regulates the strength of the cell wall by being involved in xyloglucan, which supports the load between the cellulose microfibers in the cell wall (Uozu et al., 2000; Vissenberg et al., 2000). Strengthening of the cell wall is a very important factor during the early stages of plant defense. In a study

comparing histological changes in susceptible and resistant *P. thunbergii*, the resistant *P. thunbergii* effectively inhibited the initial migration of PWN by strengthening the cell wall via lignification (Kusumoto et al., 2014). In addition, migration and reproduction of PWN are important factors that determine the survival of pine trees (Nakajima et al., 2019). Therefore, MeSA is believed to be involved in a control mechanism against PWD by rapidly inducing the expression of defense-related genes in pine trees prior to infection, promptly responding to invasion of PWN, and delaying migration and reproduction of PWN.

Overall, this study provides evidence on the effective control activity of foliar spray with MeSA against PWD under greenhouse and field conditions as possible alternative to other pesticide control methods. The mechanism of control was indicated as induction of resistance by the observed significant changes in the expression of defense-related genes without direct nematicidal activity. The optimum formulation, concentration and treatment time were adjusted for improvement of the control activity. The provided results represent an important step toward the establishment of effective eco-friendly and applicable control method for PWD under field conditions.

## CONCLUSION

MeSA was selected from 12 candidate elicitors via *in vivo* screening using *P. densiflora* seedlings. MeSA 20 DC formulation showed a control efficacy of 60% in field tests using 10-year-old *P. densiflora*. The optimal formulation and processing conditions for treatment were established as 0.1 mM MeSA 20 EC at 2 and 1 WBI with PWN. In addition, qRT-PCR analysis showed that MeSA induced elevated expression of various defense-related genes in pine leaves. The high expression of various plant defense-related and cell wall-related genes suggests that PWD can be controlled by inhibiting the migration and reproduction of PWN. Collectively, these results suggest that foliar application of MeSA may reduce the incidence of PWD by inducing resistance, thereby providing an economically feasible alternative to trunk-injection agents for the management of PWD.

## DATA AVAILABILITY STATEMENT

The original contributions presented in the study are included in the article/Supplementary Material, further inquiries can be directed to the corresponding author/s.

## AUTHOR CONTRIBUTIONS

Y-SS and J-CK conceived the study. HJ, AP, MS, NK, GH, and JK performed the experiments. HJ, AP, Y-SS, and J-CK analyzed the data. HJ wrote the manuscript. AP, Y-SS, YK, and J-CK reviewed and edited the manuscript. J-CK acquired the funds. All authors have read and agreed to the published version of the manuscript.

## FUNDING

This research was supported by a grant funded by National Institute of Forest Science, South Korea (FE0702-2016-02).

## ACKNOWLEDGMENTS

The pinewood nematode, *Bursaphelenchus xylophilus*, used in this experiment was kindly provided by Dr. Kim Junheon, National Institute of Forest Science, South Korea. We would like to thank the director of Yoosung Chemical R&T Co., Ltd., Mr. Moon Sung Kang, for his help in preparing the formulations.

## SUPPLEMENTARY MATERIAL

The Supplementary Material for this article can be found online at: <https://www.frontiersin.org/articles/10.3389/fpls.2021.812414/full#supplementary-material>

## REFERENCES

Abbott, W. S. (1925). A method of computing the effectiveness of an insecticide. *J. Econ. Entomol.* 18, 265–267. doi: 10.1093/jee/18.2.265a

Abelleira, A., Picoaga, A., Mansilla, J., and Aguin, O. (2011). Detection of *Bursaphelenchus xylophilus*, causal agent of pine wilt disease on *Pinus pinaster* in Northwestern Spain. *Plant Dis.* 95, 776–776. doi: 10.1094/PDIS-12-10-0902

Agati, G., Azzarello, E., Pollastri, S., and Tattini, M. (2012). Flavonoids as antioxidants in plants: location and functional significance. *Plant Sci.* 196, 67–76. doi: 10.1016/j.plantsci.2012.07.014

Azevedo, H., Lino-Neto, T., and Tavares, R. M. (2003). An improved method for high-quality RNA isolation from needles of adult maritime pine trees. *Plant Mol. Biol. Rep.* 21, 333–338. doi: 10.1007/bf02772582

Baermann, G. (1917). Eine einfache methode zur auffindung von *Ancylostomum* (Nematoden) larven in erdproben. *Geneesk. Tijdschr. Ned. Indie.* 57, 131–137.

Cannon, M. C., Terneus, K., Hall, Q., Tan, L., Wang, Y., Wegenhart, B. L., et al. (2008). Self-assembly of the plant cell wall requires an extensin scaffold. *Proc. Natl. Acad. Sci.* 105, 2226–2231. doi: 10.1073/pnas.0711980105

Chandrasekhar, B., Umesha, S., and Kumar, H. N. (2017). Proteomic analysis of salicylic acid enhanced disease resistance in bacterial wilt affected chilli (*Capsicum annuum*) crop. *Physiol. Mol. Plant Pathol.* 98, 85–96. doi: 10.1016/j.pmp.2017.04.002

Cheng, H., Lin, M., Li, W., and Fang, Z. (1983). The occurrence of a pine wilting disease caused by a nematode found in Nanjing. *For. Pest Dis.* 4, 1–5.

Chin, S., Behm, C. A., and Mathesius, U. (2018). Functions of flavonoids in plant–nematode interactions. *Plants* 7:85. doi: 10.3390/plants7040085

Deepak, S., Shailasree, S., Kini, R. K., Muck, A., Mithöfer, A., and Shetty, S. H. (2010). Hydroxyproline-rich glycoproteins and plant defence. *J. Phytopathol.* 158, 585–593. doi: 10.1111/j.1439-0434.2010.01669.x

Dempsey, D. M. A., and Klessig, D. F. (2012). SOS—too many signals for systemic acquired resistance? *Trends Plant Sci.* 17, 538–545. doi: 10.1016/j.tplants.2012.05.011

García-Pastor, M. E., Giménez, M. J., Zapata, P. J., Guillén, F., Valverde, J. M., Serrano, M., et al. (2020). Preharvest application of methyl salicylate, acetyl salicylic acid and salicylic acid alleviated disease caused by *Botrytis cinerea* through stimulation of antioxidant system in table grapes. *Int. J. Food Microbiol.* 334:108807. doi: 10.1016/j.ijfoodmicro.2020.108807

Hamamouch, N., Li, C., Seo, P. J., Park, C. M., and Davis, E. L. (2011). Expression of *Arabidopsis* pathogenesis-related genes during nematode infection. *Mol. Plant Pathol.* 12, 355–364. doi: 10.1111/j.1364-3703.2010.00675.x

Hayat, S., and Ahmad, A. (2007). *Salicylic acid—a plant hormone*. New York, NY: Springer Science & Business Media.

Heil, M., and Ton, J. (2008). Long-distance signalling in plant defence. *Trends Plant Sci.* 13, 264–272. doi: 10.1016/j.tplants.2008.03.005

Hirao, T., Fukatsu, E., and Watanabe, A. (2012). Characterization of resistance to pine wood nematode infection in *Pinus thunbergii* using suppression subtractive hybridization. *BMC Plant Biol.* 12:1–14. doi: 10.1186/1471-2229-12-13

Ikenaka, Y., Miyabara, Y., Ichise, T., Nakayama, S., Nimako, C., Ishizuka, M., et al. (2019). Exposures of children to neonicotinoids in pine wilt disease control areas. *Environ. Toxicol. Chem.* 38, 71–79. doi: 10.1002/etc.4316

Ji, H., Kyndt, T., He, W., Vanholme, B., and Gheysen, G. (2015).  $\beta$ -Aminobutyric acid–induced resistance against root-knot nematodes in rice is based on increased basal defense. *Mol. Plant Microbe Interact.* 28, 519–533. doi: 10.1094/MPMI-09-14-0260-R

Jung, H. W., Tschaplinski, T. J., Wang, L., Glazebrook, J., and Greenberg, J. T. (2009). Priming in systemic plant immunity. *Science* 324, 89–91. doi: 10.1126/science.1170025

Jung, J. K., Lee, U. G., Cha, D., Kim, D. S., and Jung, C. (2021). Can insecticide applications used to kill vector insects prevent pine wilt disease? *Pest Manag. Sci.* 77, 4923–4929. doi: 10.1002/ps.6532

Kalaivani, K., Kalaiselvi, M. M., and Senthil-Nathan, S. (2016). Effect of methyl salicylate (MeSA), an elicitor on growth, physiology and pathology of resistant and susceptible rice varieties. *Sci. Rep.* 6, 1–11. doi: 10.1038/srep34498

Kim, J., Jung, Y. H., and Lee, S.-M. (2021). Diel Rhythmicity of Field Responses to Synthetic Pheromone Lures in the Pine Sawyer *Monochamus saltuarius*. *Insects* 12:441. doi: 10.3390/insects12050441

Kim, J., Seo, S.-M., and Park, I.-K. (2011). Nematicidal activity of plant essential oils and components from *Gaultheria fragrantissima* and *Zanthoxylum alatum* against the pine wood nematode *Bursaphelenchus xylophilus*. *Nematology* 13, 87–93. doi: 10.1163/138855410x504907

Kim, N., Jeon, H. W., Manna, M., Jeong, S. I., Kim, J., Kim, J., et al. (2019). Induction of resistance against pine wilt disease caused by *Bursaphelenchus xylophilus* using selected pine endophytic bacteria. *Plant Pathol.* 68, 434–444. doi: 10.1111/ppa.12960

Korea Forest Service (2013). *Guideline for the control of forest diseases and insect pests*. Dunsan-dong: Korea Forest Service, Daejeon, Republic of Korea, 325.

Kusumoto, D., Yonemichi, T., Inoue, H., Hirao, T., Watanabe, A., and Yamada, T. (2014). Comparison of histological responses and tissue damage expansion between resistant and susceptible *Pinus thunbergii* infected with pine wood nematode *Bursaphelenchus xylophilus*. *J. For. Res.* 19, 285–294. doi: 10.1007/s10310-013-0417-y

Kwon, H. R., Choi, G. J., Choi, Y. H., Jang, K. S., Sung, N. D., Kang, M. S., et al. (2010). Suppression of pine wilt disease by an antibacterial agent, oxolinic acid. *Pest Manag. Sci.* 66, 634–639. doi: 10.1002/ps.1920

Kwon, T.-S., Song, M.-Y., Shin, S.-C., and Park, Y.-S. (2005). Effects of aerial insecticide sprays on ant communities to control pine wilt disease in Korean pine forests. *Appl. Entomol. Zool.* 40, 563–574. doi: 10.1303/aez.2005.563

Lee, I. H., Han, H., Koh, Y. H., Kim, I. S., Lee, S.-W., and Shim, D. (2019). Comparative transcriptome analysis of *Pinus densiflora* following inoculation with pathogenic (*Bursaphelenchus xylophilus*) or non-pathogenic nematodes (*B. thailandae*). *Sci. Rep.* 9, 1–11. doi: 10.1038/s41598-019-48660-w

Lee, S.-M., Kim, D.-S., Lee, S.-G., Park, N.-C., and Lee, D.-W. (2009). Selection of trunk injection pesticides for preventive of pine wilt disease, *Bursaphelenchus xylophilus* on Japanese black pine (*Pinus thunbergii*). *Korean J. Pestic Sci.* 13, 267–274.

Li, M., Li, H., Sheng, R.-C., Sun, H., Sun, S.-H., and Chen, F.-M. (2020). The first record of *Monochamus saltuarius* (Coleoptera; Cerambycidae) as vector of *Bursaphelenchus xylophilus* and its new potential hosts in China. *Insects* 11:636. doi: 10.3390/insects11090636

Livak, K. J., and Schmittgen, T. D. (2001). Analysis of relative gene expression data using real-time quantitative PCR and the  $2^{-\Delta \Delta CT}$  method. *Methods* 25, 402–408. doi: 10.1006/meth.2001.1262

Maehara, N., and Futai, K. (2000). Population changes of the pinewood nematode, *Bursaphelenchus xylophilus* (Nematoda: Aphelenchoididae), on fungi growing in pine-branch segments. *Appl. Entomol. Zool.* 35, 413–417. doi: 10.1303/aez.2000.413

Mamiya, Y. (1988). History of pine wilt disease in Japan. *J. Nematol.* 20:219.

Molinari, S., Fanelli, E., and Leonetti, P. (2014). Expression of tomato salicylic acid (SA)-responsive pathogenesis-related genes in *Mi-1*-mediated and SA-induced resistance to root-knot nematodes. *Mol. Plant Pathol.* 15, 255–264. doi: 10.1111/mpp.12085

Mota, M., Burgermeister, W., Braasch, H., Sousa, E., Penas, A. C., Metge, K., et al. (1999). First report of *Bursaphelenchus xylophilus* in Portugal and in Europe. *Nematology* 1, 727–734. doi:

10.1163/156854199508757

Nakajima, G., Iki, T., Yamanobe, T., Nakamura, K., and Aikawa, T. (2019). Spatial and temporal distribution of *Bursaphelenchus xylophilus* inoculated in grafts of a resistant clone of *Pinus thunbergii*. *J. For. Res.* 24, 93–99. doi: 10.1080/13416979.2019.1578136

Ojha, S., and Chatterjee, N. C. (2012). Induction of resistance in tomato plants against *Fusarium oxysporum* f. sp. *lycopersici* mediated through salicylic acid and *Trichoderma harzianum*. *J. Plant Prot. Res.* 52:3. doi: 10.2478/v10045-012-0034-3

Okai, Y., Kolai, H., Bar-Eyal, M., Mor, M., Sharon, E., Chet, I., et al. (2000). New strategies for the control of plant-parasitic nematodes. *Pest. Manag. Sci.* 56, 983–988. doi: 10.1002/1526-4998(200011)56:11<983::AID-PS233<3.0.CO;2-X

Park, J., Jeon, H. W., Jung, H., Lee, H. H., Kim, J., Park, A. R., et al. (2020). Comparative Transcriptome Analysis of Pine Trees Treated with Resistance-Inducing Substances against the Nematode *Bursaphelenchus xylophilus*. *Genes* 11:1000. doi: 10.3390/genes11091000

Park, S.-W., Kaimoyo, E., Kumar, D., Mosher, S., and Klessig, D. F. (2007). Methyl salicylate is a critical mobile signal for plant systemic acquired resistance. *Science* 318, 113–116. doi: 10.1126/science.1147113

Proença, D. N., Francisco, R., Santos, C. V., Lopes, A., Fonseca, L., Abrantes, I. M., et al. (2010). Diversity of bacteria associated with *Bursaphelenchus xylophilus* and other nematodes isolated from *Pinus pinaster* trees with pine wilt disease. *PLoS One.* 5:e15191. doi: 10.1371/journal.pone.0015191

Shaw, G. R. (1914). *The genus Pinus*. Riverside: Riverside Press.

Shulaev, V., Silverman, P., and Raskin, I. (1997). Airborne signalling by methyl salicylate in plant pathogen resistance. *Nature* 385, 718–721. doi: 10.1038/385718a0

Spoel, S. H., and Dong, X. (2012). How do plants achieve immunity? Defence without specialized immune cells. *Nat. Rev. Immunol.* 12, 89–100. doi: 10.1038/nri3141

Tao, Y., Xie, Z., Chen, W., Glazebrook, J., Chang, H.-S., Han, B., et al. (2003). Quantitative nature of *Arabidopsis* responses during compatible and incompatible interactions with the bacterial pathogen *Pseudomonas syringae*. *Plant Cell* 15, 317–330. doi: 10.1105/tpc.007591

Tzean, S., and Jan, S. (1985). “The occurrence of pine wood nematode, *Bursaphelenchus xylophilus*,” in *Proceedings of the 6th ROC symposium of electron microscopy*, (Taiwan), 38–39.

Uehara, T., Sugiyama, S., Matsuura, H., Arie, T., and Masuta, C. (2010). Resistant and susceptible responses in tomato to cyst nematode are differentially regulated by salicylic acid. *Plant Cell Physiol.* 51, 1524–1536. doi: 10.1093/pcp/pcq109

Uozu, S., Tanaka-Ueguchi, M., Kitano, H., Hattori, K., and Matsuoka, M. (2000). Characterization of XET-related genes of rice. *Plant Physiol.* 122, 853–860. doi: 10.1104/pp.122.3.853

Van Loon, L. C., Rep, M., and Pieterse, C. M. (2006). Significance of inducible defense-related proteins in infected plants. *Annu. Rev. Phytopathol.* 44, 135–162. doi: 10.1146/annurev.phyto.44.070505.143425

Vissenberg, K., Martinez-Vilchez, I. M., Verbelen, J.-P., Miller, J. G., and Fry, S. C. (2000). *In vivo* colocalization of xyloglucan endotransglycosylase activity and its donor substrate in the elongation zone of *Arabidopsis* roots. *Plant Cell* 12, 1229–1237. doi: 10.2307/3871267

Vlot, A. C., Sales, J. H., Lenk, M., Bauer, K., Brambilla, A., Sommer, A., et al. (2021). Systemic propagation of immunity in plants. *New Phytol.* 229, 1234–1250. doi: 10.1111/nph.16953

Yang, B., and Wang, Q. (1989). Distribution of the pinewood nematode in China and susceptibility of some Chinese and exotic pines to the nematode. *Can. J. For. Res.* 19, 1527–1530. doi: 10.1139/x89-232

Yano, S. (1913). Investigation on pine death in Nagasaki prefecture. *Sanrin-Kouhou.* 4, 1–14.

Yi, C. K., Byun, B. H., Park, J. D., Yang, S., and Chang, K. H. (1989). First finding of the pine wood nematode, *Bursaphelenchus xylophilus* (Steiner et Buhrer) Nickle and its insect vector in Korea. *Res. Rep. For. Res. Inst. Seoul.* 38, 141–149.

**Conflict of Interest:** The authors declare that the research was conducted in the absence of any commercial or financial relationships that could be construed as a potential conflict of interest.

**Publisher's Note:** All claims expressed in this article are solely those of the authors and do not necessarily represent those of their affiliated organizations, or those of the publisher, the editors and the reviewers. Any product that may be evaluated in this article, or claim that may be made by its manufacturer, is not guaranteed or endorsed by the publisher.

*Copyright © 2022 Jeon, Park, Sung, Kim, Manna, Han, Kim, Koo, Seo and Kim. This is an open-access article distributed under the terms of the Creative Commons Attribution License (CC BY). The use, distribution or reproduction in other forums is permitted, provided the original author(s) and the copyright owner(s) are credited and that the original publication in this journal is cited, in accordance with accepted academic practice. No use, distribution or reproduction is permitted which does not comply with these terms.*

ORIGINAL RESEARCH

published: 08 February 2022

doi: 10.3389/fpls.2021.822289



# Virulence Biomarkers of *Bursaphelenchus xylophilus*: A Proteomic Approach

**Joana M. S. Cardoso<sup>1</sup>\*, Sandra I. Anjo<sup>2</sup>, Bruno Manadas<sup>2</sup>, Hugo Silva<sup>1</sup>, Isabel Abrantes<sup>1</sup>, Katsunori Nakamura<sup>3</sup> and Luís Fonseca<sup>1</sup>**

<sup>1</sup>Department of Life Sciences, Centre for Functional Ecology, University of Coimbra, Coimbra, Portugal

<sup>2</sup>CNC-Center for Neuroscience and Cell Biology, University of Coimbra, Coimbra, Portugal

<sup>3</sup>Tohoku Research Center, Forestry and Forest Products Research Institute, Morioka, Japan

**Edited by:**

Margarida Espada, University of Évora, Portugal

**Reviewed by:**

Lee Robertson, National Institute of Agricultural and Food Research and Technology, Spain

Ryoji Shinya, Meiji University, Japan

**\*Correspondence:** Joana M. S. Cardoso, joana.cardoso@uc.pt

**Specialty section:** This article was submitted to Plant Pathogen Interactions, a section of the journal *Frontiers in Plant Science*

**Received:** 25 November 2021

**Accepted:** 28 December 2021

**Published:** 08 February 2022

**Citation:** Cardoso JMS, Anjo SI, Manadas B, Silva H, Abrantes I, Nakamura K and Fonseca L (2022) Virulence Biomarkers of *Bursaphelenchus xylophilus*: A Proteomic Approach. *Front. Plant Sci.* 12:822289. doi: 10.3389/fpls.2021.822289

The pinewood nematode (PWN), *Bursaphelenchus xylophilus*, one of the most serious forest pests worldwide, is considered the causal agent of the pine wilt disease (PWD). The main host species belong to

the genus *Pinus*, and a variation in the susceptibility of several pine species to PWN infection is well-known. It is also recognized that there is variation in the virulence among *B. xylophilus* isolates. In the present study, we applied a quantitative mass spectrometry-based proteomics approach to perform a deep characterization of proteomic changes across two *B. xylophilus* isolates with different virulence from different hosts and geographical origins. A total of 1,456 proteins were quantified and compared in the two isolates secretomes, and a total of 2,741 proteins were quantified and compared in the nematode proteomes in pine tree extract and fungus stimuli conditions. From the proteomic analyses, a group of proteins was selected and identified as potential virulence biomarkers and shed light on putative most pathogenic proteins of this plant-parasitic nematode. Proteomic data are available *via* ProteomeXchange with identifier PXD029377.

**Keywords:** pinewood nematode, pine trees, pine wilt disease, plant–nematode interactions, proteomics, secretome, virulence

## INTRODUCTION

The pinewood nematode (PWN), *Bursaphelenchus xylophilus*, is the causal agent of the pine wilt disease (PWD), one of the most serious forest pests in the world and responsible for high economic and ecological losses. It is vectored by insects mainly belonging to the genus *Monochamus* and has, as main host species, trees of the genus *Pinus*. Native from North America, at the beginning of the 20<sup>th</sup> century, PWN was introduced in Japan, which became responsible for massive mortality of native pine trees, and then spread to neighboring East Asian countries (China, Taiwan, South Korea) during the 1980s (Futai, 2013). Probably, with a Japanese origin (Mallez et al., 2021), PWN was first reported in Europe, in continental Portugal, in 1999 (Mota et al., 1999) and spread to Spain (Abelleira et al., 2011; Robertson et al., 2011) and Madeira Island (Fonseca et al., 2012). Listed by the European and Mediterranean Plant Protection Organization (EPPO) as an A2 quarantine pest (EPPO, 2021), it represents a huge threat to forest ecosystems worldwide.

*Bursaphelenchus xylophilus* is a migratory endoparasitic nematode that is able to feed on parenchyma cells of live pine trees, migrating and spreading

throughout the xylem tissues, causing cell destruction, and also to feed on fungi colonizing the dead or dying trees. During the last 20 years, advances have been made for understanding the molecular bases of these PWN-host interactions and pathogenic mechanisms. Main advances emerged from transcriptomic and genomic studies on *B. xylophilus* (Kikuchi et al., 2007, 2011; Kang et al., 2009; Figueiredo et al., 2013; Espada et al., 2016; Tsai et al., 2016), which revealed some special features of *B. xylophilus* such as the possession of cell wall-degrading enzymes, its evolutionary origin, and also constituted fundamental data that allowed the development of postgenomic studies (Shinya et al., 2013a).

Proteins are the final product of gene regulation and provide the final evidence of the function of a gene. Therefore, proteomic studies are fundamental to find out what proteins are produced and clarify which molecules are directly involved in the parasite-host interaction. From these, the secreted proteins have been of particular interest as they are directly involved in this interaction. The first complete profile of *B. xylophilus* secretome was achieved by Shinya et al. (2013b) that identified several secreted proteins potentially associated with *B. xylophilus* pathogenicity. In another study, a quantitative and comparative proteomic analysis of the secretome of *B. xylophilus* with the secretome of the closely related but non-pathogenic nematode, *B. mucronatus*, was performed, and proteins associated with peptidase activity, glycosyl hydrolase activity, and with peptidase inhibitor activity were found increased in *B. xylophilus* secretome (Cardoso et al., 2016). Additionally, the secretomes of *B. xylophilus* under the stimuli of pine species with different kinds of susceptibility to PWN were also compared, and differences detected in these secretomes highlighted diverse responses from the nematode to overcome host defenses with different susceptibilities (Silva et al., 2021).

Besides the variation in PWN host susceptibility, the nematodes themselves present a variation in their virulence level among isolates (Aikawa et al., 2003a). Several studies reported that the virulence level is usually correlated with the ability of the pathogen to multiply within the host, varies among isolates, and can be related with the geographical isolation, host trees, and environmental stresses (Kiyohara and Bolla, 1990; Aikawa et al., 2003a; Wang et al., 2005; Aikawa and Kikuchi, 2007; Shinya et al., 2012; Filipiak, 2015). Differences in gene expression patterns and genetic diversity between virulent and avirulent isolates have been reported and showed that the most

significant variation between the two forms was observed in growth, reproduction, and oxidoreductase activities (Ding et al., 2016). Furthermore, some genes affected by genomic variation had potential roles in pathogenesis, such as putative effectors or digestive peptidases, which could lead avirulent isolates to display low ingestion of nutrients and provoke a delay in development (Palomares-Rius et al., 2015; Filipiak et al., 2021). Recently, in a semi-quantitative proteomic study, the comparative secretome analysis among four *B. xylophilus* isolates with different levels of virulence has been carried out and four candidate virulence determinants identified: one lipase, two cysteine peptidases, and glycoside hydrolase family 30 (Shinya et al., 2021).

In this study, a short-GeLC approach, in combination with the Sequential Window Acquisition of All Theoretical Mass Spectra (SWATH-MS) acquisition method, was used to perform a deep characterization of proteomic changes across two *B. xylophilus* isolates with different virulence and in different conditions, pine extract (PE), and fungus stimuli to discover virulence biomarkers and shed light on the most pathogenic proteins of this plant-parasitic nematode.

## MATERIALS AND METHODS

### Nematode Cultures and Reproductive Ability Assays

Nematodes from the Portuguese virulent isolate BxPt17AS (BxV) originally isolated from *P. pinaster* and the avirulent Japanese isolate C14-5 (BxAv) originally isolated from the insect vector *M. alternatus* emerged from *P. densiflora* (Aikawa et al., 2003b; Aikawa and Kikuchi, 2007) were maintained in culture plates of the fungus *Botrytis cinerea* grown on Malt Extract Agar medium at 25°C. The BxPt17AS was used in previous studies as a virulent isolate (Cardoso et al., 2016, 2019, 2020; Silva et al., 2021) and the C14-5 as an avirulent isolate (Mota et al., 2006; Aikawa and Kikuchi, 2007; Filipiak, 2015).

To confirm the virulence status of each isolate, the reproductive ability in the fungus *B. cinerea* and in *P. pinaster* seedlings was determined. In the case of the fungus, 10 adult females and 10 adult males/isolate were individually separated under stereomicroscope, hand-picked, and placed in individual plates colonized with *B. cinerea* (10 plates/isolate). Twenty-one days after

inoculation, nematodes were collected with sterile water (SW) from the fungus plates. The resulting nematode suspension was then sieved through a 20- $\mu$ m sieve and quantified.

In the case of the *P. pinaster* seedlings, nematodes of each isolate were collected from fungus plates, used for maintenance of the isolates, and washed with SW. The resulting nematode suspension was sieved through a 20- $\mu$ m sieve and used to inoculate 2-3-year-old *P. pinaster* seedlings. Approximately 3,000 nematodes (mixed developmental stages) were inoculated/seedling (5 seedlings/isolate). As control, 5 seedlings were inoculated with SW. The inoculation procedure was performed as described in Pimentel et al. (2017). Pinewood nematode inoculated and control seedlings were kept in a greenhouse at a temperature range of 20–25°C, randomly distributed, and watered two times/week. The development of the symptomatology (yellowing/browning of the leaves) was examined and registered weekly. The reproductive ability of each isolate in *P. pinaster* was assessed 32 days after inoculation. The seedlings were cut at the soil surface level, and the aerial part (main stem and branches) and roots were separated. Nematodes were extracted from the entire seedlings (aerial part and roots) using the Whitehead and Hemming tray method (Whitehead and Hemming, 1965; EPPO, 2013) and quantified.

Statistical analyses on the reproductive ability of BxPt17As and C14-5 isolates in the fungus *B. cinerea* and in *P. pinaster* seedlings were performed independently, using ANOVA (significance level  $p < 0.05$ ). To achieve homogeneity of variance, a Log10 transformation was done. Statistical analyses were conducted using software IBM SPSS Statistics for Windows, version 28.0 (IBM Corp).

### **Pine Extract Stimuli Assay**

Pine extracts were prepared from 2-year-old *P. pinaster* seedlings as previously described (Cardoso et al., 2016), and the obtained solution was used as a pine stimulus. Mixed developmental nematode stages of each isolate (BxPt17As and C14-5) were collected from fungal cultures as described above and washed with SW. About  $10^6$  nematodes/replicate were resuspended with 5 ml of PE previously prepared and incubated overnight at 25°C in 10-cm Petri dishes. Six replicates/stimulus were performed. Nematodes were then sedimented by centrifugation and separated from the supernatant containing the secreted proteins ( $\pm$  5 ml). Samples having the secreted

proteins and samples with the nematodes were stored at  $-80^{\circ}\text{C}$  until the proteomic analysis of the secreted proteins (secretome) and whole nematode proteins (proteome), respectively. Nematodes from each isolate collected from fungus cultures and not exposed to PE were also stored at  $-80^{\circ}\text{C}$  for analysis of the whole nematode proteins (proteome) under fungus conditions.

## Sample Preparation for Proteomic Analysis

For the preparation of secreted proteins, an internal standard [(IS) – the recombinant protein maltose-binding protein fused with green fluorescent protein (MBP-GFP)] was added in equal amounts (1  $\mu\text{g}$  of recombinant protein) to each sample (Anjo et al., 2019), and the supernatants with the secreted proteins were completely dried under a vacuum using a Speedvac Concentrator Plus (Eppendorf). The resulting pellets were resuspended in an SDS-Sample buffer, aided by steps of ultrasonication (using a 750W Ultrasonic processor) and denaturation at  $95^{\circ}\text{C}$ . In addition to the individual replicates (6 in the case of the BxAv isolates and 4 replicates of the BxV), two pooled samples were created for protein identification and library creation by combining one-sixth of each replicate.

For preparation of whole nematode proteome, nematode pellets were lysed in 1-mM Tris-HCl pH 7.4 as described in Anjo et al. (2017), followed by protein precipitation using TCA-Acetone (Anjo et al., 2016). Protein pellets were resuspended as described above, and 50  $\mu\text{g}$  of total protein/sample (6 replicates/condition) was used for SWATH-MS. Four pooled samples were also created for protein identification/library creation by combining 15  $\mu\text{g}$  of each replicate. All samples were spiked with equal amounts of internal standard (1  $\mu\text{g}$  of MBP-GFP) prior to protein digestion.

Samples were then digested as previously described (Anjo et al., 2015; Cardoso et al., 2016).

## Protein Quantification by Sequential Windowed Acquisition of All Theoretical Mass Spectra

All samples were analyzed on a NanoLC<sup>TM</sup> 425 System coupled to a Triple TOF<sup>TM</sup> 6600 mass spectrometer (Sciex<sup>®</sup>) using two acquisition modes: (i) the pooled samples were analyzed by information-dependent acquisition (IDA), and (ii) the individual samples by the SWATH-MS mode. The ionization source was the OptiFlow<sup>®</sup> Turbo V Ion Source equipped with the SteadySpray<sup>TM</sup> Micro Electrode (1–50  $\mu\text{L}$ ). The chromatographic separation

was carried out on a YMC-Triart C18 Capillary Column 1/32" (12 nm, 5–3  $\mu$ m, 150 mm  $\times$  0.3 mm) and using a YMC-Triart C18 Capillary Guard Column (0.5  $\mu$ m  $\times$  5 mm, 3  $\mu$ m, 12 nm) at 50°C. The flow rate was set to 5  $\mu$ l min<sup>-1</sup>, and mobile phases A and B were 5% DMSO plus 0.1% formic acid in water or acetonitrile, respectively. The LC program was performed as follows: 5–35% of B (0–40 min), 35–90% of B (40–41 min), 90% of B (41–45 min), 90–5% of B (45–46 min), and 5% of B (46–50 min). The ionization source was operated in the positive mode set to an ion spray voltage of 4,500 V, 10 psi for nebulizer gas 1 (GS1), 15 psi for nebulizer gas 2 (GS2), 25 psi for the curtain gas (CUR), and source temperature (TEM) at 100°C.

For IDA experiments, the mass spectrometer was set to scanning full spectra (m/z 350–1,250) for 250 ms, followed by up to 100 MS/MS scans (m/z 100–1,500) per cycle, in order to maintain a cycle time of 3.298 s. The accumulation time of each MS/MS scan was adjusted in accordance with the precursor intensity (minimum of 30 ms for a precursor above the intensity threshold of 1,000). Candidate ions with a charge state between +1 and +5 and counts above a minimum threshold of 10 counts/s were isolated for fragmentation, and one MS/MS spectrum was collected before adding those ions to the exclusion list for 15 s (a mass spectrometer operated by Analyst<sup>®</sup> TF 1.7, Sciex). The rolling collision was used with a collision energy spread (CES) of 5. For SWATH experiments, the mass spectrometer was operated in a looped product ion mode (Gillet et al., 2012) and specifically tuned to a set of 90 overlapping windows, covering the precursor mass range of 350–1,250 m/z. A 50 ms survey scan (350–1,250 m/z) was acquired at the beginning of each cycle, and SWATH-MS/MS spectra were collected from 100 to 1,800 m/z for 35 ms, resulting in a cycle time of 3.251 s. The collision energy for each window was determined according to the calculation for a charge +2 ion centered upon the window with variable CES according to the window.

Peptide identification and library generation were accomplished by searching all the IDA samples using the ProteinPilot<sup>TM</sup> software (v5.1, ABSciex<sup>®</sup>) with the following parameters: (i) search against the annotated *B. xylophilus* protein database obtained from Wormbase Parasite derived from BioProject PRJEA64437 (Kikuchi et al., 2011) and MBP-GFP (IS); (ii) acrylamide alkylated cysteines as fixed modification; and (iii) trypsin as digestion type. An independent False Discovery Rate (FDR) analysis using the target-decoy approach provided with Protein Pilot software was used to assess the quality of the identifications, and positive identifications were

considered when identified proteins and peptides reached 5% local FDR (Tang et al., 2008).

Quantitative data processing was conducted using SWATH™ processing plug-in for PeakView™ (v2.0.01, ABSciex®) (Lambert et al., 2013). After retention time adjustment using the MBP-GFP peptides, up to 15 peptides, with up to five fragments each, were chosen/protein, and quantitation was attempted for all proteins in the library file that were identified from ProteinPilot™ search. Only proteins with at least one confidence peptide (FDR < 0.01) in no less than three of the four/six replicates condition and with at least three transitions were considered. Peak areas of the target fragment ions (transitions) of the retained peptides were extracted across the experiments using an extracted-ion chromatogram (XIC) window of 3 min with 100 ppm XIC width.

The proteins' levels were estimated by summing all the transitions from all the peptides for a given protein that met the criteria described above (an adaptation of Collins et al., 2013) and normalized to the levels of the internal standard or total intensity of each replicate, in the case of secretome or proteome samples, respectively.

For the analysis of the protein results and identification of the differentially regulated proteins, two non-parametric statistical tests were employed, considering the number of comparisons. A Mann-Whitney U test performed in InfernoRDN (version 1.1.5581.33355) (Polpitiya et al., 2008) was used in the case of the secretome samples. For the proteome analysis, a Kruskal-Wallis test was made to select the proteins, which were statistically different between all the comparisons, followed by the Dunn's test of Multiple Comparisons, with Benjamini-Hochberg *p*-value adjustment, to determine in which comparisons statistical differences were found. All the analyses were completed using the normalized protein levels, and a *p*-value of 0.05 was defined as a cut-off.

The heatmaps from the quantified proteins were performed in Morpheus (2021), and each row corresponds to a different protein, with its normalized protein levels.

Mass spectrometry proteomics data have been deposited to the ProteomeXChangeConsorsium through the PRIDE (Perez-Riverol et al., 2019) partner repository with the data set identifier PXD029377.

## Functional Annotation

The Gene Ontology (GO) annotations were achieved with OmicsBox (2019) based on the BLAST against the non-redundant protein database NCBI and the InterPro database using the default settings in each step. The GO analysis was done in three categories: (i) molecular function, which defines molecular activities of gene products; (ii) a cellular component, which describes where gene products are active; and (iii) the biological process, which clarifies the pathways and larger processes made up of the activities of multiple gene products. Gene ontology enrichment analysis was conducted for the proteins increased in a condition against the total of quantified proteins. It was performed in OmixBox using statistical Fisher's Exact Test associated and a *p*-value of 0.05 as a cut-off (Götz et al., 2008). Functional annotation of selected proteins was complemented with Kyoto Encyclopedia of Genes and Genomes (KEGG) pathway analysis (Kanehisa and Goto, 2000) using OmixBox.

## RESULTS

### ***Bursaphelenchus xylophilus* Isolates Reproductive Ability on Fungus and on *Pinus pinaster***

The number of nematodes, recovered from *B. cinerea* cultures of BxPt17AS isolate, was higher than the number of nematodes from C14-5 isolate. Additionally, the number of nematodes/g, extracted from the entire *P. pinaster* seedlings with C14-5 isolate, was significantly lower than from BxPt17AS-inoculated seedlings (Table 1). These results reflect the higher reproductive ability of Bx17AS (BxV) over C14-5 (BxAv) in both fungus and *P. pinaster*.

**TABLE 1.** Number of *Bursaphelenchus xylophilus* recovered from *Botrytis cinerea* cultures and from *Pinus pinaster*-inoculated seedlings.

Conditions	<i>Bursaphelenchus xylophilus</i> isolates	
	BxPt17AS (BxV)	C14-5 (BxAv)
<i>Botrytis cinerea</i>	2,656.4 $\pm$ 1042.4 <sup>a</sup>	22.7 $\pm$ 12.8 <sup>b</sup>
<i>Pinus pinaster</i> seedlings	405.1 $\pm$ 239.1 <sup>1</sup>	128.3 $\pm$ 48.6 <sup>2</sup>

Statistical analysis based on ANOVA for the average number of *B. xylophilus* ( $\pm$  standard deviation) recovered from one plate of fungus (different letters for  $p < 0.05$ ) and per gram of pine seedling (different numbers for  $p < 0.05$ ).

## Differentially Secreted Proteins

From the SWATH-MS analysis of the secreted proteins, a total of 1,456 proteins were quantified and compared between BxV and BxAv secretomes (Supplementary Table 1). From these, 669 were differentially expressed ( $p < 0.05$ ), 656 increased in BxAv secretome (Sec\_BxAv), and 13 in BxV secretome (Sec\_BxV) (Figure 1).

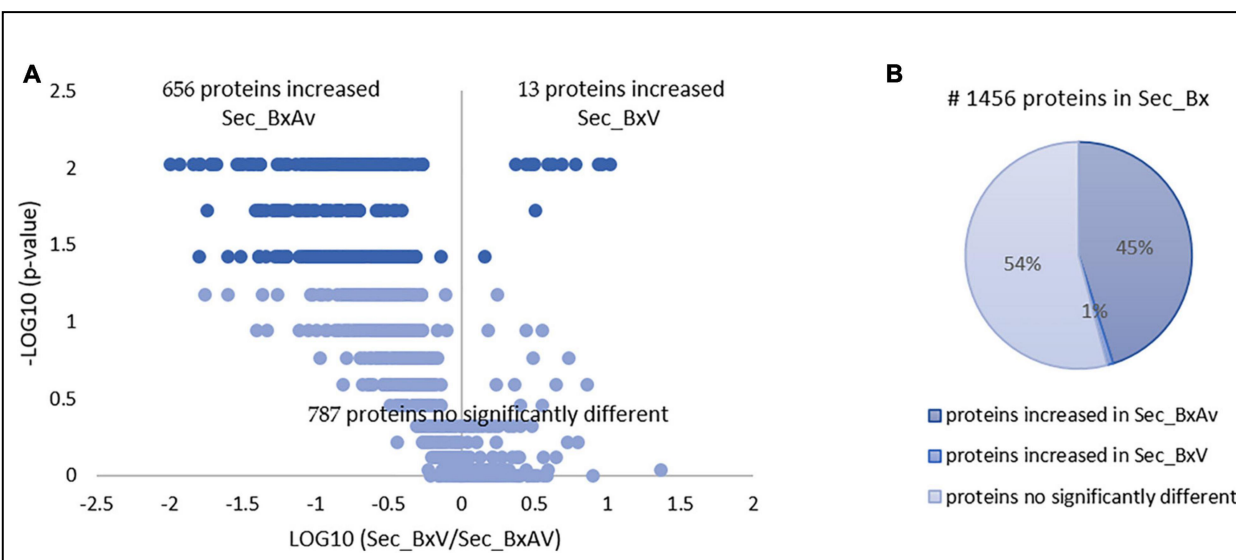


**FIGURE 1.** Quantitative analysis of secreted proteins of *Bursaphelenchus xylophilus* isolates. Volcano plot (A) and pie chart (B) reflecting the results from the statistical analysis of the 1,456 proteins quantified among the secretomes of *B. xylophilus* virulent (Sec\_BxV) and avirulent (Sec\_BxAv) isolates. Statistical analysis was performed by the Mann-Whitney U test, and statistical significance was considered for  $p < 0.05$ .

From the 13 proteins found increased in BxV secretome, five were associated with peptidase activity, belonging to three groups: serine, aspartic, and cysteine peptidases. One cellulase, two proteins with lipase activity, and a venom allergen-like protein were also found increased in BxV secretome. Additionally, a  $\gamma$ -interferon-inducible lysosomal thiol reductase (GILT) was identified. Three of the 13 proteins could not be identified (Table 2).

**TABLE 2.** Description of increased proteins in *Bursaphelenchus xylophilus* virulent secretome (Sec\_BxV) based on functional annotation.

Activity	Description	Protein ID
Peptidase	Serine peptidase	BXY_0963700.1
	Serine peptidase	BXY_1121700.1
	Serine peptidase	BXY_1703500.1
	Aspartic peptidase	BXY_0579700.1
	Cysteine peptidase	BXY_0101000.1
	Cellulase (GH45)	BXY_1261000.1
Glycoside hydrolase	Lipase	BXY_0707300.1
	Lipase	BXY_0824600.1
Unknown	Venomallergen-likeprotein	BXY_1378500.1
Oxidoreductase	$\gamma$ -interferon-inducible lysosomal thiol reductase (GILT)	BXY_0504300.1
Putative proteins with no description		BXY_0927300.1
		BXY_0174200.1
		BXY_0073000.1

After KEGG analysis, three of these proteins were associated with five metabolic pathways: the GILT BXY\_BXY\_0504300.1 associated with antigen processing and the presentation pathway (Ko4612); the cellulase BXY\_1261000.1 with starch and sucrose metabolism (Ko00500); and (iii) the lipase BXY\_0707300.1 with lysosome (Ko04142), cholesterol metabolism (Ko04979), and steroid biosynthesis (Ko00100).

In order to find which group of proteins are overrepresented in the 656 increased proteins in BxAv secretome, a GO enrichment analysis was done against the 1,456 quantified proteins. This analysis revealed an enrichment of

proteins associated with peptidase activity, peptidase inhibitor activity, oxidoreductase activity, and binding activity, among others (Figure 2) with GO terms associated with endopeptidase activity and endopeptidase inhibitor activity being significantly more enriched (Supplementary Table 2).

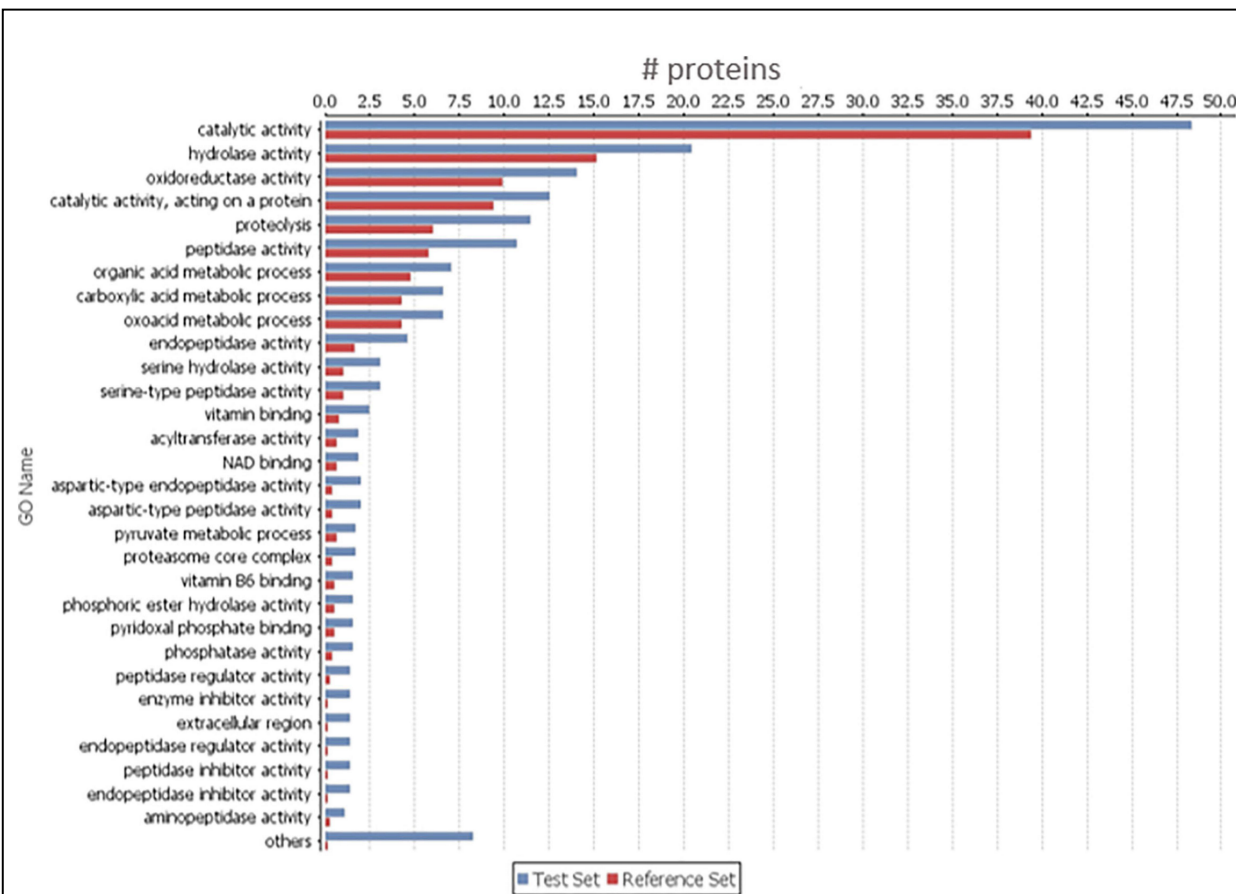


**FIGURE 2.** Gene ontology (GO) enrichment analysis of the 656 increased proteins in *Bursaphelenchus xylophilus* avirulent secretome (Sec\_BxAv). An enriched bar chart reflecting GO enrichment analysis of the 656 proteins increased in Sec\_BxAv performed against all the 1,456 quantified proteins in the secretomes using the statistical Fisher's Exact Test with  $p < 0.05$ .

## Proteome Differentially Expressed Proteins

From the SWATH-MS analysis of whole nematode proteins, a total of 2,741 proteins were quantified and compared between the nematode proteomes in different conditions: two isolates (BxV and BxAv) under fungal (fungus) or under PE stimulus (Supplementary Table 3). From these 2,741 proteins, 1,892 were differentially expressed ( $p < 0.05$ ), considering all conditions. In pairwise comparisons, a higher number of differentially expressed protein

was found between different isolates and then those of the same isolate under different condition (Figure 3).

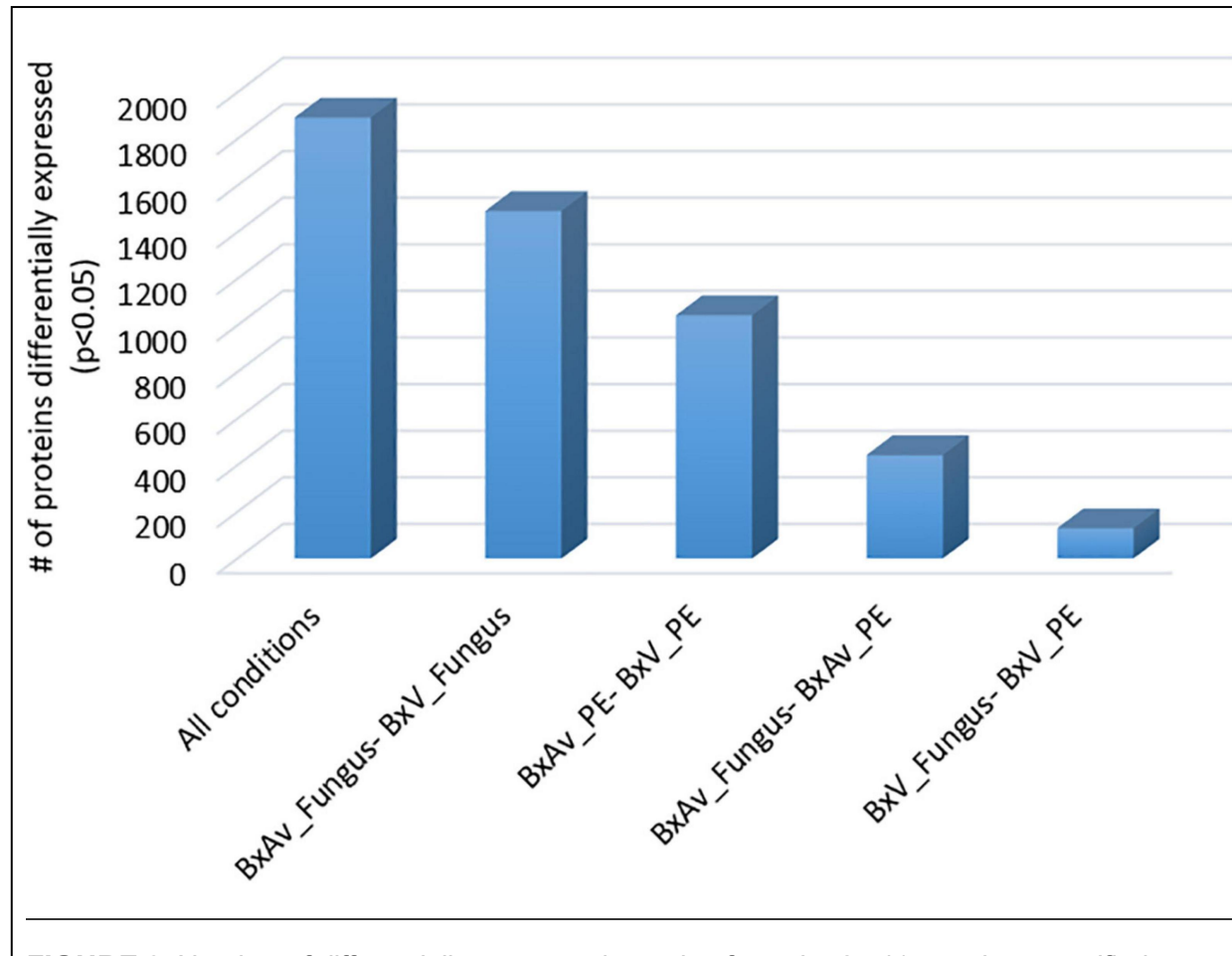
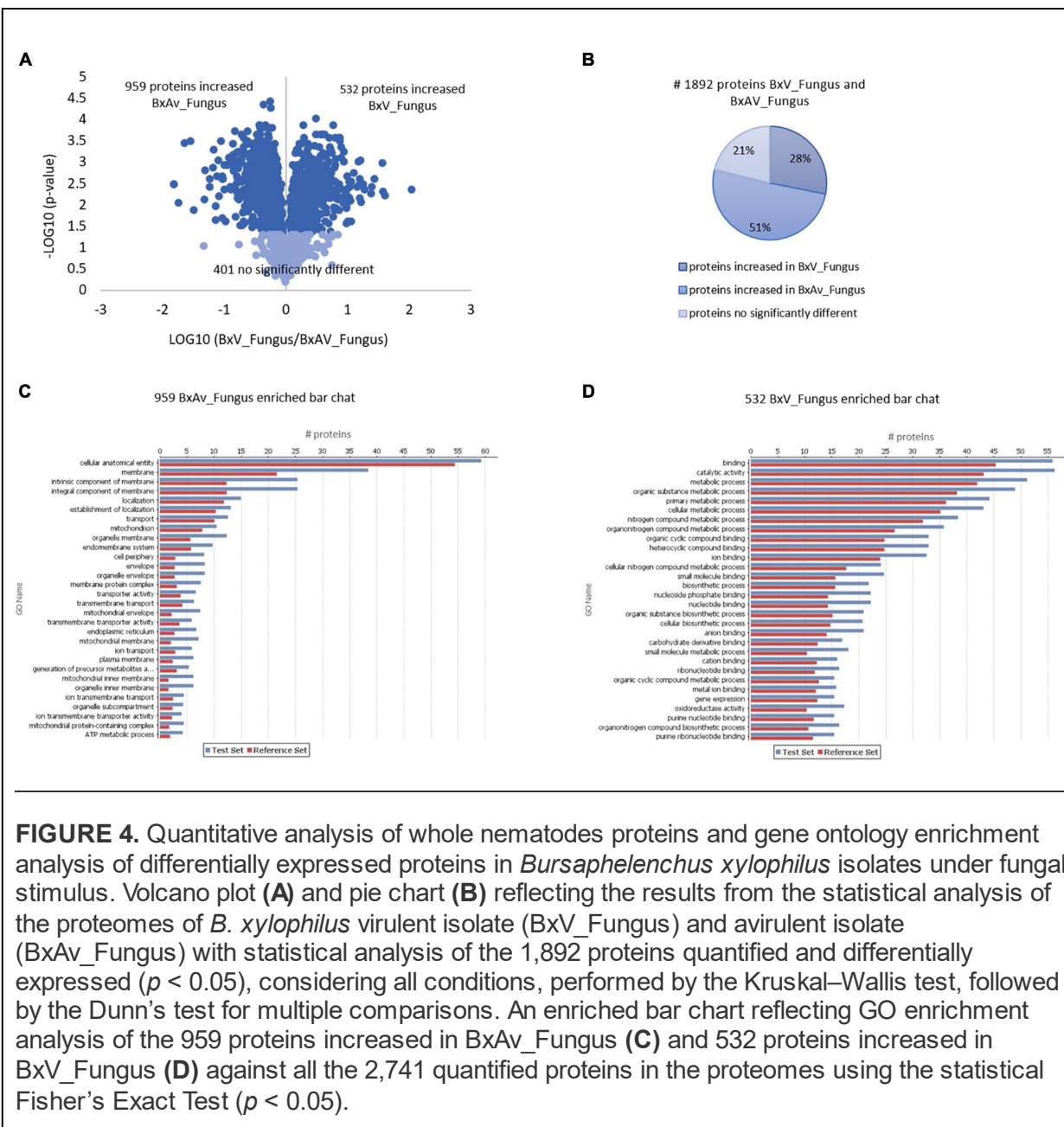


**FIGURE 3.** Number of differentially expressed proteins from the 2,741 proteins quantified among the proteomes of virulent *Bursaphelenchus xylophilus* isolate (BxV) and avirulent isolate (BxAv) under fungal (fungus) or under pine extract (PE) stimulus. Statistical analysis was performed by a Kruskal–Wallis test followed by the Dunn's test of multiple comparisons, and statistical significance was considered for an adjusted  $p < 0.05$ .

When comparing both isolates under fungal condition, a higher number of proteins (959) were found increased in BxAv\_Fungus than the proteins found increased (532) in BxV\_Fungus. From GO enrichment analysis, differences were noticed mainly associated with a cellular component in the increased BxAv\_Fungus proteins and associated with cellular and metabolic processes and catalytic and binding activity GO terms in increased BxV\_Fungus proteins (Figure 4).



Comparing the proteomes of these two isolates under PE stimuli, 571 proteins were increased in BxAv\_PE and 473 increased in BxV\_PE (Figure 5). From GO enrichment analysis, an enrichment of proteins mainly associated with a cellular component in the increased BxAv\_PE proteins and associated with cellular and metabolic processes and catalytic and binding activities in increased BxV\_PE proteins was found (Figure 5). Overall differences in the distribution of enriched GO terms between the two isolates were similar under the two stimuli.

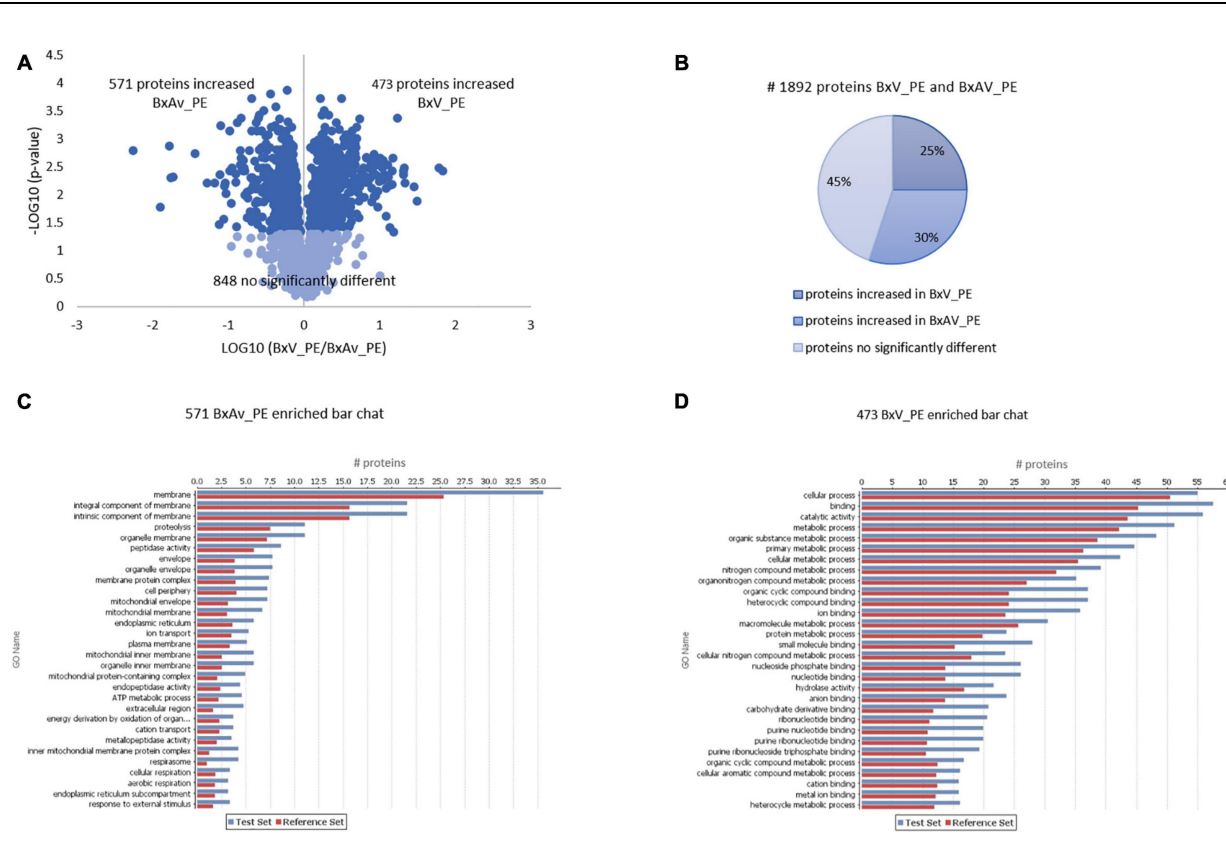


**FIGURE 5.** Quantitative analysis of whole nematodes proteins and gene ontology enrichment analysis of differentially expressed proteins in *Bursaphelenchus xylophilus* isolates under pine extract (PE) stimulus. Volcano plot (**A**) and pie chart (**B**) reflecting the results from the statistical analysis of the proteomes of *B. xylophilus* virulent isolate (BxV\_PE) and avirulent isolate (BxAv\_PE) with statistical analysis of the 1,892 proteins quantified and differentially expressed ( $p < 0.05$ ), considering all conditions, performed by the Kruskal–Wallis test followed by the Dunn's test for multiple comparisons. An enriched bar chart reflecting GO enrichment analysis of the 571 proteins increased in BxAv\_PE (**C**) and 473 proteins increased in BxV\_PE (**D**) against all the 2,741 quantified proteins in the proteomes using the statistical Fisher's Exact Test ( $p < 0.05$ ).

A comparison of increased proteins between isolates for each pair of conditions (BxV\_PE/BxAv\_PE and BxV\_Fungus/BxAv\_Fungus) revealed that most of the increased proteins of one isolate is common in both conditions, fungus, and PE (Figure 6). Moreover, the 146 proteins that were found increased in BxV proteome compared to BxAv under PE stimuli and were not increased in this isolate compared to BxAv under fungal condition were further explored as their increase could be associated with virulence status of each isolate under PE condition.

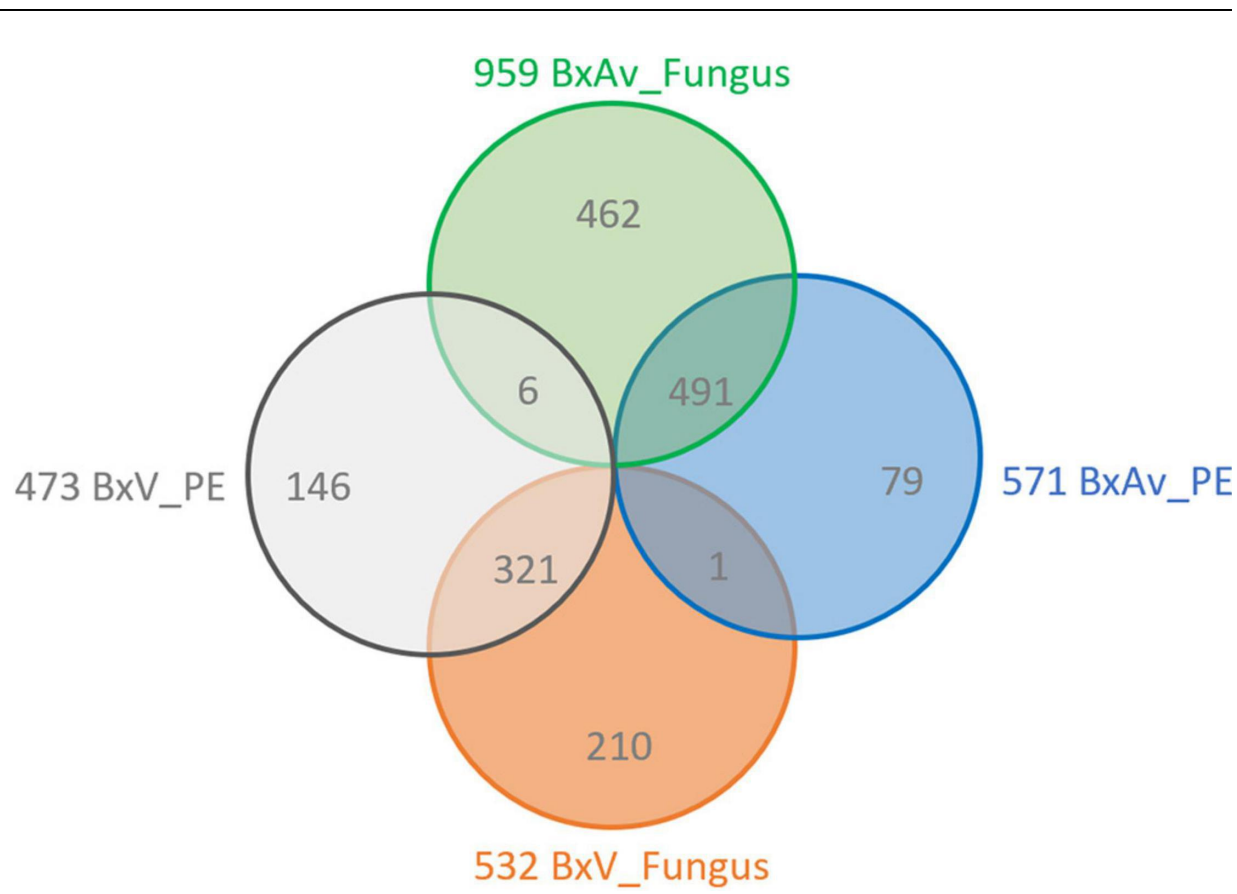


**FIGURE 6.** Increased proteins between each pair of conditions. A Venn diagram showing the number of unique and overlapping increased proteins between the proteomes of *Bursaphelenchus xylophilus* virulent isolate (BxV) and avirulent isolate (BxAv) under fungus (BxV\_Fungus/BxAv\_Fungus) and BxV and BxAv under pine extract (PE) (BxV\_PE/BxAv\_PE).

Quantitative differences on these 146 proteins among the four conditions revealed that most of the proteins are present in higher levels in BxV\_PE (Figure 7A). Thirty of these proteins are statistically increased in BxV\_PE compared to BxV\_Fungus condition (Figure 7B). The GO analysis of these proteins showed that they were mainly proteins associated with cellular and metabolic processes on biological process GO terms, binding and catalytic activities on molecular function GO terms and a cellular anatomical entity and protein-containing complex on cellular component GO terms (Figure 7C). From the proteins associated with catalytic activity, there were four with peptidase activity, two aspartic peptidases (BXY\_1580100.1, BXY\_0718400.1), and two cysteine peptidases (BXY\_1052500.1, BXY\_1408300.1); one protein with cellulase activity (BXY\_0433800.1); and one cytochrome P450 with oxidoreductase activity (BXY\_0110800.1).

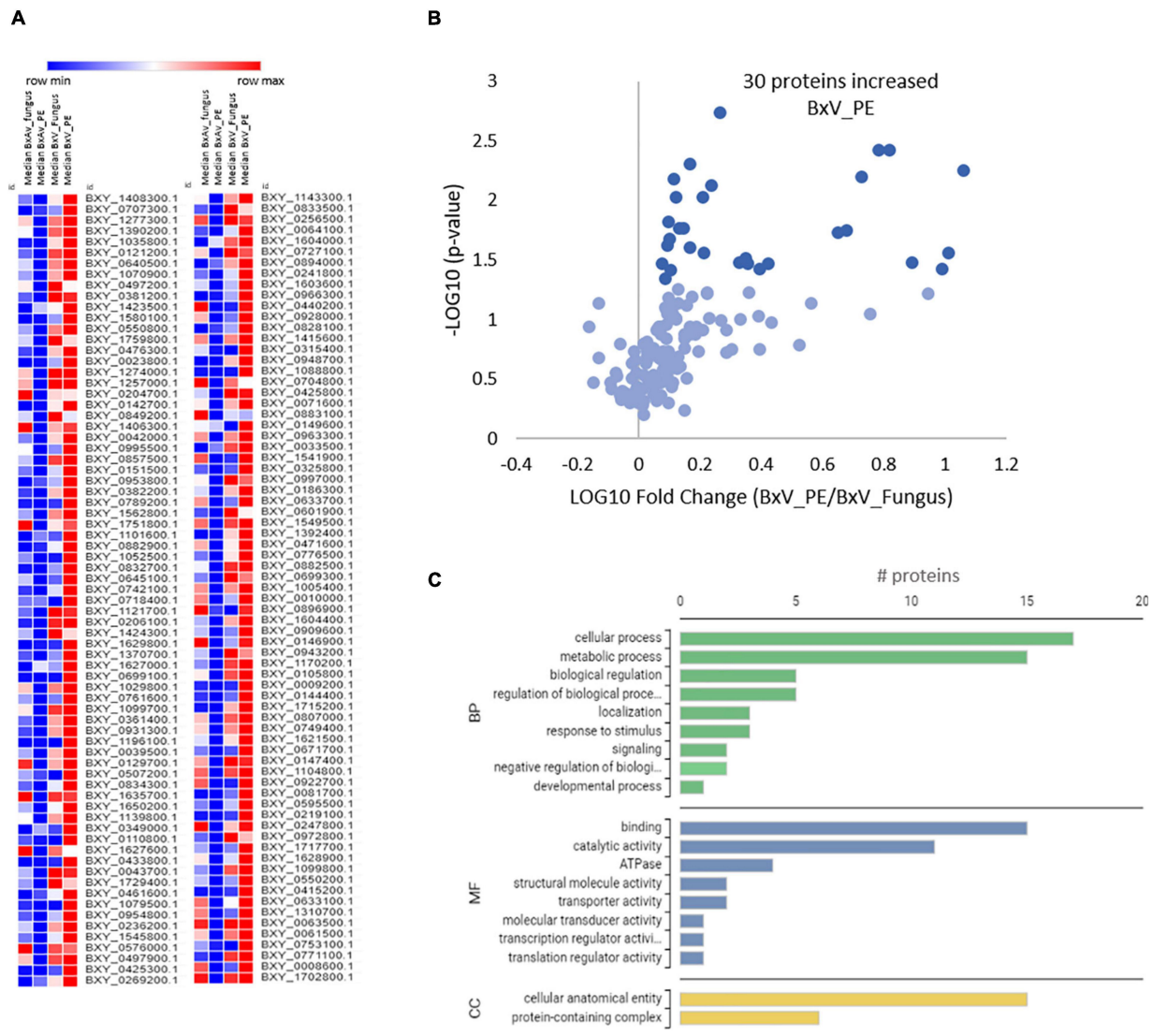


**FIGURE 7.** Quantitative analysis of selected 146 nematode proteins and gene ontology (GO) enrichment analysis of 30 differentially expressed proteins in *Bursaphelenchus xylophilus* isolates under pine extract (PE) stimulus. Heatmap of a normalized protein level in the proteomes of *B. xylophilus* in the four conditions: avirulent isolate under fungal stimulus (BxAv\_Fungus) and under PE stimulus (BxAv\_PE) and virulent isolate under fungal stimulus (BxV\_Fungus) and under PE stimulus (BxV\_PE) (A). Volcano plot reflecting the results from the statistical analysis of the proteomes of BxV\_PE and BxV\_Fungus performed by the Kruskal–Wallis test followed by the Dunn's test for multiple comparisons and with statistical significance considered for a  $p < 0.05$  (B). Gene Ontology distribution of the 30 selected proteins increased in virulent proteome (BxV) based on functional annotation with biological process (BP), molecular function (MF), and cellular component (CC) GO terms (C).

After KEGG analysis, aspartic peptidase BXY\_1580100.1 was found associated with autophagy (ko04140, ko04138), protein digestion and

absorption (ko04974), sphingolipid signaling pathway (ko04071), lysosome (ko04142), and apoptosis (ko04210). The cysteine peptidase BXY\_1052500.1 associated with plant-pathogen interaction (ko04626) and the lysosome (ko04142) and apoptosis (ko04210) pathways. The cellulase BXY\_0433800.1 associated with starch and sucrose metabolism (ko00500).

## DISCUSSION

Significant differences in the reproductive ability of BxV (Bx17AS) and BxAv (C14-5) isolates in both fungus cultures and pine seedlings were registered, indicating the higher virulence of the isolate Bx17AS, confirmed as a virulent isolate, over the isolate C14-5. However, the isolate C14-5, described as a reference avirulent isolate, was able to reproduce in *P. pinaster* seedlings. The reproductive ability of this isolate and its avirulent status were already described on the fungus *B. cinerea* and *P. thunberggi* seedlings (Mota et al., 2006; Aikawa and Kikuchi, 2007) and also on *P. sylvestris* (Filipiak, 2015), and very low or no reproduction in both fungus and pine seedlings was reported. The reproduction of C14-5 isolate in *P. pinaster* seedlings observed in this study and not reported in other hosts could be due to the conditions of the seedlings, environmental conditions, or due to the susceptibility of the host. Avirulent isolates are known to cause the death of pine seedlings when these are exposed to stresses like low light conditions (Ikeda, 1996).

Nevertheless, differences in the level of virulence of these two *B. xylophilus* isolates in *P. pinaster* were demonstrated, and how this is reflected at the proteomic level was further explored. A highly sensitive quantitative and comparative proteomic approach was applied to analyze the secretomes and proteomes of these two *B. xylophilus* isolates with different virulence and in different conditions.

From the 1,456 proteins quantified in BxV and BxAv secretomes, 787 were secreted in similar amounts by both isolates, 656 increased in BxAv secretome, and only 13 increased in BxV secretome. Interestingly, a much higher number of proteins was secreted in larger amounts by the avirulent isolate in comparison to the virulent one. Gene ontology enrichment analysis of these increased proteins in an avirulent isolate revealed that there was an enrichment of several GO categories and terms with those more significantly enriched being associated with molecular functions such as endopeptidase

activity and endopeptidase inhibitor activity. A significantly more enriched number of GO categories and terms of avirulent isolates compared to virulent ones has been previously reported compared to genomes of virulent and avirulent *B. xylophilus* isolates (Filipiak et al., 2021). Also, in accordance with our results, Filipiak et al. (2021) reported that in avirulent isolates most highly represented GO terms in molecular function category were related to endopeptidases and other peptidases. Earlier studies on genomic variations among different *B. xylophilus* isolates reported that avirulent isolates share SNPs that introduce frame shift or stop codon mutations affecting protein structures and functions (Palomares-Rius et al., 2015). This same study suggested that in avirulent isolates several proteins related to proteolysis such as endopeptidases would display loss of function, and that could lead avirulent isolates to display low ingestion of nutrients and provoke a delay in development. So, the lack of function of some of these proteins in an avirulent isolate may serve as a stimulus for overexpression of that kind of proteins and consequent increased in these protein levels but, at the same time, be responsible for nematodes' lower capacity of feeding activity and consequent lower virulence.

From the 13 proteins that were significantly increased in the secretome of the virulent isolate, five were associated with peptidase activity. Peptidases are known to be expanded in *B. xylophilus* secretome in comparison to other nematode secretomes (Shinya et al., 2013b; Cardoso et al., 2016), and 30 proteins with peptidase activity were increased in the secretome of *B. xylophilus* in comparison to *B. mucronatus*, a related but non-pathogenic nematode (Cardoso et al., 2016). In addition, five proteins also with peptidase activity were found increased in the secretome of *B. xylophilus* under *P. pinaster* stimuli in comparison to the *B. xylophilus* secretome under the stimuli of *P. pinea*, a less susceptible pine species (Silva et al., 2021). Our results support these findings, and the importance of these groups of proteins in the virulence of *B. xylophilus*, with five of the proteins increased in the secretome of the virulent isolate being associated with peptidase activity. Moreover, from the proteome analysis of both isolates in fungus and in pine extract, other four proteins with peptidase activity were found increased among the 30 proteins selected in the BxV proteome as putatively related to its virulence, two cysteine peptidases (BXY\_1052500.1, BXY\_1408300.1) and two aspartic peptidases (BXY\_1580100.1, BXY\_0718400.1). Shinya et al. (2021) reported two cysteine peptidases, Bx-CAT1 (corresponding to BXY\_1052500.1) and BxCAT-2 (BXY\_06188000.1), identified as potential

virulent determinants and suggested their involvement in food digestion and reproductive ability. In the present study, aspartic peptidase BXY\_1580100.1 was associated with several KEGG pathways, such as autophagy, protein digestion and absorption, sphingolipid signaling pathway, lysosome, and apoptosis. Autophagy is essential for feeding, fecundity, egg hatching, and survival of *B. xylophilus* under oxidative stress, contributing to its resistance to the oxidative stress induced by pine ROS metabolism, thus promoting virulence (Liu et al., 2020). As the autophagy, the programmed cell death (apoptosis) is also an important cellular mechanism in host-parasites interaction. To survive within their hosts, parasites demonstrated an ability to modulate host apoptosis pathways to their own advantage, preventing apoptosis in host cells that are inhabited by parasites and promoting apoptosis in host immune cells programmed to attack them (James and Green, 2004). The cysteine peptidase BXY\_1052500.1 was reported associated with the apoptosis pathways and also with plant-pathogen interaction, lysosome, highlighting the multifunctional role of these peptidases and their potential involvement in nematode pathogenesis.

A comparative genomic study between *B. xylophilus* virulent and avirulent isolates suggested the influence of digestive proteases in the virulence of the isolates (Palomares-Rius et al., 2015). To better know the characteristics of these important proteins, a group of cysteine peptidases and aspartic peptidases secreted by *B. xylophilus* were previously characterized (Cardoso et al., 2018, 2019). From these, the cysteine peptidase BxCP11 (BXY\_1052500) and the aspartic peptidase BxASP102 (BXY\_0579700) were also found increased in *B. xylophilus* virulent isolate in comparison to the avirulent isolate, reinforcing their role on the pathogenicity and their potential as a possible target for the nematode control. The ability of disrupting peptidases for plant-nematode control *via* the expression of peptidase inhibitors in transgenic plants has been mentioned (Fuller et al., 2008) and should be further explored for the development of new control strategies for this important forest pathogen.

Cellulases belonging to glycoside hydrolase family 45 (GH45) degrade cellulose, one of the main constituents of the plant cell walls, and are characteristic of *B. xylophilus*, as other cellulases in plant-parasitic nematodes, such as *Meloidogyne*, *Globodera*, *Heterodera*, or *Pratylenchus*, belong to the GH5 family (Kikuchi et al., 2011; Fanelli et al., 2014). In our study, two cellulases (GH45) have been found as putative virulent biomarkers

as they are increased in the secretome (BXY\_1261000.1) and proteome (BXY\_0433800.1) of the virulent isolate. Several *B. xylophilus* cellulases have been characterized and are suggested to have putative parasitic secretory functions that facilitate the feeding and migration processes within the pine tree (Kikuchi et al., 2004; Shibuya and Kikuchi, 2008; Cheng et al., 2010; Ma et al., 2011). The increase of these cell wall-degrading enzymes in the virulent isolate may reflect the higher capacity of this isolate to feed on plant cells and cause destruction.

Two lipases (BXY\_0707300.1, BXY\_0824600.1) were also found as putative virulent biomarkers as they were increased in BxV secretome. Another lipase called Bx-lip1 and corresponding to BXY\_0630900.1 was identified as a potential virulent determinant by Shinya et al. (2021). Additionally, a lipase corresponding to BXY\_1125700.1 was increased in *B. xylophilus* secretome under *P. pinaster* stimuli in comparison to the secretome under stimuli of *P. pinea* (Silva et al., 2021). Lipids are the main constituents of cell membranes and are known to influence pathogenesis and resistance mechanisms associated with plant-microbe interactions (Shah, 2005). Lipases can hydrolyze long-chain acyl-triglycerides into di- and monoglycerides, glycerol, and free fatty acids in many important biological processes, such as routine metabolism of dietary triglycerides to cell signaling and inflammation (Pascoal et al., 2018). The extracellular lipases of some plant pathogens such as *Fusarium graminearum* and others from the genus *Phytophthora* have been proposed as potential virulence factors (Voigt et al., 2005; Pascoal et al., 2018). In parasitic nematode species, their precise function remains to be recognized, and further functional investigations need to be implemented to investigate their ability to use the host lipids as substrate and act as virulent factors.

Another putative virulence biomarker detected in the present study was a venom allergen-like protein (BXY\_1378500.1), increased in BxV secretome. These proteins are known as putative effectors involved in *B. xylophilus* migration, probably by suppressing the pine tree defense mechanism (Kang et al., 2012). A  $\gamma$ -interferon-inducible lysosomal thiol reductase (GILT) (BXY\_0504300.1) was also found increased in the secretome of the virulent isolate and as thioredoxin-related oxidoreductase would also be associated with the detoxification against the plant defense response.

Moreover, one cytochrome P450 (BXY\_0110800.1) was selected from the increased proteins in *B. xylophilus* virulent isolate proteome. These proteins

are known to play important roles during the biotransformation of secondary metabolites (Urlacher and Girhard, 2012) and *B. xylophilus* can use these as a defense reaction to the secondary metabolites, such as terpenoids and cyclic aromatics, produced by the pine trees to prevent the nematode invasion (Santos et al., 2012). Some cytochrome P450 genes were overexpressed in *B. xylophilus*-infecting trees (Qiu et al., 2013) and were associated with vitality, dispersal ability, reproduction, pathogenicity, and pesticide metabolism (Xu et al., 2015).

The identification of *B. xylophilus* putative virulence proteins presented here provides a better understanding of the mechanisms that underlie the nematode infection of pine trees; however, with the lack of effective functional analysis in *B. xylophilus*, the molecular mode of action of many of these putative effectors remains to be clarified. Nevertheless, virulence biomarkers constitute key nematode targets that should be further explored for the development of new control strategies for this important forest pathogen.

## DATA AVAILABILITY STATEMENT

Mass spectrometry proteomics data have been deposited to the ProteomeXChange Consortium through the PRIDE partner repository with the data set identifier PXD029377 (<https://www.ebi.ac.uk/pride/archive/projects/PXD029377>).

## AUTHOR CONTRIBUTIONS

JC, SA, BM, IA, KN, and LF conceived and designed the experiments and revised and edited the manuscript. HS, SA, and JC performed the experiments and analyzed the data. JC wrote the original draft. All the authors have read and approved the final version of the manuscript.

## FUNDING

This research was supported by Portuguese Foundation for Science and Technology (FCT) through national funds and the co-funding by FEDER,

PT2020, and COMPETE 2020 under the projects POINTERS- PTDC/ASP-SIL/31999/2017 (POCI-01-145-FEDER-031999), UIDB/04004/2020 and UIDB/04539/2020; Project ReNATURE – Valorization of the Natural Endogenous Resources of the Centro Region (Centro 2020, Centro-01-0145-FEDER-000007), Instituto do Ambiente, Tecnologia e Vida, and the National Mass Spectrometry Network (RNEM) under contract POCI-01-0145-FEDER-402-022125 (Ref. ROTEIRO/0028/2013).

## ACKNOWLEDGMENTS

We would like to thank the Forestry and Forest Products Research Institute (FFPRI), National Research and Development, Japan, for providing the *B. xylophilus* C14-5 isolate used in this study.

## SUPPLEMENTARY MATERIAL

The Supplementary Material for this article can be found online at: <https://www.frontiersin.org/articles/10.3389/fpls.2021.822289/full#supplementary-material>

## REFERENCES

Abelleira, A., Picoaga, A., Mansilla, J. P., and Aguin, O. (2011). Detection of *Bursaphelenchus xylophilus*, causal agent of pine wilt disease on *Pinus pinaster* in Northwestern Spain. *Plant Dis.* 95, 776–777. doi: 10.1094/PDIS-12-10-0902

Aikawa, T., and Kikuchi, T. (2007). Estimation of virulence of *Bursaphelenchus xylophilus* (Nematoda: Aphelenchoididae) based on its reproductive ability. *Nematology* 9, 371–377.

Aikawa, T., Kikuchi, T., and Kosaka, H. (2003a). Demonstration of interbreeding between virulent and avirulent populations of *Bursaphelenchus xylophilus* (Nematoda: Aphelenchoididae) by {PCR-RFLP} method. *Appl. Entomol. Zool.* 38, 565–569. doi: 10.1303/aez.2003.565

Aikawa, T., Togashi, K., and Kosaka, H. (2003b). Different developmental responses of virulent and avirulent isolates of the pinewood nematode, *Bursaphelenchus xylophilus* (Nematoda: Aphelenchoididae), to the insect vector, *Monochamus alternatus* (Coleoptera: Cerambycidae). *Environ. Entomol.* 32, 96–102.

Anjo, S. I., Lourenço, A. S., Melo, M. N., Santa, C., and Manadas, B. (2016). “Unraveling mesenchymal stem cells’ dynamic secretome through nontargeted proteomics profiling,” in *Mesenchymal Stem*

*Cells: Methods and Protocols*, Vol. 1416, ed. M. Gneccchi (New York, NY: Human Press), 521–549. doi: 10.1007/978-1-4939-3584-0\_32

Anjo, S. I., Santa, C., and Manadas, B. (2015). Short GeLC-SWATH: A fast and reliable quantitative approach for proteomic screenings. *Proteomics* 15, 757–762. doi: 10.1002/pmic.201400221

Anjo, S. I., Santa, C., Saraiva, S. C., Freitas, K., Barah, F., Carreira, B., et al. (2017). “Neuroproteomics using short GeLC-SWATH: from the evaluation of proteome changes to the clarification of protein function,” in *Current Proteomic Approaches Applied to Brain Function*, Vol. 127, eds E. Santamaría and J. Fernández-Irigoyen (New York, NY: Human Press), 107–138. doi: 10.1007/978-1-4939-7119-0\_8

Anjo, S. I., Simões, I., Castanheira, P., Grãos, M., and Manadas, B. (2019). Use of recombinant proteins as a simple and robust normalization method for untargeted proteomics screening: exhaustive performance assessment. *Talanta* 205:120163. doi: 10.1016/j.talanta.2019.120163

Cardoso, J. M. S., Anjo, S. I., Fonseca, L., Egas, C., Manadas, B., and Abrantes, I. (2016). *Bursaphelenchus xylophilus* and *B. mucronatus* secretomes: a comparative proteomic analysis. *Sci. Rep.* 6:39007. doi: 10.1038/srep39007

Cardoso, J. M. S., Fonseca, L., and Abrantes, I. (2019). Aspartic peptidases of the pinewood nematode *Bursaphelenchus xylophilus*: Molecular characterization and in silico structural analysis. *For. Pathol.* 49:e12545. doi: 10.1111/efp.12545

Cardoso, J. M. S., Fonseca, L., and Abrantes, I. (2021).  $\alpha$ -L-Fucosidases from *Bursaphelenchus xylophilus* secretome-molecular characterization and their possible role in breaking down plant cell walls. *Forests* 11:265. doi: 10.3390/f11030265

Cardoso, J. M. S., Fonseca, L., Egas, C., and Abrantes, I. (2018). Cysteine proteases secreted by the pinewood nematode, *Bursaphelenchus xylophilus*: in silico analysis. *Comput. Biol. Chem.* 77, 291–296. doi: 10.1016/J.COMPBIOLCHEM.2018.10.011

Cheng, X.-Y., Dai, S. M., Xiau, L., and Xie, B.-Y. (2010). Influence of cellulase gene knockdown by dsRNA interference on the development and reproduction of the pine wood nematode, *Bursaphelenchus xylophilus*. *Nematology* 12, 225–233.

Collins, B. C., Gillet, L. C., Rosenberger, G., Rost, H. L., Vichalkovski, A., Gstaiger, M., et al. (2013). Quantifying protein interaction dynamics by SWATH mass spectrometry: application to the 14-3-3 system. *Nat. Methods* 10, 1246–1253. doi: 10.1038/nmeth.2703

Ding, X., Ye, J., Lin, S., Wu, X., Li, D., and Nian, B. (2016). Deciphering the molecular variations of pine wood nematode *Bursaphelenchus xylophilus* with different virulence. *PLoS One* 11:e0156040. doi: 10.1371/journal.pone.0156040

EPPO (2013). PM 7/4 (3) *Bursaphelenchus xylophilus*. *EPPO Bull.* 43, 105–118. doi: 10.1111/epp.12024

EPPO (2021). *Bursaphelenchus xylophilus*. EPPO Datasheets on pests Recommended for Regulation. Available online at: <https://gd.eppo.int> (accessed November 3, 2021).

Espada, M., Silva, A. C., Eves van den Akker, S., Cock, P. J. A., Mota, M., and Jones, J. T. (2016). Identification and characterization of parasitism genes from the pinewood nematode *Bursaphelenchus xylophilus* reveals a multilayered detoxification strategy. *Mol. Plant Pathol.* 17, 286–295. doi: 10.1111/mpp.12280

Fanelli, E., Troccoli, A., Picardi, E., Pousis, C., and De Luca, F. (2014). Molecular characterization and functional analysis of four  $\beta$ -1,4-endoglucanases from the root-lesion nematode *Pratylenchus vulnus*. *Plant Pathol.* 63, 1436–1445. doi: 10.1111/ppa.12222

Figueiredo, J., Simões, M. J., Gomes, P., Barroso, C., Pinho, D., Conceição, L., et al. (2013). Assessment of the geographic origins of pinewood nematode isolates via single nucleotide polymorphism in effector genes. *PLoS One* 8:e83542. doi: 10.1371/journal.pone.0083542

Filipiak, A. (2015). Pathogenicity of selected isolates of the quarantine pinewood nematode *Bursaphelenchus xylophilus* to Scots pine (*Pinus sylvestris* L.). *J. Plant Prot. Res.* 55, 378–382. doi: 10.1515/jppr-2015-0050

Filipiak, A., Malewski, T., Matczyńska, E., and Tomalak, M. (2021). Molecular variation among virulent and avirulent strains of the quarantine nematode *Bursaphelenchus xylophilus*. *Mol. Genet. Genomics* 296, 259–269. doi: 10.1007/s00438-020-01739-w

Fonseca, L., Cardoso, J. M. S., Lopes, A., Pestana, M., Abreu, F., Nunes, N., et al. (2012). The pinewood nematode, *Bursaphelenchus xylophilus*, in Madeira Island. *Helminthologia* 49, 96–103. doi: 10.2478/s11687-012-0020-3

Fuller, V. L., Lilley, C. J., and Urwin, P. E. (2008). Nematode resistance. *New Phytol.* 180, 27–44. doi: 10.1111/j.1469-8137.2008.02508.x

Futai, K. (2013). Pine wood nematode, *Bursaphelenchus xylophilus*. *Annu. Rev. Phytopathol.* 51, 61–83. doi: 10.1146/annurev-phyto-081211-172910

Gillet, L. C., Navarro, P., Tate, S., Rost, H., Selevsek, N., Reiter, L., et al. (2012). Targeted data extraction of the MS/MS spectra generated by data-independent acquisition: a new concept for consistent and accurate proteome analysis. *Mol. Cell Proteomics* 11:O111.016717. doi: 10.1074/mcp.O111.016717

Götz, S., García-Gómez, J. M., Terol, J., Williams, T. D., Nagaraj, S. H., Nueda, M. J., et al. (2008). High-throughput functional annotation and data mining with the Blast2GO suite. *Nucleic Acids Res.* 36, 3420–3435. doi: 10.1093/nar/gkn176

Ikeda, T. (1996). Responses of water-stressed *Pinus thunbergii* to inoculation with avirulent pine wood nematode (*Bursaphelenchus xylophilus*): water relations and xylem histology. *J. For. Res.* 1, 223–226. doi: 10.1007/BF02348329

James, E. R., and Green, D. R. (2004). Manipulation of apoptosis in the host–parasite interaction. *Trends Parasitol.* 20, 280–287. doi: 10.1016/j.pt.2004.04.004

Kanehisa, M., and Goto, S. (2000). KEGG: kyoto encyclopedia of genes and genomes. *Nucleic Acids Res.* 28, 27–30. doi: 10.1093/nar/28.1.27

Kang, J. S., Koh, Y. H., Moon, Y. S., and Lee, S. H. (2012). Molecular properties of a venom allergen-like protein suggest a parasitic function in the pinewood nematode *Bursaphelenchus xylophilus*. *Int. J. Parasitol.* 42, 63–70. doi: 10.1016/j.ijpara.2011.10.006

Kang, J. S., Lee, H., Moon, I. S., Lee, Y., Koh, Y. H., Je, Y. H., et al. (2009). Construction and characterization of subtractive stage-specific expressed sequence tag (EST) libraries of the pinewood nematode *Bursaphelenchus xylophilus*. *Genomics* 94, 70–77. doi: 10.1016/j.ygeno.2009.03.001

Kikuchi, T., Aikawa, T., Kosaka, H., Pritchard, L., Ogura, N., and Jones, J. T. (2007). Expressed sequence tag (EST) analysis of the pine wood nematode *Bursaphelenchus xylophilus* and *B. mucronatus*. *Mol. Biochem. Parasitol.* 155, 9–17. doi: 10.1016/j.molbiopara.2007.05.002

Kikuchi, T., Cotton, J. A., Dalzell, J. J., Hasegawa, K., Kanzaki, N., McVeigh, P., et al. (2011). Genomic insights into the origin of parasitism in the emerging plant pathogen *Bursaphelenchus xylophilus*. *PLoS Pathog.* 7:e1002219. doi: 10.1371/journal.ppat.1002219

Kikuchi, T., Jones, J. T., Aikawa, T., Kosaka, H., and Ogura, N. (2004). A family of glycosyl hydrolase family 45 cellulases from the pine wood nematode *Bursaphelenchus xylophilus*. *FEBS Lett.* 572, 201–205. doi: 10.1016/j.febslet.2004.07.039

Kiyohara, T., and Bolla, R. I. (1990). Pathogenic variability among populations of the pinewood nematode, *Bursaphelenchus xylophilus*. *For. Sci.* 36, 1061–1076. doi: 10.1093/forestscience/36.4.1061

Lambert, J.-P., Ivosev, G., Couzens, A. L., Larsen, B., Taipale, M., Lin, Z.-Y., et al. (2013). Mapping differential interactomes by affinity purification coupled with data-independent mass spectrometry acquisition. *Nat. Methods* 10, 1239–1245. doi: 10.1038/nmeth.2702

Liu, H. B., Rui, L., Feng, Y. Q., and Wu, X. Q. (2020). Autophagy contributes to resistance to the oxidative stress induced by pine reactive oxygen species metabolism, promoting infection by *Bursaphelenchus xylophilus*. *Pest Manag. Sci.* 76, 2755–2767. doi: 10.1002/ps.5823

Ma, H. B., Lu, Q., Liang, J., and Zhang, X. Y. (2011). Functional analysis of the cellulose gene of the pine wood nematode, *Bursaphelenchus xylophilus*, using RNA interference. *Genet. Mol. Res.* 10, 1931–1941. doi: 10.4238/vol10-3gmr1367

Mallez, S., Castagnone, C., Lombaert, E., Castagnone-Sereno, P., and Guillemaud, T. (2021). Inference of the worldwide invasion routes of the pinewood nematode *Bursaphelenchus xylophilus* using approximate Bayesian computation analysis. *bioRxiv* [Preprint]. doi: 10.1101/452326v4.full

Morpheus (2021). *Versatile Matrix Visualization and Analysis Software*. Available online at: <https://software.broadinstitute.org/morpheus> (accessed November 30, 2021).

Mota, M. M., Takemoto, S., Takeuchi, Y., Hara, N., and Futai, K. (2006). Comparative studies between Portuguese and Japanese isolates of the pinewood nematode, *Bursaphelenchus xylophilus*. *J. Nematol.* 38, 429–433.

Mota, M., Braasch, H., Bravo, M. A., Penas, A. C., Burgermeister, W., Metge, K., et al. (1999). First report of *Bursaphelenchus xylophilus* in Portugal and in Europe. *Nematology* 1, 727–734. doi: 10.1163/156854199508757

OmicsBox (2019). *Bioinformatics Made Easy, BioBam Bioinformatics*. Available online at: <https://www.biobam.com/omicsbox> (accessed October 8, 2021).

Palomares-Rius, J. E., Tsai, I. J., Karim, N., Akiba, M., Kato, T., Maruyama, H., et al. (2015). Genome-wide variation in the pinewood nematode *Bursaphelenchus xylophilus* and its relationship with pathogenic traits. *BMC Genomics* 16:845. doi: 10.1186/s12864-015-2085-0

Pascoal, A., Estevinho, L. M., Martins, I. M., and Choupina, A. B. (2018). REVIEW: novel sources and functions of microbial lipases and their role in the infection mechanisms. *Physiol. Mol. Plant Pathol.* 104, 119–126. doi: 10.1016/j.pmpp.2018.08.003

Perez-Riverol, Y., Csordas, A., Bai, J., Bernal-Llinares, M., Hewapathirana, S., Kundu, D. J., et al. (2019). The PRIDE database and related tools and resources in 2019: improving support for quantification data. *Nucleic Acids Res.* 47, D442–D450. doi: 10.1093/nar/gky1106

Pimentel, C. S., Gonçalves, E. V., Firmino, P. N., Calvão, T., Fonseca, L., Abrantes, I., et al. (2017). Differences in constitutive and inducible defences in pine species determining susceptibility to pinewood nematode. *Plant Pathol.* 66, 131–139. doi: 10.1111/ppa.12548

Polpitiya, A. D., Qian, W. J., Jaityl, N., Petyuk, V. A., Adkins, J. N., Camp, D. G., et al. (2008). DAnTE: A statistical tool for quantitative analysis of -omics data. *Bioinformatics* 24, 1556–1558. doi: 10.1093/bioinformatics/btn217

Qiu, X., Wu, X., Huang, L., Tian, M., and Ye, J. (2013). Specifically expressed genes of the nematode *Bursaphelenchus xylophilus* involved with early interactions with pine trees. *PLoS One* 8:e78063. doi: 10.1371/journal.pone.0078063

Robertson, L., Escuer, M., Abelleira, A., Santiago Merino, R., Cobacho Arcos, S., Navas, A., et al. (2011). Incidence of the pinewood nematode *Bursaphelenchus xylophilus* Steiner & Buhrer, 1934 (Nickle, 1970) in Spain. *Nematology* 13, 755–757. doi: 10.1163/138855411X578888

Santos, C. S., Pinheiro, M., Silva, A. I., Egas, C., and Vasconcelos, M. W. (2012). Searching for resistance genes to *Bursaphelenchus xylophilus* using high throughput screening. *BMC Genomics* 13:599. doi: 10.1186/1471-2164-13-599

Shah, J. (2005). Lipids, lipases, and lipid-modifying enzymes in plant disease resistance. *Annu. Rev. Phytopathol.* 43, 229–260. doi: 10.1146/annurev.phyto.43.040204.135951

Shibuya, H., and Kikuchi, T. (2008). Purification and characterization of recombinant endoglucanases from the pine wood nematode *Bursaphelenchus xylophilus*. *Biosci. Biotechnol. Biochem.* 72,

1325–1332. doi: 10.1271/bbb.70819

Shinya, R., Kirino, H., Morisaka, H., Takeuchi-Kaneko, Y., Futai, K., and Ueda, M. (2021). Comparative secretome and functional analyses reveal glycoside hydrolase family 30 and cysteine peptidase as virulence determinants in the pinewood nematode *Bursaphelenchus xylophilus*. *Front. Plant Sci.* 12:640459. doi: 10.3389/fpls.2021.640459

Shinya, R., Morisaka, H., Kikuchi, T., Takeuchi, Y., Ueda, M., and Futai, K. (2013b). Secretome analysis of the pine wood nematode *Bursaphelenchus xylophilus* reveals the tangled roots of parasitism and its potential for molecular mimicry. *PLoS One* 8:e67377. doi: 10.1371/journal.pone.0067377

Shinya, R., Morisaka, H., Takeuchi, Y., Futai, K., and Ueda, M. (2013a). Making headway in understanding pine wilt disease: What do we perceive in the postgenomic era? *J. Biosci. Bioeng.* 116, 1–8. doi: 10.1016/j.jbiosc.2013.01.003

Shinya, R., Takeuchi, Y., Ichimura, K., Takemoto, S., and Futai, K. (2012). Establishment of a set of inbred strains of the pine wood nematode, *Bursaphelenchus xylophilus* (Aphelenchida: Aphelenchoididae), and evidence of their varying levels of virulence. *Appl. Entomol. Zool.* 47, 341–350. doi: 10.1007/s13355-012-0124-8

Silva, H., Anjo, S. I., Manadas, B., Abrantes, I., Fonseca, L., and Cardoso, J. M. S. (2021). Comparative analysis of *Bursaphelenchus xylophilus* secretome under *Pinus pinaster* and *P. pinea* stimuli. *Front. Plant Sci.* 12:668064. doi: 10.3389/fpls.2021.668064

Tang, W. H., Shilov, I. V., and Seymour, S. L. (2008). Nonlinear fitting method for determining local false discovery rates from decoy database searches. *J. Proteome Res.* 7, 3661–3667. doi: 10.1021/pr070492f

Tsai, I. J., Tanaka, R., Kanzaki, N., Akiba, M., Yokoi, T., Espada, M., et al. (2016). Transcriptional and morphological changes in the transition from mycetophagous to phytophagous phase in the plant-parasitic nematode *Bursaphelenchus xylophilus*. *Mol. Plant Pathol.* 17, 77–83. doi: 10.1111/mpp.12261

Urlacher, V. B., and Girhard, M. (2012). Cytochrome P450 monooxygenases: an update on perspectives for synthetic application. *Trends Biotechnol.* 30, 26–36. doi: 10.1016/j.tibtech.2011.06.012

Voigt, C. A., Schäfer, W., and Salomon, S. (2005). A secreted lipase of *Fusarium graminearum* is a virulence factor required for infection of cereals. *Plant J.* 42, 364–375. doi: 10.1111/j.1365-313X.2005.02377.x

Wang, Y., Yamada, T., Sakaue, D., and Suzuki, K. (2005). Variations in life history parameters and their influence on rate of population increase of different pathogenic isolates of the pine wood nematode, *Bursaphelenchus xylophilus*. *Nematology* 7, 459–467. doi: 10.1163/156854105774355545

Whitehead, A. G., and Hemming, J. R. (1965). A comparison of some quantitative methods of extracting small vermiform nematodes from soil. *Ann. Appl. Biol.* 55, 25–38. doi: 10.1111/j.1744-7348.1965.tb07864.x

Xu, X.-L., Wu, X.-Q., Ye, J.-R., and Huang, L. (2015). Molecular characterization and functional analysis of three pathogenesis-related cytochrome P450 genes from *Bursaphelenchus xylophilus* (Tylenchida: Aphelenchoidoidea). *Int. J. Mol. Sci.* 16, 5216–5234. doi: 10.3390/ijms16035216

**Conflict of Interest:** The authors declare that the research was conducted in the absence of any commercial or financial relationships that could be construed as a potential conflict of interest.

**Publisher's Note:** All claims expressed in this article are solely those of the authors and do not necessarily represent those of their affiliated organizations, or those of the publisher, the editors and the reviewers. Any product that may be evaluated in this article, or claim that may be made by its manufacturer, is not guaranteed or endorsed by the publisher.

*Copyright © 2022 Cardoso, Anjo, Manadas, Silva, Abrantes, Nakamura and Fonseca. This is an open-access article distributed under the terms of the Creative Commons Attribution License (CC BY). The use, distribution or reproduction in other forums is permitted, provided the original author(s) and the copyright owner(s) are credited and that the original publication in this journal is cited, in accordance with accepted academic practice. No use, distribution or reproduction is permitted which does not comply with these terms.*

## HYPOTHESIS AND THEORY

published: 10 March 2022

doi: 10.3389/fpls.2022.841707



# Differential Impact of the Pinewood Nematode on *Pinus* Species Under Drought Conditions

**Mariana Estorninho<sup>1</sup>, Sergio Chozas<sup>1</sup>, Angela Mendes<sup>1</sup>, Filipe Colwell<sup>2</sup>, Isabel Abrantes<sup>3</sup>, Luís Fonseca<sup>3</sup>, Patrícia Fernandes<sup>1</sup>, Catarina Costa<sup>1</sup>, Cristina Máguas<sup>1</sup>, Otilia Correia<sup>1</sup> and Cristina Antunes<sup>1\*</sup>**

<sup>1</sup>Centre for Ecology, Evolution and Environmental Changes, Faculdade de Ciências, Universidade de Lisboa, Lisbon, Portugal

<sup>2</sup>Infarm, Crop Science Team, Amsterdam, Netherlands

<sup>3</sup>Centre for Functional Ecology, Department of Life Sciences, University of Coimbra, Coimbra, Portugal

**Edited by:**

Ryoji Shinya, Meiji University, Japan

**Reviewed by:**

Kenji Fukuda, The University of Tokyo, Japan

Sofia R. Costa, University of Minho, Portugal

**\*Correspondence:** Cristina Antunes, cmaantunes@fc.ul.pt

**Specialty section:** This article was submitted to Plant Pathogen Interactions, a section of the journal *Frontiers in Plant Science*

**Received:** 22 December 2021

**Accepted:** 10 February 2022

**Published:** 10 March 2022

**Citation:** Estorninho M, Chozas S, Mendes A, Colwell F, Abrantes I, Fonseca L, Fernandes P, Costa C, Máguas C, Correia O and Antunes C (2022) Differential Impact of the Pinewood Nematode on *Pinus* Species Under Drought Conditions. *Front. Plant Sci.* 13:841707. doi: 10.3389/fpls.2022.841707

The pinewood nematode (PWN), *Bursaphelenchus xylophilus*, responsible for the pine wilt disease (PWD), is a major threat to pine forests worldwide. Since forest mortality due to PWN might be exacerbated by climate, the concerns regarding PWD in the Mediterranean region are further emphasized by the projected scenarios of more drought events and higher temperatures. In this context, it is essential to better understand the pine species vulnerability to PWN under these conditions. To achieve that, physiological responses and wilting symptoms were monitored in artificially inoculated *Pinus pinaster* (*P. pinaster*), *Pinus pinea* (*P. pinea*), and *Pinus radiata* (*P. radiata*) saplings under controlled temperature (25/30°C) and water availability (watered/water stressed). The results obtained showed that the impact of PWN is species-dependent, being infected *P. pinaster* and *P. radiata* more prone to physiological and morphological damage than *P. pinea*. For the more susceptible species (*P. pinaster* and *P. radiata*), the presence of the nematode was the main driver of photosynthetic responses, regardless of their temperature or water regime conditions. Nevertheless, water potential was revealed to be highly affected by the synergy of PWN and the studied abiotic conditions, with higher temperatures (*P. pinaster*) or water limitation (*P. radiata*) increasing the impact of nematodes on trees' water status. Furthermore, water limitation had an influence on nematodes density and its allocation on trees' structures, with *P. pinaster* revealing the highest nematode abundance and inner dispersion. In inoculated *P. pinea* individuals, nematodes' population decreased significantly, emphasizing this species resistance to PWN. Our findings revealed a synergistic impact of PWN infection and stressful environmental conditions, particularly on the water status of *P. pinaster* and *P. radiata*, triggering disease symptoms and mortality of these species. Our results suggest that predicted drought conditions might facilitate proliferation and exacerbate the impact of PWN on these two species, through xylem cavitation, leading to strong changes in pine forests of the Mediterranean regions.

**Keywords:** *Bursaphelenchus xylophilus*, climate change, physiological responses, pine wilt disease, *Pinus pinaster*, *Pinus pinea*, *Pinus radiata*, wilting symptoms

## INTRODUCTION

Pine wilt disease (PWD) results from the infection of *Pinus* species by the pinewood nematode (PWN), *Bursaphelenchus xylophilus* (*B. xylophilus*). Currently, *B. xylophilus*, a phytophagous and mycophagous nematode, is declared a major threat to pine forests worldwide (Braasch, 2008; Carnegie et al., 2018; European and Mediterranean Plant Protection Organization [EPPO], 2021). Once inside the plant, its feeding and rapid multiplication in the cortex and in resin ducts may lead to a series of biochemical (Pimentel et al., 2017; Gaspar et al., 2020), physiological (Fukuda, 1997), and histological (Myers, 1986) changes. The damage of the resin ducts by the nematode strongly constrains water conduction in the xylem, embracing a series of physiological alterations such as leaf water potential (Fukuda, 1997; Suzuki, 2002; Menéndez-Gutiérrez et al., 2018; Yazaki et al., 2018), transpiration, and photosynthesis decrease (Fukuda, 1997; Suzuki, 2002; Yazaki et al., 2018). These physiological changes are usually responsible for visible symptoms such as discoloring and wilting of needles, loss of resin exudation from the wounded bark, and at an advanced stage death (Mamiya, 1983; Woo et al., 2010; Zas et al., 2015; Menéndez-Gutiérrez et al., 2018). Nevertheless, the period from infection to appearance of symptoms and tree death varies with a combination of biotic and abiotic factors such as trees' susceptibility, the number of nematodes transmitted by the insect vector, *Monochamus* spp., and climatic conditions (Mamiya, 1983; Menéndez-Gutiérrez et al., 2017).

Forest mortality, attributed to PWN infection, and the fast spread of PWD cannot be dissociated from the effects of climate, topography, and human activities (i.e., infected timber exports) (Tóth, 2011; Calvão et al., 2019). However, the success of its establishment is mainly related to the development of the nematode–host species interaction (Futai, 2013), anatomy and health conditions of host trees (Nunes da Silva et al., 2015; Zas et al., 2015), PWN virulence (Aikawa and Kikuchi, 2007; Filipiak, 2015), and climatic conditions (Kiyohara and Bolla, 1990; Wang, 2014). In particular, PWD dynamics and its impact on trees was shown to be highly dependent on

different climatic conditions such as light intensity (Kaneko, 1989; Kanzaki et al., 2012) and temperature, with significant disease expression restricted to areas above the isotherm of 20°C (Rutherford and Webster, 1987; Soliman et al., 2012) and a lethal effect above 21°C (Sikora and Malek, 1991). Under higher temperatures, a faster dispersion and multiplication of PWNs inside pine seedlings (day, 30°C; night, 25°C) than at low temperatures (day, 25°C; night, 20°C) might occur (Ichihara et al., 2000). Temperature is also known to have a crucial role in nematode–vector interaction, with an increase in nematode transmission, and vector's life span under 20–26°C (Jikumaru and Togashi, 2000; Ohsawa and Akiba, 2014), longer vector's flight seasons, and higher nematode loads in warmer areas (Rutherford and Webster, 1987; Pimentel et al., 2014). At lower temperatures, the development of the symptoms is slower, with no disease development in infected trees maintained at 18°C or below, whereas at 30–32°C PWD incidence and tree mortality are highest and symptoms development is faster (Rutherford and Webster, 1987; Pimentel and Ayres, 2018). Besides temperature, several studies settled that dry conditions (i.e., low water availability) result in an increase in nematode population, faster PWD progress, advanced disease symptoms, and higher tree mortality rate (Mamiya, 1983; Ikeda, 1996; Braasch, 2000; Suzuki, 2002; Wang, 2014; Yazaki et al., 2018). However, there are still unanswered questions related to how high temperatures, low water availability, and their combined effect influence PWD development in pine species occurring in the Mediterranean region.

In the Mediterranean basin, where there is a strong seasonal drought period, with warm dry summers, and where pine forests are one of the major wood resources, PWD is a current important issue. Concerns regarding insect and pests outbreaks are further emphasized by the projected scenarios of increasing drought episodes and rise of temperature for this region (Intergovernmental Panel on Climate Change [IPCC], 2014; Anderegg et al., 2015b). In Europe, PWD was detected for the first time in Portugal in 1999 (Mota et al., 1999) later in Spain (Abelleira et al., 2011) and in Madeira Island (Fonseca et al., 2012). Its expansion to all Europe is a worry (Vicente et al., 2012), but, so far, the disease remains epidemic in a restricted area. In Portugal, its limits had extended since the first report causing a regression of pine forest (Mota and Vieira, 2008b; Vicente et al., 2012). These impacts are expected to be aggravated in the next years (De la Fuente and Beck, 2018) with forecasted losses over 80% of the total stock of coniferous trees in Portugal, leading to a negative economic and ecological impact (Soliman et

al., 2012). The maritime pine, *Pinus pinaster* (*P. pinaster*) Aiton, is a thermophilic, light demanding, and fast-growing species whose plantation has increased due to its versatility. Nevertheless, is considered very susceptible to pests and diseases, being one of the most significant species affected by PWN in Europe (Vicente et al., 2012; Nunes da Silva et al., 2015; Pimentel et al., 2017). In addition, under the current and projected climatic context, other coexisting *Pinus* species might become more vulnerable to the nematode infection and consequently to PWD. This is particularly important for species that, although currently considered less susceptible to PWN, have an important role in the economy, such as stone pine, *Pinus pinea* (*P. pinea*) L. and radiata pine, *Pinus radiata* (*P. radiata*) D. Don (Mota and Vieira, 2008a; Mota et al., 2009; dos Santos and de Vasconcelos, 2012; Menéndez-Gutiérrez et al., 2018). Contrary to *P. pinaster* and *P. radiata*, *P. pinea* is considered a slow-growth species able to thrive in dry conditions and with a strong resistance to pests and diseases (Abad Viñas et al., 2016). Hence, contrasting susceptibility of these three species to PWN is expected to be related in one hand to their defenses (anatomical, constitutive, and chemical), enabling the tree to reduce the nematode's ability to migrate and proliferate within the tree, and on the other hand to their drought resistance strategies, enabling the tree to be generally less vulnerable to external biotic pressure (Nunes da Silva et al., 2015; Pimentel et al., 2017; Menéndez-Gutiérrez et al., 2018).

In this context, it is essential to better understand the vulnerability of pine species to PWN under different scenarios of environmental conditions. Therefore, the main objective of this study was to evaluate the physiological impacts of PWN on different pine species under high temperatures and drought (low water availability) and to study their combined effect on the severity of nematode's infection. To achieve that we investigated physiological responses and wilting symptoms of *P. pinaster*, *P. pinea*, and *P. radiata* to the interaction between nematode infection and two key environmental factors: temperature and water availability. We hypothesized that (i) physiological susceptibility to PWN will depend upon *Pinus* species, being the species considered more drought and nematode resistant the one that will show lower impacts of PWN on photosynthetic activity and water status, and (ii) the combination of higher temperature and water stress will enhance PWD development, with a greater and faster onset of physiological and morphological symptoms and higher tree mortality in all the studied pine species.

# MATERIALS AND METHODS

## Pinewood Nematode Inoculum

The *B. xylophilus* isolate (BxPt17AS), a virulent PWN isolate (Cardoso et al., 2016, 2022; Pimentel et al., 2017; Silva et al., 2021), used in this experiment was obtained from infected maritime pine from Alcácer do Sal (Portugal). The isolate was established and maintained in cultures of *Botrytis cinerea* Pars. grown on malt extract agar medium and incubated at 25°C (Fonseca et al., 2012; Cardoso et al., 2016; Silva et al., 2021).

## Experimental Design

The study was conducted in 5-year-old plants of three pine species with similar intraspecific heights (*P. pinaster*:  $2.05 \pm 0.2$  m; *P. pinea*:  $1.61 \pm 0.1$  m; *P. radiata*:  $1.32 \pm 0.1$  m). One month before the PWN artificial inoculation, 40 plants of each species were divided into two groups. One group was acclimated at 25°C and the other at 30°C in two separate compartments of a greenhouse at the Faculty of Science of the University of Lisbon. Climatic conditions were continuously monitored with HOBO® data loggers (Onset, MA, United States). On the 25°C treatment, the maximum and minimum temperatures reached were 15.2 and 31.1°C and the mean daily temperature was  $22.9 \pm 4$ °C. The 30°C greenhouse had a daily mean temperature of  $25.6 \pm 7$ °C and the maximum and minimum temperatures registered were 16 and 40.1°C, respectively. In both cases, plants were under natural photoperiod and solar radiation, and the air relative humidity (RH) was preserved at 50–60%. During the trial, the plants were kept in pots with the soil of the forest nursery from where they came (Aliança, Grupo Portucel Soporcel, Portugal).

Seventeen days before the PWN artificial inoculation, two water regime treatments were added to each pine species at both temperatures: (i) watered (W,  $n = 10/\text{species}$ ); and (ii) water stressed (WS,  $n = 10/\text{species}$ ). To maintain the assigned treatments, soil volumetric moisture was regularly monitored with a ThetaProbe MLX2 (LAB-EL Laboratory Electronics, Poland) before watering, allowing to control and adjust irrigation during the experiment. In the W regime, the trees were watered, with tap water, three times a week and the WS plants twice a week. The mean soil water content in W plants was  $0.17 \pm 0.09 \text{ m}^3 \text{m}^{-3}$ , while in WS plants was  $0.07 \pm 0.08 \text{ m}^3 \text{m}^{-3}$ .

To initiate the trial (day 0), eight treatments were established: (i) watered plants at 25°C non-inoculated (W25N–); (ii) watered plants at 25°C

inoculated with PWN (W25N+); (iii) WS plants at 25°C non-inoculated (WS25N-); (iv) WS plants at 25°C inoculated with PWN (WS25N+); (v) Watered plants at 30°C non-inoculated (W30N-); (vi) Watered plants at 30°C inoculated with PWN (W30N+); (vii) WS plants at 30°C non-inoculated (WS30N-); and (viii) WS plants at 30°C inoculated with PWN (WS30N+) (Figure 1). The PWN inoculation of the trees ( $n = 5 \times 3 \times 4 = 60$ ) in the treatments W25N+, WS25N+, W30N+, and WS30N+ was performed artificially. The trees ( $n = 5 \times 3 \times 4 = 60$ ) of the control treatments (W25N-, WS25N-, W30N-, and WS30N-) were inoculated with sterilized water.

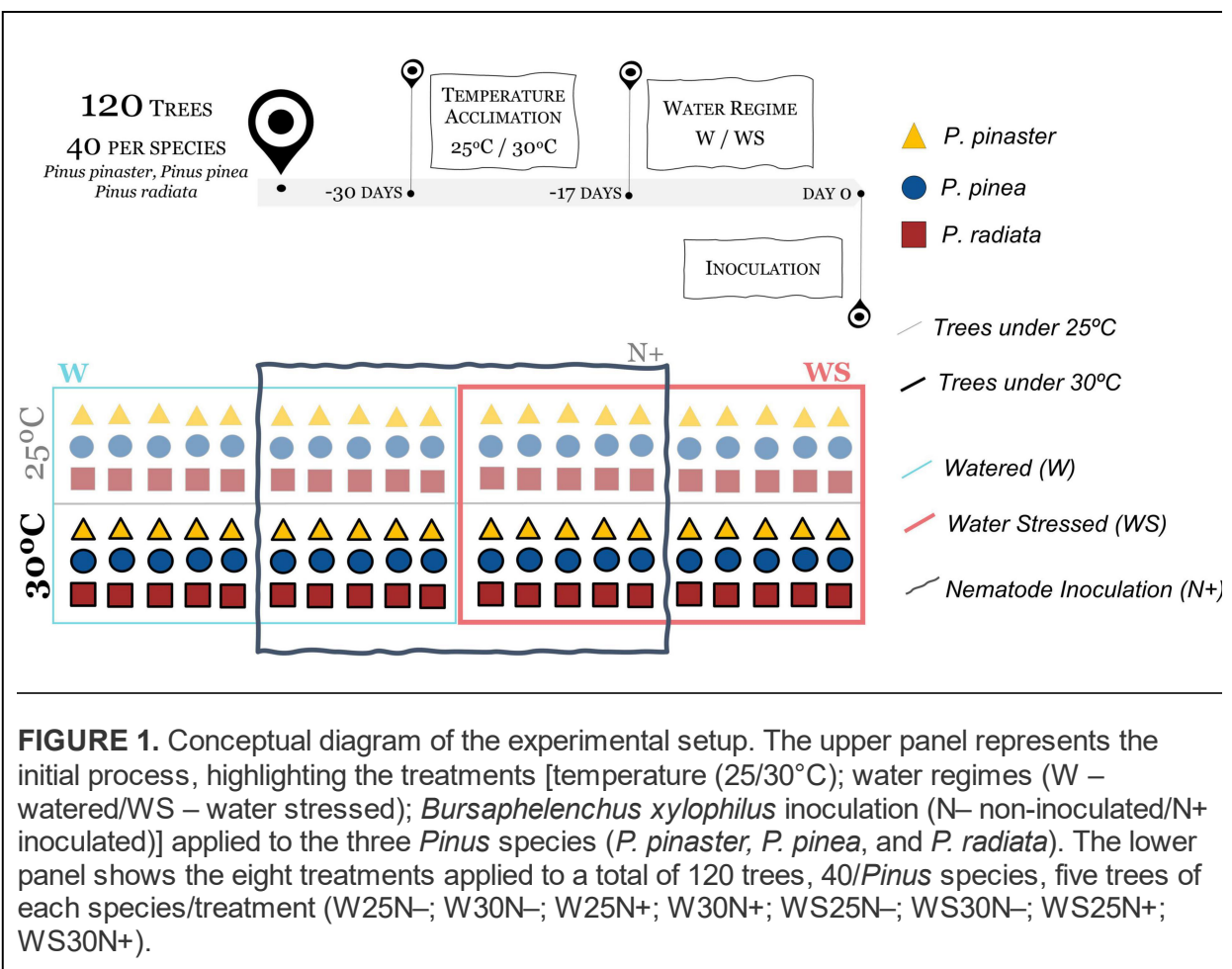


**FIGURE 1.** Conceptual diagram of the experimental setup. The upper panel represents the initial process, highlighting the treatments [temperature (25/30°C); water regimes (W – watered/WS – water stressed); *Bursaphelenchus xylophilus* inoculation (N– non-inoculated/N+ inoculated)] applied to the three *Pinus* species (*P. pinaster*, *P. pinea*, and *P. radiata*). The lower panel shows the eight treatments applied to a total of 120 trees, 40/*Pinus* species, five trees of each species/treatment (W25N-; W30N-; W25N+; W30N+; WS25N-; WS30N-; WS25N+; WS30N+).

## Artificial Inoculation

For tree inoculation, a wound was made on the main stem of each plant by removing an area of bark (2 cm × 1 cm), and a piece of cotton was placed in the wound. Then, the nematode suspension, already adjusted with sterilized water to achieve a concentration of 6,000 (mixed developmental stages)/100

$\mu\text{L}$ , or sterilized water was pipetted onto the cotton and covered with parafilm to prevent desiccation (Woo et al., 2008; Yazaki et al., 2018).

## **Assessment of Plant Physiological Performance**

Physiological measurements were taken twice a week in three (for gas-exchange measures) or five (for water potential and reflectance index) plants of the three *Pinus* species at each treatment. The sampling stopped when the individuals died or 75 days after inoculation.

### **Leaf Water Potential**

Predawn leaf water potential ( $\Psi_{pd}$ ) was measured before sunrise with a Scholander pressure chamber (Manofrígido, Lisboa, Portugal). Water potential was assessed in 1-year-old needles in all plants.

### **Gas Exchange**

Three plants of each pine species in each treatment were randomly selected, and gas-exchange measurements were performed between 10:00 a.m. and 12:30 a.m. with a portable infrared gas analyzer (GFS-3000, Walz, Effeltrich, Germany). Carbon assimilation (A,  $\mu\text{mol m}^{-2} \text{ s}^{-1}$ ), leaf transpiration rates (E,  $\text{mmol m}^{-2} \text{ s}^{-1}$ ), and stomatal conductance (gs,  $\text{mmol m}^{-2} \text{ s}^{-1}$ ) were measured with an incident photosynthetic photon flux density (PPFD) of  $1000 \mu\text{mol m}^{-2} \text{ s}^{-1}$ , a flow of  $700 \mu\text{mol/s}$ , and under greenhouse  $\text{CO}_2$  concentration and RH conditions (in a leaf chamber of  $8 \text{ cm}^2$ ). The measures were taken in two needles of each tree and their specific leaf areas (accessed with a leaf area meter) were used to estimate respective A, E, and gs (and the mean value was considered for further analysis).

### **Photochemical Reflectance Index**

Reflectance was assessed using a spectroradiometer (UNISPEC-SC Spectral Analysis System, PP Systems, United States) 15 days after the inoculation. The measurements were carried out in 5 needles/plant/treatment (mean value was considered for further analysis). Photochemical Reflectance Index (PRI) was calculated as  $\text{PRI} = (\text{R531} - \text{R570}) / (\text{R531} + \text{R570})$ , being R531 and R570 reflectance at wavelengths of 531 and 570 nm, respectively. PRI is based on carotenoids estimation and is highly associated with photosynthetic light use efficiency (Peñuelas and Filella, 1998). Thus, it can be used as an index of photosynthetic activities in which low PRI values are associated with

responses to stress factors such as high temperatures, water stress, excess of light exposition, salinity, and presence of pests (Wong and Gamon, 2015; Sukhova and Sukhov, 2018).

## **Wilting Symptoms**

To compare PWD development across species under different conditions over time, wilt symptoms were examined visually and recorded for all pine trees under the nematode treatments (W25N<sup>+</sup>; WS25N<sup>+</sup>; W30N<sup>+</sup>; WS30N<sup>+</sup>) and the control situation (W25N<sup>-</sup>). The symptoms considered were alteration of leaf color, from green to yellow and brown, followed by canopy foliage loss (Mamiya, 1983). These symptoms of needle dehydration were classified into a six class scale based on wilting and percentage of brown needles in the tree: 0 – tree without symptoms, I – <10% brown leaves, II – 10–50% brown leaves, III – 50–80% brown leaves, IV – >80% brown leaves, and V – dead tree without leaves (Proen  a et al., 2010). We considered the trial to be ended when tree mortality was verified within the water regime trial-set of 10 trees (i.e., in WS25N<sup>+</sup>//W25N<sup>+</sup> or WS30N<sup>+</sup>//W30N<sup>+</sup>). After 75 days, even if there were plants still alive the assessment stopped.

## **Pinewood Quantification**

Pinewood nematode was quantified in plants inoculated with the nematode (N<sup>+</sup>,  $n = 60$ ), by the end of each trial. We considered the trial to be ended when tree mortality was verified within the water regime trial set of 10 trees (in WS25N<sup>+</sup>//W25N<sup>+</sup> or WS30N<sup>+</sup>//W30N<sup>+</sup>). Plants were removed from pots and the respective stem, branches, and roots separated. Each component of the plant was sliced into 5 mm thick, and nematodes extracted, using the tray method (Whitehead and Hemming, 1965), identified, and quantified under a stereomicroscope. After 75 days, all the plants still alive were also cut and the same procedure was applied.

## **Statistical Analysis**

Aiming at identifying physiological patterns among the species and treatments, and to reduce and integrate the physiological parameters, a principal component analysis (PCA) was performed based on all physiological variables (PRI, A, gs, E, and  $\Psi_{pd}$ ), using the mean (representative of the data set) and minimum (lowest physiological performance reached) of individual data measured throughout the experiment, using facto extra R package

(Kassambara and Mundt, 2019). Individual coordinates of the axis that accounted for the highest percentage of variance explained (in this case the first axis of the PCA, PC1) were extracted and used in further statistical analysis.

The effects of the interaction Species\*Inoculation\* Temperature\*Water Regime on PC1 (a synthesis trait for plants' photosynthetic performance); the effects of the interaction of the treatments applied (Inoculation\*Temperature\*Water Regime) by species on (i) PC1 and (ii)  $\Psi_{pd}$  (a parameter not integrated in the PC1, reflecting plant water status); and the effects of the interaction Temperature\*Water Regime on the number of nematodes/g (considering inoculated plants), were tested through an Analysis of Variance of Aligned Rank Transformed Data for a non-parametric factorial analysis [using ART package by Villacorta (2015)].

To assess the nematode effect on A and  $\Psi_{pd}$  under the treatment conditions, the variation of these parameters (physiological components related with carbon acquisition and plant water status, respectively) was calculated at each time point by subtracting the respective species control value to each measure (i.e., the difference between the inoculated plants and non-inoculated plants under the same water regime and temperature treatment), with negative values representing lower values compared to the control situation.

All the statistical analyses were conducted using R (R Core Team, 2019).

## RESULTS

Our results showed a distinct physiological performance and severity of the infection among the three *Pinus* species under different temperatures and water regimes.

### **The Physiological Impact of Pinewood Nematode on the *Pinus* Species**

Through the multivariate approach, we found a differentiation among species and inoculation treatments. The first two axis of the PCA (PC1 and PC2) accounted for 82.8% of the total variance (65.8 and 17%, respectively, Figure 2 and Supplementary Table 1). PC1 represented a physiological gradient related to gas exchange and photosynthetic activity, showing increasing values

of carbon assimilation (A), transpiration (E), and stomatal conductance (gs), whereas PC2 was mainly reflecting predawn water potential ( $\Psi_{pd}$ ). A significant effect of the interaction species  $\times$  nematode infection on PC1 was found ( $F$ -value = 24;  $p < 0.001$ ; Supplementary Table 2). Accordingly, significant differences were found among the pine species depending on the inoculation treatment, with the nematode inoculation significantly reducing the physiological status of *P. pinaster* and *P. radiata*, but not of *P. pinea* (Figure 2 and Supplementary Figures 1, 2). The *Pinus* species segregated along the physiological axis, with a clear differentiation of *P. radiata*, showing higher values of photosynthetic activity under non-infected conditions and a higher decrease of A and gs under nematode inoculation (Figures 2, 3 and Supplementary Figures 1, 2).

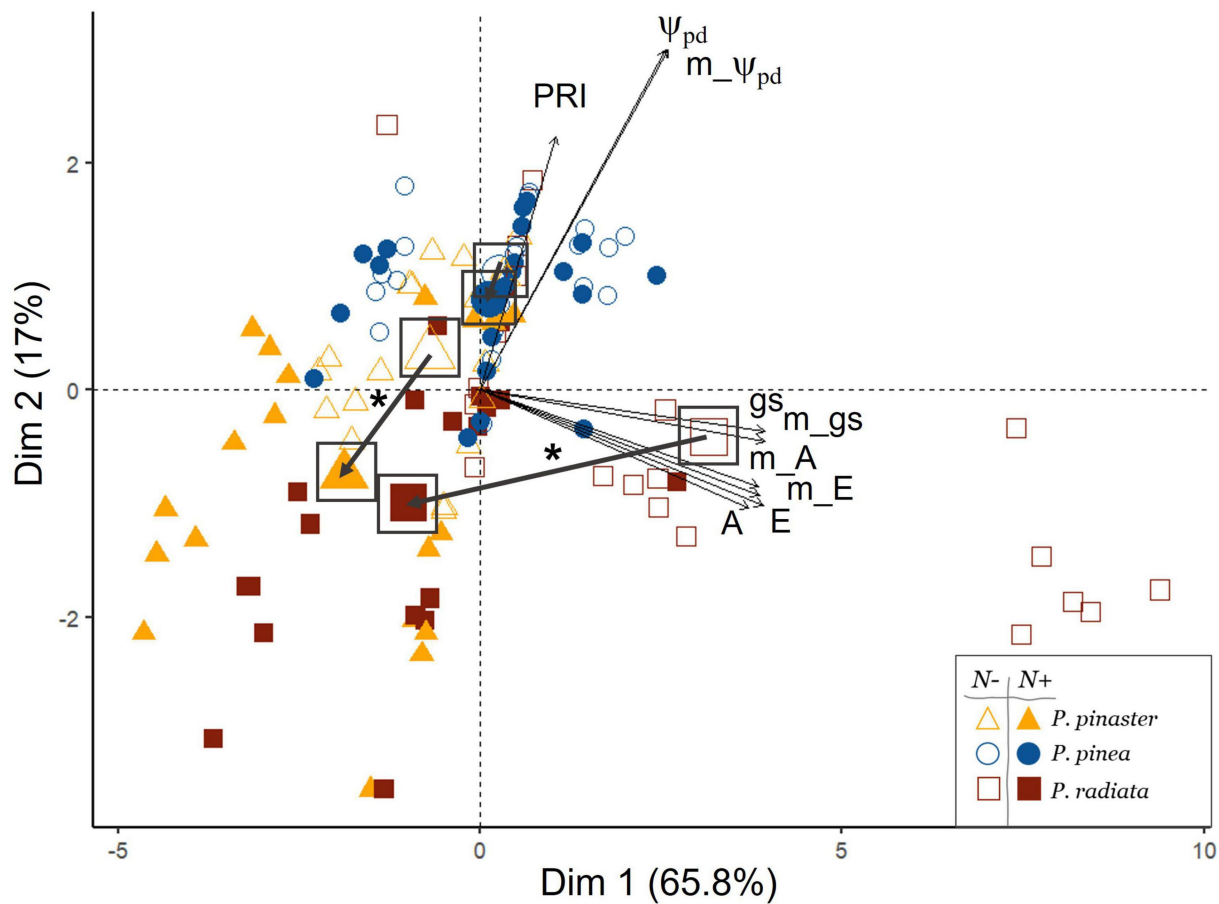


**FIGURE 2.** Principal component analysis (PCA) of ecophysiological parameters of the three *Pinus* species, considering the *Bursaphelenchus xylophilus* inoculation treatment (N- non-inoculated/N+ inoculated). Mean values of each group (inoculation treatment by species) are represented by a bigger symbol and highlighted by a square; an arrow represents the bidimensional difference between mean values of each group and an asterisk (\*) represents significant differences of PC1 and/or PC2 between groups. Physiological parameters abbreviations: PRI, photochemical reflectance index;  $\Psi_{pd}$ , water potential predawn; gs, leaf conductance; E, transpiration; A, carbon assimilation; m, minimum.

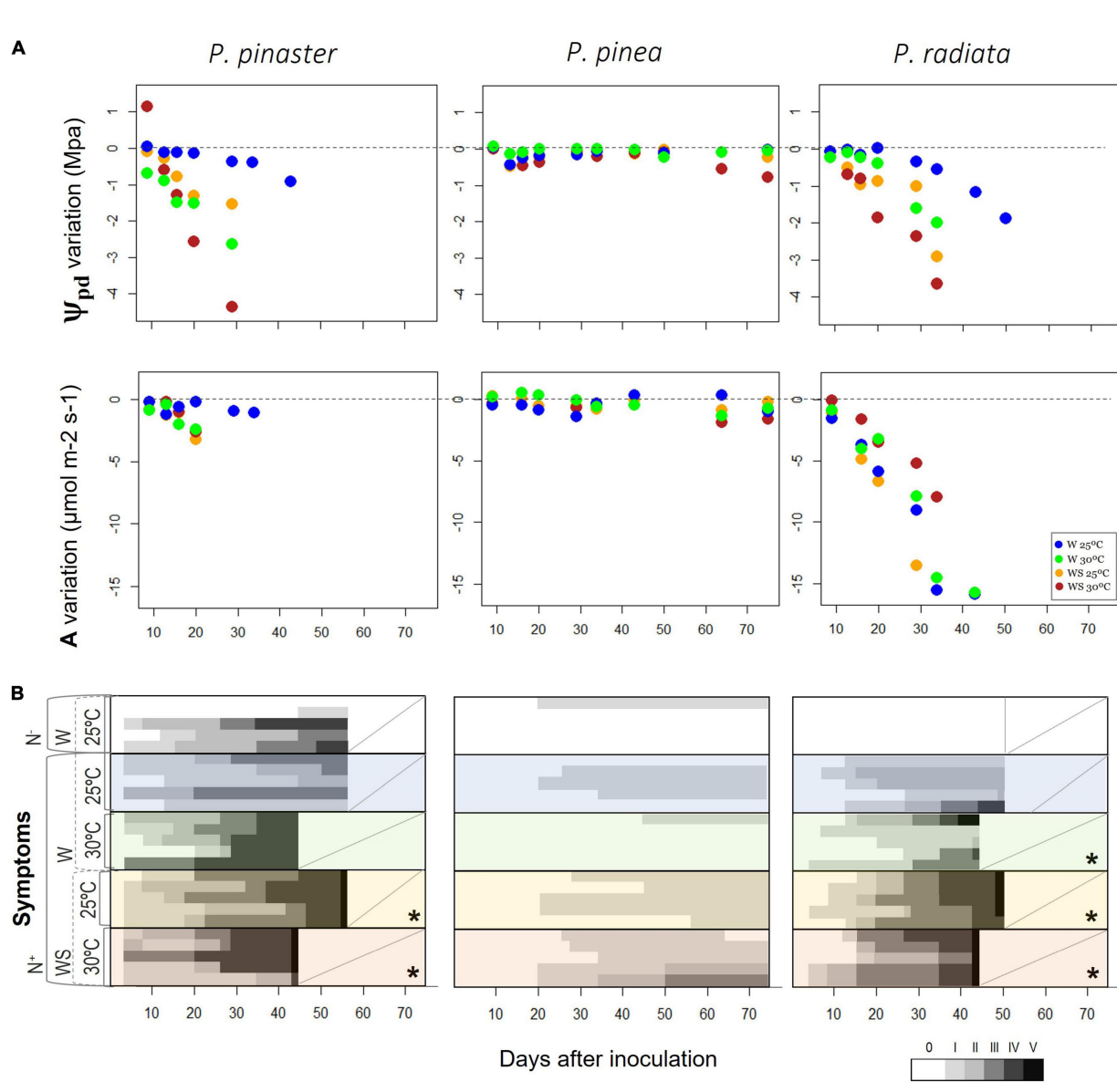


**FIGURE 3.** Variation over time of main physiological variables and visible symptoms. **(A)** Pre-dawn water potential ( $\Psi_{pd}$ ) and carbon assimilation ( $\Delta$ ) from the controlled abiotic conditions to the respective inoculated treatment, i.e., the difference of  $\Psi_{pd}$  and  $\Delta$  between the inoculated treatments and the associated control (W25: N– vs. N+, WS25: N– vs. N+, W30: N– vs. N+, WS30: N– vs. N+) and **(B)** wilting symptoms after inoculation. Classification of wilting symptoms based on six scaled classes: 0 – tree without symptoms; I – <10% brown leaves; II – 10–50% brown leaves; III – 50–80% brown leaves; IV – >80% brown leaves; V – dead tree without leaves (Proença et al., 2010). An asterisk represents the presence of severe symptoms, with plants reaching death. A diagonal line indicates that the trial was finished, and the trees were removed. See section “Materials and Methods” for detailed information about each treatment and respective abbreviations.

## Influence of Temperature and Drought on the Severity of the Pinewood Nematode Infection

Only *P. pinaster* and *P. radiata* overall photosynthetic performance were negatively influenced by the nematode, regardless of their temperature and water regime, as no interaction effect was found for any of the species (Table 1 and Supplementary Figure 4). Alongside, WS plants from all pine species presented lower gas exchange rates and lower  $\Psi_{pd}$ , indicating a common physiological response to water stress (Supplementary Figures 1, 2).

**TABLE 1.** Effects of temperature (25°C/30°C), water regimes (W – watered/WS – water stressed), *Bursaphelengus xylophilus* inoculation (N– non-inoculated/N+ inoculated) and their interaction on PC1 values extracted from first PCA axis, and on pre-dawn Water Potential ( $\Psi_{pd}$ ).

PC1 (gas exchange)	Df	<i>P. pinaster</i>			<i>P. pinea</i>			<i>P. radiata</i>		
		SSq	F-value	p-value	SSq	F-value	p-value	SSq	F value	p-value
Nematode inoculation	1	1254.4	10.01	0.003**	136.9	0.846	0.365	2160.9	22.53	0.000***
Temperature	1	980.1	7.24	0.011*	84.1	0.517	0.478	12.1	0.07	0.787
Water regime	1	1587.6	13.80	0.001***	4000	97.146	0.000***	1562.5	14.02	0.001***
Nematode inoculation: temperature	1	291.6	1.87	0.181	6.4	0.039	0.845	14.4	0.09	0.768
Nematode inoculation: water regime	1	193.6	1.22	0.278	10	0.060	0.807	202.5	1.27	0.267
Temperature: water regime	1	136.9	0.86	0.360	40	0.244	0.625	48.4	0.30	0.587
Nematode inoculation: temperature: water regime	1	90	0.56	0.458	0.90	0.005	0.942	0.9	0.01	0.941
Residuals	32									
<b>Predawn water potential (<math>\Psi_{pd}</math>)</b>										
Nematode inoculation	1	864.0	49.46	0.000***	505.2	17.70	0.001***	958.09	52.08	0.000***
Temperature	1	816.7	40.06	0.000***	440.6	12.79	0.003**	712.97	23.64	0.000***
Water regime	1	864	49.46	0.000***	746.8	45.05	0.000***	964.52	52.32	0.000***
Nematode inoculation: temperature	1	682.7	23.57	0.000***	3.92	0.06	0.811	237.12	4.25	0.055
Nematode inoculation: water regime	1	48.2	0.73	0.406	165.7	3.15	0.096	621.94	20.57	0.000***
Temperature: water regime	1	54	0.84	0.374	62.75	1.09	0.314	181.72	3.24	0.090
Nematode inoculation: temperature: water regime	1	104.2	1.67	0.214	102.0	1.83	0.196	36.17	0.51	0.484
Residuals	16				15			17		

Data analyzed separated by *Pinus* species. F-values are reported with the corresponding p-value and significance: \* $p < 0.05$ , \*\* $p < 0.01$ , and \*\*\* $p < 0.001$ .

Over time, the decrease of  $\Psi_{pd}$  in infected plants was more evident in *P. radiata* and *P. pinaster*, while *P. pinea* maintained its  $\Psi_{pd}$  values similar to the control plants along with the experiment (Figure 3A and Supplementary Figure 1). A higher drop of  $\Psi_{pd}$  was observed in infected *P. radiata* and *P. pinaster* under 30°C and water stress (Figure 3A). During the experiment, the highest differences of A compared to their respective control plants were observed in *P. radiata* under water stress. *Pinus pinaster* reached values below -4 MPa only when inoculated with the nematode (Supplementary Figure 1), and the highest decrease was observed in the infection treatment under water and temperature treatments (with a relative decrease of 4 MPa,

reaching values of  $-8$  MPa by the end of the experiment; Figure 3A and Supplementary Figure 1). These observed low  $\Psi_{pd}$  values could then be linked to the development of foliar damage and earlier tree mortality compared to the other species (Figure 3). Symptom development was different among the pine species, as *P. pinaster* and *P. radiata* plants exhibited PWD severe symptoms, while *P. pinea* plants showed no severe symptoms (Figure 3B and Supplementary Figure 5). In *P. pinaster* and *P. radiata*, the progressive severity of the infection was higher under water stress, and tree mortality was observed as earlier as 43 days after inoculation in WS plants under higher temperatures (Figure 3B).

Associated with these symptoms, proliferation of the nematode was verified in the trunk and branches of both *P. pinaster* and *P. radiata* (Figure 4 and Supplementary Table 3). The highest number of nematodes was found in their trunks with water stress promoting nematodes proliferation (no significant effect of the interaction Temperature\*Water Regime on nematode number was found, Supplementary Table 4). Moreover, *P. pinaster* was the species with a higher density of nematodes and the only one holding an expressive number of individuals in the roots (Figure 4). Contrastingly, most *P. pinea* plants presented zero nematodes at the end of the experiment (Figure 4).

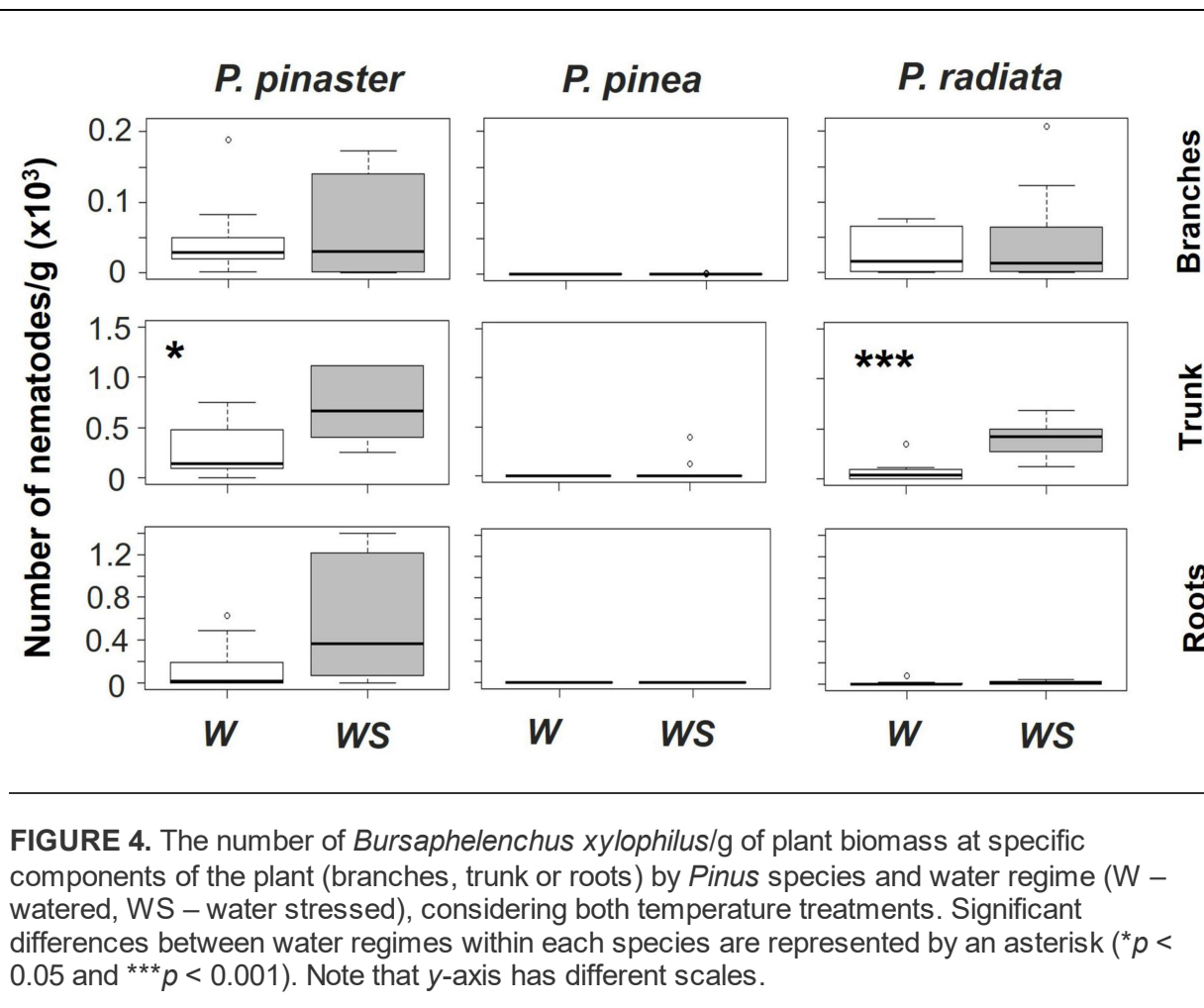


**FIGURE 4.** The number of *Bursaphelenchus xylophilus*/g of plant biomass at specific components of the plant (branches, trunk or roots) by *Pinus* species and water regime (W – watered, WS – water stressed), considering both temperature treatments. Significant differences between water regimes within each species are represented by an asterisk (\* $p < 0.05$  and \*\*\* $p < 0.001$ ). Note that y-axis has different scales.

## DISCUSSION

Susceptibility to PWN was found to be dependent on pine species, being infected *P. pinaster* and *P. radiata* more prone to physiological damages and morphological severe symptoms than *P. pinea*. The impact of nematode inoculation on *P. pinaster* and *P. radiata* was extremely notable, as nematode presence led to a quick physiological performance decrease and to crown discoloration. On the contrary, *P. pinea* expressed almost no wilting symptoms throughout the experiment and was able to keep their physiological performance when infected (Figures 2, 3 and Supplementary Figure 1). Remarkably, *P. pinea* showed to be able to reduce the nematode infection to numbers close to zero even under stressful conditions such as high temperatures and low water availability (Figure 4). These results reinforce

that *P. pinea* is the most resistant species to PWN and *P. pinaster* and *P. radiata* are more susceptible to the pathogen.

*Pinus pinea* resistance to PWN is known to be linked to its drought-resistance strategies, generally associated with slow-growing rates and high investment in constitutive defenses (Awada et al., 2003; Tapias et al., 2004; Endara and Coley, 2011). Specifically, the higher concentration of phenolics and tannins, which *P. pinea* can produce, strongly contributed to its lower susceptibility to PWN, compared to the two faster-growing species, *P. pinaster* and *P. radiata* (Tapias et al., 2004; Pimentel et al., 2017). Importantly, our results indicate that the presence of nematode was the main driver of photosynthetic responses in both *P. pinaster* and *P. radiata*, regardless of their temperature or water regime (Figure 2 and Table 1). This result highlights the impact that the nematode has on gas-exchange rates, particularly on *P. radiata*, independently of plants' temperature or water conditions. It supports the idea that PWN infection promotes a significant and continuous decline in photosynthetic and transpiration rates (Woo et al., 2010), especially in the fast-growing and acquisitive but less chemically defended pines. Generally, fast-growing species must maintain high C uptakes through high rates of carbon assimilation at the cost of decreasing midday leaf water potential (Attia et al., 2015) to promote biomass production. Compared to *P. pinaster*, *P. radiata* showed to be a species with considerably high rates of gas exchange under non-inoculated conditions and showed a stronger gas exchange regulation and decline of carbon assimilation under the presence of the nematode (Figures 2, 3 and Supplementary Figure 1). Thus, *P. radiata* is the most impacted on gas-exchange processes by the presence of the nematode, and through A rate decline measures, the PWN infection could be early detectable in this species.

Nevertheless, it is important to look at other vitality attributes such as plants' water status. Nematode presence negatively affected  $\Psi_{pd}$  of all the pine species, being *P. pinaster* and *P. radiata* the most affected with a significant decline of their water status (Table 1, Figure 3, and Supplementary Figure 1). In this case, the synergy of water stress and PWN infection and the interaction of temperature and nematode infection played a relevant role in the significant decrease of the water status of *P. radiata* and *P. pinaster*, respectively. Thus, even though there was no enhancement of the nematode effect with stress climatic conditions on the photosynthetic performance of these species, the interaction of climatic stressful conditions and PWN-

enhanced negative impacts on plants' water status. The low  $\Psi_{pd}$  values observed for these species exposed their incapacity of nighttime recovery through water refilling and their higher susceptibility to xylem cavitation when infected under stressful environmental conditions. The anatomical deterioration of PWN infected trees can more easily permit xylem cavitation through the increase of water tension and/or the increase of vulnerability with the denaturation of living cells in the xylem (Fukuda et al., 2007; Umebayashi et al., 2011) which is exacerbated by water limitation in *P. radiata* and water stress and high temperatures in *P. pinaster*. The dysfunctional water conduction in the xylem embraces a series of physiological alterations such as leaf water potential (Fukuda, 1997; Suzuki, 2002; Menéndez-Gutiérrez et al., 2018; Yazaki et al., 2018), transpiration, and photosynthesis decrease (Fukuda, 1997; Suzuki, 2002; Yazaki et al., 2018).

High temperatures in *P. pinaster* and low water availability in *P. radiata* are therefore expected to further increase the negative impact of the nematode presence through hydraulic failure (Martínez-Vilalta et al., 2009; Choat et al., 2018). The differential nematode effects, which depends on different abiotic factors, are linked to their resistance strategies and physiological response capacity. On one hand, *P. radiata*, with an isohydric response (Brodribb et al., 2014), promptly closed their stomata accompanied by a sharp decrease of  $gs$  and  $A$ , in the presence of the nematode and particularly under water-limited conditions (Supplementary Figure 1). However, was not able to maintain high levels of  $\Psi_{pd}$  (mean value for W25N–:  $-1.06$  MPa), and the decrease in  $A$  was followed by a decrease in  $\Psi_{pd}$ , which denotes a great plant stress affecting both carbon assimilation and water status of the plants (Supplementary Figure 1). Similar to other pine species (such as *Pinus halepensis* and *Pinus edulis*), there are response mechanisms involving carbon starvation from low assimilation and transpiration rates (Skelton et al., 2015; Birami et al., 2018; Breshears et al., 2021) accompanied by hydraulic failure in the shoot. On the other hand, infected *P. pinaster* did not show a great  $A$  decrease (through the absence of a strong stomatal control), while losing water, particularly under high temperatures. Stressful temperature conditions are known to promote stomatal opening (Feller, 2006), and the increase in leaf temperatures may decouple net photosynthesis from stomatal conductance, as seen in *Pinus taeda* (Urban et al., 2017). Also, *P. pinaster* is known to have a low genetic variation of cavitation resistance between climatically contrasting populations and very limited phenotypic plasticity

(Lamy et al., 2013), conferring this species with low capacity to enable short-term acclimatization and adaptive plasticity to deal with the infection under high temperature and low water availability. *Pinus pinaster* experienced a great decline of water potential (Figure 3A and Supplementary Figure 1), reaching values known to be indicative of high vulnerability to xylem cavitation in *P. pinaster*, way beyond the reference values of  $P_{50}$  of  $-3.8$  MPa (Martínez-Vilalta et al., 2009; Corcuera et al., 2011; Bouche et al., 2016), when inoculated with the nematode. The low values of  $\Psi_{pd}$  observed in infected plants when under water limitation or high temperature, further associated with unhealthy symptoms (Figure 3B) denotes a process of hydraulic failure occurring under these conditions (Martínez-Vilalta et al., 2009; Choat et al., 2018). This species is therefore highly prone to hydraulic failure, rather than to carbon starvation, when infected by the nematode under high temperatures.

Importantly, associated with the physiological decline of both PWN infected *P. pinaster* and *P. radiata* under drought, we observed severe wilting symptoms, culminating in tree mortality (Figure 3). Under water stress and high temperatures, there was a faster onset of the wilting symptoms (and mortality) compared to no water limitation and mild temperature. Water deficiency is considered a key factor in tree mortality (Futai, 2013; Anderegg et al., 2015a) with morphological symptoms, like the browning of needles, as one of the main consequences. It is expected that xylem cavitation has started before a significant decrease in needle water potential, as also reported in *Pinus thunbergii* (Fukuda et al., 2007) and water shortages affected the progression of disease symptoms because water stress of the trees decreased its tolerance to the disease (Yazaki et al., 2018). As the decline in water status was observed in both affected species,  $\Psi_{pd}$  represented a physiological trait more sensitive to environmental conditions (extra exogenous plant stressors), with the impact of the infection further decreasing trees' water status under higher temperatures (*P. pinaster*) or water limitation (*P. radiata*). As this physiological response anticipated visible symptoms in needles (discoloration), early observations of plants water status (through for example water potential measurements) could serve as potential physiological indicators for an early detection of PWN infected trees, mitigating the decline of Portuguese pine forests observed in recent years (Futai, 2008; Institute for Nature Conservation and Forests [ICNF], 2019).

The total number of nematodes and their allocation on species structure was also different among the pine species and influenced by water limitation (Figure 4). *Pinus pinaster* had the most nematode density and migration to several components of the plants, followed by *P. radiata* and in last *P. pinea*. Besides the lower susceptibility of *P. pinea* to PWN, our results emphasize an intrinsic resistance to this pathogen. Only trees under 30°C and WS were still infected by the end of the experiment, and even in this scenario, nematode populations decreased considerably. This response is likely linked to *P. pinea* anatomy of resin canals (Son et al., 2015) and to the production of constitutive defenses (Pimentel et al., 2017). The most negatively affected species (*P. pinaster* and *P. radiata*) displayed a higher density of nematodes on the main trunk and a proliferation to the branches. Additionally, in *P. pinaster* individuals it was verified a proliferation of nematodes from trunk to roots which could be linked to specific traits such as wider axial resin canals (Nunes da Silva et al., 2015). Proliferation and fast dispersion of nematodes are connected to the weakening and death of seedlings and young trees (Futai, 2013) with distinct species having different tolerances (Nunes da Silva et al., 2015). Furthermore, nematodes' proliferation of both susceptible species was significantly improved not only by water limitation but also by time course, resulting in a larger number of nematodes in water-stressed plants. In accordance with other studies, water limitation has a crucial role in *B. xylophilus* dynamics (proliferation and migration within tree host) (Fukuda et al., 2007; Futai, 2013; Yazaki et al., 2018), which will consequently have a strong influence on the development of the observed wilting symptoms. Moreover, variation in PWN isolates' reproductive ability in *Pinus* spp. and their virulence can occur (e.g., significant higher numbers of nematodes after artificial inoculations are excepted for virulent isolates when compared with avirulent PWN isolates) (Aikawa and Kikuchi, 2007; Filipiak, 2015; Cardoso et al., 2022). Thus, intraspecific PWN variability (and the existence of intraspecific variability in the virulence level of certain PWN isolates) might have implications on the effects observed. Nevertheless, we show that the synergy between PWN infection and abiotic conditions, particularly water stress, is relevant for the development of PWD in *P. pinaster* and *P. radiata*.

## CONCLUSION

The negative impact of the presence of the nematode on physiological traits is observed in both *P. pinaster* and *P. radiata*. *Pinus pinea* showed to be able to resist PWN even under the treatments of higher temperatures and lower water. The presence of the nematode has a particularly strong negative effect on the gas-exchange rates of *P. radiata* and the PWN effect on this species' water status is exacerbated by water limitation. Additionally, *P. pinaster* water status is significantly affected by PWN under high temperatures. The extra influence of these abiotic factors is also felt on nematode proliferation, on the visible wilting symptoms, and on higher mortality for both species. Our results suggest that, although through different physiological mechanisms (mostly hydraulic failure in *P. pinaster*, and both hydraulic failure and carbon limitation in *P. radiata*), drought increases the susceptibility of these species to PWN. Moreover, this study suggests that the decrease of vitality and mortality due to PWN in *P. pinaster* and *P. radiata*'s can be exacerbated by climate, with the spread of PWD in pine forests of the Mediterranean regions being possibly facilitated by predicted drought conditions (i.e., high temperatures and low water availability). Apart from having different abiotic requests (Keeley, 2012; Vergarechea et al., 2019), the studied pine species showed distinct physiological susceptibilities to PWN, and its species-specific response to PWN under particular environmental pressures are essential and should be considered when defining sustainable forest management strategies.

## DATA AVAILABILITY STATEMENT

The raw data supporting the conclusions of this article will be made available by the authors, upon request to the corresponding author.

## AUTHOR CONTRIBUTIONS

ME and CA: formal analysis, investigation, and writing – original draft, review, and editing. SC: formal analyses and writing – original draft, review, and editing. AM: laboratory work and writing – review and editing. FC: laboratory work and writing – original draft. IA and LF: conceptualization, laboratory work, investigation, and writing – review and editing. PF and CC:

field and laboratory work and writing – original draft. CM and OC: conceptualization, investigation, and writing – review and editing. All authors contributed to the article and approved the submitted version.

## **FUNDING**

This study was financially supported by the “Fundação para a Ciência e a Tecnologia” (FCT, Portugal), through the projects: ClimPest “Climate change and its impact on coastal pine forests in west Portugal: the case of two recently emerged pests” (PTDC/BIA-ECO/31655/2017), POINTERS “Host tree-pinewood nematode interactions: searching for sustainable approaches for pine wilt disease management” (PTDC/ASP-SIL/31999/2017) and ReNATURE “Valorization of the Natural Endogenous Resources of the Centro Region” through FEDER funds – Programa Operacional Factores de Competitividade (COMPETE), Centro 2020, Centro-01-0145-FEDER-000007, project FCOMP-01-0124-FEDER-008794 (FCT PTDC/AGR-FL/098916/2008), PTDC/AGRCFL/098869/2008. ME was supported by the FCT project ClimPest through a fellowship (PTDC/BIA-ECO/31655/2017), SC supported by the FCT project PORBIOTA through a postdoctoral fellowship (POCI-01-0145-FEDER-022127), and CA was funded by the European Commission Research Executive Agency, through a Marie Skłodowska-Curie Actions individual fellowship (Grant Number 101003298 – HyChanCEs project). We also acknowledge the support from FCT through the strategic projects UIDB/00329/2020 and UIDB/04004/2020 granted to cE3c and CFE, respectively, and to “Instituto do Ambiente, Tecnologia e Vida”.

## **SUPPLEMENTARY MATERIAL**

The Supplementary Material for this article can be found online at: <https://www.frontiersin.org/articles/10.3389/fpls.2022.841707/full#supplementary-material>

## **REFERENCES**

Abad Viñas, R., Caudullo, G., Oliveira, S., and de Rigo, D. (2016). "Pinus pinea in Europe: distribution, habitat, usage and threats," in *European Atlas of Forest Tree Species*, eds A. San-Miguel-Ayanz, J. de Rigo, D. Caudullo, G. Houston Durrant, and T. Mauri (Luxembourg: Publication Office of the European Union).

Abelleira, A., Picoaga, A., Mansilla, J., and Aguin, O. (2011). Detection of *Bursaphelenchus xylophilus*, causal agent of pine wilt disease on *Pinus pinaster* in Northwestern Spain. *Plant Dis.* 95:776. doi: 10.1094/PDIS-12-10-0902

Aikawa, T., and Kikuchi, T. (2007). Estimation of virulence of *Bursaphelenchus xylophilus* (Nematoda: aphelenchoididae) based on its reproductive ability. *Nematology* 9, 371–377. doi: 10.1163/156854107781352007

Anderegg, W. R. L., Flint, A., Huang, C. Y., Flint, L., Berry, J. A., Davis, F. W., et al. (2015a). Tree mortality predicted from drought-induced vascular damage. *Nat. Geosci.* 8, 367–371. doi: 10.1038/ngeo2400

Anderegg, W. R. L., Hicke, J. A., Fisher, R. A., Allen, C. D., Aukema, J., Bentz, B., et al. (2015b). Tree mortality from drought, insects, and their interactions in a changing climate. *New Phytol.* 208, 674–683. doi: 10.1111/nph.13477

Attia, Z., Domec, J., Oren, R., Way, D. A., and Moshelion, M. (2015). Growth and physiological responses of isohydric and anisohydric poplars to drought. *J. Exp. Bot.* 66, 4373–4381. doi: 10.1093/jxb/erv195

Awada, T., Radoglou, K., Fotelli, M. N., and Constantindou, H. A. (2003). Ecophysiology of seedlings of three Mediterranean pine species in contrasting light regimes. *Tree Physiol.* 23, 33–41. doi: 10.1093/treephys/23.1.33

Birami, B., Gattmann, M., Heyer, A. G., Grote, R., Arneth, A., and Ruehr, N. K. (2018). Heat waves alter carbon allocation and increase mortality of aleppo pine under dry conditions. *Front. For. Glob. Chang.* 1:8. doi: 10.3389/ffgc.2018.00008

Bouche, P. S., Delzon, S., Choat, B., Badel, E., Brodribb, T. J., Burlett, R., et al. (2016). Are needles of *Pinus pinaster* more vulnerable to xylem embolism than branches? New insights from X-ray computed tomography. *Plant Cell Environ.* 39, 860–870. doi: 10.1111/pce.12680

Braasch, H. (2000). Influence of temperature and water supply on mortality of 3-year-old pines inoculated with *Bursaphelenchus xylophilus* and *B. mucronatus*. *Nachrichtenblatt Dtsch. Pflanzenschutzdienstes* 52, 244–249.

Braasch, H. (2008). *Bursaphelenchus* species in conifers in Europe: distribution and morphological relationships. *EPPO Bull.* 31, 127–142. doi: 10.1111/j.1365-2338.2001.tb00982.x

Breshears, D. D., Fontaine, J. B., Ruthrof, K. X., Field, J. P., Feng, X., Burger, J. R., et al. (2021). Underappreciated plant vulnerabilities to heat waves. *New Phytol.* 231, 32–39. doi: 10.1111/nph.17348

Brodribb, T., McAdam, S., Jordan, G., and Martins, S. (2014). Conifer species adapt to low-rainfall climates by following one of two divergent pathways. *Proc. Natl. Acad. Sci. U.S.A.* 111, 1–5. doi: 10.1073/pnas.1407930111

Calvão, T., Duarte, C., and Pimentel, C. (2019). Climate and landscape patterns of pine forest decline after invasion by the pinewood nematode. *For. Ecol. Manage.* 433, 43–51. doi: 10.1016/j.foreco.2018.10.039

Cardoso, J. M. S., Anjo, S. I., Fonseca, L., Egas, C., Manadas, B., and Abrantes, I. (2016). *Bursaphelenchus xylophilus* and *B. mucronatus* secretomes: a comparative proteomic analysis. *Sci. Rep.* 6:39007. doi: 10.1038/srep39007

Cardoso, J. M. S., Anjo, S. I., Manadas, B., Silva, H., Abrantes, I., Nakamura, K., et al. (2022). Virulence biomarkers of *bursaphelenchus xylophilus*: a proteomic approach. *Front. Plant Sci.* 12:822289. doi: 10.3389/fpls.2021.822289

Carnegie, A., Venn, T., Lawson, S., Nagel, M., Wardlaw, T., Cameron, N., et al. (2018). An analysis of pest risk and potential economic impact of pine wilt disease to *Pinus* plantations in Australia. *Aust. For.* 81, 1–13. doi: 10.1080/00049158.2018.1440467

Choat, B., Brodribb, T. J., Brodersen, C. R., Duursma, R. A., López, R., and Medlyn, B. E. (2018). Triggers of tree mortality under drought. *Nature* 558, 531–539. doi: 10.1038/s41586-018-0240-x

Corcuera, L., Cochard, H., Gil-Pelegrin, E., and Notivol, E. (2011). Phenotypic plasticity in mesic populations of *Pinus pinaster* improves resistance to xylem embolism (P50) under severe drought. *Trees - Struct. Funct.* 25, 1033–1042. doi: 10.1007/s00468-011-0578-2

De la Fuente, B., and Beck, P. S. A. (2018). Invasive species may disrupt protected area networks: insights from the pine wood nematode spread in Portugal. *Forests* 9, 1–15. doi: 10.3390/f9050282

dos Santos, C. S. S., and de Vasconcelos, M. W. (2012). Identification of genes differentially expressed in *Pinus pinaster* and *Pinus pinea* after infection with the pine wood nematode. *Eur. J. Plant Pathol.* 132, 407–418. doi: 10.1007/s10658-011-9886-z

Endara, M. J., and Coley, P. D. (2011). The resource availability hypothesis revisited: a meta-analysis. *Funct. Ecol.* 25, 389–398. doi: 10.1111/j.1365-2435.2010.01803.x

European and Mediterranean Plant Protection Organization [EPPO] (2021). *Bursaphelenchus xylophilus. EPPO Datasheets Pests RECOMM. Regul.* Paris: European and Mediterranean Plant Protection Organization.

Feller, U. (2006). Stomatal opening at elevated temperature: an underestimated regulatory mechanism. *Genet. Plant Physiol.* 32, 19–31.

Filipiak, A. (2015). Pathogenicity of selected isolates of the quarantine pinewood nematode *Bursaphelenchus xylophilus* to Scots pine (*Pinus sylvestris L.*). *J. Plant Prot. Res.* 55, 378–382. doi: 10.1515/jppr-2015-0050

Fonseca, L., Cardoso, J. M. S., Lopes, A., Pestana, M., Abreu, F., Nunes, N., et al. (2012). The pinewood nematode, *Bursaphelenchus xylophilus*, in Madeira Island. *Helminthologia* 49, 96–103. doi: 10.2478/s11687-012-0020-3

Fukuda, K. (1997). Physiological process of the symptom development and resistance mechanism in pine wilt disease. *J. For. Res.* 2, 171–181. doi: 10.1007/BF02348216

Fukuda, K., Utsuzawa, S., and Sakaue, D. (2007). Correlation between acoustic emission, water status and xylem embolism in pine wilt disease. *Tree Physiol.* 27, 969–976. doi: 10.1093/treephys/27.7.969

Futai, K. (2008). “Pine Wilt in Japan: from first incidence to the present,” in *Pine Wilt Disease*, eds B. G. Zhao, K. Futai, J. R. Sutherland, and Y. Takeuchi (Tokyo: Springer Japan), 5–12. doi: 10.1007/978-4-431-75655-2\_2

Futai, K. (2013). Pine wood nematode, *Bursaphelenchus xylophilus*. *Annu. Rev. Phytopathol.* 51, 61–83. doi: 10.1146/annurev-phyto-081211-172910

Gaspar, M. C., Agostinho, B., Fonseca, L., Abrantes, I., de Sousa, H. C., and Braga, M. E. M. (2020). Impact of the pinewood nematode on naturally-emitted volatiles and scCO<sub>2</sub> extracts from *Pinus pinaster* branches: a comparison with *P. pinea*. *J. Supercrit. Fluids* 159:104784. doi: 10.1016/j.supflu.2020.104784

Ichihara, Y., Fukuda, K., and Suzuki, K. (2000). Early symptom development and histological changes associated with migration of *Bursaphelenchus xylophilus* in seedling tissues of *Pinus thunbergii*. *Plant Dis.* 84, 675–680. doi: 10.1094/PDIS.2000.84.6.675

Ikeda, T. (1996). Responses of water-stressed *Pinus thunbergii* to inoculation with avirulent pine wood nematode (*Bursaphelenchus xylophilus*): water relations and xylem histology. *J. For. Res.* 1, 223–226. doi: 10.1007/BF02348329

Institute for Nature Conservation and Forests [ICNF] (2019). *Inventário Florestal Nacional (IFN6)–Principais Resultados – Relatório Sumário*. Lagos: ICNF, 34.

Intergovernmental Panel on Climate Change [IPCC] (2014). *Climate Change 2014: Synthesis Report. Contribution of Working Groups I, II and III to the Fifth Assessment Report of the Intergovernmental Panel on Climate Change* [Core writing team, R.K. Pachauri and L.A. Meyer (eds.)]. Geneva: IPCC.

Jikumaru, S., and Togashi, K. (2000). Temperature effects on the transmission of *Bursaphelenchus xylophilus* (Nemata: aphelenchoididae) by *Monochamus alternatus* (Coleoptera: cerambycidae). *J. Nematol.* 32, 110–116.

Kaneko, S. (1989). Effect of light intensity on the development of pine wilt disease. *Can. J. Bot.* 67, 1861–1864. doi: 10.1139/b89-235

Kanzaki, N., Tanaka, R., and Sahashi, N. (2012). Mortality of shaded pine trees inoculated with virulent and less-virulent isolates of pine wood nematodes. *Environ. Entomol.* 41, 828–832. doi: 10.1603/EN12031

Kassambara, A., and Mundt, F. (2019). *Factoextra: Extract and Visualize the Results of Multivariate Data Analyses. R Package Version 1.0.6.* Available online at: <https://cran.r-project.org/package=factoextra%0A>

Keeley, J. E. (2012). Ecology and evolution of pine life histories. *Ann. For. Sci.* 69, 445–453. doi: 10.1007/s13595-012-0201-8

Kiyohara, T., and Bolla, R. I. (1990). Pathogenic variability among populations of the pinewood nematode, *Bursaphelenchus xylophilus*. *For. Sci.* 36, 1061–1076.

Lamy, J.-B., Delzon, S., Pauline, S. B., Alia, R., Giovanni Giuseppe, V., Cochard, H., et al. (2013). Limited genetic variability and phenotypic plasticity detected for cavitation resistance in a Mediterranean pine. *New Phytol.* 201, 874–886. doi: 10.1111/nph.12556

Mamiya, Y. (1983). Pathology of the pine wilt disease caused by *Bursaphelenchus xylophilus*. *Annu. Rev. Phytopathol.* 21, 201–220. doi: 10.1146/annurev.py.21.090183.001221

Martínez-Vilalta, J., Cochard, H., Mencuccini, M., Sterck, F., Herrero, A., Korhonen, J. F. J., et al. (2009). Hydraulic adjustment of Scots pine across Europe. *New Phytol.* 184, 353–364. doi: 10.1111/j.1469-8137.2009.02954.x

Menéndez-Gutiérrez, M., Alonso, M., Jiménez, E., Toval, G., Mansilla, P., Abelleira, A., et al. (2018). Interspecific variation of constitutive chemical compounds in *Pinus* spp. xylem and susceptibility to pinewood nematode (*Bursaphelenchus xylophilus*). *Eur. J. Plant Pathol.* 150, 939–953. doi: 10.1007/s10658-017-1334-2

Menéndez-Gutiérrez, M., Alonso, M., Toval, G., and Díaz, R. (2017). Variation in pinewood nematode susceptibility among *Pinus pinaster* Ait. provenances from the Iberian Peninsula and France. *Ann. For. Sci.* 74, 1–15. doi: 10.1007/s13595-017-0677-3

Mota, M. M., and Vieira, P. C. (2008a). “Pine wilt disease in Portugal,” in *Pine Wilt Disease*, eds B. G. Zhao, K. Futai, J. R. Sutherland, and Y. Takeuchi (Tokyo: Springer Japan), 33–38. doi: 10.1371/journal.pone.0067377

Mota, M.M., and Vieira, P.C. (2008b). *Pine Wilt Disease: A Worldwide Threat to Forest Ecosystems*. Berlin: Springer.

Mota, M. M., Braasch, H., Bravo, M. A., Penas, A. C., Burgermeister, W., Metge, K., et al. (1999). First report of *Bursaphelenchus xylophilus* in Portugal and in Europe. *Nematology* 1, 727–734. doi: 10.1163/156854199508757

Mota, M. M., Futai, K., and Vieira, P. (2009). “Pine wilt disease and the pinewood nematode, *Bursaphelenchus Xylophilus*,” in *Integrated Management of Fruit Crops Nematodes*, eds A. Ciancio and K. G. Mukerji (Dordrecht: Springer Netherlands), 253–274. doi: 10.1007/978-1-4020-9858-1\_11

Myers, R. F. (1986). Cambium destruction in conifers caused by pinewood nematodes. *J. Nematol.* 18, 398–402.

Nunes da Silva, M., Solla, A., Sampedro, L., Zas, R., and Vasconcelos, M. W. (2015). Susceptibility to the pinewood nematode (PWN) of four pine species involved in potential range expansion across Europe. *Tree Physiol.* 35, 987–999. doi: 10.1093/treephys/tpv046

Ohsawa, M., and Akiba, M. (2014). Possible altitude and temperature limits on pine wilt disease: the reproduction of vector sawyer beetles (*Monochamus alternatus*), survival of causal nematode (*Bursaphelenchus xylophilus*), and occurrence of damage caused by the disease. *Eur. J. For. Res.* 133, 225–233. doi: 10.1007/s10342-013-0742-x

Peñuelas, J., and Filella, L. (1998). Technical focus: visible and near-infrared reflectance techniques for diagnosing plant physiological status. *Trends Plant Sci.* 3, 151–156. doi: 10.1016/S1360-1385(98)01213-8

Pimentel, C., Gonçalves, E., Firmino, P., Calvão, T., Fonseca, L., Abrantes, I., et al. (2017). Differences in constitutive and inducible defences in pine species determining susceptibility to pinewood nematode. *Plant Pathol.* 66, 131–139. doi: 10.1111/ppa.12548

Pimentel, C. S., and Ayres, M. P. (2018). Latitudinal patterns in temperature-dependent growth rates of a forest pathogen. *J. Therm. Biol.* 72, 39–43. doi: 10.1016/j.jtherbio.2017.11.018

Pimentel, C. S., Ayres, M. P., Vallery, E., Young, C., and Streett, D. A. (2014). Geographical variation in seasonality and life history of pine sawyer beetles *Monochamus* spp: its relationship with phoresy by the pinewood nematode *Bursaphelenchus xylophilus*. *Agric. For. Entomol.* 16, 196–206. doi: 10.1111/afe.12049

Proença, D. N., Francisco, R., Santos, C. V., Lopes, A., Fonseca, L., Abrantes, I. M. O., et al. (2010). Diversity of bacteria associated with *bursaphelenchus xylophilus* and other nematodes isolated from *Pinus pinaster* trees with pine wilt disease. *PLoS One* 5:e15191. doi: 10.1371/journal.pone.0015191

R Core Team (2019). *R: A Language and Environment for Statistical Computing*. Vienna: R Foundation for Statistical Computing. Available online at: <https://www.R-project.org/>

Rutherford, T. A., and Webster, J. M. (1987). Distribution of pine wilt disease with respect to temperature in North America, Japan, and Europe. *Can. J. For. Res.* 17, 1050–1059. doi: 10.1139/x87-161

Sikora, E. J., and Malek, R. B. (1991). Influence of temperature on development of pine wilt in scots pine. *J. Nematol.* 23, 188–193.

Silva, H., Anjo, S. I., Manadas, B., Abrantes, I., Fonseca, L., and Cardoso, J. M. S. (2021). Comparative Analysis of *Bursaphelenchus xylophilus* Secretome Under *Pinus pinaster* and *P. pinea* Stimuli. *Front. Plant Sci.* 12:668064. doi: 10.3389/fpls.2021.668064

Skelton, R. P., West, A. G., and Dawson, T. E. (2015). Predicting plant vulnerability to drought in biodiverse regions using functional traits. *Proc. Natl. Acad. Sci. U.S.A.* 112, 5744–5749. doi: 10.1073/pnas.1503376112

Soliman, T., Mourits, M. C. M., van der Werf, W., Hengeveld, G. M., Robinet, C., and Lansink, A. G. J. M. O. (2012). Framework for modelling economic impacts of invasive species, applied to pine wood nematode in Europe. *PLoS One* 7:e45505. doi: 10.1371/journal.pone.0045505

Son, J. A., Matsushita, N., and Hogetsu, T. (2015). Migration of *Bursaphelenchus xylophilus* in cortical and xylem axial resin canals of resistant pines. *For. Pathol.* 45, 246–253. doi: 10.1111/efp.12164

Sukhova, E., and Sukhov, V. (2018). Connection of the photochemical reflectance index (PRI) with the photosystem II quantum yield and nonphotochemical quenching can be dependent on variations of Photosynthetic parameters among investigated plants: a Meta-Analysis. *Remote Sens.* 10:771. doi: 10.3390/rs10050771

Suzuki, K. (2002). Pine wilt disease – a threat to pine forest in Europe. *Dendrobiology* 48, 71–74.

Tapias, R., Climent, J., Pardos, J., and Gil, L. (2004). Life histories of Mediterranean pines. *Plant Ecol.* 171, 53–68. doi: 10.1023/B:VEGE.0000029383.72609.f0

Tóth, A. (2011). *Bursaphelenchus xylophilus*, the pinewood nematode: its significance and a historical review. *Acta Biol. Szeged.* 55, 213–217.

Umebayashi, T., Fukuda, K., Haishi, T., Sotooka, R., Zuhair, S., and Otsuki, K. (2011). The developmental process of xylem embolisms in pine wilt disease monitored by multipoint imaging using compact magnetic resonance imaging. *Plant Physiol.* 156, 943–951. doi: 10.1104/pp.110.170282

Urban, J., Ingwers, M. W., McGuire, M. A., and Teskey, R. O. (2017). Increase in leaf temperature opens stomata and decouples net photosynthesis from stomatal conductance in *Pinus taeda* and *Populus deltoides x nigra*. *J. Exp. Bot.* 68, 1757–1767. doi: 10.1093/jxb/erx052

Vergarechea, M., del Río, M., Gordo, J., Martín, R., Cubero, D., and Calama, R. (2019). Spatio-temporal variation of natural regeneration in *Pinus pinea* and *Pinus pinaster* Mediterranean forests in Spain. *Eur. J. For. Res.* 138, 313–326. doi: 10.1007/s10342-019-01172-8

Vicente, C., Espada, M., Vieira, P., and Mota, M. (2012). Pine wilt disease: a threat to European forestry. *Eur. J. Plant Pathol.* 133, 89–99. doi: 10.1007/s10658-011-9924-x

Villacorta, P. J. (2015). *ART: Aligned Rank Transform for Nonparametric Factorial Analysis. R Package Version 1.0*. Available online at: <https://cran.r-project.org/package=ART>

Wang, F. (2014). Pine wilt in meteorological hazard environments. *Nat. Hazards* 72, 723–741. doi: 10.1007/s11069-014-1032-8

Whitehead, A. G., and Hemming, J. R. (1965). A comparison of some quantitative methods of extracting small vermiform nematodes from soil. *Ann. Appl. Biol.* 55, 25–38. doi: 10.1111/j.1744-7348.1965.tb07864.x

Wong, C. Y. S., and Gamon, J. A. (2015). The photochemical reflectance index provides an optical indicator of spring photosynthetic activation in evergreen conifers. *New Phytol.* 206, 196–208. doi: 10.1111/nph.13251

Woo, K.-S., Lee, D.-H., Koo, Y.-B., and Yeo, J.-K. (2008). Inoculation of seven pine species or hybrid seedlings with Korean isolates of pinewood nematode under greenhouse conditions. *Ann. For. Sci.* 65:811. doi: 10.1051/forest:2008072

Woo, S.-Y., Lee, S., Han, H., and Baek, S. (2010). Comparison in disease development and gas exchange rate of *Pinus densiflora* seedlings artificially inoculated with *Bursaphelenchus xylophilus* and *B. mucronatus*. *For. Sci. Technol.* 6, 110–117. doi: 10.1080/21580103.2010.9671978

Yazaki, K., Takanashi, T., Kanzaki, N., Komatsu, M., Levia, D. F., Kabeya, D., et al. (2018). Pine wilt disease causes cavitation around the resin canals and irrecoverable xylem conduit dysfunction. *J. Exp. Bot.* 69, 589–602. doi: 10.1093/jxb/erx417

Zas, R., Moreira, X., Ramos, M., Lima, M. R. M., Nunes da Silva, M., Solla, A., et al. (2015). Intraspecific variation of anatomical and chemical defensive traits in maritime pine (*Pinus pinaster*) as factors in susceptibility to the pinewood nematode (*Bursaphelenchus xylophilus*). *Trees* 29, 663–673. doi: 10.1007/s00468-014-1143-6

**Conflict of Interest:** FC was employed by company Infarm.

The remaining authors declare that the research was conducted in the absence of any commercial or financial relationships that could be construed as a potential conflict of interest.

**Publisher's Note:** All claims expressed in this article are solely those of the authors and do not necessarily represent those of their affiliated organizations, or those of the publisher, the editors and the reviewers. Any product that may be evaluated in this article, or claim that may be made by its manufacturer, is not guaranteed or endorsed by the publisher.

*Copyright © 2022 Estorninho, Chozas, Mendes, Colwell, Abrantes, Fonseca, Fernandes, Costa, Máguas, Correia and Antunes. This is an open-access article distributed under the terms of the Creative Commons Attribution License (CC BY). The use, distribution or reproduction in other forums is permitted, provided the original author(s) and the copyright owner(s) are credited and that the original publication in this journal is cited, in accordance with accepted academic practice. No use, distribution or reproduction is permitted which does not comply with these terms.*

ORIGINAL RESEARCH

published: 18 March 2022

doi: 10.3389/fpls.2022.856109



# Rapid On-Site Detection of the *Bursaphelenchus xylophilus* Using Recombinase Polymerase Amplification Combined With Lateral Flow Dipstick That Eliminates Interference From Primer-Dependent Artifacts

**Qinzheng Zhou, Ya Liu, Zheng Wang, Huimin Wang, Xingyao Zhang and Quan Lu\***

*Key Laboratory of Forest Protection of National Forestry and Grassland Administration, Research Institute of Forest Ecology, Environment and Nature Conservation, Chinese Academy of Forestry, Beijing, China*

**Edited by:**

Anna Filipiak, Institute of Plant Protection – National Research Institute, Poland

**Reviewed by:**

Lee Robertson, National Institute of Agricultural and Food Research and Technology, Spain  
Ju-Yeon Yoon, Jeonbuk National University, South Korea

**\*Correspondence:** Quan Lu, [luquan@caf.ac.cn](mailto:luquan@caf.ac.cn)

**Specialty section:** This article was submitted to Plant Pathogen Interactions, a section of the journal *Frontiers in Plant Science*

**Received:** 16 January 2022

**Accepted:** 17 February 2022

**Published:** 18 March 2022

**Citation:** Zhou Q, Liu Y, Wang Z, Wang H, Zhang X and Lu Q (2022) Rapid On-Site Detection of the *Bursaphelenchus xylophilus* Using Recombinase Polymerase Amplification Combined

The pine wood nematode (PWN), *Bursaphelenchus xylophilus*, is one of the most lethal nematode species, which causes pine wilt disease (PWD), a devastating forest disease. To date, no effective methods have been developed to control the disease; hence, rapid precise detection of *B. xylophilus* is of great significance. Traditional molecular diagnostic methods are time-consuming and require sophisticated instruments or skilled operators, which are unavailable in resource-limited settings. A specific, sensitive, and field-applicable diagnostic method is urgently needed. In this study, we developed a diagnostic method using recombinase polymerase amplification combined with lateral flow dipstick (RPA-LFD) for the rapid on-site detection of *B. xylophilus*. The false-positive signals from primer-dependent artifacts were eliminated using a probe, and base substitutions were included in the primer and probe. The entire detection process for the RPA-LFD assay can be completed under 38°C within approximately 30 min, including 15 min for crude nematode genomic DNA (gDNA) extraction and master mix preparation, 15 min for the RPA-LFD assay. This assay displayed high specificity toward *B. xylophilus* and showed no cross-reactions with closely related species, including *Bursaphelenchus mucronatus* and *Bursaphelenchus douei*. The sensitivity of this assay had a detection limit as low as 1 pg of *B. xylophilus* purified genomic DNA. Furthermore, the application of the RPA-LFD assay in simulated spiked pinewood samples showed accurate detection results. The RPA-LFD assay in this study successfully detected *B. xylophilus* in less than 30 min, providing a novel alternative for the simple, sensitive, and specific detection of *B. xylophilus* and showed potential for *B. xylophilus* point-of-care testing (POCT) in resource-limited areas or in field.

**Keywords:** pine wilt disease, rapid diagnostic, recombinase polymerase amplification, lateral flow dipstick, *Bursaphelenchus xylophilus*, POCT, false positive

# INTRODUCTION

Pine wilt disease (PWD) is a devastating forest disease caused by the pine wood nematode (PWN) (Mota and Vieira, 2008). The spread of PWNs is mainly caused by increased global trade. As PWD is regarded as an “incurable disease,” rapid and accurate detection, quarantine, and monitoring can manage disease spread (Futai, 2013; Yazaki et al., 2018; Kim et al., 2020). Therefore, the primary task in PWD control is to accurately detect PWN.

Various *Bursaphelenchus xylophilus* diagnostic methods have been developed, including morphological methods using microscopic observations and molecular diagnostic methods using diverse molecular markers (Inácio et al., 2015; Lee et al., 2021). However, due to the similar morphological characteristics of *B. xylophilus* and its closely related species, *Bursaphelenchus mucronatus*, accurately identifying *B. xylophilus* requires specialized knowledge and professional skills (Gu et al., 2011; Gu and Wang, 2011; Wang et al., 2012; Gu, 2014; Li et al., 2021). Furthermore, molecular methods require sophisticated equipment and are not suitable for implementation in the field, causing delayed detection and response to PWD pandemics (Sultana et al., 2013). Therefore, a specific, sensitive, and field-applicable diagnostic method is needed to improve the efficiency of *B. xylophilus* detection and quarantine.

Alternatively, isothermal DNA amplification techniques that do not require the use of thermal cycling apparatus have been applied to detect *B. xylophilus*. These include loop-mediated isothermal amplification (LAMP) (Kikuchi et al., 2009; Meng et al., 2018; Ahuja and Somvanshi, 2021), denaturation bubble-mediated strand exchange amplification (SEA) (Liu C. et al., 2019), and recombinase polymerase amplification (RPA) (Cha et al., 2019, 2020; Fang et al., 2021). RPA, an isothermal nucleic acid amplification method that has attracted much attention because it is sensitive, rapid, works at isothermal temperature (Piepenburg et al., 2006; Glökler et al., 2021). In addition, RPA assays have been developed to detect some plant-parasitic and animal-parasitic nematodes, including *B. xylophilus* (Cha et al., 2019, 2020), *Meloidogyne enterolobii* (Subbotin, 2019), *Meloidogyne* spp. (*M. incognita*, *M. arenaria*, *M. javanica*, and *M. enterolobii*) (Ju et al., 2019), *Meloidogyne javanica* (Chi et al., 2020), *Meloidogyne hapla* (Song et al., 2020; Subbotin

and Burbridge, 2021), *Angiostrongylus cantonensis* (Jarvi et al., 2021), and *Trichinella* spp. (Li et al., 2019).

Recombinase polymerase amplification amplicons can be visualized using lateral flow dipstick (LFD), with results could be directly interpreted by the naked eye within a few minutes (Daher et al., 2016). LFDs are products based on lateral flow technology using gold nanoparticles and can promptly detect amplification products making results easy to interpret (Qi et al., 2018).

The LFD assay requires a special nfo probe with a fluorescein amidites (FAM) (carboxyfluorescein) antigen label at the 5'-end, a tetrahydrofuran (THF) spacer (abasic site) in the middle, a C3 spacer (amplification blocker) at the 3'-end, and reverse primer labeled with biotin at the 5'-end. RPA amplicons are amplified using two primers and a probe, which contains both biotin and FAM, and the mouse anti-FAM antibody is enveloped with AuNPs. After reaction mixture is added to the sample well, they are driven by capillary force to move across the conjugate pad and bind to the anti-FAM AuNPs. The test line, which is enveloped with streptavidin, captures molecules with a biotin label when the amplification products go through. The control line, which is used to validate LFD detection, only captures the anti-FAM antibody enveloped with AuNPs because the anti-FAM antibody is from a mouse (Figure 1; Dai et al., 2019; Miao et al., 2019).

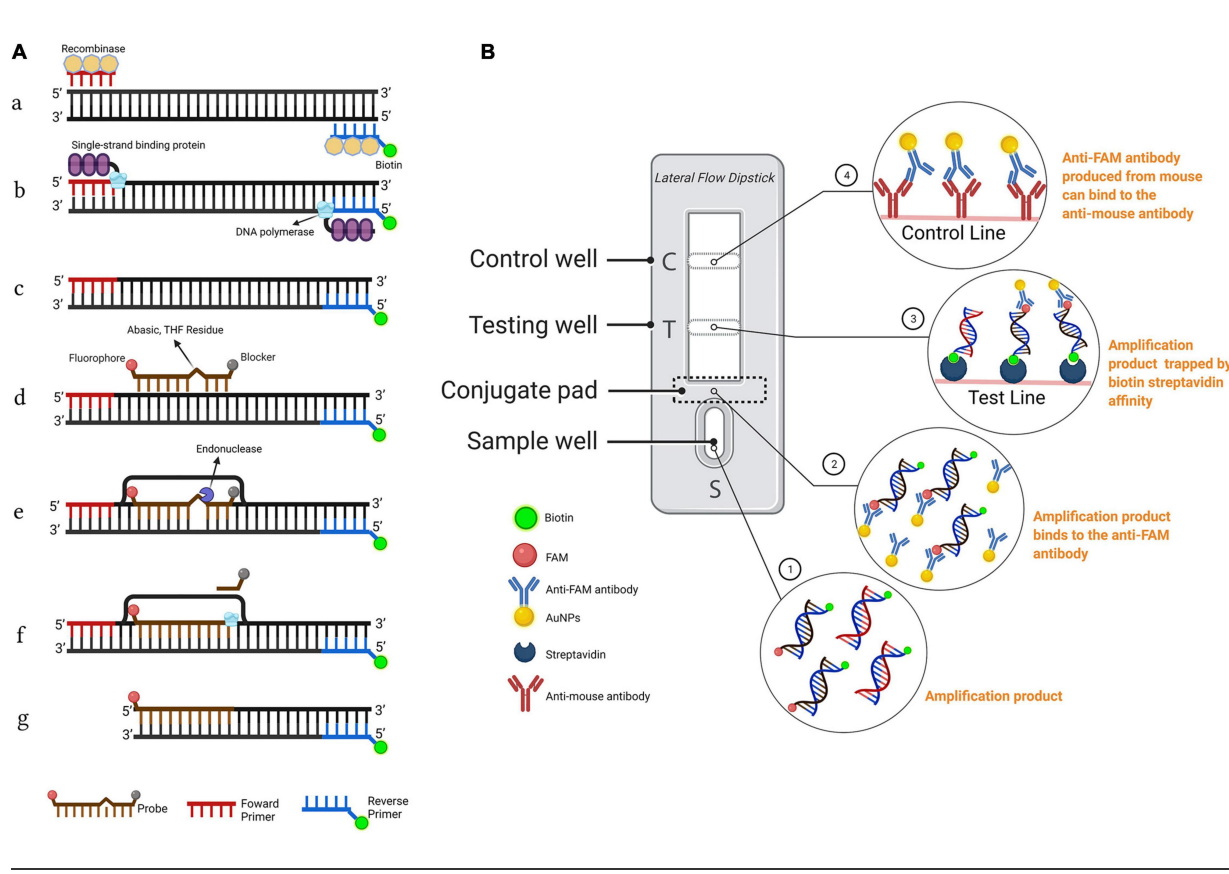


**FIGURE 1.** Schematic representation of the recombinase polymerase amplification combined with lateral flow dipstick (RPA-LFD) assay. **(A)** Principle of RPA. DNA strands are represented by horizontal lines, and base pairings are represented by short vertical lines between DNA strands. The forward primer (F), reverse primer (R), probe (P), nfo, single strand DNA-binding protein (SSB), polymerase, recombinase, fluorophore, blocker, and tetrahydrofuran (THF) residue are shown by various color and forms and text annotation. Created with BioRender.com. **(B)** Schematic representation of the lateral flow dipstick working principle. Lateral flow dipstick was painted after real ones. The segment names are displayed on the left of the dipstick drawing. The direction of liquid migration is from the sample well, through the conjugate pad, to the test and control wells. The coating material on each segment of the dipstick is shown in the image to the right. Molecules and their symbolic shape are displayed in the lower-left corner. Dipstick created with BioRender.com.

It should be noted that false-positive signals from the self-linked primer–probe complex should be considered a vital inherent defect of the RPA-LFD assay (Wu et al., 2020). Without the temperature cycles in PCR-based methods, primer combination in RPA is performed at ambient temperature, which does not provide an opportunity for dissociation if mispairing occurs and may generate a false-positive signal. In addition, LFD could not differentiate the size of the amplification product that releases signal.

Furthermore, the RPA-LFD assay is overly sensitive; thus, interference from false-positive signals due to primer-dependent artifacts must be avoided (Poritz and Ririe, 2014; Wang et al., 2020).

In this study, we developed a simple, rapid, specific, and sensitive RPA-LFD assay to detect *B. xylophilus*. This method eliminated false-positive signals from non-specific primer–probe complexes due to an elaborate design and strict screening of primers and probe, as well as by bringing in base substitutions on the reverse primer and probe. The specificity and sensitivity of the assay were also investigated. The practicability was also analyzed by detecting *B. xylophilus* in spiked pine wood samples.

## MATERIALS AND METHODS

### Specimen Collection and DNA Extraction

*Bursaphelenchus xylophilus*, *B. mucronatus*, and *Bursaphelenchus doui* were provided by the Key Laboratory of Forest Protection of National Forestry and Grassland Administration, Chinese Academy of Forestry, China. A total of 17 nematode isolates representing three *Bursaphelenchus* species, collected from multiple sites in China, were used in this study (Table 1). Nematode isolates were reared on *Botrytis cinerea* mycelia cultured on potato dextrose agar (PDA) plates at 25°C for 5–7 days and were identified using morphological methods and molecular diagnostic methods. Nematodes were then separated using the Baermann funnel technique (Viglierchio and Schmitt, 1983), and 500 µl of nematodes were collected in a 1.5 ml Eppendorf tube after being washed three times in sterilized water and stored at 4°C for future use.

**TABLE 1.** Nematode species used in *B. xylophilus* recombinase polymerase amplification combined with lateral flow dipstick (RPA-LFD) detection assay.

Species	Isolate	Host	Origin
<i>Bursaphelenchus xylophilus</i>	Bx-HS	<i>Pinus massoniana</i>	Huangshan, Jiangsu
	Bx-LY	<i>P. massoniana</i>	Liyang, Jiangsu
	Bx-CD9	<i>P. thunbergii</i>	Changdao, Yantai
	Bx-ZJ	<i>P. massoniana</i>	Fuyang, Zhejiang
	Bx-HZ	<i>P. massoniana</i>	Hangzhou, Zhejiang
	Bx-NB	<i>P. massoniana</i>	Ningbo, Zhejiang
	Bx-AMA3	<i>P. hwangshanensis</i>	Maanshan, Anhui
	Bx-YW4	<i>P. massoniana</i>	Kunming, Yunnan
<i>Bursaphelenchus mucronatus</i>	Bm-DB	<i>P. sylvestris</i> var. <i>mongolica</i>	Jiagedaqi, Heilongjiang
	Bm-NB	<i>P. massoniana</i>	Ningbo, Zhejiang
	Bm-BM7	<i>P. massoniana</i>	Wuhu, Anhui
	Bm-BM9	<i>P. massoniana</i>	Zigong, Sichuan
	Bm-JHL10	<i>P. elliottii</i>	Nanjing, Jiangsu
<i>Bursaphelenchus doui</i>	Bd-NJ	<i>P. massoniana</i>	Nanjing, Jiangsu
	Bd-CQ	<i>P. massoniana</i>	Yunyang, Chongqing
	Bd-ZG1	<i>P. elliottii</i>	Zigong, Sichuan
	Bd-ZG4	<i>P. elliottii</i>	Zigong, Sichuan

Genomic DNA (gDNA) was extracted from approximately 500 nematodes of each nematode species (*B. xylophilus*, *B. mucronatus*, and *B. doui*) using the TIANamp Genomic DNA Kit [Tiangen Biotech (Beijing) Co. Ltd., Beijing, China] according to the manufacturer's instructions. The DNA concentration and purity were quantified using a NanoDrop2000 spectrophotometer (Thermo Fisher Scientific, Waltham, MA, United States). The DNA was diluted to 10 ng/μl with distilled water and stored at –20°C for future use.

## Designing of Recombinase Polymerase Amplification Primers

To design specific primers for RPA, the previously identified conserved gene encoding synaptic guidepost protein (SYG-2), was selected as the target segment (Gou, 2014; Meng et al., 2018). The syg-2 gene part sequences were amplified using PCR primer pairs syg2-part-f/syg2-part-r, and the PCR cycle conditions were set as described by Gou (2014). The PCR products (25  $\mu$ l) were electrophoresed on a 2% agarose gel, and the amplified products were recovered using a PCR Cleaning Kit [Tiangen Biotech (Beijing) Co., Ltd., Beijing, China] and sequenced [Sangon Biotech (Shanghai) Co. Ltd., Shanghai, China], and the sequences were aligned using the ClustalW program implemented in MEGA version 7.0.14. RPA-basic assays require forward and reverse primers; accordingly, the RPA primers were designed using Primer Premier 5.0 (Premier Biosoft, Palo Alto, CA, United States) according to the TwistDx instruction manual (Cambridge, United Kingdom). RPA primer length was 30–36 bp, the primer GC content was 30–70%, and the amplicon length was between 150 and 300 bp.

### **Recombinase Polymerase Amplification Procedure and Electrophoresis**

The Basic RPA 50- $\mu$ l reaction volume was prepared according to the instructions for the RPA-basic kit (#WLN8201KIT; AMP-Future Biotech Co. Ltd., Weifang, China). It consisted of 29.4  $\mu$ l rehydration buffer, 2  $\mu$ l forward primer, 2  $\mu$ l reverse primer (primer concentration, 10  $\mu$ M), one lyophilized enzyme pellet, 1  $\mu$ l DNA template, and 13.1  $\mu$ l nuclease-free water; the reaction was initiated by adding 2.5  $\mu$ l magnesium acetate. After incubation at 38°C for 30 min, amplicons were purified using spin columns before electrophoresis on 1.5% agarose gels.

### **Probe Designing**

The probes were designed using Primer Premier 5.0 software (Premier Biosoft). The size of the probe was set as 46–53 nt, GC content was 20–80%, and  $T_m$  set as 50–80°C. Maximum hairpin and primer dimer parameters were set at  $\leq 4$  bonds near 3'-end. Other settings were set as default. Following design, primers and probes were assessed using the OligoAnalyzer Tool (IDT) and screened depending on their binding score for continuous base pairings between the probe and reverse primer. The RPA primers and nfo probe were synthesized and provided by Sangon Biotech (Shanghai) Co. Ltd.

## **Recombinase Polymerase Amplification-Lateral Flow Dipstick Procedure**

Recombinase polymerase amplification-lateral flow dipstick assays were carried out in a 50  $\mu$ l reaction volume using the RPA nfo kit (#WLN8203KIT: AMP-Future Biotech Co. Ltd.) according to the manufacturer's instructions. The reaction mixture comprised 29.4  $\mu$ l rehydration buffer, 2.5  $\mu$ l magnesium acetate, 2  $\mu$ l each primer pair (10  $\mu$ M), 0.6  $\mu$ l nfo probe (10  $\mu$ M), 12.5  $\mu$ l nuclease-free water, and 1.0  $\mu$ l DNA template. All reagents except the DNA template and magnesium acetate were prepared in a master mix, which was subsequently dispensed into reaction tubes containing a dried enzyme pellet provided with the kit. After adding 1  $\mu$ l of the nucleic acid template to the tubes and pipetting 2.5  $\mu$ l of magnesium acetate into the tube lids, the lids were closed carefully, and the tubes were inverted several times and briefly centrifuged at 6,000 rpm for 30 s.

Post-amplification results were visually interpreted using Hybridetect LFD (kit #WLFS8201; AMP-Future Biotech Co. Ltd.). Thereafter, 10  $\mu$ l of reaction solution was added to a centrifuge tube containing 190  $\mu$ l ddH<sub>2</sub>O, after which 50  $\mu$ l diluted solution was pipetted onto the LFD sample well and incubated for 3–5 min at ambient temperature. If both test and control line are visible, it is positive; if only the control line is visible, it is negative; and if the control line is not visible, it is invalid. A repeat test would then be conducted using a new dipstick in an invalid situation.

## **Introduction of Base Substitutions to Probe and Reverse Primer**

Recombinase polymerase amplification can tolerate several base mispairings in primers without noticeably influencing accuracy (Daher et al., 2015; Liu X. et al., 2019). Therefore, base substitutions were introduced into the probe and reverse primer according to previous research (Wu et al., 2020). The probe and primer with base substitution were evaluated for false-positive signals using no template control (NTC).

## **Optimization of Recombinase Polymerase Amplification-Lateral Flow Dipstick Assays**

To investigate the optimal conditions of the RPA-LFD assay, different reaction temperatures (15, 20, 25, 30, 35, 40, and 45°C) and reaction times (5, 10, 15, 20, 25, 30, and 35 min) were assessed. For determination of optimal reaction

temperature, all treatments were reacted for 30 min. After the reaction, tubes were immediately put on ice to stop the reaction.

### **Specificity of Recombinase Polymerase Amplification-Lateral Flow Dipstick Assay**

To investigate the specificity of the assay, nematode genomic DNA was prepared from 17 nematode isolates, including eight *B. xylophilus*, five *B. mucronatus*, and four *B. doui* isolates, were used as DNA templates, as described above. Specificity tests were repeated three times.

### **Analysis of Recombinase Polymerase Amplification-Lateral Flow Dipstick Assay Sensitivity**

The sensitivity of the RPA assay was investigated using the RPA nfo kit by testing a 10-fold serial dilution of gDNA extracted from *B. xylophilus*. Genomic DNA extracted from *B. xylophilus* was diluted into seven concentrations with sterile distilled water, including  $10, 1, 10^{-1}, 10^{-2}, 10^{-3}, 10^{-4}$ , and  $10^{-5}$  ng, respectively. Each dilution and sterile distilled water as the NTC, were used as templates in the RPA-LFD assay, respectively, as described previously. The sensitivity tests were repeated thrice.

### **Preparation of Pinewood Spiked Sample for Recombinase Polymerase Amplification-Lateral Flow Dipstick Evaluation**

To investigate the interference from the DAP buffer or pine wood, which includes humic acid, ethanol, polysaccharides, and polyphenols (Cha et al., 2019). Pine wood chips (100 mg) from healthy pine trees were placed in a 2 ml tube filled with 1 ml DAP buffer (20 mM sodium hydroxide, 5% polyethylene glycol 200, and 5% dimethyl sulfoxide) (Cha et al., 2019), and 10 ng of pure gDNA of different *B. xylophilus* or *Bursaphelenchus* spp. isolates was spiked into the lysates. The tubes were then vibrantly mixed and incubated at ambient temperature for 10 min. Subsequently, 2.5  $\mu$ l of lysate solution was used as the RPA template (the final concentration of gDNA was 25 pg in each RPA reaction).

## **RESULTS**

### **Primer Design and Screening**

Using Primer Premier 5.0, six potential primer pairs were obtained (Table 2). They were screened using basic RPA (Figure 2). The image showed amplification of the syg-2 (synaptic guidepost protein) target fragments, which have a typical ladder pattern, comprised multimers of the amplicon-sized monomer, probably because the protocadherin gene family which syg-2 belongs to is arrayed in tandem on the chromosome (Figure 2; Yamagata et al., 2003). However, five of them showed primer dimer bands under specific amplification bands. Primer pair S1F/R amplified specific products and showed no obvious primer-dimer (Figure 2). In order to use LFD to interpret results, the reverse primer was labeled at the 5'-end with biotin.

**TABLE 2.** Sequences of the primers and probes used in *B. xylophilus* recombinase polymerase amplification (RPA) assay.

Assay	Primer/ Probe	Sequences 5'-3'	Length (bp)	Amplicon size (bp)
Basic RPA	S1F	TCTTAAGTCAGCAAATGA ATAAATTAGGAGGAATC	36	194
	S1R	ATAGGCAGCAGAAGTTA GACAATCGGGAAT	30	
	S2F	TCTTAAGTCAGCAAATGA ATAAATTAGGAGGAATC	36	208
	S2R	CGGAAAATACAAAAATA GGCAGCAGAAGTTAGA	33	
	S3F	TCTTAAGTCAGCAAATGA ATAAATTAGGAGGAATC	36	209
	S3R	TCGGAAAATACAAAAATA GGCAGCAGAAGTT	31	
	S4F	ATTCTTAAGTCAGCAAAT GAAATAATTAGGAGGAA	36	210
	S4R	CGGAAAATACAAAAATAG GCAGCAGAAGTTAGA	33	
	S5F	ATTCTTAAGTCAGCAAAT TGAAATAATTAGGAGGAA	36	211
	S5R	TCGGAAAATACAAAAATA GGCAGCAGAAGTT	31	
RPA-LFD	S6F	CTGTCAAGCAAATGAAATAA TTAGGAGGAATCCAATT	36	203
	S6R	CGGAAAATACAAAAATAG GCAGCAGAAGTTAGA	33	
	S1R-nfo	[Biotin]ATAGGCAGCAGAAGT TAGACAATCGGGAAT	36	138
	S1-nfo-P	[FAM]GTATATTCTATAATAGA TTGTAAACACCGT[THF]TA AAGGAATTAGTTT[C3 Spacer]	45	
Modified RPA-LFD	mS1R- nfo	[Biotin]ATAGGCAGCAGAAG TAAGACAATCGGGAAT	36	138
	mS1-nfo- P	[FAM]GTATATTCTATAATAGAG TTGTAAACACCGT[THF]GATA GGAATTAGTTT[C3 Spacer]	30	

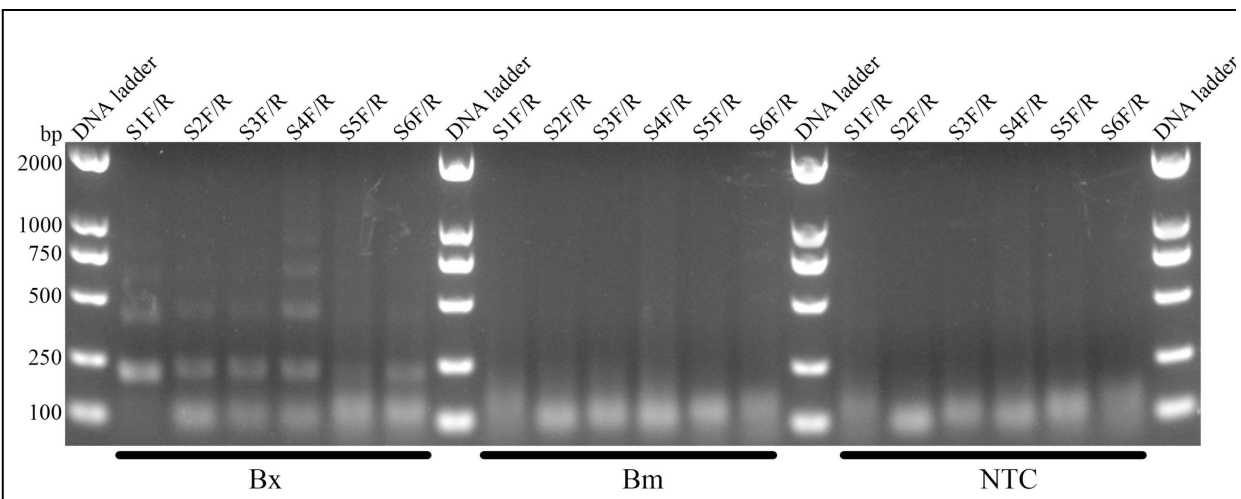
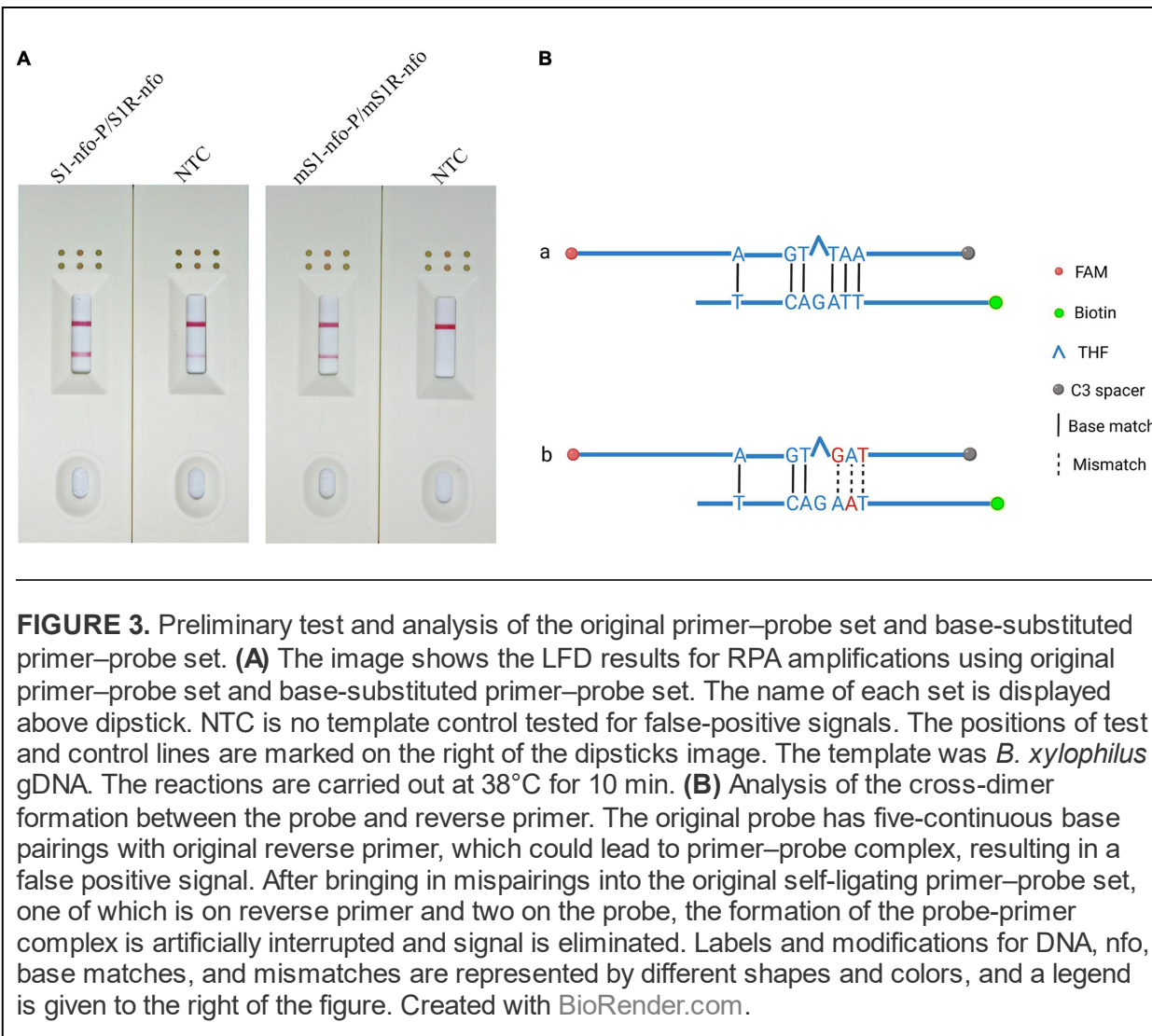


**FIGURE 2.** Screening of primer pairs by Basic-RPA. The image shows amplification bands targeting the *syg-2* gene. The primer name is shown above each lane. The following Bx, Bm, and NTC lanes are *B. xylophilus*, *B. mucronatus* genomic DNA, and no template controls for corresponding primer pairs, respectively. Band sizes for DNA ladders are shown on the left.

## **Addition of a Probe Into the Recombinase Polymerase Amplification Reaction**

The nfo probe (S1-nfo-P) was between the forward and reverse primers and comprised of an oligonucleotide with a 5'-FAM as antigenic label and a 3'-C3 spacer that could block extension. An THF spacer (tetrahydrofuran) was placed on the probe to replace a guanine. The nfo enzyme activated after bases flanking THF matching with complementary bases and would cut THF site, removing probe 3'-end blocker for extension (Figure 1A). The specific RPA primers, nfo probe, and their sequences are listed in Table 2.

For the newly added probe, the RPA-LFD assay was carried out to evaluate the amplification signal and false-positive signal. The amplification signal was evident for primer-probe set S1R-nfo/S1-nfo-P; however, the false-positive signal also existed for NTC (Figure 3A). Cross dimer analysis showed that there was still a continuous base match between the probe and primer. Furthermore, the matched bases were located on two sides of THF site, facilitating the nfo enzyme cutting activity (Figure 3B).



### Elimination of False-Positive Signals With Base Mismatches

The results showed that false-positive signal was eliminated by bringing mispairings on probe and reverse primer (mS1-nfo-P/mS1R-nfo) (Figures 3A,B, substituted bases in red). The sequences of the modified probe (mS1-nfo-P) and reverse primer (mS1R-nfo) are listed in Table 2. These base substitutions did not influence amplification accuracy and efficiency by observing band color density (Figure 3A). Therefore, this primer and probe were used for the following RPA-LFD reactions in this study.

### Optimization of Recombinase Polymerase Amplification-Lateral Flow Dipstick Assay for *Bursaphelenchus xylophilus* Detection

The RPA-LFD assays were tested at temperature range from 15 to 45°C at 5°C intervals for 30 min. Results showed that test lines were visible from 20 to 45°C, color density of the test line did not increase noticeably from 35 to 45°C. Therefore, 38°C was selected as the optimal temperature (Figure 4A). Moreover, the RPA-LFD reaction time was tested from 5 to 35 min at 5 min intervals at 38°C. Results showed that test lines were visible when the reaction time was 10–35 min; therefore, 10 min was selected as the optimal time for the RPA-LFD assay of *B. xylophilus* detection considering rapid diagnostics (Figure 4B).

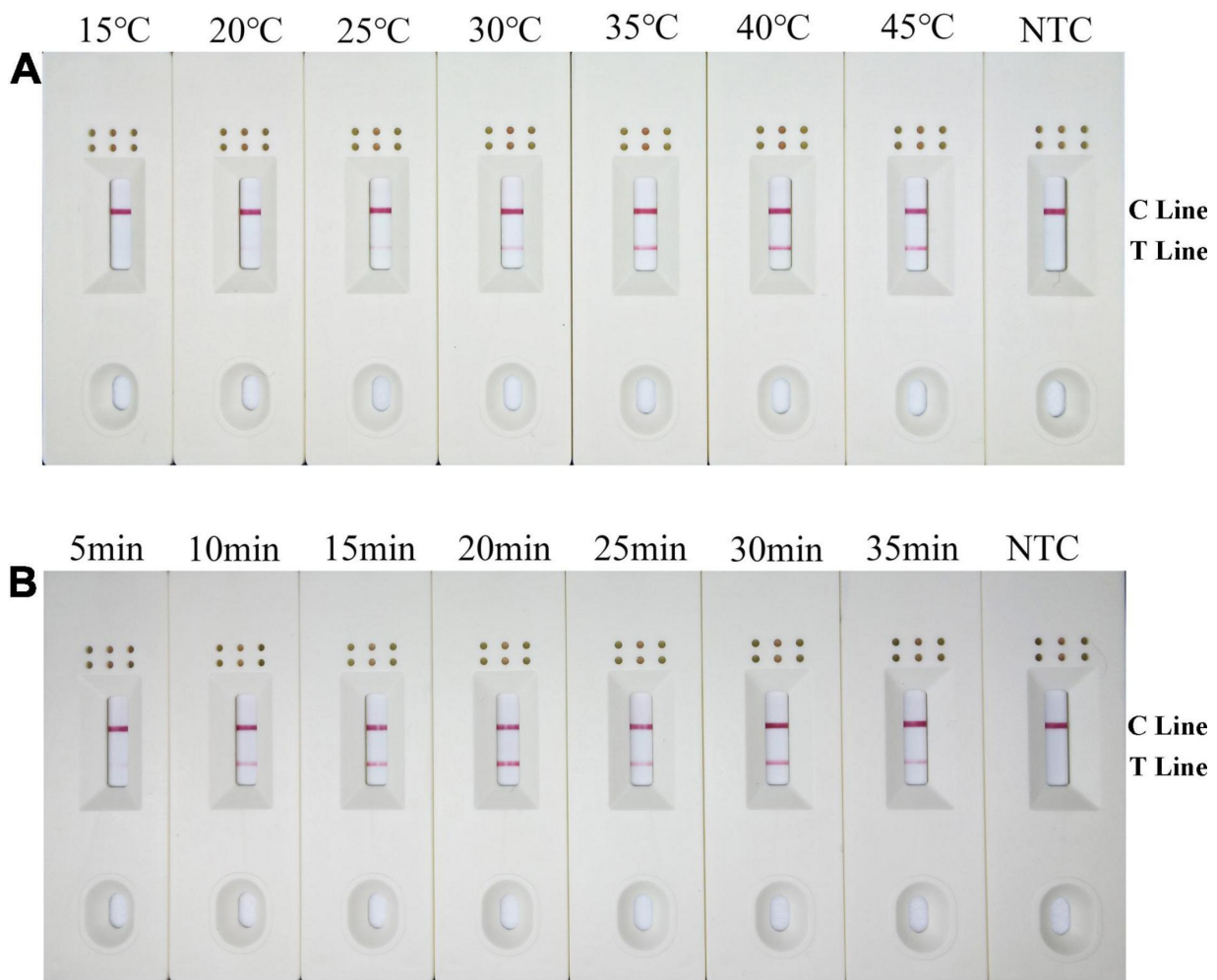


**FIGURE 4.** Optimization of the modified primer–probe set in RPA–LFD assay. **(A)** Optimal reaction temperature of the RPA–LFD assay. The figure shows the LFD results of RPA amplification at different temperatures. The temperature is displayed at the top of each dipstick. The amplification template is *B. xylophilus* gDNA. The NTC band is no template control carried out at 38°C. The positions of the control and test lines are shown on the right side of the dipstick. **(B)** Optimal reaction time of the RPA–LFD assay. The image shows the LFD results of RPA amplifications with different times. The time to perform the RPA reaction is displayed at the top of each dipstick. The amplification template is *B. xylophilus* gDNA. NTC dipsticks are performed for 10 min without template. The positions of the control and test lines are shown on the right side of the dipstick.

## Analytical Specificity of Recombinase Polymerase Amplification-Lateral Flow Dipstick Assay

To assess the RPA-LFD analytical specificity, gDNA was prepared using several nematode species, including eight *B. xylophilus*, five *B. mucronatus*,

and four *B. doui* isolates (Table 1). Only when *B. xylophilus* gDNA as DNA template can produce red test lines on dipsticks, indicating positive results. When other nematode species gDNA or NTC as DNA template, no red test lines were seen on dipsticks (Figure 5), indicating that this primer–probe combination had good specificity toward *B. xylophilus* and had no cross-reactions with other nematode species.

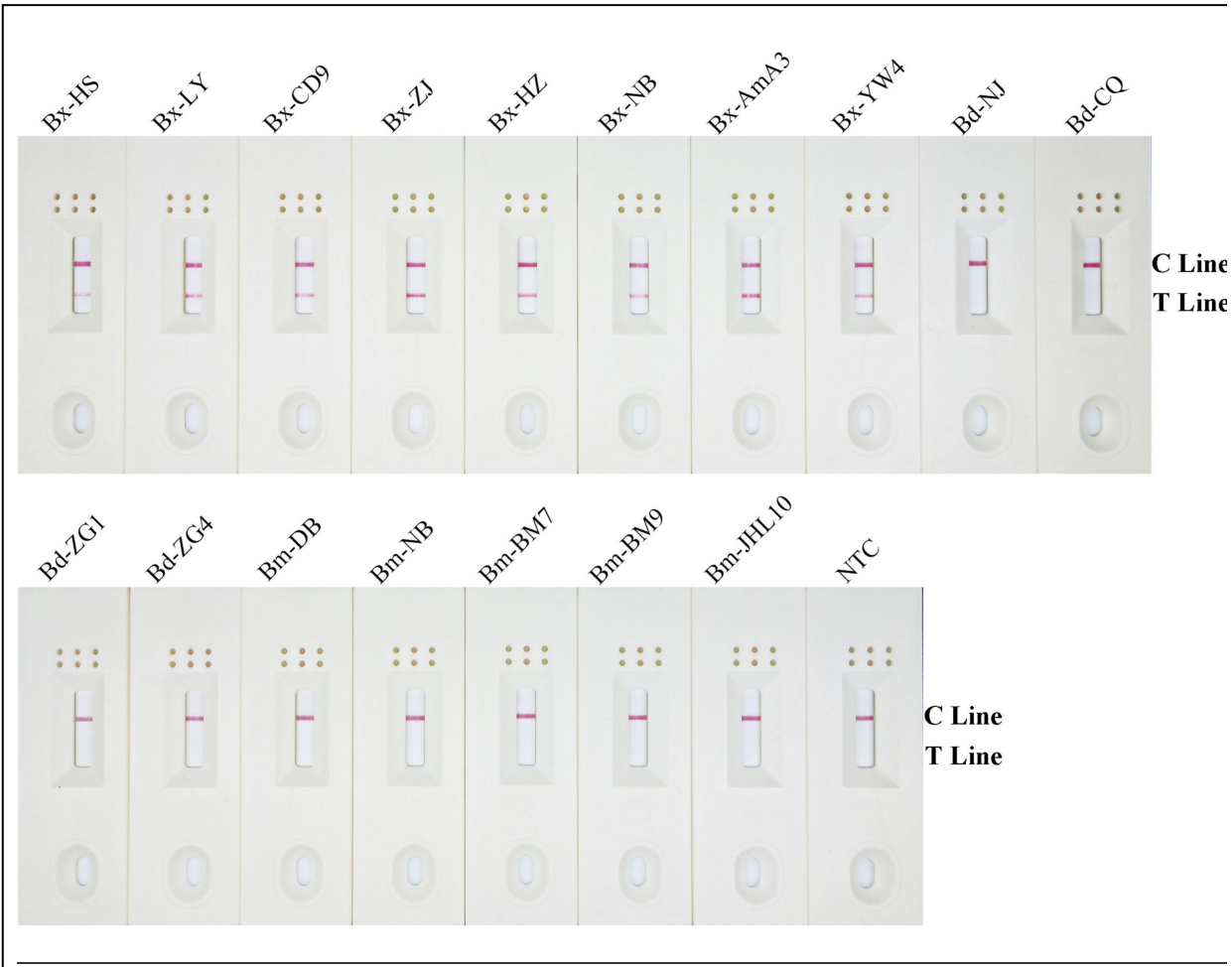


**FIGURE 5.** Detection specificity of the modified primer–probe set in RPA–LFD assay. Specificity determination of RPA-LFD using different nematode isolates gDNA templates. The isolate of nematode is marked above each dipstick. The NTC dipstick is no template control. The positions of test and control lines are shown on the right side of dipstick. Reactions are carried out at 38°C for 10 min.

## Detection Limit of Recombinase Polymerase Amplification-Lateral Flow Dipstick Assay

Results showed that the LFD test and control lines were displayed from 10 to  $10^{-3}$  ng gDNA. Furthermore, the red color of the test line lightened with

decreasing *B. xylophilus* concentrations, and *B. xylophilus* gDNA as low as 1 pg ( $10^{-3}$  ng) could be detected (Figure 6). Therefore, the detection limit of the RPA-LFD assay for *B. xylophilus* was 1 pg of gDNA.

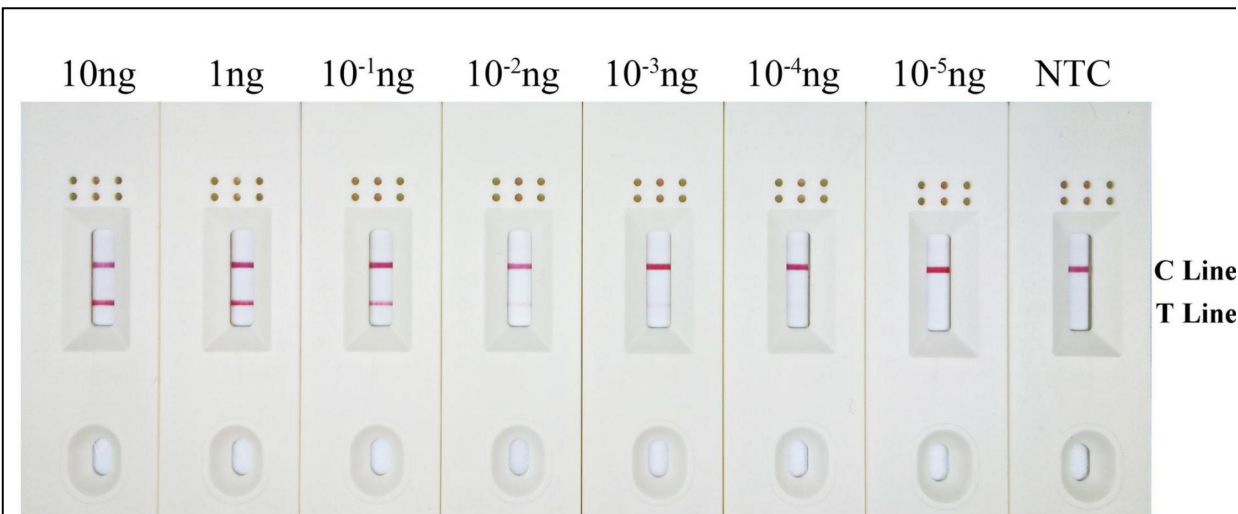


**FIGURE 6.** Detection limit of the RPA–LFD assay. The image shows the LFD results of RPA amplification with different concentrations of *B. xylophilus* gDNA. The DNA concentration used as template is shown above each dipstick. NTC is the no template control. The reactions are carried out at 38°C for 10 min. Test line and control lines are shown on the right side of dipstick.

### Application Simulation of the Recombinase Polymerase Amplification-Lateral Flow Dipstick Test for *Bursaphelenchus xylophilus* Detection

Using an application simulation, the RPA-LFD test was applied for *B. xylophilus* detection using artificially spiked pine wood samples. Thirteen healthy pine wood samples were prepared, of which eight were artificially spiked with *B. xylophilus* gDNA, two with *B. mucronatus* gDNA, another two with *B. doui* gDNA, and one with sterilized distilled water as NTC. The results of the RPA-LFD assay were consistent with those of the spiked gDNA species and all eight *B. xylophilus* gDNA spiked pine wood samples were successfully detected (Figure 7).

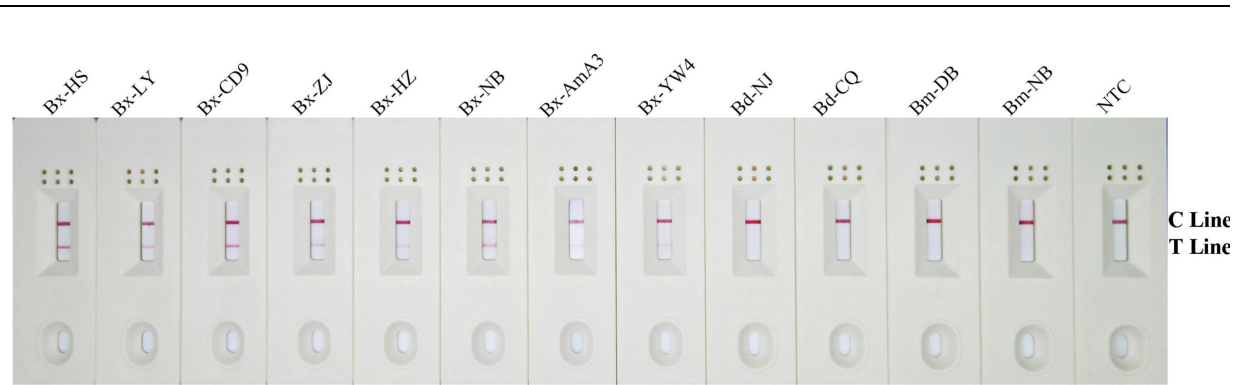


**FIGURE 7.** Detection of *B. xylophilus* purified gDNA in spiked pinewood samples. Images of the LFD results of RPA amplification of healthy pinewood samples spiked with gDNA of various nematode isolates. The spiked gDNA species are shown at the top of each dipstick. The double-distilled water was used as the no-template control, corresponding to the NTC dipstick. The positions of the control and test lines are shown on the right side of the image. The reactions are carried out at 38°C for 10 min.

## DISCUSSION

*Bursaphelenchus xylophilus* induced PWD has destroyed numerous pine trees and has spread to 18 provinces and 693 counties in China over the past 40 years, causing considerable economic losses of hundreds of billions of yuan [Announcement of the State Forestry and Grassland Administration (No. 6 of 2021), 2021]. Therefore, a primary procedure for disease prevention and quarantine comprising an accurate, rapid, sensitive, and convenient method for detecting *B. xylophilus* in pine wood is urgently needed.

Polymerase chain reaction-based amplification is considered the gold standard of molecular diagnostics; however, it requires trained personnel and specialized, expensive equipment generally unavailable outside laboratory settings (Patel et al., 2014). As an emerging isothermal amplification technique, RPA has displayed many strengths, such as short detection time, high sensitivity, easy operation, and minimum instrument needed. Besides, the RPA amplification results could be interpreted using LFD within a few mins. All these characteristics make RPA-LFD very suitable for on-site detection (James and Macdonald, 2015; Li et al., 2019).

The choice of detection target is crucial for specific diagnostics. Several genes have been selected as biomarkers for PWN detection, including 5S

rRNA, hsp70, satellite DNA, ITS rRNA, topoisomerase I, syg-2, and pel-3 (Kang et al., 2004; Castagnone et al., 2005; Leal et al., 2007; Huang et al., 2010; Zhuo et al., 2011; Kang et al., 2015; Meng et al., 2018). Among these, the syg-2 gene has been reported to have superior performance in the LAMP method and was thus selected as the target in this study. To identify regions specific to *B. xylophilus*, the syg-2 gene sequence of *B. xylophilus* was amplified using the PCR primers designed by Gou (2014) and then compared with two closely related species, after which the diverged region specific to *B. xylophilus* was selected (Supplementary Figure 1). The diverged region was considered a possible target area for designing primer and probe in the assay. Since the protocadherin DNA family has been shown to consist of tandemly arranged repeats, the amplification of a ladder of multimers of the amplicon-sized monomer was observed in basic-RPA experiments using the designed primers (Figure 2; Hirano et al., 2003; Washbourne et al., 2004).

On the LFD, the control line is enveloped with anti-mouse antibody, and the test line was enveloped with streptavidin. The test line first captures products labeled with biotin when the reaction mixture passes through. If the products also had a FAM label, it will combine with the AuNPs, which are enveloped with anti-FAM antibody, led to the enrichment of AuNPs at the test line, showing a red line (Wang et al., 2020). The control line is used to validate LFD detection, only captures the anti-FAM antibody enveloped with AuNPs, because the anti-FAM antibody is from a mouse (Figure 1).

Nonetheless, the RPA-LFD method has a non-ignorable inherent defect of primer-dependent artifacts. In the RPA-basic-based LFD reaction, forward and reverse primers were labeled with FAM and biotin at 5'-end, respectively. Amplicons are labeled with both biotin and FAM, if primer dimers are formed, it also produces a positive signal (Figures 8A,B). No matter how cautious the screening of primer is, it is nearly impossible to prevent primer dimers in the DNA amplification process (Meagher et al., 2018). Thermal cycling strategies could prevent primer-dimer formation in PCR but are unsuitable for RPA because RPA works at an isothermal temperature of about 38°C, and mispaired primers are difficult to dissociate (Brownie et al., 1997). Furthermore, the LFD method cannot differentiate the size of the molecule emitting signal and treats each molecule as a positive signal (Safenkova et al., 2020). Considering the RPA-LFD method is highly sensitive (Miao et al., 2019), any interference from primer-dependent artifacts could result in false-positive detection.

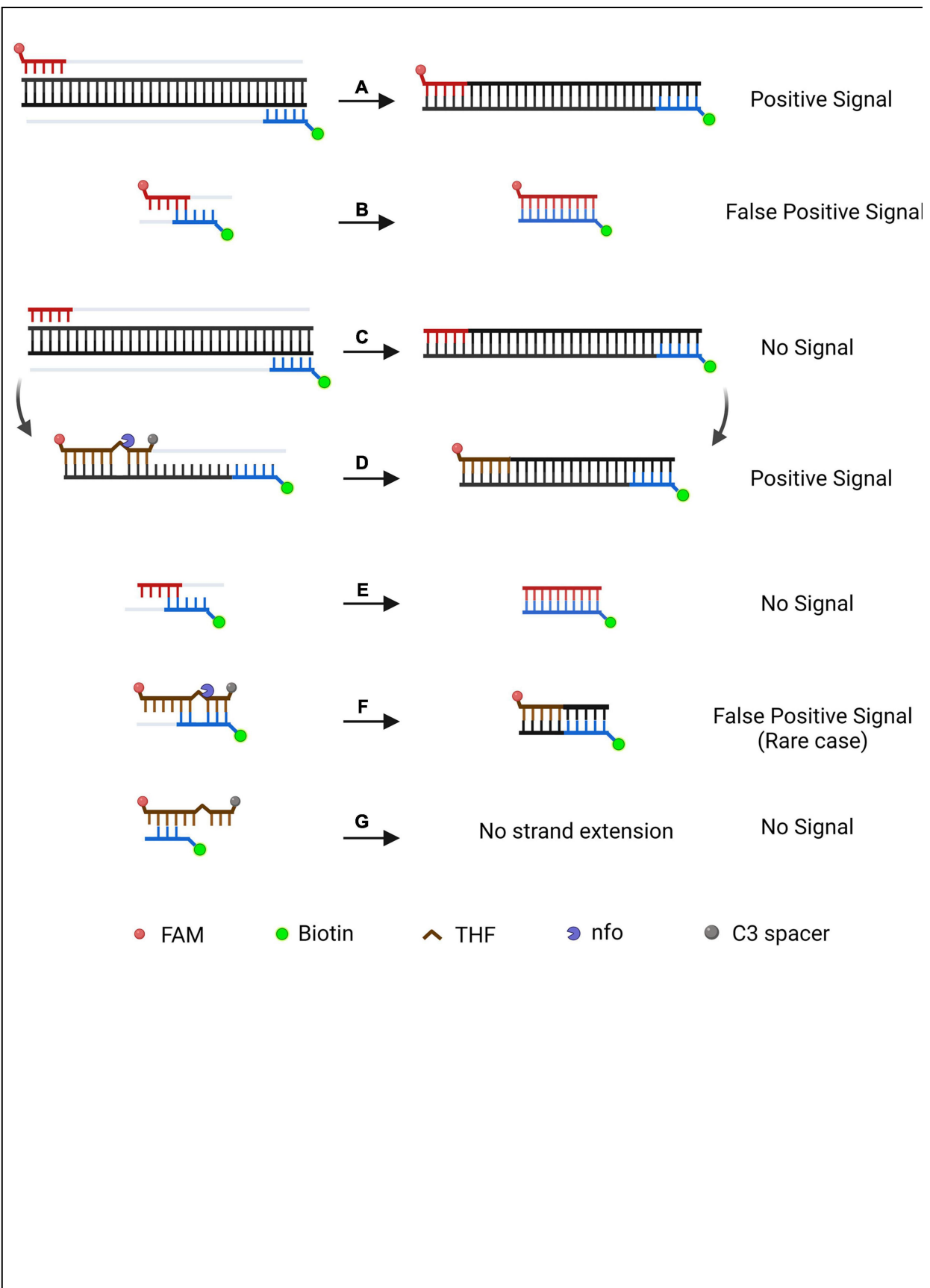


**FIGURE 8.** Schematic illustration of a specially designed probe that reduces false-positive signals from primer-dependent artifacts. In the RPA-Basic-based LFD reaction, both the amplification products (**A**) and the primer-dimers (**B**) can give positive signals. By using a probe in RPA reaction, amplification of the target DNA from the primers does not yield a positive signal (**C**). The amplification product is subjected to another round of amplification under the guidance of the probe and shows a positive signal (**D**). Primer dimers in the probe-based RPA reaction give no positive signal (**E**). In most cases, the primer–probe complex will not give a positive signal (**G**). The complex gives a positive signal when the primer and probe pairing multiple bases flanking the THF site (**F**). DNA strands are represented by horizontal lines, and matching bases are represented by short vertical lines between the DNA strands. The expected amplification of the DNA strand is indicated by the gray line. Modification group and nfo are represented by different colors and forms, and a legend is given at the bottom of the figure. Created with BioRender.com. Picture inspired by Wu et al. (2020).

Research has shown that introducing a probe in RPA would enhance specificity and decrease non-specific amplification products (Figures 8C,D; Piepenburg et al., 2006; Ivanov et al., 2021). FAM was labeled at the 5'-end of the probe, while the C3-spacer was labeled at the 3'-end of the probe that block extension. The THF site was placed on the probe to be cut by nfo enzyme. In this way, amplification led by primer pair would result in a product that only has biotin label, which would not generate a signal on the LFD (Figure 8C). The probe fully pairing amplified DNA strand can be cut by nfo at THF site (nfo was activated if bases flanking THF site paired with complementary bases), freeing the 3'-end for the extension to produce a positive signal on the LFD (Figure 8D). Using this probe-guided amplification, primer-dimers did not produce a signal (Figure 8E). The partly matched primer–probe complex could not be amplified (Figure 8G). Only in the rare case, the primer and probe paired several bases flanking the THF site (Figure 8F), and this would generate false-positive signal (Wu et al., 2020).

Therefore, elimination of the false-positive signal could not only count on using a probe, elaborate design and strict screening are still essential to prevent false-positive scenarios (Figure 8). Based on previous research, we inferred that the false-positive signal occurred in this study should be caused by the probe-primer complex since the labels were on the probe and reverse primer (Wu et al., 2020). By setting stringent parameters, probes were designed to have the lowest theoretical chance of primer pairing. However, cross-dimer analysis displayed many possible primer–probe dimer scenarios between the nfo probe and the reverse primer, and some cross-dimers fit the special case of false-positive signals. That is, the reverse primer formed mismatches with bases flanking the THF site on the probe, which could

elucidate why the original primer–probe set (S1-nfo-P/S1R-nfo) displayed false-positive signals.

The probe needed to be in the middle of two primers. However, obtaining an ideal probe without any continuous bases pairing to the reverse primer was scarcely possible. Nonetheless, we could exploit the tolerance of RPA to certain base mispairings on primers against the template, and attempt to bring in base substitutions in RPA-LFD method (Daher et al., 2015; Liu X. et al., 2019). By imitating a previously described method of bringing in three mismatches (Wu et al., 2020) in which two are in the probe and one in the reverse primer, the probe-primer dimer ligation was artificially interrupted, and false-positive was avoided. In addition, the RPA-LFD efficacy was not noticeably influenced when compared the color difference between the S1-nfo-P/S1R-nfo line and mS1-nfo-P/mS1R-nfo line, as shown in Figure 3.

Primer-dependent artifacts were successfully eliminated, resulting in the establishment of the RPA-LFD method. The analytical specificity test showed that the assay displayed high specificity toward *B. xylophilus* and avoided cross-reactions with the other two *Bursaphelenchus* species tested. A previous study reported that the detection limit of the RPA assay is approximately 1.6 fg ( $1.6 \times 10^{-6}$  ng) of gDNA from *B. xylophilus* (using pure gDNA) (Cha et al., 2020). However, in our RPA-LFD assay, a sensitivity test using *B. xylophilus* gDNA showed that the detection limit was 1 pg. This is probably because the RPA probe-based approach had a lower sensitivity than the approach with labeled primers (Ivanov et al., 2021).

The whole procedure for the RPA-LFD assay could be finished under 38°C within about 30 min, including 15 min for nematode gDNA extraction and master mix preparation, 15 min for the RPA-LFD assay (10 min for RPA reaction, 5 min for visual detection on the LFDs) (Figure 9). Compared with other diagnostic methods for *B. xylophilus* detection, the time needed for RPA-LFD detection was the shortest. Furthermore, RPA displayed tolerance to interference from pinewood (Figure 7), presenting an opportunity for further investigation into the prevalence of *B. xylophilus*, especially in new areas of occurrence.

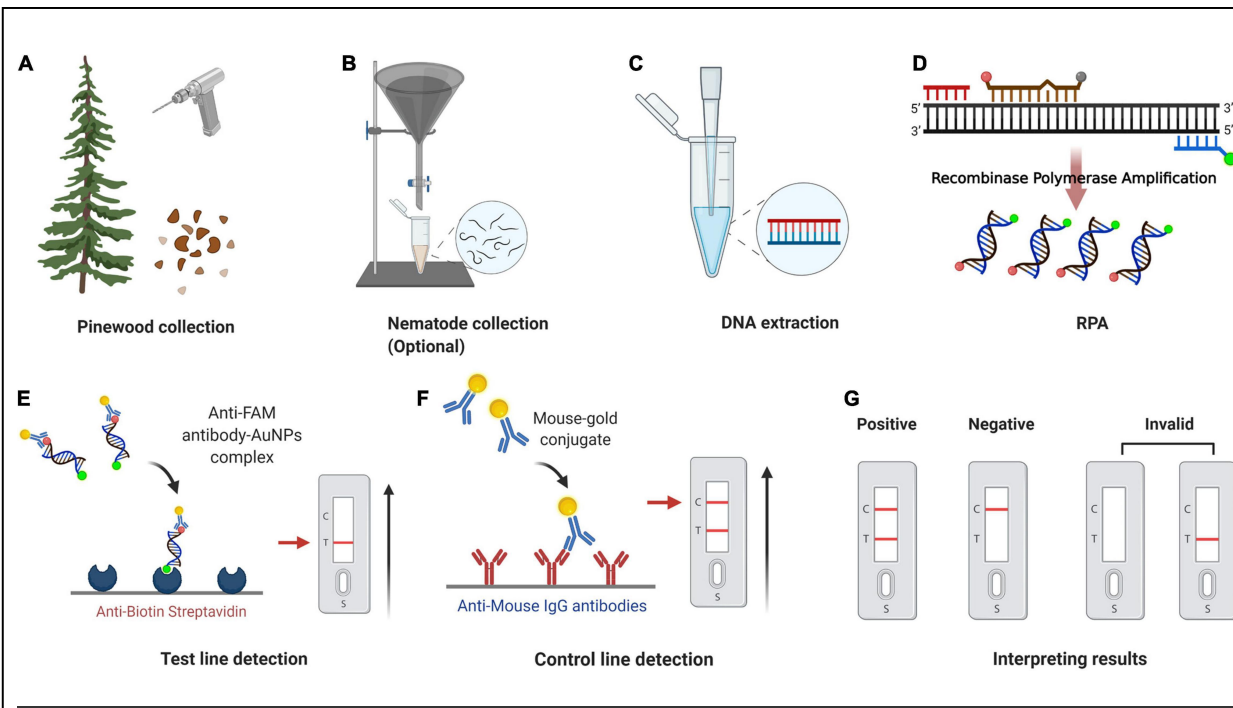


**FIGURE 9.** Point-of-Care testing workflow for pinewood nematode detection. **(A)** Pinewood chips are collected from trees using an electric drill or axe. **(B)** Nematodes are collected from pinewood chips using Baermann funnel method (optional). **(C)** gDNA is extracted from nematode/pinewood using DAP lysis buffer. **(D)** Recombinase polymerase amplification. **(E)** The sample enters testing well (T) and anti-FAM antibody-AuNPs complex binds to immobilized anti-biotin streptavidin. **(F)** Mouse antibody-gold conjugate binds to immobilized anti-mouse IgG antibodies. **(G)** Positive result: one dipstick each in C line and T line; Negative result: one dipstick in C line; Invalid result: no dipstick in C line despite the T line. The whole procedure for the RPA-LFD assay could be finished under 38°C within about 30 min, including 15 min for nematode gDNA extraction and master mix preparation, 15 min for the RPA-LFD assay (10 min for RPA reaction, 5 min for visual detection on the LFDs). Adapted from “COVID-19 Serologic Diagnostic Test through Antibody Detection,” by BioRender.com (2020). Retrieved from <https://app.biorender.com/biorender-templates>.

However, applying RPA-LFD detection to PWN diagnostics still faces some issues, with the expense being a major one. Reagent costs for RPA-LFD assays are approximately 50 RMB per reaction at present, even when using the RPA nfo kit manufactured locally, which are higher than those for polymerase chain reaction. However, when considering instrumentation costs, the RPA-LFD method becomes relatively more affordable. Even though PCR is currently considered the gold standard for nematode diagnostics, thermocycling instruments are expensive. Local forestry bureaus or quarantine departments are not commonly equipped with these, results usually take days to weeks to obtain due to the shortage of instruments. The minimal equipment needed for conducting RPA-LFD assays would allow reactions to be

completed timely in the field or at quarantine departments for point-of-care diagnostics within minutes rather than days.

The relatively low cost of RPA-LFD assay can be used by more people to support extensive surveillance across the country, whether in areas known to have high levels of PWD infection, such as Zhejiang Province, or in areas with relatively low levels of infection regions, supporting decision-making. In addition, detection capability in remote areas with limited resources could drastically increase with the emergency deployment of RPA-LFD assay kits. Thus, the RPA-LFD assay developed here has potential applications in the field and areas with limited resources.

## CONCLUSION

In conclusion, a rapid, on-site RPA-LFD assay for specific and sensitive detection of *B. xylophilus* was developed. The RPA-LFD assay prevents the risk of false-positive results from primer-dependent artifacts by using a probe and bringing base substitutions in the primer and probe. Furthermore, the assay successfully detected *B. xylophilus* with high specificity and sensitivity in less than 30 min at an isothermal temperature of 38°C. The developed RPA-LFD assay can provide a novel alternative for PWN point-of-care testing that has a simple read-out system and can be performed under field conditions without any special instrumentation or in areas with minimal laboratory infrastructure.

## DATA AVAILABILITY STATEMENT

The original contributions presented in the study are included in the article/Supplementary Material, further inquiries can be directed to the corresponding author.

## AUTHOR CONTRIBUTIONS

QZ conceptualized and designed the research, analyzed the data, interpreted the results, and wrote the manuscript. QZ and YL performed the experiments. QL, YL, ZW, and HW participated in the discussion for experimental design.

XZ helped funding acquisition. QL revised the manuscript and directed the project. All authors contributed to the article and approved the submitted version.

## FUNDING

This study was supported by grants from Zhejiang Science and Technology Program (2020C02007) and Fundamental Research Funds of Chinese Academy of Forestry (CAFYBB2021ZG001).

## ACKNOWLEDGMENTS

We thank Fengmao Chen of Nanjing Forestry University, Zhenyu Liu of Shandong Agricultural University, Laifa Wang and Xizhuo Wang of Chinese Academy of Forestry for their kind support on nematode isolates of *Bursaphelenchus* species. We also thank Tingting Dai of Nanjing Forestry University for providing guidance on RPA-LFD methodology.

## SUPPLEMENTARY MATERIAL

The Supplementary Material for this article can be found online at: <https://www.frontiersin.org/articles/10.3389/fpls.2022.856109/full#supplementary-material>

**Supplementary Figure 1** | Nucleotide sequence alignment of the syg-2 gene part sequence from *Bursaphelenchus xylophilus* (Bx), *Bursaphelenchus mucronatus* (Bm), and *Bursaphelenchus douei* (Bd). Location of S1F/R primers and S1-nfo-P are marked by black arrow lines, respectively. Gaps in sequence alignment were indicated by dots.

## REFERENCES

Ahuja, A., and Somvanshi, V. S. (2021). Diagnosis of plant-parasitic nematodes using loop-mediated isothermal amplification (LAMP): a review. *Crop Protect.* 147:105459. doi: 10.1016/j.cropro.2020.105459

Announcement of the State Forestry and Grassland Administration (No. 6 of 2021) (2021). *Announcement of the State Forestry and Grassland Administration (No. 6 of 2021)*. Available online at: <http://www.forestry.gov.cn/main/3457/20210329/152323508644481.html> (accessed March 29, 2021).

Brownie, J., Shawcross, S., Theaker, J., Whitcombe, D., Ferrie, R., Newton, C., et al. (1997). The elimination of primer-dimer accumulation in PCR. *Nucleic Acids Res.* 25, 3235–3241. doi: 10.1093/nar/25.16.3235

Castagnone, C., Abad, P., and Castagnone-Sereno, P. (2005). Satellite DNA-based species-specific identification of single individuals of the pinewood nematode *Bursaphelenchus xylophilus* (Nematoda: aphelenchoididae). *Eur. J. Plant Pathol.* 112, 191–193. doi: 10.1007/s10658-004-0580-2

Cha, D., Kim, D., Choi, W., Park, S., and Han, H. (2020). Point-of-care diagnostic (POCD) method for detecting *Bursaphelenchus xylophilus* in pinewood using recombinase polymerase amplification (RPA) with the portable optical isothermal device (POID). *PLoS One* 15:e0227476. doi: 10.1371/journal.pone.0227476

Cha, D., Kim, D., Lee, S., and Han, H. (2019). A new on-site detection method for *Bursaphelenchus xylophilus* in infected pine trees. *For. Pathol.* 49:e12503. doi: 10.1111/efp.12503

Chi, Y., Zhao, W., Ye, M., Ali, F., Wang, T., and Qi, R. (2020). Evaluation of recombinase polymerase amplification assay for detecting *Meloidogyne Javanica*. *Plant Dis.* 104, 801–807. doi: 10.1094/PDIS-07-19-1473-RE

Daher, R. K., Stewart, G., Boissinot, M., and Bergeron, M. G. (2016). Recombinase polymerase amplification for diagnostic applications. *Clin. Chem.* 62, 947–958. doi: 10.1373/clinchem.2015.245829

Daher, R. K., Stewart, G., Boissinot, M., Boudreau, D. K., and Bergeron, M. G. (2015). Influence of sequence mismatches on the specificity of recombinase polymerase amplification technology. *Mol. Cell. Probes* 29, 116–121. doi: 10.1016/j.mcp.2014.11.005

Dai, T., Yang, X., Hu, T., Jiao, B., Xu, Y., Zheng, X., et al. (2019). Comparative evaluation of a novel recombinase polymerase amplification-lateral flow dipstick (RPA-LFD) assay, LAMP, conventional PCR, and leaf-disc baiting methods for detection of *Phytophthora sojae*. *Front. Microbiol.* 10:1884. doi: 10.3389/fmicb.2019.01884

Fang, Y., Wu, X., Lin, Y., Wang, H., Wu, H., and Ju, Y. (2021). Duplex-RPA Detection for *Bursaphelenchus xylophilus* and *Bursaphelenchus mucronatus*. *Biotechnol. Bull.* 37:183. doi: 10.13560/j.cnki.biotech.bull.1985.2021-0579

Futai, K. (2013). Pine wood nematode, *Bursaphelenchus xylophilus*. *Annu. Rev. Phytopathol.* 51, 61–83. doi: 10.1146/annurev-phyto-081211-172910

Glöckler, J., Lim, T. S., Ida, J., and Frohme, M. (2021). Isothermal amplifications—a comprehensive review on current methods. *Crit. Rev. Biochem. Mol. Biol.* 56, 543–586. doi: 10.1080/10409238.2021.1937927

Gou, D. (2014). *A New Method to Extract Genomic DNA of Bursaphelenchus xylophilus from the Pine Wood and the Establishment of the LAMP Detection System*. Master's thesis. Sichuan: Sichuan Agricultural University.

Gu, J. (2014). *Identification Techniques of Bursaphelenchus xylophilus and its Approximate Species*. Xiamen: Xiamen University Press.

Gu, J., and Wang, J. (2011). *Morphological and Molecular Identification of Bursaphelenchus Species*. Xiamen: Xiamen University Press.

Gu, J., Wang, J., Braasch, H., Burgermeister, W., and Schröder, T. (2011). Morphological and molecular characterisation of mucronate isolates ('M' form) of *Bursaphelenchus xylophilus* (Nematoda: aphelenchoididae). *Russian J. Nematol.* 19, 103–120.

Hirano, S., Suzuki, S. T., and Redies, C. (2003). The cadherin superfamily in neural development: diversity, function and interaction with other molecules. *Front. Biosci.* 8:d306–d355. doi: 10.2741/972

Huang, L., Ye, J., Wu, X., Xu, X., Sheng, J., and Zhou, Q. (2010). Detection of the pine wood nematode using a real-time PCR assay to target the DNA topoisomerase I gene. *Eur. J. Plant Pathol.* 127, 89–98. doi: 10.1007/s10658-009-9574-4

Inácio, M., Nobrega, F., Vieira, P., Bonifacio, L., Naves, P., Sousa, E., et al. (2015). First detection of *Bursaphelenchus xylophilus* associated with *Pinus nigra* in Portugal and in Europe. *For. Pathol.* 45, 235–238. doi: 10.1111/efp.12162

Ivanov, A. V., Safenkova, I. V., Zherdev, A. V., and Dzantiev, B. B. (2021). Recombinase polymerase amplification assay with and without nuclease-dependent-labeled oligonucleotide probe. *Int. J. Mol. Sci.* 22:11885. doi: 10.3390/ijms222111885

James, A., and Macdonald, J. (2015). Recombinase polymerase amplification: emergence as a critical molecular technology for rapid, low-resource diagnostics. *Expert Rev. Mol. Diagnostics* 15, 1475–1489. doi: 10.1586/14737159.2015.1090877

Jarvi, S. I., Atkinson, E. S., Kaluna, L. M., Snook, K. A., and Steel, A. (2021). Development of a recombinase polymerase amplification (RPA-EXO) and lateral flow assay (RPA-LFA) based on the ITS1 gene for the detection of *Angiostrongylus cantonensis* in gastropod intermediate hosts. *Parasitology* 148, 251–258. doi: 10.1017/S0031182020002139

Ju, Y., Lin, Y., Yang, G., Wu, H., and Pan, Y. (2019). Development of recombinase polymerase amplification assay for rapid detection of *Meloidogyne incognita*, *M. javanica*, *M. arenaria*, and *M. enterolobii*. *Eur. J. Plant Pathol.* 155, 1155–1163. doi: 10.1007/s10658-019-01844-6

Kang, J., Kim, A. Y., Han, H., Moon, Y., and Koh, Y. (2015). Development of two alternative Loop-mediated isothermal amplification tools for detecting pathogenic pine wood nematodes. *For. Pathol.* 45, 127–133. doi: 10.1111/efp.12147

Kang, J. S., Choi, K. S., Shin, S. C., Moon, I. S., Lee, S. G., and Lee, S. H. (2004). Development of an efficient PCR-based diagnosis protocol for the identification of the pinewood nematode, *Bursaphelenchus xylophilus* (Nematoda: aphelenchoididae). *Nematology* 6, 279–285. doi: 10.1163/1568541041217915

Kikuchi, T., Aikawa, T., Oeda, Y., Karim, N., and Kanzaki, N. (2009). A rapid and precise diagnostic method for detecting the pinewood nematode *Bursaphelenchus xylophilus* by loop-mediated isothermal amplification. *Phytopathology* 99, 1365–1369. doi: 10.1094/PHYTO-99-12-1365

Kim, B.-N., Kim, J. H., Ahn, J.-Y., Kim, S., Cho, B.-K., Kim, Y.-H., et al. (2020). A short review of the pinewood nematode, *Bursaphelenchus xylophilus*. *Toxicol. Environ. Health Sci.* 12, 1–8. doi: 10.1007/s13530-020-00068-0

Leal, I., Green, M., Allen, E., Humble, L., and Rott, M. (2007). Application of a real-time PCR method for the detection of pine wood nematode, *Bursaphelenchus xylophilus*, in wood samples from lodgepole pine. *Nematology* 9, 351–362. doi: 10.1163/156854107781352098

Lee, J. P., Sekhon, S. S., Kim, J. H., Kim, S. C., Cho, B. K., Ahn, J. Y., et al. (2021). The pine wood nematode *Bursaphelenchus xylophilus* and molecular diagnostic methods. *Mol. Cell. Toxicol.* 17, 1–13. doi: 10.1007/s13273-020-00110-9

Li, T. T., Wang, J. L., Zhang, N. Z., Li, W. H., Yan, H. B., Li, L., et al. (2019). Rapid and visual detection of *Trichinella* spp. using a lateral flow strip-based recombinase polymerase amplification (LF-RPA) assay. *Front. Cell. Infect. Microbiol.* 9:1. doi: 10.3389/fcimb.2019.00001

Li, Y. L., Fan, C. J., Jiang, X. H., Tian, X. Y., and Han, Z. M. (2021). *Bursaphelenchus xylophilus*: an important pathogenic factor of pine wilt disease and its relationship with *bursaphelenchus mucronatus*. *Plant Dis.* 105, 3055–3062. doi: 10.1094/PDIS-02-21-0396-RE

Liu, C., Hu, Z., Wang, X., Geng, Y., Ma, C., Wang, Z., et al. (2019). The rapid detection of the *Bursaphelenchus xylophilus* by denaturation bubble-mediated strand exchange amplification. *Anal. Sci.* 35, 449–453. doi: 10.2116/analsci.18P461

Liu, X., Yan, Q., Huang, J., Chen, J., Guo, Z., Liu, Z., et al. (2019). Influence of design probe and sequence mismatches on the efficiency of fluorescent RPA. *World J. Microbiol. Biotechnol.* 35, 1–11. doi: 10.1007/s11274-019-2620-2

Meagher, R. J., Priye, A., Light, Y. K., Huang, C., and Wang, E. (2018). Impact of primer dimers and self-amplifying hairpins on reverse transcription loop-mediated isothermal amplification detection of viral RNA. *Analyst* 143, 1924–1933. doi: 10.1039/C7AN01897E

Meng, F., Wang, X., Wang, L., Gou, D., Liu, H., Wang, Y., et al. (2018). A loop-mediated isothermal amplification-based method for detecting *Bursaphelenchus xylophilus* from *Monochamus alternatus*. *For. Pathol.* 48:e12404. doi: 10.1111/efp.12404

Miao, F., Zhang, J., Li, N., Chen, T., Wang, L., Zhang, F., et al. (2019). Rapid and sensitive recombinase polymerase amplification combined with lateral flow strip for detecting African swine fever virus. *Front. Microbiol.* 10:1004. doi: 10.3389/fmicb.2019.01004

Mota, M. M., and Vieira, P. (2008). *Pine Wilt Disease: A Worldwide Threat to Forest Ecosystems*. Berlin: Springer.

Patel, S. K., Pratap, C. B., Jain, A. K., Gulati, A. K., and Nath, G. (2014). Diagnosis of *Helicobacter pylori*: what should be the gold standard? *World J. Gastroenterol.: WJG* 20:12847. doi: 10.3748/wjg.v20.i36.12847

Piepenburg, O., Williams, C. H., Stemple, D. L., and Armes, N. A. (2006). DNA detection using recombination proteins. *PLoS Biol.* 4:e204. doi: 10.1371/journal.pbio.0040204

Poritz, M. A., and Ririe, K. M. (2014). Getting things backwards to prevent primer dimers. *J. Mol. Diagnostics* 16, 159–162. doi: 10.1016/j.jmoldx.2014.01.001

Qi, Y., Yin, Q., Shao, Y., Li, S., Chen, H., Shen, W., et al. (2018). Rapid and visual detection of *Coxiella burnetii* using recombinase polymerase amplification combined with lateral flow strips. *BioMed Res. Int.* 2018:6417354. doi: 10.1155/2018/6417354

Safenkova, I. V., Ivanov, A. V., Slutskaya, E. S., Samokhvalov, A. V., Zherdev, A. V., and Dzantiev, B. B. (2020). Key significance of DNA-target size in lateral flow assay coupled with recombinase polymerase amplification. *Anal. Chim. Acta* 1102, 109–118. doi: 10.1016/j.aca.2019.12.048

Song, Z., Yang, X., Zhang, X., Luan, M., Guo, B., Liu, C., et al. (2020). Rapid and visual detection of *Meloidogyne hapla* using recombinase polymerase amplification combined with a lateral flow dipstick (RPA-LFD) assay. *Plant Dis.* 105, 2697–2703. doi: 10.1094/PDIS-06-20-1345-RE

Subbotin, S. A. (2019). Recombinase polymerase amplification assay for rapid detection of the root-knot nematode *Meloidogyne enterolobii*. *Nematology* 21, 243–251. doi: 10.1163/15685411-00003210

Subbotin, S. A., and Burbridge, J. (2021). Sensitive, accurate and rapid detection of the northern root-knot nematode, *meloidogyne hapla*, using recombinase polymerase amplification assays. *Plants* 10:336. doi: 10.3390/plants10020336

Sultana, T., Han, H., and Park, J. K. (2013). Comparison of complete mitochondrial genomes of pine wilt nematode *Bursaphelenchus xylophilus* and *Bursaphelenchus mucronatus* (Nematoda: aphelenchoidea) and development of a molecular tool for species identification. *Gene* 520, 39–46. doi: 10.1016/j.gene.2013.02.006

Viglierchio, D., and Schmitt, R. V. (1983). On the methodology of nematode extraction from field samples: baermann funnel modifications. *J. Nematol.* 15:438.

Wang, J., Gu, J., Chen, X., and Duan, W. (2012). Identification of East Asian and European types of *Bursaphelenchus mucronatus* by morphological and ITS PCR-RFLP methods. *Sci. Silvae Sin.* 48, 113–117.

Wang, L., Zhao, P., Si, X., Li, J., Dai, X., Zhang, K., et al. (2020). Rapid and specific detection of *Listeria monocytogenes* with an isothermal amplification and lateral flow strip combined method that eliminates false-positive signals from primer-dimers. *Front. Microbiol.* 10:2959. doi: 10.3389/fmicb.2019.02959

Washbourne, P., Dityatev, A., Scheiffele, P., Biederer, T., Weiner, J. A., Christopherson, K. S., et al. (2004). Cell adhesion molecules in synapse formation. *J. Neurosci.* 24, 9244–9249. doi: 10.1523/JNEUROSCI.3339-04.2004

Wu, H., Zhao, P., Yang, X., Li, J., Zhang, J., Zhang, X., et al. (2020). A recombinase polymerase amplification and lateral flow strip combined method That Detects *Salmonella enterica* serotype *typhimurium* with no worry of primer-dependent artifacts. *Front. Microbiol.* 11:1015. doi: 10.3389/fmicb.2020.01015

Yamagata, M., Sanes, J. R., and Weiner, J. A. (2003). Synaptic adhesion molecules. *Curr. Opinion Cell Biol.* 15, 621–632. doi: 10.1016/S0955-0674(03)00107-8

Yazaki, K., Takanashi, T., Kanzaki, N., Komatsu, M., Levia, D. F., Kabeya, D., et al. (2018). Pine wilt disease causes cavitation around the resin canals and irrecoverable xylem conduit dysfunction. *J. Exp. Bot.* 69, 589–602. doi: 10.1093/jxb/erx417

Zhuo, K., Luo, M., Cui, R., and Liao, J. (2011). A multiplex one-step PCR method for the simultaneous identification of *Bursaphelenchus xylophilus*, *B. mucronatus* and *B. douei*—three species within the *xylophilus* group. *For. Pathol.* 41, 66–69. doi: 10.1111/j.1439-0329.2009.00638.x

**Conflict of Interest:** The authors declare that the research was conducted in the absence of any commercial or financial relationships that could be construed as a potential conflict of interest.

**Publisher's Note:** All claims expressed in this article are solely those of the authors and do not necessarily represent those of their affiliated organizations, or those of the publisher, the editors and the reviewers. Any product that may be evaluated in this article, or claim that may be made by its manufacturer, is not guaranteed or endorsed by the publisher.

Copyright © 2022 Zhou, Liu, Wang, Wang, Zhang and Lu. This is an open-access article distributed under the terms of the Creative Commons Attribution License (CC BY). The use, distribution or reproduction in other forums is permitted, provided the original author(s) and the copyright owner(s) are credited and that the original publication in this journal is cited, in accordance with accepted academic practice. No use, distribution or reproduction is permitted which does not comply with these terms.

ORIGINAL RESEARCH

published: 05 April 2022

doi: 10.3389/fpls.2022.850660



# Quantitative Trait Loci Analysis Based on High-Density Mapping of Single-Nucleotide Polymorphisms by Genotyping-by-Sequencing Against Pine Wilt Disease in Japanese Black Pine (*Pinus thunbergii*)

**Tomonori Hirao<sup>1</sup>\*, Koji Matsunaga<sup>2</sup> and Kenta Shirasawa<sup>3</sup>**

<sup>1</sup> Forest Bio-Research Center, Forestry and Forest Products Research Institute, Hitachi, Japan

<sup>2</sup> Kyushu Regional Breeding Office, Forest Tree Breeding Center, Forestry and Forest Products Research Institute, Koshi, Japan

<sup>3</sup> Department of Frontier Research and Development, Kazusa DNA Research Institute, Kisarazu, Japan

**Edited by:**

Margarida Espada, University of Évora, Portugal

**Reviewed by:**

David M. Francis, The Ohio State University, United States

Peng Qi, University of Georgia, United States

**\*Correspondence:** Tomonori Hirao, [hiratomo@affrc.go.jp](mailto:hiratomo@affrc.go.jp)

**Specialty section:** This article was submitted to Plant Pathogen Interactions, a section of the journal *Frontiers in Plant Science*

**Received:** 08 January 2022

**Accepted:** 09 March 2022

**Published:** 05 April 2022

**Citation:** Hirao T, Matsunaga K and Shirasawa K (2022) Quantitative Trait Loci Analysis Based on High-Density Mapping of Single-Nucleotide Polymorphisms by Genotyping-by-Sequencing Against Pine Wilt Disease in Japanese Black Pine (*Pinus thunbergii*). *Front. Plant Sci.* 13:850660. doi: 10.3389/fpls.2022.850660

Identifying genes/loci for resistance to pine wilt disease (PWD) caused by the pine wood nematode (PWN) is beneficial for improving resistance breeding in *Pinus thunbergii*, but to date, genetic information using molecular markers has been limited. Here, we constructed a high-density linkage map using genotyping-by-sequencing (GBS) and conducted quantitative trait loci (QTL) analysis for PWD resistance for the self-pollinated progeny of “Namikata 73,” which is the most resistant variety among resistant varieties of *P. thunbergii*, following inoculation tests with PWN. An  $S_1$  mapping population consisting of the 116 progenies derived from self-pollination of the resistant variety, “Namikata 73” (resistance rank 5 to PWN), was inoculated with PWN isolate Ka-4 and evaluated for disease symptoms. To construct a high-density linkage map, we used single-nucleotide polymorphisms (SNPs) identified by GBS based on next-generation sequencing technology and some anchor DNA markers, expressed sequence tag (EST)-derived SNP markers and EST-derived simple sequence repeat (SSR) markers, and genomic SSR markers. The linkage map had 13 linkage groups (LGs) consisting of 2,365 markers including 2,243 GBS-SNP markers over a total map distance of 1968.4 centimorgans (cM). Results from QTL analysis using phenotype data and the linkage map indicated that PWD resistance is controlled by a single locus located on LG-3, as identified in a previous study. This locus showed overdominant genetic action in the present study. With the confirmation of *PWD1* in two different mapping populations (present study and a previous study), the locus associated with this region is thought to be a good target for marker-assisted selection in *P. thunbergii* breeding programs in order to obtain high levels of resistance to PWD caused by PWN.

**Keywords:** genotyping-by-sequencing, genetic linkage map, pine wood nematode, pine wilt disease, PWD resistance

## INTRODUCTION

The conifer species *Pinus thunbergii* Parl (Japanese black pine) was widely planted in coastal areas of Japan to prevent land erosion and to provide protection from wind-blown sand and tidal waves. However, since around 1970, the spread of pine wilt disease (PWD) caused by the pine wood

nematode (PWN) *Bursaphelengus xylophilus* has become a chronic problem in pine forests in Japan (Kiyohara and Tokushige, 1971). Control measures for PWD have taken the form of breeding programs to select and develop more resistant pine varieties, and genetic analysis has been implemented to improve cost-effectiveness.

The first breeding project to develop pine varieties resistant to PWD was started in 1978 in southwest Japan (Fujimoto et al., 1989), and as the damage has spread, related projects have been promoted throughout Japan with the exception of on Hokkaido Island (Kurinobu, 2008; Forestry Agency Ministry of Agriculture, Forestry and Fisheries of Japan, 2010). In the first breeding project conducted from 1978 to 1984 in southwest Japan, 16 resistant clones were selected from 15,000 candidate *P. thunbergii* trees and were further developed as resistant varieties (Fujimoto et al., 1989). As of March, 2019, 171 resistant individuals have been selected from pine forests with severe PWD damage from all over Japan (Forest Tree Breeding Center, Forestry and Forest Products Research Institute, 2019).

*P. thunbergii* has 12 basic chromosomes ( $2n=24$ ) and an estimated genome size of approximately 25 Gbps (Neale and Wheeler, 2019). The reference genome of this species has not yet been determined. To date, several genetic linkage maps have been constructed using DNA markers (Kondo et al., 2000; Hayashi et al., 2004; Hirao et al., 2019), with the genetic linkage map identifying the locus for resistance to PWN in *P. thunbergii* by Hirao et al. (2019) being the only genetic study to date to identify resistance to PWD using genetic markers. The genetic linkage map was constructed using the genomic simple sequence repeat (SSR) and expressed sequence tag (EST)-derived single-nucleotide polymorphism (SNP) markers in resistant  $F_1$  families, and the locus related to PWD resistance, *PWD1*, was mapped on linkage group (LG) 3. It is necessary to accumulate more knowledge of the genetics of *P. thunbergii* in order to elucidate the mechanism of PWD resistance and to improve breeding success for resistance traits.

Through gene-assisted selection (GAS) and marker-assisted selection (MAS) tools, improved genetics and more cost-effective breeding programs can be developed. Furthermore, more effective genome-wide and high-density linkage mapping with more effective genotyping methods are needed to more accurately detect PWD-resistant loci.

The use of SNPs is advantageous over many other markers due to their abundance in the genome, their ubiquitous distribution throughout the genome, and their typical biallelic and co-dominant characteristics. Recently, new approaches, such as restriction site-related DNA sequencing (RADseq) and genotyping-by-sequencing (GBS), have led to the discovery of thousands of SNPs and the cost-effective genotyping of some crops (Davey et al., 2011; Andrews et al., 2016). Among the different approaches, GBS is the simplest and most cost-effective approach due to simple procedures to prepare the library and a high level of multiplexing capacity, as well as its effectiveness in organisms for which complete genome sequencing is lacking (Elshire et al., 2011). The GBS approach is widely used in many crops in breeding and molecular genetics studies, genetic diversity studies, trait mapping, and genome-wide association studies (Poland and Rife, 2012; He et al., 2014; Chung et al., 2017), and it has also been attempted in coniferous species with large and complex genomes (Pan et al., 2015; Hall et al., 2020). Identifying the genetic factors for PWD resistance is critical for the development of PWD-resistant clones of *P. thunbergii*.

In a previous study, QTL analysis for resistance to PWD in *P. thunbergii* was conducted using the  $F_1$  population of crosses between resistant varieties with a pseudo-testcross strategy (Hirao et al., 2019). Employing a pseudo-testcross strategy (Grattapaglia and Sederoff, 1994) for linkage mapping in a controlled cross between two outbred parents is widely utilized for mapping quantitative trait loci (QTL) in outcrossing species. However, the  $F_1$  population often displays many different types of segregation because outcrossing species are highly heterozygous. Some loci may have four different alleles between the crossing parents, generating four genotype classes in the progeny. Many others may also follow the  $F_2$  pattern in a 1:2:1 ratio and the backcross pattern in a 1:1 ratio (Lu et al., 2004; Wu et al., 2010). Although *P. thunbergii* is an outcrossing species, it is known to have the potential to develop a self-fertilizing population by artificial self-pollination (Katsuta, 1964). Lacking a reference sequence for applying a genome-wide GBS approach, we considered that using a self-fertilized  $S_1$  population would simplify detection of genetic segregation and the locus related to PWD resistance in *P. thunbergii*. Utilizing this approach also broadens the range of genetic approaches for targeted loci detection, and facilitates the further accumulation of genetic knowledge on loci associated with PWD resistance.

In the present study, the GBS approach was used for SNP identification and genotyping of the  $S_1$  mapping population of the most highly resistant variety of *P. thunbergii*. The identified SNPs were used to construct high-density genetic maps, and SNP genotyping data and phenotyping data for the  $S_1$  populations were used to identify the locus related to PWD resistance in *P. thunbergii*.

## MATERIALS AND METHODS

### Plant Material

Sixteen resistant varieties of *P. thunbergii* were selected for the first breeding program and were ranked with regard to resistance (levels 1–5) based on the survival rate of openly pollinated progeny following inoculation with PWN with higher survival rates indicating greater resistance (Toda, 2004). Using self-pollination of the most highly resistant variety, “Namikata 73,” an  $S_1$  population of 135 progenies was seeded in March 2012 and planted in pots with a diameter of 15 cm and a height of 30 cm in a greenhouse at the Forest Products Research Institute, Forest Tree Breeding Center (FFPRI-FTBC) in Ibaraki, Japan in April 2014. Total genomic DNA of the  $S_1$  population was extracted from needles using the DNeasy Plant Mini Kit (Qiagen, Hilden, Germany) and subjected to polymorphism analyses, as described below.

### Artificial Inoculation and Phenotyping

The Ka-4 isolate of PWN, which has been used in PWD resistance breeding projects since 2003, was inoculated on the main stems at 5 cm above the ground on 15 June 2014. The bark was shaved with a knife to expose cambium cells, and 5,000 nematodes suspended in 50  $\mu$ l of sterile water were introduced to the shaved area. Counts of progenies showing resistance (survival) and susceptibility (mortality) were evaluated at 70 days post-inoculation (dpi) with PWN. The count data were subjected to the chi-squared test to assess goodness of fit to the expected Mendelian ratios with a significance threshold of  $p = 0.05$ .

### Genotyping-by-Sequencing

The GBS library was prepared following a method adapted from Elshire et al. (2011) using 100 ng of genomic DNA per individual and the *ApeKI* restriction enzyme. Individual libraries were barcoded, amplified, and normalized before pooling and sequencing in order to reduce the range in per sample coverage (Nicotra et al., 2016). The GBS libraries of 136 multiplexed samples including the parent sample were sequenced on an Illumina HiSeq 2,500 (Illumina, San Diego, CA, United States) using 100 bp paired-end reads and two lanes by Hokkaido System Science Co., Ltd. (Sapporo, Hokkaido, Japan) and on an Illumina HiSeq 4000 (Illumina) using 100 bp paired-end reads and four lanes by Macrogen (Seoul, South Korea).

A schematic of the progeny sample processing is shown in Supplementary Figure 1. First, four progenies were removed from analysis due to contamination discovered in SSR genotyping, and the sequence data of the parent and 131 progeny GBS raw sequence reads were subjected to a quality check using FastQC (v0.11.2). For SNP calling, samples with target reads that accounted for less than 10% of the mean sequenced reads in the sequencing lane were considered as failed sequencing reactions and removed from analysis (Elshire et al., 2011). In our testing, only two samples were excluded from further consideration for this reason. The final 130 samples (129 S<sub>1</sub> and one parent) were analyzed using Universal Network Enabled Analysis Kit (UNEAK) pipeline in the TASSEL 3.0 analysis package (Bradbury et al., 2007; Lu et al., 2013). This pipeline permits SNP calling based solely on GBS tag sequence data without requiring a reference genome sequence. Parameters in the UNEAK pipeline to select SNPs were set at a minimum read depth of 5, minimum/maximum minor allele frequencies (MAF, 0.01 and 0.5, respectively), and minimum/maximum call rates (0 and 1, respectively). The MAF and call rate were set at a low values for global analysis because these parameters were filtered within populations at later steps. As filtering was applied before genetic analysis, SNPs that were not heterozygous in the parent genotype and those with a proportion of missing data points greater than 20% were removed from subsequent data analysis. Further, samples showing missing data for more than 20% of all genotypes were removed by manual filtering on Excel.

Raw GBS data, excluding the contaminated progenies, have been submitted to the DDBJ Sequence Read Archive under accession numbers DRA012628, DRA012645, and DRA012646.

A total of 87 genomic DNA-derived SSR markers (Lian et al., 2000; Watanabe et al., 2006; Iwaizumi et al., 2013, 2018; Hirao et al., 2019) were used for segregation analysis in the present study. Multiplex PCR with three or four SSR primer pairs was performed using a Multiplex PCR Kit (Qiagen, Hilden, Germany), with 2× QIAGEN multiplex PCR master mix, 0.25 µm each primer pair, and 40 ng of genomic DNA in a total volume of 10 µl. Amplification was performed on a Veriti thermal cycler (Thermo Fisher Scientific, Waltham, MA, United States) using an initial denaturation step at 95°C for 15 min, followed by 30 cycles of denaturation at 94°C for 30 s, annealing at 57°C for 1.5 min, and extension at 72°C for 1 min, with a final extension at 60°C for 30 min. PCR products (1 µl) were mixed with 0.2 µl GeneScan 500 LIZ size standard (Thermo Fisher Scientific) and 9.8 µl of Hi-Di formamide (Thermo Fisher Scientific) prior to electrophoresis. The length of the amplified fragments was analyzed on an ABI 3130xl sequencer (Thermo Fisher Scientific) and alleles were scored with GeneMapper v5.0 software (Thermo Fisher Scientific). Four samples showing contamination were eliminated from further consideration.

For EST-derived SNP genotyping, we used an array of 768 SNPs on Illumina's GoldenGate platform (Hirao et al., 2019). Genotyping of the SNP markers was carried out using the custom oligonucleotide pooled assay (OPA; Illumina Inc., San Diego, CA) containing the allele-specific and locus-specific oligos for use in the Illumina GoldenGate assay and Illumina's BeadArray Express Reader according to standard manufacturer protocol. Automatic allele calling for each locus was inferred with GenomeStudio Software (Illumina).

## Linkage Map Construction

GBS-based genotype data were integrated with the genotyping of SSR markers and EST-derived SNP markers and were applied to genetic analysis. Data could not be obtained for three samples in the GoldenGate assay, and finally, 116 samples were applied to genetic analysis. Linkage analysis was conducted using JoinMap 4.1 (Van Ooijen, 2006) with the genotype data coded as an  $F_2$  intercross population type. Genotypic data completeness was filtered as 99% on 116 samples, and aberrant segregated loci ( $p < 0.05$ ) were removed by the chi-squared test. Grouping was performed using independent logarithm of odds (LOD) scores from 2 to 20 with a step size of 1, after which the minimum LOD score of 10 was used to determine the autonomous

LGs. The groups were converted to maps at LOD using a regression algorithm with the following settings: linkages with recombination frequency (<0.4), LOD (>0.01) threshold for removal of loci with respect to jumps in goodness-of-fit (5.0) and performing a ripple after adding 1 locus. Distance was calculated using Kosambi's mapping function. A map was drawn using Mapchart 2.32 (Voorrips, 2002) based on the genetic location determined by JoinMap 4.1.

The numbering of the linkage group and the order of the DNA markers in the linkage map constructed in the present study were determined by comparison with a previously constructed linkage map of *P. thunbergii* (Hirao et al., 2019). Based on information of common markers mapped on the two linkage maps, the number and orientation of the linkage group or the relative order and location of the mapped genes in *P. thunbergii* were compared to the consensus linkage map in previous study.

## QTL Analysis

QTL analysis was performed using MapQTL 6.0 software (Van Ooijen, 2009). To perform the binary trait method in the present QTL analysis, resistant and susceptible phenotypes were assigned values of 0 and 1, respectively, and two different methods were used. First, interval mapping (IM) at 1 cM intervals was carried out to detect putative QTL regions. The genome-wide and LG-specific LOD thresholds for each QTL were calculated using a permutation test with 1,000 repetitions at  $p < 0.05$  (5%). Closely flanking markers were then selected as cofactors and multiple QTL mapping (MQM) also known as composite interval mapping was performed. The confidence interval for each resulting QTL was determined by a decrease in 1 LOD unit from the QTL LOD peak. Second, the non-parametric Kruskal–Wallis (KW) test module was applied to traits to confirm the significance of the marker within the confidence interval. The allelic effect for the QTL was calculated in MapQTL6 based on the genotypes of loci detected with significance by the KW test using the formula proposed by Knott et al. (1998). Additive and dominance effects, as well as the degree of dominance of the QTLs, were calculated as described in Stuber et al. (1987) and Frérot et al. (2010).

## RESULTS

## Construction of a GBS-SNP-Based Genetic Linkage Map

Barcode GBS libraries were constructed for 135 *P. thunbergii* progenies and their parent using the enzyme *ApeKI* and pooling for sequencing. Raw data of Illumina sequences of all 136 libraries totaled  $1.8 \times 10^9$  reads and 177.5 GB, and after removing four samples that were contaminated and two samples with low quality, the raw sequences of 129 progenies and the parent were processed using *de novo* SNP calling and the UNEAK algorithm implemented in TASSEL 3.0. A total of 535,452 SNPs were obtained with the default setting but with the minimum tag count set to five. After application of a series of filters, which removed another 10 progenies, a total of 27,827 high-quality SNPs were obtained from 119 progenies.

Of the 87 genomic SSR markers, genotyping was performed on 131 individuals excluding four contaminated samples. Fifty-four (62.07%) markers showed clear amplification, were heterozygous in the parent genotype and had the possibility of showing expected genetic segregation. Those markers were integrated with EST-derived SNP markers, and GBS-based genotype data for further genetic filtering.

For EST-derived SNP markers using Illumina's GoldenGate platform, genotyping was performed on 129 individuals, excluding four contaminated samples and two samples with insufficient data in GBS. Firstly, three samples with missing data for more than 20% of all genotypes were removed from subsequent data analysis. Of the 768 loci, 599 SNPs (77.99%) that were not heterozygous in the parent genotype and those with more than 20% missing data points were removed from subsequent data analysis. The genotype data of 169 markers (22.01%) that passed this filtering were integrated into the genomic SSR genotype data and GBS-based genotype data, and further filtering for the expected Mendelian segregation ratio was performed to construct a linkage map.

GBS-based genotype data were integrated with genotyping of SSR markers and EST-derived SNP markers, and this data set was used for genetic analysis. No data could be obtained for three samples with the GoldenGate assay (for genotyping EST-derived SNPs), and we finally used markers from 116 samples for construction of a linkage map. The number of samples in the analysis leading to the construction of the linkage map is shown in Supplementary Figure 1. For construction of the genetic map, distorted markers that did not show the expected 1:2:1 segregation pattern (at

a threshold of  $p < 0.05$ ), and markers with data set completeness of less than 99% were removed from those obtained from the 116 samples. A total of 2,397 markers (34 SSR markers, 107 GG markers, and 2,256 GBS-SNP markers) from the remaining 116 progenies were used to construct the genetic map.

A total of 17 markers (1 genomic SSR marker, 3 EST-derived SNP markers and 13 GBS-SNP markers) of 2,397 markers were not grouped, 15 markers (4 genomic SSR markers, 10 EST-derived SNP markers, and 1 GBS-SNP marker) of 2,380 markers were removed due to having the same similarity loci, and the remaining 2,365 markers (29 SSR markers, 93 GG markers, and 2,243 GBS-SNP markers) were distributed over 13 LGs and had a minimum LOD score of 10.0 (Figure 1; Table 1; Supplementary Tables S1A–C). The linkage map spanned a cumulative distance of 1,968.4 centimorgans (cM), with each LG ranging from 81.07 cM (LG-6) and 122 markers to 198.11 cM (LG-3) and 243 markers. The average distance between the markers ranged from 0.59 (LG-1) to 0.88 (LG-5), and the average spacing between two adjacent markers was 0.79 cM across 13 LGs with the largest gap being 14.15 cM (on LG-5).

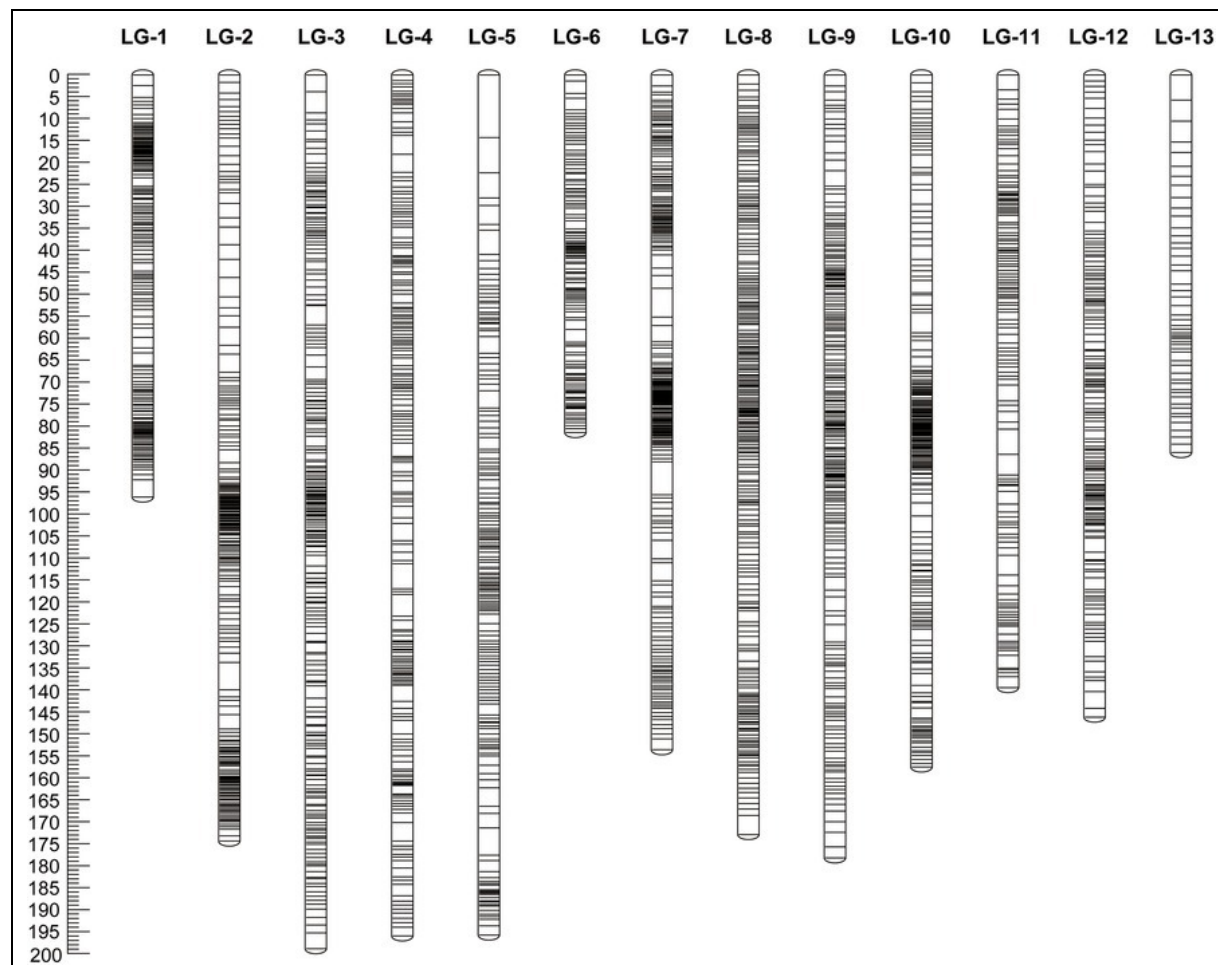


**FIGURE 1.** Genetic map constructed in the  $S_1$  mapping population derived from self-pollination of “Namikata 73.” The map includes 2,365 markers (29 SSR, 93 EST- SNP, and 2,243 GBS- SNP) across 13 LGs for a total length of 1,968.4 cM.

**TABLE 1.** Characterization of the genetic linkage map of ‘Namikata 73’.

Linkage group	Number of Markers			Length (cM)	Avg. marker distance (cM)	Max. gap (cM)
	gSSR	EST derived SNPs	GBS-SNPs			
1	1	6	155	95.68	0.59	3.90
2	2	5	201	173.72	0.73	6.20
3	4	8	231	198.11	0.77	4.85
4	5	10	183	195.17	0.82	5.63
5	1	4	163	195.01	0.88	14.15
6	0	7	115	81.07	0.86	2.92
7	2	10	227	153.04	0.82	7.50
8	1	13	242	172.22	0.80	4.31
9	6	8	204	177.49	0.80	4.02
10	0	4	199	156.88	0.80	4.59
11	2	9	122	138.87	0.81	5.76
12	5	7	152	145.56	0.82	3.81
13	0	2	49	85.62	0.84	5.66
Total	29	93	2,243	1968.43	—	—

We compared the constructed linkage map in the present study to the previously constructed a genetic linkage map of *P. thunbergii* (Hirao et al., 2019). The position of 25 genomic SSR markers and 44 EST-derived SNP markers mapped on the *P. thunbergii* linkage map constructed in the present study were used to identify the numbering of the linkage group and the order of the DNA markers. The relative order of mapped markers on the linkage maps for the two types was highly correlated,  $R^2 = 0.888\text{--}0.999$  (Supplementary Table S2), although there were not enough markers to compare the relative order of the mapped genes in some linkage groups (LG-10). In addition, since the markers that can be compared to the linkage map of the previous study were not mapped for the 13 linkage groups, it was not possible to verify the original linkage group identification (which linkage group should be integrated with this linkage group) or the order of the DNA markers.

## Evaluation of PWD Resistance in the Population

Although the inoculation test was originally started with 131  $S_1$  progenies (see Supplementary Figure 1 for analysis schematic), only 116 progenies were used to construct the genetic linkage map after removing samples due to contamination and poor or missing genotype data for genotyping. Results of the inoculation test and genetic segregation for the 116 progenies used to construct the genetic linkage map are shown in Table 2, Supplementary Table S3, and results for the original 131 progenies are shown in Supplementary Table S4. To test whether the resistance trait is controlled by a single gene, the chi-squared test was applied to phenotypic data of resistant (survival, 1) and susceptible (mortality, 0) states with the null hypothesis that the ratio of susceptible to resistant individuals used to make the linkage map should have a 1:1 segregation ratio. On the other hand, the null hypothesis of a 3:1 ratio of susceptible to resistant individuals was rejected. These results indicate that PWD resistance in the  $S_1$  population is controlled by a major gene.

**TABLE 2.** Segregation ratio of PWD resistance in the 'Namikata 73'  $S_1$  mapping population ( $n = 116$ ).

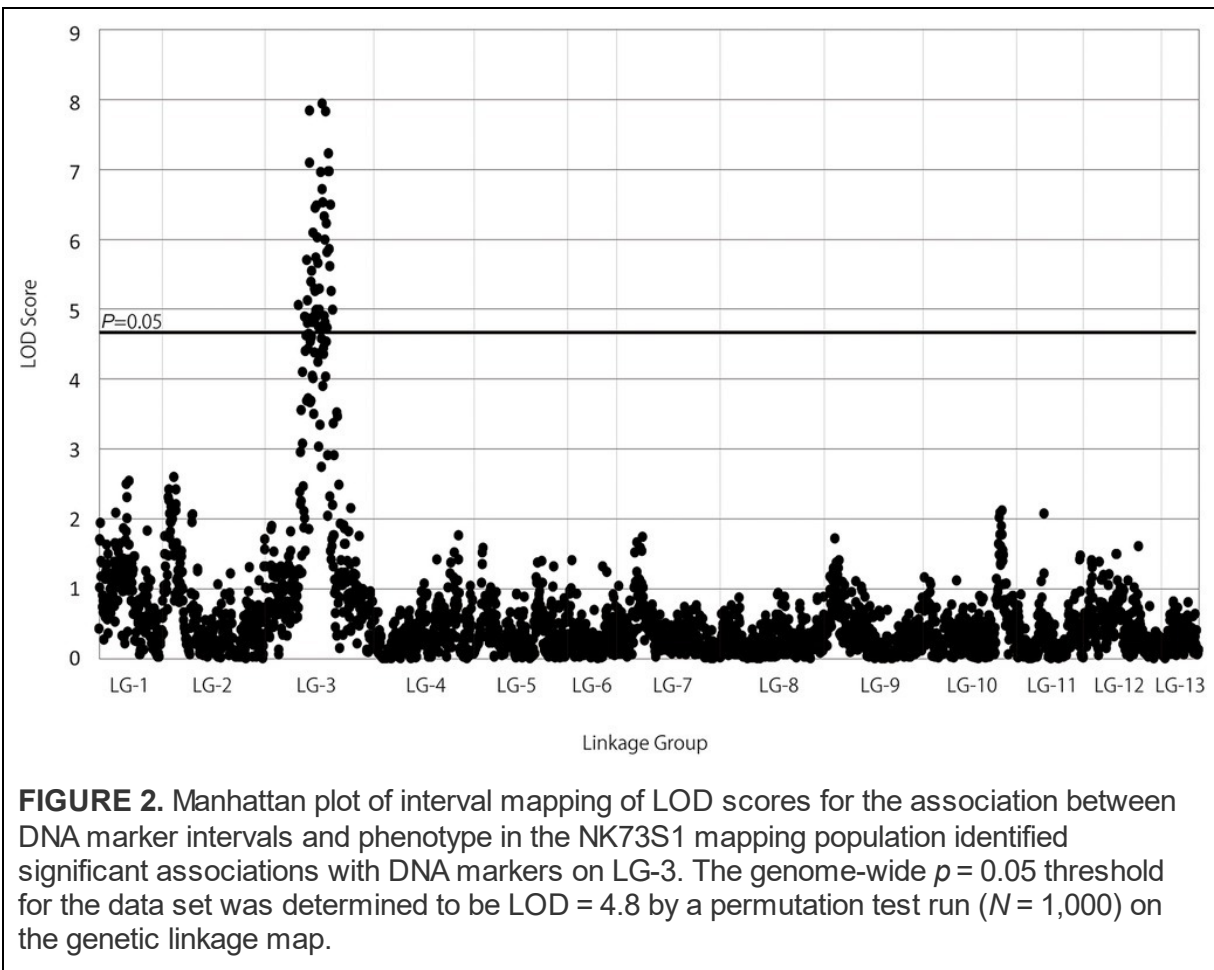
Progeny	Binary standard <sup>a</sup>		Total	Expected ratio (1:1) <sup>*</sup>		Expected ratio (3:1) <sup>*</sup>	
	Resistant (Survival; 1)	Susceptible (Mortality; 0)		$\chi^2$	<i>p</i> -value	$\chi^2$	<i>p</i> -value
$S_1$ population	57	59	116	0.03	0.85	36.05	1.927e-9

<sup>a</sup>Resistant and susceptible are evaluated based on mortality.

<sup>\*</sup>Chi-squared and *p*-values (one degree of freedom) are calculated under the assumption of Mendelian 1:1 and 3:1 segregation ratios.

## **Identification of a Locus for PWD Resistance in the NK73-S<sub>1</sub> Mapping Population**

QTL analysis performed using the constructed genetic linkage map and phenotypic data from a PWN inoculation test revealed a locus for PWD resistance on LG-3 (Figure 2) and a maximum plateau LOD score of 7.9. Permutation tests with 1,000 permutations yielded an LOD score threshold with statistical significance of  $\alpha = 0.05$  for PWD resistance of 4.8, which was used as the threshold to detect QTL for PWD resistance with genome-wide significance. MQM mapping confirmed the location of the major QTL that explains up to 27.0% of the total phenotypic variance observed for PWD resistance with a maximum LOD of 7.9 at 101.87 cM on LG-3 (Figure 3; Table 3). Based on all scores, MQM mapping identified marker TP105701 as a cofactor for this region. The QTL regions defined by a 1-LOD confidence interval around a significant QTL LOD peak contained three GBS-SNP markers, one EST-derived SNP marker, and one genomic SSR marker, respectively (Figure 3; Table 3).



### LG-3

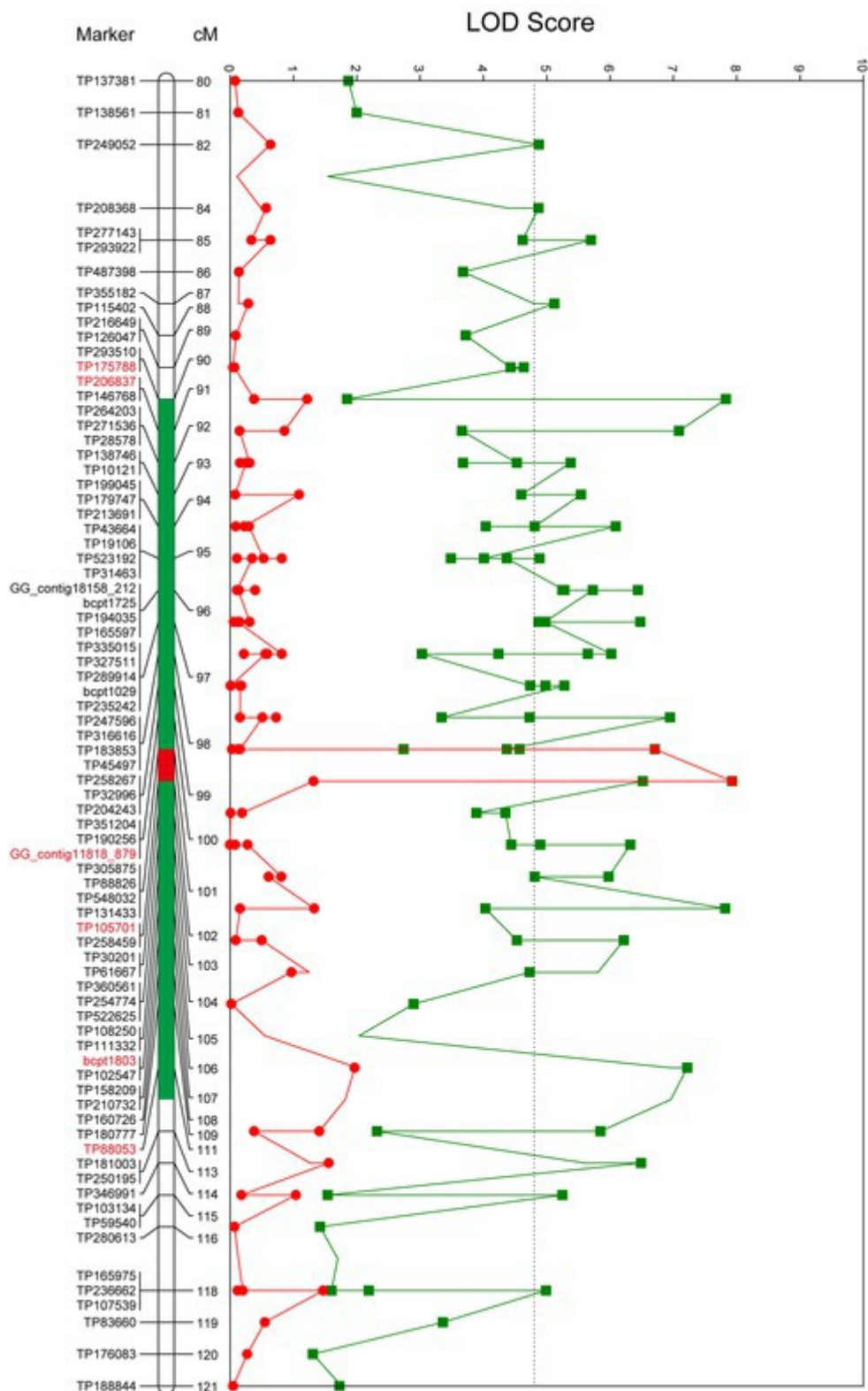


**FIGURE 3.** Localization of QTLs for PWD resistance identified in resistant variety “Namikata 73.” Only the area around the QTL was detected are displayed, and the red marker is located in the *PWD1* interval. The line trace in green shows the LOD score determined by interval mapping. The line trace in red shows the LOD score determined by multiple QTL mapping. Green tones and red tone as colored bars indicates a 1-LOD confidence interval of interval mapping and multiple QTL mapping. The genome-wide  $p = 0.05$  threshold for the data set was determined to be LOD = 4.8. The genetic linkage maps are in centimorgans (cM).

**TABLE 3.** Quantitative trait loci (QTLs) detected for PWD resistance in ‘Namikata 73’ S1 mapping population on the linkage group 3.

LG <sup>a</sup>	Locus	Marker type	Position (cM)	allele1	allele_2	LOD	PVE (%) <sup>b</sup>	K <sup>c</sup>	Signif. KW <sup>d</sup>	Df <sup>e</sup>	Genotype score <sup>f</sup>			Additive	Dominance	Allelic effects <sup>g</sup>
											Mean-hom-allele1	Mean-hetero	Mean-hom-allele2			
3	TP175788	GBS-SNP	90.06	T	A	7.83	26.7	30.729	*****	2	3.800	1.931	2.393	-0.704	-1.165	OD (1.656)
3	TP206837	GBS-SNP	90.72	T	C	7.09	24.5	28.209	*****	2	3.719	1.981	2.219	-0.750	-0.988	OD (1.317)
3	GG_	EST-derived	100.10	C	T	6.95	24.1	27.733	*****	2	3.793	2.034	2.241	0.776	-0.983	OD (1.267)
	contig11818_879	SNP														
3	TP105701	GBS-SNP	101.87	C	T	7.93	27.0	31.069	*****	2	3.727	1.889	2.345	0.691	-1.147	OD (1.660)
3	bcp1803	genomic SSR	105.67	235	237	7.82	26.7	30.695	*****	2	3.893	2.033	2.222	0.835	-1.025	OD (1.227)
3	TP88053	GBS-SNP	111.33	C	T	7.22	24.9	28.660	*****	2	3.793	1.984	2.385	0.704	-1.105	OD (1.569)

<sup>a</sup>Linkage group.

<sup>b</sup>Percentage of the phenotypic variation explained by the QTL.

<sup>c</sup>Kruskal-Wallis analysis (K<sup>c</sup>) test regarded as nonparametric equivalent of one-way analysis of variance (Van Ooijen, 2009).

<sup>d</sup>Significant markers \*\*\*\*\* $p < 0.0001$ .

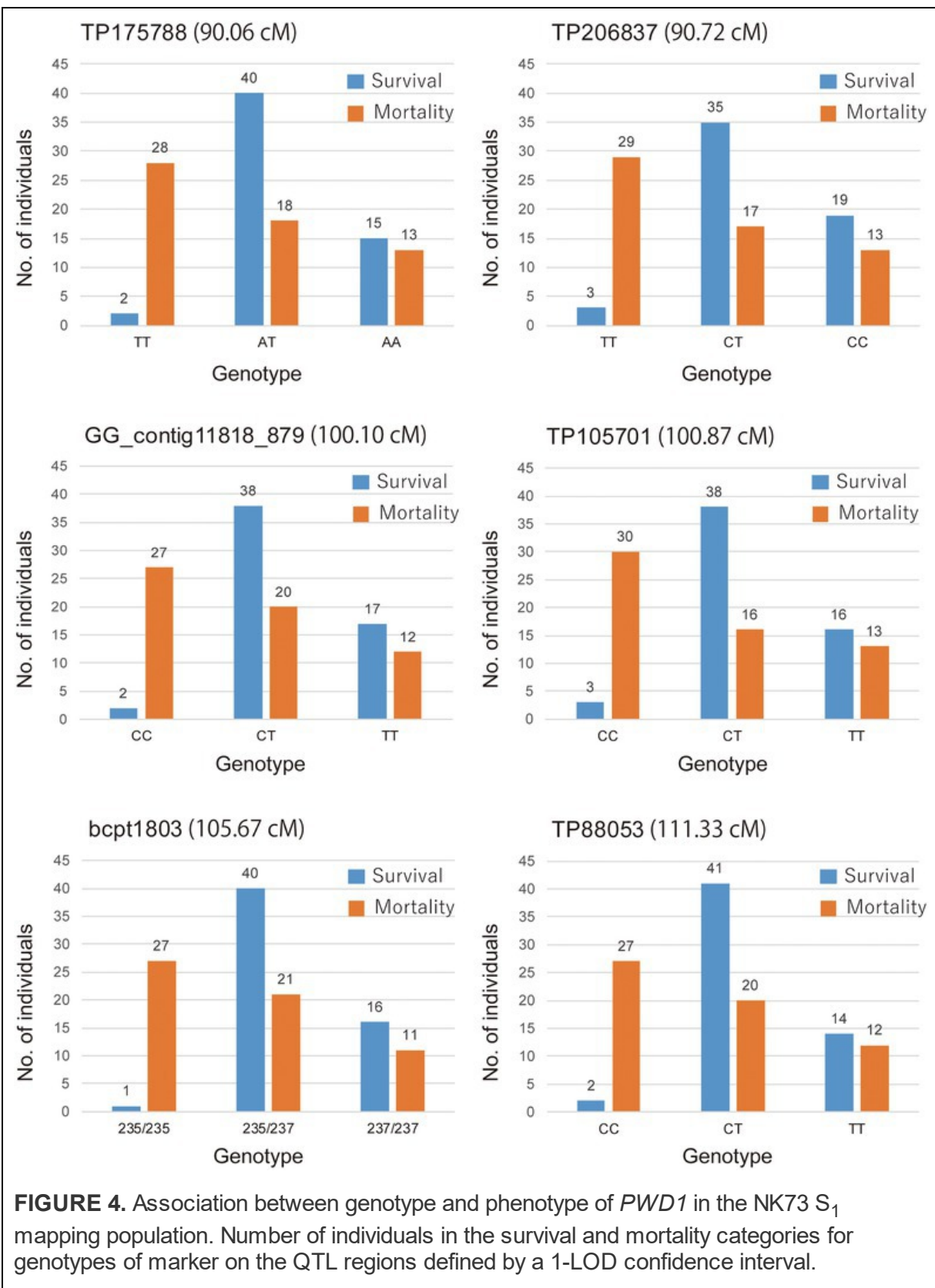
<sup>e</sup>Degree of freedom.

<sup>f</sup>Arithmetic mean of the distribution of the quantitative trait associated with homozygous of allele 1, heterozygous, and homozygous of allele 2, respectively.

<sup>g</sup>Allelic effects: additive effect (a), dominance effect (d), average degree of dominance (k), allelic interaction, average of disease severity, and mean severity reduction. Average degree of dominance (k) was estimated according to the formula  $k = [df/a]$ , indicating the following allelic interaction possibilities for a marker associated with QTL: absence of dominance (AD) if  $k = 0$ , partial dominance (PD) if  $0 < k < 1.0$ , complete dominance (CD) if  $k = 1.0$ , and overdominance (OD) if  $k > 1.0$ . (Stuber et al., 1987; Frérot et al., 2010).

The marker (TP105701) with a maximum LOD and the other five markers in the QTL regions defined by a 1-LOD confidence interval were converted to the actual detected allele, and those were shown to be significantly associated with the corresponding phenotypic data by the KW test and exhibited an overdominance effect (Table 3). The genotype of the nearest marker (TP105701) corresponded to genotype a (CC), h (CT), and b (TT) respectively. The highest LOD peak marker TP105701 was recorded with genotype 33 “CC”: 54 “CT”: 29 “TT.” Based on the allelic test of marker (TP105701) by the  $2 \times 2$  chi-squared test, the “T” of allele-1 was shown to be significantly associated with PWD resistance while the “C” of allele-2 was associated with PWD susceptibility ( $\chi^2 = 15.46$ ,  $p = 0.000084$ ). Similar results were shown for the other five markers ( $\chi^2 = 12.533$ – $17.660$ ,  $p = 0.0004$ – $0.000026$ ). The genotype–phenotype relationship was visualized by the real number of progeny for the mortality and survival groups for each locus genotype in a bar graph (Figure 4). These results indicate that the homozygous genotype of allele-1 actually confers susceptibility, but homozygous genotype allele-2 does not confer resistance, and heterozygous genotypes of allele-1 and allele-2 confer resistance, which corroborates the

results above that the effect of the allele was detected as an overdominance effect.



## DISCUSSION

The resistant variety “Namikata 73” used in this study is one of the 16 resistant varieties selected from 14,620 candidate trees collected from affected forests of southwest Japan over 7 years from 1978 to 1985 (Fujimoto et al., 1989). In a previous study, the heritability of resistance traits in resistant varieties was evaluated based on the survival rates of open-pollinated progenies with the survival rate of open-pollinated progeny in “Namikata 73” being the highest at 68.9%, compared to 38.5 to 61.1% for other resistant varieties and 12.5% for susceptible pines (Toda and Kurinobu, 2002). Results of previous studies indicate that this variety may carry a highly effective resistance gene/locus, but so far, the locus of this variety has not been clarified by molecular genetic approaches. On the other hand, a very effective defense response against PWN infection by this variety when compared to susceptible trees has been characterized at the transcriptional level (Hirao et al., 2012) as being a moderate defense response mediated by pathogenesis-related protein expression, followed by significant upregulation of cell wall-related genes induced by ROS. These results provide important insights for the resistance or defense response against PWD in other varieties or other *Pinus* species. Thus, identifying the resistance locus of this variety is an important clue for systematically elucidating the resistance mechanism to pine wilt disease.

To date, there have been few reports of linkage mapping in *P. thunbergii*. A genetic linkage map constructed using genomic SSR, EST-derived SSR, or SNP markers for  $F_1$  mapping with co-dominant markers and showing 12 LGs spanning over 1403.6 cM was recently reported by Hirao et al. (2019). Here, we applied high-throughput GBS technology with type-II restriction endonuclease *ApeKI* (GCWGC; Elshire et al., 2011) to identify SNPs in  $S_1$  segregated populations for the PWN resistance trait. In addition, genomic SSR markers and EST-derived SNP markers were also applied as anchor markers for comparison purposes with the consensus linkage map of *P. thunbergii* constructed in the previous study (Hirao et al., 2019). Since the draft genome of *P. thunbergii* has not yet been determined, we performed non-reference based GBS with the UNEAK pipeline (Lu et al., 2013), and a total of 2,243 GBS-SNP markers were used to construct 13 LGs spanning over 1,968.43 cM.

When comparing the order of the markers that are commonly mapped on the two maps for the linkage maps constructed in this study and the linkage maps constructed in the previous study by Hirao et al. (2019), the relative order in which markers were mapped on these two linkage maps were highly correlated. Linkage group 10 has not been fully validated as there were not enough markers to compare the relative order of the mapped markers. The length of the linkage map (1,968.43 cM) in the present study was approximately 500–560 cM longer than previously published linkage maps (1469.8 cM in Kondo et al., 2000 and 1403.6 cM in Hirao et al., 2019). GBS used in the present study provided a high mean marker density genetic map of 0.79 markers/cM, which is higher than the 15.6 and 3.26 mean marker density obtained on a previously constructed RAPD (random amplified polymorphic DNA)-based map (Kondo et al., 2000) or microsatellite-and EST-based map (Hirao et al., 2019). We considered that this is due primarily to a larger number of SNP markers being placed on the genetic map.

Although the 13 linkage groups constructed in the present study did not converge to the 12 basic chromosomes of *P. thunbergii*, we can assume that they may constitute one linkage group considering that LG-6 and LG-13 have shorter overall lengths than the other LGs. The EST-derived SNP marker (GG\_contig11987\_905) on LG-13 could not be associated with the consensus linkage map of *P. thunbergii* constructed in a previous study (Hirao et al., 2019), but we showed correspondence with the locus/gene (0\_17469) with high homology for LG-6 in the linkage map of *P. taeda* (Neves et al., 2014; Westbrook et al., 2015; data not shown). LG-6 and LG-13 correspond to the bottom and the upper parts, respectively, of *P. taeda* LG-6. The reason that LG-6 does not converge to one linkage group may be a sufficient number of polymorphisms that could not be detected by the GBS approach with type-II restriction endonuclease *Ape*KI or the presence of a lethal gene.

The genome-wide genotyping and construction of high-density linkage maps is an essential initial step in advancing fundamental genetics research and breeding programs for PWD resistance. Sequencing-based genotyping technology, such as GBS and RADseq, may result in large amounts of missing data, and missing data along with genotyping errors often leads to inaccurate ordering of markers of linkage maps. Although utilizing high-quality SNPs with <20% missing data without imputation has been attempted as an alternative for improving the data quality in a previous study (Liu et al.,

2014), we eventually utilized GBS-SNPs with completeness of 99% integrity to construct the linkage map for delineating *PWD1* in the present study. With this approach, we considered that the negative effect caused by missing data could be minimized. Furthermore, we were able to sufficiently narrow down the genetic polymorphisms and particular genome regions that are candidates for PWD resistance based on comparisons with results of previous constructed linkage maps in pine species.

As shown in the present study, PWD resistance in the  $S_1$  mapping population might be controlled by a major gene, as genetic analysis suggests good fit to a Mendelian ratio of 1:1 with a chi-squared value of 0.03 and probability of 0.85. Regarding the phenotype evaluation, assessment of external wilting symptoms after artificial inoculation is the most commonly used method for evaluating susceptibility and resistance in the host pine, and genetic analysis based on mortality evaluation (survival and mortality) confirmed that PWD resistance is a heritable trait (Toda and Kurinobu, 2001; Kurinobu, 2008; Menéndez-Gutiérrez et al., 2017). Binary data based on mortality were used for the actual QTL analysis in this study, and we succeeded in detecting a major locus that contributes to PWD resistance.

As a result of linkage analysis with the constructed genetic linkage map and phenotypic data in the resistant variety “Namikata 73”  $S_1$  mapping population, the PWD resistance locus was localized to LG-3 with a map distance of 101.87 cM. In addition to the GBS-SNP marker; TP105701 which has the highest LOD value and the highest contribution to trait, five markers (three GBS-SNP markers, one EST-derived SNP marker, and one genomic SSR marker) were detected as effective markers under the QTL confidence interval on LG-3. These QTLs have been detected over the range of 90.06 to 111.33 cM (interval of approximately 21 cM). The locus associated with PWD resistance detected in the present study was found to be on the same locus (*PWD1*: *PINE WILT DISEASE 1*) as in a previous study (Hirao et al., 2019) by making a comparison with the position of EST-derived SNP markers and genomic SSR markers used for mapping the  $F_1$  population in a previous study. In that previous study, a major *PWD1* locus for PWD resistance was detected over a confidence interval corresponding to a span of approximately 40 cM on the constructed map of LG-3 and corresponding to the maternal “Tanabe 54” based on maternal segregation. “Tanabe 54” was another one of the resistant varieties selected along with “Namikata 73” for use in the breeding project conducted in the 1970s. While

the survival rate of open-pollinated progenies of “Tanabe 54” was 38.5%, it showed the lowest heritability among the other 15 resistant varieties. The results of the present study indicate that the PWD resistance locus is identical to the PWD resistance locus in “Tanabe 54” with low heritability (38.5%) and in “Namikata 73” with high heritability (68.9%), which is an important clue for elucidating genes and their inheritance patterns for PWD resistance in the future.

For GBS-SNP marker TP105701, which has the highest LOD value and the highest contribution to trait, the “C” of the actual allele is clearly shown to be the susceptibility factor in *PWD1* in the present study, the overdominant gene action of resistance conferred by the “T” allele appears in the heterozygous genotype. On the other hand, the resistance effect of the homozygous “TT” genotype in *PWD1* was almost as ineffective as the heterozygous “CT” genotype. The genetic action of this locus was detected as being overdominant according to the degree of dominance in QTL analysis. Overdominance has been recognized as the allelic interaction explanation for hybrid vigor or heterosis; allele “A” and “B” at a locus can interact to cause a superior phenotype compared with both the “AA” and “BB” homozygous states (Birchler et al., 2006; Lippman and Zamir, 2007; Crow, 2010). In the present study, the “C” and “T” alleles at the *PWD1* locus have some interaction, and the heterozygous “CT” genotype exhibited overdominant action for PWD resistance. On the other hand, overdominance is also sometimes actually considered to be pseudo-overdominance. In pseudo-overdominance, repulsion-phase linkage (trans-complementation) of dominant and deleterious genes represent non-additive allelic action and occur when the active parts of a locus are interrupted by inactive parts such that heterozygosity becomes necessary for completion of chain transcription (Jones, 1917; Fasoula and Fasoula, 1983; Birchler et al., 2006; Lippman and Zamir, 2007; Crow, 2010). In *PWD1* of “Namikata 73,” the dominant gene (linked with allele “T”) suppresses the function of the susceptible gene (linked with allele “C”), and the susceptible gene may be linked in the repulsion phase, such that heterozygous  $S_1$  progenies obtained by self-pollination of “Namikata 73” may have the same high resistance as “Namikata 73” itself. Detailed examination of the genetic hypothesis (e.g., overdominance or pseudo-overdominance and epistatic action) needs to be conducted multi-generationally in order to separate out repulsion-phase linkage.

The other five markers in the QTL confidence interval (3 GBS-SNPs, 1 EST-derived marker, and 1 genomic SSR marker) showed similar trends and effects as TP105701. In addition, many markers have been detected in KW analysis, a non-parametric test. There are 65 markers associated with resistance traits at the level of  $p < 0.0001$ , including the above 6 markers, including 60 GBS-SNPs, 2 EST-derived SNPs, and 3 genomic SSR markers (Supplementary Table S5). Those GBS markers will be important information in identifying resistance candidate regions in more detail when the whole genome of *P. thunbergii* will have been determined in the future (Supplementary Table S1 and Supplementary File 1). Regarding EST-derived markers, contig11818 has been targeted polymorphisms on genes homologous to phenylalanine ammonia-lyase, and contig18158 has been targeted polymorphisms on genes homologous to hypothetical protein ARALYDRAFT\_891246. (See Supplementary Material of Hirao et al. (2019) for the information on the Illumina GoldenGate assay). It is unclear at this time whether these genes are involved in PWD resistance, but markers on highly conserved genes provide important information for comparison with genomic information of other pine species and other tree species. Furthermore, SSR marker shows co-dominant inheritance, robust and high reproducibility, high polymorphism, transferability between species, and low requirements of expertise and instrumentation, which are all characters that make it attractive as a marker. In addition, SSR markers are relatively low cost for genotyping and can be used by small labs. Although population-wide scoring of the SSR markers detected in the present study is a time-consuming, labor-intensive, and costly process, the information gained will support fundamental genetics research and breeding for PWD resistance (See Supplementary Material of Hirao et al. (2019) for information on genomic SSR markers).

As one of the genetic approaches in outbreeding plant species, such as trees, the pseudo-testcross strategy (Grattapaglia and Sederoff, 1994) with pseudo-testcross linkage analyses for each of two parents in an  $F_1$  full-sib family is used. In a previous study, inheritance patterns of PWD resistance traits were investigated by a two-way pseudo-testcross strategy using an  $F_1$  mapping population derived from resistant varieties cross, “Tanabe 54”  $\times$  “Tosashimizu 64” (Hirao et al., 2019). Although linkage analysis for PWD resistance using an  $S_1$  mapping population was first attempted in *P. thunbergii* in the present study, the PWD resistance trait was clearly

segregated, and the GBS-derived SNP markers were closely mapped to *PWD1* on LG-3. These results suggest a genetic approach using a self-pollinated family as one of the simplest and most effective approaches for detecting a major locus related to PWD resistance.

The result that the resistance locus was localized to LG-3 in both “Namikata 73” and “Tanabe 54,” the varieties with the highest and lowest heritability, respectively, for progeny for resistance is an unexpected new finding. In order to clarify the genetic mechanism at this locus, it is necessary to obtain genomic information of *P. thunbergii* and to clarify the genomic structure and genetic variation in this QTL region and to furthermore verify its heredity over multiple generations. Furthermore, in addition to the genome-wide genotyping system used in this study, the use of a large single cross to build genetic maps is also an important factor for constructing a high-density and high accuracy linkage map, which has been shown to be effective in the study of other tree species (Bartholomé et al., 2015; Pavy et al., 2017). By developing these verifications, it is possible to develop a more accurate marker system related to resistance traits for realizing resistance breeding by GAS and MAS, and we can thus advance PWN-resistant breeding in *P. thunbergii*.

## CONCLUSION

In this study, we constructed a high-density linkage map for *P. thunbergii* using GBS-SNP markers, along with anchor markers, such as genomic SSR markers and co-dominant SNP markers derived from ESTs. The use of a high-density sequence-based genetic map facilitated anchoring the QTLs to a physical map and provided a means for making an alignment with previously reported QTLs. Further, the locus for PWD resistance was identified on LG-3 by QTL analysis of the  $S_1$  mapping population using the constructed genetic linkage map and phenotypic data from a PWN inoculation test. The QTL on LG-3 was co-located with *PWD1*, which was detected in a previous study. The high-resolution genetic map of the  $S_1$  mapping population also enabled identification of QTLs in a narrower physical interval than for QTLs previously identified with SSR markers. Further, the susceptibility gene and the gene that suppresses the susceptibility gene were suggested to be “pseudo-overdominance” linked in the repulsion phase, although the genetic

pattern at this locus was determined to be overdominance. This study thus provides an important clue for elucidating genes and their inheritance patterns for PWD resistance in the future.

## **DATA AVAILABILITY STATEMENT**

The datasets presented in this study can be found in online repositories. The names of the repository/repositories and accession number(s) can be found in the article/Supplementary Material.

## **AUTHOR CONTRIBUTIONS**

TH conducted sampling and inoculation tests, as well as evaluation of phenotypes, prepared DNA, genotyped each DNA marker, constructed linkage maps, performed QTL analysis, and drafted the manuscript. KM mapped population development and seed materials. KS generated GBS genotyping data and constructed linkage maps. All authors assisted with manuscript preparation and read and approved the final manuscript.

## **FUNDING**

This research was supported financially by the Ministry of Agriculture, Forestry and Fisheries of Japan as part of the “Project to advance the development of technology for varieties of Japanese black pine and red pine resistant to the pine wood nematode.” This work was also supported by JSPS KAKENHI Grant Number 16K07792.

## **ACKNOWLEDGMENTS**

We thank A. Watanabe at the Kyushu University and M. Takahashi of FTBC, FFPRI for their coordination of the research project. We also thank M. Yano and Y. Katayose of the National Institute of Agrobiological Sciences for

GoldenGate SNP genotyping and for granting us use of their bead array reader. We thank T. Yamanobe of FTBC, FFPRI for the inoculation test of PWN. We also thank our colleagues in the field management section of FTBC for the production and cultivation of plant materials.

## SUPPLEMENTARY MATERIAL

The Supplementary Material for this article can be found online at: <https://www.frontiersin.org/articles/10.3389/fpls.2022.850660/full#supplementary-material>

**Supplementary Figure 1 |** Outline of the sample used for the construction of the linkage map and 731 QTL analysis in this study.

## REFERENCES

Andrews, K. R., Good, J. M., Miller, M. R., Luikart, G., and Hohenlohe, P. A. (2016). Harnessing the power of RADseq for ecological and evolutionary genomics. *Nat. Rev. Genet.* 17, 81–92. doi: 10.1038/nrg.2015.28

Bartholomé, J., Mandrou, E., Mabiala, A., Jenkins, J., Nabihoudine, I., Klopp, C., et al. (2015). High-resolution genetic maps of eucalyptus improve *Eucalyptus grandis* genome assembly. *New Phytol.* 206, 1283–1296. doi: 10.1111/nph.13150

Birchler, J. A., Yao, H., and Chudalayandi, S. (2006). Unraveling the genetic basis of hybrid vigor. *Proc. Natl. Acad. Sci.* 103, 12957–12958. doi: 10.1073/PNAS.0605627103

Bradbury, P. J., Zhang, Z., Kroon, D. E., Casstevens, T. M., Ramdoss, Y., and Buckler, E. S. (2007). TASSEL: software for association mapping of complex traits in diverse samples. *Bioinformatics* 23, 2633–2635. doi: 10.1093/bioinformatics/btm308

Chung, Y. S., Choi, S. C., Jun, T. H., and Kim, C. (2017). Genotyping-by-sequencing: a promising tool for plant genetics research and breeding. *Hortic. Environ. Biotechnol.* 58, 425–431. doi: 10.1007/s13580-017-0297-8

Crow, J. F. (2010). The rise and fall of overdominance. *Plant Breed. Rev.* 17, 225–257. doi: 10.1002/9780470650134.ch5

Davey, J. W., Hohenlohe, P. A., Etter, P. D., Boone, J. Q., Catchen, J. M., and Blaxter, M. L. (2011). Genome-wide genetic marker discovery and genotyping using next-generation sequencing. *Nat. Rev. Genet.* 12, 499–510. doi: 10.1038/nrg3012

Elshire, R. J., Glaubitz, J. C., Sun, Q., Poland, J. A., Kawamoto, K., Buckler, E. S., et al. (2011). A robust, simple genotyping-by-sequencing (GBS) approach for high diversity species. *PLoS One* 6:e19379. doi: 10.1371/journal.pone.0019379

Fasoula, D. A., and Fasoula, V. A. (1983). Gene action and plant breeding. *Plant Breed. Rev.* 15, 315–374.

Forest Tree Breeding Center, Forestry and Forest Products Research Institute (2019). Available at: <http://www.ffpri.affrc.go.jp/ftbc/business/sinhijnnssyu/teikousei.html> (Accessed September 27, 2019).

Forestry Agency Ministry of Agriculture, Forestry and Fisheries of Japan (2010). Annual report on trends of forest and forestry-fiscal year 2009. Tokyo: Forestry Agency, Ministry of Agriculture, Forestry and Fisheries of Japan. (in Japanese).

Frérot, H., Faucon, M. P., Willems, G., Godé, C., Courseaux, A., Darracq, A., et al. (2010). Genetic architecture of zinc hyperaccumulation in *Arabidopsis halleri*: The essential role of QTL × environment interactions. *New Phytol.* 187, 355–367. doi: 10.1111/j.1469-8137.2010.03295.x

Fujimoto, K., Toda, T., Nishimura, K., Yamate, H., and Fuyuno, S. (1989). Breeding project on resistance to the pine-wood nematode. –An outline of the research and the achievement of the project for ten years. *Bull. For. Tree Breed. Inst.* 7, 1–84.

Grattapaglia, D., and Sederoff, R. (1994). Genetic linkage maps of *Eucalyptus grandis* and *Eucalyptus urophylla* using a pseudo-testcross: mapping strategy and RAPD markers. *Genetics* 137:1121. doi: 10.1093/genetics/137.4.1121

Hall, D., Zhao, W., Wennström, U., Andersson Gull, B., and Wang, X. R. (2020). Parentage and relatedness reconstruction in *Pinus sylvestris* using genotyping-by-sequencing. *Heredity* 124, 633–646. doi: 10.1038/s41437-020-0302-3

Hayashi, E., Kondo, T., Terada, K., Kuramoto, N., and Kawasaki, S. (2004). Identification of AFLP markers linked to a resistance gene against pine needle gall midge in Japanese black pine. *Theor. Appl. Genet.* 108, 1177–1181. doi: 10.1007/s00122-003-1537-0

He, J., Zhao, X., Laroche, A., Lu, Z.-X., Liu, H., and Li, Z. (2014). Genotyping-by-sequencing (GBS), an ultimate marker-assisted selection (MAS) tool to accelerate plant breeding. *Front. Plant Sci.* 5:484. doi: 10.3389/fpls.2014.00484

Hirao, T., Fukatsu, E., and Watanabe, A. (2012). Characterization of resistance to pine wood nematode infection in *Pinus thunbergii* using suppression subtractive hybridization. *BMC Plant Biol.* 12:13. doi: 10.1186/1471-2229-12-13

Hirao, T., Matsunaga, K., Hirakawa, H., Shirasawa, K., Isoda, K., Mishima, K., et al. (2019). Construction of genetic linkage map and identification of a novel major locus for resistance to pine wood nematode in Japanese black pine (*Pinus thunbergii*). *BMC Plant Biol.* 19:424. doi: 10.1186/s12870-019-2045-y

Iwaizumi, M. G., Miyata, S., Hirao, T., Tamura, M., and Watanabe, A. (2018). Historical seed use and transfer affects geographic specificity in genetic diversity and structure of old planted *Pinus thunbergii* populations. *For. Ecol. Manag.* 408, 211–219. doi: 10.1016/j.foreco.2017.10.026

Iwaizumi, M. G., Tsuda, Y., Ohtani, M., Tsumura, Y., and Takahashi, M. (2013). Recent distribution changes affect geographic clines in genetic diversity and structure of *Pinus densiflora* natural populations in Japan. *For. Ecol. Manag.* 304, 407–416. doi: 10.1016/j.foreco.2013.05.026

Jones, D. F. (1917). Dominance of linked factors as a means of accounting for heterosis. *Proc. Natl. Acad. Sci. U. S. A.* 3, 310–312. doi: 10.1073/pnas.3.4.310

Katsuta, M. (1964). Self-fertilization in *Pinus thunbergii* and *P. densiflora*. *Bull. Tokyo Univ. Forest* 15, 23–35.

Kiyohara, T., and Tokushige, Y. (1971). Inoculation experiments of a nematode, *Bursaphelenchus* sp., onto pine trees. *J. Forestry Soc.* 53, 210–218.

Knott, S. A., Marklund, L., Haley, C. S., Andersson, K., Davies, W., Ellegren, H., et al. (1998). Multiple marker mapping of quantitative trait loci in a cross between outbred wild boar and large white pigs. *Genetics* 149, 1069–1080. doi: 10.1093/genetics/149.2.1069

Kondo, T., Terada, K., Hayashi, E., Kuramoto, N., Okamura, M., and Kawasaki, H. (2000). RAPD markers linked to a gene for resistance to pine needle gall midge in Japanese black pine (*Pinus thunbergii*). *Theor. Appl. Genet.* 100, 391–395. doi: 10.1007/s001220050051

Kurinobu, S. (2008). Current status of resistance breeding of Japanese pine species to pine wilt disease. *Forest Sci. Technol.* 4, 51–57. doi: 10.1080/21580103.2008.9656338

Lian, C., Miwa, M., and Hogetsu, T. (2000). Isolation and characterization of microsatellite loci from the Japanese red pine, *Pinus densiflora*. *Mol. Ecol.* 9, 1186–1187. doi: 10.1046/j.1365-294x.2000.00954-10.x

Lippman, Z. B., and Zamir, D. (2007). Heterosis: revisiting the magic. *Trends Genet.* 23, 60–66. doi: 10.1016/J.TIG.2006.12.006

Liu, H., Bayer, M., Druka, A., Russell, J. R., Hackett, C. A., Poland, J., et al. (2014). An evaluation of genotyping by sequencing (GBS) to map the Breviaristatum-e (ari-e) locus in cultivated barley. *BMC Genomics* 15:104. doi: 10.1186/1471-2164-15-104

Lu, Q., Cui, Y., and Wu, R. (2004). A multilocus likelihood approach to joint modeling of linkage, parental diplotype and gene order in a full-sib family. *BMC Genet.* 5:20. doi: 10.1186/1471-2156-5-20

Lu, F., Lipka, A. E., Glaubitz, J., Elshire, R., Cherney, J. H., Casler, M. D., et al. (2013). Switchgrass genomic diversity, Ploidy, and evolution: novel insights from a network-based SNP discovery protocol. *PLoS Genet.* 9:e1003215. doi: 10.1371/journal.pgen.1003215

Menéndez-Gutiérrez, M., Alonso, M., Toval, G., and Díaz, R. (2017). Variation in pinewood nematode susceptibility among *Pinus pinaster* Ait. Provenances from the Iberian Peninsula and France. *Ann. For. Sci.* 74:76. doi: 10.1007/s13595-017-0677-3

Neale, D. B., and Wheeler, N. C. (2019). “Genomes: Classical Era,” in *The Conifers: Genomes, Variation and Evolution*. eds. D. B. Neale and N. C. Wheeler (Cham: Springer International Publishing), 25–42.

Neves, L. G., Davis, J. M., Barbazuk, W. B., and Kirst, M. (2014). A high-density gene map of loblolly pine (*Pinus taeda* L.) based on exome sequence capture genotyping. *G3* 4, 29–37. doi: 10.1534/g3.113.008714

Nicotra, A. B., Chong, C., Bragg, J. G., Ong, C. R., Aitken, N. C., Chuah, A., et al. (2016). Population and phylogenomic decomposition via genotyping-by-sequencing in Australian pelargonium. *Mol. Ecol.* 25, 2000–2014. doi: 10.1111/mec.13584

Pan, J., Wang, B., Pei, Z.-Y., Zhao, W., Gao, J., Mao, J.-F., et al. (2015). Optimization of the genotyping-by-sequencing strategy for population genomic analysis in conifers. *Mol. Ecol. Resour.* 15, 711–722. doi: 10.1111/1755-0998.12342

Pavy, N., Lamothe, M., Pelgas, B., Gagnon, F., Birol, I., Bohlmann, J., et al. (2017). A high-resolution reference genetic map positioning 8.8 K genes for the conifer white spruce: structural genomics implications and correspondence with physical distance. *Plant J.* 90, 189–203. doi: 10.1111/tpj.13478

Poland, J. A., and Rife, T. W. (2012). Genotyping-by-sequencing for plant breeding and genetics. *Plant Genome J.* 5:92. doi: 10.3835/plantgenome2012.05.0005

Stuber, C. W., Edwards, M. D., and Wendel, J. F. (1987). Molecular marker-facilitated investigations of quantitative trait loci in maize. II. Factors influencing yield and its component traits 1. *Crop Sci.* 27, 639–648. doi: 10.2135/cropsci1987.0011183x002700040006x

Toda, T. (2004). Studies on breeding for resistance to pine wilt disease in *Pinus densiflora* and *P. thunbergii*. *Bull For Tree Breed Cent.* 20, 83–217.

Toda, T., and Kurinobu, S. (2001). Genetic improvement in pine wilt disease resistance in *Pinus thunbergii*: The effectiveness of pre-screening with an artificial inoculation at the nursery. *J. For. Res.* 6, 197–201. doi: 10.1007/BF02767093

Toda, T., and Kurinobu, S. (2002). Realized genetic gains observed in progeny tolerance of selected red pine (*Pinus densiflora*) and black pine (*P. thunbergii*) to pine wilt disease. *Silvae Genet.* 51, 42–44.

Van Ooijen, J. (2006). *JoinMap 4: Software for the Calculation of Genetic Linkage Maps in Experimental Populations*. Wageningen: Kyazma BV.

Van Ooijen, J. W. (2009). *MapQTL Version 6.0, Software for the Mapping of Quantitative Trait Loci in Experimental Populations of Diploid Species*. Wageningen, Netherlands: Kyazma BV.

Voorrips, R. E. (2002). MapChart: software for the graphical presentation of linkage maps and QTLs. *J. Hered.* 93, 77–78. doi: 10.1093/jhered/93.1.77

Watanabe, A., Ubukata, M., Kondo, T., Lian, C., and Hogetsu, T. (2006). Isolation of microsatellite markers from *Pinus densiflora* Sieb. Et Zucc. Using a dual PCR technique. *Mol. Ecol. Notes* 6, 80–82. doi: 10.1111/j.1471-8286.2005.01145.x

Westbrook, J. W., Chhatre, V. E., Wu, L.-S., Chamala, S., Neves, L. G., Muñoz, P., et al. (2015). A consensus genetic map for *Pinus taeda* and *Pinus elliottii* and extent of linkage disequilibrium in two genotype-phenotype discovery populations of *Pinus taeda*. *G3* 5, 1685–1694. doi: 10.1534/g3.115.019588

Wu, S., Yang, J., Huang, Y., Li, Y., Yin, T., Wullschleger, S. D., et al. (2010). An improved approach for mapping quantitative trait loci in a pseudo-testcross: revisiting a poplar mapping study. *Bioinform. Biol. Insights.* 4, 1–8. doi: 10.4137/BBI.S4153

**Conflict of Interest:** The authors declare that the research was conducted in the absence of any commercial or financial relationships that could be construed as a potential conflict of interest.

**Publisher's Note:** All claims expressed in this article are solely those of the authors and do not necessarily represent those of their affiliated organizations, or those of the publisher, the editors and the reviewers. Any product that may be evaluated in this article, or claim that may be made by its manufacturer, is not guaranteed or endorsed by the publisher.

*Copyright © 2022 Hirao, Matsunaga and Shirasawa. This is an open-access article distributed under the terms of the Creative Commons Attribution License (CC BY). The use, distribution or reproduction in other forums is permitted, provided the original author(s) and the copyright owner(s) are credited and that the original publication in this journal is cited, in accordance with accepted academic practice. No use, distribution or reproduction is permitted which does not comply with these terms.*

ORIGINAL RESEARCH

published: 25 April 2022

doi: 10.3389/fpls.2022.872076



# Novel Functional Analysis for Pathogenic Proteins of *Bursaphelenchus xylophilus* in Pine Seed Embryos Using a Virus Vector

Haru Kirino<sup>1</sup>, Ken-ichi Konagaya<sup>2</sup> and Ryoji Shinya<sup>1\*</sup>

<sup>1</sup> School of Agriculture, Meiji University, Kawasaki, Japan

<sup>2</sup> Forest Bio-Research Center, Forestry and Forest Products Research Institute, Hitachi, Japan

**Edited by:**

Shahid Siddique, University of California, Davis, United States

**Reviewed by:**

Lee Robertson, National Institute of Agricultural and Food Research and Technology, Spain

Joana M. S. Cardoso, University of Coimbra, Portugal

**\*Correspondence:** Ryoji Shinya, shinya@meiji.ac.jp

**Specialty section:** This article was submitted to Plant Pathogen Interactions, a section of the journal *Frontiers in Plant Science*

**Received:** 09 February 2022

**Accepted:** 04 April 2022

**Published:** 25 April 2022

**Citation:** Kirino H, Konagaya K and Shinya R (2022) Novel Functional Analysis for Pathogenic Proteins of *Bursaphelenchus xylophilus* in Pine Seed Embryos Using a Virus Vector. *Front. Plant Sci.* 13:872076. doi: 10.3389/fpls.2022.872076

Pine wilt disease (PWD), which is caused by the pine wood nematode *Bursaphelenchus xylophilus*, is among the most serious tree diseases worldwide. PWD is thought to be initiated by sequential excessive hypersensitive responses to *B. xylophilus*. Previous studies

have reported candidate pathogenic molecules inducing hypersensitive responses in pine trees susceptible to *B. xylophilus*. The functions of some of these molecules have been analyzed in model plants using transient overexpression; however, whether they can induce hypersensitive responses in natural host pines remains unclear due to the lack of a suitable functional analysis method. In this study, we established a novel functional analysis method for susceptible black pine (*Pinus thunbergii*) seed embryos using transient overexpression by the *Apple latent spherical virus* vector and investigated five secreted proteins of *B. xylophilus* causing cell death in tobacco to determine whether they induce hypersensitive responses in pine. We found that three of five molecules induced significantly higher expression in pathogenesis-related genes ( $p < 0.05$ ), indicating hypersensitive response in pine seed embryos compared with mock and green fluorescence protein controls. This result suggests that tobacco-based screening may detect false positives. This study is the first to analyze the function of pathogenic candidate molecules of *B. xylophilus* in natural host pines using exogenous gene expression, which is anticipated to be a powerful tool for investigating the PWD mechanism.

**Keywords:** pine wilt disease, pine wood nematode, exogenous gene expression, hypersensitive responses, pathogenesis-related genes, *apple latent spherical virus*

## INTRODUCTION

Pine wilt disease (PWD), which is caused by the pine wood nematode *Bursaphelenchus xylophilus*, is a serious threat to pine forests worldwide (Kiyohara and Tokushige, 1971; Yi et al., 1989; Burgermeister et al., 1999; Abelleira et al., 2011). The mechanism by which *B. xylophilus* kills host pine trees has been extensively studied during the past 50 years. Based on physiological and histological observation, sequential excessive hypersensitive responses to the spread of *B. xylophilus* through the tree are thought to lead, eventually, to the death of susceptible pine trees (Myers,

1988; Futai, 2013). The expression levels of pathogenesis-related (PR) genes, that is the landmark of hypersensitive responses, have been found to be much higher in susceptible trees inoculated with nematodes than in resistant trees (Hirao et al., 2012). Furthermore, Yamaguchi et al. (2019) showed that all of pine seedling, that increased the number of *B. xylophilus* and expression levels of PR genes after nematodes inoculation, exhibited external symptoms. Accordingly, identifying *B. xylophilus* molecules that induce hypersensitive responses in host pine trees is important for predicting PWD occurrence, and the range of candidate molecules has been narrowed down using genomic, transcriptome, and proteome methods (Kikuchi et al., 2011; Shinya et al., 2013, 2021; Palomares-Rius et al., 2015; Cardoso et al., 2016, 2021; Ding et al., 2016; Espada et al., 2016, 2018; Filipiak et al., 2020; Silva et al., 2021). Recent functional analyses of these candidate molecules have mainly applied RNAi in *B. xylophilus* or examined the expression of its virulence factors in plants (Ma et al., 2011; Huang et al., 2019; Qiu et al., 2019). Because *B. xylophilus* RNAi effects are generally transient and weak, functional analysis using plants appears to be a more suitable approach for this research (Park et al., 2008).

The overexpression of foreign genes in plants is a major biotechnological tool in molecular functional analysis. For example, leaf-disk assays based on transient overexpression in the model plant *Nicotiana benthamiana* have been applied to investigate whether pathogenic candidate molecules of *B. xylophilus* induce cell death (Hu et al., 2019; Kirino et al., 2020; Shinya et al., 2021). Such studies have successfully narrowed the field of candidate molecules; however, whether they induce hypersensitive responses in natural pines remains unclear. Therefore, the next challenge is to develop a method for expressing *B. xylophilus* protein in pine trees and to perform functional analysis of the pathogenic candidate molecules. Because transgenic pine seedling production requires substantial time and effort, they are unsuitable for screening *B. xylophilus* pathogenic candidates. Therefore, in this study, we focused on pine seed embryos instead of pine seedlings. Exogenous proteins such as green fluorescent protein (GFP) can be transiently expressed in pine seed embryos using the *apple latent spherical virus* (ALSV) vector (Konagaya, 2017). ALSV is a small spherical virus (diameter, 25 nm) originally isolated from apple trees (Li et al., 2000, 2004) and has two ssRNA species (pEALSR1 and pEALSR2). ALSV-based vectors can be used to infect experimentally a broad range of plant species without causing

symptoms, effectively inducing stable virus-induced expression of foreign genes in plants (Takahashi and Yoshikawa, 2008). Therefore, we hypothesized that an ALSV-based method is suitable for identifying pathogenic molecules in *B. xylophilus*.

To evaluate the effectiveness of this method using pine seed embryos with ALSV for the functional analysis of pathogenic molecules in *B. xylophilus*, we selected five proteins secreted by *B. xylophilus* causing cell death in tobacco (Kirino et al., 2020; Shinya et al., 2021) and expressed them in susceptible black pine (*Pinus thunbergii*) seed embryos through transient overexpression using the ALSV vector. Because *B. xylophilus* protein expression induced using the ALSV vector is transient and insufficient for inducing cell death, genetic markers are more suitable for evaluating host responses. Then, we examined whether hypersensitive response could be induced through the expression of each *B. xylophilus* protein based on expression of PR-1b (enigmatic biochemical function), PR-2 (beta-1,3-glucanase), PR-3 (classes I and IV chitinase), PR-4 (chitinase types I and II), PR-5 (thaumatin-like protein), and PR-6 (type II proteinase inhibitor family protein) in pine seed embryos because the expression of these genes was induced more quickly and to a higher level in susceptible than in resistant trees following infection by a virulent isolate of *B. xylophilus*, suggesting that the expression of these PR genes is good indicators of hypersensitive response that precede pine wilt (Hirao et al., 2012). To our knowledge, this is the first report of functional analysis using recombinant pathogenic candidate molecules of *B. xylophilus* in host pines. This method is anticipated to be a powerful tool for investigating the PWD mechanism.

## MATERIALS AND METHODS

### Nematode Strains and Culturing

We used the virulent Ka4 isolate of *B. xylophilus*, which was propagated on the BC-3 strain of the fungus *Botrytis cinerea*, grown at 25°C on malt extract agar (MEA) plates (Difco Laboratories) containing 100 µg/ml chloramphenicol in 90-mm petri dishes.

### Nematode Sterilization

Nematodes grown for 3–5 days in mixed culture were collected into 15-mL tubes containing sterile water. The tubes were centrifuged at 2,000 rpm for 2 min. The supernatant was discarded, with nematodes retained at the bottom of the tube. We added 5 ml of a solution consisting of 0.002% mercuric chloride, 0.0025% sodium azide, and 0.001% Triton X-100 in sterile water; the solution was allowed to stand for 10 min. The nematodes were washed with sterile water three times. Then, a nematode solution in 5 ml sterile water containing 5  $\mu$ l of 1,000 ppm streptomycin was incubated at 12°C overnight. The nematodes were again washed with sterile water three times and then re-suspended in sterile water and used for inoculation into pine seed embryos.

### **Pine Seed Sterilization**

We used a PWD-susceptible black pine Taga-1 isolate of *P. thunbergii* in this study. Pine seeds were immersed in 70% ethanol and shaken for 3 min. Floating seeds were discarded. The remaining seeds were immersed in 5% hydrogen peroxide solution in sterile water containing a drop of Tween 20 and shaken for 10 min. The seeds were washed with sterile water five times, immersed in sterile water at 4°C for 1 week, and then used for nematode or biolistic inoculation.

### **Nematode Inoculation to Pine Seed Embryos**

For each sterilized pine seed, the seed coat and endosperm were removed and the embryo was extracted using tweezers and knife. These pine seed embryos were sown on a 60-mm mGD plate (Konagaya et al., 2020) containing 10  $\mu$ g/ml benomyl and 100  $\mu$ g/ml chloramphenicol. Twelve pine seed embryos were inoculated approximately 500 nematodes per plant under aseptic conditions, and six were not inoculated nematodes (mock control) with one replicate per experiment. The embryos were placed into a growth chamber (25°C, 24 h light).

### **Nematode Total RNA Extraction and cDNA Synthesis**

Mixed-stage nematodes grown for 5 days on MEA plates were collected with sterile water, sedimented by centrifugation at 2,500 rpm for 2 min, and re-suspended in fresh sterile water. This procedure was repeated three times. After the final wash, the nematode pellet was homogenized using a mortar and pestle after freezing with liquid nitrogen. Total RNA was extracted from

homogenized nematodes and purified using the RNeasy Mini Kit (Qiagen), according to the manufacturer's protocol. Reverse transcription was performed using 1 µg of total RNA and the PrimeScript II first-strand cDNA Synthesis Kit (Takara Bio Inc.), according to the manufacturer's protocol. The transcribed cDNA was adjusted to a concentration of 200 ng/µL and subjected to PCR amplification.

## Construction of ALSV Vectors

The candidate proteins (Table 1) were proteins secreted by *B. xylophilus* that were found to cause tobacco cell death in our previous studies (Kirino et al., 2020; Shinya et al., 2021). The sequence of *Bx-CPI* included signal peptide because it induced cell death in *N. benthamiana* only when signal peptide was present. Signal peptides of the other proteins were removed. All sequences including the GFP control were amplified by PCR from cDNA extracted from *B. xylophilus* or pRSET-EmGFP (Thermo Fisher Scientific). All PCR assays were performed using Takara PrimeSTAR GXL DNA polymerase, according to the manufacturer's protocol (Takara Bio Inc.). The PCR components were as follows: 10 µl 5 × Prime STAR GXL buffer, 4 µl dNTP Mixture (2.5 mM each), 1 µl forward primer (10 µM), 1 µl reverse primer (10 µM), 1 µl Prime STAR GXL Polymerase, 1 µl cDNA template (200 ng/µL), and 32 µl H<sub>2</sub>O. The cycling conditions were as follows: 35 cycles at 98°C for 10 s, 55°C for 15 s, and 68°C for 60 s/kb. The primers were designed using the Primer 3 Plus software (<http://www.bioinformatics.nl/cgi-bin/primer3plus/primer3plus.cgi>). The primers are listed in Table 2. The DNA products from *B. xylophilus* were inserted into the pEALSR2L5R5 vector (Yamagishi and Yoshikawa, 2013) using the In-Fusion HD Cloning Kit (Takara Bio Inc.) under the following conditions: 37°C for 15 min and 42°C for 15 min. The amplified GFP was digested with *Xho* I and *Bam* HI, and ligated to pEALSR2L5R5 vectors restricted with the same enzymes following previous research (Li et al., 2004). The resulting clones were designated pEALSR2-BxTH1, pEALSR2-BxTH2, pEALSR2-BxCPI, pEALSR2-BxGH30, and pEALSR2-BxGST. Gene sequences were confirmed by sanger sequence analysis using primer pair; Virus FP and Virus RP in Table 2 (Yamagishi et al., 2014). Both pEALSR1 and the constructed pEALSR2 that ALSV consists of were transformed in *Escherichia coli* JM109 and purified from large-scale cultures using the Plasmid Mini Kit (Qiagen); each was mixed at a

concentration of 0.5 µg/µL and then mechanically inoculated into *Chenopodium quinoa* leaves at the eight true leaf stage for propagating ALSV vectors (25°C, 16 h:8 h light:dark). Three independent plants were inoculated per vectors. Leaves with chlorotic spots were homogenized by shaking twice at 1,500 rpm for 3 min with 15 iron balls (diameter, 5 mm) in 15-mL tubes, and RNA was extracted using the RNeasy Mini Kit.

**TABLE 1.** Candidate pathogenic molecules secreted by *Bursaphelenchus xylophilus*.

Gene DB accession	Full-length base sequences (bp)	Protein annotation
BUX.s00036.89	441	thaumatin-like (Bx-TH1)
BUX.s00036.92	258	thaumatin-like (Bx-TH2)
BUX.s00351.347	375	cysteine protease inhibitor-like (Bx-CPI)
BUX.s00647.112	717	glutathione s-transferase (Bx-GST)
BUX.s00713.1066	1,545	o-glycosyl hydrolase family 30 (Bx-GH30)

**TABLE 2.** List of primers used in this study.

Primer name	Sequence (5' to 3')	References
Bx-TH1 FP	<u>TTCACACTCGAGCCC</u> ATGGGATATA <u>CGAGCTTCG</u>	–
Bx-TH1 RP	<u>TAGCAGGGAT</u> CCCCCAGGACAGTAGATGACGTAG	–
Bx-TH2 FP	<u>TGATTTCA</u> ACTCGAGATGGAGTTCTCTTGAGA	–
Bx-TH2 RP	CTTCTAGCAGGGAT <u>CCGCAGAAGTACAAGTCGAAC</u>	–
Bx-CPI FP	TTCACACTCGAGCCC <u>ATGTTGTTCAAAGTTACTGTG</u>	–
Bx-CPI RP	<u>TAGCAGGGAT</u> CCCCCTTTGCTGACGATTTCGG	–
Bx-GST FP	<u>TGATTTCA</u> ACTCGAGATGTTAGAGCTGTATTATTC	–
Bx-GST RP	CTTCTAGCAGGGAT <u>CCCTGAGTGGCATTGAAATAATG</u>	–
Bx-GH30 FP	<u>TGATTTCA</u> ACTCGAGATGACGCC <u>TTGCAAGAAGG</u>	–
Bx-GH30 RP	CTTCTAGCAGGGAT <u>CCACTATTGTTGAAGATGATGGT</u>	–
GFP FP	CCCTCGAGAT <u>CGT</u> GAGCAAGGGCAGGA	Li et al., 2004
GFP RP	<u>CGGGAT</u> CCCTTGTA <u>CGCTCGTCCA</u>	Li et al., 2004
Elongation factor-1 alpha FP	GGGAAGGCC <u>ACCCAAAGTTT</u>	Hirao et al., 2012
Elongation factor-1 alpha RP	TACATGGGAAGACGCC <u>GAAT</u>	Hirao et al., 2012
PR-2 family FP	CGACAA <u>ACATT</u> CGCC <u>CCCTTCT</u>	Hirao et al., 2012
PR-2 family RP	CTGCAGCG <u>GGTTGAATAT</u>	Hirao et al., 2012
PR-4 family FP	CCCCGTT <u>ACTGTCAATTGCAT</u>	Hirao et al., 2012
PR-4 family RP	AAAGCGT <u>GACGGTGC</u> GTATT	Hirao et al., 2012
PR-5 family FP	GAACCA <u>GTGCC</u> ATACACAGTCT	Hirao et al., 2012
PR-5 family RP	CCTGCC <u>GAACGTTAAAGTC</u>	Hirao et al., 2012
PR-6 family FP	TGCTGGCG <u>GCATCTATTTA</u>	Hirao et al., 2012
PR-6 family RP	TAACAC <u>CTGGCAATGCA</u>	Hirao et al., 2012
Virus FP (4F6150(+))	CGATGA <u>ATCTCCCTG</u> ATAGA	Yamagishi et al., 2014
Virus RP (4R6279(-))	AGAGTAGTGG <u>TCTCCAGCAA</u>	Yamagishi et al., 2014

The underlined sequences indicate restriction sites.

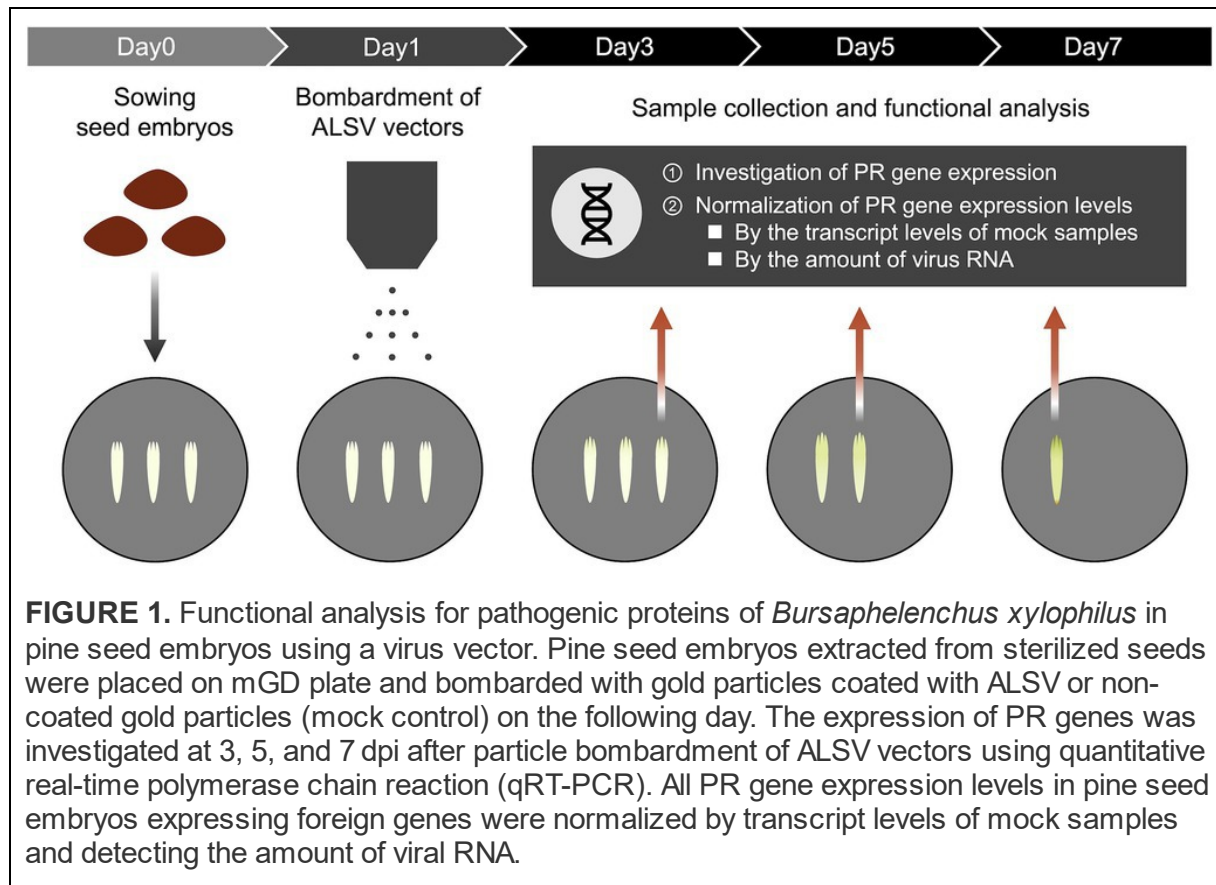
## Biostatic Inoculation of Pine Seed Embryos With ALSV

Biostatic inoculation of pine seed embryos with ALSV-RNAs was performed as described previously (Yamagishi et al., 2010), with modifications. We added 2 mg of gold particles (diameter, 0.6  $\mu$ m) and 12.5  $\mu$ l RNase-free H<sub>2</sub>O into a 2-mL microcentrifuge tube. The tube was then vortexed vigorously using a MicroMixer E-36 (Taitec) for 5 min and then sonicated for at least 5 min. During vortexing, 33  $\mu$ l of 1.5  $\mu$ g/ $\mu$ L total RNA solution extracted from ALSV-infected *C. quinoa* leaves, 11  $\mu$ l of 10 M ammonium acetate, and 113  $\mu$ l of 2-propanol were added to the tube sequentially. After continual vortexing for 7–10 min, gold particles coated with the RNAs were stored at –20°C for 1 h to overnight. The pellet of gold particles was washed gently three times with 1 ml of 100% ethanol and the pellet was re-suspended in 66  $\mu$ l of 100% ethanol. Pine seed embryos extracted from sterilized seeds were placed on a 90-mm mGD plate containing 10  $\mu$ g/ml benomyl and 0.4 M maltose and inoculated biolistically with ALSV on the following day. Fifteen pine seed embryos were bombarded with gold particles coated with total RNAs from ALSV-infected leaves per different ALSV vectors, and nine were bombarded with non-coated gold particles (mock control) at a pressure of approximately 1,100 psi using the PDS-1000/He Particle Delivery system (Bio-Rad) with one replicate per experiment. Pine seed embryos were bombarded in two shots, each containing 0.3 mg of particles. Next, the pine seed embryos were placed in a growth chamber (25°C, 24 h light). The next day, pine seed embryos were placed on a 90-mm mGD plate containing 10  $\mu$ g/ml benomyl and returned to the growth chamber. GFP fluorescence was observed using a MS FLIII fluorescence stereomicroscope (Leica Microsystems) with a GFP2 Plus filter system (excitation filter, 480/40 nm; emission filter, 510 nm). The GFP signal was imaged using a DC300 F digital camera system (Leica Microsystems).

## **Quantitative Reverse-Transcription Polymerase Chain Reaction and Normalization**

For quantitative reverse-transcription polymerase chain reaction (qRT-PCR) analysis, samples were collected from pine seed embryos at 3 and 5 days post-*B. xylophilus* infection (dpi), or at 3, 5, and 7 dpi after particle bombardment with ALSV vectors. Total RNA was isolated from pine seed embryos using the RNeasy Plant Mini Kit (Qiagen) following the manufacturer's protocol. RT-PCR was performed using total pine seed embryo RNA. Total RNA was reverse-transcribed using the PrimeScript II

first-strand cDNA synthesis kit (TaKaRa) according to the manufacturer's protocol and qRT-PCR was performed using the Power SYBR Green PCR Master Mix (Applied Biosystems) on the StepOnePlus Real-Time PCR System (Applied Biosystems). The PCR mixtures were prepared according to the manufacturer's instructions and contained 300 nM each of the forward and reverse gene-specific primers and 4  $\mu$ l of the 20-fold diluted reverse-transcription reaction (total, 5 ng) for a final volume of 20  $\mu$ l. All reactions were heated to 95°C for 10 min; this denaturation step was followed by 40 cycles of 95°C for 15 s and 60°C for 1 min. The PCR products were subjected to melting curve analysis under the following conditions: 60–95°C at a temperature increment of 1.6°C/s. Elongation factor 1-alpha (FY842441.1) was used as the reference gene for normalizing the transcript profiles. Primer pairs were designed as described previously (Hirao et al., 2012; Table 2). Real-time PCR data were calibrated against the transcript levels of mock samples; the  $2^{-\Delta\Delta C_t}$  method was used to quantify relative transcript abundance. Pine seed embryos expressing GFP were used as a control sample to distinguish specific and non-specific induced expression changes. All PR gene expression levels in pine seed embryos expressing foreign genes were normalized by detecting the amount of viral RNA. Primer pairs for detecting the amount of viral RNA were designed as described previously (Yamagishi et al., 2014; Table 2). Figure 1 shows an outline of the experiment method.



## RESULTS

### ***PR-2, PR-4, PR-5, and PR-6 Reacted to *B. xylophilus* in Pine Seed Embryos***

To identify suitable marker genes to react to *B. xylophilus* invasion in pine seed embryos, we assayed the expression of six PR genes in pine seed embryos using qRT-PCR. The expression of these PR genes has been suggested to be a good indicator of hypersensitive response that precede pine wilt (Hirao et al., 2012). In this study, the expression levels of four genes (*PR-2*, *PR-4*, *PR-5*, and *PR-6*) were markedly upregulated following inoculation with *B. xylophilus* into pine seed embryos (Figure 2). The expression levels of *PR-2* and *PR-6* in pine seed embryos infected with *B. xylophilus* were  $>10$ -fold higher than those of the mock control (non-inoculated) at 3 and 5 days post-*B. xylophilus* infection (dpi;  $p < 0.05$ ). The expression levels of *PR-4* and *PR-5* were significantly higher than those of

the mock control only at 5 dpi ( $p < 0.05$ ). Expression data for *PR-1b* and *PR-3* were omitted from Figure 2 due to their unstable expression in pine seed embryos, irrespective of the presence of *B. xylophilus*. Therefore, we used *PR-2*, *PR-4*, *PR-5*, and *PR-6* as marker genes for subsequent molecular functional analyses.

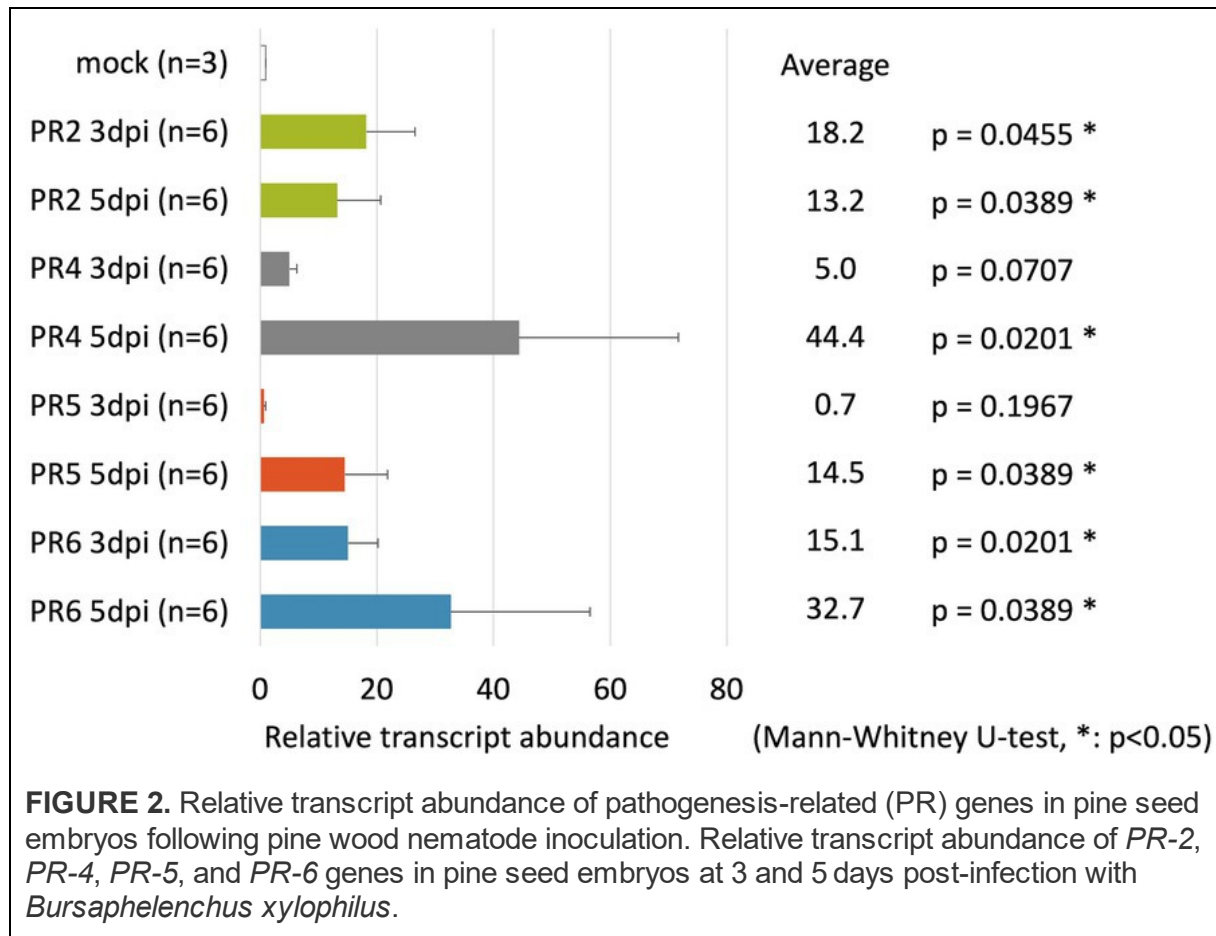
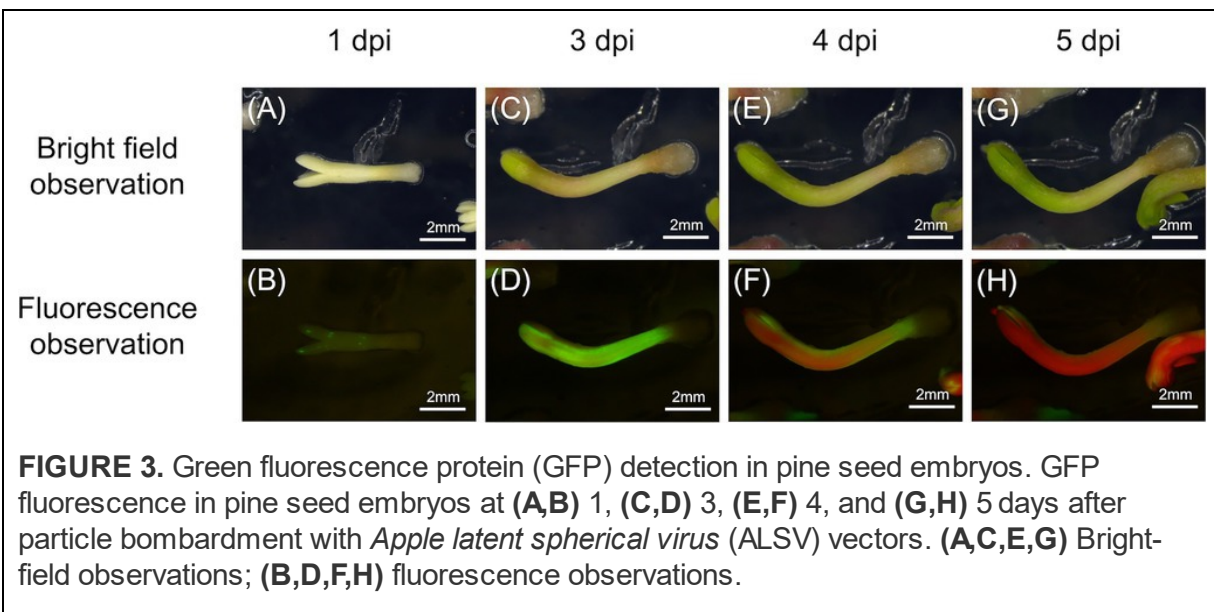


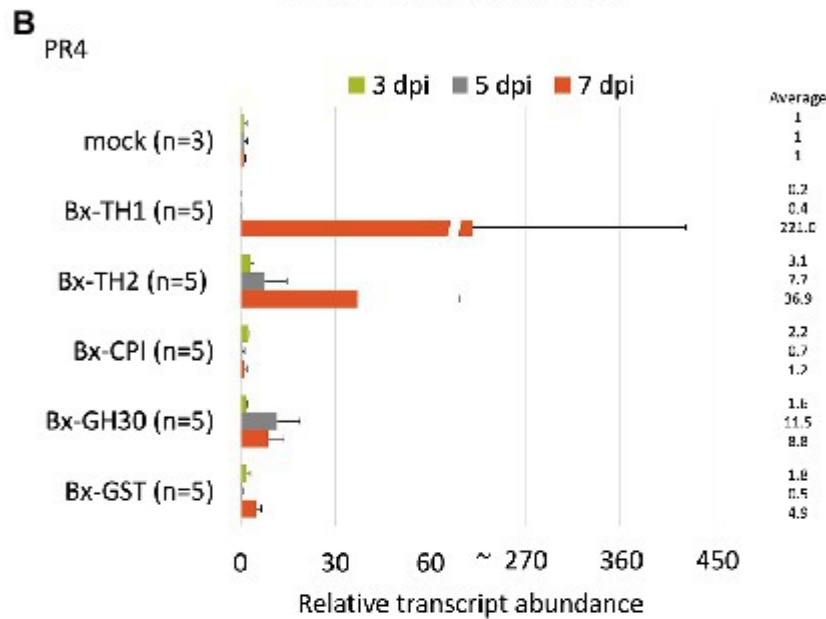
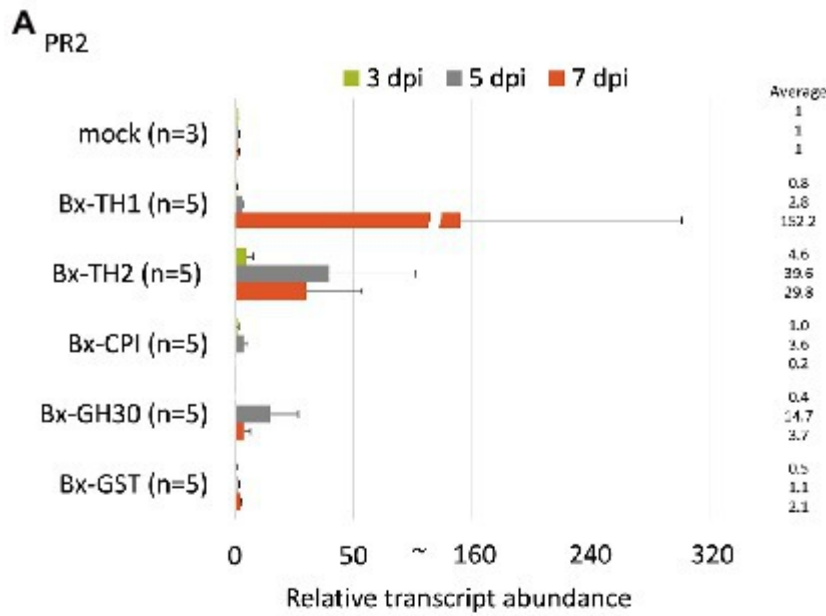
**FIGURE 2.** Relative transcript abundance of pathogenesis-related (PR) genes in pine seed embryos following pine wood nematode inoculation. Relative transcript abundance of *PR-2*, *PR-4*, *PR-5*, and *PR-6* genes in pine seed embryos at 3 and 5 days post-infection with *Bursaphelenchus xylophilus*.

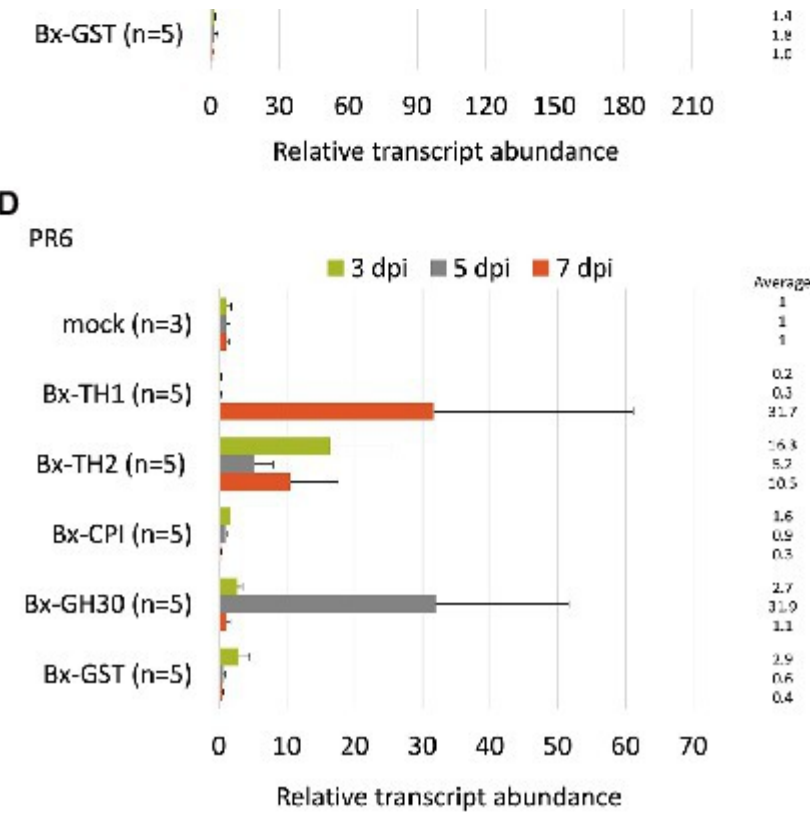
## Bx-TH1, Bx-TH2, and Bx-GH30 Induced PR Gene Expression in Pine Seed Embryos

To determine whether *B. xylophilus* secreted proteins causing cell death in tobacco could induce the expression of PR genes in pine seed embryos, we constructed and transformed six ALSV vectors, coding sequences of *Bx-TH1*, *Bx-TH2*, *Bx-CPI*, *Bx-GH30*, *Bx-GST*, and *GFP* (control) in pine seed embryos. GFP fluorescence in pine seed embryos was observed from 1 dpi after particle bombardment with ALSV vectors (Figure 3), and almost no GFP signal was observed at 7 dpi. To analyze the function of pathogenic *B. xylophilus* candidate proteins, we investigated the expression of four PR

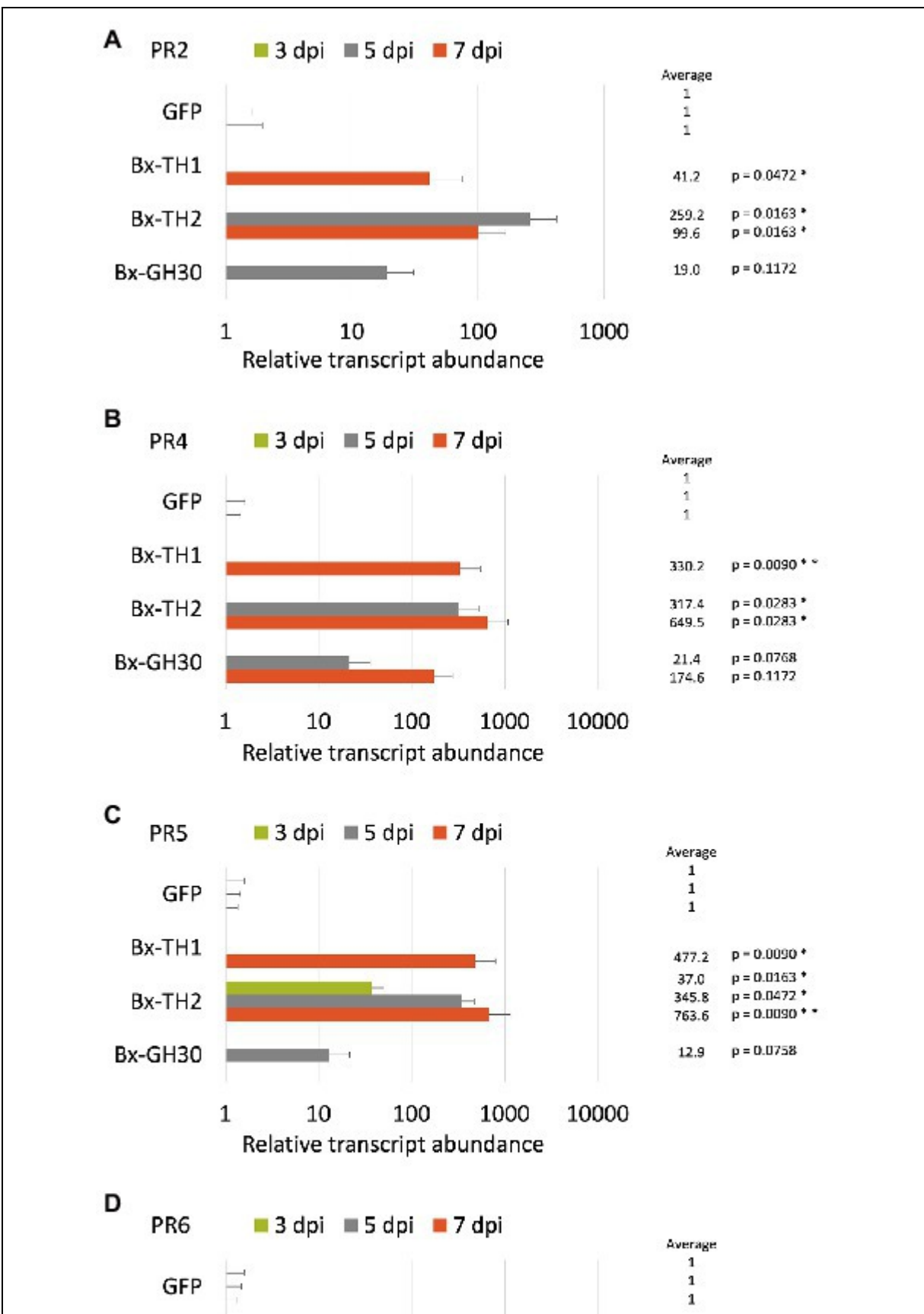
genes (*PR-2*, *PR-4*, *PR-5*, and *PR-6*) at 3, 5, and 7 dpi after ALSV vector particle bombardment using qRT-PCR. Expression levels of the four PR genes in pine seed embryos expressing Bx-TH1, Bx-TH2, and Bx-GH30 were  $>5$ -fold higher than those of mock following normalization by the reference gene elongation factor 1-alpha (Figure 4) and GFP controls following normalization of expression levels according to the amount of viral RNA detected (Figure 5). Though no discrepancies were found between the normalized results using the expression levels of the reference gene elongation factor 1-alpha (mock control) and the amount of viral RNA (GFP control), variation of relative transcript abundance among replicates was lower when normalized with GFP control. When we normalized the gene expression levels by the reference gene elongation factor 1-alpha, no statistically significant difference was observed in relative transcript abundance due to the large variations (Figure 4). When we normalized the gene expression levels by the amount of viral RNA, Bx-TH1 induced significantly higher expression levels of the four PR genes only at 7 dpi than GFP control ( $p < 0.05$ ; Figure 5). Bx-TH2 induced high expression of *PR-5* in pine seed embryos at all time points, and significantly higher expression of *PR-2*, *PR-4*, and *PR-6* at 5 and 7 dpi than GFP control ( $p < 0.05$ ; Figure 5). Bx-GH30 induced high expression of *PR-4* at 5 and 7 dpi, and the other PR genes only at 5 dpi, although these differences were not significant than GFP control, except *PR-6* expression at 7 dpi ( $p < 0.05$ ; Figure 5). *Bx-CPI* and *Bx-GST* did not induce PR gene expression in pine seed embryos.







**FIGURE 4.** Relative transcript abundance of PR genes between pine seed embryos expressing pathogenic candidate proteins and mock control. Expression levels of (A) *PR-2*, (B) *PR-4*, (C) *PR-5*, and (D) *PR-6* in pine seed embryos expressing pathogenic candidate proteins, compared with mock control, using the reference gene elongation factor 1-alpha to normalize results. No statistically significant difference was observed ( $p > 0.05$ , Mann-Whitney U-test).



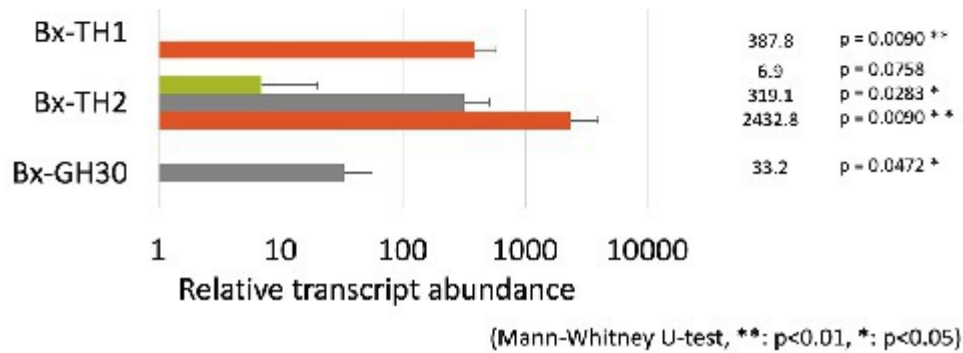


**FIGURE 5.** Relative transcript abundance of PR genes between pine seed embryos expressing pathogenic candidate proteins and GFP control. Expression levels of (A) *PR-2*, (B) *PR-4*, (C) *PR-5*, and (D) *PR-6* in pine seed embryos expressing pathogenic candidate proteins, compared with GFP control, using the amount of viral RNA detected to normalize results. \**p* < 0.05 and \*\**p* < 0.01 (Mann-Whitney U-test).

## DISCUSSION

To develop a method for expressing *B. xylophilus* proteins in pine trees, which are its natural hosts, we conducted transient overexpression of five proteins secreted by *B. xylophilus* causing cell death in tobacco in susceptible black pine seed embryos using the ALSV vector and investigated whether a hypersensitive response could be induced by these proteins expression based on the transcript level of PR genes on pine seed embryos.

Previous studies using tobacco adopted cell death as an indicator for screening nematode pathogenic factors; however, exogenous gene expression was found to be transient and insufficient for inducing cell death during *B. xylophilus* protein expression in pine seed embryos using the ALSV vector. Instead, we constructed a GFP expression vector and bombarded ALSV particles into pine seed embryos and clearly observed the GFP signal at 1–7 dpi. This result suggests that pine embryos suppress the expression of foreign genes through post-transcription gene silencing (PTGS). PTGS is commonly observed when plants are transformed using foreign genes (Depicker and Van Montagu, 1997). For example, when ALSV with GFP or yellow fluorescent protein (YFP) was inoculated to tobacco leaves, both types of fluorescence gradually faded after 10 dpi (Takahashi et al., 2007; Yaegashi et al., 2007). Several pine species were transformed inefficiently and unstably using *Agrobacterium*, possibly due to gene silencing, including *P. halepensis*

(Tzfira et al., 1996), *P. taeda* (Wenck et al., 1999), *P. strobus* (Levée et al., 1997), and *P. pinaster* (Trontin et al., 2002). Therefore, we focused on PR gene expression in host pine embryos as an indicator for screening nematode pathogenic factors. A previous study showed that the expression of antimicrobial peptides and putative PR genes (e.g., *PR-1b*, *PR-2*, *PR-3*, *PR-4*, *PR-5*, and *PR-6*) was higher in susceptible pine trees than in resistant trees after *B. xylophilus* infection (Hirao et al., 2012). Therefore, we used *PR-1b*, *PR-2*, *PR-3*, *PR-4*, *PR-5*, and *PR-6* as candidate marker genes for *B. xylophilus* invasion into pine seed embryos. We found that the expression levels of *PR-2*, *PR-4*, *PR-5*, and *PR-6* were significantly increased in susceptible pine seed embryos following *B. xylophilus* infection ( $p < 0.05$ ). *PR-1b* and *PR-3* expression levels were not stably detected, perhaps because they were too weak for detection by qRT-PCR. *PR-2*, *PR-4*, *PR-5*, and *PR-6* showed similar responses to those in pine seedlings following *B. xylophilus* inoculation; therefore, we used these four genes as indicators of the pine hypersensitive response in subsequent analyses.

Next, we expressed candidate pathogenic *B. xylophilus* molecules in pine seed embryos and assessed their functions by detecting the expression patterns of *PR-2*, *PR-4*, *PR-5*, and *PR-6*. The expression levels of PR genes in pine seed embryos expressing Bx-TH1, Bx-TH2 and Bx-GH30 were  $> 5$ -fold higher than those of the mock and GFP controls. This result is consistent with our previous report that these three molecules induced cell death in *N. benthamiana* (Kirino et al., 2020). Further studies with many pathogenic molecules of *B. xylophilus* are necessary to make the consistency of the results obtained in tobacco and pine seed embryo more clear.

The two remaining pathogenic candidate proteins examined in this study (Bx-CPI and Bx-GST) did not increase PR gene expression in pine seed embryos relative to the mock and GFP controls. This result is inconsistent with the previous *N. benthamiana* functional screening result. Woody plants such as pines and herbaceous plants such as *N. benthamiana* differ in structure, lifespan, and defense systems. Generally, the defenses of slow-growing woody plants are typically quantitative and are affected by genetic variation, whereas those of fast-growing herbaceous plants are qualitative and influenced by environmental variation (Massad et al., 2011). This difference in defense systems between pine seed embryos and *N. benthamiana* may have influenced our functional screening results, suggesting that screening using *N. benthamiana* may result in false positives,

although results can vary between tobacco and pine seed embryos depending on the type of gene expressed.

Although the assay system established in this study is useful, it has two limitations. First, this method tends to produce large variation in gene expression levels. Expression levels of the four selected PR genes differed among individuals and transgenes at each time point. When qRT-PCR is performed, individual variation in endogenous PR gene expression levels should be considered. Because ALSV vectors were introduced into pine seed embryos biolistically, the amount of vector introduced into each embryo is variable, leading to variation in *B. xylophilus* protein expression. The expression efficiency of each gene introduced into a pine seed embryo may also differ among genes. To reduce this variability in gene expression, we normalized PR gene expression based on the amount of viral RNA in each pine seed embryo (Figure 5), which produced more stable gene expression patterns. The second limitation consists of the differential characteristics between seed embryos and seedlings. Our previous studies showed that changes in the subcellular localization of candidate proteins can alter their ability to induce cell death in tobacco (Kirino et al., 2020; Shinya et al., 2021). As seed embryos are composed of undifferentiated tissue, the localization of *B. xylophilus* protein expressed in seed embryos may differ from that in seedlings. Therefore, to clarify whether candidate molecules that induced hypersensitive responses in seed embryos exhibit the same function in pine seedlings, it is necessary to compare their localization. Furthermore, though many reports have suggested the relationship between the hypersensitive response and pine wilt, there is still no direct evidence to prove it due to technical limitations. The method we have developed using ALSV vectors in this study may contribute to proving this in the future because ALSV vectors have been shown to effectively induce stable virus-induced gene silencing in various plants (e.g., Sasaki et al., 2011).

In summary, we report a novel functional analysis that uses recombinant pathogenic candidate molecules of *B. xylophilus* in host pines. The results of our investigation of tobacco and pine seed embryos suggest that tobacco-based screening for pathogenic *B. xylophilus* molecules may result in false positives. Although the proposed method has limitations that must be resolved in future research, it has potential as a powerful tool for screening pathogenic molecules of *B. xylophilus* in their native host.

# DATA AVAILABILITY STATEMENT

The original contributions presented in the study are included in the article/supplementary material; further inquiries can be directed to the corresponding author.

# AUTHOR CONTRIBUTIONS

HK, KK, and RS designed the study and wrote the manuscript. HK and KK performed the research and analyzed the data. All authors contributed to the article and approved the submitted version.

# FUNDING

This study was funded by grants from JSPS Grant-in-Aid for Early-Career Scientists JP19K15853 (to RS), JSPS Grant-in-Aid for JSPS Research Fellow JP21J20926 (to HK), and JST PRESTO grant no. JPMJPR17Q5 (to RS).

# ACKNOWLEDGMENTS

We would like to thank Tomonori Hirao (FFPRI) and Nobuyuki Yoshikawa (Iwate University) for generously providing me with pine seeds and ALSV vectors (pEALSR1 and pEALSR2L5R5), respectively. We thank the Forest Tree Gene Bank Program, Forest Tree Breeding Center, and Forest Products Research Institute in Japan for donating the black pine seeds.

# REFERENCES

Abelleira, A., Picoaga, A., Mansilla, J. P., and Aguin, O. (2011). Detection of *Bursaphelenchus xylophilus*, causal agent of pine wilt disease on *Pinus pinaster* in northwestern Spain. *Plant Dis.* 95:776. doi: 10.1094/PDIS-12-10-0902

Burgermeister, W., Braasch, H., Sousa, E., Penas, A. C., Mota, M., Metge, K., et al. (1999). First report of *Bursaphelenchus xylophilus* in Portugal and in Europe. *Nematology* 1, 727–734. doi: 10.1163/156854199508757

Cardoso, J., Anjo, S., Fonseca, L., Egas, C., Manadas, B., and Abrantes, I. (2016). *Bursaphelenchus xylophilus* and *B. mucronatus* secretomes: a comparative proteomic analysis. *Sci. Rep.* 6:39007. doi: 10.1038/srep39007

Cardoso, J., Anjo, S., Manadas, B., Silva, H., Abrantes, I., Nakamura, K., et al. (2021). Virulence biomarkers of *Bursaphelenchus xylophilus*: a proteomic approach. *Front. Plant Sci.* 12:822289. doi: 10.3389/fpls.2021.822289

Depicker, A., and Van Montagu, M. (1997). Post-transcriptional gene silencing in plants. *Curr. Opin. Cell Biol.* 9, 373–382. doi: 10.1016/S0955-0674(97)80010-5

Ding, X., Ye, J., Lin, S., Wu, X., Li, D., and Nian, B. (2016). Deciphering the molecular variations of pine wood nematode *Bursaphelenchus xylophilus* with different virulence. *PLoS One* 11:e0156040. doi: 10.1371/journal.pone.0156040

Espada, M., Eves-van den Akker, S., Maier, T., Vijaypalani, P., Baum, T., Mota, M., et al. (2018). STATAWAARS: a promoter motif associated with spatial expression in the major effector-producing tissues of the plant-parasitic nematode *Bursaphelenchus xylophilus*. *BMC Genom.* 19:553. doi: 10.1186/s12864-018-4908-2

Espada, M., Silva, A. C., van den Akker, S. E., Cock, P. J. A., Mota, M., Jones, J. T., et al. (2016). *Mol. Plant Pathol.* 17, 286–295. doi: 10.1111/mpp.12280

Filipiak, A., Malewski, T., Matczyńska, E., and Tomalak, M. (2020). Molecular variation among virulent and avirulent strains of the quarantine nematode *Bursaphelenchus xylophilus*. *Mol. Gen. Genomics.* 296, 259–269. doi: 10.1007/s00438-020-01739-w

Futai, K. (2013). Pine wood nematode, *Bursaphelenchus xylophilus*. *Annu. Rev. Phytopathol.* 51, 61–83. doi: 10.1146/annurev-phyto-081211-172910

Hirao, T., Fukatsu, E., and Watanabe, A. (2012). Characterization of resistance to pine wood nematode infection in *Pinus thunbergii* using suppression subtractive hybridization. *BMC Plant Bio.* 12:13. doi: 10.1186/1471-2229-12-13

Hu, L. J., Wu, X. Q., Li, H. Y., Zhao, Q., Wang, Y. C., and Ye, J. R. (2019). An effector, BxSapB1, induces cell death and contributes to virulence in the pine wood nematode *Bursaphelenchus xylophilus*. *Mol. Plant Microbe. Interact.* 32, 452–463. doi: 10.1094/MPMI-10-18-0275-R

Huang, X., Hu, L., and Wu, X. (2019). Identification of a novel effector BxSapB3 that enhances the virulence of pine wood nematode *Bursaphelenchus xylophilus*. *Acta. Bioch. Bioph. Sin.* 51, 1071–1078. doi: 10.1093/abbs/gmz100

Kikuchi, T., Cotton, J. A., Dalzell, J. J., Hasegawa, K., Kanzaki, N., McVeigh, P., et al. (2011). Genomic insights into the origin of parasitism in the emerging plant pathogen *Bursaphelenchus xylophilus*. *PLoS Pathog.* 7:e1002219. doi: 10.1371/journal.ppat.1002219

Kirino, H., Yoshimoto, K., and Shinya, R. (2020). Thaumatin-like proteins and a cysteine protease inhibitor secreted by the pine wood nematode *Bursaphelenchus xylophilus* induce cell death in *Nicotiana benthamiana*. *PLoS One* 15:e0241613. doi: 10.1371/journal.pone.0241613

Kiyohara, T., and Tokushige, Y. (1971). Inoculation experiments of a nematode, *Bursaphelenchus* sp., onto pine trees. *J. Jpn. For. Soc.* 53, 210–218. doi: 10.11519/jjfs1953.53.7\_210

Konagaya, K. (2017). A trial of forest tree breeding research by applying virus. *Rinbokuikushu-joho (in Japanese)* 23:5.

Konagaya, K., Nanasato, Y., and Taniguchi, T. (2020). A protocol for *Agrobacterium*-mediated transformation of Japanese cedar, Sugi (*Cryptomeria japonica* D. Don) using embryogenic tissue

explants. *Plant Biotechnol.* 37, 147–156. doi: 10.5511/plantbiotechnology.20.0131a

Levée, V., Lelu, M. A., Jouanin, L., Cornu, D., and Pilate, G. (1997). *Agrobacterium tumefaciens*-mediated transformation of hybrid larch (*Larix kaempferi* × *L. decidua*) and transgenic plant regeneration. *Plant Cell Rep.* 16, 680–685. doi: 10.1007/s002990050301

Li, C., Sasaki, N., Isogai, M., and Yoshikawa, N. (2004). Stable expression of foreign proteins in herbaceous and apple plants using apple latent spherical virus RNA2 vectors. *Arch. Virol.* 149, 1541–1558. doi: 10.1007/s00705-004-0310-2

Li, C., Yoshikawa, N., Takahashi, T., Ito, T., Yoshida, K., and Koganezawa, H. (2000). Nucleotide sequence and genome organization of apple latent spherical virus: a new virus classified into the family Comoviridae. *J. Gen. Virol.* 81, 541–547. doi: 10.1099/0022-1317-81-2-541

Ma, H. B., Lu, Q., Liang, J., and Zhang, X. Y. (2011). Functional analysis of the cellulose gene of the pine wood nematode, *Bursaphelenchus xylophilus*, using RNA interference. *Genet. Mol. Res.* 10, 1931–1941. doi: 10.4238/vol10-3gmr1367

Massad, T. J., Fincher, R. M., Smilanich, A. M., and Dyer, L. (2011). A quantitative evaluation of major plant defense hypotheses, nature versus nurture, and chemistry versus ants. *Arthropod-Plant Interact.* 5, 125–139. doi: 10.1007/s11829-011-9121-z

Myers, R. F. (1988). Pathogenesis in pine wilt caused by pinewood nematode, *Bursaphelenchus xylophilus*. *J. Nematol.* 20, 236–244.

Palomares-Rius, J. E., Tsai, I. J., Karim, N., Akiba, M., Kato, T., Maruyama, H., et al. (2015). Genome-wide variation in the pinewood nematode *Bursaphelenchus xylophilus* and its relationship with pathogenic traits. *BMC Genom.* 16:845. doi: 10.1186/s12864-015-2085-0

Park, J. E., Lee, K. Y., Lee, S. J., Oh, W. S., Jeong, P. Y., Woo, T., et al. (2008). The efficiency of RNA interference in *Bursaphelenchus xylophilus*. *Mol. Cells* 26, 81–86.

Qiu, X., Yang, L., Ye, J., Wang, W., Zhao, T., Hu, H., et al. (2019). Silencing of cyp-33C9 Gene affects the reproduction and pathogenicity of the pine wood nematode, *Bursaphelenchus xylophilus*. *Int. J. Mol. Sci.* 20:4520. doi: 10.3390/ijms20184520

Sasaki, S., Yamagishi, N., and Yoshikawa, N. (2011). Efficient virus-induced gene silencing in apple, pear and Japanese pear using apple latent spherical virus vectors. *Plant Meth.* 7:15. doi: 10.1186/1746-4811-7-15

Shinya, R., Kirino, H., Morisaka, H., Takeuchi-Kaneko, Y., Futai, K., and Ueda, M. (2021). Comparative secretome and functional analyses reveal glycoside hydrolase family 30 and cysteine peptidase as virulence determinants in the pinewood nematode *Bursaphelenchus xylophilus*. *Front. Plant Sci.* 12:640459. doi: 10.3389/fpls.2021.640459

Shinya, R., Morisaka, H., Kikuchi, T., Takeuchi, Y., Ueda, M., and Futai, K. (2013). Secretome analysis of the pine wood nematode *Bursaphelenchus xylophilus* reveals the tangled roots of parasitism and its potential for molecular mimicry. *PLoS One* 8:e67377. doi: 10.1371/journal.pone.0067377

Silva, H., Anjo, S. I., Manadas, B., Abrantes, I., Fonseca, L., and Cardoso, J. (2021). Comparative analysis of *Bursaphelenchus xylophilus* secretome under *Pinus pinaster* and *P. pinea* stimuli. *Front. Plant Sci.* 12:668064. doi: 10.3389/fpls.2021.668064

Takahashi, T., Sugawara, T., Yamatsuta, T., Isogai, M., Natsuaki, T., and Yoshikawa, N. (2007). Analysis of the spatial distribution of identical and two distinct virus populations differently labeled with cyan and yellow fluorescent proteins in coinfected plants. *Phytopathology* 97, 1200–1206. doi: 10.1094/PHYTO-97-10-1200

Takahashi, T., and Yoshikawa, N. (2008). “Analysis of cell-to-cell and long-distance movement of apple latent spherical virus in infected plants using green, cyan, and yellow fluorescent proteins,” in *Plant*

*Virology Protocols: From Viral Sequence to Protein Function.* eds. G. D. Foster, I. E. Johansen, Y. Hong, and P. D. Nagy (Totowa, NJ: Humana Press), 545–554.

Trontin, J. F., Harvengt, L., Garin, E., Lopez-Vernaza, M., Arancio, L., Hoebeke, J., et al. (2002). Towards genetic engineering of maritime pine (*Pinus pinaster* Ait.). *Ann. For. Sci.* 59, 687–697. doi: 10.1051/forest:2002057

Tzfira, T., Yarnitzky, O., Vainstein, A., and Altman, A. (1996). *Agrobacterium rhizogenes*-mediated DNA transfer in *Pinus halepensis* mill. *Plant Cell Rep.* 16, 26–31. doi: 10.1007/BF01275443

Wenck, R. A., Quinn, M., Whetten, R. W., Pullman, G., and Sederoff, R. (1999). High-efficiency *Agrobacterium*-mediated transformation of Norway spruce (*Picea abies*) and loblolly pine (*Pinus taeda*). *Plant Mol. Biol.* 39, 407–416. doi: 10.1023/A:1006126609534

Yaegashi, H., Yamatsuta, T., Takahashi, T., Li, C., Isogai, M., Kobori, T., et al. (2007). Characterization of virus-induced gene silencing in tobacco plants infected with apple latent spherical virus. *Arch. Virol.* 152, 1839–1849. doi: 10.1007/s00705-007-1011-4

Yamagishi, N., Kishigami, R., and Yoshikawa, N. (2014). Reduced generation time of apple seedlings to within a year by means of a plant virus vector: a new plant-breeding technique with no transmission of genetic modification to the next generation. *Plant Biotechnol. J.* 12, 60–68. doi: 10.1111/pbi.12116

Yamagishi, N., Sasaki, S., and Yoshikawa, N. (2010). Highly efficient inoculation method of apple viruses to apple seedlings. *J. K. Arch.* 427, 226–229.

Yamagishi, N., and Yoshikawa, N. (2013). “Highly efficient virus-induced gene silencing in apple and soybean by apple latent spherical virus vector and biolistic inoculation,” in *Virus-Induced Gene Silencing: Methods and Protocols*. ed. A. Becker (Totowa, NJ: Humana Press), 167–181.

Yamaguchi, R., Matsunaga, K., Hirao, T., Tamura, M., and Watanabe, A. (2019). Spatiotemporal analysis of pine wilt disease: relationship between pinewood nematode distribution and defence response in *Pinus thunbergii* seedlings. *Forest Pathol.* 49:e12518. doi: 10.1111/efp.12518

Yi, C. K., Byun, B. H., Park, J. D., Yang, S. I., and Chang, K. H. (1989). First finding of the pine wood nematode, *Bursaphelenchus xylophilus* (Steiner et Buhler) Nickle and its insect vector in Korea. *For. Res. Ins.* 38, 141–149.

**Conflict of Interest:** The authors declare that the research was conducted in the absence of any commercial or financial relationships that could be construed as a potential conflict of interest.

**Publisher’s Note:** All claims expressed in this article are solely those of the authors and do not necessarily represent those of their affiliated organizations, or those of the publisher, the editors and the reviewers. Any product that may be evaluated in this article, or claim that may be made by its manufacturer, is not guaranteed or endorsed by the publisher.

Copyright © 2022 Kirino, Konagaya and Shinya. This is an open-access article distributed under the terms of the Creative Commons Attribution License (CC BY). The use, distribution or reproduction in other forums is permitted, provided the original author(s) and the copyright owner(s) are

*credited and that the original publication in this journal is cited, in accordance with accepted academic practice. No use, distribution or reproduction is permitted which does not comply with these terms.*

ORIGINAL RESEARCH

published: 25 April 2022

doi: 10.3389/fpls.2022.856826



# Parallel Evolution of C-Type Lectin Domain Gene Family Sizes in Insect-Vectored Nematodes

**Jing Ning<sup>1,2†</sup>, Jiao Zhou<sup>1,2†</sup>, Haixiang Wang<sup>3</sup>, Yaning Liu<sup>1,2</sup>, Faheem Ahmad<sup>4</sup>, Xiaohui Feng<sup>1,2</sup>, Yu Fu<sup>1,2,5</sup>, Xiaoting Gu<sup>1,2</sup> and Lilin Zhao<sup>1,2\*</sup>**

<sup>1</sup> State Key Laboratory of Integrated Management of Pest Insects and Rodents, Institute of Zoology, Chinese Academy of Sciences, Beijing, China

<sup>2</sup> CAS Center for Excellence in Biotic Interactions, University of Chinese Academy of Sciences, Beijing, China

<sup>3</sup> College of Forestry, Shanxi Agricultural University, Taigu, China

<sup>4</sup> Department of Biosciences, COMSATS University Islamabad (CUI), Islamabad, Pakistan

<sup>5</sup> School of Life Sciences, Division of Life Sciences and Medicine, University of Science and Technology of China, Hefei, China

**Edited by:**

Margarida Espada, University of Évora, Portugal

**Reviewed by:**

Nicolaas A. van der Merwe, University of Pretoria, South Africa

Xuehuan Feng, University of Nebraska-Lincoln, United States

Juan Emilio Palomares-Rius, Spanish National Research Council (CSIC), Spain

**\*Correspondence:** Lilin Zhao, zhaoll@ioz.ac.cn

**†**These authors have contributed equally to this work

**Specialty section:** This article was submitted to Plant Pathogen Interactions, a section of the journal *Frontiers in Plant Science*

**Received:** 17 January 2022

**Accepted:** 11 March 2022

**Published:** 25 April 2022

**Citation:** Ning J, Zhou J, Wang H, Liu Y, Ahmad F, Feng X, Fu Y, Gu X and Zhao L (2022) Parallel Evolution of C-Type Lectin Domain Gene Family Sizes in Insect-Vectored Nematodes. *Front. Plant Sci.* 13:856826. doi: 10.3389/fpls.2022.856826

The dispersal stage of pathogens is crucial for the successful spread and infection of their hosts. Some plant-parasitic nematodes (PPNs) have evolved specialized dispersal stages to reach healthy hosts by being carried out by insect vectors. Because gene gain and loss is a major factor contributing to the evolution of novel characteristics, it is essential to clarify the gene family characteristics among nematodes with different dispersal modes to disentangle the evolution of insect-mediated dispersal. Here, the size of the C-type lectin (CTL) family genes of insect-vectored nematodes was found to be drastically reduced compared with those of self-dispersing nematodes, whereas the diversity of their functional domains was significantly higher. The gene family sizes of vector-dispersed nematodes were only a twentieth of the size of that of a self-dispersing (i.e., without a biotic vector) nematode model *Caenorhabditis elegans*, and these genes were inactive during the dispersal stage. Phylogenetic analysis showed that some CTL genes of vector-borne PPNs shared higher homology to the animal parasitic nematodes compared with other PPNs. Moreover, homology modeling predicted that the CTLs of insect-vectored nematodes bear remarkable structural similarity to the lectin genes of their vector's immune system. Because CTL genes are important sugar-binding proteins for the innate immune response of *C. elegans*, the loss of some CTL genes of vector-transmitted PPNs might be responsible for their parallel adaptations to a mutualistic relationship with their vector. These results expand our understanding of the evolutionary benefits of vector-mediated transmission for the nematode and vector-nematode co-evolution.

**Keywords:** C-type lectin, gene family, insect vector, co-evolution, parallel evolution

## INTRODUCTION

Due to globalization, insect-vectored plant and animal diseases have become one of the major threats for biosafety, ecosystem function and stability as well as human health (Blaxter et al., 1998; Jones et al., 2014). One of the

major pests threatening the safety of horticultural and forest ecosystem is plant-parasitic nematodes (PPNs), which have caused extensive damage to agricultural and cash crops worldwide (Jones et al., 2014). Over 4,100 species of PPNs have been described to date, which collectively pose a serious threat to global food and ecological security (Demangeat et al., 2010). Global agricultural economic losses caused by PPNs have been estimated to cost more than US\$ 157 billion per year (Abad et al., 2008). Due to accelerated globalization and, hence, increased spread of these pests, this estimate is expected to increase in the future.

The PPNs have evolved a variety of dispersal strategies that help them expand their distribution. Some of the PPNs are self-dispersed (i.e., not using plant or animal vectors), such as some root-knot nematodes, which have a very short free-living stage in the soil. These PPNs can be transported to new uninfested areas by water or by clinging to soil particles (Dutta et al., 2012). However, the vast majority of PPN species have a wide parasitic range (i.e., number of suitable hosts) and are transmitted vertically from mother to offspring *via* seeds and/or horizontally *via* intermediate hosts. The stem and bulb nematode, *Ditylenchus dipsaci*, e.g., is known to infect more than 500 plant species and can use weeds as an intermediate, yet non-preferred, hosts and as vectors until a preferred host is available (Trankner, 1992; Vovlas et al., 2011). However, a few species have become more specialized with more limited host repertoire and have secondarily lost the ability for wide-range dispersal. For example, the hosts of *Bursaphelenchus* spp., such as *Bursaphelenchus xylophilus* (pinewood nematode) and *Bursaphelenchus cocophilus*, are limited to a few species of *Pinus* and *Palmae*, respectively. These PPNs have significantly improved the efficiency of their transmission by evolving special dispersal stages that are carried out to the healthy hosts by insect vectors (Jordaan et al., 1987; Moens and Perry, 2009). However, evidence of evolution behind the transition from self-dispersing to vector-mediated dispersal of nematodes is lacking.

Changes in the number of gene copies in a specific gene family represent a raw source of evolutionary innovations (Kondrashov et al., 2002; Chen et al., 2010). More copies of a specific gene could increase the content of the associated protein, which may improve the performance of the animal in a task in which the protein is needed (Ollivier et al., 2016; Cheng et al., 2017). However, a reduction in gene family size does not necessarily mean the loss of its biological function. Growing body of research shows that gene loss can

be beneficial by providing an evolutionary mechanism for phenotypic adaptations (Chen et al., 2010; Sharma et al., 2019). For example, sperm whales, *Physeter macrocephalus*, have lost the gene AMPD3 which encodes an erythrocyte-specific enzyme related to O<sub>2</sub> affinity of hemoglobin. This is probably an adaptation to sustained diving because lower affinity facilitates O<sub>2</sub> release from hemoglobin to O<sub>2</sub>-depleted tissues (O'Brien et al., 2015; Sharma et al., 2019). In addition, a reduction in the size of hair- and epidermis-related gene families has likely facilitated the adaptation of cetaceans to the aquatic environment, resulting in a thicker and smoother epidermis that can better cope with water pressure and drag force (Sharma et al., 2019). This “less is more” principle can shed light on possible molecular and cellular mechanisms underlying various adaptations and, therefore, investigating gene losses has a great potential to reveal the genomic basis of evolutionary processes.

Despite the genomes of numerous nematode species have been sequenced and are available in repositories, the genomic basis of the evolutionary transition from self-dispersing to insect-vectored dispersal is not clear. However, the availability of these genomes enables the use of comparative genomics to associate genomic differences with the different nematode dispersal modes. We suggest three approaches that are most suitable for this task, namely, first, comparison of the genomes of nematode species differing in their dispersal strategies (e.g., self-dispersed without a biotic vector vs. insect-vectored) and lifestyles (insect- and/or plant-parasitic and free-living); second, comparison of gene expression of dispersal and propagative stages within insect-vectored nematode species; and finally, analysis of molecules that parasitic nematodes excrete and secrete when encountering the vector and host. Following these approaches, we explored genetic factors that influence the successful loading of nematodes to their insect vector. We focused on the C-type lectin (CTL) family because these genes play important roles in avoiding vector immunity. We found that the size of the CTL family was drastically reduced among insect-vectored nematodes compared with that of self-dispersing nematodes, while the high diversity of its functional domains was retained. The CTL genes of insect-vectored nematodes were not expressed during the dispersal stage, i.e., when being transported to a new host tree *via* an insect. Moreover, the CTL protein structures of insect-vectored parasitic nematodes were similar to their vector's homologous protein. Our results suggest that gene family reduction

and lower expression of CTLs are mechanism that has likely contributed to the adaptation of nematodes from self-dispersing to insect-vectored dispersal strategy.

## MATERIALS AND METHODS

### Collection of Genomic Data

We collected the protein sequence of 12 nematode species from NCBI (<https://www.ncbi.nlm.nih.gov/>) and WormBase (<https://www.wormbase.org/>), including two PPNs vectored by *Monochamus alternatus* (i.e., *B. xylophilus* and *Bursaphelenchus mucronatus*), two animal-parasitic nematodes vectored by blood-feeding insects (i.e., *Brugia malayi* and *Loa loa*), and self-dispersing nematodes spreading without a biotic vector, including two PPNs (i.e., *Meloidogyne arenaria* and *Meloidogyne javanica*), two animal-parasitic nematodes (i.e., *Steinernema carpocapsae* and *Enterobius vermicularis*), four free-living nematodes (i.e., *Caenorhabditis elegans*, *Caenorhabditis brenneri*, *Caenorhabditis remanei*, and *Pristionchus pacificus*), and one outgroup *Echinococcus granulosus* (Supplementary File 1).

### Phylogenetic Analysis

A phylogenetic tree was constructed with program RAxML using the maximum-likelihood (ML) algorithm and estimation of multiple sequence alignment (MSA) with a self-expanding bootstrap of 200 and substitution model from ProtTest using *E. granulosus* as an outgroup (Stamatakis, 2006). This ML tree was converted into an ultrametric time-scaled phylogenetic tree by r8s using the calibrated times from the TimeTree (<http://timetree.org/>) website. Finally, Evolview was used to display the phylogenetic tree (Subramanian et al., 2019). The Café (version 3.0) program was used to analyze the expansion and contraction of gene families (De Bie et al., 2006).

### Gene Family Clustering and Orthology Prediction

To understand the evolutionary relationships among insect-vectored and self-dispersing nematodes, we performed systematic gene comparisons among these groups. Proteins shorter than 30aa or with frameshifts were removed.

The All-vs.-All similarity alignment of protein sequences was constructed using Diamond (1e-5) (Buchfink et al., 2015). Orthofinder was used to infer the orthologous genes within the species and obtain the gene family based on the similarity of protein sequence alignments (Emms and Kelly, 2019). Based on the gene family clustering results, the candidate-contracted gene families of the four insect-vectored nematodes were identified by comparing them with corresponding candidate genes from self-dispersing nematodes (using a *t*-test in SPSS version 20.0 to compare the gene numbers among the two groups of species).

## Identification of CTLs

Blastp and HMMScan (version 3.0) were used to search for CTL genes of *B. xylophilus*, *B. mucronatus*, *B. malayi*, *L. loa*, *S. carpocapsae*, *E. vermicularis*, *M. arenaria*, and *M. javanica* based on those from of *C. elegans*, *C. remanei*, *C. brenneri*, and *P. pacificus* (Johnson et al., 2010). In addition, domain analyses of these proteins were carried out with NCBI Conserve-Domain Tool (<https://www.ncbi.nlm.nih.gov/cdd>) and Pfam (<http://www.sanger.ac.uk/Software/Pfam/>). Signal peptides (SPs) were analyzed using SignalP version 3.0 (<http://www.cbs.dtu.dk/services/SignalP>), and transmembrane domain was searched by TMHMM server version 2.0 (<http://www.cbs.dtu.dk/services/TMHMM/>). Domain pattern was re-drawn using TBtools version 0.53 (Chen et al., 2020). The 3D structure prediction for the CTLs was carried out in the SWISS-MODEL workspace (<http://swissmodel.expasy.org/workspace/>) (Waterhouse et al., 2018). The subcellular location of nematode CTL proteins was predicted using WoLF PSORT ([http://www.genscript.com/psort/wolf\\_psort.html](http://www.genscript.com/psort/wolf_psort.html)). MSAs were executed using MUSCLE software (Edgar, 2004). Phylogenetic trees were constructed by the neighbor-joining (NJ) method in MEGA 6, 1,000 repetitions of bootstrap (Tamura et al., 2013). All CTL domain (CTLD) sequences from other model species used in this study are provided as Supplementary File 2.

## Transcriptomic Data Collection

The PPNs (*B. xylophilus*) were collected from infected trees in the Zhashui area of Shangluo City in Shaanxi Province (33°35'31"N, 108°49'25"E). The propagative (i.e., non-dispersal) stages (L<sub>1</sub>-L<sub>4</sub>) of the nematodes were

cultured on *Botrytis cinerea* plates and retrieved using a modified Baermann funnel technique (Baermann, 1917). The third-stage dispersal juveniles (L<sub>III</sub>) were collected from infected pine trees. The chunks were cut into wood chips, and the nematodes were extracted using the Baermann's funnel technique. In addition, the fourth-stage dispersal juveniles (L<sub>IV</sub>) were collected from the trachea of newly emerged vector beetles (*M. alternatus*). Impurities were removed from the nematodes by sucrose flotation, and then they were washed using phosphate-buffered saline, flash-frozen with Trizol, and stored at -80°C until used in experiments.

Total RNA samples were extracted from propagative (L<sub>2</sub>, L<sub>3</sub>, L<sub>4</sub>, both female and male) and dispersal (L<sub>III</sub> and L<sub>IV</sub>) stages of *B. xylophilus* using Trizol reagent (Thermo Fisher Scientific) according to the manufacturer's instructions. The integrity of RNA was assessed using a NanoDrop ND-1000 spectrophotometer (NanoDrop Technologies, Inc., Wilmington, DE 19810, USA). The A260/A280 ratio of the RNA was between 1.8 and 2.0. A dynabeads messenger RNA (mRNA) purification kit was used to purify mRNA (RiboPureTM Kit Family Ambion, Life Technology, Waltham, MA, USA). Then, RNA-seq libraries were constructed and sequenced on the Illumina Hiseq 2000 platform (Illumina, San Diego, CA, USA) in the Beijing Institutes of Biological Sciences (Chinese Academy of Sciences) (Hou et al., 2015). Raw data were processed to trim short or terminal low-quality bases and adapter sequences. Microbial contaminants with identity 95% and coverage 90% were removed by Blast. The clean data were assembled by Trinity (version 2.6.5) (Grabherr et al., 2011) to obtain reference transcripts due to the reference transcriptome (PRJNA381109). The differentially expressed transcripts (DETs) were analyzed using DEG-seq2, and differentially expressed mRNAs were finally selected with fold change > 2 and *p-adjusted* < 0.05 (Wang et al., 2010).

The RNA-seq data of *M. alternatus* with different life stages and with/without *B. xylophilus* were collected from the SRA database of the NCBI (Supplementary File 4) and processed by the same methods with *B. xylophilus*. The Illumina paired-end transcriptomic data of *B. malayi* were collected from the SRA database of the NCBI (Supplementary File 4). The RNA samples from the abovementioned sequences were extracted from different life stages. All the transcriptomic sequencing reads were trimmed to remove low-quality data and adaptor sequences using the IlluQC\_PRLL.pl of

NGS QC Toolkit and an in-house Perl script “QC\_remove\_low\_quality.pl” ([https://github.com/jianbone/L\\_vannamei\\_genome](https://github.com/jianbone/L_vannamei_genome)). Reads were mapped to the annotated *B. malayi* genome assemblies with Bowtie2 (Langdon, 2015). The relative change in gene expression was analyzed using the pheatmap package in R environment.

### **Quantitative Real-Time Polymerase Chain Reaction**

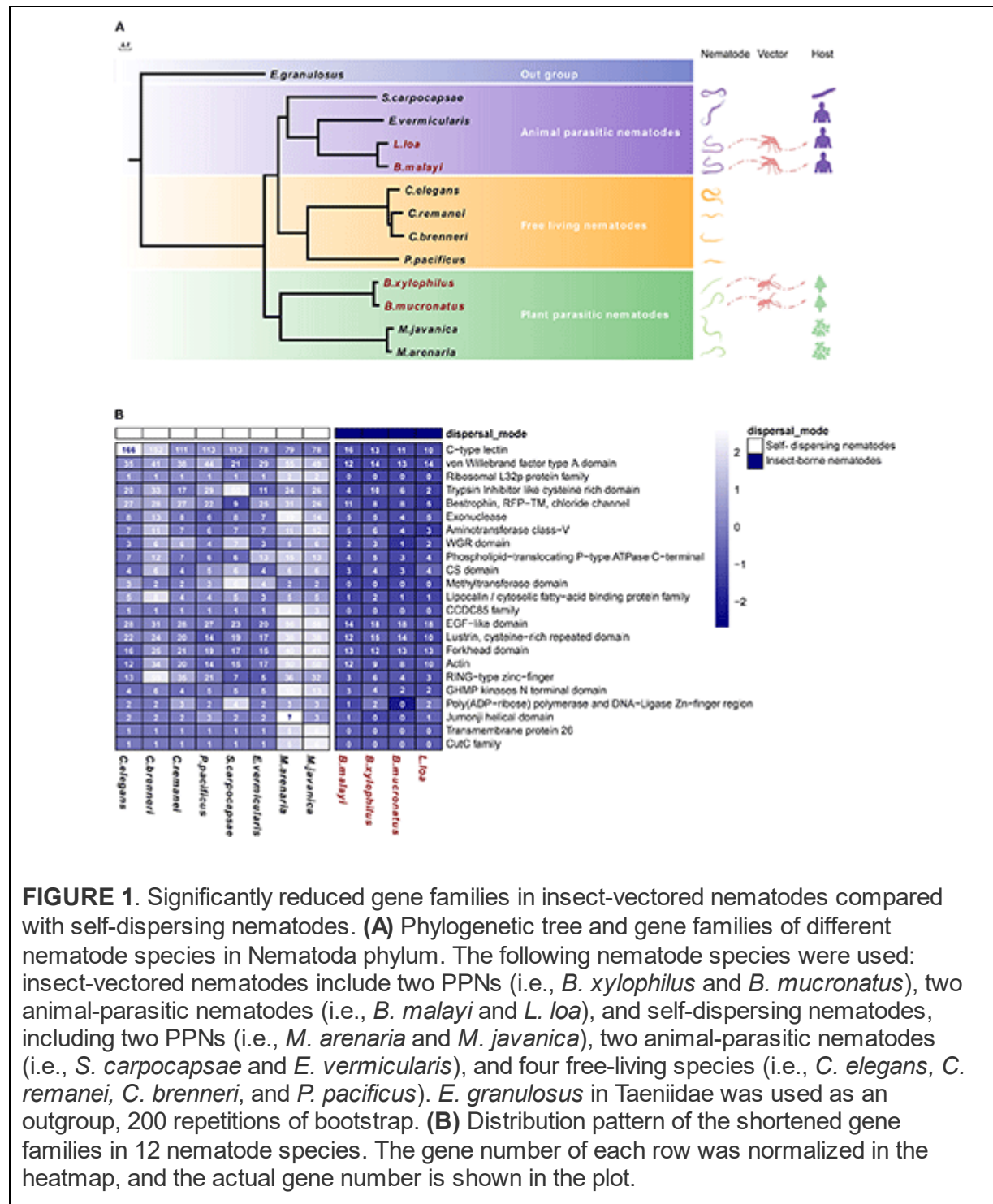
Quantitative real-time polymerase chain reaction (qPCR) was performed in triplicate for each sample using SYBR PrimeScript RT-PCR Kit (TaKaRa, Dalian, China) on an MX3000P Thermal cycler (Stratagene, La Jolla, California, USA) with designed specific primers (Supplementary Table 1). Thermal cycling was performed at 95°C for 30 s, followed by 40 cycles of 95°C for 5 s, 60°C for 20 s, and 95°C for 1 min, 55°C for 30 s, and 95°C for 30 s.  $\beta$ -actin of *B. xylophilus* was used as an internal control. The expression values were calculated using the  $2^{-\Delta\Delta CT}$  method and normalized to  $\beta$ -actin expression levels (Livak and Schmittgen, 2001). One-way ANOVA (SPSS version 20.0) with Tukey's multiple comparison test was used to compare the number of relative fold changes in gene expression. Data were considered significant when  $p < 0.05$ .

## **RESULTS**

### **Phylogeny of the Nematodes**

Compared with other nematodes, insect-vectored parasites were expected to show adaptations, i.e., genetic changes to this new method of transmission compared with self-dispersing (ancestral trait) nematodes. Therefore, comparing the genomes of insect-vectored nematodes with other nematodes could help to reveal the molecular basis of nematode-vector transmission. We compared the genome among nematodes differing in their dispersal strategy and lifestyle (plant- or animal-parasitic or free-living), including two PPNs vectored by *M. alternatus* (i.e., *B. xylophilus* and *B. mucronatus*), two animal-parasitic nematodes vectored by blood-feeding insects (i.e., *B. malayi* and *L. loa*), and self-dispersing nematodes spreading without a biotic vector, including two plant-parasitic nematodes (i.e., *M. arenaria* and *M. javanica*), two animal-parasitic nematodes (i.e., *S.*

*carpocapsae* and *E. vermicularis*), and four free-living nematodes (i.e., *C. elegans*, *C. remanei*, *C. brenneri*, and *P. pacificus*). A total of 104,444 gene families were clustered among these species using OrthoFinder. The species with similar lifestyle were clustered into monophyletic groups, and the four vector-dispersed nematode species were also clustered with their corresponding suborders. This observation suggests that the four insect-vectored nematodes do not originate from the same common ancestor and that their ancestors may have been different from those of the self-dispersing nematodes (Figure 1A).



A genome-wide comparison revealed large and frequent changes in the size of the gene families. These changes resulted from the high rate of gene gain (through duplication) and loss (through deletion or pseudogenization) and the evolution of completely new genes. Based on the gene family

clustering resulting, we identified 23 gene families whose sizes were significantly reduced among the four insect-vectored nematodes. Many of the reduced gene families were found to be involved in nucleotide repair, gene expression regulation, and immune system (Figure 1B). Exonuclease and DNA ligase and phospholipid-translocating ATPase were two reduced gene families that participate in nucleotide repair. Fork head domain is a common type of protein domain that is often found in transcription factors. Its purpose is to bind DNA, while the Zinc-finger domain-containing proteins function in gene transcription, translation, and other functions (Klug and Rhodes, 1987; Kaufmann and Knochel, 1996). CTLD and epidermal growth factor (EGF)-like domain are two major reduced gene families involved in the immune system. The newly completed *C. elegans* genome sequence encodes 278 predicted proteins containing the CTLD domain, which is the seventh most abundant domain (Zelensky and Gready, 2005; Brown et al., 2018). In addition, the EGF-like domain plays an important role in the immune system and apoptosis. Both EGF and the von Willebrand factor type A (VWA) domains are common additional domains of CTLs (Stetak et al., 2006; Lenting et al., 2015).

### C-Type Lectin Gene Family Contraction

To estimate the gene family contraction of the CTL accurately, we identified all CTL genes and classified them according to their domain characteristics. The most common type of CTL contains one CTLD domain, whereas other types also contain additional CTLDs, complement C1r/C1s Uegf Bmp1 (CUB), or VWA domains or some uncommon domains. Among the 12 nematodes with whole-genome sequence-based data used here, the size of the CTL family was highly reduced among insect-vectored nematodes compared with the self-dispersing nematodes. The order of species based on the number of CTLs from highest to lowest was *C. elegans*, *C. brenneri*, *S. carpocapsae*, *P. pacificus*, *C. remanei*, *M. arenaria*, *M. javanica*, *E. vermicularis*, *B. malayi*, *B. xylophilus*, *B. mucronatus*, and *L. loa* with 166, 152, 113, 111, 110, 79, 78, 77, 16, 12, 12, and 10 CTLs, respectively. Despite this, the species with the highest ratio of complex structure of CTLs were *B. xylophilus* and *B. mucronatus* (6/12) (Figure 2). The subcellular localizations of nematode CTL proteins were predicted using WoLF PSORT (Table 1). Most of them had a high probability to be located in the extracellular matrix based on signalP results. Except for extracellular CTLs,

most proteins are located on the surface of the plasma membrane, which is common for CTL receptors (CLRs) (Geijtenbeek and Gringhuis, 2016). Transmembrane CLRs can use various intracellular signaling pathways to directly modulate cellular, developmental, homeostatic, and immunological responses (Osorio and Sousa, 2011). However, the rest of the proteins were presumably located in mitochondria, cytoplasm, endoplasmic, cytoskeleton, nucleus, and peroxisome.

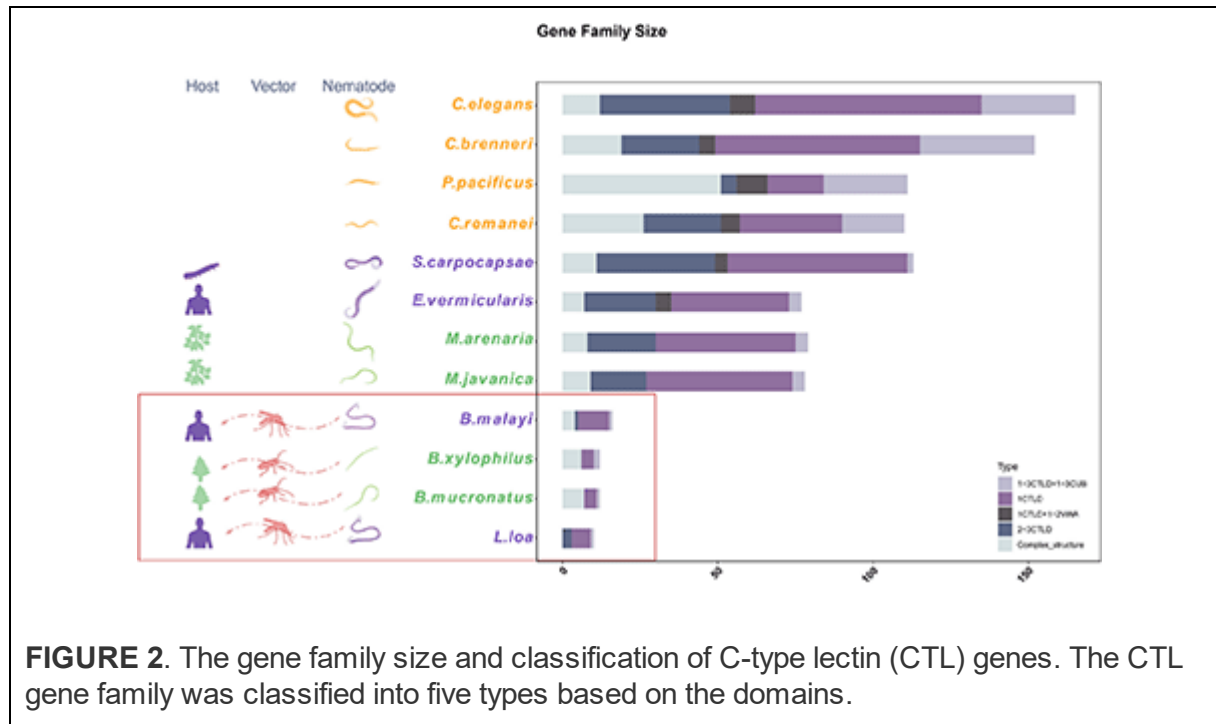


**FIGURE 2.** The gene family size and classification of C-type lectin (CTL) genes. The CTL gene family was classified into five types based on the domains.

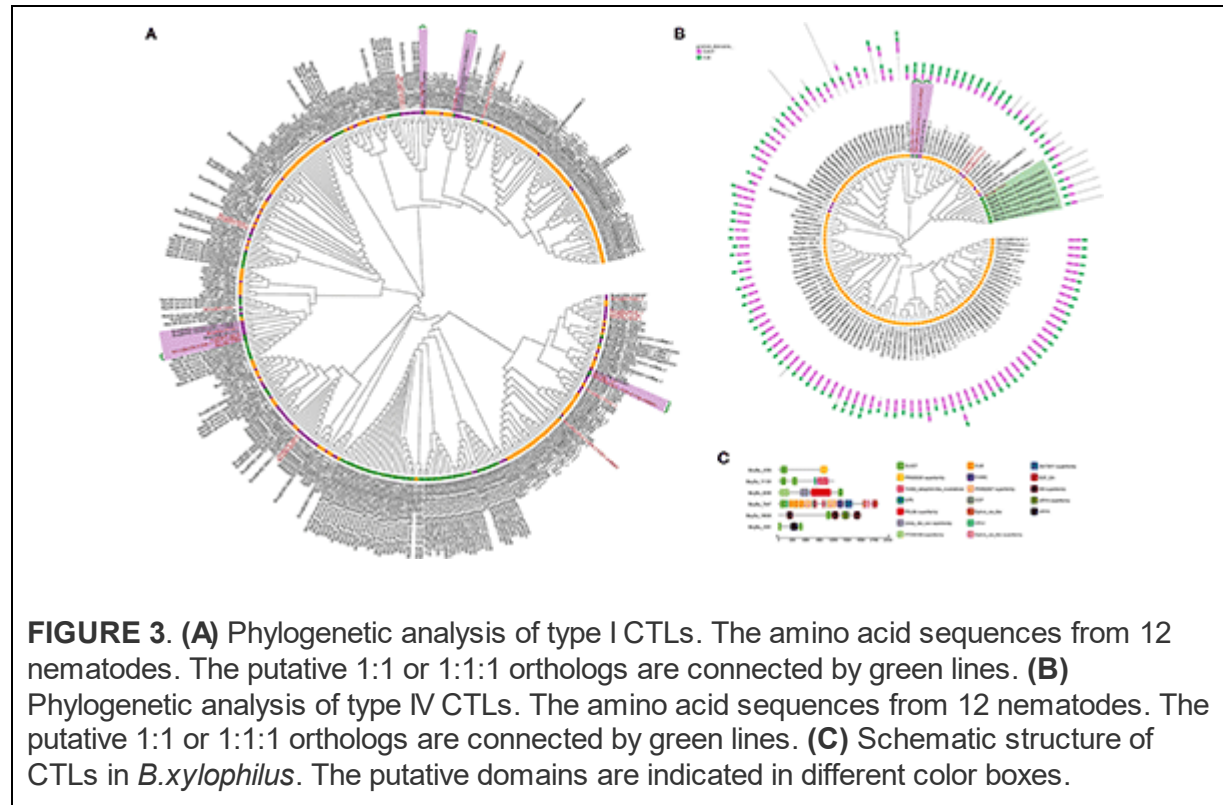
**Table 1.** Subcellular localization of C-type lectins.

	Cel	Cbn	Cre	Ppa	Sca	Mar	Mja	Eve	Bma	Bxy	Bmu	Llo
Extracellular	98	88	57	34	81	25	33	31	6	6	5	3
Plasma membrane	64	46	38	66	15	31	25	14	7	3	4	2
Mitochondrion	3	1	2	1	3	0	1	1	0	1	0	0
Cytoplasm	0	11	4	4	5	14	8	18	1	1	2	4
Endoplasmic	0	0	2	1	0	3	0	0	0	1	0	0
Cytoskeleton	0	0	0	0	0	0	0	1	1	0	0	1
Nucleus	1	5	5	6	7	4	8	7	1	0	1	0
Cytosolic or nuclear	0	1	3	1	2	2	3	4	0	0	0	0
Endoplasmic or Mitochondrion	0	0	0	0	0	0	0	1	0	0	0	0
Peroxisome	0	0	0	0	0	0	0	1	0	0	0	0

## Phylogenetic Analysis of CTL Genes

To elucidate the evolutionary history of nematode CTLs, phylogeny analysis of five protein types from 12 sequenced species was performed using

maximum likelihood (ML) methods. Among them, the members from type I contained one CTLD domain, which identified 401 sequences in this study. In the phylogenetic analysis, Bxy|Bu\_1183 shared 1:1 orthology with Sca|L596\_010888 and Bxy|Bu\_842 shared 1:1:1 orthology with Eve|EVEC\_0000020501-mRNA-1 and Sca|L596\_010190. In addition, Bxy|Bu\_2162 and Bxy|Bu\_717 shared 1:1 orthology with *B. mucronatus* while being in the same clade with several CTL genes of animal parasitic nematodes (Figure 3A). Type III members contain 1–3 CTLD domains and 1–3 CUB domains. CUB domains can mediate protein–protein interactions in various extracellular proteins and are involved in a variety of major biological functions, including immunity and development, as well as in various cancer types (Gaboriaud et al., 2011). Such CTLs are very rare in parasitic nematodes. The phylogenetic tree showed that Bxy|Bu\_1341, Bmu|BmChr6\_6706.5\_1338.mRNA1, and Sca|L596\_027679 were 1:1:1 orthologs, whereas Bxy|Bu\_3303 was in the same clade with CTL genes of PPNs (Figure 3B). The phylogenetic analysis of type II and type IV members is attached in Supplementary Figure 1. Phylogenetic analysis of CTL among nematodes shows that these genes are evolutionarily conserved. Interestingly, these CTL genes were not species-specifically expanded or contracted, and these genes from the same species were not clustered together but nested with the genes from other nematode species. Therefore, these results suggested that the reduction of these genes is a common phenomenon shared by insect-vectored nematodes investigated here, and may be associated with parallel adaptation to live inside the insect vector environment rather than adaptation among specific nematode-host species pairs.



To get a better overview of the characteristics of the complicated structure of CTLs, we further analyzed their sequence features in *B. xylophilus*. The CTLs show surprisingly high diversity in protein secondary structure and may have the potential to generate immune specificity. These proteins contain additional CTLDs, extracellular domains (CUB), low-density lipoprotein (LDL) receptor motifs, EGF-like domains, or VWA. Nine proteins contained a signal sequence and were thus secreted, and three proteins contained a transmembrane-spanning region (Table 2). Previous studies have considered that these secreted proteins may contribute to both recognition and antimicrobial activity (Nicholas and Hodgkin, 2004; Schulenburg and Ewbank, 2004; O'Rourke et al., 2006). In addition, Bxy|Bu\_11124 had two CTLDs, one G Protein-Coupled Receptor (GPCR) proteolysis site (GPS), and one 7tmB2\_latrophilin-like\_invertebrate (GPCR), indicating that Bxy|Bu\_11124 might be anchored to the cell membrane. Latrophilin, also called lectomedins, belongs to adhesion GPCRs. GPCRs are important regulators that couple cellular adhesion toward intracellular events (Langenhan et al., 2013, 2016). Bxy|Bu\_7847 had a very complex structure, which contains CTLD, CUB, LDL, EGF,

complement control protein (CCP) domain, and ephrin-receptor-like domain (Figure 3C).

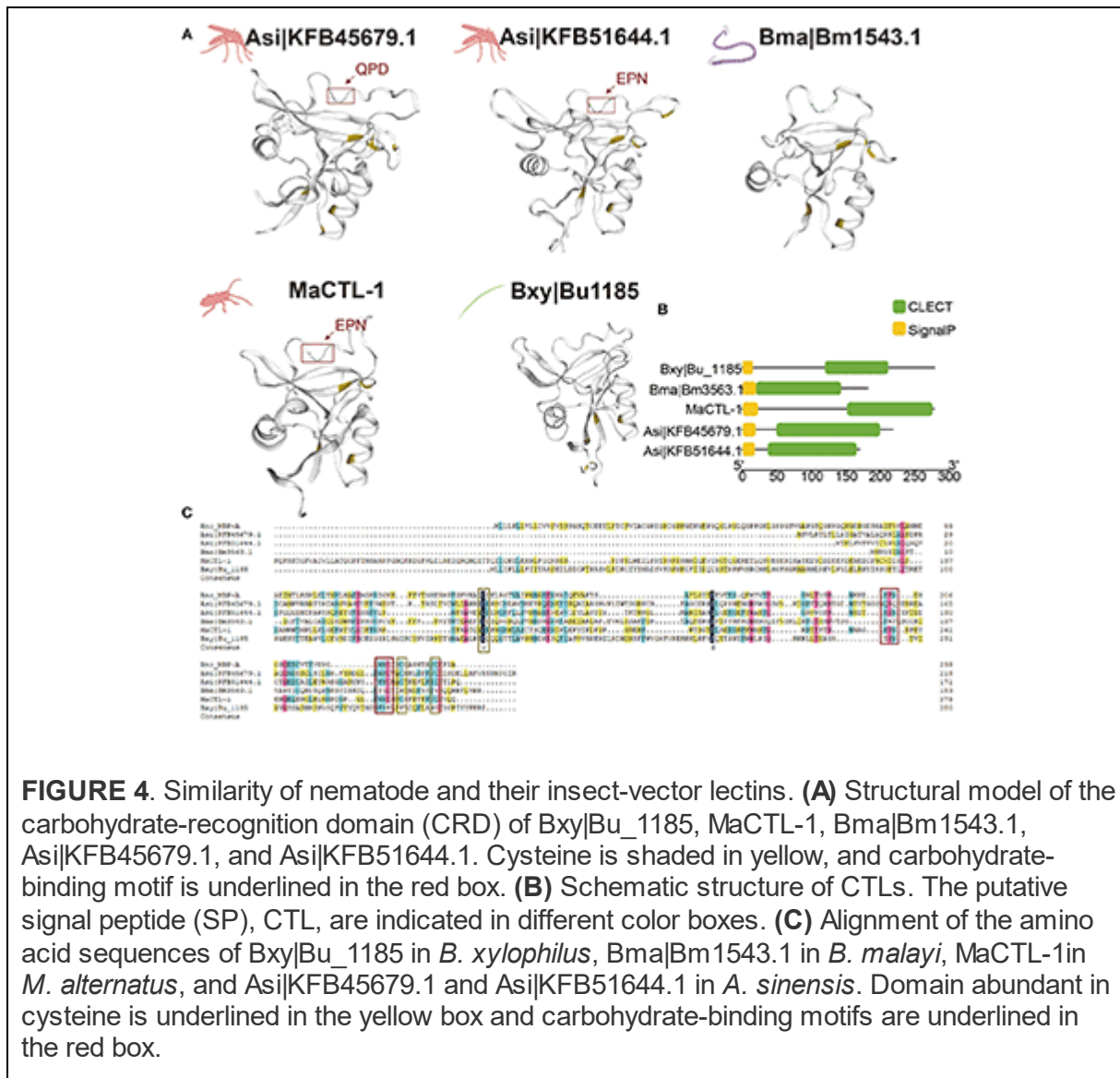
**Table 2.** Subcellular localization of *B.xylophilus* C-type lectins.

	Genomic		Proteomic
	SignalP	Transmembrane	Secreted protein
Bxy Bu_1185	✓		
Bxy Bu_842			
Bxy Bu_2162	✓		
Bxy Bu_717	✓		
Bxy Bu_3303	✓	✓	
Bxy Bu_1341	✓		
Bxy Bu_11124	✓	✓	
Bxy Bu_1991			
Bxy Bu_6499		✓	
Bxy Bu_7847	✓		
Bxy Bu_18638	✓		✓
Bxy Bu_4785	✓		

## Structural Conservation Among Nematode and Insect-Vector Lectins

We aligned the CTLs of two representative insect-borne nematodes, namely, *B. xylophilus* and *B. malayi*, and their insect vector, namely, *M. alternatus* and *Anopheles sinensis*. The structures were aligned with the known structure of these proteins and modeled accordingly (Figure 4A). Based on these predictions, Bxy|Bu\_1185 and Bma|Bml543.1 showed a remarkable structural similarity to MaCTL-1, Asi|KFB45679.1, and Asi|KFB51644.1, with the major beta sheets and alpha helices being in corresponding positions. All of these lectins have four cysteine residues, and the three lectins of vector contain a motif QPD (Gln-Pro-Asp) and EPN (Glu-Pro-Asn) which confer specificity for carbohydrates for these proteins (Brown et al., 2018). In addition, all of these five lectins had a SP but no transmembrane domains which were probably secreted (Figure 4B). The

carboxy-terminal domain had strong similarities to nematode and insect vector and mammalian CTLs, including the Bxy|Bu\_1185, Bma|Bm1543.1, MaCTL-1, Asi|KFB45679.1, Asi|KFB51644.1, and rat mannose-binding protein-A (Rno-MBP-A) (Weis et al., 1991). Maximal amino-acid identity was 20.35% among these CTLs (Figure 4C).



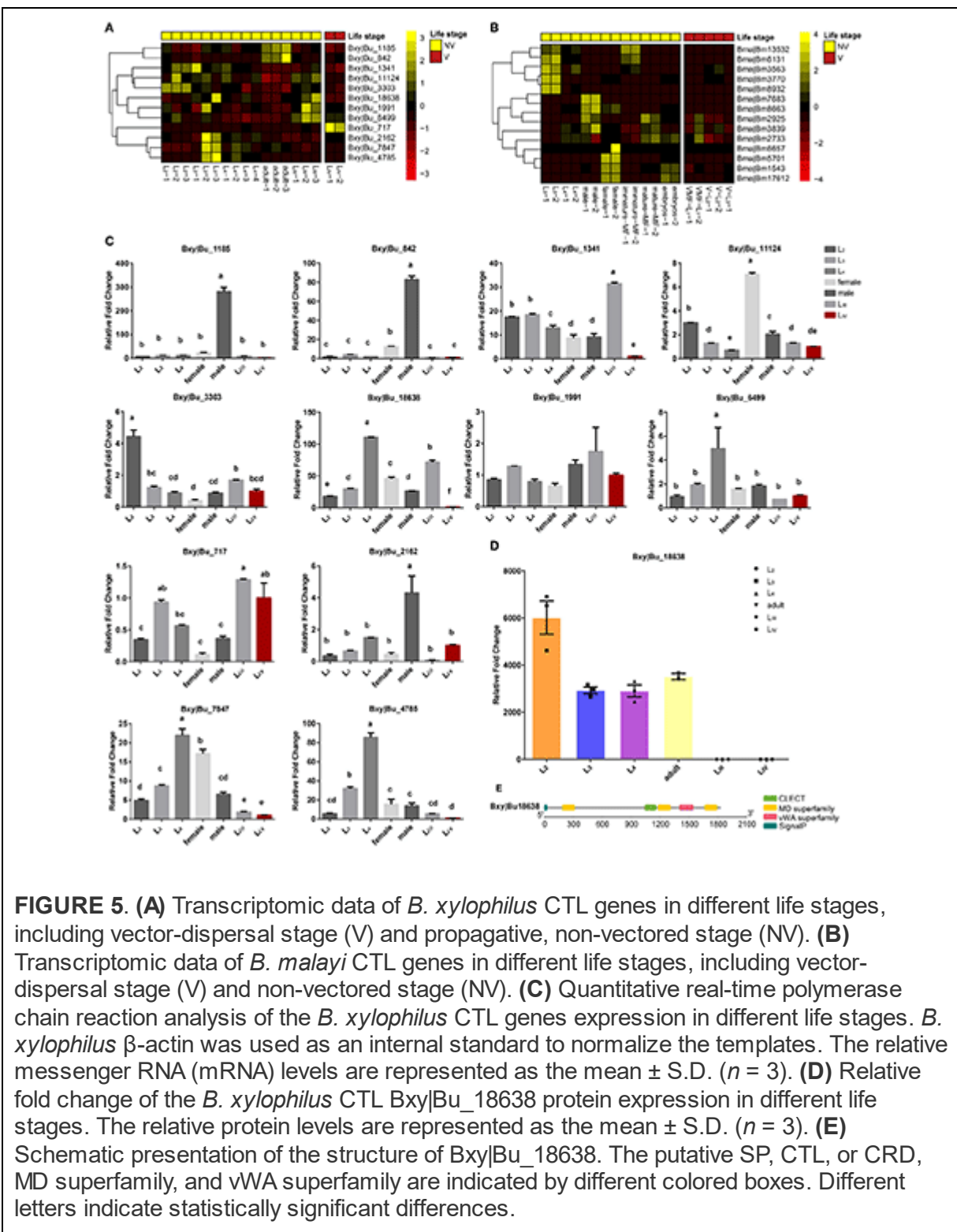
## Comparison of CTLs Between Dispersal and Propagative Life Stages of Insect-Vectored Nematodes

This approach exploits the fact that many species of parasitic nematodes have life cycles where some stages are propagative and some are dispersive (which are transmitted to a new host by the insect vectors) (Sommer and

Streit, 2011). Comparing the gene expression in dispersive and propagative life cycle stages might, therefore, identify the genes and proteins used or not used by the dispersal stage. A characteristic component of the innate immune system is that some of the genes are transcriptionally upregulated after microbial invasion (Zou et al., 2007). For the model free-living nematode *C. elegans*, 104 clec genes were only upregulated, and 103 clec genes were both upregulated and downregulated following an infection with different pathogens (Pees et al., 2016). Each life stage had a specific upregulated expression of CTL genes (Supplementary Figure 2). However, our transcriptomic analysis of *B. xylophilus* and *B. malayi* with different life histories did not find the same gene expression pattern.

Besides the propagative stages (L<sub>1</sub>-L<sub>4</sub>), *B. xylophilus* has two dispersal life stages, namely, the third- and fourth-stage dispersal juveniles (L<sub>III</sub> and L<sub>IV</sub>) (Futai, 2013). L<sub>III</sub> larvae are attracted to mature vector-beetle larvae and aggregate around their pupal chambers, whereas in the next stage, L<sub>IV</sub> larvae are only attracted to the newly enclosed adults which carry the nematodes in their trachea to new hosts trees (Zhao et al., 2007). Comparison of the transcriptome of these dispersive and propagative life stages of *B. xylophilus* showed that CTL genes are not activated in the L<sub>IV</sub> stage except for Bxy|Bu\_717 (Figure 5A). However, most of these lectin genes are activated by *Stenotrophomonas maltophilia*, which is one of the most dominant bacteria in *B. xylophilus* (Supplementary Figure 3), indicating that these genes may be related to the pathogen recognition in *B. xylophilus* (Cheng et al., 2013). The CTL genes of *B. xylophilus* were taken to perform qPCR experiments to validate the transcription level, and the results were generally in agreement with that from transcriptomic analysis (Figure 5C). *B. malayi* is a filarial (arthropod-vector) nematode and one of the three causative agents of lymphatic filariasis in humans. The development and replication of *B. malayi* occur in the two discrete phases, i.e., in the mosquito vector and in the human main host. Both stages are essential to the life cycle of the parasite (Edeson and Wilson, 1964). The mosquito serves as both a biological vector and an intermediate host, and is required for the developmental cycle and transmission of *B. malayi*. Once the mosquito feeds on human blood and ingests microfilariae (MF) of *B. malayi*, the MF develop into infective larvae (L<sub>1</sub> to L<sub>3</sub>), which is then transmitted into humans when the mosquito takes another blood meal (Sommer and Streit,

2011). Comparison of the transcriptome of these dispersive and propagative life stages of *B. malayi* showed that the expression of CTLs is not activated in MF and infective larval (L<sub>1</sub>-L<sub>3</sub>) stages (Figure 5B). In other words, the immune response of a vector may not always be effective because of the ability of the nematode to survive or overcome the immune defense.

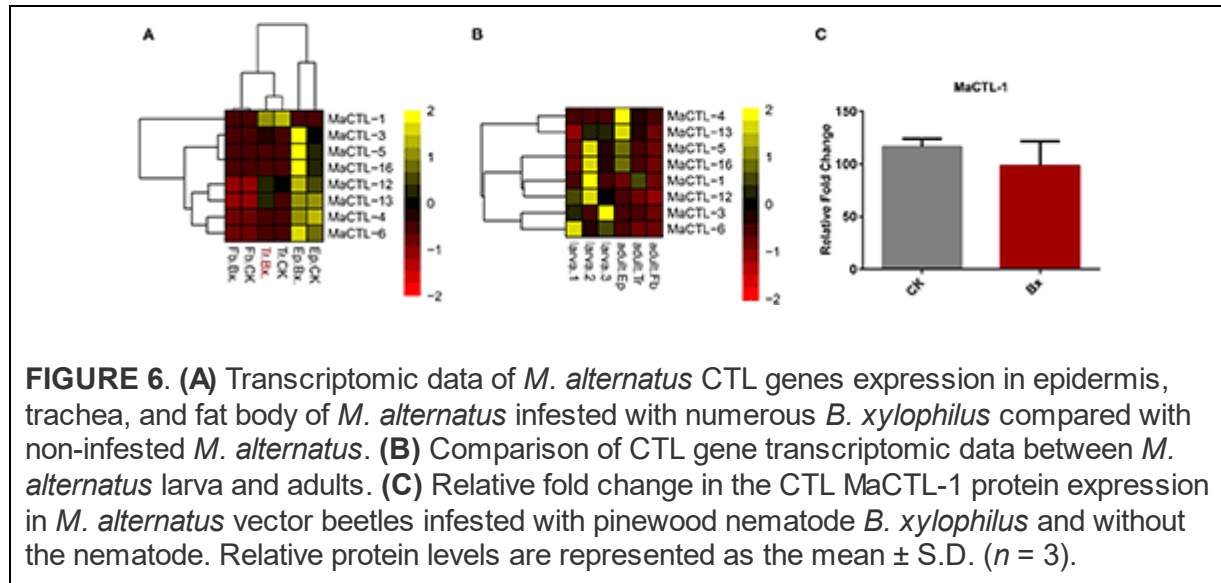


Identification of the molecules that nematode parasites secrete into their vectors can help us to understand the interactive interface between parasites

and their vectors. Among these CTL genes of *B. xylophilus*, we identified 6 secreted proteins (Table 2). By using the secretory proteomics analysis of nematodes of different stages (unpublished data), we found one of the secreted proteins, Bxy|Bu\_18638. In addition to a CTLD, this secreted protein also has 3 MD domains and one VWA domain. This protein can only be detected during the propagative stage and may be related to the complex environment of the host pine tree during the corresponding propagative stage.

### **The Vector Responses to Nematodes**

The insect-vectored nematodes showed high specificity with their insect vectors (Kariuki et al., 2010; Zhou et al., 2018b). The successful boarding and transmission of parasitic nematodes depend on the immune recognition of the insect vector during parasitic invasion. This step is often mediated by pattern recognition proteins (PRPs), including peptidoglycan recognition proteins (PGRPs),  $\beta$ -glucan recognition proteins ( $\beta$ GRPs), CTLs, and galectins (Brown et al., 2018). Previous studies have shown that the vector beetle, i.e., *M. alternatus*, has fewer CTL genes compared with five other insect species not vectoring nematodes (Zhou et al., 2018a), but whether these genes trigger a response during nematode loading has not been studied. Therefore, to analyze whether CTL genes play a role in carrying *B. xylophilus*, a transcriptomic comparison of the vector beetle was performed with or without *B. xylophilus*. We found that *B. xylophilus* loading barely affected the transcription of CTLs of the insect vector, neither in their tracheal system, nor in epidermis and midgut (Figure 6A). In addition, we compared the CTL transcription between the larvae and adults of this vector beetle and found that the gene expression in the adult, especially the trachea, was not activated (Figure 6B). Similarly, the relative content of MaCTL-1 protein, which has high homology to *B. xylophilus* CTL, was not significantly different in the trachea with or without *B. xylophilus* (Figure 6C).



## DISCUSSION

This study found that CTL family contraction has likely contributed to the evolutionary transition from self-dispersing to vector-mediated dispersal mode in insect-vectored nematodes. CTLs are the most abundant lectins in *C. elegans* and are important for nematodes to recognize hosts or pathogens (Loukas et al., 1999; Loukas and Maizels, 2000; Zelensky and Gready, 2005; Bauters et al., 2017; Brown et al., 2018; Zhang et al., 2018; Zhuo et al., 2019). The size of this gene family was drastically reduced in insect-vectored nematodes compared with those of self-dispersing nematodes (Figure 2). The activity of these genes was also downregulated in the dispersive life stages, i.e., stages that are transmitted to a new host by the insect vectors (Figure 5). Such changes may contribute to the insensitiveness of the nematode to their vector and vice versa: lower expression or gene number of CTL genes may potentially prevent or decrease the immune response of the nematode when entering the vector and, consequently, reduce the likelihood that the vector mounts an immune response against the nematode. Desensitization toward the vector may, therefore, be the first step in the transition from self-dispersing to vector-mediated dispersal. Interestingly, however, insect-vectored nematodes retained major genes with complex domains, which may be a strategy to compensate for the gene loss by increasing their functional diversity. This “less-is-more” molecular

evolution strategy may, therefore, play an important role in the establishment of new interspecific relationships.

Our results also demonstrate a parallel evolution in CTL gene family sizes among insect-vectored nematodes. Gene family expansion and contraction can be used as a reliable index of adaptive evolution (Temperley et al., 2008). Similar evolutionary pressures, such as environmental changes and establishment of new interspecific relationships, can lead to the development of similar biological traits among phylogenetically distinct species. For example, previous studies have found contraction in the MMP12 gene family among both cetaceans and manatees. This gene family codes a potent protease-degrading elastin, a key protein necessary for the elasticity of vertebrate lung, indicating that the shared loss of MMP12 among these two lineages is likely a result of adaptation to aquatic environment (Sharma et al., 2019). Similarly, the reduction of the CTL gene family may be a driving molecular force behind the parallel evolution among nematodes adapted to vector-mediated dispersal.

Nematodes have developed a range of morphological, behavioral, physiological, and molecular defense reactions to survive and complete their life cycles within an insect vector. Correspondingly, vector insects have also evolved a variety of strategies to tolerate nematode invasion. Studies have compared CTL genes in nematodes and their vectors and found that these genes are largely identical, which may be due to the adaptation of the nematode to its vector hosts. First, gene loss events have not only occurred in the insect-vectored nematode, but also in many vector insects. For example, the size of the CTL gene family in insect vectors of *B. malayi* and *B. xylophilus*, *A. sinensis*, and *M. alternatus*, respectively, is also reduced (Zhou et al., 2014, 2018a). Second, we found that the CTL genes were not activated in the dispersive stages of these nematodes or in their insect vectors. However, these genes immediately activate once the vector is carried with intolerable nematode or the nematode loading into unmatched vector (Kariuki et al., 2010; Zhou et al., 2018b). Third, we found that these nematodes and their insect vectors had conserved lectin structures, suggesting a presence of a co-evolved nematode-vector immune-recognition strategy. In fact, many biological characteristics of insect-vectored nematodes have been degraded due to the establishment of a mutualistic relationship between nematodes and their vectors. For example, in order to reduce the likelihood of triggering its vector's immune response, pinewood

nematode *B. xylophilus* molts before entering into the vector trachea to remove most of the symbiotic microbes adhering to its body surface (Zhang et al., 2021). In addition, the nematode's oral orifice is degenerated and forms a closed body cavity, which may prevent the bacteria and/or secretions from flowing out from its intestine into the insect vector (Zhang et al., 2021). These results suggest that both nematodes and their vectors reduce immune recognition and defense against each other to balance their mutualistic relationship. This “retreat in order to advance” strategy can reveal insights into possible mechanisms underlying adaptation and deepen our understanding of coevolution.

## DATA AVAILABILITY STATEMENT

The datasets presented in this study can be found in online repositories. The names of the repository/repositories and accession number(s) can be found below: National Center for Biotechnology Information (NCBI) BioProject database under Accession Number PRJNA798902.

## AUTHOR CONTRIBUTIONS

LZ designed the research. JN performed the experiments. JN, JZ, HW, and YL analyzed the data. XF, YF, and XG collected samples. JN, JZ, FA, and LZ wrote the manuscript. All authors critically reviewed and approved the manuscript.

## FUNDING

This study was supported by the Basic Frontier Scientific Research Program of the Chinese Academy of Sciences from 0 to 1 (ZDBS-LY-SM027-03), the National Key Plan for Scientific Research and Development of China (2021YFC2600100 and 2019YFC1200504), the Natural Science Foundation of China (NSFC 31970466), the Strategic Priority Research Program of Chinese Academy of Sciences (Grant No. XDPB16), the National Youth Talent Support Program of China (Ten Thousand People Plan), and the State

Key Laboratory of Integrated Management of Pest Insects and Rodents (Grant No. Chinese IPM2111).

## SUPPLEMENTARY MATERIAL

The Supplementary Material for this article can be found online at: <https://www.frontiersin.org/articles/10.3389/fpls.2022.856826/full#supplementary-material>

**Supplementary File 1.** Genome datasets used in comparative analyses.

**Supplementary File 2.** Amino acid sequences of CTL genes in nematodes.

**Supplementary File 3.** Amino acid sequences of CTL genes in vectors.

**Supplementary File 4.** Transcriptomic datasets used in comparative analyses.

**Supplementary Table 1.** Primers used in quantitative real-time PCR analysis.

**Supplementary Figure 1.** Phylogenetic analysis of CTLs. **(A)** Phylogenetic analysis of type II CTLs. **(B)** Phylogenetic analysis of type IV CTLs.

**Supplementary Figure 2.** Specific upregulated expression of CTL genes in *C. elegans*.

**Supplementary Figure 3.** Transcriptomic data of *B. xylophilus* CTL genes under *S. maltophilia* compared with aseptic nematodes.

## REFERENCES

Abad, P., Gouzy, J., Aury, J. M., Castagnone-Sereno, P., Danchin, E. G. J., Deleury, E., et al. (2008). Genome sequence of the metazoan plant-parasitic nematode *Meloidogyne incognita*. *Nat. Biotechnol.* 26, 909–915. doi: 10.1038/nbt.1482

Baermann, G.. (1917). Eine einfache methode zur auffindung von *Ancylostomum* (Nematoden) larven in erdproben. *Geneeskd Tijdschr Ned Indie* 57, 131–137.

Bauters, L., Naalden, D., and Gheysen, G. (2017). The distribution of lectins across the phylum nematoda: a genome-wide search. *Int. J. Mol. Sci.* 18, 91. doi: 10.3390/ijms18010091

Blaxter, M. L., De Ley, P., Garey, J. R., Liu, L. X., Scheldeman, P., Vierstraete, A., et al. (1998). A molecular evolutionary framework for the phylum Nematoda. *Nature* 392, 71–75. doi: 10.1038/32160

Brown, G. D., Willment, J. A., and Whitehead, L. (2018). C-type lectins in immunity and homeostasis. *Nat. Rev. Immunol.* 18, 374–389. doi: 10.1038/s41577-018-0004-8

Buchfink, B., Xie, C., and Huson, D. H. (2015). Fast and sensitive protein alignment using DIAMOND. *Nat. Methods* 12, 59–60. doi: 10.1038/nmeth.3176

Chen, C. J., Chen, H., Zhang, Y., Thomas, H. R., Frank, M. H., He, Y. H., et al. (2020). TBtools: an integrative toolkit developed for interactive analyses of big biological data. *Mol. Plant* 13, 1194–1202. doi: 10.1016/j.molp.2020.06.009

Chen, F. C., Chen, C. J., Li, W. H., and Chuang, T. J. (2010). Gene family size conservation is a good indicator of evolutionary rates. *Mol. Biol. Evol.* 27, 1750–1758. doi: 10.1093/molbev/msq055

Cheng, T. C., Wu, J. Q., Wu, Y. Q., Chilukuri, R. V., Huang, L. H., Yamamoto, K., et al. (2017). Genomic adaptation to polyphagy and insecticides in a major East Asian noctuid pest. *Nat. Ecol. Evol.* 1, 1747–1756. doi: 10.1038/s41559-017-0314-4

Cheng, X. Y., Tian, X. L., Wang, Y. S., Lin, R. M., Mao, Z. C., Chen, N., et al. (2013). Metagenomic analysis of the pinewood nematode microbiome reveals a symbiotic relationship critical for xenobiotics degradation. *Sci. Rep.* 3, 1869. doi: 10.1038/srep01869

De Bie, T., Cristianini, N., Demuth, J. P., and Hahn, M. W. (2006). CAFE: a computational tool for the study of gene family evolution. *Bioinformatics* 22, 1269–1271. doi: 10.1093/bioinformatics/btl097

Demangeat, G., Komar, V., Van-Ghelder, C., Voisin, R., Lemaire, O., Esmenjaud, D., et al. (2010). Transmission competency of single-female xiphinema index lines for grapevine fanleaf virus. *Phytopathology* 100, 384–389. doi: 10.1094/Phyto-100-4-0384

Dutta, T. K., Ganguly, A. K., and Gaur, H. S. (2012). Global status of rice root-knot nematode, *Meloidogyne graminicola*. *Afr. J. Microbiol. Res.* 6, 6016–6021. doi: 10.5897/Ajmr12.707

Edeson, J. F. B., and Wilson, T. (1964). The epidemiology of filariasis due to *Wuchereria Bancrofti* and *Brugia Malayi*. *Annu. Rev. Entomol.* 9, 245. doi: 10.1146/annurev.en.09.010164.001333

Edgar, R. C. (2004). MUSCLE: multiple sequence alignment with high accuracy and high throughput. *Nucleic Acids Res.* 32, 1792–1797. doi: 10.1093/nar/gkh340

Emms, D. M., and Kelly, S. (2019). OrthoFinder: phylogenetic orthology inference for comparative genomics. *Genome Biol.* 20, 466201. doi: 10.1186/s13059-019-1832-y

Futai, K.. (2013). Pine Wood Nematode, *Bursaphelenchus xylophilus*. *Annu. Rev. Phytopathol.* 51, 61–83. doi: 10.1146/annurev-phyto-081211-172910

Gaboriaud, C., Gregory-Pauron, L., Teillet, F., Thielens, N. M., Bally, I., and Arlaud, G. J. (2011). Structure and properties of the  $\text{Ca}^{2+}$ -binding CUB domain, a widespread ligand-recognition unit involved in major biological functions. *Biochem. J.* 439, 185–193. doi: 10.1042/BJ20111027

Geijtenbeek, T. B. H., and Gringhuis, S. I. (2016). C-type lectin receptors in the control of T helper cell differentiation. *Nat. Rev. Immunol.* 16, 433–448. doi: 10.1038/nri.2016.55

Grabherr, M. G., Haas, B. J., Yassour, M., Levin, J. Z., Thompson, D. A., Amit, I., et al. (2011). Full-length transcriptome assembly from RNA-Seq data without a reference genome. *Nat. Biotechnol.* 29, 644–U130. doi: 10.1038/nbt.1883

Hou, Y., Wang, X. L., Saha, T. T., Roy, S., Zhao, B., Raikhel, A. S., et al. (2015). Temporal coordination of carbohydrate metabolism during mosquito reproduction. *PLoS Genet.* 11, 1005309. doi: 10.1371/journal.pgen.1005309

Johnson, L. S., Eddy, S. R., and Portugaly, E. (2010). Hidden Markov model speed heuristic and iterative HMM search procedure. *BMC Bioinform.* 11, 431. doi: 10.1186/1471-2105-11-431

Jones, J. T., Haegeman, A., Danchin, E. G. J., Gaur, H. S., Helder, J., Jones, M. G. K., et al. (2014). Top 10 Plant parasitic nematodes in molecular plant pathology. *J. Nematol.* 46, 181–181. doi: 10.1111/mpp.12057

Jordaan, E. M., Loots, G. C., Jooste, W. J., and Dewaele, D. (1987). Effects of root-lesion nematodes (pratylenchus-brachyurus godfrey and pratylenchus-zeae graham) and fusarium-moniliforme sheldon

alone or in combination, on maize. *Nematologica* 33, 213–219. doi: 10.1163/187529287x00344

Kariuki, M. M., Hearne, L. B., and Beerntsen, B. T. (2010). Differential transcript expression between the microfilariae of the filarial nematodes, *Brugia malayi* and *B. pahangi*. *BMC Genom.* 11. doi: 10.1186/1471-2164-11-225

Kaufmann, E., and Knochel, W. (1996). Five years on the wings of fork head. *Mech. Dev.* 57, 3–20. doi: 10.1016/0925-4773(96)00539-4

Klug, A., and Rhodes, D. (1987). Zinc fingers - a novel protein fold for nucleic-acid recognition. *Cold Spring Harb. Symp. Quant. Biol.* 52, 473–482. doi: 10.1101/Sqb.1987.052.01.054

Kondrashov, F. A., Rogozin, I. B., Wolf, Y. I., and Koonin, E. V. (2002). Selection in the evolution of gene duplications. *Genome Biol.* 3, 1–9. doi: 10.1186/gb-2002-3-2-research0008

Langdon, W. B.. (2015). Performance of genetic programming optimised Bowtie2 on genome comparison and analytic testing (GCAT) benchmarks. *BioData Min.* 8, 1. doi: 10.1186/s13040-014-0034-0

Langenhan, T., Aust, G., and Hamann, J. (2013). Sticky signaling—adhesion class G protein-coupled receptors take the stage. *Sci. Signal.* 6, re3-re3. doi: 10.1126/scisignal.2003825

Langenhan, T., Piao, X., and Monk, K. R. (2016). Adhesion G protein-coupled receptors in nervous system development and disease. *Nat. Rev. Neurosci.* 17, 550–561. doi: 10.1038/nrn.2016.86

Lenting, P. J., Christophe, O. D., and Denis, C. V. (2015). von Willebrand factor biosynthesis, secretion, and clearance: connecting the far ends. *Blood* 125, 2019–2028. doi: 10.1182/blood-2014-06-528406

Livak, K. J., and Schmittgen, T. D. J. (2001). Analysis of relative gene expression data using real-time quantitative PCR and the 2- $\Delta\Delta$ CT method. *Methods* 25, 402–408. doi: 10.1006/meth.2001.1262

Loukas, A., and Maizels, R. M. (2000). Helminth C-type lectins and host-parasite interactions. *Parasitol. Today* 16, 333–339. doi: 10.1016/S0169-4758(00)01704-X

Loukas, A., Mullin, N. P., Tetteh, K. K. A., Moens, L., and Maizels, R. M. (1999). A novel C-type lectin secreted by a tissue-dwelling parasitic nematode. *Curr. Biol.* 9, 825–828. doi: 10.1016/S0960-9822(99)80366-2

Moens, M., and Perry, R. N. (2009). Migratory plant endoparasitic nematodes: a group rich in contrasts and divergence. *Annu. Rev. Phytopathol.* 47, 313–332. doi: 10.1146/annurev-phyto-080508-081846

Nicholas, H. R., and Hodgkin, J. (2004). Responses to infection and possible recognition strategies in the innate immune system of *Caenorhabditis elegans*. *Mol. Immunol.* 41, 479–493. doi: 10.1016/j.molimm.2004.03.037

O'Brien, W. G., Berka, V., Tsai, A. L., Zhao, Z. Y., and Lee, C. C. (2015). CD73 and AMPD3 deficiency enhance metabolic performance via erythrocyte ATP that decreases hemoglobin oxygen affinity. *Sci. Rep.* 5, 1–11. doi: 10.1038/srep13147

Ollivier, M., Tresset, A., Bastian, F., Lagoutte, L., Axelsson, E., Arendt, M. L., et al. (2016). Amy2B copy number variation reveals starch diet adaptations in ancient European dogs. *R. Soc. Open Sci.* 3, 160449. doi: 10.1098/rsos.160449

O'Rourke, D., Baban, D., Demidova, M., Mott, R., and Hodgkin, J. (2006). Genomic clusters, putative pathogen recognition molecules, and antimicrobial genes are induced by infection of *C. elegans* with *M. nematophilum*. *Genom. Res.* 16, 1005–1016. doi: 10.1101/gr.50823006

Osorio, F., and Sousa, G. R. E. (2011). Myeloid C-type lectin receptors in pathogen recognition and host defense. *Immunity* 34, 651–664. doi: 10.1016/j.immuni.2011.05.001

Pees, B., Yang, W. T., Zarate-Potes, A., Schulenburg, H., and Dierking, K. (2016). High innate immune specificity through diversified C-type lectin-like domain proteins in invertebrates. *J. Innate Immun.* 8, 129–142. doi: 10.1159/000441475

Schulenburg, H., and Ewbank, J. J. (2004). Diversity and specificity in the interaction between *Caenorhabditis elegans* and the pathogen *Serratia marcescens*. *BMC Evol. Biol.* 4, 49. doi: 10.1186/1471-2148-4-49

Sharma, V., Hecker, N., Roscito, J. G., Foerster, L., Langer, B. E., and Hiller, M. (2019). A genomics approach reveals insights into the importance of gene losses for mammalian adaptations (vol 9, 1215, 2018). *Nat. Commun.* 10, 1. doi: 10.1038/s41467-019-13828-5

Sommer, R. J., and Streit, A. (2011). Comparative genetics and genomics of nematodes: genome structure, development, and lifestyle. *Annu. Rev. Genet.* 45, 1–20. doi: 10.1146/annurev-genet-110410-132417

Stamatakis, A.. (2006). RAxML-VI-HPC: Maximum likelihood-based phylogenetic analyses with thousands of taxa and mixed models. *Bioinformatics* 22, 2688–2690. doi: 10.1093/bioinformatics/btl446

Stetak, A., Hoier, E. F., Croce, A., Cassata, G., Di Fiore, P. P., and Hajnal, A. (2006). Cell fate-specific regulation of EGF receptor trafficking during *Caenorhabditis elegans* vulval development. *Embo J.* 25, 2347–2357. doi: 10.1038/sj.emboj.7601137

Subramanian, B., Gao, S. H., Lercher, M. J., Hu, S. N., and Chen, W. H. (2019). Evolview v3: a webserver for visualization, annotation, and management of phylogenetic trees. *Nucleic Acids Res.* 47, W270–W275. doi: 10.1093/nar/gkz357

Tamura, K., Stecher, G., Peterson, D., Filipski, A., and Kumar, S. (2013). MEGA6: molecular evolutionary genetics analysis version 6.0. *Mol. Biol. Evol.* 30, 2725–2729. doi: 10.1093/molbev/mst197

Temperley, N. D., Berlin, S., Paton, I. R., Griffin, D. K., and Burt, D. W. (2008). Evolution of the chicken Toll-like receptor gene family: a story of gene gain and gene loss. *BMC Genom.* 9, 1–12. doi: 10.1186/1471-2164-9-62

Trankner, A.. (1992). Use of agricultural and municipal organic wastes to develop suppressiveness to plant-pathogens. *Biol. Control Plant Dis.* 230, 35–42.

Vovlas, N., Troccoli, A., Palomares-Rius, J. E., De Luca, F., Liebanas, G., Landa, B. B., et al. (2011). *Ditylenchus gigas* n. sp. parasitizing broad bean: a new stem nematode singled out from the *Ditylenchus dipsaci* species complex using a polyphasic approach with molecular phylogeny. *Plant Pathol.* 60, 762–775. doi: 10.1111/j.1365-3059.2011.02430.x

Wang, L. K., Feng, Z. X., Wang, X., Wang, X. W., and Zhang, X. G. (2010). DEGseq: an R package for identifying differentially expressed genes from RNA-seq data. *Bioinformatics* 26, 136–138. doi: 10.1093/bioinformatics/btp612

Waterhouse, A., Bertoni, M., Bienert, S., Studer, G., Tauriello, G., Gumienny, R., et al. (2018). SWISS-MODEL: homology modelling of protein structures and complexes. *Nucleic Acids Res.* 46, W296–W303. doi: 10.1093/nar/gky427

Weis, W. I., Kahn, R., Fourme, R., Drickamer, K., and Hendrickson, W. A. (1991). Structure of the calcium-dependent lectin domain from a rat mannose-binding protein determined by mad phasing. *Science* 254, 1608–1615. doi: 10.1126/science.1721241

Zelensky, A. N., and Gready, J. E. (2005). The C-type lectin-like domain superfamily. *Febs Journal* 272, 6179–6217. doi: 10.1111/j.1742-4658.2005.05031.x

Zhang, C., Wickham, J. D., Zhao, L. L., and Sun, J. H. (2021). A new bacteria-free strategy induced by MaGal2 facilitates pinewood nematode escape immune response from its vector beetle. *Insect Sci.* 28, 1087–1102. doi: 10.1111/1744-7917.12823

Zhang, L., Mou, L. Y., Chen, X. Q., Yang, Y., Hu, M., Li, X. R., et al. (2018). Identification and preliminary characterization of Hc-clec-160, a novel C-type lectin domain-containing gene of the

strongyloid nematode *Haemonchus contortus*. *Parasites Vectors* 11. doi: 10.1186/s13071-018-3005-3

Zhao, L. L., Wei, W., Kang, L., and Sun, J. H. (2007). Chemotaxis of the pinewood nematode, *Bursaphelenchus xylophilus*, to volatiles associated with host pine, *Pinus massoniana*, and its vector *Monochamus alternatus*. *J. Chem. Ecol.* 33, 1207–1216. doi: 10.1007/s10886-007-9289-y

Zhou, D., Zhang, D., Ding, G., Shi, L., Hou, Q., Ye, Y., et al. (2014). Genome sequence of *Anopheles sinensis* provides insight into genetics basis of mosquito competence for malaria parasites. *BMC Genomics* 15, 42. doi: 10.1186/1471-2164-15-42

Zhou, J., Yu, H. Y., Zhang, W., Ahmad, F., Hu, S. N., Zhao, L. L., et al. (2018a). Comparative analysis of the *Monochamus alternatus* immune system. *Insect Sci.* 25, 581–603. doi: 10.1111/1744-7917.12453

Zhou, J., Zhao, L. L., Yu, H. Y., Wang, Y. H., Zhang, W., Hu, S. N., et al. (2018b). Immune tolerance of vector beetle to its partner plant parasitic nematode modulated by its insect parasitic nematode. *Faseb J.* 32, 4862–4877. doi: 10.1096/fj.201800247R

Zhuo, K., Naalden, D., Nowak, S., Huy, N. X., Bauters, L., and Gheysen, G. (2019). A *Meloidogyne graminicola* C-type lectin, Mg01965, is secreted into the host apoplast to suppress plant defence and promote parasitism. *Mol. Plant Pathol.* 20, 346–355. doi: 10.1111/mpp.12759

Zou, Z., Evans, J. D., Lu, Z. Q., Zhao, P. C., Williams, M., Sumathipala, N., et al. (2007). Comparative genomic analysis of the *Tribolium* immune system. *Genome Biol.* 8, r177. doi: 10.1186/gb-2007-8-8-r177

**Conflict of Interest:** The authors declare that the research was conducted in the absence of any commercial or financial relationships that could be construed as a potential conflict of interest.

**Publisher's Note:** All claims expressed in this article are solely those of the authors and do not necessarily represent those of their affiliated organizations, or those of the publisher, the editors and the reviewers. Any product that may be evaluated in this article, or claim that may be made by its manufacturer, is not guaranteed or endorsed by the publisher.

Copyright © 2022 Ning, Zhou, Wang, Liu, Ahmad, Feng, Fu, Gu and Zhao. This is an open-access article distributed under the terms of the Creative Commons Attribution License (CC BY). The use, distribution or reproduction in other forums is permitted, provided the original author(s) and the copyright owner(s) are credited and that the original publication in this journal is cited, in accordance with accepted academic practice. No use, distribution or reproduction is permitted which does not comply with these terms.

ORIGINAL RESEARCH

published: 11 May 2022

doi: 10.3389/fpls.2022.890949



# Genes Encoding Potential Molecular Mimicry Proteins as the Specific Targets for Detecting *Bursaphelenchus xylophilus* in PCR and Loop-Mediated Isothermal Amplification Assays

**Fanli Meng<sup>1</sup>, Zhenkai Liu<sup>2,3</sup>, Yongxia Li<sup>2,3\*</sup> and Xingyao Zhang<sup>2,3</sup>**

<sup>1</sup> The Key Laboratory for Silviculture and Conservation of Ministry of Education, College of Forestry, Beijing Forestry University, Beijing, China

<sup>2</sup> Key Laboratory of Forest Protection of National Forestry and Grassland Administration, Ecology and Nature Conservation Institute, Chinese Academy of Forestry, Beijing, China

<sup>3</sup> Co-Innovation Center for Sustainable Forestry in Southern China, Nanjing Forestry University, Nanjing, China

**Edited by:**

Anna Filipiak, Institute of Plant Protection – National Research Institute, Poland

**Reviewed by:**

Kai Guo, Zhejiang Agriculture and Forestry University, China  
Alfonso Navas, CSIC, Spain

**\*Correspondence:** Yongxia Li, lyx020419@caf.ac.cn

**Specialty section:** This article was submitted to Plant Pathogen Interactions, a section of the journal *Frontiers in Plant Science*

**Received:** 07 March 2022

**Accepted:** 05 April 2022

**Published:** 11 May 2022

**Citation:** Meng F, Liu Z, Li Y and Zhang X (2022) Genes Encoding Potential Molecular Mimicry Proteins as the Specific Targets for Detecting *Bursaphelenchus xylophilus* in PCR and Loop-Mediated Isothermal Amplification Assays. *Front. Plant Sci.* 13:890949. doi: 10.3389/fpls.2022.890949

The introduction of the pine wood nematode (*Bursaphelenchus xylophilus*) to new areas has affected the international forestry industry because this pathogen causes pine wilt disease (PWD). Therefore, methods for the accurate and reliable detection of *B. xylophilus* are essential for controlling and managing this pest. The PCR and Loop-Mediated Isothermal Amplification (LAMP) techniques developed in this study involve species-specific primer sets targeting *B. xylophilus* genes encoding potential molecular mimicry proteins (*Bx-tlp-1*, *Bx-tlp-2*, and *Bx-cpi*), which are associated with pathogenicity. The PCR and LAMP results revealed that the primers were specific for *B. xylophilus* *Bx-tlp-1*, *Bx-tlp-2*, and *Bx-cpi*. Moreover, our LAMP assay targeting *Bx-tlp-1* conducted at 63°C detected *B. xylophilus* within 20 min and *B. xylophilus* from *Monochamus alternatus* or *M. saltuarius* within 30 min. The lower limits of detection for the LAMP and PCR assays were 10 pg and 10 ng genomic DNA, respectively, implying these assays may be useful for the rapid detection of *B. xylophilus* in pine forests. Designing primers specific for *Bx-tlp-1*, *Bx-tlp-2*, and *Bx-cpi* enabled the relatively rapid detection of *B. xylophilus* isolates as well as *M. alternatus* or *M. saltuarius* carrying *B. xylophilus*. These primers, which were designed following a thorough functional analysis of key *B. xylophilus* pathogenicity-related genes, may be useful for developing improved assays for the early diagnosis and prevention of PWD.

**Keywords:** *Bursaphelenchus xylophilus*, potential molecular mimicry proteins, specific target, rapid detection, PCR and LAMP

## INTRODUCTION

Pine is among the most popular timber species worldwide. Its ecological, economic, and social benefits are internationally recognized. Additionally, pine, which is an integral component of many products influencing human lifestyles, is a major forestation species in China (Jones et al., 2008; Soliman et al., 2012). However, it is susceptible to pine wilt disease (PWD) caused by the pine wood nematode *Bursaphelenchus xylophilus*, (Nickle et al., 1981), which poses a major threat to pine forests (Mamiya and Enda, 1972; Mota et al., 1999; Futai, 2013).

As a global forest quarantine disease, PWD can adversely affect forest ecologies and prevent sustainable timber production in the Americas, Europe, and Asia. *Bursaphelenchus xylophilus* is native to North America, but it was introduced to Japan in 1905, China in 1982, South Korea in 1988, Portugal in 1999, Spain in 2008, and the Madeira islands in 2010. After it was introduced to Europe, it spread to the Mediterranean coast (Futai, 2013). Since the first outbreak of PWD in China in 1982 (Cheng et al., 1983), the disease has been detected in 726 county-level administrative regions in 19 provinces. In the winter of 2017, PWD was detected in Fushun, Liaoning province, where the annual average temperature is 8.5°C referring to China Meteorological Administration. Almost 100,000 hectares were affected by PWD, resulting in the deaths of more than 50 million pine trees and economic losses exceeding 25 billion RMB. Hence, strengthening the quarantine and preventing the spread of PWD are the primary objectives of PWD disease management program.

The beetle species *Monochamus alternatus* and *M. saltuarius* are the principal vectors of *B. xylophilus* in Asia. These insects carry the dispersal fourth-stage juveniles of *B. xylophilus* and other nematodes (Ryss and Subbotin, 2017; Kanzaki and Giblin-Davis, 2018). Therefore, reliably discriminating *B. xylophilus* from other nematodes according to their morphological characteristics is a difficult task. Examining *M. alternatus* and *M. saltuarius* for the presence of *B. xylophilus* juveniles is an important part of an effective disease control strategy. More specifically, accurately identifying the juvenile stages is crucial for halting the spread of PWD.

Nematode species are routinely identified on the basis of their morphological characteristics. More specifically, *B. xylophilus* is typically identified according to the morphological characteristics of the adult-stage nematode; however, this requires a certain level of expertise and experience. Moreover, it is impossible to accurately identify the larvae. The limitations to morphology-based methods for identifying *B. xylophilus* have necessitated the development of methods relying on immunological, physiological, biochemical, and genetic characteristics. The current accepted methods for detecting and identifying *B. xylophilus* primarily involve molecular biology techniques. For example, the PCR(Wang et al., 2009) and loop-mediated isothermal amplification (LAMP) are commonly used detection techniques.

Regarding PCR, which enables the rapid amplification of DNA, two primers specific for the target DNA must be designed. The target sequence is

then amplified by DNA polymerase (e.g., Taq DNA polymerase) in three steps (denaturation, renaturation, and extension). The amplified sequence serves as a template for the next cycle. Because each cycle takes 2–4 min to complete, the target sequence can be amplified several million times in 2–3 h. Because of it, the PCR technique is mature for clinical diagnoses and quarantine. The LAMP technique, which can be used to rapidly amplify DNA, requires four primers specific for six regions of the target DNA. The target sequence is then amplified by *Bst* DNA polymerase at a constant temperature between 60 and 65°C. As a rapid, simple, specific, sensitive, and low-cost technique, LAMP has been exploited for research regarding disease detection and gene chip development (Tomita et al., 2008).

In this study, we developed PCR- and LAMP-based methods for the direct detection of *B. xylophilus*. The proposed PCR and LAMP techniques use the species-specific primer sets targeting *B. xylophilus* genes encoding potential molecular mimicry proteins, including thaumatin-like protein-1 (*Bx-tlp-1*; accession number KM063438.1), thaumatin-like protein-2 (*Bx-tlp-2*; accession number MK000287), and a cysteine proteinase inhibitor (*Bx-cpi*; accession number MK000288). Shinya et al. (2013) performed a proteomic analysis and identified two putative *B. xylophilus* thaumatin-like proteins (TLPs) and one cysteine proteinase inhibitor with sequences that were highly similar to those of plant proteins. These proteins were subsequently determined to induce cell death in *Nicotiana benthamiana* (Kirino et al., 2020). Moreover, the TLP sequences in *B. xylophilus* and *Pinus massoniana* are reportedly similar (Wang et al., 2014). Additionally, Meng et al. (2017) cloned the gene encoding a *P. massoniana* TLP (*Pm-tlp*) and revealed that its expression is associated with the expression of the *B. xylophilus* *Bx-tlp-1*. The relatively high sequence similarity between potential molecular mimicry proteins and plant proteins suggests that they may have similar functions. An analysis of the expression of the potential molecular mimicry proteins in *B. xylophilus* infecting pine trees indicated that the temporal changes to the  $\alpha$ -pinene content in the trees are consistent with the expression levels of the genes encoding a TLP (CPI) in *B. xylophilus* and *P. massoniana*. Thus, these genes are likely important for *B. xylophilus* infections of pine species (Meng et al., 2017, 2020).

Because the potential molecular mimicry proteins are associated with *B. xylophilus* pathogenicity, we designed primers specific for the *B. xylophilus*

genome, which may be useful for developing new disease prevention and control measures.

## MATERIALS AND METHODS

### Nematodes and Beetles

Both *B. xylophilus* and *Bursaphelenchus mucronatus* were raised on a *Botrytis cinerea* mycelial lawn on potato dextrose agar medium in plates at 25°C. The nematode cultures were stored in the laboratory. *Monochamus alternatus* and *M. saltuarius* were collected in different provinces in China, such as Fujian, Anhui, Zhejiang, Shandong, Guangdong, Tianjin, and Liaoning province. For each beetle, the thorax tissues were cut into two equal parts. One-half was used to isolate and observe nematodes by microscope, and the other half was used to extract DNA for detection, which was described as Meng et al. (2018).

### Genomic DNA Extraction

Genomic DNA was extracted from the nematode and beetle tissues as described by Meng et al. (2018) with some modifications. Single nematode was isolated from the culture medium, and transferred to a 200- $\mu$ l Eppendorf tube. After adding 10  $\mu$ l TE buffer, the tube was maintained in liquid nitrogen for 1 min and then incubated at 85°C for 1 min. This freeze–thaw treatment was performed three times. The supernatant was collected as the template nematode DNA sample. Beetle thorax tissues (0.2 g) were washed in sterilized water, centrifuged to remove as much water as possible, and then transferred to a 2-ml Eppendorf tube. After adding 200  $\mu$ l TE buffer, the tube was placed in a grinder operated at 60 Hz for 5 min. After a centrifugation at 10,000 g for 1 min, the beetle samples were maintained in liquid nitrogen for 1 min and then incubated at 85°C for 1 min. This freeze–thaw treatment was performed three times, after which the samples were centrifuged at 10,000 g for 1 min. The supernatant was transferred to a 1.5-ml Eppendorf tube, and the freeze–thaw treatment and centrifugation were repeated. The supernatant was collected as the template beetle DNA sample.

### DNA Oligonucleotides

The PCR and LAMP primers designed and used in this study (Table 1) targeted *B. xylophilus* genes (*Bx-tlp-1*, *Bx-tlp-2*, and *Bx-cpi*) encoding previously identified potential molecular mimicry proteins (Meng et al., 2020). The PCR primers were designed using Primer 6.0. The six LAMP primers were designed using an online LAMP primer design program<sup>1</sup> according to previously described criteria (Notomi et al., 2000). The primer set comprised two outer primers (F3 and B3), one forward inner primer (FIP), one reverse inner primer (BIP), and two loop primers (Loop F and Loop B). These primers, which anneal specifically to six distinct regions of the target DNA sequence, were synthesized by the Beijing Genomics Institute (Beijing, China). In addition, the LAMP primers targeting *syg-2* designed by Meng et al. (2018) are provided in the Supplementary Material (Supplementary Table S1).

**TABLE 1.** Sequences of the primers used to detect nematode and beetle DNA.

Test	Target	Primer name	Oligonucleotide sequence
PCR	<i>Bx-tlp-1</i>	tlp1-F	TGTGGCTGACACTTATGG
		tlp1-R	AGTCGTCGTTGTAGTTGATA
	<i>Bx-tlp-2</i>	tlp2-F	TCACACTGCCGAGTTCTCCTTC
		tlp2-R	TCCGTGAGTCTGCTATTGTCCTCC
	<i>Bx-cpi</i>	cpi-F	CACGGCAAGTGTCTAGGTGGATT
		cpi-R	TGAGCAGCGACAACTTGATGGAA
	<i>Bx-tlp-1</i>	tlp1F3	GCTGACACTTATGGTGGATAT
		tlp1B3	CCTCCGTGCTTGATCG
		tlp1FIP	AGTTGATAGTGAACTTGCTTAGCG+ ATCGGATGTGCTATTGCC
		tlp1BIP	CGACGACTTCGTAGACACTTATGA A+CGCTGGTACAAGTCAAGTT
		tlp1LoopF	ACCGAGTGTGGTTCTTGAA
	<i>Bx-tlp-2</i>	tlp1LoopB	CAACGGCTATGACACTCCA
		tlp2F3	TGTGAAGCCTATACACTCCT
		tlp2B3	TCAGCAGAAGTACAAGTCG
		tlp2FIP	CCGCTCATAGCATCGTAAGTT+AAT GATTACTATGACTTGAGCGT
LAMP	<i>Bx-tlp-2</i>	tlp2BIP	CGGATGCCTACCAGTATCC+GTGC CTCCAGTTCTCAC
		tlp2LoopF	CTGAAGACCGAAGCGTCAT
		tlp2LoopB	CGGAGACAATAGCAAGACTCA
	<i>Bx-cpi</i>	cpiF3	TCCTTGTGGAGCCAA
		cpiB3	GCTTGACGATTCGGTGA
		cpiFIP	TTGAGCAGCGAGCACTTGAT+CAA GAAGGCTGTCCACATT
		cpiBIP	TGGTGAGAACTACGCCATCG+TCA TGCAACTGGATTACTTCTT
		cpiLoopF	CTGATGGCTTGCTTCGC
		cpiLoopB	CGTAATTGAGTCCGAATGTTACAA

## PCR and LAMP

The PCR mixture (25  $\mu$ l) consisted of the following: PrimeSTAR HS DNA (Premix; TaKaRa, Japan), 12.5  $\mu$ l; forward and reverse primers, 1  $\mu$ l each; DNA template, 1  $\mu$ l; and ddH<sub>2</sub>O, 9.5  $\mu$ l. The PCR program was as follows: 94°C for 3 min; 35 cycles of 94°C for 30 s, 55°C for 30 s, and 72°C for 1

min; 72°C for 10 min. The amplified products were analyzed by agarose gel electrophoresis.

The LAMP mixture (25  $\mu$ l) comprised the following: primers F3 and B3, 5 pmol each; primers FIP and BIP, 40 pmol each; primers Loop F and Loop B, 20 pmol each; 2  $\times$  Reaction Mix (Eiken Chemical, Japan), 12.5  $\mu$ l; and DNA template, 1  $\mu$ l. Samples were incubated at 63°C for 60 min and then at 85°C for 3 min to terminate the reaction. A positive control (purified *B. xylophilus* DNA) and a negative control (distilled water) were included in each run. The LAMP amplicons were detected by fluorescence using LightCycler 480 II system (Roche Diagnostics Ltd., Switzerland) or by a color change in the reaction mixture under natural light.

### **Analysis of PCR and LAMP Assay Specificity and Sensitivity**

To evaluate the specificity of the PCR and LAMP primer sets, the assays were performed using *M. alternatus* and *M. saltuarius* genomics DNA as well as the genomic DNA extracted from the following nematode, plant, and fungal species: *B. xylophilus*, *B. mucronatus*, *Bursaphelenchus fraudulentus*, *Bursaphelenchus conicaudatus*, *Bursaphelenchus corneolus*, *Bursaphelenchus firmae*, *Bursaphelenchus luxuriosae*, *Bursaphelenchus sexdentati*, *Aphelenchoides* sp., *Meloidogyne incongnita*, *Caenorhabditis elegans*, *Pinus thunbergii*, *Pinus massoniana*, *Helianthus annuus*, *Oryza brachyantha*, *Beauveria bassiana*, *Pochonia chlamydosporia*, *Penicillium griseofulvum*, *Paecilomyces lilacinus*, *Fusarium oxysporum* Schltl, *B. cinerea*, and *Pestalotia diospyri* (Kikuchi et al., 2009; Ye and Giblin-Davis, 2013; Meng et al., 2020). At least three replicates were analyzed for each assay.

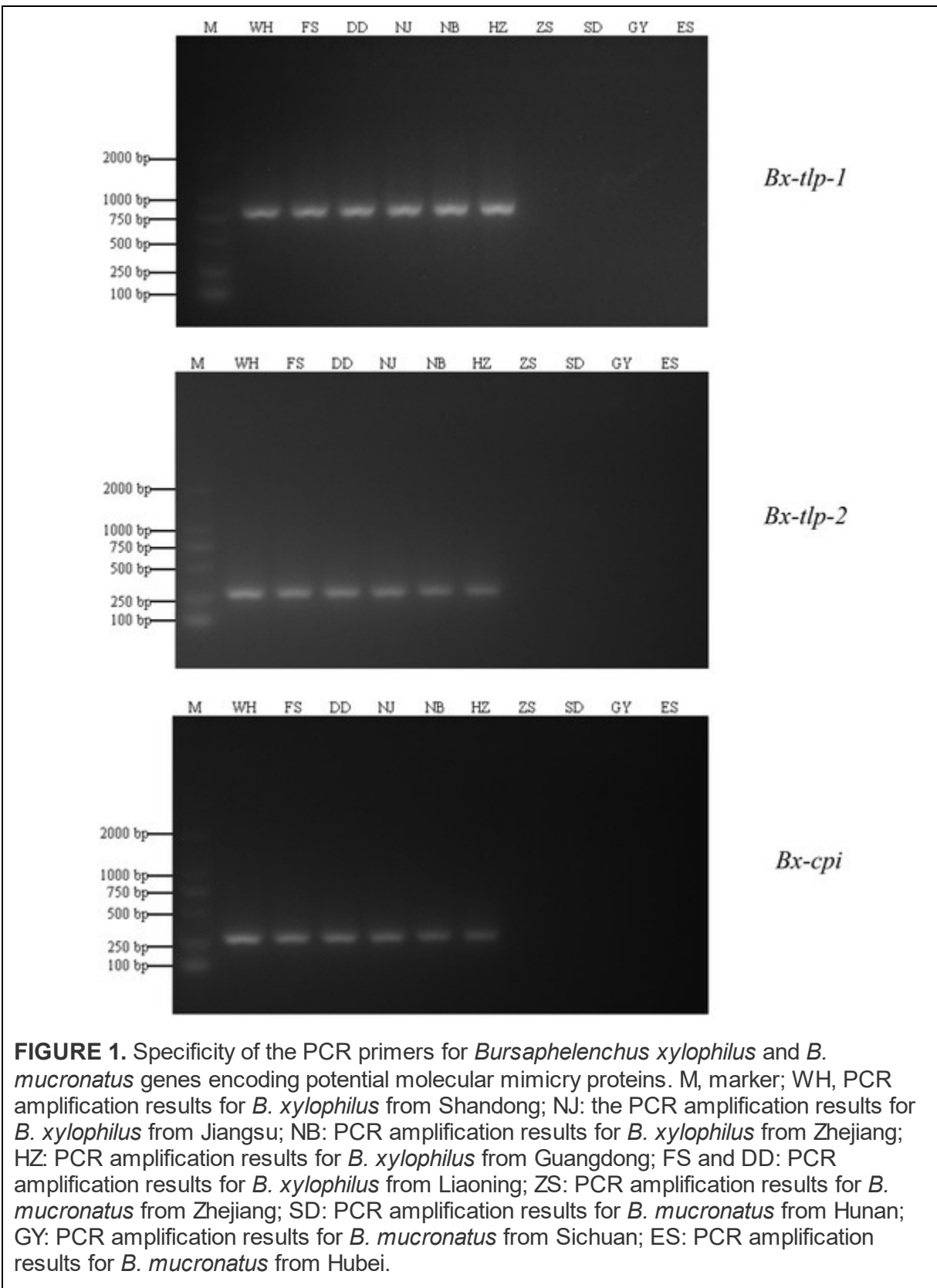
The sensitivity for the PCR and LAMP primer sets (i.e., minimal number of copies that could be detected) was assessed by performing the assays using a range of copy numbers ( $10^6$  to  $10^1$ ) per reaction.

## **RESULTS**

### **PCR Detection of the Target Genes**

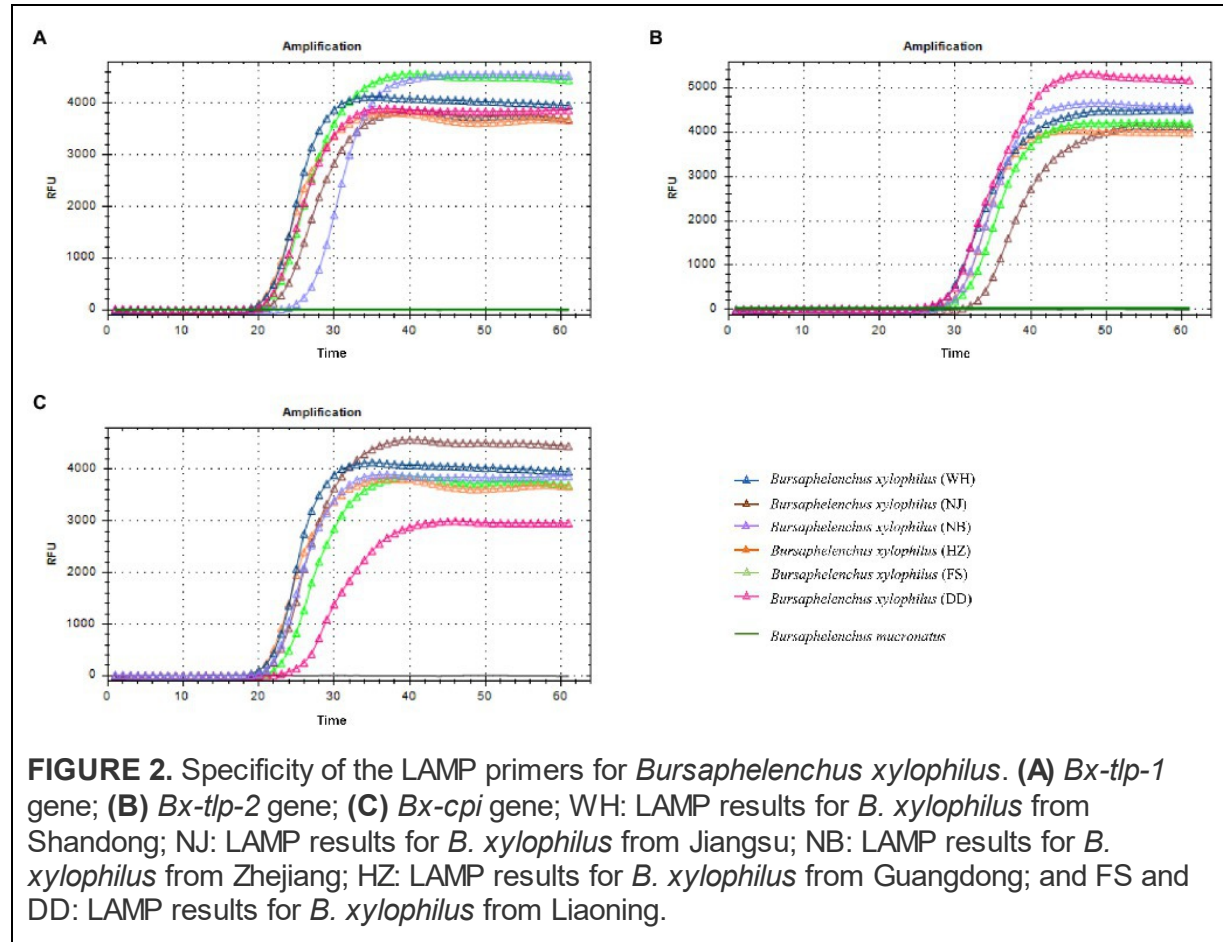
Fragments of the *B. xylophilus* genes encoding potential molecular mimicry proteins (*Bx-tlp-1*, *Bx-tlp-2*, and *Bx-cpi*) were amplified by PCR. The

amplified *Bx-tlp-1*, *Bx-tlp-2*, and *Bx-cpi* fragments were 755, 241, and 202 bp, respectively (Figure 1). The sequences of these fragments are provided in the Supplementary Material (Supplementary Figures S1–S3).



## LAMP Detection of the Target Genes

Amplified products are detectable in a LAMP assay within 60 min. In this study, the *Bx-tlp-1* and *Bx-cpi* LAMP amplicons were detectable within 20 min (Figures 2A,C), whereas the *Bx-tlp-2* LAMP amplicon was detectable within 30 min (Figure 2B).



## Specificity of the PCR and LAMP Primers for *Bursaphelenchus xylophilus*

Amplified products were obtained for the PCR analysis of genomic DNA extracted from the *B. xylophilus* isolates from Shandong, Jiangsu, Zhejiang, Guangdong, and Liaoning provinces. In contrast, PCR products were not generated for the other nematodes, plants, and fungi or for the negative control (i.e., no template). Accordingly, the PCR primers designed to target *Bx-tlp-1*, *Bx-tlp-2*, and *Bx-cpi* were specific for *B. xylophilus*. The LAMP primers targeting *syg-2* designed by Meng et al. (2018) were unable to

produce detectable amplicons within 20 min for the *B. xylophilus* isolates from Liaoning province (FS and DD; Table 2). However, *Bx-tlp-1* and *Bx-cpi* LAMP amplicons were detectable within 20 min for all *B. xylophilus* isolates, suggesting the targeted *Bx-tlp-1* and *Bx-cpi* sequences may be specific to *B. xylophilus* (Supplementary Table S2; Supplementary Figure S4).

**TABLE 2.** Specificity of the PCR and Loop-Mediated Isothermal Amplification (LAMP) assays for *Bursaphelenchus xylophilus*.

Code	Geographical origin	syg-2 (Meng et al., 2018)	Bx-tlp-1			Bx-tlp-2			Bx-cpi		
			PCR			LAMP			PCR		
			20 min	60 min	90 min	20 min	60 min	90 min	20 min	60 min	90 min
<i>Bursaphelenchus xylophilus</i>	WH	Shandong	+	+	+	+	+	+	-	+	+
<i>B. xylophilus</i>	NJ	Jiangsu	+	+	+	+	+	+	-	+	+
<i>B. xylophilus</i>	NB	Zhejiang	+	+	+	+	+	+	-	+	+
<i>B. xylophilus</i>	HZ	Guangdong	+	+	+	+	+	+	-	+	+
<i>B. xylophilus</i>	FS	Liaoning	+	-	+	+	+	+	-	+	+
<i>B. xylophilus</i>	DD	Liaoning	+	-	+	+	+	+	-	+	+
<i>Bursaphelenchus mucronatus</i>	ZS	Zhejiang	-	-	-	-	-	-	-	-	-
<i>B. mucronatus</i>	SD	Hunan	-	-	-	-	-	-	-	-	-
<i>B. mucronatus</i>	GY	Sichuan	-	-	-	-	-	-	-	-	-
<i>B. mucronatus</i>	ES	Hubei	-	-	-	-	-	-	-	-	-
<i>Bursaphelenchus fraudulentus</i>	BF	China	-	-	-	-	-	-	-	-	-
<i>Bursaphelenchus conicaudatus</i>	BC	China	-	-	-	-	-	-	-	-	-
<i>Bursaphelenchus corneolus</i>	BC2	China	-	-	-	-	-	-	-	-	-
<i>Bursaphelenchus firmae</i>	BF2	China	-	-	-	-	-	-	-	-	-
<i>Bursaphelenchus luxuriosae</i>	BL	China	-	-	-	-	-	-	-	-	-
<i>Bursaphelenchus sexdentata</i>	BS	China	-	-	-	-	-	-	-	-	-
<i>Aphelenchoides</i> sp.	ASP	China	-	-	-	-	-	-	-	-	-
<i>Meloidogyne incongrita</i>	MC	Beijing	-	-	-	-	-	-	-	-	-
<i>Caenorhabditis elegans</i>	CE	China	-	-	-	-	-	-	-	-	-
<i>Monochamus alternatus</i>	FZ	Fujian	-	-	-	-	-	-	-	-	-
<i>M. alternatus</i>	CZ	Anhui	-	-	-	-	-	-	-	-	-
<i>M. alternatus</i>	HZ	Zhejiang	-	-	-	-	-	-	-	-	-
<i>M. alternatus</i>	WD	Shandong	-	-	-	-	-	-	-	-	-
<i>M. alternatus</i>	HD	Guangdong	-	-	-	-	-	-	-	-	-
<i>Monochamus saltuarius</i>	FC	Liaoning	-	-	-	-	-	-	-	-	-
<i>M. saltuarius</i>	NZ	Liaoning	-	-	-	-	-	-	-	-	-
<i>M. saltuarius</i>	SM	Liaoning	-	-	-	-	-	-	-	-	-
<i>M. saltuarius</i>	YP	Liaoning	-	-	-	-	-	-	-	-	-
<i>M. saltuarius</i>	TJ	Tianjin	-	-	-	-	-	-	-	-	-
<i>Pinus thunbergii</i>	PT	Shandong	-	-	-	-	-	-	-	-	-
<i>Pinus masoniana</i>	PM	Zhejiang	-	-	-	-	-	-	-	-	-
<i>Helianthus annuus</i>	HA	Beijing	-	-	-	-	-	-	-	-	-
<i>Oryza brachyantha</i>	OB	China	-	-	-	-	-	-	-	-	-
<i>Beauveria bassiana</i>	BB	China	-	-	-	-	-	-	-	-	-
<i>Pochonia chlamydosporia</i>	PC	China	-	-	-	-	-	-	-	-	-
<i>Penicillium griseofulvum</i>	PG	China	-	-	-	-	-	-	-	-	-
<i>Paecilomyces lilacinus</i>	PL	China	-	-	-	-	-	-	-	-	-
<i>Oxysporum schitdzi</i>	OS	China	-	-	-	-	-	-	-	-	-
<i>Botrytis cinerea</i>	BC	China	-	-	-	-	-	-	-	-	-
<i>Pestalotiopsis diospyri</i>	PD	China	-	-	-	-	-	-	-	-	-

+, amplified product; -, no amplified product.

## Sensitivity of the PCR and LAMP Assays

On the basis of a comparative analysis of the sensitivities of the two assays, we concluded that the detection limit of the fluorochrome dye used in the LAMP assay was 10 pg for the two positive results (i.e., for *Bx-tlp-1* and *Bx-cpi*), whereas the detection limit of the PCR assay for the same genes was 10 ng (Table 3). The LAMP primers used in this study to target the genes encoding potential molecular mimicry proteins were more sensitive than the

primers designed by Meng et al. (2018), which were also associated with *B. xylophilus* pathogenicity.

**TABLE 3.** Comparison of the LAMP and PCR assay sensitivities.

Target genes	Test	Concentration of genomic DNA of <i>Bursaphelenchus xylophilus</i> after dilution					
		10 <sup>-1</sup>	10 <sup>-2</sup>	10 <sup>-3</sup>	10 <sup>-4</sup>	10 <sup>-5</sup>	10 <sup>-6</sup>
		10ng	1ng	100 pg	10 pg	1 pg	100 fg
<i>Bx-tlp-1</i>	LAMP	+	+	+	+	–	–
	PCR	+	–	–	–	–	–
<i>Bx-tlp-2</i>	LAMP	+	+	+	–	–	–
	PCR	+	–	–	–	–	–
<i>Bx-cpi</i>	LAMP	+	+	+	+	–	–
	PCR	+	–	–	–	–	–

+, amplified product; –, no amplified product.

### Utility of the PCR and LAMP Assays for Detecting *Bursaphelenchus xylophilus* From *Monochamus alternatus* or *Monochamus saltuarius*

The results of the PCR amplification conducted to detect *B. xylophilus* from *M. alternatus* or *M. saltuarius* collected from 10 regions in China are presented in Figure 3. Additionally, the LAMP assay results are presented as an amplification curve visualized using the fluorochrome dye. The results indicated that the primers targeting *Bx-tlp-1* and *Bx-cpi* were able to detect the genomic DNA of *B. xylophilus* from *M. alternatus* or *M. saltuarius* within 40 min, whereas the primers targeting *Bx-tlp-2* detected *B. xylophilus* genomic DNA within 50 min (Figure 4). The primers targeting *syg-2* (Meng et al., 2018) detected the genomic DNA of *B. xylophilus* from *M. saltuarius* within 50 min (Table 4). Hence, the primers designed for the genes encoding potential molecular mimicry proteins (*Bx-tlp-1*, *Bx-tlp-2*, and *Bx-cpi*) may be more sensitive than the primers targeting *syg-2*.

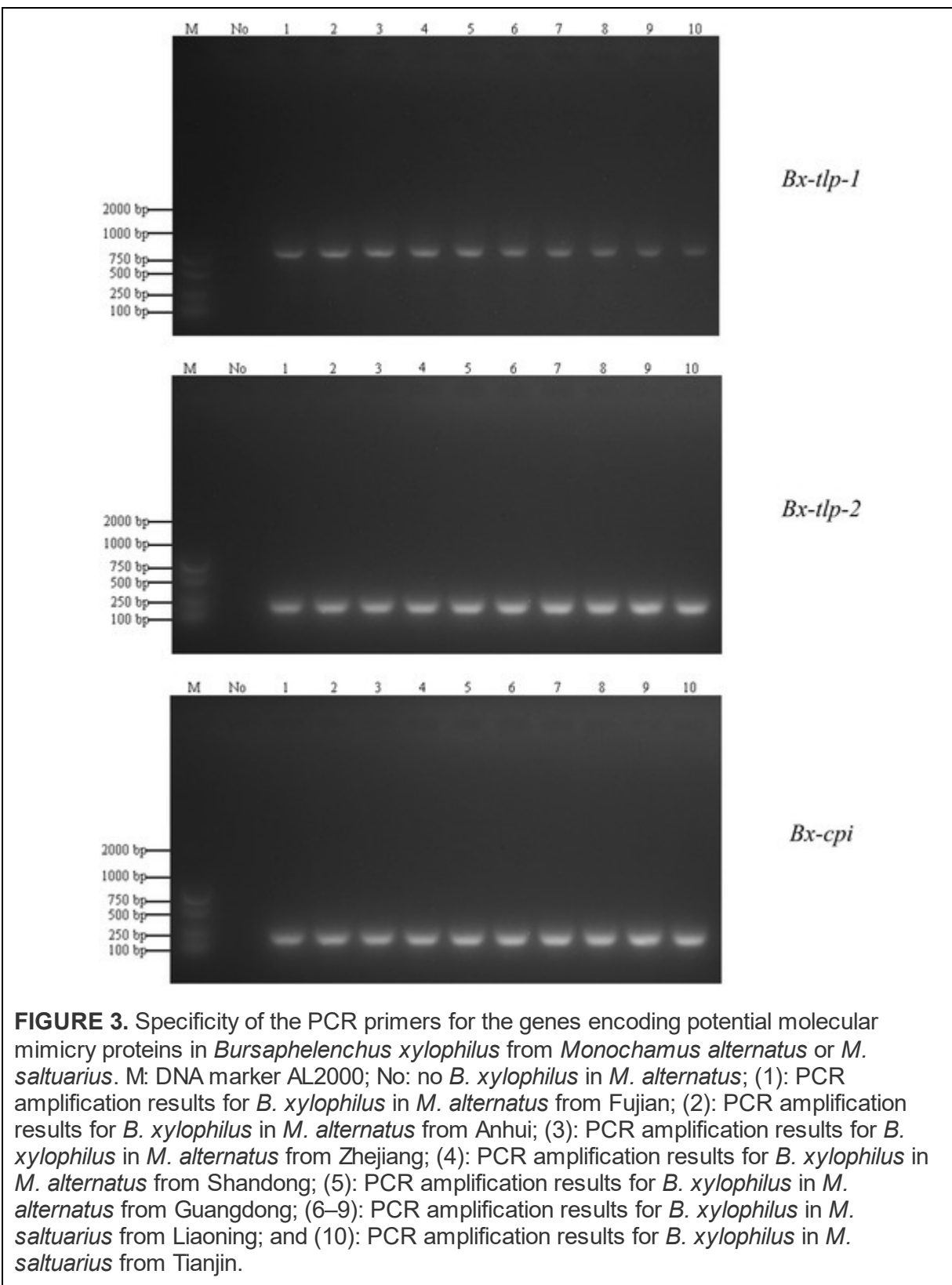


**FIGURE 3.** Specificity of the PCR primers for the genes encoding potential molecular mimicry proteins in *Bursaphelenchus xylophilus* from *Monochamus alternatus* or *M. saltuarius*. M: DNA marker AL2000; No: no *B. xylophilus* in *M. alternatus*; (1): PCR amplification results for *B. xylophilus* in *M. alternatus* from Fujian; (2): PCR amplification results for *B. xylophilus* in *M. alternatus* from Anhui; (3): PCR amplification results for *B. xylophilus* in *M. alternatus* from Zhejiang; (4): PCR amplification results for *B. xylophilus* in *M. alternatus* from Shandong; (5): PCR amplification results for *B. xylophilus* in *M. alternatus* from Guangdong; (6–9): PCR amplification results for *B. xylophilus* in *M. saltuarius* from Liaoning; and (10): PCR amplification results for *B. xylophilus* in *M. saltuarius* from Tianjin.

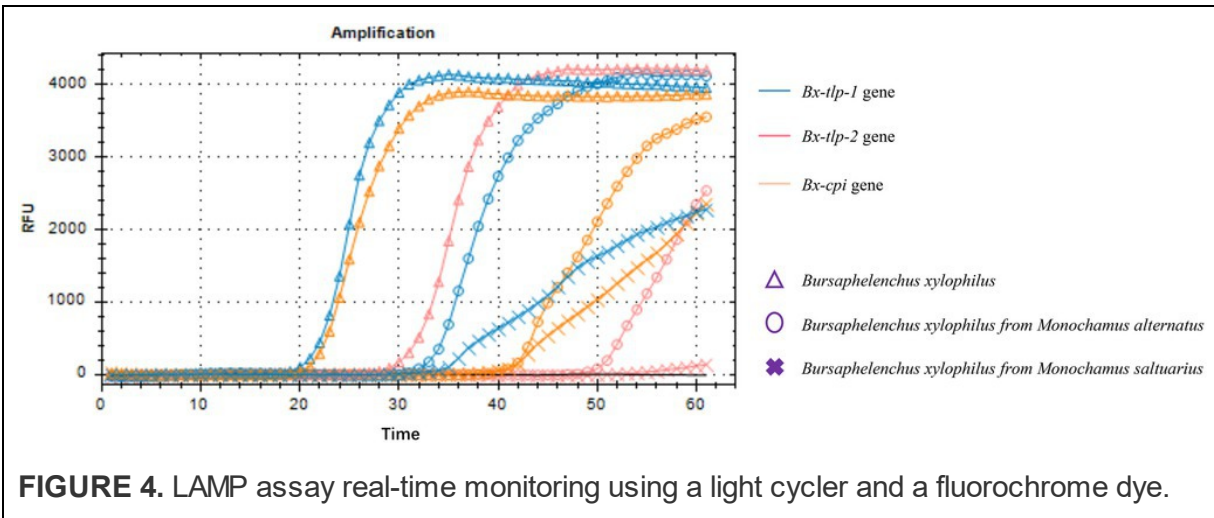


**FIGURE 4.** LAMP assay real-time monitoring using a light cycler and a fluorochrome dye.

**TABLE 4.** LAMP-based detection of *Bursaphelenchus xylophilus* from *Monochamus alternatus* or *M. saltuarius*. +, LAMP amplicon detected; -, LAMP amplicon not detected.

Code	Vectors	Host	Geographical origin	syg-2 (Meng et al., 2018)				Bx-tlp-1			Bx-tlp-2			Bx-cpi		
				30 min	40 min	50 min	30 min	40 min	50 min	30 min	40 min	50 min	30 min	40 min	50 min	
1	<i>Monochamus alternatus</i>	<i>Pinus massoniana</i>	Fujian	-	+	+	+	+	+	-	-	+	-	+	+	
2	<i>M. alternatus</i>	<i>P. massoniana</i>	Anhui	-	+	+	+	+	+	-	-	+	-	+	+	
3	<i>M. alternatus</i>	<i>P. massoniana</i>	Zhejiang	-	+	+	+	+	+	-	-	+	-	+	+	
4	<i>M. alternatus</i>	<i>P. massoniana</i>	Guangdong	-	+	+	+	+	+	-	-	+	-	+	+	
5	<i>M. alternatus</i>	<i>P. thunbergii</i>	Shandong	-	+	+	+	+	+	-	-	+	-	+	+	
6	<i>M. saltuarius</i>	<i>P. koraiensis</i>	Liaoning	-	-	+	+	+	+	-	-	+	-	+	+	
7	<i>M. saltuarius</i>	<i>P. tabuliformis</i>	Liaoning	-	-	+	+	+	+	-	-	+	-	+	+	
8	<i>M. saltuarius</i>	<i>P. tabuliformis</i>	Liaoning	-	-	+	+	+	+	-	-	+	-	+	+	
9	<i>M. saltuarius</i>	<i>P. tabuliformis</i>	Liaoning	-	-	+	+	+	+	-	-	+	-	+	+	
10	<i>M. saltuarius</i>	<i>P. tabuliformis</i>	Tianjin	-	-	+	+	+	+	-	-	+	-	+	+	

## DISCUSSION

The causative agent of PWD, *B. xylophilus*, is a prevalent organism carried by beetles (i.e., *M. alternatus* or *M. saltuarius*). Therefore, the numbers of beetles (*M. alternatus* or *M. saltuarius*) in a pine forest is a crucial indicator of the possibility of a PWD outbreak. Unless *B. xylophilus* from *M. alternatus* or *M. saltuarius* is specifically treated in the primary phase, the resulting PWD will often lead to tree death. The efficient and rapid detection of *B. xylophilus* from *M. alternatus* or *M. saltuarius* is necessary for preventing outbreaks *via* the implementation of specific treatments (Wang et al., 2009; Cardoso et al., 2012). Because death by PWD is very rapid, a novel method for detecting PWD must produce results quickly.

Proteins secreted by pathogens that are structurally or functionally similar to host defense-related proteins are called molecular mimicry proteins. Researchers identified substances released by pathogens that mimic plant defense-related compounds and disrupt physiologically important plant signaling pathways (Winn et al., 2021). Previous studies revealed the relatively high similarity between the Bx-TLP (Bx-CPI) and Pm-TLP (Pm-CPI) sequences, indicative of a similarity in their functions (Wang et al., 2014; Meng et al., 2017, 2020, 2022). Moreover, the expression of *B. xylophilus* genes encoding potential molecular mimicry proteins (*Bx-tlp-1*, *Bx-tlp-2*, and *Bx-cpi*) is responsive to  $\alpha$ -pinene, which may affect terpene metabolism in pine trees and influence the pathogenicity of *B. xylophilus* (Meng et al., 2019, 2020, 2022).

In the present study, we designed specific primer sets targeting *Bx-tlp-1*, *Bx-tlp-2*, and *Bx-cpi* for the rapid detection of *B. xylophilus* and *M. alternatus* or *M. saltuarius* carrying *B. xylophilus*. The PCR and LAMP assays specifically detected all *B. xylophilus* isolates, with no amplification for all other examined species. The high specificity of the LAMP assay was conferred by the six primers targeting six regions of the *Bx-tlp-1* and *Bx-cpi* sequences, which were specific to *B. xylophilus*. The specificity of the LAMP primers used in this work was significantly better than that reported by Kikuchi et al. (2009; Supplementary Table S2), who detected *B. mucronatus* and *B. fraudulentus* in 90 min. On the other hand, there were no amplified products in other *Bursaphelenchus* group species, such as *B. firmae*, *B. luxuriosae*, and *B. sexdentati*. Meanwhile, the average concentration of genomic DNA from a single *B. xylophilus* was about 32 ng/ $\mu$ l (the volume was 10  $\mu$ l), and the lower limits of detection for the LAMP and PCR assays were 10 pg and 10 ng genomic DNA, respectively. Moreover, LAMP primers targeting *Bx-tlp-1* or *Bx-cpi* were 5-fold more sensitive than the LAMP primers targeting *syg-2* (51.4 pg; Meng et al., 2018) and were able to rapidly detect *B. xylophilus* from *M. alternatus* or *M. saltuarius*. Thus, the key genes associated with *B. xylophilus* pathogenicity may be excellent targets for the rapid detection of the nematode because they may also be related to the fitness of the hosts, insects, and environment.

Considering the high sensitivity of the LAMP assay, the post-amplification procedures should be performed in a separate room (i.e., away from the PCR and LAMP reagents) to minimize the possibility of contamination (Kikuchi et al., 2009; Zhu et al., 2009; Meng et al., 2018). The

LAMP assay requires only a regular water bath or a heat block that maintains the temperature at 63°C. Therefore, it is more cost-effective than a conventional PCR assay. Moreover, the two additional loop primers increase the speed and specificity of the amplification, resulting in faster reactions (relative to a conventional PCR). Additionally, the key genes associated with pathogenicity (e.g., those encoding potential molecular mimicry proteins) can be used as the specific targets for detection, which may be significant for preventing or controlling disease outbreaks. Our LAMP-based method detected *B. xylophilus* *Bx-tlp-1* within 20 min and *B. xylophilus* from *M. alternatus* or *M. saltuarius* within 30 min. These results are better than the LAMP assay results obtained by Meng et al. (2018) who detected the *B. xylophilus* target gene within 25 min and *B. xylophilus* from *M. alternatus* within 50 min. Furthermore, in contrast to a conventional PCR assay, the LAMP assay enables the detection of a positive amplification by the naked eye. The reactions and results can be interpreted simply by observing the color change in the reaction mixture. In addition to eliminating the need for the time-consuming electrophoretic analysis, LAMP assays can be performed without the sophisticated equipment needed for PCR (Kang et al., 2009; Huang et al., 2010; Hu et al., 2011; Kanetani et al., 2011; Meng et al., 2018).

In conclusion, *M. alternatus* is the main insect vector for *B. xylophilus*. The number of nematodes in *M. alternatus* is an important factor related to the distribution of *B. xylophilus*. Therefore, the fast and efficient detection of *M. alternatus* carrying *B. xylophilus* is necessary for the monitoring and early detection of PWD (Kikuchi et al., 2009; Hu et al., 2011; Cardoso et al., 2012; Meng et al., 2018). In this study, we designed PCR and LAMP primers specific for the *B. xylophilus* genes encoding potential molecular mimicry proteins (*Bx-tlp-1*, *Bx-tlp-2*, and *Bx-cpi*). The specific amplified fragments for *Bx-tlp-1*, *Bx-tlp-2*, and *Bx-cpi* were 755, 241, and 202 bp, respectively. However, no specific amplification products were detected for the other analyzed nematodes (e.g., *B. mucronatus*). These findings indicate that *Bx-tlp-1*, *Bx-tlp-2*, and *Bx-cpi* can be used to specifically detect *B. xylophilus* as well as *M. alternatus* or *M. saltuarius* carrying *B. xylophilus*. Furthermore, designing primers specific for *B. xylophilus* following an in-depth analysis of the functions of key pathogenicity genes may have important implications for future attempts at developing reliable methods for the early diagnosis and prevention of PWD.

## DATA AVAILABILITY STATEMENT

The datasets presented in this study can be found in online repositories. The names of the repository/repositories and accession number(s) can be found in the article/Supplementary Material.

## AUTHOR CONTRIBUTIONS

FM, YL, and XZ: experimental design. FM and ZL: experimental implementation. ZL: material contribution. FM: data analysis and manuscript writing. All authors contributed to the article and approved the submitted version.

## FUNDING

The present research was funded by the Fundamental Research Funds for the Central Universities (2021ZY03) and China Postdoctoral Science Foundation (2020M680410).

## SUPPLEMENTARY MATERIAL

The Supplementary Material for this article can be found online at: <https://www.frontiersin.org/articles/10.3389/fpls.2022.890949/full#supplementary-material>

## FOOTNOTES

<sup>1</sup><http://primerexplorer.jp/e/>

## REFERENCES

Cardoso, J. M. S., Fonseca, L., and Abrantes, I. (2012). Direct molecular detection of the pine wood nematode, *Bursaphelenchus xylophilus*, from pine wood, bark and insect vector. *Eur. J. Plant Pathol.* 133, 419–425. doi: 10.1007/s10658-011-9915-y

Cheng, H., Lin, M., Li, W., and Fang, Z. (1983). The occurrence of a pine wilting disease caused by a nematode found in Nanjing. *Forest Pest Dis.* 4, 1–5.

Futai, K. (2013). Pine wood nematode, *Bursaphelenchus xylophilus*. *Annu. Rev. Phytopathol.* 51, 61–83. doi: 10.1146/annurev-phyto-081211-172910

Hu, Y. Q., Kong, X. C., Wang, X. R., Zhong, T. K., Zhu, X. W., Mota, M. M., et al. (2011). Direct PCR-based method for detecting *Bursaphelenchus xylophilus*, the pine wood nematode in wood tissue of *Pinus massoniana*. *Forest Pathol.* 41, 165–168. doi: 10.1111/j.1439-0329.2010.00692.x

Huang, L., Ye, J. R., Wu, X. Q., Xu, X. L., Sheng, J. M., and Zhou, Q. X. (2010). Detection of the pine wood nematode using a real-time PCR assay to target the DNA topoisomerase I gene. *Eur. J. Plant Pathol.* 127, 89–98. doi: 10.1007/s10658-009-9574-4

Jones, J. T., Moens, M., Mota, M., Li, H. M., and Kikuchi, T. (2008). *Bursaphelenchus xylophilus*: opportunities in comparative genomics and molecular host-parasite interactions. *Mol. Plant Pathol.* 9, 357–368. doi: 10.1111/j.1364-3703.2007.00461.x

Kanetani, S., Kikuchi, T., Akiba, M., Nakamura, K., Ikegame, H., and Tetsuka, K. (2011). Detection of *Bursaphelenchus xylophilus* from old discs of dead *Pinus armandii* var. *amamiana* trees using a new detection kit. *Forest Pathol.* 41, 387–391. doi: 10.1111/j.1439-0329.2010.00695.x

Kang, J. S., Moon, I. S., Lee, S. G., Shin, S. C., and Lee, S. H. (2009). Rapid and accurate prediction of the frequencies of *Bursaphelenchus xylophilus* and *B. mucronatus* in mixed nematode samples using real-time species-specific PCR. *Nematology* 11, 289–299. doi: 10.1163/156854109X429619

Kanzaki, N., and Giblin-Davis, R. M. (2018). Diversity and plant pathogenicity of *Bursaphelenchus* and related nematodes in relation to their vector bionomics. *Curr. Forest. Rep.* 4, 85–100. doi: 10.1007/s40725-018-0074-7

Kikuchi, T., Aikawa, T., Oeda, Y., Karim, N., and Kanzaki, N. (2009). A rapid and precise diagnostic method for detecting the pinewood nematode *Bursaphelenchus xylophilus* by loop-mediated isothermal amplification. *Phytopathology* 99, 1365–1369. doi: 10.1094/PHYTO-99-12-1365

Kirino, H., Yoshimoto, K., and Shinya, R. (2020). Thaumatin-like proteins and a cysteine protease inhibitor secreted by the pine wood nematode *Bursaphelenchus xylophilus* induce cell death in *Nicotiana benthamiana*. *PLoS One* 15:e0241613. doi: 10.1371/journal.pone.0241613

Mamiya, Y., and Enda, N. (1972). Transmission of *Bursaphelenchus lignicolus* (Nematoda: Aphelenchoididae) by *Monochamus alternatus* (Coleoptera: Cerambycidae). *Nematologica* 18, 159–162. doi: 10.1163/187529272X00395

Meng, F. L., Li, Y. X., Liu, Z. K., Feng, Y. Q., Wang, X., and Zhang, X. Y. (2022). Expression of the thaumatin-like protein-1 gene (*Bx-tlp-1*) from pine wood nematode *Bursaphelenchus xylophilus* affects terpene metabolism in pine trees. *Phytopathology* 112, 888–897. doi: 10.1094/PHYTO-07-21-0289-R

Meng, F. L., Li, Y. X., Liu, Z. K., Wang, X., Feng, Y. Q., Wei, Z., et al. (2020). Potential molecular mimicry proteins responsive to  $\alpha$ -pinene in *Bursaphelenchus xylophilus*. *Int. J. Mol. Sci.* 21:982. doi: 10.3390/ijms21030982

Meng, F. L., Li, Y. X., Wang, X., Feng, Y. Q., Liu, Z. K., Zhang, W., et al. (2019). Thaumatin-like protein-1 gene (*Bx-tlp-1*) is associated with the pathogenicity of *Bursaphelenchus xylophilus*. *Phytopathology* 109, 1949–1956. doi: 10.1094/PHYTO-03-19-0082-R

Meng, F. L., Wang, X. Z., Wang, L. F., Gou, D. P., Liu, H. J., Wang, Y. N., et al. (2018). A loop-mediated isothermal amplification-based method for detecting *Bursaphelenchus xylophilus* from

*Monochamus alternatus*. *For. Pathol.* 48:e12404. doi: 10.1111/efp.12404

Meng, F. L., Wang, J., Wang, X., Li, Y. X., and Zhang, X. Y. (2017). Expression analysis of thaumatin-like proteins from *Bursaphelenchus xylophilus* and *Pinus massoniana*. *Physiol. Mol. Plant Pathol.* 100, 178–184. doi: 10.1016/j.pmpp.2017.10.002

Mota, M. M., Braasch, H., Bravo, M. A., Penas, A. C., Burgermeister, W., Metge, K., et al. (1999). First report of *Bursaphelenchus xylophilus* in Portugal and in Europe. *Nematology* 1, 727–734. doi: 10.1163/156854199508757

Nickle, W. R., Golden, A. M., Mamiya, Y., and Wergin, W. P. (1981). On the taxonomy and morphology of the pine wood nematode, *Bursaphelenchus xylophilus* (Steiner & Buhrer 1934) Nickle 1970. *J. Nematol.* 13, 385–392.

Notomi, T., Okayama, H., Masubuchi, H., Yonekawa, T., Watanabe, K., Amino, N., et al. (2000). Loop-mediated isothermal amplification of DNA. *Nucleic Acids Res.* 28:e63. doi: 10.1093/nar/28.12.e63

Ryss, A. Y., and Subbotin, S. A. (2017). Coevolution of wood-inhabiting nematodes of the genus *Bursaphelenchus Fuchs*, 1937 with their insect vectors and plant hosts. *Zh. Obshch. Biol.* 78, 13–42.

Shinya, R., Morisaka, H., and Kikuchi, T. (2013). Secretome analysis of the pine wood nematode *Bursaphelenchus xylophilus* reveals the tangled roots of parasitism and its potential for molecular mimicry. *PLoS One* 8:e67377. doi: 10.1371/journal.pone.0067377

Soliman, T., Mourits, M. C. M., Vanderwerf, W., Hengeveld, G. M., Robinet, C., and Lansink, A. G. J. (2012). Framework for modeling economic impacts of invasive species, applied to pine wood nematode in Europe. *PLoS One* 7:e45505. doi: 10.1371/journal.pone.0045505

Tomita, N., Mori, Y., Kanda, H., and Notomi, T. (2008). Loop-mediated isothermal amplification (LAMP) of gene sequences and simple visual detection of the products. *Nat. Protoc.* 3, 877–882. doi: 10.1038/nprot.2008.57

Wang, J., Han, S., Li, Y., Deng, X., and Zhang, X. Y. (2014). Cloning of TLP-1 gene and prediction of TLP-1 protein structure of *Bursaphelenchus xylophilus*. *J. Sichuan Agri. Univ.* 32, 305–310. doi: 10.3969/j.issn.1000-2650.2014.03.011

Wang, X. R., Zhu, X. W., Hu, Y. Q., Huang, H. H., Kong, X. C., and Jia, W. H. (2009). A PCR-based method for detecting the pine wood nematodes—*Bursaphelenchus xylophilus* from *Monochamus alternatus*. *Sci. Silvae Sin.* 45, 70–75. doi: 10.11707/j.1001-7488.20090712

Winn, M., Rowlinson, M., Wang, F. H., Bering, L., and Micklefield, J. (2021). Discovery, characterization and engineering of ligases for amide synthesis. *Nature* 593, 391–398. doi: 10.1038/s41586-021-03447-w

Ye, W. M., and Giblin-Davis, R. M. (2013). Molecular characterization and development of real-time PCR assay for pine-wood nematode *Bursaphelenchus xylophilus* (Nematoda: parasitaphelenchidae). *PLoS One* 8:e78804. doi: 10.1371/journal.pone.0078804

Zhu, R. Y., Zhang, K. X., Zhao, M. Q., Liu, Y. H., Xu, Y. Y., Ju, C. M., et al. (2009). Use of visual loop-mediated isothermal amplification of rimM sequence for rapid detection of *mycobacterium tuberculosis* and *Mycobacterium bovis*. *J. Microbiol. Methods* 78, 339–343. doi: 10.1016/j.mimet.2009.07.006

**Conflict of Interest:** The authors declare that the research was conducted in the absence of any commercial or financial relationships that could be construed as a potential conflict of interest.

**Publisher's Note:** All claims expressed in this article are solely those of the authors and do not necessarily represent those of their affiliated organizations, or those of the publisher, the editors and the reviewers. Any product that may be evaluated in this article, or claim that may be made by its manufacturer, is not guaranteed or endorsed by the publisher.

*Copyright © 2022 Meng, Liu, Li and Zhang. This is an open-access article distributed under the terms of the Creative Commons Attribution License (CC BY). The use, distribution or reproduction in other forums is permitted, provided the original author(s) and the copyright owner(s) are credited and that the original publication in this journal is cited, in accordance with accepted academic practice. No use, distribution or reproduction is permitted which does not comply with these terms.*

ORIGINAL RESEARCH

published: 20 May 2022

doi: 10.3389/fpls.2022.856841



# Invasion History of the Pinewood Nematode *Bursaphelenchus xylophilus* Influences the Abundance of *Serratia* sp. in Pupal Chambers and Tracheae of Insect-Vector *Monochamus alternatus*

**Haokai Tian<sup>1,2†</sup>, Tuuli-Marjaana Koski<sup>1,2†</sup>, Lilin Zhao<sup>1,2</sup>, Ziying Liu<sup>1,2</sup> and Jianghua Sun<sup>1,3\*</sup>**

<sup>1</sup> State Key Laboratory of Integrated Management of Pest Insects and Rodents, Institute of Zoology, Chinese Academy of Sciences, Beijing, China

<sup>2</sup> CAS Center for Excellence in Biotic Interactions, University of Chinese Academy of Sciences, Beijing, China

<sup>3</sup> College of Life Science, Institute of Life Science and Green Development, Hebei University, Baoding, China

**Edited by:**

Claudia S. L. Vicente, University of Évora, Portugal

**Reviewed by:**

Manuel G. M. Mota, University of Évora, Portugal

Margarida Espada, University of Évora, Portugal

Pablo Castillo, Institute for Sustainable Agriculture (CSIC), Spain

**\*Correspondence:** Jianghua Sun, sunjh@ioz.ac.cn

**†**These authors have contributed equally to this work

**Specialty section:** This article was submitted to Plant Pathogen Interactions, a section of the journal *Frontiers in Plant Science*

**Received:** 17 January 2022

**Accepted:** 30 March 2022

**Published:** 20 May 2022

**Citation:** Tian H, Koski T-M, Zhao L, Liu Z and Sun J (2022) Invasion History of the Pinewood Nematode *Bursaphelenchus xylophilus* Influences the Abundance of *Serratia* sp. in Pupal Chambers and Tracheae of Insect-Vector *Monochamus alternatus*. *Front. Plant Sci.* 13:856841. doi: 10.3389/fpls.2022.856841

Pine wilt disease (PWD) has caused extensive mortality in pine forests worldwide. This disease is a result of a multi-species interaction among an invasive pinewood nematode (PWN) *Bursaphelenchus xylophilus*, its vector *Monochamus* sp. beetle, and the host pine tree (*Pinus* sp.). In other systems, microbes have been shown to attenuate negative impacts on invasive species after the invasion has reached a certain time point. Despite that the role of PWD associated microbes involved in the PWD system has been widely studied, it is not known whether similar antagonistic “hidden microbial players” exist in this system due to the lack of knowledge about the potential temporal changes in the composition of associated microbiota. In this study, we investigated the bacteria-to-fungi ratio and isolated culturable bacterial isolates from pupal chambers and vector beetle tracheae across five sampling sites in China differing in the duration of PWN invasion. We also tested the pathogenicity of two candidate bacteria strains against the PWN-vector beetle complex. A total of 118 bacterial species belonging to 4 phyla, 30 families, and 54 genera were classified based on 16S sequencing. The relative abundance of the genus *Serratia* was lower in pupal chambers and tracheae in newly PWN invaded sites (<10 years) compared to the sites that had been invaded for more than 20 years. *Serratia marcescens* strain AHPC29 was widely distributed across all sites and showed nematicidal activity against PWN. The insecticidal activity of this strain was dependent on the life stage of the vector beetle *Monochamus alternatus*: no insecticidal activity was observed against final-instar larvae, whereas *S. marcescens* was highly virulent against pupae. Our findings improved the understanding of the temporal variation in the microbial community associated with the PWN-vector beetle complex and the progress of PWD and can therefore facilitate the development of biological control agents against PWN and its vector beetle.

**Keywords:** *Serratia marcescens*, pinewood nematode, *Monochamus alternatus*, pathogenicity, bacteria isolation, invasion time

# INTRODUCTION

The pinewood nematode (PWN), *Bursaphelenchus xylophilus* (Steiner and Buhrer) Nickle, is native to North America and is the causal agent of a highly destructive pine wilt disease (PWD). This nematode has become an invasive global quarantine pest and has damaged pine forests in Japan, South Korea, China, and recently also in Portugal and Spain (Mota et al., 1999; Zhao et al., 2014). In China, despite tremendous prevention and control efforts implemented during the past 40 years, PWN has recently spread from its initial southern distribution range to the high-altitude range in the northern part of the country (Zhao et al., 2014; Pan et al., 2020). Compared to many other plant-parasitic nematodes, PWN has a complex life cycle including both intermediate vector (*Monochamus* sp. beetle) and primary (*Pinus* sp.) hosts, to which PWN life stages are tightly connected. Propagative stages (egg to adult) live exclusively within the host pine whereas the dispersal life stages ( $J_{III}$  and  $J_{IV}$ ) are also associated with the vector beetle. Under unfavorable conditions, propagative stages molt to third-stage dispersal juveniles ( $J_{III}$ ) and aggregate around the pupal chamber to wait for beetle pupation. Once the vector beetle has reached the late pupal stage or early adulthood,  $J_{III}$  molts to fourth-stage dispersal juveniles ( $J_{IV}$ ) and enters the vector beetle's tracheae system. After the vector beetles mature and emerge from the PWN invaded trees, they find suitable trees to feed and oviposit and transport  $J_{IV}$  in their tracheae to new pine trees where the nematodes start a new life cycle (Zhao et al., 2013b, 2016). Besides needing to balance the different environmental conditions generated by the host tree and insect vector, PWN also encounters various microbiota in both environments, which may influence their invasion success. For example, bacteria and fungi associated with PWD can influence nematode reproduction and virulence, the population size and prevalence of the PWN-vector beetle complex, the severity of PWD, and the resistance of host pine (Vicente et al., 2012; Zhao et al., 2013a; Nascimento et al., 2015; Alves et al., 2018; Zhang et al., 2020b).

After the successful colonization, the population size of an invasive species usually increases but may eventually start to decline after the invasion has reached a certain time point (Knevel et al., 2004; Nijjer et al., 2007; Diez et al., 2010; Zhao et al., 2019). This decline may be related to the

biological resistance formed by the native biotic and abiotic factors (Mitchell et al., 2010). One of such factors can be an antagonistic microorganism associated with the invasive species. Past studies have shown that the initial dominance of an invasive species can later be reversed by stabilizing processes, which in some cases are mediated by changes in associated microbiota. For example, the biomass accumulation of invasive plants in the invaded habitat can decrease due to an increase in the abundance of local soil pathogens (Nijjer et al., 2007; Diez et al., 2010; Mitchell et al., 2010). In the PWD system, only a few studies have investigated the changes in the microbial community during the progress of PWD, leaving the temporal effects on microbiota composition unknown. However, pupal chambers in sites with a longer duration of PWN invasion significantly harbor fewer nematodes compared to sites with a shorter duration of invasion (data not shown). Because PWN is also in contact with various microbial associates, it is possible that similar to the example from some invasive plants, the increased proportion of antagonistic microorganisms may also explain the lower abundance of PWN in these sites.

Pinewood nematodes and vector beetles are known to be associated with several fungi, many of which are shown to be beneficial for this disease complex. Some fungi such as *Ophiostoma ips*, *Ophiostoma minus*, and *Ceratocystis* sp. act as a nutritional source for the mycophagous phases of PWN (Vicente et al., 2021). Ophiostomatoid fungi (i.e., *Sporothrix* sp. 1), dominating in pupal chambers and vector beetle tracheae, also positively influence the reproduction of PWN and increase the growth and survival rate of its vector beetle (Futai, 2013; Zhao et al., 2013a). Regarding PWN associated bacteria, the genus *Serratia* widely exists across all stages of PWN's life cycle (i.e., both propagative and dispersal stages) and appears to be a close associate of PWN, having increased relative abundance in pines with PWD (Guo et al., 2020; Zhang et al., 2020b). Some *Serratia* species help PWN to survive from high oxidative stress (Vicente et al., 2013), whereas some species of this genus are potentially harmful to PWN while being beneficial to the host plant (Paiva et al., 2013; Akduman et al., 2018; Liu et al., 2019). *Serratia plymuthica* M24T3, for instance, is nematicidal but its presence can improve the tolerance and the growth of its host plant, *Arabidopsis thaliana* (Proenca et al., 2019). Similarly, *Serratia quinivorans* BXF1 is antagonistic to fungi and bacteria but promotes the growth of plant

roots and can also opportunistically colonize the same host pine species together with PWN (Nascimento et al., 2016). Besides being potentially antagonistic to PWN, some *Serratia* species may also be harmful to PWN's vector beetle (*Monochamus* sp.), because bacteria of this genus are conditionally pathogenic to more than 70 species of insects (Grimont and Grimont, 1978). For example, *Serratia marcescens* is lethal if it enters the hemolymph and can successfully evade the immune system of the insect (Raymann et al., 2017, 2018). Interestingly, some vector beetle adults and larvae (e.g., *M. alternatus*, *M. galloprovincialis*, and *M. saltuarius*) that have a phoretic relationship with PWN can also carry genus *Serratia* in their gut microbiota (Vicente et al., 2013; Alves et al., 2016; Guo et al., 2020; Ge et al., 2021) without adverse effects under normal conditions.

So far, no research has focused on PWN associate bacteria-to-fungi ratio or investigated the temporal changes in their abundances as the PWN invasion progresses. Despite the positive effects of the dominating Ophiostomatoid fungal associates, we speculated that bacteria unfavorable to the PWN-vector beetle complex may be the “hidden players” behind the observed lower PWN abundance in areas with a longer duration of PWN invasion. More specifically, we hypothesized that some bacteria (i.e., *Serratia* sp.) pathogenic to PWN and its vector beetle will increase in abundance as the invasion progresses, being more abundant in the sites with a longer duration of PWN invasion. We tested this hypothesis by investigating the microbiota community in pupal chambers and vector beetle tracheae in sites differing in the duration of PWN invasion, as well as using candidate bacterial isolates from these samples to investigate their pathogenicity to PWN and its vector beetle. We focused on the genus *Serratia* because of the frequent association of these bacteria with PWD as well as the high potential of these bacteria to negatively influence both PWN and its vector, therefore being excellent biocontrol candidates against PWD.

## MATERIALS AND METHODS

All samples in this study were collected from five locations in China in the spring for 2 years (March to April 2018–2019). These five sites varied in the duration of PWN invasion: Liaoning (LN): 1–5 years of invasion; Shaanxi (SX) and Anhui (AH): 5–10 years of invasion; Zhejiang (ZJ): 15–20 years of

invasion; and Jiangsu (JS): 25–30 years of invasion (Supplementary Figure 1). Thirty trees with signs of late-stage PWD infection (recently dead and leafless) with a diameter at breast height (DBH) of 10–15 cm were sampled per location. Two or three logs of 20–30 cm long and of 5–10 cm in diameter were chosen from each tree (Zhao et al., 2013a). The pine species in each location were LN: *Pinus tabuliformis*, *Pinus koraiensis*; SX: *Pinus tabuliformis* and *Pinus armandi*; AH, ZJ, and JS: *Pinus massoniana* (Supplementary Figure 1). The logs from each site were kept at 4°C until used for pupal chamber samples and J<sub>III</sub> collection (2018–2020). The rest of the logs were kept in the glasshouse for vector beetle collection (2018–2019).

### **Collection of Pupal Chamber Samples**

Each year, pupal chamber samples of *Monochamus* sp. vector beetles were collected from the randomly chosen logs from each site. Sawdust was scraped using a sterile scalpel and forceps from the surface of pupal chambers across multiple logs, and tissues from three to five pupal chambers were pooled as one sample. In total, five to seven samples were collected from each site per year, resulting in a total of 87 samples from the five sites across the two sampling years (2018 and 2019).

### **Collection of Vector Beetle Tracheae Samples**

The vector beetles (*M. alternatus* and *M. saltuarius*) were surface-sterilized by using ethanol and then rinsed three times with sterile water. Tracheae of vector beetles were extracted under the CKX53 microscope (Olympus, Tokyo, Japan) (Zhou et al., 2018; Zhang et al., 2020a). In total, we collected 394 vector beetles. From each beetle, we extracted one trachea sample including all tracheal tissue, resulting in a minimum of 30 tracheae samples from each site per year.

### **Nematode Collection**

J<sub>III</sub>s were collected in the tissues surrounding pupal chambers from the same logs in which pupal chambers were sampled. In brief, 20 g of wood tissue around each pupal chamber was used to recover PWN by the using Baermann funnel technique (Zhao et al., 2013a,b). After collection, J<sub>III</sub> was examined under a microscope for morphological confirmation.

## **Fecundity of Nematodes Collected From Sites Varying in the Duration of PWN Invasion**

The J<sub>III</sub>s were cultured with the fungus *Botrytis cinerea* on potato dextrose agar (PDA) plates in which they can molt to propagative stages. Periodic investigation of nematode fecundity was made by choosing 12 individuals (nine females and three males) of PWNs to a PCR tube containing 150 µl of phosphate-buffered saline with tween-20 (PBST). Each treatment was repeated 10 times, the total number of eggs at the bottom of each tube was counted under a microscope (Meng et al., 2020). To confirm whether the potential differences in fecundity were related to the differences in the duration of PWN invasion, we compared the fecundity (mean number of eggs) of PWN harvested from different sites after these nematode populations were cultured in the lab for 7 days and again after 30 days of culturing.

## **Quantification of Relative Bacterial and Fungal Abundances**

The DNA extraction of the pupal chamber and tracheae samples was performed using the High Pure PCR Template Preparation Kit (Roche Applied Science, Mannheim, Germany) following the manufacturer's procedures. The DNA samples extracted from pupal chambers and tracheae used for Illumina sequencing for microbiota investigation were also used for the PCR analysis of bacterial and fungal abundance. According to previous studies, the bacterial genus *Serratia* and the fungal genus *Sporothrix* are widespread and dominant taxa in the pupal chambers (Zhao et al., 2013a; Guo et al., 2020), which is why these taxa were used for plasmid synthesis. For the bacterial standard, a 203-bp, the double-stranded plasmid was synthesized to span the 16S region of the *S. marcescens* genome. For the fungal standard, a 333-bp, double-stranded DNA plasmid was synthesized to span the 18S internal transcribed spacer (ITS) region and the 5.8S rRNA gene of *Sporothrix* sp. 1. The standard recombinant plasmids of two strains were performed using *pEASY-T5* Zero Cloning Kit according to the manufacturer's instructions (Transgene, Beijing, China). For each taxon's standard, the lyophilized material was used to prepare a 10 nM stock solution that was serially diluted to produce 10 standards spanning the 10<sup>-1</sup>-10<sup>8</sup> copy number range (Ledon-Rettig et al., 2018; Tkacz et al., 2018). Plots of Cp vs. log 10 (copy number) afforded linear calibration curves with amplification efficiencies between 91–95% and 72–73% for *S. marcescens*

and *Sporothrix* sp.1, respectively, and  $R^2$  values of 1 and 0.96–0.98 for these taxon standards, respectively. Based on the melting-curve analyses, we found no evidence for primer dimers. We estimated fungal and bacterial abundance based on the estimated gene copy number from their respective standard curves and used these values to calculate bacteria-to-fungi ratios (Fierer et al., 2005).

The samples used for microbial profiling were used for RT-qPCR (five biological replicates). The RT-qPCR annealing temperature was 49°C and the extension time was 45 s. A fragment of the 16S ribosomal ribonucleic acid (rRNA) gene was amplified using the primers Eub338 (5'-ACTCCTACGGGAGGCAGCAG-3') and Eub518 (5'-ATTACCGCGGCTGCTGG-3') for bacteria and a fragment spanning the SSU internal transcribed spacer (ITS) region and the 5.8S rRNA gene for fungi using primers ITS1f (5'-TCCGTAGGTGAAACCTGCGG-3') and 5.8S (5'-CGCTGCGTTCTTCATCG-3') (Fierer et al., 2005).

### **Analysis of Relative Abundance of the Genus *Serratia* Among Different Sites**

The microbiota data from the pupal chamber and vector beetle tracheae samples used in this study have been submitted to the NCBI BioProject under accession number PRJNA720535. The relative abundance of genus *Serratia* involved in pupal chambers and tracheae of vector beetles have based on the ASV table of our other experiment (Tian et al. unpublished data). The ASV tables used for analyses in this study are available at [https://github.com/Haokai-Tian/Tian2022\\_microbiome.git](https://github.com/Haokai-Tian/Tian2022_microbiome.git), but the results are presented here (Figure 4) for a demonstration of the microbial community differences among the sites.

### **Isolation and Identification of Bacteria From the Pupal Chamber and Tracheae Samples**

Pupal chamber and beetle tracheae samples were surface-disinfected with 70% ethanol and then rinsed several times in sterile water before sampling. Five to ten samples of pupal chambers and 10–15 beetles in each site per year were used for bacterial isolation. The chips of the pupal chamber and tracheae samples were infiltrated in 1 ml and 40  $\mu$ l of 10% phosphate-buffered saline (PBS) separately, and the samples were sonicated for 1 min

and vortexed at a medium speed for 10 s. The suspension was then plated (dilution factors varied from  $10^1$  to  $10^3$ ) on the Luria-Bertani medium (LB) and tryptic soy agar (TSA). The nystatin and cycloheximide were added for preventing the growth of fungus and yeast (Liu et al., 2021). All plates were incubated at 28°C for 15–20 days. For each morphotype, at least two cultures from different samples were selected and identified by 16S ribosomal DNA (rDNA) sequencing, and the samples were stored at  $-80^{\circ}\text{C}$  in TSA broth with 20–30% glycerin.

DNA was extracted using a MightyPrep reagent for DNA (TaKaRa, Dalian, China) following the instruction. We selected 16S rDNA sequences to compare with the type strains in EzBioCloud database (<https://www.ezbiocloud.net/>) and combine phylogenetic relationships to identify bacteria. The 16S rDNA was amplified with primers 8F (5'-GCGGATCCGGCCGCTGCAGAGTTGATCCTGGCTCAG-3') and 1492R (5'-GGCTCGAGCGGCCGCCGGGTTACCTTGTACGACTT-3') (Weisburg et al., 1991). The reaction mixture for PCR contained 12.5  $\mu\text{l}$  of 2  $\times$  MightyAmp Buffer Ver.3, 0.5  $\mu\text{l}$  of MightyAmp DNA Polymerase Ver.3, 1  $\mu\text{l}$  of each primer (10  $\mu\text{M}$ /each), and 2.5  $\mu\text{l}$  of 10  $\times$  Additive for High Specificity (TaKaRa, China).

## Phylogenetic Analyses

National Center for Biotechnology Information (NCBI) and the EzBioCloud database were used to obtain sequences of the closest type strains for phylogenetic analysis (Yoon et al., 2017). A total of 118 sequences obtained from this study and 119 sequences downloaded from EzBioCloud were homologously aligned and de-tailed using MUSCLE v3.5.1 (<http://www.drive5.com/muscle/>) and trimAL v1.3 (<http://trimal.cgenomics.org/downloads>) (Edgar, 2004; Capella-Gutierrez et al., 2009). The alignment length is 1,267 bp. Finally, the phylogenetic tree (1,000 replicates) using the Maximum Likelihood (ML) method was constructed by the GTR GAMMA model in IQTree v2.1.3 (<http://www.iqtree.org>) (Nguyen et al., 2015; Chernomor et al., 2016). Confidence at each node was assessed by 1,000 bootstrap replicates (Zhou et al., 2021). *Anabaena affinis* (AF247591) was chosen as the outgroup. The resulting tree was visualized and edited with iTol (<https://itol.embl.de>) (Letunic and Bork, 2019). Bacterial sequences from pupal chambers and

vector beetle tracheae used in this study have been deposited in the GenBank database under the accession numbers OM319701-OM319818.

### **Nematicidal Activity of Two *Serratia* Strains**

Two *Serratia* strains, *S. marcescens* strain AHPC29 and *Serratia nematodiphila* strain ZJPC33, isolated from the pupal chambers in this study were used for nematicidal activity tests. The target strain was cultured in a shaker at 28°C and 150 rpm for 24 h. After centrifuging the bacteria solution, the supernatant was removed, and the remaining bacteria pellet was resuspended in 0.9% physiological saline solution. The final bacterial concentration was diluted to 0.5 OD. The propagative stages of the PWNs used in this experiment were cultured with the fungus *Botrytis cinerea* on PDA plates at 25°C (Meng et al., 2020). Before the test, the nematodes were washed with 3% hydrogen peroxide for 10 min followed by washes with sterilized 0.03 M MgSO<sub>4</sub> (Nascimento et al., 2016). After this, 200–300 nematodes were added to a 96-well sterile microplate. The ratio of nematodes to bacterial suspension was 1:1 (or control: PWN in 0.03 M MgSO<sub>4</sub> solution), and the total volume was 100 ul, with five replicates per treatment. The final concentration of bacterial strains was 0.5 OD. The sterile microplates were incubated at room temperature, and nematode mortality was determined after 24 h.

### **Survival Assays of Vector Beetles Exposed to Pathogenic *S. marcescens***

The two *Serratia* strains used in the nematicidal activity test were also used in survival assays of the vector beetles. The final concentration of bacterial strains for this test was consistent with the nematicidal activity test mentioned above.

The final instar larvae, early pupae (max. 2 days after pupation), and newly eclosed adults of *M. alternatus* were soaked in 70% alcohol for 30 s and then rinsed with sterile 0.9% physiological saline solution. These beetles were then added to the solution of *Serratia* bacterial cells at an OD of 0.5 in 2 ml Falcon tubes or 0.9% saline solution for control. The tubes were lightly shaken for 30 s and placed on a Petri dish (90 mm). Each treatment was replicated three times, with each replicate consisting of five

beetles. Beetle survival was monitored every day for 10 days (Pineda-Castellanos et al., 2015; Raymann et al., 2018).

## Statistical Analysis

Statistical analysis was performed in R (version 3.6.1) (<http://www.r-project.org>) and GraphPad Prism 7. A one-way ANOVA with Tukey's multiple comparison test was used for the analysis of nematode reproduction and bacteria-to-fungi ratio, and the Kruskal-Wallis *H*-test was used for the relative abundance of the genus *Serratia* genus. The two-tailed paired *t*-test was used for the nematicidal analysis of the bacterial strains against PWN and vector beetle. The Kaplan-Meier method was used for the analysis of survival curves, and the log-rank test was applied to evaluate the significance of testing. All figures and graphs were made in GraphPad Prism 7 and adapted in Adobe Illustrator (version 23.0.5).

# RESULTS

## Fecundity Comparison Among Sites Differing in the Duration of PWN Invasion

We compared the fecundity of PWNs collected from different sampling sites, ranging from 2 to 30 years since the PWN invasion. PWNs from sites with a longer duration of PWN invasion (>10 years) produced significantly fewer eggs compared to the PWNs collected from more recently invaded sites (<10 years) (Figure 1A,  $p < 0.05$ ). However, after being cultured in lab conditions for 1 month, these differences in fecundity among sites disappeared (Figure 1B).

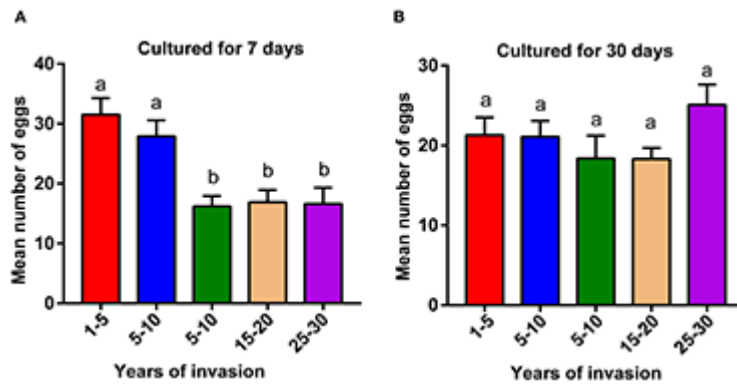


**FIGURE 1.** Comparison of pinewood nematode (PWN) fecundity collected from sites differing in the duration of PWN invasion. Fecundity of **(A)** wild population of PWN cultured in laboratory conditions for 7 days and **(B)** after the same populations were cultured in laboratory conditions for 30 days. A one-way ANOVA with Tukey's multiple comparison test,  $p < 0.05$ . Data are presented as means  $\pm$  SEM. Different letters indicate significant differences. The numbers in the x-axis indicate the duration of PWN invasion in years (1–5: 1–5 years of invasion).

## The Bacteria-to-Fungi Ratio in Pupal Chambers and Tracheae Among Sites Differing in the Duration of PWN Invasion

The bacteria-to-fungi ratio of the pupal chamber and tracheae samples were highest in the sites with the longest duration of invasion (25–30 years) and lowest in the sites with the shortest duration of invasion (1–5 years) (Figures 2A,B). Along with the increasing duration of PWN invasion, the bacteria-to-fungi ratio of pupal chamber and tracheae samples also gradually increased. The bacteria-to-fungi ratio in pupal chambers from the two sites with a shorter duration of invasion (<10 years) was lower than 1.5 (Figure 2A). In general, the total content of bacteria was higher compared to fungi (bacteria-to-fungi ratio  $>1$ ) in all pupal chamber and tracheae samples (Figures 2A,B). The total bacteria content (estimated number of copies) in pupal chamber samples was highest in the sites with the longest duration of invasion (25–30 years), whereas the total bacteria content was lowest in sites with the shortest duration of invasion (<5 years) (Figure 2C). For the samples of vector beetle tracheae, there were no significant differences in total bacterial content among different sites, except for the site with 15–20 years of invasion, which had lower bacteria abundance compared to other sites (Figure 2D).

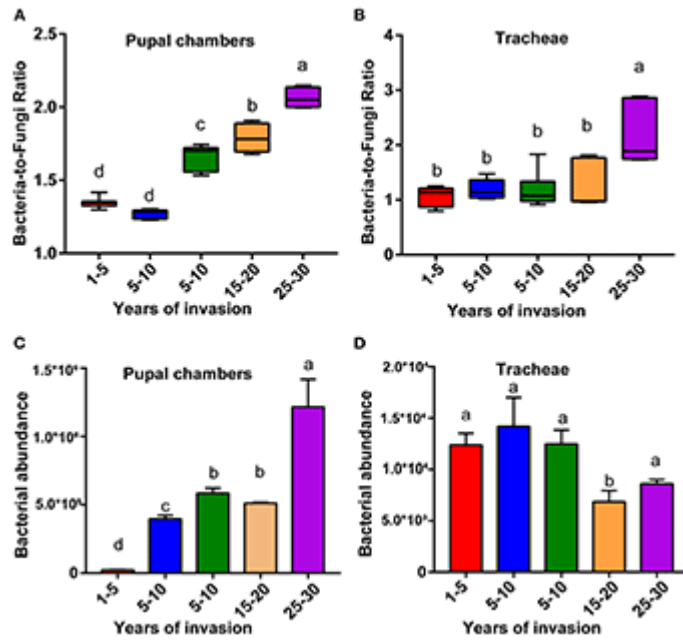


**FIGURE 2.** The relative bacterial and fungal abundance of pupal chambers and tracheae in sites differing in the duration of PWN invasion. The bacteria-to-fungi ratio of pupal chambers (A) and tracheae (B) samples in sites differing in the duration of PWN invasion (years of invasion in the X-axis). The total bacteria content of pupal chamber (C) and tracheae (D) samples from different sites differed in the duration of PWN Sinvasion. The abundance of bacterial and fungal biomass was estimated by RT-qPCR. Different letters indicate statistically significant differences from the one-way ANOVA with Tukey's multiple comparison test,  $p < 0.05$ . Data are presented as means  $\pm$  SEM.

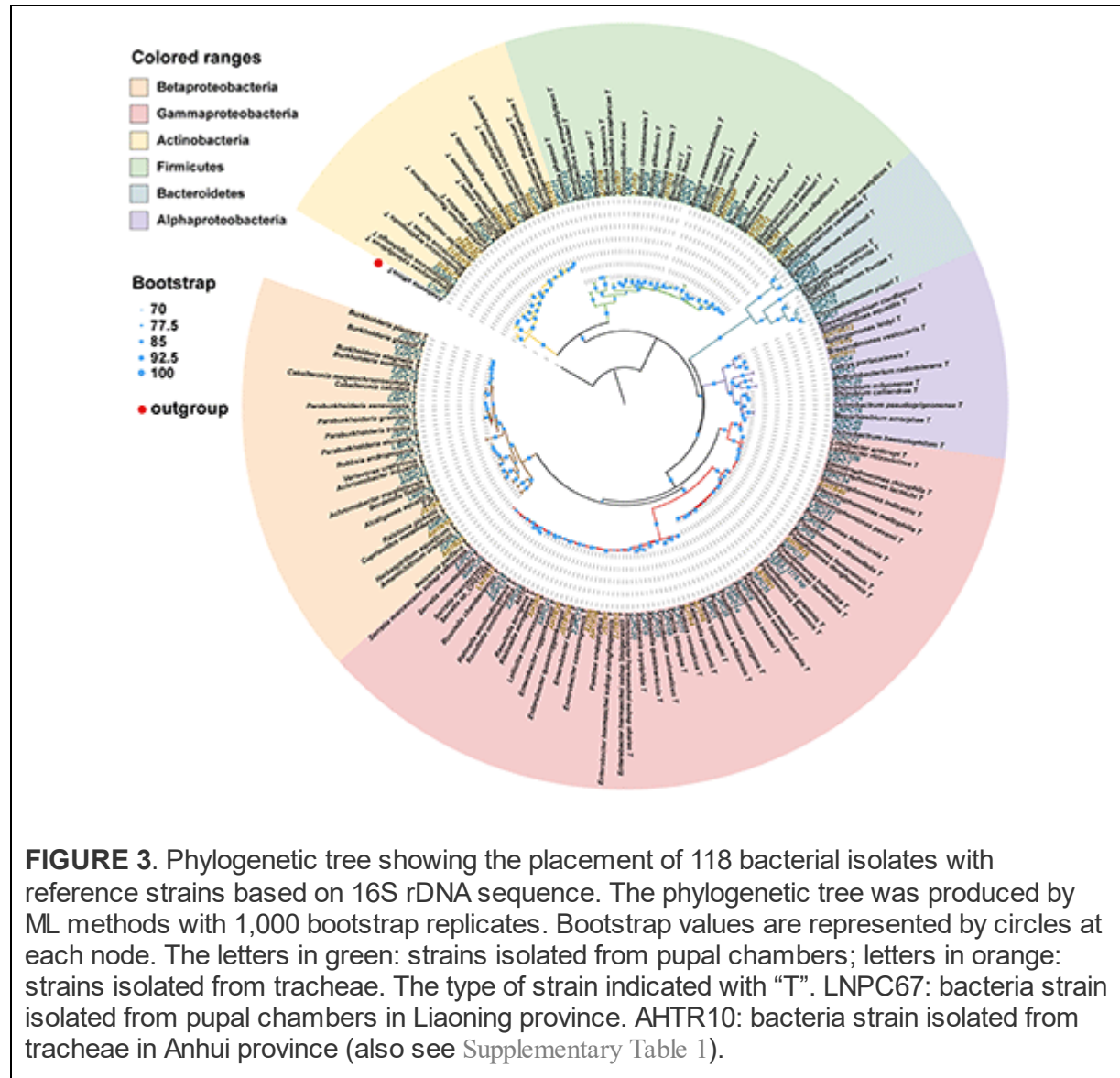
## Isolation and Identification of Bacterial Species

We isolated and cultivated 118 bacterial strains in total, belonging to 54 genera in 30 families and from four phyla. In general, the majority of the strains belonged to the three classes of the phylum Proteobacteria, and the class of Gammaproteobacteria included six families and 15 genera (44 species). The class of Betaproteobacteria included six families and 12 genera (21 species). The class of Alphaproteobacteria included seven families and eight genera (11 species). The phylum of Actinobacteria included four families and six genera (13 species). The phylum of Firmicutes included five families and nine genera. The phylum of Bacteroidetes included two families and four genera (six species) (Table 1). A total of 28 strains belong to two or more source groups. The top five genera were *Enterobacter* (7 species), *Pseudomonas* (13 species), *Bacillus* (11 species),

*Microbacterium* (6 species), and *Stenotrophomonas* (5 species) (Figure 3; Supplementary Table 1).

**Table 1.** The taxonomic distribution of bacterial isolates.

Phylum/class	Family	Genus	Isolate
Gammaproteobacteria	6	15	44
Betaproteobacteria	6	12	21
Alphaproteobacteria	7	8	11
Actinobacteria	4	6	13
Firmicutes	5	9	23
Bacteroidetes	2	4	6



This phylogenetic relationship between isolated strains and their closest type strains shown in the phylogenetic tree was also consistent with the blast result in EzBioCloud (Figure 3; Supplementary Table 1). Most phylum or class clusters strains were isolated from both pupal chamber and tracheae, except for the phylum Bacteroidetes which was only isolated from pupal chambers. The result of the phylogenetic tree showed that we isolated two species of *Serratia*, *S. marcescens* and *S. nematodiphila*, which had closely phylogenetic relationships (Figure 3). *Serratia marcescens* strain AHPC29 was isolated in pupal chambers and tracheae of the vector beetle from three sites with the longest duration of PWN invasion and was also found in the vector beetle tracheae in site (LN) with the shortest duration of the invasion.

*S. nematodiphila* strain ZJPC33 was only isolated in the pupal chamber of ZJ in this study (Supplementary Table 1).

### The Distribution of the Genus *Serratia* Among Sites Varying in the Duration of PWN Invasion

We analyzed the relative abundance of genus *Serratia* in the pupal chamber and vector beetle samples across the five sites differing in the duration of PWN invasion. In fact, for pupal chambers, the relative abundance of genus *Serratia* increased with the increasing duration of PWN invasion, being significantly higher in sites with the longest duration of invasion compared to sites with the shortest duration of invasion (<5 years) (Figure 4A). Only 0.093% of the genus *Serratia* was found in pupal chambers collected from sites with the shortest duration of invasion (<5 years), whereas 8.33% of this genus was detected in pupal chamber samples from areas over 20 years since invasion (Figure 4A). The relative abundance of the genus *Serratia* in vector beetle tracheae was highest in the sites with moderate (5–10 years) and the longest duration of PWN invasion (25–30 years) compared to other sites, and hence, the abundance of the genus *Serratia* did not consistently increase as the invasion progressed (Figure 4B).

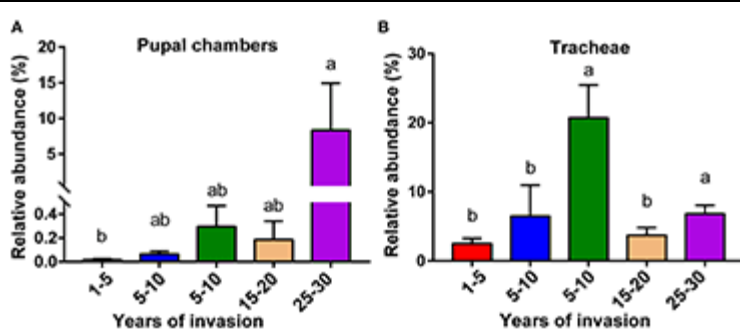


**FIGURE 4.** The relative abundance of genus *Serratia* involved in pupal chambers (A) and tracheae (B) from sites differing in the duration of PWN invasion (years of invasion in the X-axis). Data are presented as means  $\pm$  SEM, Kruskal-Wallis *H*-test,  $p < 0.05$ . Different letters indicate statistically significant differences.

### Pathogenicity of Two *Serratia* Strains to PWN and Its Vector Beetle

We tested the nematicidal activity of the two *Serratia* species (strains AHPC29 and ZJPC33) most commonly found with pupal chambers and

tracheae against PWN. The two species did not differ in nematicidal activity, *S. marcescens* strains AHPC29 caused 39.4% of mortality to PWN and *S. nematodiphila* strain ZJPC33 caused 42.3% mortality (Figure 5A).

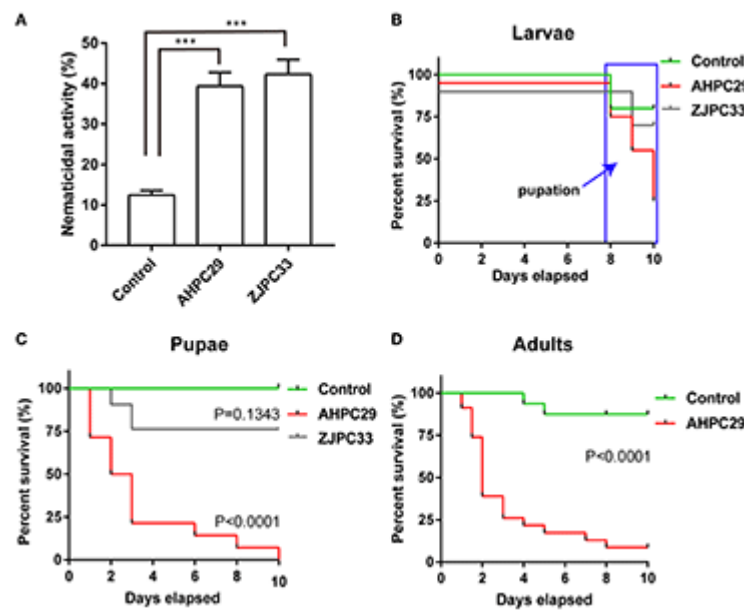


**FIGURE 5.** Pathogenicity of *Serratia marcescens* strain to PWN and its vector beetle. **(A)** The mortality assay of PWN with two *Serratia* strains AHPC29 and ZJPC33. AHPC29: *Serratia marcescens* strain AHPC29; ZJC33: *Serratia nematodiphila* strain ZJPC33. Nematicidal activity of bacterial solution monitored after 24 h. Two-tailed paired *t*-test, \*\*\**p* < 0.001. **(B,C)** Meier survival curves of vector beetle last-instar larvae and pupae exposed to AHPC29 and ZJPC33. **(D)** Meier survival curves of vector beetle adults exposed to AHPC29. Survivorship was monitored daily for 10 days. The log-rank test was used for the comparison of survival curves.

We also tested the pathogenicity of two *Serratia* strains to vector beetle *M. alternatus*. Final-instar larvae were resistant to the AHPC29 and ZJPC33 (no mortality observed before pupation), but the resistance started to decline after pupation (Figure 5B). For the pupae stage, the ZJPC33 strain showed much lower mortality compared to the strain AHPC29 (log-rank test, AHPC29: *p* < 0.0001; ZJPC33: *p* > 0.05) (Figures 5B,C). The vector beetle adults exposed to AHPC29 showed high death rates (*p* < 0.0001; Figure 5D). Most pupae and adults died during the first 5 days post-infection of AHPC29 according to the Kaplan-Meier survival curves (log-rank test, *p* < 0.0001) (Figures 5C,D).

## DISCUSSION

In our related previous study, we showed that the pupal chambers in sites with a longer duration of PWN invasion harbored fewer PWNs compared to sites with more recent PWN invasion (data not shown, Tian et al., Unpublished data), indicating the presence of a hidden microbial player causing negative effects to the PWN-vector beetle complex. In this study, using both quantitative detection and culture-dependent methods, we explored this possibility by investigating PWN fecundity as well as the composition and abundance of associated bacteria and fungi across five sites varying in the duration of PWN invasion (2–30 years post-invasion). PWNs collected from the sites with the longest duration of invasion had the lowest fecundity compared to PWNs collected from sites with a shorter duration of the invasion. These differences disappeared over time when the nematodes were cultured in laboratory conditions, indicating that the nematode fecundity was related to the nematode's environment within the host tree rather than site-specific genetic difference. We found indirect evidence that the reduced PWN fecundity together with the previously found lower PWN abundance may be related to the changes in the associated microbiota community and increased abundance of an antagonistic microorganism in sites with a longer duration of PWN invasion. Firstly, the bacteria-to-fungi ratio and the total bacteria content were significantly higher in sites with the longest duration of the invasion. Second, *S. marcescens*, a common bacteria found in our pupal chamber and tracheae samples, not only had the highest abundance in these sites but was also shown to be lethal to both PWN and its vector after direct exposure. Therefore, despite pupal chambers and tracheae also harboring beneficial Ophiostomatoid fungi (Zhao et al., 2013a), our results indicated that the negative effects caused by bacteria of the genus *Serratia* may override these effects and may be the “hidden players” limiting the success of the PWN-vector beetle complex when the PWN invasion has reached a certain time point.

Similar results have been demonstrated on invasive plants, showing that, as the invasion progresses over time, the initial dominance of an invasive plant species can later be reversed by stabilizing processes that are related to changes in the microbial composition (Knevel et al., 2004; Nijjer et al., 2007; Dostál et al., 2013). Soil-plant models have shown that compared to bacterial communities, fungal diversities in soil or roots are more influenced

by the variation caused by the geographic location (Hu et al., 2019; Thiergart et al., 2020). Similarly, previous studies have shown that the genus *Serratia* is widespread across PWN-invaded sites (as also confirmed in the current study), whereas the dominant beneficial Ophiostomatoid fungi of the PWN-vector beetle complex are more dependent on the geographic location (Zhao et al., 2013a, 2018). This indicates that PWD-associated bacterial community may be more robust against environmental compared to fungal community and hence, may play an important role in PWD progression. However, the influence of the variation in abiotic factors, such as rainfall and temperature, among different sites may influence the abundance of bacterial and fungal associates of bark beetles (Six and Bentz, 2007; Öhrn et al., 2021), and their effects on PWD complex should also therefore be considered in future studies. Nevertheless, although not much is known about the changes in the bacterial and fungal community of invasive species in general or in terms of PWD, the increase in bacteria-to-fungi ratio in the sites with a longer duration of invasion indicates the existence of temporal change in the microbiota community in relation to the progression of PWD, and depending on the outcome of such community change, may be detrimental to the PWN-vector complex.

Similar to previous studies (Nascimento et al., 2015; Proença et al., 2017), we found that the genus *Serratia* had a strong association with both PWN and its vector beetle. The increase in the abundance of pathogenic *Serratia* bacteria in pupal chambers and tracheae in sites with a longer duration of PWN invasion, suggests that antagonistic effects against the PWN-vector beetle complex will be enhanced as PWD progresses. Besides the direct lethal effects of these bacteria on the PWN-vector beetle complex mentioned above, changes in the bacteria-to-fungi ratio may have resulted in increased microbe-microbe competition, as shown in other systems (Durán et al., 2018). This in turn may have resulted in the depletion of Ophiostomatoid fungal food source for PWN, therefore contributing to the lower abundance of PWN in sites with a longer duration of the invasion. Whether *Serratia* sp. competes with PWN-associated fungi and results in depletion of PWN's food resources or whether the lower nematode abundance and fecundity in sites with a longer duration of PWN invasion are purely caused by the nematicidal activity of such bacteria remains to be tested in future studies. The genus *Serratia* has highly diverse interactions among other organisms, depending on the interacting partner and *Serratia* species or strain. For example,

although *S. marcescens* strain AHPC29 used in this study was found to be highly antagonistic to PWN and its vector, another *S. marcescens* strain associated with PWN (PWN146) has been suggested to be mutualistic, improving the virulence of PWN while being phytotoxic to pine seedlings (Vicente et al., 2012). Another *Serratia* species, *S. quinivorans* strain BXF1, is not lethal to PWN, suggesting that it may be a non-specific transient mutualist of the nematode (Nascimento et al., 2016). In addition, the genus *Serratia*, including *S. marcescens*, is also commonly found in the gut of PWNs and *Monochamus* beetles, without showing adverse effects under normal conditions (Alves et al., 2018; Guo et al., 2020; Ge et al., 2021). Considering these diverse interactions of the genus *Serratia*, the role of different species of this genus for the different players involved in PWD (host tree, PWN, and vector beetle), as well as its potential competition with the PWD associated fungi, warrant further studies. Similar to the nematicidal and insecticidal activities of *S. marcescens* demonstrated here, the pathogenicity of this species to insects has been demonstrated in other studies (Raymann et al., 2018). Several genes related to the toxicity of *Serratia* have been identified, such as those that function in lipopolysaccharide (LPS) biosynthesis, iron absorption, and hemolysin production (Hejazi and Falkiner, 1997; Kurz et al., 2003). For PWN, a kind of serine protease was found to be majorly responsible for the toxicity of the *S. marcescens* (Paiva et al., 2013), whereas, for insects, the lethal effect of this pathogen may be caused by a chitinase it produces (Hejazi and Falkiner, 1997; Lacey et al., 2015). Some studies suggest that successful colonization and pathogenicity of this bacterium may depend on the gut microbiome composition of the host (Raymann et al., 2017; Heu et al., 2021). Another mutually non-inclusive possibility is that the immune system of the inactive pupae is weaker compared to active last instar larvae, and it is also possible that *S. marcescens* is virulent only when present in the bloodstream (Raymann et al., 2018). However, because *S. marcescens* was also found to be lethal to adult beetles, further investigation is needed to confirm the mechanism behind the variation in susceptibility (e.g., immunity, cuticle thickness influencing direct exposure, and gut microbiome, among others) of different PWN vector life stages to this bacterium. Compared to previous studies investigating the nematicidal activity of *S. marcescens* using its metabolites, we used actual bacterial suspension to study its nematicidal and insecticidal activities. These differences in methodologies (different concentrations of the effective

substance and/or use of different *S. marcescens* strains) may explain the relatively lower virulence observed in this study compared to previous studies, yet the virulence is within the range reported in other *Serratia* studies (Paiva et al., 2013; Proen  a et al., 2017; Liu et al., 2019). However, the use of live bacteria, as used in this study, is likely more ecologically relevant, more accurately mimicking the type of exposure of how the PWN and vector beetle encounter these bacteria in nature. Although the use of H<sub>2</sub>O<sub>2</sub> to surface sterilize the nematodes resulted in some mortality in the control group, all nematodes were disinfected with this same method and hence were likely to have no significant influence on the observed mortality pattern.

The nematicidal and insecticidal *S. marcescens* strain AHPC29 used in our study could potentially be used as a biological agent against PWN and its vector beetle. One advantage of using a bacterium as a biocontrol agent is that it can more easily enter the host pine compared to chemical pesticides and is less likely to cause toxics to non-target organisms, especially because this bacterium appears to be a predominant associate of the PWN-vector complex. In addition, some studies have found that genetically engineered bacteria can improve the control of plant diseases and their insect vectors (Wang et al., 2017; Kwak et al., 2018). Therefore, the *S. marcescens* strain could also potentially be genetically engineered to carry nematicidal or insecticidal protein into host pine to control PWD. Moreover, the abundance dynamics of bacteria and fungi demonstrated in our study could reflect the prevalence of the PWN-vector beetle complex and indicate the progress of PWD. Similar to the studies showing that variation in soil and root microbiome could reflect the health status of the host plant and predict future disease outcomes (Wei et al., 2019), our results on the bacteria-to-fungi ratio could also provide important information for the evaluation of the degree of PWN invasion in field condition. Our results also found that *S. marcescens* strain AHPC29 was highly virulent for the pupae stage of vector beetle, suggesting that spring (when *Monochamus* sp. usually pupae) is likely the optimal time window for applying this control method. Future studies should investigate the pathogenicity of this strain in field conditions using different life stages of PWN and its vector beetle to confirm its applicability for PWD biocontrol.

# CONCLUSION

In conclusion, our results show that variation in the duration of PWN invasion can drastically alter the microbial composition and the prevalence of PWD. In addition, a common bacterial associate of PWN and its vector, *S. marcescens* (strain AHPC29), can act as an antagonistic to both of these partners required for the initiation of PWD. This lethal strain found in this study should therefore be tested in future studies (e.g., in field conditions) for its application as a biocontrol agent against PWN and its vector beetle. Our research can also indicate that microbial composition could be used as a tool to determine the progression of plant disease. For the progress of PWD, the estimate could be done by using the abundance of the genus *Serratia* as a biomarker.

# DATA AVAILABILITY STATEMENT

The datasets presented in this study can be found in online repositories. The names of the repository/repositories and accession number(s) can be found below: Bacterial 16S rRNA gene sequencing data have been submitted to the NCBI BioProject under accession number PRJNA720535. Bacterial sequences from pupal chambers and vector beetle tracheae used in this study have been deposited in the GenBank database under the accession numbers OM319701-OM319818. The ASV tables used for analyses in this study are available at [https://github.com/Haokai-Tian/Tian2022\\_microbiome.git](https://github.com/Haokai-Tian/Tian2022_microbiome.git).

# AUTHOR CONTRIBUTIONS

HT, LZ, and JS designed the research. HT performed experiments and analyzed the data. HT, T-MK, and JS wrote the manuscript. All authors read and approved the final manuscript.

# FUNDING

This work was supported by the National Natural Science Foundation of China (32088102 and 32061123002) and the National Key Research and Development Program of China (2021YFC2600100).

## SUPPLEMENTARY MATERIAL

The Supplementary Material for this article can be found online at: <https://www.frontiersin.org/articles/10.3389/fpls.2022.856841/full#supplementary-material>

## REFERENCES

Akduman, N., Rödelsperger, C., and Sommer, R. J. (2018). Culture-based analysis of pristionchus-associated microbiota from beetles and figs for studying nematode-bacterial interactions. *PLoS ONE* 13, e0198018. doi: 10.1371/journal.pone.0198018

Alves, M., Pereira, A., Matos, P., Henriques, J., Vicente, C., Aikawa, T., et al. (2016). Bacterial community associated to the pine wilt disease insect vectors *Monochamus galloprovincialis* and *Monochamus alternatus*. *Sci. Rep.* 6, 23908. doi: 10.1038/srep23908

Alves, M., Pereira, A., Vicente, C., Matos, P., Henriques, J., Lopes, H., et al. (2018). The role of bacteria in pine wilt disease: Insights from microbiome analysis. *FEMS Microbiol. Ecol.* 94, ffy077. doi: 10.1093/femsec/ffy077

Capella-Gutierrez, S., Silla-Martinez, J. M., and Gabaldon, T. (2009). Trimal: a tool for automated alignment trimming in large-scale phylogenetic analyses. *Bioinformatics* 25, 1972–1973. doi: 10.1093/bioinformatics/btp348

Chernomor, O., Von Haeseler, A., and Minh, B. Q. (2016). Terrace aware data structure for phylogenomic inference from supermatrices. *Syst. Biol.* 65, 997–1008. doi: 10.1093/sysbio/syw037

Diez, J. M., Dickie, I., Edwards, G., Hulme, P. E., Sullivan, J. J., and Duncan, R. P. (2010). Negative soil feedbacks accumulate over time for non-native plant species. *Ecol. Lett.* 13, 803–809. doi: 10.1111/j.1461-0248.2010.01474.x

Dostál, P., Müllerová, J., Pyšek, P., Pergl, J., and Klinarová, T. (2013). The impact of an invasive plant changes over time. *Ecol. Lett.* 16, 1277–1284. doi: 10.1111/ele.12166

Durán, P., Thiergart, T., Garrido-Oter, R., Agler, M., Kemen, E., Schulze-Lefert, P., et al. (2018). Microbial interkingdom interactions in roots promote arabidopsis survival. *Cell* 175, 973. doi: 10.1016/j.cell.2018.10.020

Edgar, R. C. (2004). Muscle: multiple sequence alignment with high accuracy and high throughput. *Nucleic Acids Res.* 32, 1792–1797. doi: 10.1093/nar/gkh340

Fierer, N., Jackson, J. A., Vilgalys, R., and Jackson, R. B. (2005). Assessment of soil microbial community structure by use of taxon-specific quantitative pcr assays. *Appl. Environ. Microbiol.* 71, 4117. doi: 10.1128/AEM.71.7.4117-4120.2005

Futai, K. (2013). Pine wood nematode, *Bursaphelenchus xylophilus*. *Annu. Rev. Phytopathol.* 51, 61–83. doi: 10.1146/annurev-phyto-081211-172910

Ge, S. X., Shi, F. M., Pei, J. H., Hou, Z. H., Zong, S. X., and Ren, L. L. (2021). Gut bacteria associated with *Monochamus saltuarius* (coleoptera: Cerambycidae) and their possible roles in host plant adaptations. *Front. Microbiol.* 12, e687211. doi: 10.3389/fmicb.2021.687211

Grimont, P. A. D., and Grimont, F. (1978). Genus *Serratia*. *Annu. Rev. Microbiol.* 32:221–248. doi: 10.1146/annurev.mi.32.100178.001253

Guo, Y., Lin, Q., Chen, L., Carballar-Lejarazu, R., Zhang, A., Shao, E., et al. (2020). Characterization of bacterial communities associated with the pinewood nematode insect vector *Monochamus alternatus* hope and the host tree *Pinus massoniana*. *BMC Genomics* 21, 1–13. doi: 10.1186/s12864-020-6718-6

Hejazi, A., and Falkiner, F. R. (1997). *Serratia marcescens*. *J. Med. Microbiol.* 46, 903–912. doi: 10.1099/00222615-46-11-903

Heu, K., Romoli, O., Schonbeck, J. C., Ajenoe, R., Epelboin, Y., Kircher, V., et al. (2021). The effect of secondary metabolites produced by *Serratia marcescens* on *Aedes aegypti* and its microbiota. *Front. Microbiol.* 12, e645701. doi: 10.3389/fmicb.2021.645701

Hu, Y., Veresoglou, S. D., Tedersoo, L., Xu, T., Ge, T., Liu, L., et al. (2019). Contrasting latitudinal diversity and co-occurrence patterns of soil fungi and plants in forest ecosystems. *Soil Biol. Biochem.* 131, 100–110. doi: 10.1016/j.soilbio.2019.01.001

Knevel, I. C., Lans, T., Menting, F. B. J., Hertling, U. M., and Van Der Putten, W. H. (2004). Release from native root herbivores and biotic resistance by soil pathogens in a new habitat both affect the alien *Anmophila arenaria* in south africa. *Oecologia* 141, 502–510. doi: 10.1007/s00442-004-1662-8

Kurz, C. L., Chauvet, S., Andres, E., Aurouze, M., Vallet, I., Michel, G. P. F., et al. (2003). Virulence factors of the human opportunistic pathogen *Serratia marcescens* identified by *in vivo* screening. *EMBO J.* 22, 1451–1460. doi: 10.1093/emboj/cdg159

Kwak, M. J., Kong, H. G., Choi, K., Kwon, S. K., Song, J. Y., Lee, J., et al. (2018). Rhizosphere microbiome structure alters to enable wilt resistance in tomato. *Nat. Biotechnol.* 36, 1100. doi: 10.1038/nbt.4232

Lacey, L. A., Grzywacz, D., Shapiro-Ilan, D. I., Frutos, R., Brownbridge, M., and Goettel, M. S. (2015). Insect pathogens as biological control agents: back to the future. *J. Invertebr. Pathol.* 132, 1–41. doi: 10.1016/j.jip.2015.07.009

Ledon-Rettig, C. C., Moczek, A. P., and Ragsdale, E. J. (2018). Diplogastrellus nematodes are sexually transmitted mutualists that alter the bacterial and fungal communities of their beetle host. *Proc. Natl. Acad. Sci. USA* 115, 10696–10701. doi: 10.1073/pnas.1809606115

Letunic, I., and Bork, P. (2019). Interactive tree of life (itol) v4: recent updates and new developments. *Nucleic Acids Res.* 47, W256–W259. doi: 10.1093/nar/gkz239

Liu, Y., Ponpandian, L. N., Kim, H., Jeon, J., Hwang, B. S., Lee, S. K., et al. (2019). Distribution and diversity of bacterial endophytes from four *pinus* species and their efficacy as biocontrol agents for devastating pine wood nematodes. *Scientific. Rep.* 9, 12461. doi: 10.1038/s41598-019-48739-4

Liu, Y., Xu, L., Zhang, Z., Huang, Z., Fang, D., Zheng, X., et al. (2021). Isolation, identification, and analysis of potential functions of culturable bacteria associated with an invasive gall wasp, *Leptocycbe invasa*. *Microb. Ecol.* 83, 151–166. doi: 10.1007/s00248-021-01715-w

Meng, J., Wickham, J. D., Ren, W., Zhao, L., and Sun, J. (2020). Species displacement facilitated by ascarosides between two sympatric sibling species: a native and invasive nematode. *J. Pest Sci.* 93, 1059–1071. doi: 10.1007/s10340-020-01206-w

Mitchell, C. E., Blumenthal, D., Jarosik, V., Puckett, E. E., and Pysek, P. (2010). Controls on pathogen species richness in plants' introduced and native ranges: roles of residence time, range size and host traits. *Ecol. Lett.* 13, 1525–1535. doi: 10.1111/j.1461-0248.2010.01543.x

Mota, M. M., Braasch, H., Bravo, M. A., Penas, A. C., Burgermeister, W., Metge, K., et al. (1999). First report of *Bursaphelenchus xylophilus* in portugal and in europe. *Nematology* 1, 727–734. doi: 10.1163/156854199508757

Nascimento, F. X., Espada, M., Barbosa, P., Rossi, M. J., Vicente, C. S. L., and Mota, M. (2016). Non-specific transient mutualism between the plant parasitic nematode, *Bursaphelenchus xylophilus*, and the opportunistic bacterium *Serratia quinivorans* bxfl, a plant-growth promoting pine endophyte with antagonistic effects. *Environ. Microbiol.* 18, 5265–5276. doi: 10.1111/1462-2920.13568

Nascimento, F. X., Hasegawa, K., Mota, M., and Vicente, C. S. L. (2015). Bacterial role in pine wilt disease development – review and future perspectives. *Environ. Microbiol. Rep.* 7, 51–63. doi: 10.1111/1758-2229.12202

Nguyen, L. T., Schmidt, H. A., Von Haeseler, A., and Minh, B. Q. (2015). Iq-tree: a fast and effective stochastic algorithm for estimating maximum-likelihood phylogenies. *Mol. Biol. Evol.* 32, 268–274. doi: 10.1093/molbev/msu300

Nijjer, S., Rogers, W. E., and Siemann, E. (2007). Negative plant-soil feedbacks may limit persistence of an invasive tree due to rapid accumulation of soil pathogens. *Proc. Royal Soc. B Biol. Sci.* 274, 2621–2627. doi: 10.1098/rspb.2007.0804

Öhrn, P., Berlin, M., Elfstrand, M., Krokene, P., and Jönsson, A.M. (2021). Seasonal variation in norway spruce response to inoculation with bark beetle-associated bluestain fungi one year after a severe drought. *For. Ecol. Manage.* 496, 119443. doi: 10.1016/j.foreco.2021.119443

Paiva, G., Proença, D. N., Francisco, R., Verissimo, P., Santos, S. S., Fonseca, L., et al. (2013). Nematicidal bacteria associated to pinewood nematode produce extracellular proteases. *PLoS ONE* 8, e79705. doi: 10.1371/journal.pone.0079705

Pan, L., Li, Y., Cui, R., Liu, Z., and Zhang, X. (2020). Monochamus saltuarius endangers *Pinus tabuliformis* carr. and carries *Bursaphelenchus xylophilus* (steiner and buhrer) in China. *Forests* 11, 1051. doi: 10.3390/f11101051

Pineda-Castellanos, M. L., Rodriguez-Segura, Z., Villalobos, F. J., Hernandez, L., Lina, L., and Nunez-Valdez, M. E. (2015). Pathogenicity of isolates of *Serratia marcescens* towards larvae of the scarab *Phyllophaga Blanchardi* (coleoptera). *Pathogens* 4, 210–228. doi: 10.3390/pathogens4020210

Proença, D. N., Grass, G., and Morais, P. V. (2017). Understanding pine wilt disease: roles of the pine endophytic bacteria and of the bacteria carried by the disease-causing pinewood nematode. *Microbiol. Open* 6, e00415. doi: 10.1002/mbo3.415

Proenca, D. N., Schwab, S., Vidal, M. S., Baldani, J. I., Xavier, G. R., and Morais, P. V. (2019). The nematicide *Serratia plymuthica* M24T3 colonizes arabidopsis thaliana, stimulates plant growth, and presents plant beneficial potential. *Braz. J. Microbiol.* 50, 777–789. doi: 10.1007/s42770-019-00098-y

Raymann, K., Coon, K. L., Shaffer, Z., Salisbury, S., and Moran, N. A. (2018). Pathogenicity of *Serratia marcescens* strains in honey bees. *Mbio* 9, e01649–e01618. doi: 10.1128/mBio.01649-18

Raymann, K., Shaffer, Z., and Moran, N. A. (2017). Antibiotic exposure perturbs the gut microbiota and elevates mortality in honeybees. *PLoS Biol.* 15, e2001861. doi: 10.1371/journal.pbio.2001861

Six, D. L., and Bentz, B. J. (2007). Temperature determines symbiont abundance in a multipartite bark beetle-fungus ectosymbiosis. *Microb. Ecol.* 54, 112–118. doi: 10.1007/s00248-006-9178-x

Thiergart, T., Durán, P., Ellis, T., Vannier, N., Garrido-Oter, R., Kemen, E., et al. (2020). Root microbiota assembly and adaptive differentiation among european arabidopsis populations. *Nat. Ecol. Evol.* 4, 122–131. doi: 10.1038/s41559-019-1063-3

Tkacz, A., Hortala, M., and Poole, P. S. (2018). Absolute quantitation of microbiota abundance in environmental samples. *Microbiome* 6, 110. doi: 10.1186/s40168-018-0491-7

Vicente, C. S. L., Nascimento, F., Espada, M., Barbosa, P., Mota, M., Glick, B. R., et al. (2012). Characterization of bacteria associated with pinewood nematode *Bursaphelenchus xylophilus*. *PLoS ONE* 7, e46661. doi: 10.1371/journal.pone.0046661

Vicente, C. S. L., Nascimento, F. X., Espada, M., Barbosa, P., Hasegawa, K., Mota, M., et al. (2013). Characterization of bacterial communities associated with the pine sawyer beetle *Monochamus galloprovincialis*, the insect vector of the pinewood nematode *Bursaphelenchus xylophilus*. *FEMS Microbiol. Lett.* 347, 130–139. doi: 10.1111/1574-6968.12232

Vicente, C. S. L., Soares, M., Faria, J. M. S., Ramos, A. P., and Inacio, M. L. (2021). Insights into the role of fungi in pine wilt disease. *J. Fungi* 7, 780. doi: 10.3390/jof7090780

Wang, S., Dos-Santos, A. L. A., Huang, W., Liu, K. C., Oshaghi, M. A., Wei, G., et al. (2017). Driving mosquito refractoriness to *Plasmodium falciparum* with engineered symbiotic bacteria. *Science* 357, 1399. doi: 10.1126/science.aan5478

Wei, Z., Gu, Y., Friman, V. P., Kowalchuk, G. A., Xu, Y., Shen, Q., et al. (2019). Initial soil microbiome composition and functioning predetermine future plant health. *Sci. Adv.* 5, eaaw0759. doi: 10.1126/sciadv.aaw0759

Weisburg, W. G., Barns, S. M., Pelletier, D. A., and Lane, D. J. (1991). 16s ribosomal DNA amplification for phylogenetic study. *J. Bacteriol.* 173, 697–703. doi: 10.1128/jb.173.2.697-703.1991

Yoon, S. H., Ha, S. M., Kwon, S., Lim, J., Kim, Y., Seo, H., et al. (2017). Introducing ezbiocloud: a taxonomically united database of 16s rrna gene sequences and whole-genome assemblies. *Int. J. Syst. Evol. Microbiol.* 67, 1613–1617. doi: 10.1099/ijsem.0.001755

Zhang, C., Wickham, J. D., Zhao, L., and Sun, J. (2020a). A new bacteria-free strategy induced by magal2 facilitates pinewood nematode escape immune response from its vector beetle. *Insect Sci.* 28, 1087–1102. doi: 10.1111/1744-7917.12823

Zhang, W., Wang, X., Li, Y., Liu, Z., Li, D., Wen, X., et al. (2020b). Pinewood nematode alters the endophytic and rhizospheric microbial communities of *Pinus massoniana*. *Microb. Ecol.* 81, 807–817. doi: 10.1007/s00248-020-01619-1

Zhao, L., Ahmad, F., Lu, M., Zhang, W., Wickham, J. D., and Sun, J. (2018). Ascarosides promote the prevalence of ophiostomatoid fungi and an invasive pathogenic nematode, *Bursaphelenchus xylophilus*. *J. Chem. Ecol.* 44, 701–710. doi: 10.1007/s10886-018-0996-3

Zhao, L., Lu, M., Niu, H., Fang, G., Zhang, S., and Sun, J. (2013a). A native fungal symbiont facilitates the prevalence and development of an invasive pathogen-native vector symbiosis. *Ecology* 94, 2817–2826. doi: 10.1890/12-2229.1

Zhao, L., Mota, M., Vieira, P., Butcher, R. A., and Sun, J. (2014). Interspecific communication between pinewood nematode, its insect vector, and associated microbes. *Trends Parasitol.* 30, 299–308. doi: 10.1016/j.pt.2014.04.007

Zhao, L., Zhang, S., Wei, W., Hao, H., Zhang, B., Butcher, R. A., et al. (2013b). Chemical signals synchronize the life cycles of a plant-parasitic nematode and its vector beetle. *Curr. Biol.* 23, 2038–2043. doi: 10.1016/j.cub.2013.08.041

Zhao, L., Zhang, X., Wei, Y., Zhou, J., Zhang, W., Qin, P., et al. (2016). Ascarosides coordinate the dispersal of a plant-parasitic nematode with the metamorphosis of its vector beetle. *Nat. Commun.* 7, 12341. doi: 10.1038/ncomms12341

Zhao, M., Lu, X., Zhao, H., Yang, Y., Hale, L., Gao, Q., et al. (2019). *Ageratina Adenophora* invasions are associated with microbially mediated differences in biogeochemical cycles. *Sci. Total Environ.* 677, 47–56. doi: 10.1016/j.scitotenv.2019.04.330

Zhou, J., Zhao, L., Yu, H., Wang, Y., Zhang, W., Hu, S., et al. (2018). Immune tolerance of vector beetle to its partner plant parasitic nematode modulated by its insect parasitic nematode. *FASEB J.* 32, 4862–4877. doi: 10.1096/fj.201800247R

Zhou, X., Ma, Z. Y., Qi, Z. H., Liu, Y. X., and Cai, L. (2021). Construction and display of phylogenetic tree based on amplicon data. *Microbiome Protocols eBook. Bio-101* e2003730. doi: 10.21769/BioProtoc.2003730

**Conflict of Interest:** The authors declare that the research was conducted in the absence of any commercial or financial relationships that could be construed as a potential conflict of interest.

**Publisher's Note:** All claims expressed in this article are solely those of the authors and do not necessarily represent those of their affiliated organizations, or those of the publisher, the editors and the reviewers. Any product that may be evaluated in this article, or claim that may be made by its manufacturer, is not guaranteed or endorsed by the publisher.

*Copyright © 2022 Tian, Koski, Zhao, Liu and Sun. This is an open-access article distributed under the terms of the Creative Commons Attribution License (CC BY). The use, distribution or reproduction in other forums is permitted, provided the original author(s) and the copyright owner(s) are credited and that the original publication in this journal is cited, in accordance with accepted academic practice. No use, distribution or reproduction is permitted which does not comply with these terms.*

ORIGINAL RESEARCH

published: 23 May 2022

doi: 10.3389/fpls.2022.886867



# Simulating Pine Wilt Disease Dispersal With an Individual-Based Model Incorporating Individual Movement Patterns of Vector Beetles

**Chunlei Xia<sup>1</sup>, Tae-Soo Chon<sup>2\*</sup>, Fugo Takasu<sup>3</sup>, Won Il Choi<sup>4</sup> and Young-Seuk Park<sup>5\*</sup>**

<sup>1</sup> Yantai Institute of Coastal Zone Research, Chinese Academy of Sciences, Yantai, China

<sup>2</sup> Ecology and Future Research Institute, Busan, South Korea

<sup>3</sup> Department of Environmental Science, Nara Women's University, Nara, Japan

<sup>4</sup> Division of Forest Ecology, National Institute of Forest Science, Seoul, South Korea

<sup>5</sup> Department of Biology, Kyung Hee University, Seoul, South Korea

**Edited by:**

Anna Filipiak, Institute of Plant Protection–National Research Institute, Poland

**Reviewed by:**

Yasir Khan, Zhejiang University, China

Muhammad Ozair, COMSATS University Islamabad, Pakistan

**\*Correspondence:** Young-Seuk Park, parkys@khu.ac.kr

Tae-Soo Chon, tschon.chon@gmail.com

**Specialty section:** This article was submitted to *Plant Pathogen Interactions*, a section of the journal *Frontiers in Plant Science*

**Received:** 01 March 2022

**Accepted:** 19 April 2022

**Published:** 23 May 2022

**Citation:** Xia C, Chon T-S, Takasu F, Choi WI and Park Y-S (2022) Simulating Pine Wilt Disease Dispersal With an Individual-Based Model Incorporating Individual Movement Patterns of Vector Beetles. *Front. Plant Sci.* 13:886867. doi: 10.3389/fpls.2022.886867

Individual movements of the insect vector pine sawyer beetles were incorporated into an individual-based model (IBM) to elucidate the dispersal of pine wilt disease (PWD) and demonstrate the effects of control practices. The model results were compared with the spatial data of infested pine trees in the Gijang-gun area of Busan, Republic of Korea. Step functions with long- and middle-distance movements of individual beetles effectively established symptomatic and asymptomatic trees for the dispersal of PWD. Pair correlations and pairwise distances were suitable for evaluating PWD dispersal between model results and field data at short and long scales, respectively. The accordance between model and field data was observed in infestation rates at 0.08 and 0.09 and asymptomatic rates at 0.16–0.17 for disease dispersal. Eradication radii longer than 20 m would effectively control PWD dispersal for symptomatic transmission and 20–40 m for asymptomatic transmission. However, the longer eradication radii were more effective at controlling PWD. Therefore, to maximize control effects, a longer radius of at least 40 m is recommended for clear-cutting eradication. The IBM of individual movement patterns provided practical information on interlinking the levels of individuals and populations and could contribute to the monitoring and management of forest pests where individual movement is important for population dispersal.

**Keywords:** forest pests, dispersal model, forest management, dispersal of invasive species, asymptomatic rate, control of pine wilt disease dispersal

## INTRODUCTION

Populations cause critical damage to forests because of the vulnerability of spatially contagious vegetation to disease occurrence (Bruce and Ruth, 2009). For example, pine wilt disease (PWD), caused by the pinewood nematode *Bursaphelenchus xylophilus*, is a key pest of pine trees in East Asia and Europe. PWD is vectored by the Japanese pine sawyer *Monochamus alternatus* (Mamiya, 1988; Togashi, 1988), and the spread of the disease is complex, such as association among nematodes, vectors, and host plants.

Modeling with PWD was initiated in conjunction with biological invasion processes, such as emergence, survival, dispersal, reproduction, and disease transmission (Togashi and Magira, 1981; Togashi and Shigesada, 2006). The development of the mechanistic models for PWD has two tracks. In one track, mathematical structure models were used to address overall disease transmission controlled by key parameters. Deterministic population dynamics models have been originally devised to investigate the range expansion of infected trees of PWD (Yoshimura et al., 1999a; Takasu et al., 2000). Recently, mathematical structure models have been extensively conducted for PWD, regarding global transmission dynamics, system stability and sensitivity, and optimal control strategies (e.g., Lee and Kim, 2013; Lee, 2014; Khan et al., 2018, 2020, 2021).

The second track involves the construction of spatially explicit models to present spatial heterogeneity with local rules (e.g., individual behavior) for expressing the complex dispersal processes of PWD. Two types of spatially explicit models have been developed: lattice models and individual-based models (IBMs). Regarding lattice models, Lee et al. (2007) proposed a simulation model for PWD and the pine needle gall midge based on cellular automata to illustrate the expansion of the infested area during population dispersal under field conditions. Considering the influence of infested neighborhoods and short- and long-distance movements, Nguyen et al. (2017) developed a lattice model to address the role of the asymptomatic carrier in the spread of PWD. In addition, IBMs have been developed to simulate PWD dispersal and are generally more flexible in expressing behaviors at the individual level owing to the incorporation of local rules and their link to the population level. In the present study, we incorporated a new individual movement pattern into an IBM. This study is a continuation of the work reported by Takasu (2009) in which a theoretical distribution pattern of movement was used in an IBM.

Although individual variation is an important factor in an IBM (DeAngelis and Gross, 1992; Grimm and Railsback, 2005), specific individual movement patterns, *per se*, have not been extensively incorporated into the model. Breckling et al. (1997) devised an object-oriented modeling strategy to depict the activity patterns of organisms in heterogeneous environments. Strategic forager movements (e.g., hungry and satiated exploration) were simulated in an IBM to generate home range areas responding to the distribution of food densities (South, 1999). Watkins and

Rose (2017) linked strategic movement patterns (e.g., restricted-area search and kinesis) to an IBM to demonstrate individual fitness (i.e., egg production in prey-predator dynamics). Heinz et al. (2007) incorporated individual movement patterns (e.g., correlated, spiral, and loop-like movements) specifically into IBMs to characterize generic dispersal functions in landscapes. The individual–population relationships were further analyzed to reveal the functional relationship between the parameters of the dispersal function and movement details (Heinz et al., 2007). Usually, movement patterns are situation-oriented (e.g., finding food) or theoretical (e.g., correlated random walk), and not spatially explicit in presenting individual movements.

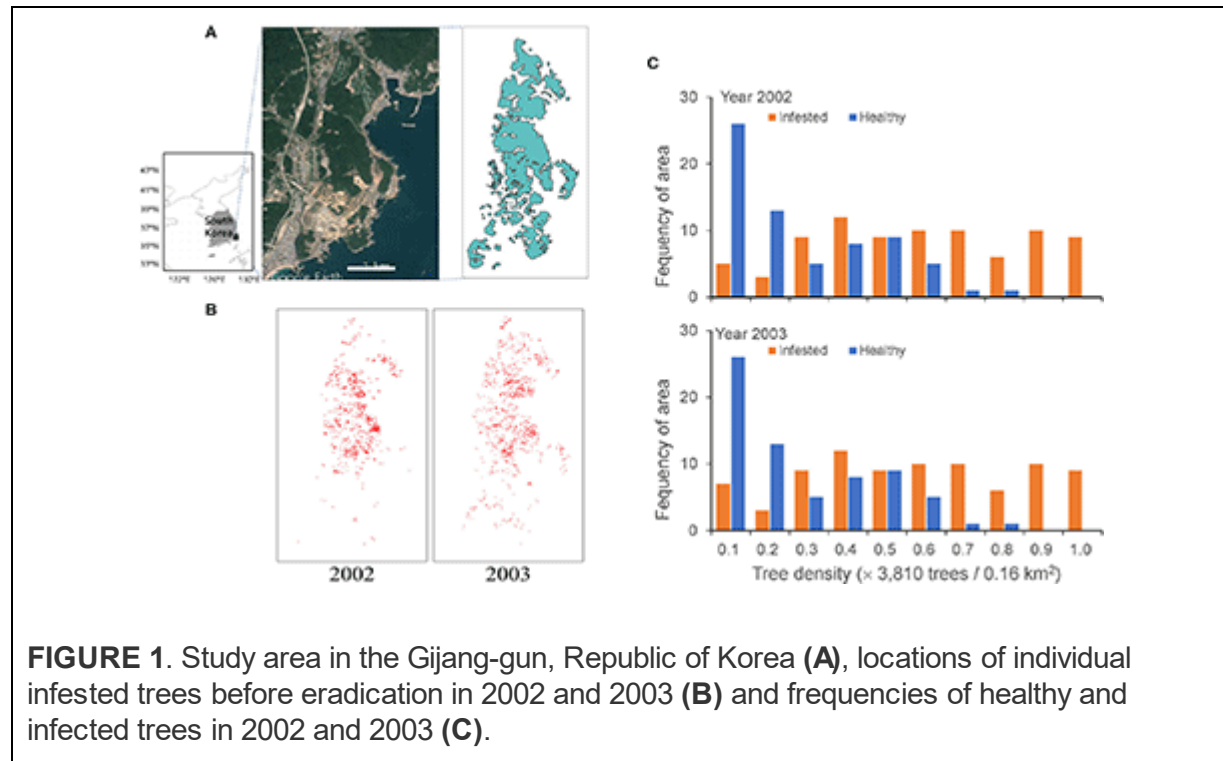
Regarding IBMs applied to PWD, Takasu (2009) linked vector beetle mobility to demonstrate the importance of the Allee effect by considering mechanistic interactions at the individual level. The IBMs were further developed by incorporating the Lévy flight of pine sawyer beetles to disperse PWD (Chon et al., 2009). We aimed to incorporate spatially explicit movement patterns of vector beetle individuals to introduce PWD expansion in forests to evaluate control practices. Specifically, in this study, (1) we hypothesized that individual movement patterns of vector beetles would be over short and long distances, (2) the individual movement patterns were incorporated into IBM to reveal PWD dispersal at the population level with symptomatic and asymptomatic transmissions, (3) model results were evaluated by comparison with field data, and (4) the models were used to recommend suitable control practices to minimize PWD infestation.

## MATERIALS AND METHODS

### Field Data of Pine Wilt Disease

Spatial data of pine trees affected by PWD in the Gijang-gun area ( $50 \text{ km}^2$ ), Busan, the southeastern corner of the Korean peninsula, were used for modeling (Figure 1). Data were obtained from the National Institute of Forest Science, Republic of Korea. The infested pine trees were individually identified in a grid of  $2 \text{ m} \times 2 \text{ m}$  using a photo-scanning technique (resolution of  $20 \mu\text{m}$  corresponding to  $12 \text{ cm}$  on the ground) from November 2002 to November 2003 (Lee and Cho, 2006) (Figure 1). Extensive control practices

were conducted by clear-cutting and infested trees were entirely burned for control at the end of each year (Kwon et al., 2006). However, PWD was still dispersed, even after extensive control, as shown in Figure 1.



## Model Development

The model was developed according to IBM guidelines, such as process overview, system definition, state variables, rules of life events, and stochasticity (Grimm et al., 2006; Chon et al., 2009).

## Process Overview

The IBM was designed to introduce the PWD dispersal by incorporating individual life events of pine sawyer beetles (*M. alternatus*), such as emergence, reproduction, movement, and infestation. Individual movement patterns were hypothesized to simulate visits to infested trees in the model. In addition, the control practices of cutting down infested trees were applied to the model, considering the extensive control practices conducted at the end of each year in Republic of Korea (Kwon et al., 2011).

## System Definition

The model was applied to field data with a width of 40 ( $= 4 \times 10$ ) km<sup>2</sup> in two dimensions (Figure 1A), assuming that every single tree is represented by a unit cell in a lattice of 2 m  $\times$  2 m. The infested trees were individually recognized in a grid of 2 m  $\times$  2 m from the high spatial resolution remote sensing data (Lee and Cho, 2006) and the data were transformed to 2,000  $\times$  5,000 cells for 40 ( $= 4 \times 10$ ) km<sup>2</sup>. The individual infested trees are presented in a lattice map from 2002 to 2003 (Figure 1B). The red dots on the map, representing infested trees, overlapped at some places due to the aggregation of infested trees.

Considering that the beetles actively move from late May to the beginning of November, the simulation period was 24 weeks (Choi and Park, 2012), assuming 4 weeks in 1 month in this model. The unit time step was defined as 1 week. The emergence of the next generation was simulated in the year following the control practices. Simulations were conducted over 2 years, matching the field survey from November 2002 to November 2003 (Figure 1) to evaluate the model results with field data, and additionally for 10 years to estimate control effects based on the selected parameters.

Absorbing boundary conditions were adopted; once any individual moved outside the study area, the individual would never return to the study area again, being considered either drowned in the sea or lost in the city. The descriptions of the variables and parameters are provided in Table 1.

**Table 1.** Component description in individual-based model (IBM) applied to the sawyer beetle transmitting pine wilt disease (PWD).

Component	Subcomponent	Description
<b>System environment</b>		
Domain	Space	2D, Lattice; 2,000 × 5,000 cells (unit: 2 × 2 m <sup>2</sup> )
	Time (t)	24-time steps per year (1 week/step)
Constraint	Boundary	Absorbing boundary
<b>Variables</b>		
Individual level	Beetle position	x, y coordinates, 2D
	Beetle status	Healthy or infested
	No. of movement	5
	Lattice status	Empty, Healthy, Symptomatic, Asymptomatic
	Asymptomatic period	1 year
	Number of beetle offspring	20 individuals/tree
	Beetle	Number of individuals
Population level	Infested trees	Number of trees (symptomatic or asymptomatic)
	Reproduction	20 progenies per tree
	Emergence period	Last week, May–1 <sup>st</sup> week, Aug.
	Dispersal distance	Step functions
	Asymptomatic trees	Random selection according to asymptomatic rate
	Control	Eradication
<b>Parameter and data</b>		
Initial conditions	Position of symptomatic trees	Randomly selected from field data
Parameters	Infestation rate (beetle visit)	0.08–0.12
	Asymptomatic rate	0.08–0.17
	Control radius	0–35 cells
Output	Population of infested trees	Number of trees (Symptomatic/Asymptomatic)
	Pair correlation of infested trees	Coefficients (not normalized)
	Pairwise distance of infested trees	Frequency of distances

## State Variables

Individual sawyer beetles were considered an entity in the model. Each individual's position, age, and movement distance were assigned as attributes. At the population level, the dispersal of PWD, either symptomatic or asymptomatic transmission by vector beetles, was presented as the predicted variable.

## Initial Distribution

The field data of the infested trees were used as the input data for the initial conditions (Figures 1A,B). Figure 1C shows the frequency of healthy and infected tree densities per unit area of 0.16 km<sup>2</sup>. A substantial proportion was similarly infected between the 2 years with 33.2 and 34.08% of infestation in 2002 and 2003, respectively. Noteworthy, the proportion of infected trees increased with an increase in total density; at a total density of 0.9–1.0 (normalized) and a maximum density of 38,130 trees per 0.16 km<sup>2</sup>, no healthy trees remained. The proportion of areas without trees was 39% of

the study area. We assumed 10% of infested trees (Korea Forest Service, 2003; Kwon et al., 2011) in November 2002 were the asymptomatic trees originating in 2001 for simulation, and the asymptotic trees were randomly selected at the beginning of the simulation period. The consecutive simulation results for the 2 years (2002 and 2003) before eradication (i.e., November) were compared with the corresponding field data.

## Life Events

The life events of sawyer beetles were simulated, such as emergence, reproduction, movement, and infestation (Kishi, 1995), to demonstrate vector dispersal and disease transmission at the population level in the model.

### ***Emergence***

Adult beetles emerged from dead (infested) pine trees in summer according to the Gaussian distribution ( $\sigma^2 = 3$ ,  $\mu = 5.5$ ) in each lattice (Naves et al., 2008):

$$f(x) = \frac{1}{\sqrt{2\pi}\sigma} \exp\left(-\frac{(x - \mu)^2}{2\sigma^2}\right) \quad (1)$$

where  $x$  is the number of adult beetles. At the beginning of each year, the emergence time of each beetle was randomly assigned within 1–10 time steps, from late May to early August.

The emerged beetles,  $F(n)$ , from each tree were calculated as follows (Yoshimura et al., 1999b; Takasu, 2009):

$$F(n) = \frac{bn}{1 + an} \quad (2)$$

where  $n$  is the number of ovipositions,  $b$  is the net reproductive success, and  $a$  is a parameter that controls the maximum number of beetles emerging from a tree (Takasu, 2009). The hyperbolic function of equation (2) shows that the emerged beetles saturated as the number of oviposition  $n$  increased owing to density-dependent mortality of the beetle larva within a tree. In our model, we assumed 20 beetles emerging from a tree with PWD in the simulation every year (Takasu, 2009), representing reproduction for the simulation in the model.

### ***Beetle Movement***

Considering that nematodes cannot move and are carried mainly by pine sawyer beetles, the movement of individual beetles plays a key role in determining the dispersal of PWD (Park et al., 2013; Choi et al., 2017; Lee et al., 2017). Therefore, we hypothesized that spatially explicit movement patterns of beetle individuals would contribute to PWD dispersal at the population level and would subsequently play a key role in controlling PWD. Emerged beetles dispersed to find trees for feeding ~1 week after emergence in the active period from May to November (Nguyen, 2010; Choi and Park, 2012; Choi et al., 2019). Infested beetles can infest healthy trees during these visits. Based on preliminary tests of movements and the literature, we assumed that an adult beetle could disperse five times randomly during the active period based on the number of movements (Togashi, 1990; Kwon et al., 2018).

Regarding the movement distance, short and long movements of the beetle were incorporated into the model. Short- and long-distance movements have been reported in the field and used for modeling (Choi et al., 2017; Nguyen et al., 2017; Lee et al., 2021). Spatially explicit movement of sawyer beetles has not been extensively reported. However, other studies have adopted a theoretical distribution, such as Gaussian (Takasu, 2009) and Lévy flight (Chon et al., 2009), as the dispersal kernel for sawyer beetle movements.

The step-function movements were devised to generate the movement patterns in this study (Figure 2). The probabilities of short and long movements are presented according to step functions; if a higher probability is given to a short distance, the individuals will move more in short distances in nearby areas and vice versa in wide areas. According to probabilities in association with distance, movement patterns of “S (1–24 cells),” “M (14–31 cells),” and “L (17–39 cells)” are presented to indicate the short, middle, and long distances, respectively (Figure 2). The pattern “W” was separately assigned to the movement demonstrating a wide range of possibilities, and the possibility of moving 10–13 cells in addition to the distance range covered by “M.” Different maximum movement distances were assigned to each minimum movement type (S, M, L, and W) with 30, 40, and 50 cells. The distances and probabilities of movements were empirically determined based on previous reports (Togashi and Magira, 1981; Yoshimura et al., 1999a; Choi et al., 2017; Lee et al., 2017) and the experience of field experts. For simplicity, numbers 3, 4, and 5 (in 10 units) were used throughout the text and figures instead of 30, 40, and 50 cells, respectively.

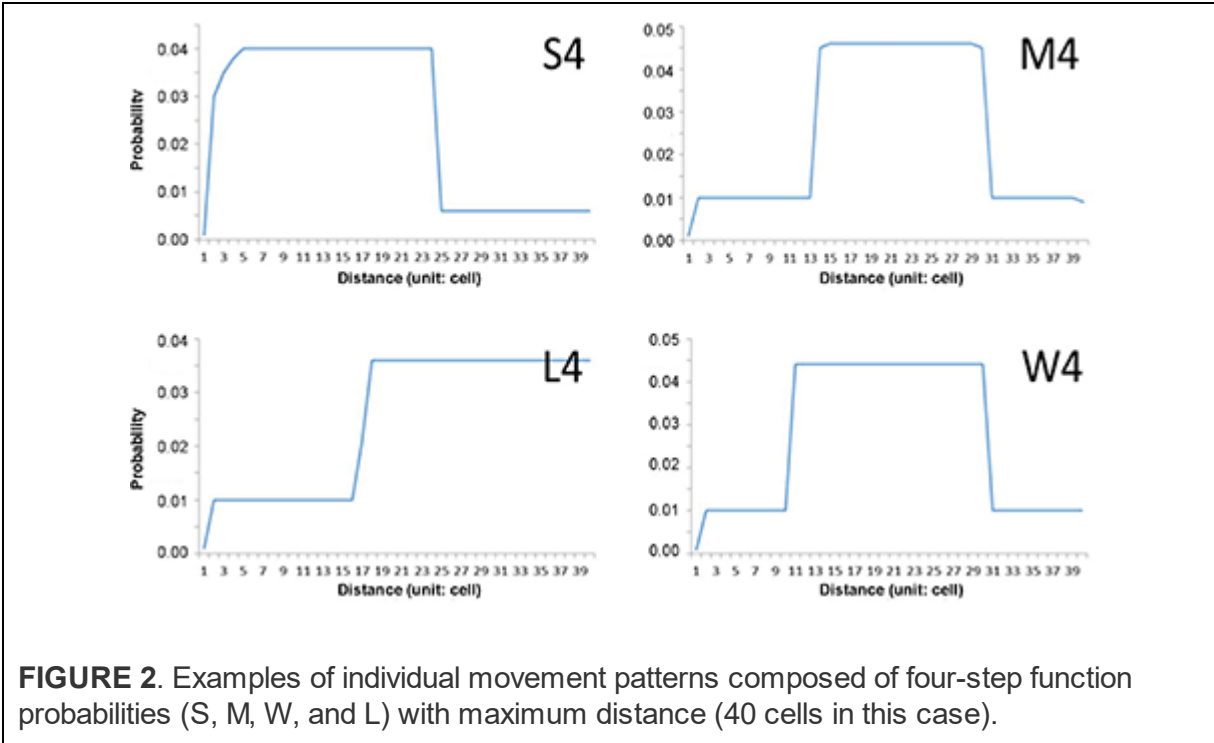


**FIGURE 2.** Examples of individual movement patterns composed of four-step function probabilities (S, M, W, and L) with maximum distance (40 cells in this case).

### **Infestation**

Healthy trees were affected by PWD after visits by nematode-carrying beetles. Most trees showed symptoms after infection in the same year. However, some infested trees did not present with symptoms of PWD in the same year but showed symptoms in the following year. These trees were considered to be asymptomatic carriers. These asymptomatic trees play an important role in the spread of PWD the following year under field conditions (Futai, 2003; Nguyen et al., 2017).

Although all symptomatic trees were removed at the end of each year according to the eradication protocols of the government, some beetles still emerged in both infested and non-infested areas. The proportion was low but sufficient to cause further dispersal in the following years (Shin, 2008; Kwon et al., 2011; Choi and Park, 2012), as shown in Figure 1. Therefore, we hypothesized that asymptomatic trees would contribute to PWD dispersal and incorporated both symptomatic and asymptomatic infestations into the model. Asymptomatic trees were determined by random choice among infested trees according to an asymptomatic rate between 0.08 and 0.17 based on field data (Shin, 2008; Nguyen et al., 2017), whereas the rest of the infested trees were set to show symptoms in the current year. The beetles moved randomly at an arbitrary angle with the assigned movement distance in each movement to

visit the infested tree in a unit cell. If there was no infested tree, then the movement was continued until the beetle found the tree with a maximum of five movements (Table 1).

### **Determining Infested Trees**

The infested tree was determined by applying the tree infestation rate by beetles at each visit. A field study showed that a proportion of pine trees that beetles attacked could survive the disease (Yoshimura et al., 1999b). When the susceptible trees had more visitors, the trees had a higher chance of infestation. The lattice state was defined as empty, healthy, symptomatic, or asymptomatic based on the infestation state (Table 1).

### **Control**

Eradication of the infested trees was used as a control method in this study and was carried out at the end of each year for the simulation period. Symptomatic trees and all their neighbors within the control radius ( $r$ ) cells were cut down. The eradication process was given as:

$$\text{Tree}(i, j) = 0; \text{ if } \sqrt{(i - x)^2 + (j - y)^2} \leq r \quad (3)$$

where  $(x, y)$  indicates the position of a symptomatic and  $(i, j)$  represents any cell in the spatial map.

The model was tested using different levels of  $r$  from 0 to 35 cells at intervals of five cells. When  $r = 0$ , cutting was conducted only on the symptomatic trees (Table 1).

### **Output Data**

The spatial dispersal pattern was analyzed using pairwise distance and pair correlation density functions. The pairwise distance (Law and Dieckmann, 2000; Nguyen et al., 2017) calculates the distances from all possible pairs of infested trees between 2 years of data:

$$D_{ij} = \sum_{i=1, j=1}^{M, N} \sqrt{(x_{1,i} - x_{2,j})^2 + (y_{1,i} - y_{2,j})^2} \quad (4)$$

where  $(x_1, i, y_1, j)$  and  $(x_2, i, y_2, j)$  are the coordinates of diseased trees between the first and second years, respectively, and  $M$  and  $N$  represent the total number of diseased trees each year. In this study, data for the consecutive years of 2002 and 2003 were used for calculating pairwise

distance, considering that these last 2 years in the survey period had data for both symptomatic and asymptomatic trees from the simulation, as stated above.

The pair correlation function,  $C(\xi, p)$ , measures the degree of association between the occurrence of infested trees across two consecutive times and is expressed as a product of pairs of densities of individuals at different locations, averaged over a spatial region (Law and Dieckmann, 2000; Nguyen et al., 2017):

$$C(\xi, p) = \frac{1}{A} \int p(x, t)[p(x+\xi, t+\tau) - \delta_x(x + \xi)]dx \quad (5)$$

where  $p(x, t)$  is the density of lattice  $i$  (or  $j$ ) at position  $x$  (or  $x + \xi$ ) at time  $t$  (or  $t + \tau$ ), and  $\xi$ ,  $\delta$ ,  $\tau$ , and  $A$  represent the space difference, time difference, Kronecker delta, and spatial region, respectively. In this study, the time difference was considered to be 1 year. Pearson's correlation coefficients were calculated to evaluate the fittings between the field data and model results for both pairwise distance and pair correlation functions.

## Stochasticity

Stochasticity was applied to the model through life events, such as emergence time and short- and long-movements with different angles. In addition, symptomatic and asymptomatic trees were randomly chosen as the initial conditions.

# RESULTS

## Pairwise Distance of Infested Trees

The dispersal of infested trees according to individual movement patterns was evaluated using field data at the population level between 2002 and 2003. Pairwise distances were compared between the model output and field data according to movement patterns (S, M, L, and W) at different maximum distances (Figure 3). Overall, the pairwise distances were in accordance with the field and model data across the different maximum distances ( $r > 0.98$ ,  $p < 0.001$ ). The frequencies of pairwise distances sharply increased to reach a peak at  $\sim 1,200$  m (arrow in Figure 3 shown at S3 as an example of

the peak). After the peak, the distances slowly decreased to reach a minimal frequency beyond 6,000 m. Overall, the model results tended to slightly overestimate compared with the field data as the distance was longer than the peak distance of 1,200 m (the dotted ellipse shown in S4 in Figure 3 as an example). S3 showed the minimum difference between the model results and field data among all movement patterns (top left panel, Figure 3).

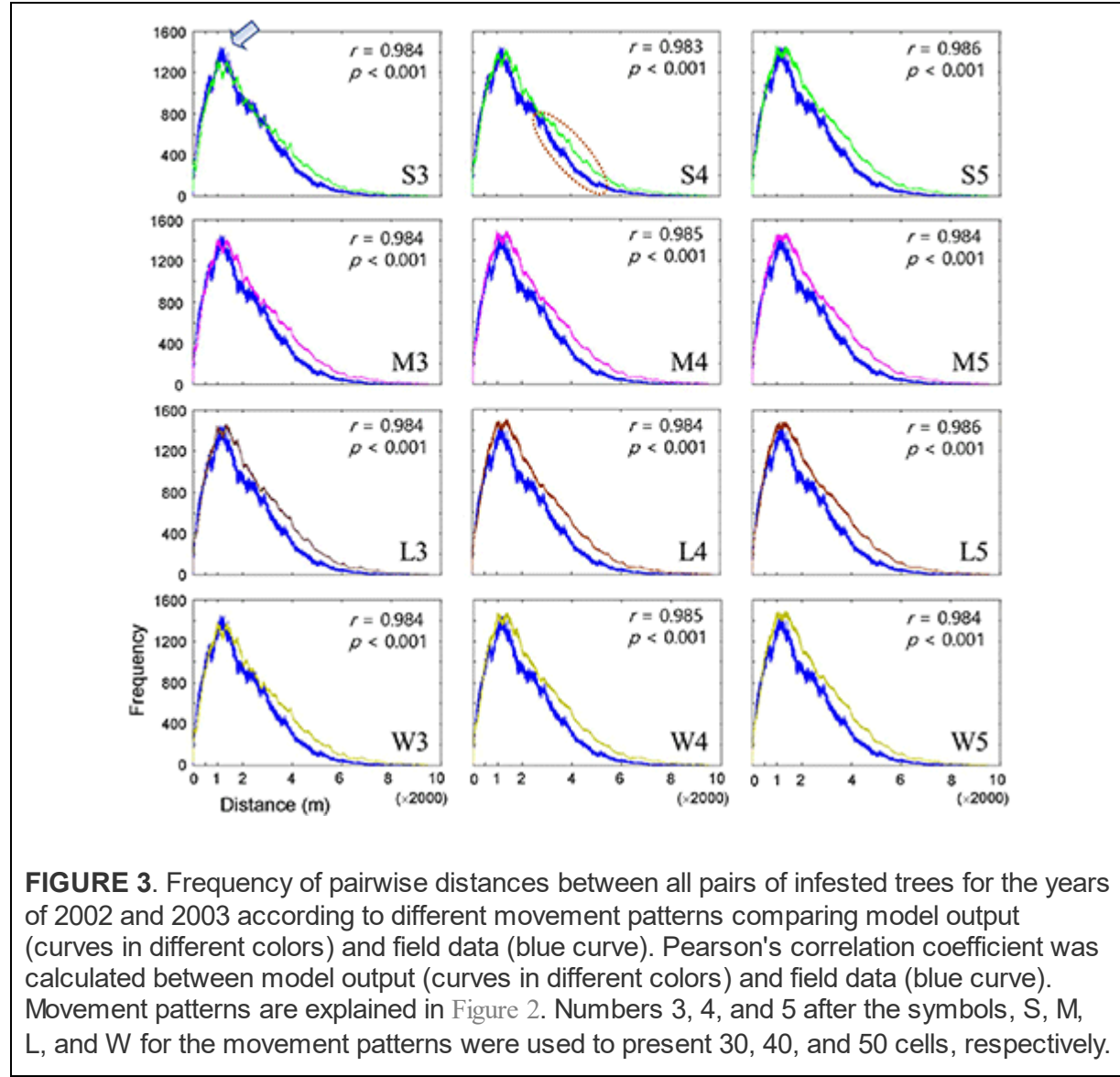
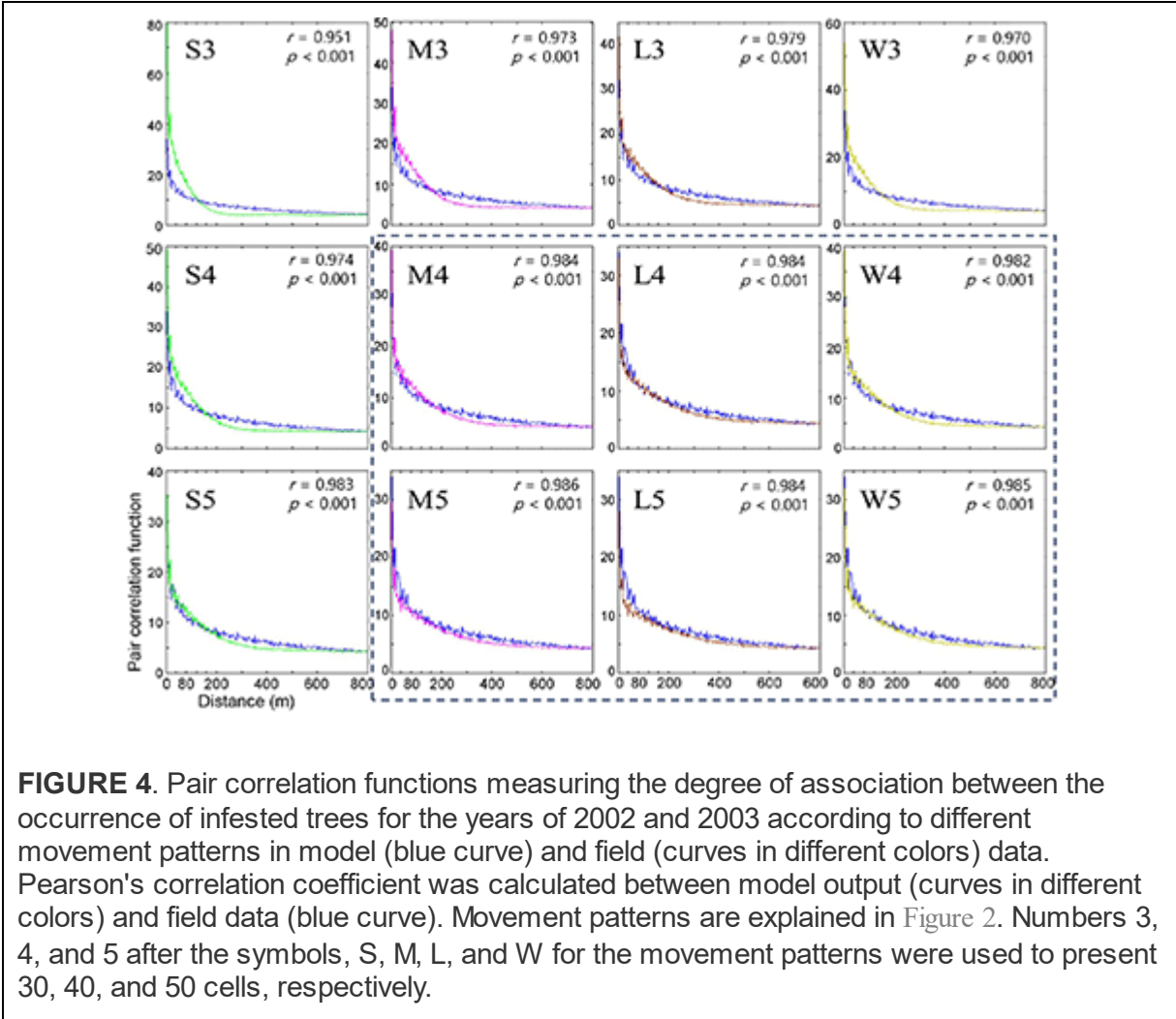


**FIGURE 3.** Frequency of pairwise distances between all pairs of infested trees for the years of 2002 and 2003 according to different movement patterns comparing model output (curves in different colors) and field data (blue curve). Pearson's correlation coefficient was calculated between model output (curves in different colors) and field data (blue curve). Movement patterns are explained in Figure 2. Numbers 3, 4, and 5 after the symbols, S, M, L, and W for the movement patterns were used to present 30, 40, and 50 cells, respectively.

## Pair Correlation

Subsequently, the pair correlation functions (not normalized) according to the distances between infested trees were compared between the model and field data between 2002 and 2003 (Figure 4). The model's correlation coefficients

were similar to those of the field data ( $r > 0.95$ ,  $p < 0.001$ ). However, the correlations decreased rapidly as distance increased. Although rapidly decreasing, correlation coefficients remained at a substantial level  $\sim 100$  m, indicating spatial associations in disease occurrence between the previous and current years in a short distance.



Overall, the fittings between the field data and model results for the pair correlation functions were close to M, L, and W with maximum distances of 40 and 50 cells ( $r > 0.982$ ,  $p < 0.001$ ) (Figure 4), compared with S at short maximum distances. However, for some movement patterns, the model results overestimated correlations (higher than the model results) for distances less than  $\sim 60$  m, while the model results underestimated correlations (higher than the model results) beyond this distance. This

discrepancy was more clearly observed with the S pattern and the maximum distance of 30 cells ( $r = 0.951, p < 0.001$ ) (S3, top left panel, Figure 4).

When the degree of fitting was directly compared between the pairwise distance (Figure 3) and correlation functions (Figure 4), the pattern of discrepancy was comparable between the two evaluation methods. For example, for pattern S3, the pairwise distance from the model was fairly close between the field data and model results with slight overestimation over a relatively long-range, 3,000 – 6,000 m. In contrast, the correlation function obtained from the model was differentiated from the field data in a short spatial scale, with overestimation at less than 60 m and underestimation beyond 60 m.

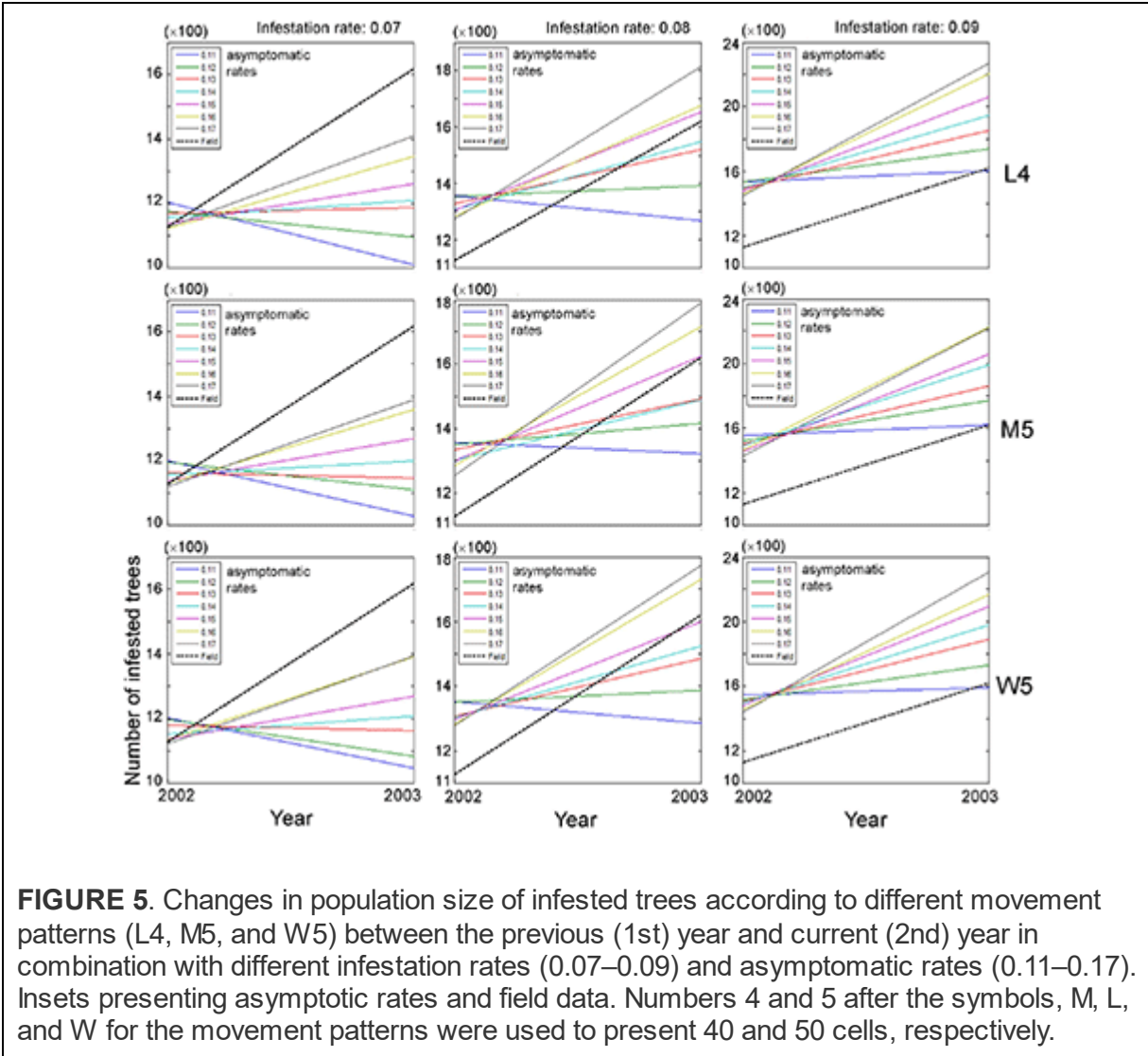
Considering the closest fitting for the pair correlation function for the movement patterns M, L, and W, a maximum distance of 50 cells was matched to M and W, whereas 40 cells were assigned to L, with the highest degree of closeness in the correlation function between the field data and model results for each movement pattern (Figure 4). Compared with S3, the fittings by M5, W5, and L4 were fairly close between the model results and field data for both pairwise distances and pair correlations, except for a slight overestimation in pairwise distances in the long-range after the peak.

Notably, the pairwise distance and correlation functions have different roles in fitting the field data by considering the spatial scale. The pair correlation had higher values at short distances (1–400 m range), indicating the reliability of the fitting at short distances. In contrast, pairwise distance represents fitting over a broad range with a long distance (1–8,000 m) (Figures 3, 4).

The results stated above can be summarized as follows. First, the model fitting was closer to the real data according to the correlation functions and pairwise distances. Second, pairwise distance revealed the model fitting broadly on the long scale, whereas the correlation function was more suitable for fitting to field data on a short scale. Third, the movement patterns with long movements, such as M, L, and W, were more closely fitted to the field data than S but there was no notable difference among them. Fourth, the maximum distances of 40 and 50 cells had a better fitting than the short maximum distance of 30 cells.

## **Population Size According to Individual Movement Patterns**

Based on the closeness between model and field data, we selected movement patterns (L4, M5, and W5), and the dispersal of PWD was simulated at the population level. The asymptomatic and infestation rates were optimally adjusted in combination with 0.11–0.17 and 0.07–0.09, respectively, to fit the field data. Changes in the population size of infested trees were evaluated between the previous (2002) and current (2003) years across different asymptomatic and infestation rates (Figure 5). Overall, the absolute densities of infested trees were not in accord with the simulation output and field data, as shown by the substantial difference in the intercept between the model results and field data (dotted lines, Figure 5). Instead, the trends of density changes between the 2 years had some meaningful results: the slopes in population densities were comparable between model output and field data. Overall, accordance between model and field data was observed in infestation rates of 0.08 and 0.09, and high asymptotic rates of 0.16–0.17 (Figure 5). However, the slopes were not in accordance with the case of an infestation rate equal to 0.07 across different ranges of asymptotic rates (left panels, Figure 5).

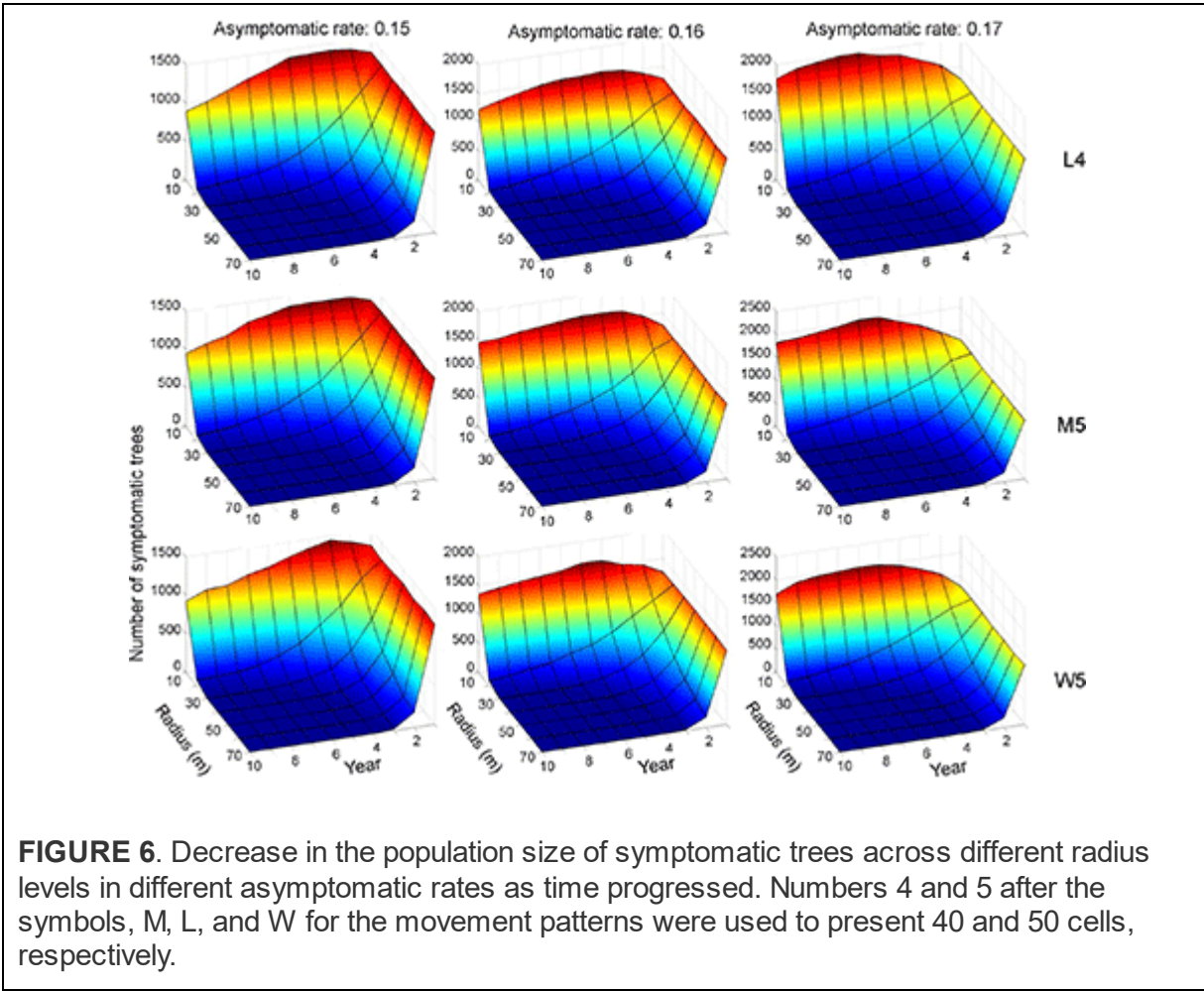


The overall optimum value of the infestation rate observed was 0.09 in fitting the population of diseased trees in field conditions compared with the infestation rates of 0.07 and 0.08, since the increasing trend of the diseased population between 2 years was more consistently observed in a narrower range across different asymptomatic ranges with the infestation rate equal to 0.09 (right panels, Figure 5).

## Control Effects

Control practices were conducted with different eradication radii ( $r$ ) between 10 and 70 m. Simulations were run for 10 years separately for each movement pattern (L4, M5, and W5). Figures 6, 7 show symptomatic and asymptomatic population densities, respectively, according to different

parameters suggested in the previous section (infestation rate equal to 0.09, asymptotic rates equal to 0.15, 0.16, and 0.17). In total, 20 simulations were performed for each parameter combination, and the averages are shown in Figures 6, 7. Regarding symptomatic trees, if the radius was equal to or longer than 20 m, then the eradication practices led to control effects across different parameter levels by showing low densities. The longer radius elicited a more effective control effect. The densities of infested trees were close to zero, mostly starting with the 2nd year, without much difference in movement patterns (Figure 6).



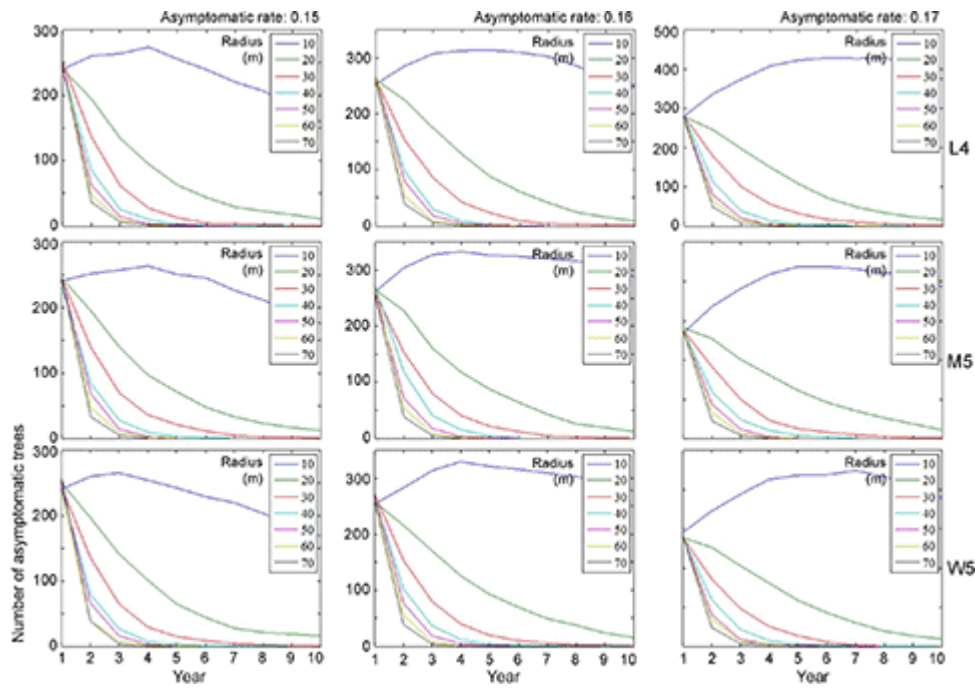


**FIGURE 7.** Decrease in the population size of asymptomatic trees across different radius levels in different asymptomatic rates as time progressed. Insets indicating control radius (m). Numbers 4 and 5 after the symbols, M, L, and W for the movement patterns were used to present 40 and 50 cells, respectively.

Regarding asymptomatic trees, an eradication radius  $> 20$  m also showed a substantial decrease in the densities of asymptomatic trees starting from the 2nd year (Figure 7). In the last 10 years of simulation, the densities approached zero across all different movement patterns and asymptotic rates. Furthermore, infestation population size decreased with the increasing eradication radius, more rapidly with a longer radius (Figure 7). In contrast, with a control radius of 10 m, the densities of asymptomatic trees were invariably high across different parameter levels.

Although there was some variability, the asymptomatic densities decreased immediately after the 2nd year when the control radius was equal to or  $> 40$  m (Figure 7). With a shorter eradication radius of 20–30 m, the densities decreased by  $\sim 50\%$  between the 3rd and 5th years. Notably, the densities of asymptomatic trees tended to decrease linearly as time progressed when the radius was 20 m. A radius of 30 m showed a rapid decrease in asymptomatic trees compared with a 20-m radius within 3–4 years. Regarding maximum control,  $\sim 87\%$  of infested trees would be

controlled in the 2nd year if the radius was equal to 70 m, with an asymptomatic rate equal to 0.15 (Figure 7).

## DISCUSSION

The present study demonstrated an individual-population relationship, specifically interlinking individual movement behavior to infested population dispersal. Individual movement patterns were effectively incorporated into the IBM to demonstrate the population dispersal of infested trees with the symptomatic and asymptomatic transmission of PWD. Evaluation with the pairwise distance and pair correlation function (Figures 3, 4) suggested suitable movement types with long-distance movement and high levels of maximum distances (i.e., M5, L4, and W5).

Although previous IBM studies have been applied to PWD using Gaussian distribution (Takasu, 2009) and Lévy flight (Chon et al., 2009), this type of step function has never been incorporated into IBMs. Pairwise distances and correlation functions were specifically effective at different spatial scales in presenting closeness to field data at the population level; the pair correlation function was effective at revealing the model performance over short distances, while pairwise distance represented the fitting at long distances in a broad range (Figures 3, 4). These types of spatial fitting would suggest an effective means of evaluating individual-population relationships addressed by IBMs across spatial distances.

Pairwise distances were slightly overestimated by the model beyond the peak at a distance of 1,200 m across different movement types (dotted ellipse in the middle subfigure of the top row in Figure 3 as an example) compared with the field data. These results indicated that simulated beetles moved more broadly as they dispersed away from their initial positions compared with the field data, but clear reasons for this discrepancy were not found in the current study. Future studies should be carried out on spatial analyses of simulated movements of individuals in combination with field experiments.

Notably, the pair correlation function frequencies were overestimated at distances  $< 80$  m and underestimated at distances  $> 80$  m, as representatively observed with S3 (Figures 3, 4). It remains unclear why this type of discrepancy was more strongly observed at short maximum distances for S3 and M3 but was not evident for M, L, and W over long distances of 40 and

50 cells (Figure 4). Further studies are warranted to carry out spatiotemporal analyses of the model results.

The IBM linked to individual movement patterns was effective at finding suitable ranges for controlling PWD. The model suggested that control practices using an eradication radius of 20 m with an infestation rate equal to 0.09 and an asymptotic rate of 0.15–0.17 across different movement patterns (M5, L4, and W5) would be effective for both symptomatic and asymptomatic transmissions (Figures 5, 6). Although short eradication radii in the range of 20–40 m would effectively control asymptomatic transmission, it would take a longer time (i.e., several years) to completely eradicate the PWD (Figure 7). Therefore, longer radii, at least 40 m, would be needed for clear-cutting eradication. Overall, the model results are consistent with those reported by Kwon et al. (2011) regarding the effectiveness of eradicating all trees surrounding the infested trees. IBMs incorporating individual movement patterns were informative for designing control practices under field conditions.

The step function was compared with alternative functions (e.g., Gaussian and exponential) regarding the probability of determining different movement distances in the preliminary tests. However, we could not produce similar patterns for PWD dispersal with these alternative functions. In particular, the sharp peak at a short distance in pairwise distances (arrow in Figure 3 as an example) was unproduceable under similar simulation conditions. A comparison of different movement types to reveal population dispersion will be carried out in a future study. In our model, the absolute densities could not be estimated close to the actual values under field conditions (Figure 5). Numerous factors would be involved in determining densities under field conditions in a complex manner, such as reproduction of vector beetles and nematodes, the transmission of PWD through trees and vectors, environmental effects, and control efforts. Further studies regarding additional modeling and field surveys are warranted. Along with obtaining more detailed output from IBMs, mathematical structure models could be developed to simulate system stability realistically and provide optimal control strategies for field conditions in the future (Khan et al., 2018, 2020, 2021).

## CONCLUSION

Individual movements of the insect vector and pine sawyer beetle, were incorporated into an IBM in  $2\text{ m} \times 2\text{ m}$  units to elucidate the dispersal of trees infested with PWD and evaluate forest pest control practices. Individual movement patterns over short and long distances consisting of step functions were effective at presenting the dispersal of vector beetles under field conditions. After evaluating the field data for each infested tree, a close-fitting between the model results and field data was observed with pair correlation and pairwise distances. Pair correlation effectively fitted PWD dispersal, presenting correlational relationships over a short distance (i.e., 100 m). Pairwise distances were available for fitting the model results and field data over a long-range (1–8,000 m), including peaking distances between infested trees. The accordance between model and field data was observed through the simulation of infestation rates at 0.08 and 0.09 and asymptotic rates at 0.16–0.17. An eradication radius longer than 20 m would effectively control PWD dispersal for symptomatic transmission and one of 20–40 m would work for asymptomatic transmission. However, to maximize the control effects, longer radii of at least 40 m are recommended for clear-cutting eradication. Further studies are required to estimate absolute densities and analyze partially observed over- and under-estimations in the pair correlation and pairwise distances. Additional analyses on system stability and optimized control strategies could be conducted with further development of mathematical structure models coupled with the accumulation of information from IBMs. IBMs incorporating individual movement patterns effectively provided practical information for pest management by interlinking information on individual-population relationships and would contribute to develop monitoring and managing strategies for forest pests when individual movement is important for population dispersal.

## DATA AVAILABILITY STATEMENT

The original contributions presented in the study are included in the article/supplementary material, further inquiries can be directed to the corresponding authors.

# AUTHOR CONTRIBUTIONS

CX, T-SC, and Y-SP designed the concept and wrote the article with contributions from FT and WC. CX developed and simulated the model. FT and WC revised the model and its parameters. T-SC and Y-SP prepared the visualization. All authors contributed to the article and approved the submitted version.

# FUNDING

This study was supported by the National Institute of Forest Science and the R&D Program for Forest Science Technology (FTIS 2017042A00-1823-CA01) provided by the Korea Forest Service (Korea Forestry Promotion Institute).

# ACKNOWLEDGMENTS

We are grateful to the late Dr. Heung-Soo Kim for his contribution to this study regarding movement model design and testing.

# REFERENCES

Breckling, B., Reuter, H., and Middelhoff, U. (1997). An object oriented modelling strategy to depict activity pattern of organisms in heterogeneous environments. *Environ. Model. Assess.* 2, 95–104. doi: 10.1023/A:1019092823578

Bruce, H., and Ruth, M. (2009). *Dynamic Modeling of Disease and Pests*. New York: Springer.

Choi, W. I., Nam, Y., Lee, C. Y., Choi, B. K., Shin, Y. J., Lim, J.-H., et al. (2019). Changes in major insect pests of pine forests in Korea over the last 50 years. *Forests*. 10, 692. doi: 10.3390/f10080692

Choi, W. I., and Park, Y.-S. (2012). Dispersal patterns of exotic forest pests in South Korea. *Insect Sci.* 19, 535–548. doi: 10.1111/j.1744-7917.2011.01480.x

Choi, W. I., Song, H. J., Kim, D. S., Lee, D.-S., Lee, C.-Y., Nam, Y., et al. (2017). Dispersal patterns of pine wilt disease in the early stage of its invasion in South Korea. *Forests*. 8, 411. doi: 10.3390/f8110411

Chon, T.-S., Lee, S. H., Jeoung, C., Cho, H. K., and Chung, Y.-Y. (2009). “Individual based models,” in *Handbook of Ecological Modeling and Informatics*, eds. S.E. Jørgensen, T.-S. Chon and F. Recknagel (Southampton, UK: WIT Press), 99–114. doi: 10.2495/978-1-84564-207-5/07

DeAngelis, D. L., and Gross, L. J. (1992). *Individual-Based Models and Approaches in Ecology: Populations, Communities and Ecosystems*. New York: Chapman and Hall. doi: 10.1007/978-1-4757-0869-1

Futai, K. (2003). Role of asymptomatic carrier trees in epidemic spread of pine wilt disease. *J. For. Res.* 8, 253–260. doi: 10.1007/s10310-003-0034-2

Grimm, V., Berger, U., Bastiansen, F., Eliassen, S., Ginot, V., Giske, J., et al. (2006). A standard protocol for describing individual-based and agent-based models. *Ecol. Modell.* 198, 115–126. doi: 10.1016/j.ecolmodel.2006.04.023

Grimm, V., and Railsback, S. F. (2005). *Individual-Based Modeling and Ecology*. Princeton, NJ: Princeton University Press. doi: 10.1515/9781400850624

Heinz, S., Wissel, C., Conradt, L., and Frank, K. (2007). Integrating individual movement behaviour into dispersal functions. *J. Theor. Biol.* 245, 601–609. doi: 10.1016/j.jtbi.2006.12.009

Khan, M. A., Ahmed, L., Mandal, P. K., Smith, R., and Haque, M. (2020). Modelling the dynamics of Pine Wilt Disease with asymptomatic carriers and optimal control. *Sci. Rep.* 10, 11412–11412. doi: 10.1038/s41598-020-67090-7

Khan, M. A., Khan, R., Khan, Y., and Islam, S. (2018). A mathematical analysis of Pine Wilt disease with variable population size and optimal control strategies. *Chaos, Solitons and Fractals*. 108, 205–217. doi: 10.1016/j.chaos.2018.02.002

Khan, R. A., Hussain, T., Ozair, M., Tasneem, F., and Faizan, M. (2021). Dynamical features of pine wilt disease through stability, sensitivity and optimal control. *Adv. Differ. Equ.* 2021, 261. doi: 10.1186/s13662-021-03411-y

Kishi, Y. (1995). *The Pine Wood Nematode and the Japanese Pine Sawyer*. Tokyo, Japan: Thomas Company Limited.

Korea Forest Service. (2003). *Effect of Chemical Treatment of Wilt Pine Trees on Epidemic Activity of Pine Wilt Disease Caused by Pine Wood Nematode*. Daejeon, Korea (in Korean).

Kwon, H. J., Jung, J.-K., Jung, C., Han, H., and Koh, S.-H. (2018). Dispersal capacity of *Monochamus saltuarius* on flight mills. *Entomol. Exp. Appl.* 166, 420–427. doi: 10.1111/eea.12686

Kwon, T.-S., Shin, J. H., Lim, J.-H., Kim, Y.-K., and Lee, E. J. (2011). Management of pine wilt disease in Korea through preventative silvicultural control. *For. Ecol. Manag.* 261, 562–569. doi: 10.1016/j.foreco.2010.11.008

Kwon, T. S., Lim, J. H., Sim, S. J., Kwon, Y. D., Son, S. K., Lee, K. Y., et al. (2006). Distribution patterns of *Monochamus alternatus* and *M. saltuarius* (Coleoptera: Cerambycidae) in Korea. *Jour. Korean For. Soc.* 95, 543–550. Available online at: <https://www.koreascience.or.kr/article/JAKO200610103460923.page>

Law, R., and Dieckmann, U. (2000). “Moment Approximations of Individual-based Models,” in *The Geometry of Ecological Interactions: Simplifying Spatial Complexity*, eds. U. Dieckmann, R. Law and J. Metz (Cambridge: Cambridge University Press), 252–270. doi: 10.1017/CBO9780511525537.017

Lee, D.-S., Choi, W. I., Nam, Y., and Park, Y.-S. (2021). Predicting potential occurrence of pine wilt disease based on environmental factors in South Korea using machine learning algorithms. *Ecol. Inform.* 64, 101378. doi: 10.1016/j.ecoinf.2021.101378

Lee, D.-S., Nam, Y., Choi, W. I., and Park, Y.-S. (2017). Environmental factors influencing on the occurrence of pine wilt disease in Korea. *Korean J. Ecology and Environment*. 50, 374–380. doi: 10.11614/KSL.2017.50.4.374

Lee, K. S. (2014). Stability analysis and optimal control strategy for prevention of pine wilt disease. *Abstr. Appl. Anal.* 2014, 182680. doi: 10.1155/2014/182680

Lee, K. S., and Kim, D. (2013). Global dynamics of a pine wilt disease transmission model with nonlinear incidence rates. *Appl. Math. Model.* 37, 4561–4569. doi: 10.1016/j.apm.2012.09.042

Lee, S. D., Park, S., Park, Y.-S., Chung, Y.-J., Lee, B.-Y., and Chon, T.-S. (2007). Range expansion of forest pest populations by using the lattice model. *Ecol. Modell.* 203, 157–166. doi: 10.1016/j.ecolmodel.2006.04.031

Lee, S. H., and Cho, H. K. (2006). “Detection of the pine trees damaged by pine wilt disease using high spatial remote sensing data”, in *ISPRS Commission VII Mid-TermSymposia Remote Sensing from Pixels to Processes*, eds N. Kerle and A. Skidmore (Enschede: ISPRS), 8–11.

Mamiya, Y. (1988). History of pine wilt disease in Japan. *J. Nematol.* 20, 219–226. Available online at: <https://pubmed.ncbi.nlm.nih.gov/19290205/>

Naves, P. M., Sousa, E., and Rodrigues, J. M. (2008). Biology of *Monochamus galloprovincialis* (Coleoptera, Cerambycidae) in the pine wilt disease affected zone, southern Portugal. *Silva Lusiana.* 16, 133–148.

Nguyen, T. V. (2010). *Dispersal of pine wilt disease using spatially explicit model and cross-correlation analysis*(Ph.D. thesis). Pusan National University, Busan, Republic of Korea.

Nguyen, T. V., Park, Y.-S., Jeoung, C.-S., Choi, W.-I., Kim, Y.-K., Jung, I.-H., et al. (2017). Spatially explicit model applied to pine wilt disease dispersal based on host plant infestation. *Ecol. Modell.* 353, 54–62. doi: 10.1016/j.ecolmodel.2016.10.022

Park, Y.-S., Chung, Y.-J., and Moon, Y.-S. (2013). Hazard ratings of pine forests to a pine wilt disease at two spatial scales (individual trees and stands) using self-organizing map and random forest. *Ecol. Inform.* 13, 40–46. doi: 10.1016/j.ecoinf.2012.10.008

Shin, S. C. (2008). “*Pine Wilt Disease in Korea*,” in *Pine Wilt Disease*, eds B.G. Zhao, K. Futai, J.R. Sutherland and Y. Takeuchi (Tokyo, Japan: Springer).

South, A. (1999). Extrapolating from individual movement behaviour to population spacing patterns in a ranging mammal. *Ecol. Modell.* 117, 343–360. doi: 10.1016/S0304-3800(99)00015-0

Takasu, F. (2009). Individual-based modeling of the spread of pine wilt disease: vector beetle dispersal and the Allee effect. *Popul. Ecol.* 51, 399–409. doi: 10.1007/s10144-009-0145-5

Takasu, F., Yamamoto, N., Kawasaki, K., Togashi, K., Kishi, Y., and Shigesada, N. (2000). Modeling the expansion of an introduced tree disease. *Biol. Invasions.* 2, 141–150. doi: 10.1023/A:1010048725497

Togashi, K. (1988). Population density of *Monochamus alternatus* adults (Coleoptera: Cerambycidae) and incidence of pine wilt disease caused by *Bursaphelenchus xylophilus* (Nematoda: Aphelenchoididae). *Res. Popul. Ecol.* 30, 177–192. doi: 10.1007/BF02513243

Togashi, K. (1990). A field experiment on dispersal of newly emerged adults of *Monochamus alternatus* (Coleoptera: Cerambycidae). *Popul. Ecol.* 32, 1–13. doi: 10.1007/BF02512586

Togashi, K., and Magira, H. (1981). Age-specific survival rate and fecundity of the adult Japanese pine sawyer *Monochamus alternatus* Hope (Coleoptera: Cerambycidae), at different emergence times. *Appl. Entomol. Zool.* 16, 351–361. doi: 10.1303/aez.16.351

Togashi, K., and Shigesada, N. (2006). Spread of the pinewood nematode vectored by the Japanese pine sawyer: modeling and analytical approaches. *Popul. Ecol.* 48, 271–283. doi: 10.1007/s10144-006-0011-7

Watkins, K. S., and Rose, K. A. (2017). Simulating individual-based movement in dynamic environments. *Ecol. Modell.* 356, 59–72. doi: 10.1016/j.ecolmodel.2017.03.025

Yoshimura, A., Kawasaki, K., Takasu, F., Togashi, K., Futai, K., and Shigesada, N. (1999a). Modeling the spread of pine wilt disease caused by nematodes with pine sawyers as vector. *Ecology.* 80. doi: 10.1890/0012-9658(1999)080(1691:MTSOPW)2.0.CO

Yoshimura, A., Kawasaki, K., Takasu, F., Togashi, K., Futai, K., and Shigesada, N. (1999b). Modeling the spread of pine wilt disease caused by nematodes with pine sawyers as vector. *Ecology*. 80, 1691–1702. doi: 10.1890/0012-9658(1999)080(1691:MTSOPW)2.0.CO;2

**Conflict of Interest:** The authors declare that the research was conducted in the absence of any commercial or financial relationships that could be construed as a potential conflict of interest.

**Publisher's Note:** All claims expressed in this article are solely those of the authors and do not necessarily represent those of their affiliated organizations, or those of the publisher, the editors and the reviewers. Any product that may be evaluated in this article, or claim that may be made by its manufacturer, is not guaranteed or endorsed by the publisher.

*Copyright © 2022 Xia, Chon, Takasu, Choi and Park. This is an open-access article distributed under the terms of the Creative Commons Attribution License (CC BY). The use, distribution or reproduction in other forums is permitted, provided the original author(s) and the copyright owner(s) are credited and that the original publication in this journal is cited, in accordance with accepted academic practice. No use, distribution or reproduction is permitted which does not comply with these terms.*

ORIGINAL RESEARCH

published: 31 May 2022

doi: 10.3389/fpls.2022.862594



# UGT440A1 Is Associated With Motility, Reproduction, and Pathogenicity of the Plant-Parasitic Nematode *Bursaphelenchus xylophilus*

**Min Wang<sup>1</sup>, Guicai Du<sup>2</sup>, Junna Fang<sup>3</sup>, Linsong Wang<sup>4</sup>, Qunqun Guo<sup>2</sup>, Tingting Zhang<sup>2</sup> and Ronggui Li<sup>2\*</sup>**

<sup>1</sup>Medical College, Qingdao University, Qingdao, China

<sup>2</sup>College of Life Sciences, Qingdao University, Qingdao, China

<sup>3</sup>Qingdao JiMo People's Hospital, Qingdao, China

<sup>4</sup>Institute of Oceanology, Chinese Academy of Sciences, Qingdao, China

**Edited by:**

Ryoji Shinya, Meiji University, Japan

**Reviewed by:**

Lee Robertson, National Institute of Agricultural and Food Research and Technology, Spain

Claudia S. L. Vicente, University of Évora, Portugal

**\*Correspondence:** Ronggui Li, lrg@qdu.edu.cn

**Specialty section:** This article was submitted to Plant Pathogen Interactions, a section of the journal *Frontiers in Plant Science*

**Received:** 26 January 2022

**Accepted:** 11 May 2022

**Published:** 31 May 2022

**Citation:** Wang M, Du G, Fang J, Wang L, Guo Q, Zhang T and Li R (2022) UGT440A1 Is Associated With Motility, Reproduction, and Pathogenicity of the Plant-Parasitic Nematode *Bursaphelenchus xylophilus*. *Front. Plant Sci.* 13:862594. doi: 10.3389/fpls.2022.862594

Pine wilt disease (PWD) caused by *Bursaphelenchus xylophilus* is considered a major threat to pine forests worldwide. Uridine diphosphate (UDP)-glycosyltransferases (UGTs) catalyze the conjugation of small lipophilic compounds with sugars and play crucial roles in the detoxification and homeostatic processes in all living organisms. We investigated the molecular characteristics and biological functions of the gene *UGT440A1* that encodes UGTs in *B. xylophilus*. The *in situ* hybridization results indicated that *UGT440A1* is expressed in all developmental stages of *B. xylophilus*, particularly in the head, intestine, and hypodermis of the second-stage of juveniles (J2), third-stage of juveniles (J3) and fourth-stage of juveniles (J4) females and in almost the whole body of J4 males and adults. Recombinant *UGT440A1* was observed mainly in the inclusion bodies, and the enzyme activity assay revealed that *UGT440A1* could catalyze the glycosylation reaction of two types of flavonols (kaempferol and quercetin). RNA interference (RNAi) of *UGT440A1* suppressed motility, feeding, and reproduction of *B. xylophilus*. Furthermore, *UGT440A1* knockdown caused a delay in the development of PWD symptoms in the pine seedlings inoculated with the nematodes. These results suggest that *UGT440A1* is involved in the pathogenic process of *B. xylophilus* and the information may facilitate a better understanding of the molecular mechanism of PWD.

**Keywords:** *Bursaphelenchus xylophilus*, UDP-glycosyltransferase, motility, reproduction, pathogenicity

## INTRODUCTION

Pine wilt disease (PWD) caused by pine wood nematode (PWN) *Bursaphelenchus xylophilus* is one of the most serious diseases that has caused considerable damage to pine forests in East Asia, North America, and Europe (Nickle et al., 1981; Mamiya, 1983; Mota et al., 1999; Penas et al., 2004; Zhao et al., 2008; Futai, 2013). Owing to the rapid spread of PWD and high mortality of host trees, this nematode is considered a major threat to pine forests worldwide and has been extensively studied (Futai, 2013; Modesto et

al., 2021; Shinya et al., 2021). Despite several attempts to control the spread of the disease, no effective control method is available to date because of the poorly understood pathogenic mechanism of PWD (Jones et al., 2008). In Asia, *B. xylophilus* is transmitted from dead to healthy pine trees by the vector beetles. The nematode migrates to pine trees through wounds created by the feeding of insect vector, *Monochamus spp.* (Futai, 2013). The life cycle of the nematode, following invasion, comprises a phytophagous phase and a mycophagous phase. In the phytophagous phase, the nematode infects a tree, feeds on the epithelial cells, and leads to lethal wilting. Subsequently, the infected pines produce ethanol, monoterpenes and other volatile compounds (Ikeda and Oda, 1980). In our recent study, we found that a low concentration of ethanol derived by the host tree could promote the growth of *B. xylophilus* population and that a UGT gene-encoded enzyme UDP-glycosyltransferase (UGT) was significantly upregulated when PWNs were treated with ethanol (Wang et al., 2022).

UGTs are generally present in diverse organisms from bacteria to humans. These enzymes catalyze the transfer of glucose from UDP-glucose or other substrate donors to the substrate acceptors and play a crucial role in detoxification of endogenous and exogenous substances (Hundle et al., 1992; Bock, 2003). *B. xylophilus* must resist or metabolize the nematicidal substances produced by the pines once it invades a pine tree (Mamiya, 2012). The detoxification process mediated by these nematodes has been divided into three phases: the addition of functional groups to molecules (phase I); the actual detoxification reactions (phase II); and efflux (phase III) (Lindblom and Dodd, 2009). UGTs are one of the two main families of enzymes involved in phase II. Studies on UGTs in nematodes have mainly focused on investigating nematode resistance to xenobiotics. In parasitic nematodes, the increased activity of UGTs could protect the nematodes against drug toxicity and contribute to drug resistance (Vokral et al., 2012). Fontaine and Choe reported a resistance-related UGT that conferred high tolerance toward albendazole to *Caenorhabditis elegans* (Fontaine and Choe, 2018). Additionally, the investigation of the UGT family in *H. contortus* revealed significant sex differences in the expression levels of several UGTs (Matouskova et al., 2018). However, the molecular characteristics and biological functions of UGT gene in the nematodes remain poorly understood.

Based on the transcriptome analysis results for *B. xylophilus* related to the response to host-derived ethanol, we hypothesize that the upregulated UGT

gene might not only participate in the detoxification process but also be associated with the reproduction of *B. xylophilus*. We cloned the gene according to the sequence obtained by the transcriptome analysis and submitted the sequences to the UDP-glycosyltransferase Nomenclature Committee<sup>1</sup> to assign a name to the gene. The gene was named as *UGT440A1* by the committee. Furthermore, to elucidate the molecular and biological functions of *UGT440A1* in *B. xylophilus*, we expressed the recombinant *UGT440A1*, examined its spatiotemporal expression in different developmental stages of *B. xylophilus*, and investigated the influences on motility, reproduction, and pathogenicity of *B. xylophilus* after suppression of *UGT440A1* through RNA interference (RNAi).

## MATERIALS AND METHODS

### Culture and Collection of Nematodes

The highly virulent *B. xylophilus* strain AMA3 was isolated from diseased *Pinus thunbergii* seedlings in Nanjing, China. The nematodes were cultured on *Botrytis cinerea* in potato dextrose agar (PDA) plates at 25°C in the dark for 7–9 days at Qingdao University (Qingdao, Shandong Province, China) (Guo et al., 2017). Then, the mixed-stage nematodes were separated using the Baermann funnel technique (Viglierchio and Schmitt, 1983). The nematodes were placed in Petri dishes for 1 h at 25°C in the dark to obtain eggs, as described previously (Futai, 1980; Tang et al., 2020). The collected eggs were hatched in the absence of food for 24 h in the dark at 25°C to obtain J2 larvae. Subsequently, the J2 larvae were cultured for 48 h at 25°C in the dark to obtain J4 worms. After the male and female J4 nematodes were distinguished, they were transferred to the PDA plates containing *B. cinerea* separately for 24 h at 25°C in the dark. Then, virgin adult worms were collected using two Baermann funnels (Zhu et al., 2016). Two-year-old *Pinus thunbergii* (*P. thunbergii*) seedlings were grown in the greenhouse at 25°C.

### **UGT440A1 Gene Cloning**

DNA was extracted from nematodes with the method described previously (Huang et al., 2010). Total RNA was extracted using TRIzol® Reagent (Invitrogen, Waltham, MA, United States) and treated with DNase I (Cwbio, Beijing, China), according to the manufacturer's protocol. DNA and RNA

were examined through electrophoresis on a 1.5% denaturing agarose gel and quantified by measuring ultraviolet absorbance at 260/280-nm wavelength (NanoDrop® ND-2000, Thermo Fisher, USA). The synthesis of first-strand cDNA was performed, as described previously (Tang et al., 2020). According to the *UGT440A1* sequence obtained through the transcriptome analysis and the *B. xylophilus* genome data from WormBase ParaSite<sup>2</sup>, a pair of specific primers (forward: 5'-CCGGAATTCAATTAAACCAACATAATATGTTG-3'; reverse: primer 5'-GCTCTAGAAAAGCTATTATTAAATTCTATTCTCAGA CA-3') was used to amplify the complete *UGT440A1* through polymerase chain reaction (PCR) from *B. xylophilus* genomic DNA. The PCR conditions were as follows: pre-denaturation at 94°C for 5 min, followed by 30 cycles of denaturation at 94°C for 45 s; annealing at 56°C for 45 s; extension at 72°C for 150 s, and a final extension at 72°C for 10 min. To further analyze the UGT440A1 protein, the coding sequence of the gene was amplified by PCR using cDNA reverse-transcribed from mRNA of *B. xylophilus*. The primers (forward: 5'-CCCAAGCTTATGCGCGCCTTCTGC -3'; reverse: 5'-CC GGAATTCTTACTCCGCTTGACCTTGG-3') were designed based on the ORF region of *UGT440A1*. The PCR conditions were as follows: pre-denaturation at 94°C for 5 min, followed by 30 cycles of denaturation at 94°C for 45 s; annealing at 60°C for 45 s; extension at 72°C for 90 s, and a final extension at 72°C for 10 min. The amplified products were cloned into a pMD®18-T Simple Vector (Takara, Dalian, China) and then sequenced.

### **Sequence Analysis of *UGT440A1***

The program open reading frame (ORF) Finder<sup>3</sup> was utilized to analyze the ORF of *UGT440A1*. The *B. xylophilus* genome from WormBase ParaSite was used for the structural analysis of *UGT440A1*. The protein sequences of *UGT440A1* were deduced from the nucleotide sequences by using the Basic Local Alignment Search Tool<sup>4</sup>. Protein sequences of other species utilized in alignments were obtained from the NCBI<sup>5</sup>. Conserved domains were identified using the conserved domain database of NCBI<sup>6</sup>. DNAMAN9 software was used to perform multiple alignments, and MEGA-X software was utilized to construct a phylogenetic tree with the neighbor joining method. Physicochemical characteristics of *UGT440A1* were obtained from ProtParam<sup>7</sup>. Signal peptides and transmembrane helices were predicted using SignalP Server<sup>8</sup> and THHMM Server<sup>9</sup>, respectively. The deduced amino acid

sequence of *UGT440A1* was modeled using the SWISS-MODEL program<sup>10</sup> and further analyzed using the PyMOL 2.3.2 software.

### Fluorescence *in situ* Hybridization

mRNA FISH was performed to determine the spatial expression patterns of *UGT440A1* at different developmental stages of *B. xylophilus*. A red fluorescence-labeled probe (5'-Cy3-CGCTGATAGTCATCTCGCTTCCATGATCGTCGTCC ATGCCT-3') was generated from the cloned sequence of *UGT440A1* and designed using Primer Premier 5.0 software (Primer, Canada). *B. xylophilus* at different developmental stages were collected and centrifuged in 1.5-mL centrifuge tubes. The nematodes were fixed with the RNase-free paraformaldehyde solution (4%) at 5°C for 16 h and then pretreated at room temperature for 4 h. Smeared 50 µL suspension of nematodes (approximately 200 nematodes) in a microscope slide and baked the nematodes at 56°C on a slide warmer. FISH was performed using FISH *in situ* hybridization kit C007 (Gefan, Shanghai, China), according to the manufacturer's protocol. The nematodes were incubated in 200 mM hydrochloric acid for 15 min in a humidified box containing 5 × saline sodium citrate (SSC) and formamide, and then washed twice with diethylpyrocarbonate (DEPC)-treated water. Proteinase K (0.5 mg mL<sup>-1</sup>) was used to digest the nematodes at 37°C for 20 min, followed by washing with 100 mM glycine for 1 min and twice washing with phosphate buffer saline (PBS) for 2 min. The nematodes were incubated in RNase-free paraformaldehyde solution (4%) for 10 min, and then washed twice with PBS for 3 min. Incubation of the nematodes with acetic anhydride (0.25%) for 10 min were performed to reduce the non-specific binding, following five times washing with PBS for 5 min and twice washing with 5 × SSC for 2 min. The nematodes then were pre-hybridized in hybridization buffer at 65°C for 1 h. *In situ* hybridization was performed with rotation and probe concentration of 1.0 µg mL<sup>-1</sup> for 48 h at 65°C. After hybridization, the nematodes were washed three times with a mixture of formamide and 4 × SSC (1:1) at 65°C for 15 min and five times with PBS for 5 min at room temperature. Counterstaining was carried out with 4',6-diamidino-2-phenylindole (2.0 µg mL<sup>-1</sup>) for 5 min. The nematodes were examined under a Nikon light microscope (Eclipse Ci, Nikon, Japan). The sense probe (5'-Cy3-AGGCATGGACGACGATCATGGAAGCGAGATGACTTACTA TCAGCG-3') was used as a negative control.

## Expression and Purification of UGT440A1

The *UGT440A1* coding region without the putative signal sequence was amplified through PCR from the original plasmid by using specific primers (forward: 5'- ATGGA GAAGATCTTACTCTTAAATGC GGCGAGAAC-3'; reverse: 5'- ATTGCCGACGCCGTGATTACTT-3') and inserted into the pET-15b (Invitrogen, United States) vector. Plasmid was transformed into *Escherichia coli* (*E. coli*) BL21 (DE3) Plyss (Solarbio, Beijing, China). Expression of the recombinant UGT and collection of inclusion bodies were performed using the method described in a study, with some modifications (Liu et al., 2015). The recombinant UGT440A1 was overexpressed in *E. coli* BL21 (DE3) harboring pET-15b-UGT through Isopropyl- $\beta$ -D-thiogalactopyranoside (IPTG) induction at 37°C. The inclusion bodies were dissolved in 10 mL solution buffer (20 mM Tris, 5 mM DTT, 8 M urea, pH 8.0) at 4°C overnight. The supernatant was collected through centrifugation at 10000 g for 15 min at room temperature and diluted with refolding buffer (20 mM Tris-HCl, 150 mM NaCl, pH 8.0) to gradually reduce the concentration of urea from 8 M to 1 M. The refolded protein was purified through Ni-NTA affinity chromatography and analyzed through SDS-PAGE (12% gel) (Liu et al., 2015).

## Activity Assay of UGT440A1 Recombinant Protein

UGT activity was assayed according to a method reported previously, with some modifications (Real et al., 1991). The reaction mixture, with the final volume of 0.2 mL, comprised 100 mM Tris-HCl buffer (pH 7.4), 10 mM MgCl<sub>2</sub>, 5 mM D-gluconic acid lactone, 500  $\mu$ M uridine diphosphate- $\alpha$ -D-glucose (UDPG), 100 mM substrate (kaempferol or quercetin), and 100  $\mu$ L recombinant UGT. The reaction mixtures were incubated for 1 h at 37°C, and the reaction was terminated by adding 1 vol. methanol. Proteins and insoluble materials were removed through centrifugation at 15,000 g for 5 min at 4°C. Ten microliter of the filtered supernatant fraction was used for high-performance liquid chromatography (HPLC) analysis of the reaction products. Reactions performed in the absence of UDPG or recombinant UGT440A1 served as the control.

## Double-Stranded RNA Synthesis

By using pET-15b-*UGT440A1* as the template, a 368-bp DNA fragment was amplified through PCR with T7-labeled gene-specific primers (forward: 5'-

TAATACGACTCACTATAGGGAAGTAATCACGGCGTCGGC-3'; reverse: 5'-TAATACGACTCACTATAGGGAAGCACATGGT CTCTTCC-3'). A pair of T7-labeled gene-specific primers was used to amplify the 323-bp DNA fragment of green fluorescent protein gene (*Bxy-gfp*), with pET-15b-*gfp* as the template (forward 5'-TAATACGACTCACTATAGGGAACGG CCACAAGTTCAGC-3'; reverse 3'-TAATACGACTCACTATA GGGAAAGTCGATGCCCTTCAGC-3'). The amplified products were used as the templates for double-stranded RNA (dsRNA) synthesis. The dsRNA was synthesized using the MEGAscript (TM) RNAi Kit (Invitrogen, Vilnius, Lithuania), according to the manufacturer's instructions. Fluorescent dsRNA labeled with cyanine dyes 3 (Cy3) was constructed by adding Cy3-dCTP in the reaction system. The integrity of dsRNAs was visualized in a 1.5% agarose gel.

### **Efficiency Assessment of RNAi**

Approximately 4000 *B. xylophilus* (a mixture of juveniles and adults) were soaked in 50  $\mu$ L soaking buffer (0.05% gelatin, 3 mM spermidine, 0.25  $\times$  Mg<sup>2+</sup>-free M9) containing *UGT* dsRNA (1.0  $\mu$ g/ $\mu$ L) and then incubated for 48 h at 25°C (Huang et al., 2019; Park et al., 2008). Afterward, *B. xylophilus* were washed with sterile water several times. Nematodes soaked in soaking buffer containing ddH<sub>2</sub>O and *gfp* dsRNA were used as double negative controls. The nematodes were rinsed four times with sterilized water and photographed under a fluorescence microscope to assess the efficiency of the dsRNA uptake. QRT-PCR was used to verify the effect of *UGT440A1* silencing through RNAi on mRNA levels. PCR was performed using TB Green Premix Ex Taq II (TaKaRa, Dalian, China), with 0.4  $\mu$ M each of forward and reverse primer (forward: 5'-CTCGCGGAAGCGGGTTACAA-3'; reverse: 5'-CTGGTCGCGACACCCAAAGTT-3'). The actin gene amplified by the primer pair (forward: 5'-CTGCTGAGCGTGAAATCGT-3' and reverse: 5'-GTTGTAGGTGGTCTCGTGG-3') was used as the internal control. The PCR program was set as follows: 30 s at 95°C, followed by 40 cycles of 5 s at 95°C and 34 s at 60°C. Each experiment was performed thrice.

### **Assay for Motility After RNAi**

Approximately 40 nematodes (a mix of juvenile and adult nematodes) were observed under a stereo microscope after the nematodes were soaked in buffer with dsRNA (as described above) for 48 h at 25°C in the dark. The head

thrashing frequency ( $> 120^\circ$  within a single head swing) in 30 s was used to measure the vitality of *B. xylophilus* (Tang et al., 2020). Nematodes soaked in buffer containing ddH<sub>2</sub>O and *gfp* dsRNA were used as double negative controls. Each assay was repeated three times.

### **Assay for Feeding and Reproduction After RNAi**

Twenty pairs of virgin male and female nematodes were soaked separately in buffer containing dsRNA (1.0  $\mu\text{g}/\mu\text{L}$ ) for 48 h (Huang et al., 2019). Thereafter, the nematodes were washed several times to remove external dsRNA. Then, 10 pairs of nematodes were cultured in a PDA plate with *B. cinerea* at 25°C in the dark. The feeding area of *B. xylophilus* was photographed daily. After culturing for 9 days, the nematodes were isolated from the PDA plates and counted under an optical microscope. The other 10 pairs were transferred onto a glass dish with ddH<sub>2</sub>O for 48 h in the dark at 25°C to allow the nematodes to lay eggs, and the number of eggs was counted under an optical microscope. To determine the effect of *UGT* dsRNA on egg hatching of *B. xylophilus*, thirty pairs of virgin male and female nematodes were soaked separately in buffer containing dsRNA for 48 h. Following treatment, the nematodes were transferred onto a glass dish for 16 h to lay eggs, then eggs were incubated at 25°C for 20 h for hatching, and the hatching rate was calculated (Huang et al., 2019). The same quantity of nematodes soaked in buffer containing ddH<sub>2</sub>O and *gfp* dsRNA served as negative controls. Each experiment was performed three times.

### **Assay on the Pathogenicity After RNAi**

Approximately 3000 *B. xylophilus* (a mix of juvenile and adult nematodes) were soaked in 50  $\mu\text{L}$  soaking buffer containing *UGT* dsRNA (1.0  $\mu\text{g}/\mu\text{L}$ ) and then incubated for 48 h at 25°C (Huang et al., 2019). Afterward, *B. xylophilus* were washed with sterile water several times. Thereafter, the nematodes were inoculated into 2-year-old *P. thunbergii* seedlings. Sterile water without nematodes and nematodes soaked in buffer containing ddH<sub>2</sub>O and *gfp* dsRNA were used as negative controls. Each treatment was replicated three times. Each *P. thunbergii* seedling was inoculated with 200  $\mu\text{L}$  suspension of mixed-stage nematodes (approximately 1,000 nematodes). Approximately 2-cm-long wounds on *P. thunbergii* at 30–50 cm above the soil level were inoculated and sealed with parafilm (Qiu et al., 2016). The inoculated *P. thunbergii* seedlings were grown in the greenhouse at 25°C. Wilting symptoms

developing on the pine woods that were inoculated with the nematodes were observed daily. The PWD symptoms were evaluated and categorized into four groups: 0 = all of the needles were green; 1 = 0%–25% of the needles were discolored and turning yellow; 2 = 26%–50% of the needles had turned yellow; 3 = 51%–75% of the needles had turned yellow; and 4 = 76%–100% of the needles had turned yellow (Yu et al., 2012). The infection rates and the disease severity index (DSI) of the *P. thunbergii* seedlings were calculated with a method described previously (Yu et al., 2012).

## Statistical Analysis

All experiments involving *B. xylophilus* included three replicates, with each treatment replicated three times. All values of the repeated experiments are expressed as means  $\pm$  standard deviation (S.D.), and all statistical analyses were performed using SPSS 19.0 software (SPSS, Chicago, IL, USA). The independent sample *t*-test and one-way analysis of variance were used to assess differences between the groups. A *P* value of  $< 0.05$  was considered to denote statistical significance.

# RESULTS

## Alignment and Phylogenetic Analysis of *UGT440A1*

The DNA sequence of *UGT440A1* was successfully amplified by PCR (Supplementary Figure 1). The sequence analysis showed that the PCR product comprises 2,231 bp containing a 1,566-bp ORF which encoded 521 amino acids. The structural analysis showed that *UGT440A1* (*BXY\_1088500.1*) comprised seven exons and six introns and contained 50 bp of the 5' untranslated region and 50 bp of the 3' untranslated region (Figure 1A). The coding sequence of *UGT440A1* was submitted to NCBI Genbank under the accession number MZ467299. The conserved domain search showed that *UGT440A1* belonged to the glycosyltransferases B (GTB) superfamily (the members of this family share a common GTB topology) of glycosyltransferase and the coding sequence of *UGT440A1* consisted of the GT1-Gtf-like Pfam domain, which was localized between amino acids 22 and 443. The alignment of multiple amino acid sequences revealed the homology of *UGT440A1* with a range of UGTs (Figure 1B). Furthermore, sequence analysis revealed the presence of a typical UGT signature sequence in

*UGT440A1*: [FVA]-[LIVMF]-[TS]-[HQ]-[SGAC]-G-x(2)-[STG]-x(2)-[DE]-x(6)-P-[LIVMFA]-[LIVMFA]-x(2)-P-[LMVFIQ]-x(2)-[DE]-Q (the amino acids in the square brackets can be arbitrary, and x stands for any base) (Mackenzie et al., 1997; Figure 1B). The further bioinformatics analysis showed the presence of a signal peptide and a transmembrane region in the deduced amino acid sequence of *UGT440A1* (Figure 1B), which indicated that *UGT440A1* is a transmembrane protein. The phylogenetic relationship of *UGT440A1* with other UGT proteins revealed that *UGT440A1* formed a well-founded cluster with UGT of other nematodes (Figure 2). And UGT proteins in nematode species apparently separated those of plant-parasitic nematodes, including *B. xylophilus*, *Aphelenchus avenae*, *Meloidogyne enterolobii* and *Meloidogyne graminicola* from those of other nematode species. Notably, the UGT protein of *Aphelenchus avenae* was the closest protein to *UGT440A1* among the 18 family members examined. In addition, four outgroups, namely Chordata, Arthropoda, Bacteria, and Fungi were observed (Figure 2). The analysis showed that the *UGT440A1* sequences are more closely related to fungal and bacterial sequences compared with animal sequences.

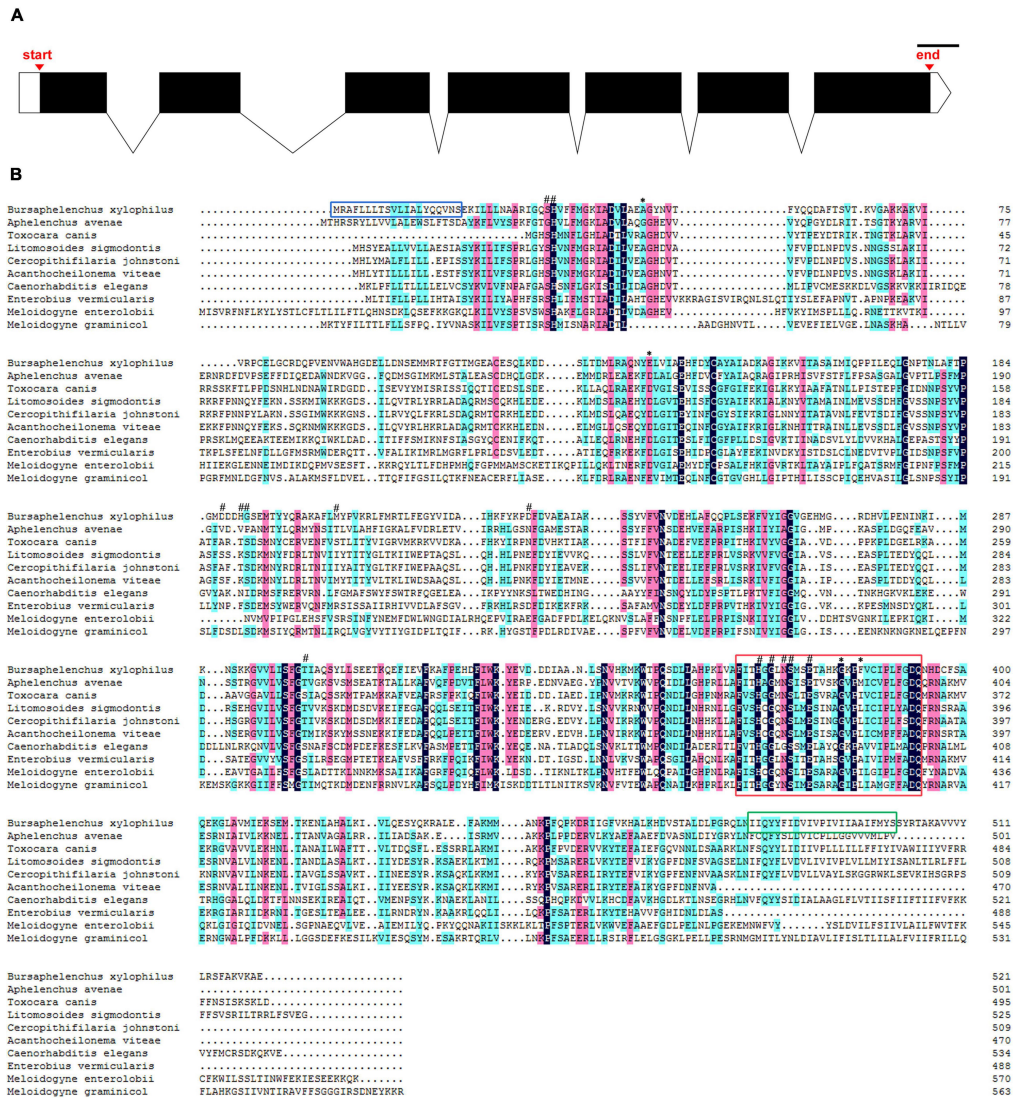


**FIGURE 1.** Sequence analysis of *UGT440A1*. **(A)** Genomic DNA structure of *UGT440A1*. White boxes indicate exons, the black region corresponds to the coding sequences, and the lines indicate introns; scale bar = 100 bp. **(B)** Alignment of *UGT440A1* with homologs. The alignment compares *UGT440A1* (MZ467299) with the UGT proteins of *Aphelenchus avenae* (KAH7725749.1), *Toxocara canis* (KHN83392.1), *Litomosoides sigmodontis* (VDK69150.1), *Cercopithifilaria johnstoni* (CAG9530659), *Acanthocheilonema viteae* (VBB30777.1), *Caenorhabditis elegans* (NP\_506211.1), *Enterobius vermicularis* (VDD95930.1), *Meloidogyne enterolobii* (CAD2191161.1) and *Meloidogyne graminicola* (KAF7639096.1). Black, red, and blue shadings indicate fully conserved, strongly conserved, and weakly conserved amino acids, respectively. Signal peptide sequences, transmembrane region, and typical signature of UGT are enclosed by the blue, green, and red boxes, respectively. The predicted active sites and polypeptide binding sites are indicated by (#) and (\*), respectively.

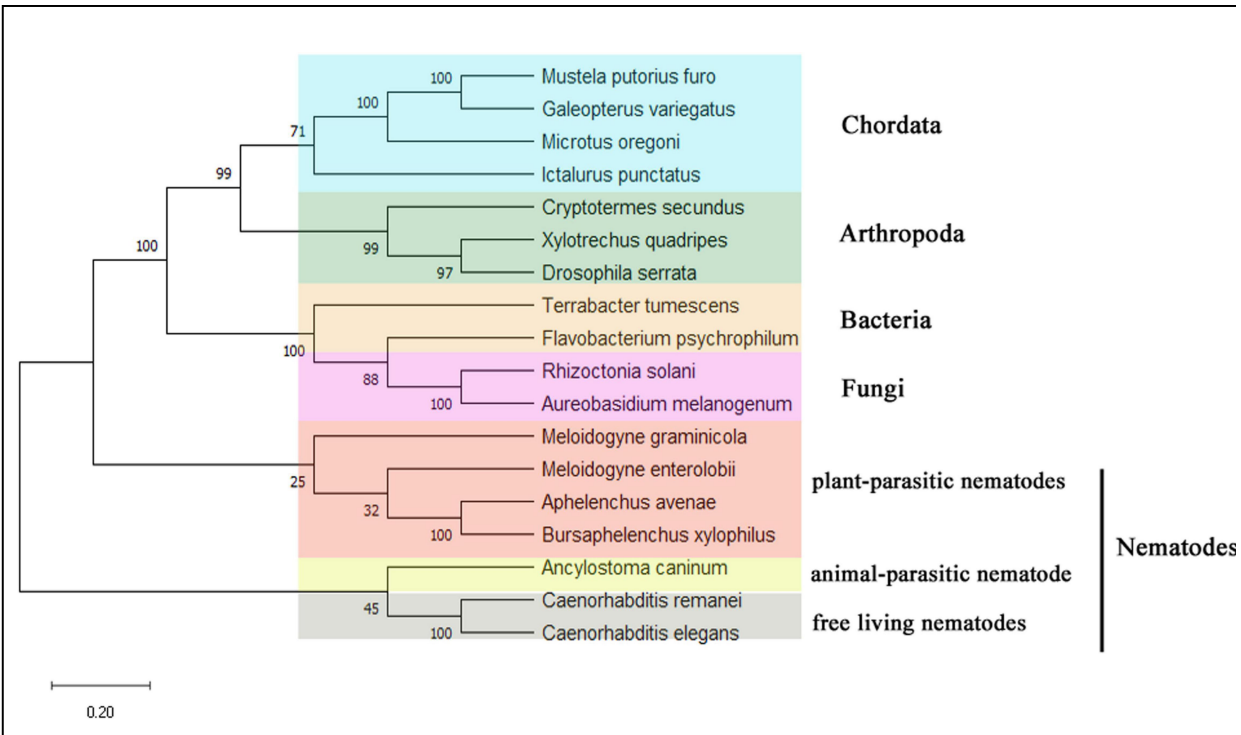


**FIGURE 2.** Unrooted phylogenetic analysis of UGT440A1 protein. Percentage nodal support is based on 500 bootstrap replicates. The scale bar indicates the evolutionary distance (0.2 substitutions per position). *Mustela putorius furo* (XP\_004738075.1); *Galeopterus variegatus* (XP\_008590698.1); *Microtus oregoni* (XP\_041487187.1); *Ictalurus punctatus* (ABI51987.1); *Cryptotermes secundus* (XP\_023705394.1); *Xylotrechus quadripes* (QIK00375.1); *Drosophila serrata* (XP\_020813000.1); *Terrabacter tumescens* (GGM90420.1); *Flavobacterium psychrophilum* (WP\_227038871.1); *Rhizoctonia solani* (CUA68035.1); *Aureobasidium melanogenum* (AQQ13387.1); *Meloidogyne graminicola* (KAF7639096.1); *Meloidogyne enterolobii* (CAD2191161.1); *Aphelenchus avenae* (KAH7725749.1); *Bursaphelenchus xylophilus* (MZ467299); *Ancylostoma caninum* (RCN52832.1); *Caenorhabditis remanei* (KAF1754268.1); *Caenorhabditis elegans* (NP\_506211.1).

## Molecular Modeling of *UGT440A1*

The tertiary structure of *UGT440A1* was predicted with the crystal structure of macrolide glycosyltransferase (PDB ID: 2iya.1) as a template by using the online program SWISS-MODEL (Figure 3A). The theoretical tertiary structure consisted of 15 alpha-helices and 13 beta-strands. The N-terminal domain had 7 beta-strands and surrounded by 8 alpha-helices, and the C-terminal domain was made up of 7 alpha-helices and 6 beta-strands. The molecular surface of *UGT440A1* was assessed using the PyMOL program, as the protein was in a cell environment. Molecular surface modeling revealed mainly the presence of white patches, along with slight red and blue patches, which indicated the presence of both neutral and charged regions (Figure 3B).

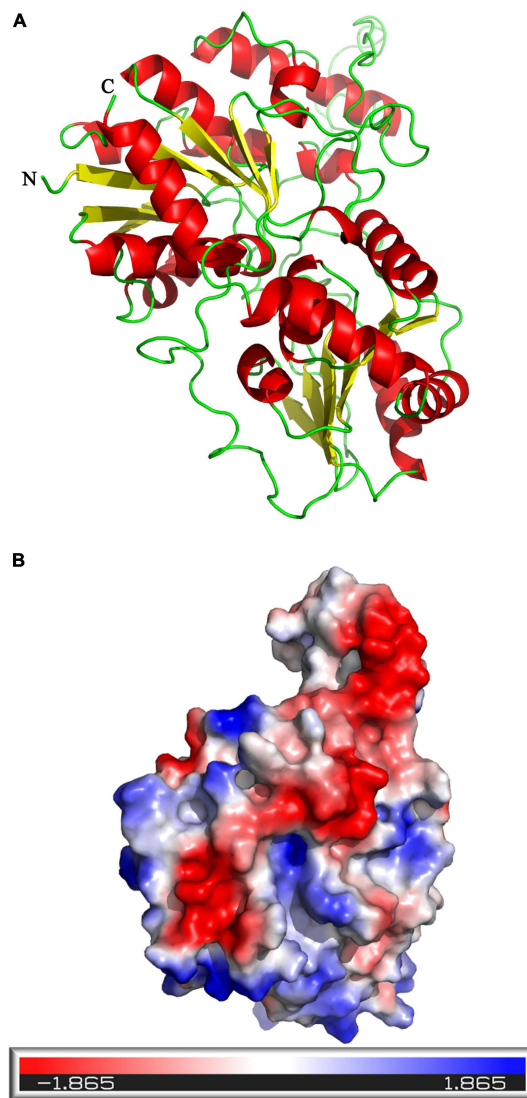


**FIGURE 3.** Predicted structure of *UGT440A1*. **(A)** Three-dimensional structure of *UGT440A1*, with macrolide glycosyltransferase (PDB ID: 2iya.1) as a template. **(B)** The electrostatic potential surface of *UGT440A1*. The color gradient ranging from red to blue corresponds to negatively charged regions ( $-5K_BT/e$ ) to positively charged regions ( $+ 5 K_BT/e$ ), and white color indicates neutral regions.

### Gene Expression Pattern of *UGT440A1* in PWNs

Fluorescence *in situ* hybridization (FISH) was used to identify the spatiotemporal expression of *UGT440A1*. Hybridization signals were detected from embryo until adult *B. xylophilus* were formed. The red fluorescence-labeled probe stained nearly the whole embryo (Figure 4A), whereas a restricted staining pattern was observed in juvenile nematodes (J2, J3, and J4

females), wherein the hybridization signals were detected in the head, intestine, and subcutaneous tissues (Figures 4B,C,E). However, the hybridization signals were detected nearly throughout the body of J4 males and adults (Figures 4D,F,G). No hybridization signal was observed in the negative controls (Figures 4H,I).

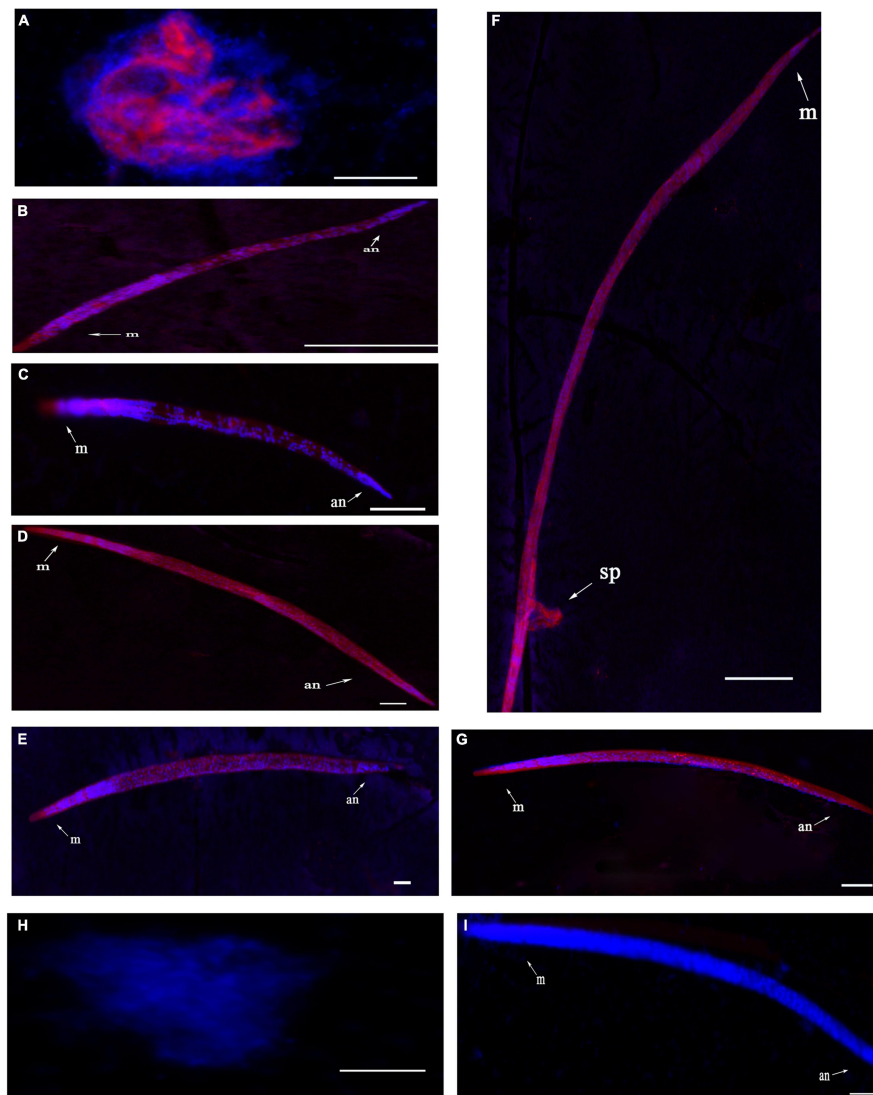


**FIGURE 4.** Localization of *UGT440A1* mRNA in *B. xylophilus* determined through fluorescence *in situ* hybridization. Hybridization with the red fluorescence-labeled probes in the embryo (A), J2 juvenile (B), J3 juvenile (C), male J4 juvenile (D), female J4 juvenile (E), male adult (F), and female adult (G). Hybridization in embryo (H) and female adult (I) in the negative control. m, metacorpus; an, anus; sp, spicules. Scale bar = 20  $\mu$ m (A–E, H), 50  $\mu$ m (F,G,I).

## Expression, Purification, and Activity of the Recombinant *UGT440A1*

The *UGT440A1* coding region without the putative signal sequence was amplified through PCR and cloned into the vector pET-15b to construct pET-15b-UGT. The recombinant UGT440A1 was overexpressed in *E. coli* BL21 (DE3) through IPTG induction at 37°C. The SDS-PAGE analysis indicated that the recombinant protein had the expected molecular mass of 53 kDa, which corresponded to 51.5 kDa from the *UGT440A1* ORF and 1.5 kDa encoded by the expression vector, including a His<sub>6</sub>tag (Figure 5A). The expressed recombinant protein was found mainly in the inclusion bodies, which could be refolded by stepwise dilution with refolding buffer (Figure 5A). The renatured recombinant UGT440A1 was then purified through Ni<sup>2+</sup> affinity chromatography, and the electrophoretic homogeneity was verified through SDS-PAGE (Figure 5A). To assay the activity of UGT440A1, two types of flavonols, quercetin and kaempferol, which are the parent nuclei of flavonoids in pine wood, were selected as substrates to detect whether recombinant UGT440A1 had the catalytic activity. Because the polarity of flavonoids increases when they combine with glucose, the product is expected to peak earlier in case of a glycosylation reaction. The HPLC results indicated that the expressed recombinant protein could catalyze the two substrates, as more than one products were detected (Figure 5B).

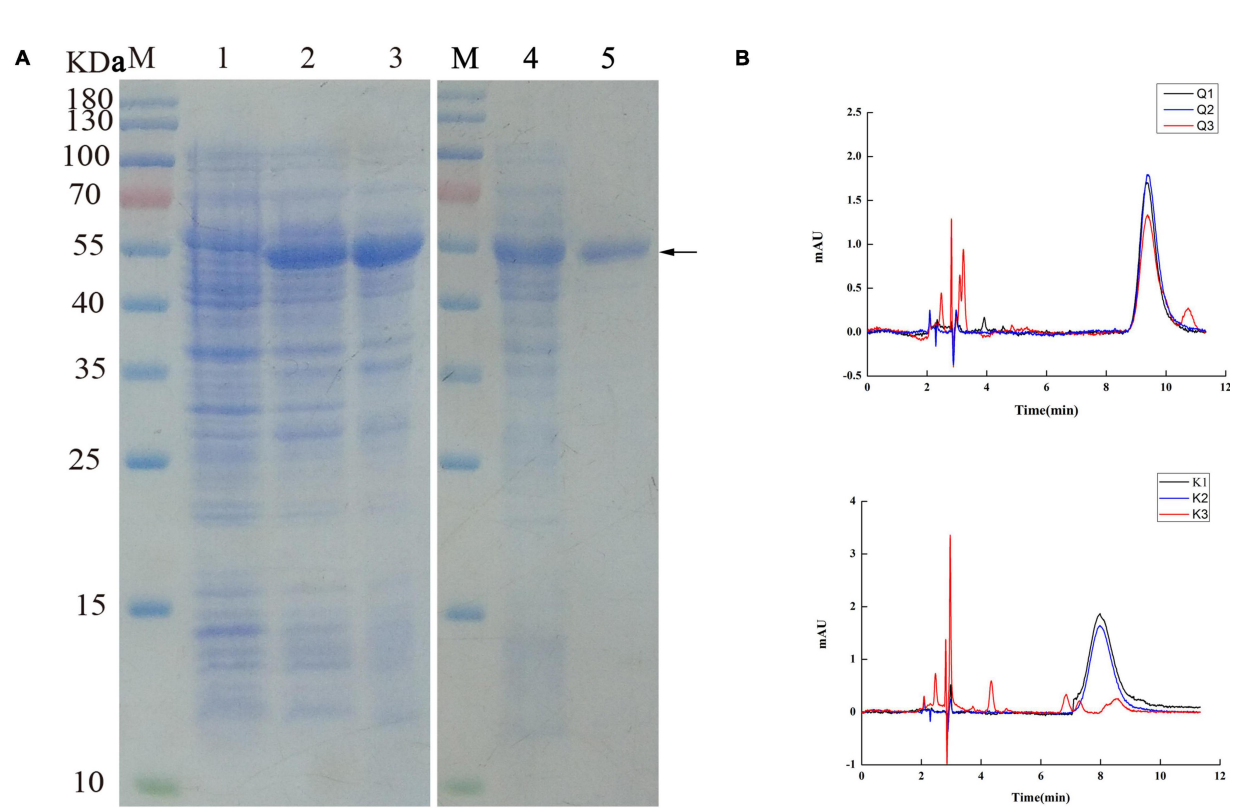


**FIGURE 5.** Purification and activity assay of the recombinant UGT440A1. **(A)** SDS-PAGE analysis of the expression and purification of recombinant UGT440A1. M, standard proteins; 1, total proteins of *E. coli* BL21 (DE3); 2, total proteins of *E. coli* BL21 (DE3) harboring pET-15b-*UGT440A1*; 3, inclusion bodies; 4, washed inclusion bodies; 5, purified recombinant UGT440A1. **(B)** Detection of the recombinant *UGT440A1* activity through HPLC analysis. Overlapping chromatogram of reaction products, with quercetin (Q) or kaempferol (K) as the substrate; reaction performed in the absence of UDPG (Q1 and K1); the absence of recombinant UGT440A1 (Q2 and K2); and complete reaction mixtures (Q3 and K3).

## Efficiency Assessment of RNAi

To verify that the dsRNA could be transferred effectively into *B. xylophilus*, nematodes were observed under a fluorescence microscope. The patterns of fluorescein indicated that Cy3 labeled dsRNA was taken up by the nematodes effectively (Figures 6B,D). No fluorescence was detected in the nematode soaked in sterilized water (Figure 6F). And no phenotypic changes were detected in the nematodes after RNAi of *UGT440A1* (Figures 6A,C,E). The RNAi efficiency on the *UGT440A1* expression level was evaluated through QRT-PCR. The results showed that compared with the expression level of *UGT440A1* in the nematodes soaked in sterilized water, that in the nematodes soaked in *UGT440A1* dsRNA was only 0.15 (Figure 7A) ( $p < 0.001$ ). This

result indicated that the expression of *UGT440A1* in nematodes could be strongly inhibited by soaking the nematodes in *UGT440A1* dsRNA. The *gfp* dsRNA, as one of the negative controls, demonstrated no significant effects on the expression level of *UGT440A1* compared with sterilized water (Figure 7A) ( $p > 0.05$ ).

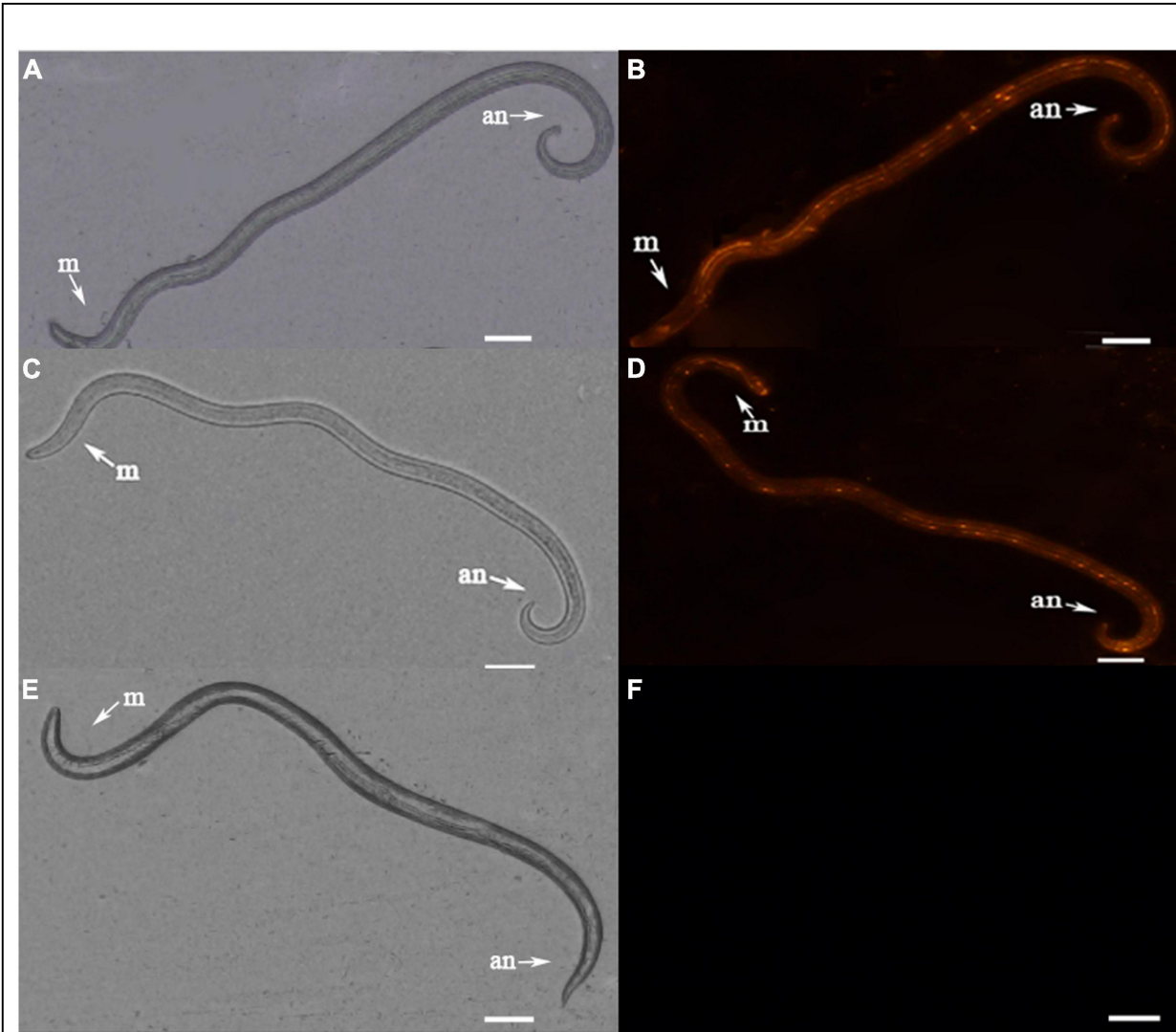


**FIGURE 6.** Fluorescence micrographs of *B. xylophilus* after RNAi. **(A)** Morphology of nematode soaked in *UGT440A1* dsRNA. **(B)** The red fluorescence indicates the Cy3-labeled *UGT440A1* dsRNA entry into the nematode. **(C)** Morphology of nematode soaked in *gfp* dsRNA. **(D)** The red fluorescence indicates the Cy3-labeled *gfp* dsRNA entry into the nematode. **(E)** Morphology of nematode soaked in sterilized water. **(F)** No fluorescence was detected in the nematode soaked in sterilized water. m, metacorpus; an, anus. Scale bar = 50  $\mu$ m.

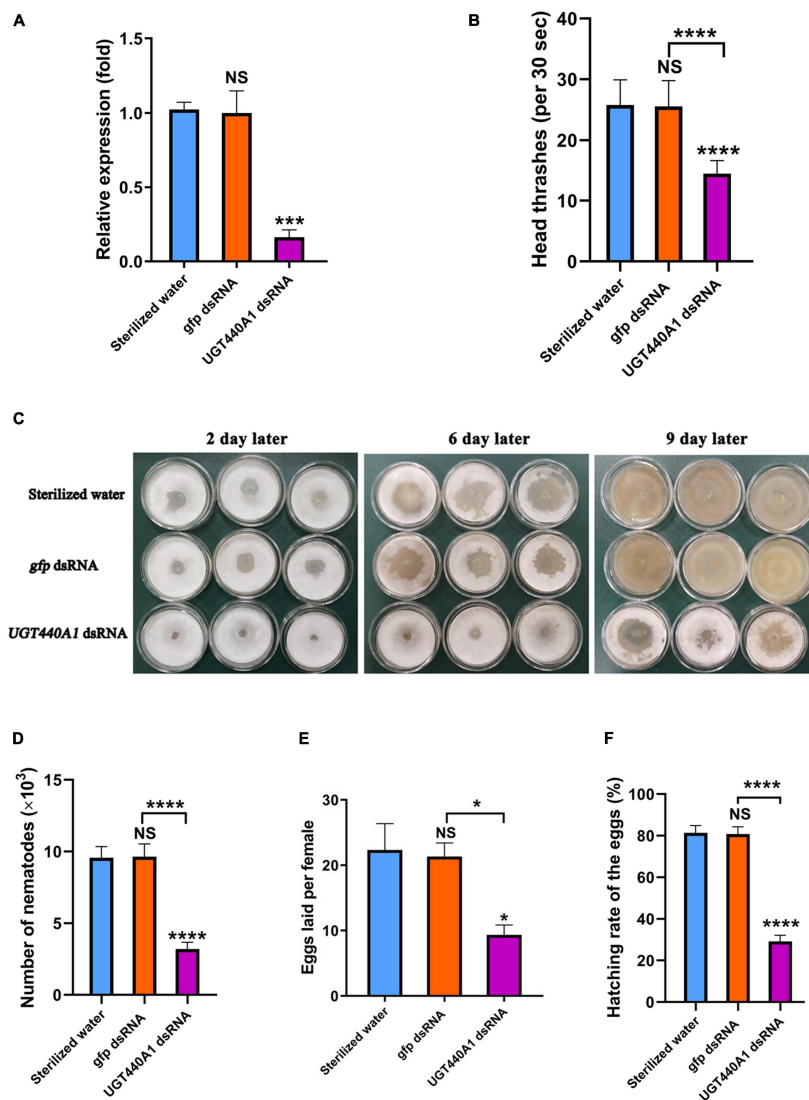


**FIGURE 7.** Expression and function analysis of *UGT440A1* after RNAi. **(A)** Relative expression of *UGT440A1* after RNAi. **(B)** The motility of *B. xylophilus* assessed on the basis of the number of head thrashes per 30 s after RNAi. **(C)** Feeding of *B. cinerea* by *B. xylophilus* soaked in sterilized water, *gfp* dsRNA, and *UGT440A1* dsRNA solutions. **(D)** Reproductive assay of *B. xylophilus* after RNAi. **(E)** The ability of egg laying measured by the number of eggs laid per female after RNAi. **(F)** The ability of egg hatching after RNAi. Asterisks indicate statistically significant differences (\* $P < 0.05$ , \*\* $P < 0.001$  and \*\*\* $P < 0.0001$ ), and NS denotes no significant difference.

## ***UGT440A1* Is Required for Motility of *Bursaphelenchus xylophilus***

To analyze the influence of *UGT440A1* on the locomotion of *B. xylophilus*, the head thrashing frequency of the nematodes was observed under a stereo

microscope. The nematodes soaked in dsRNA exhibited difficulties in motility. The head thrashing frequencies in the *UGT440A1* dsRNA, sterilized water, and *gfp* dsRNA groups were  $14.53 \pm 0.19$ ,  $25.82 \pm 0.37$ , and  $25.59 \pm 0.38$  times per 30 s, respectively (Figure 7B). These results indicated that *UGT440A1* is crucial for *B. xylophilus* motility.

### ***UGT440A1* Is Crucial for Feeding and Reproduction of *Bursaphelenchus xylophilus***

The nematode feeding areas were observed after the nematodes soaked in the dsRNA of *UGT440A1* were transferred to the PDA plate. The feeding rate of the treatment groups was obviously slower than that of the negative controls (Figure 7C). At the ninth day, almost all of the hyphae had been consumed by *B. xylophilus* in the sterilized water and *gfp* dsRNA groups, whereas in the *UGT440A1* dsRNA group, only a part of the hyphae was consumed (Figure 7C). The same day, the nematodes were collected and counted in each group; the number of nematodes in the *UGT440A1* dsRNA, sterilized water and *gfp* dsRNA groups was  $3,192 \pm 111$ ,  $9,572 \pm 182$ , and  $9,642 \pm 210$ , respectively (Figure 7D). Sterilized water and *gfp* dsRNA were not found to have significant influences on the feeding and reproduction of *B. xylophilus* ( $p > 0.05$ ). These results indicated that *UGT440A1* is essential for feeding and reproduction of *B. xylophilus*.

Furthermore, to evaluate the effects of *UGT440A1* on egg laying and hatching abilities of the nematodes, we treated the virgin adults with *UGT440A1* dsRNA. The number of eggs laid by an individual female nematode in the treatment, sterilized water, and *gfp* dsRNA groups was  $9.33 \pm 1.52$ ,  $22.33 \pm 4.04$ , and  $21.33 \pm 2.08$ , respectively (Figure 7E). The hatching rates for the *UGT440A1* dsRNA, sterilized water, and *gfp* dsRNA groups were  $29.11\% \pm 3.01\%$ ,  $81.33\% \pm 3.53\%$ , and  $80.78\% \pm 3.49\%$ , respectively (Figure 7F). These results suggested that *UGT440A1* is vital for the egg laying and hatching potential of *B. xylophilus*.

### ***UGT440A1* Is Involved in *Bursaphelenchus xylophilus* Pathogenicity**

To examine the virulence of the nematodes, *B. xylophilus* treated with *UGT440A1* dsRNA were inoculated into 2-year-old *P. thunbergii* seedlings (Figure 8A). Twelve days after inoculation, the pine seedlings inoculated with nematodes that were treated with sterile water and *gfp* dsRNA exhibited clear

symptoms of PWD. The infection rate of both the sterilized water and *gfp* dsRNA treatment groups was 33.3%, whereas the DSi for the two groups was  $16.67 \pm 16.67$  and  $8.33 \pm 8.33$ , respectively (Table 1) ( $p < 0.05$ ). The *UGT440A1* dsRNA treatment group exhibited no PWD symptom in at this time point; however, this group exhibited leaf yellowing 18 days after inoculation. Furthermore, the pine seedlings inoculated with nematodes that were treated with sterilized water and *gfp* dsRNA exhibited higher infection rates and DSi, respectively, than those treated with *UGT440A1* dsRNA at 20 and 40 days after inoculation (Table 1 and Figures 8B,C) ( $p < 0.05$ ). On day 60, all the pine seedlings in the sterilized water and *gfp* dsRNA groups died, whereas the *UGT440A1* dsRNA-treated seedlings were still alive, despite the obvious symptoms of PWD (Figure 8D). The pine seedlings inoculated with sterile water without nematodes did not exhibit any PWD symptom throughout the experimental period. These results indicated that PWD onset was delayed after RNAi of *UGT440A1*.

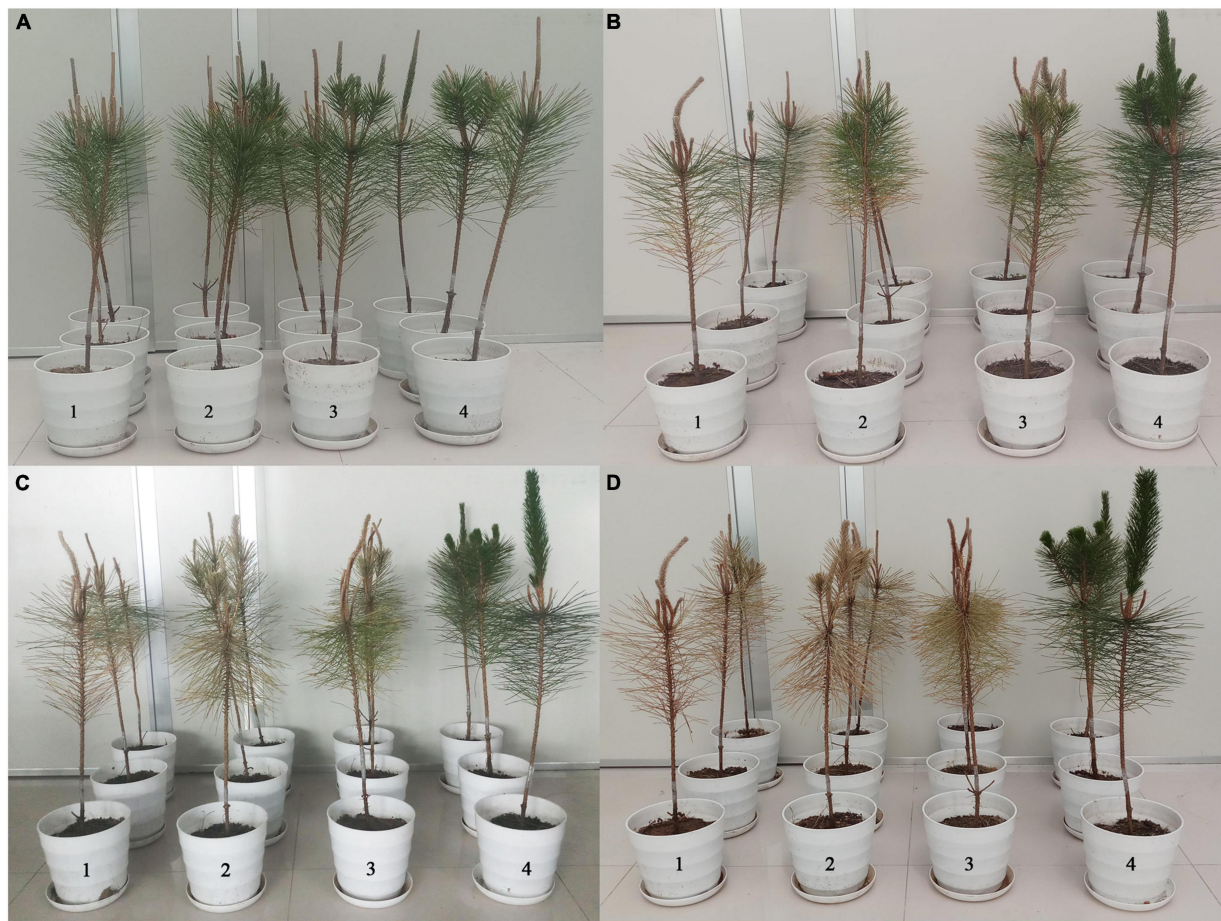


**FIGURE 8.** Pathogenicity assay of *B. xylophilus* after RNAi of *UGT440A1*. Wilting symptoms in *P. thunbergii* seedlings produced at 1 day (**A**), 20 days (**B**), 40 days (**C**), and 60 days (**D**) after inoculation with *B. xylophilus* soaked in sterilized water (1), *gfp* dsRNA (2), *UGT440A1* dsRNA (3), and sterilized water without *B. xylophilus* (4).

**TABLE 1.** Infection rates and disease severity index of *Pinus thunbergii* seedlings inoculated with *Bursaphelenchus xylophilus* under different treatments.

Treatment	Infection Rates (%)				Disease Severity Index (DSI)			
	12th Day	20th Day	40th Day	60th Day	12th Day	20th Day	40th Day	60th Day
<b>ddH<sub>2</sub>O</b>	33.3	66.6	100	100	16.67 ± 16.67 <sup>a</sup>	41.67 ± 9.64 <sup>a</sup>	68.81 ± 3.52 <sup>a</sup>	100 ± 0.00 <sup>a</sup>
<b>gfp dsRNA</b>	33.3	66.6	100	100	8.33 ± 8.33 <sup>a</sup>	27.78 ± 8.98 <sup>a</sup>	62.43 ± 4.91 <sup>a</sup>	100 ± 0.00 <sup>a</sup>
<b>UGT440A1dsRNA</b>	0	33.3	66.6	100	0 ± 0.00 <sup>a</sup>	13.89 ± 6.33 <sup>b</sup>	37.50 ± 6.87 <sup>b</sup>	100 ± 0.00 <sup>a</sup>

Different letters indicate significant differences ( $p < 0.05$ ) among treatments.

## DISCUSSION

UGTs catalyze the conjugation of small lipophilic compounds with sugars and play vital roles in the detoxification and homeostatic processes in all living organisms (Meech et al., 2012; Guillemette, 2003). The nucleotide sugars could be UDP-galactose, UDP-glucose, UDP-glucolonic acid, UDP-xylose, or UDP-rhamnose (Mackenzie et al., 1997). Mammalian UGTs mainly use UDP-glucuronic acid as the sugar donor, whereas invertebrate and plant UGTs mainly use glucose. Although UGTs in plants and mammals, particularly in humans, have been studied extensively in the past decades, little is known about the molecular features and biological functions of UGTs in *B. xylophilus* (Bock, 2016). In this study, we reported a *UGT440A1* gene encoding UGT from *B. xylophilus* and investigated the molecular features and biological roles of this gene for the first time.

UGT440A1 is evolutionarily conserved across species of different phyla. The relatively conserved functional domain of *UGT440A1* protein was found in the region of the *UGT440A1* signature motif, which was located at the C terminal. Multiple alignments of the UGT protein sequences revealed that the C-terminal domain (sugar donor-binding domain) was more conserved than the N-terminal domain (substrate-binding domain), which might be related to the diversity of substrate structures. The phylogenetic analysis showed that UGT440A1 forms a branch with UGT of other nematodes, which revealed a nematode-specific divergence for UGTs. UGT440A1 and its homolog UGTs from *Aphelenchus avenae*, *Meloidogyne enterolobii* and *Meloidogyne graminicola* were grouped in the same sub-clade, which was separated from all the other nematode homologs. UGT440A1 is closely related to the UGT gene of the *Aphelenchus avenae*. A recent study reported that compared to the other nematode species, *B. xylophilus* and *Aphelenchus avenae* had the highest synteny and shared the highest number of gene families (Wan et al., 2021). A signal peptide and a transmembrane domain, which were distributed in the protein sequences, were also predicted. The signal peptide regulated the integration of *UGT440A1* precursors in the endoplasmic reticulum compartment, whereas the transmembrane domain anchored the protein to the endoplasmic reticulum. Most human UGTs are predominantly expressed in the liver and kidney, which are the major organs involved in detoxification (Meech et al., 2019). In insects, the UGTs are expressed in the fat body, midgut, and other tissues. A study revealed that UGTs are expressed preferentially in the olfactory organ (antenna), indicating that UGTs may be associated with the deactivation of pheromones (Younus et al., 2014). Another study reported the expression of *UGT13* in the hypodermis of *C. elegans*

(Hasegawa et al., 2010). In the present study, FISH analysis indicated that *UGT440A1* expresses in all developmental stages of *B. xylophilus*. *UGT440A1* was found to specifically express in the head, intestine, and hypodermis of J2, J3, and J4 females. In J4 males and adults, *UGT440A1* expressed almost in the whole body of *B. xylophilus*, especially in the spicule of adult male nematodes. The results indicated that *UGT440A1* might have multiple functions and a sex-specific role in adult nematodes that have not been identified yet. However, the exact tissue or cells where *UGT440A1* is expressed could not be determined in the present study. Thus, further research is required to determine the protein localization site in *B. xylophilus*.

*UGT440A1* plays diverse roles in motility, feeding, and reproduction of *B. xylophilus*. *UGT440A1* knockdown was found to impair the motility of the nematodes in the present study. Once *B. xylophilus* have invaded the pines, these nematodes migrate and multiply, thereby producing the symptoms of PWD (Futai, 2013). The cell death and early development of disease symptoms in host trees coincide with *B. xylophilus* migration, and avirulent nematodes migrate into the xylem resin canals much slower than virulent nematodes (Ichihara et al., 2000). This finding suggests that the migration ability may play a crucial role in *B. xylophilus* pathogenicity, especially in the early PWD stage. In *C. elegans*, muscle cell aging and death can affect motility, and reduced insulin-like growth factor (IGF) signaling can prevent muscle cell death (Oh and Kim, 2013). Upregulation of detoxification-related genes including UGTs was found in *daf-2* (the single IGF receptor in *C. elegans*) mutant adults (Gems and McElwee, 2005). The aforementioned findings indicated that *UGT440A1* regulates the motility of nematodes possibly through the IGF signaling pathway, and detoxification may be a possible longevity assurance mechanism in the muscle cells of nematodes.

*UGT440A1* knockdown was also found to reduce the feeding ability of *B. xylophilus*. The nematode feeds on healthy plant tissues of the pine cortex in the early PWD stage, whereas in the later stages of PWD, the nematodes mainly feed on fungi in host trees. A recent study demonstrated that UGTs in *B. xylophilus* are upregulated after infection and are expressed predominantly in the intestine (Espada et al., 2016). In *C. elegans*, the intestine is the first line of defense against exogenous compounds, and phase II detoxification enzymes including UGTs play a key role in this process (Crook-McMahon et al., 2014). Additionally, in the silkworm *Bombyx mori*, UGT (*UGT10286*) promotes the glucosylation of quercetin, facilitates the uptake and transport of quercetin,

and influences the overall bioavailability of flavonoids (Daimon et al., 2010). Our results also showed that *UGT440A1* could catalyze the combination of two flavonoids, kaempferol and quercetin, with glucose. These results demonstrated that *UGT440A1* may play a crucial role in digestion and detoxification in the intestine of *B. xylophilus*. However, the mechanisms through which *UGT440A1* aids digestion and detoxification remain to be investigated.

The reproduction ability is closely related to aggressiveness and pathogenicity of plant-parasitic nematodes (Wang et al., 2005). Our results indicated a decrease in the reproduction ability after RNAi of *UGT440A1* in *B. xylophilus*. UGTs play a role in steroid metabolism, whereas the sex steroids such as estrogens, androgens, and progesterones are the targets of UGT-mediated metabolism (Meech and Mackenzie, 1997; Meech et al., 2019). UGTs catalyze the glucuronidation of sex steroid hormones, which represents a major pathway of inactivation and excretion of these hormones. In humans, UGTs are expressed in the reproductive organs including uterus, ovary, cervix, placenta, testes, and breast (Meech et al., 2019). The crucial role of several UGT genes in reproduction has also been validated in insects. Knockdown of three UGT genes, namely *UGT352A1*, *UGT352B1* and *UGT354A1*, was shown to reduce the fecundity of female *Bemisia tabaci* (Gennadius) (Guo et al., 2020). Moreover, a recent study reported that UGT12 is a positive modulator of reproduction in brown planthopper because UGT12 knockdown resulted in a decrease in vitellogenin synthesis and hormone acid methyltransferase expression (Ge et al., 2019). Consequently, we speculate that *UGT440A1* influences reproduction in *B. xylophilus* by altering the levels of steroid hormones and other biomolecules.

After *B. xylophilus* invade a pine tree, the host pines generate a wide range of nematicidal and nematistatic substances, which can not only defend the invasion but also decrease the reproduction and migration rate of the nematodes (Futai, 2013; Kuwazu, 1998; He et al., 2016). Therefore, *B. xylophilus* must resist or metabolize those substances to successfully invade the host (Lindblom and Dodd, 2009; Mamiya, 2012). Detoxification-related genes, such as cytochrome P450 genes, have been demonstrated to be essential for feeding, reproduction, and pathogenicity of nematodes (Benenati et al., 2009; Ziniel et al., 2015; Qiu et al., 2019). Moreover, UGTs play a crucial role in actual detoxification reactions (phase II of the detoxification process) of nematodes. The present study demonstrated that PWD onset is markedly

delayed after *UGT440A1* knockdown, which highlights the significance of the gene in the pathogenic process of the nematode.

This study is the first to characterize UGTs in *B. xylophilus* and investigate the molecular characteristics and biological functions of *UGT440A1* in *B. xylophilus*. Our study revealed the diverse roles of *UGT440A1* in motility, feeding, and reproduction of *B. xylophilus*. These results suggest that *UGT440A1* gene is involved in the pathogenic process of *B. xylophilus* and the information may facilitate a better understanding of the molecular mechanism of PWD.

## DATA AVAILABILITY STATEMENT

The datasets presented in this study can be found in online repositories. The names of the repository/repositories and accession number(s) can be found in the article/Supplementary Material.

## AUTHOR CONTRIBUTIONS

MW, RL, and GD designed the experiment. MW and LW performed the RNAi experiments. MW and JF performed the gene cloning experiment. MW and QG performed data analysis. MW, RL, and TZ interpreted data and prepared the manuscript. All authors discussed the results and reviewed the manuscript.

## FUNDING

This study was supported by the Key Programs for Research and Development of Shandong Province, China (No. 2016GNC110024), and National Natural Science Foundation of China (Nos: 31070575 and 31901313).

## SUPPLEMENTARY MATERIAL

The Supplementary Material for this article can be found online at: <https://www.frontiersin.org/articles/10.3389/fpls.2022.862594/full#suppleme>

ntary-material

## FOOTNOTES

<sup>1</sup><https://labs.wsu.edu/ugt/>

<sup>2</sup><http://parasite.wormbase.org/index.html>

<sup>3</sup><http://www.ncbi.nlm.nih.gov/gorf/gorf.html>

<sup>4</sup><https://blast.ncbi.nlm.nih.gov/Blast.cgi>

<sup>5</sup>[www.ncbi.nlm.nih.gov/genbank/](http://www.ncbi.nlm.nih.gov/genbank/)

<sup>6</sup><https://www.ncbi.nlm.nih.gov/Structure/cdd/>

<sup>7</sup><https://web.expasy.org/protparam/>

<sup>8</sup><http://www.cbs.dtu.dk/services/SignalP/>

<sup>9</sup><http://www.cbs.dtu.dk/services/THHMM/>

<sup>10</sup><https://swissmodel.expasy.org/>

## REFERENCES

Benenati, G., Penkov, S., Muller-Reichert, T., Entchev, E. V., and Kurzchalia, T. V. (2009). Two cytochrome P450s in *Caenorhabditis elegans* are essential for the organization of eggshell, correct execution of meiosis and the polarization of embryo. *Mech. Dev.* 126, 382–393. doi: 10.1016/j.mod.2009.02.001

Bock, K. W. (2003). Vertebrate UDP-glucuronosyltransferases: functional and evolutionary aspects. *Biochem. Pharmacol.* 66, 691–696. doi: 10.1016/S0006-2952(03)00296-X

Bock, K. W. (2016). The UDP-glycosyltransferase (UGT) superfamily expressed in humans, insects and plants: animal-plant arms-race and co-evolution. *Biochem. Pharmacol.* 99, 11–17. doi: 10.1016/j.bcp.2015.10.001

Crook-McMahon, H. M., Olahova, M., Button, E. L., Winter, J. J., and Veal, E. A. (2014). Genome-wide screening identifies new genes required for stress-induced phase 2 detoxification gene expression in animals. *BMC Biol.* 12:64. doi: 10.1186/s12915-014-0064-6

Daimon, T., Hirayama, C., Kanai, M., Ruike, Y., Meng, Y., Kosegawa, E., et al. (2010). The silkworm Green b locus encodes a quercetin 5-O-glucosyltransferase that produces green cocoons with UV-shielding properties. *Proc Natl Acad Sci U.S.A.* 107, 11471–11476. doi: 10.1073/pnas.1000479107

Espada, M., Silva, A. C., Eves Van Den Akker, S., Cock, P. J., Mota, M., and Jones, J. T. (2016). Identification and characterization of parasitism genes from the pinewood nematode

*Bursaphelenchus xylophilus* reveals a multilayered detoxification strategy. *Mol. Plant Pathol.* 17, 286–295. doi: 10.1111/mpp.12280

Fontaine, P., and Choe, K. (2018). The transcription factor SKN-1 and detoxification gene ugt-22 alter albendazole efficacy in *Caenorhabditis elegans*. *Int. J. Parasitol. Drugs Drug Resist.* 8, 312–319. doi: 10.1016/j.ijpddr.2018.04.006

Futai, K. (1980). Developmental rate and population growth of *Bursaphelenchus lignicolus* (Nematoda: Aphelenchoididae) and *B. mucronatus*. *Appl. Entomol. Zool.* 15, 115–122.

Futai, K. (2013). Pine wood nematode, *Bursaphelenchus xylophilus*. *Annu. Rev. Phytopathol.* 51, 61–83. doi: 10.1146/annurev-phyto-081211-172910

Ge, L. Q., Zheng, S., Gu, H. T., Zhou, Y. K., Zhou, Z., Song, Q. S., et al. (2019). Jinggangmycin-induced UDP-Glycosyltransferase 1-2-like is a positive modulator of fecundity and population growth in *Nilaparvata lugens* (Stål) (Hemiptera: Delphacidae). *Front. Physiol.* 10:747. doi: 10.3389/fphys.2019.00747

Gems, D., and McElwee, J. J. (2005). Broad spectrum detoxification: the major longevity assurance process regulated by insulin/IGF-1 signaling? *Mech. Ageing Dev.* 126, 381–387. doi: 10.1016/j.mad.2004.09.001

Guillemette, C. (2003). Pharmacogenomics of human UDP-glucuronosyltransferase enzymes. *Pharmacogenomics J.* 3, 136–158. doi: 10.1038/sj.tpj.6500171

Guo, L., Xie, W., Yang, Z., Xu, J., and Zhang, Y. (2020). Genome-wide identification and expression analysis of Udp-Glucuronosyltransferases in the whitefly *Bemisia Tabaci* (Gennadius) (Hemiptera: Aleyrodidae). *Int. J. Mol. Sci.* 21:8492. doi: 10.3390/ijms21228492

Guo, Q., Du, G., Qi, H., Zhang, Y., Yue, T., Wang, J., et al. (2017). A nematicidal tannin from *Punica granatum* L. rind and its physiological effect on pine wood nematode (*Bursaphelenchus xylophilus*). *Pestic. Biochem. Physiol.* 135, 64–68. doi: 10.1016/j.pestbp.2016.06.003

Hasegawa, K., Miwa, S., Tsutsumiuchi, K., and Miwa, J. (2010). Allyl isothiocyanate that induces GST and UGT expression confers oxidative stress resistance on *C. elegans*, as demonstrated by nematode biosensor. *PLoS One* 5:e9267. doi: 10.1371/journal.pone.0009267

He, L. X., Wu, X. Q., Xue, Q., and Qiu, X. W. (2016). Effects of Endobacterium (*Stenotrophomonas maltophilia*) on pathogenesis-related gene expression of pine wood nematode (*Bursaphelenchus xylophilus*) and pine wilt disease. *Int. J. Mol. Sci.* 17:778. doi: 10.3390/ijms17060778

Huang, L., Wang, P., Tian, M. Q., Zhu, L. H., and Ye, J. R. (2019). Major sperm protein BxMSP10 is required for reproduction and egg hatching in *Bursaphelenchus xylophilus*. *Exp. Parasitol.* 197, 51–56. doi: 10.1016/j.exppara.2019.01.004

Huang, L., Ye, J. R., Wu, X. Q., Xu, X. L., Sheng, J. M., and Zhou, Q. X. (2010). Detection of the pine wood nematode using a real-time PCR assay to target the DNA topoisomerase I gene. *Eur. J. Plant Pathol.* 127, 89–98. doi: 10.1007/s10658-009-9574-4

Hundle, B. S., O'brien, D. A., Alberti, M., Beyer, P., and Hearst, J. E. (1992). Functional expression of zeaxanthin glucosyltransferase from *erwinia herbicola* and a proposed uridine diphosphate binding site. *Proc. Natl. Acad. Sci. U.S.A.* 89, 9321–9325. doi: 10.1073/pnas.89.19.9321

Ichihara, Y., Fukuda, K., and Suzuki, K. (2000). Early symptom development and histological changes associated with migration of *Bursaphelenchus xylophilus* in seedling tissues of *pinus thunbergii*. *Plant Dis.* 84, 675–680. doi: 10.1094/PDIS.2000.84.6.675

Ikeda, T., and Oda, K. (1980). The occurrence of attractiveness for *Monochamus alternatus* hope (Coleoptera: Cerambycidae) in nematode-infected pine trees. *J. Jpn. For. Soc.* 62, 432–434.

Jones, J. T., Moens, M., Mota, M., Li, H., and Kikuchi, T. (2008). *Bursaphelenchus xylophilus*: opportunities in comparative genomics and molecular host-parasite interactions. *Mol. Plant Pathol.* 9, 357–368. doi: 10.1111/j.1364-3703.2007.00461.x

Kuwazu, K. (1998). Pathogenic toxin of in pine wood disease. *Kagaku Sebutsu*. 36, 120–124.

Lindblom, T. H., and Dodd, A. K. (2009). Xenobiotic Detoxification in the Nematode *Caenorhabditis elegans* (vol 305A, pg 720, 2006). *J. Exp. Zool. Part A*. 311a, 312–312. doi: 10.1002/jez.528

Liu, G., Feng, K., Guo, D., and Li, R. (2015). Overexpression and activities of 1-Cys peroxiredoxin from *Pseudomonas fluorescens* GcM5-1A carried by pine wood nematode. *Folia Microbiol. (Praha)* 60, 443–450. doi: 10.1007/s12223-015-0380-4

Mackenzie, P. I., Owens, I. S., Burchell, B., Bock, K. W., Bairoch, A., Belanger, A., et al. (1997). The UDP glycosyltransferase gene superfamily: recommended nomenclature update based on evolutionary divergence. *Pharmacogenetics* 7, 255–269. doi: 10.1097/00008571-199708000-00001

Mamiya, Y. (1983). Pathology of the pine wilt disease caused by *Bursaphelenchus xylophilus*. *Annu. Rev. Phytopathol.* 21, 201–220. doi: 10.1146/annurev.py.21.090183.001221

Mamiya, Y. (2012). Scanning electron microscopy of pine seedling wood tissue sections inoculated with the pinewood nematode *Bursaphelenchus xylophilus* previously prepared for light microscopy. *J. Nematol.* 44, 255–259.

Matouskova, P., Lecova, L., Laing, R., Dimunova, D., Vogel, H., Raisova Stuchlikova, L., et al. (2018). UDP-glycosyltransferase family in *Haemonchus contortus*: phylogenetic analysis, constitutive expression, sex-differences and resistance-related differences. *Int. J. Parasitol. Drugs Drug Resist.* 8, 420–429. doi: 10.1016/j.ijpddr.2018.09.005

Meech, R., Hu, D. G., Mckinnon, R. A., Mubarokah, S. N., Haines, A. Z., Nair, P. C., et al. (2019). The UDP-Glycosyltransferase (UGT) superfamily: new members, new functions, and novel paradigms. *Physiol. Rev.* 99, 1153–1222. doi: 10.1152/physrev.00058.2017

Meech, R., and Mackenzie, P. I. (1997). Structure and function of uridine diphosphate glucuronosyltransferases. *Clin. Exp. Pharmacol. Physiol.* 24, 907–915. doi: 10.1111/j.1440-1681.1997.tb02718.x

Meech, R., Miners, J. O., Lewis, B. C., and Mackenzie, P. I. (2012). The glycosidation of xenobiotics and endogenous compounds: versatility and redundancy in the UDP glycosyltransferase superfamily. *Pharmacol. Ther.* 134, 200–218. doi: 10.1016/j.pharmthera.2012.01.009

Modesto, I., Sterck, L., Arbona, V., Gomez-Cadenas, A., Carrasquinho, I., Van De Peer, Y., et al. (2021). Insights into the mechanisms implicated in *Pinus pinaster* resistance to pinewood nematode. *Front. Plant Sci.* 12:690857. doi: 10.3389/fpls.2021.690857

Mota, M. M., Braasch, H., Bravo, M. A., Penas, A. C., Burgermeister, W., Metge, K., et al. (1999). First report of *Bursaphelenchus xylophilus* in Portugal and in Europe. *Nematology* 1, 727–734. doi: 10.1163/156854199508757

Nickle, W. R., Golden, A. M., Mamiya, Y., and Wergin, W. P. (1981). On the taxonomy and morphology of the pine wood nematode, *Bursaphelenchus xylophilus* (Steiner & Buhler 1934) Nickle 1970. *J. Nematol.* 13, 385–392.

Oh, K. H., and Kim, H. (2013). Reduced IGF signaling prevents muscle cell death in a *Caenorhabditis elegans* model of muscular dystrophy. *Proc. Natl. Acad. Sci. U.S.A.* 110, 19024–19029. doi: 10.1073/pnas.1308866110

Park, J. E., Lee, K. Y., Lee, S. J., Oh, W. S., Jeong, P. Y., Woo, T., et al. (2008). The efficiency of RNA interference in *Bursaphelenchus xylophilus*. *Mol. Cells.* 26, 81–86.

Penas, A. C., Correia, P., Bravo, M. A., Mota, M., and Tenreiro, R. (2004). Species of *Bursaphelenchus* Fuchs, 1937 (Nematoda : Parasitaphelenchidae) associated with maritime pine in Portugal. *Nematology* 6, 437–453. doi: 10.1023/B:NEMT.0000046914.00963.d

Qiu, X., Yang, L., Ye, J., Wang, W., Zhao, T., Hu, H., et al. (2019). Silencing of cyp-33C9 gene affects the reproduction and pathogenicity of the pine wood nematode, *Bursaphelenchus xylophilus*. *Int. J. Mol. Sci.* 20:4520. doi: 10.3390/ijms20184520

Qiu, X. W., Wu, X. Q., Huang, L., and Ye, J. R. (2016). Influence of Bxpell gene silencing by dsRNA interference on the development and pathogenicity of the pine wood nematode, *Bursaphelenchus xylophilus*. *Int J Mol Sci* 17, 125. doi: 10.3390/ijms17010125

Real, M. D., Ferre, J., and Chapa, F. J. (1991). UDP-glucosyltransferase activity toward exogenous substrates in *Drosophila melanogaster*. *Anal. Biochem.* 194, 349–352. doi: 10.1016/0003-2697(91)90239-p

Shinya, R., Kirino, H., Morisaka, H., Takeuchi-Kaneko, Y., Futai, K., and Ueda, M. (2021). Comparative secretome and functional analyses reveal glycoside hydrolase family 30 and cysteine peptidase as virulence determinants in the pinewood nematode *Bursaphelenchus xylophilus*. *Front. Plant Sci.* 12:640459. doi: 10.3389/fpls.2021.640459

Tang, J., Ma, R., Zhu, N., Guo, K., Guo, Y., Bai, L., et al. (2020). Bxy-fuca encoding alpha-L-fucosidase plays crucial roles in development and reproduction of the pathogenic pinewood nematode, *Bursaphelenchus xylophilus*. *Pest. Manag. Sci.* 76, 205–214. doi: 10.1002/ps.5497

Viglierchio, D. R., and Schmitt, R. V. (1983). On the methodology of nematode extraction from field samples: baermann funnel modifications. *J. Nematol.* 15, 438–444.

Vokral, I., Bartikova, H., Prchal, L., Stuchlikova, L., Skalova, L., Szotakova, B., et al. (2012). The metabolism of flubendazole and the activities of selected biotransformation enzymes in *Haemonchus contortus* strains susceptible and resistant to anthelmintics. *Parasitology* 139, 1309–1316. doi: 10.1017/S0031182012000595

Wan, X., Saito, J. A., Hou, S., Geib, S. M., Yuryev, A., Higa, L. M., et al. (2021). The *Aphelenchus avenae* genome highlights evolutionary adaptation to desiccation. *Commun. Biol.* 4:1232. doi: 10.1038/s42003-021-02778-8

Wang, M., Wang, L. S., Fang, J. N., Du, G. C., Zhang, T. T., and Li, R. G. (2022). Transcriptomic profiling of *Bursaphelenchus xylophilus* reveals differentially expressed genes in response to ethanol. *Mol. Biochem. Parasitol.* 248:111460. doi: 10.1016/j.molbiopara.2022.111460

Wang, Y., Yamada, T., Sakaue, D., and Suzuki, K. (2005). Variations in life history parameters and their influence on rate of population increase of different pathogenic isolates of the pine wood nematode, *Bursaphelenchus xylophilus*. *Nematology* 7, 459–467. doi: 10.1163/156854105774355545

Younus, F., Chertemps, T., Pearce, S. L., Pandey, G., Bozzolan, F., Coppin, C. W., et al. (2014). Identification of candidate odorant degrading gene/enzyme systems in the antennal transcriptome of *Drosophila melanogaster*. *Insect. Biochem. Mol. Biol.* 53, 30–43. doi: 10.1016/j.ibmb.2014.07.003

Yu, L. Z., Wu, X. Q., Ye, J. R., Zhang, S. N., and Wang, C. (2012). NOS-like-mediated nitric oxide is involved in *Pinus thunbergii* response to the invasion of *Bursaphelenchus xylophilus*. *Plant Cell Rep.* 31, 1813–1821. doi: 10.1007/s00299-012-1294-0

Zhao, G. B., Futai, K., Sutherland, J. R., and Takeuchi, Y. (2008). *Pine Wilt Disease*. Tokyo: Springer.

Zhu, N., Bai, L., Schutz, S., Liu, B., Liu, Z., Zhang, X., et al. (2016). Observation and quantification of mating behavior in the pinewood nematode, *Bursaphelenchus xylophilus*. *J. Vis. Exp.* 11:54842. doi: 10.3791/54842

Ziniel, P. D., Karumudi, B., Barnard, A. H., Fisher, E. M., Thatcher, G. R., Podust, L. M., et al. (2015). The schistosoma mansoni cytochrome P450 (CYP3050A1) is essential for worm survival and egg development. *PLoS Negl. Trop. Dis.* 9:e0004279. doi: 10.1371/journal.pntd.0004279

**Conflict of Interest:** The authors declare that the research was conducted in the absence of any commercial or financial relationships that could be construed as a potential conflict of interest.

**Publisher's Note:** All claims expressed in this article are solely those of the authors and do not necessarily represent those of their affiliated organizations, or those of the publisher, the editors and the reviewers. Any product that may be evaluated in this article, or claim that may be made by its manufacturer, is not guaranteed or endorsed by the publisher.

*Copyright © 2022 Wang, Du, Fang, Wang, Guo, Zhang and Li. This is an open-access article distributed under the terms of the Creative Commons Attribution License (CC BY). The use, distribution or reproduction in other forums is permitted, provided the original author(s) and the copyright owner(s) are credited and that the original publication in this journal is cited, in accordance with accepted academic practice. No use, distribution or reproduction is permitted which does not comply with these terms.*

ORIGINAL RESEARCH

published: 14 June 2022

doi: 10.3389/fpls.2022.908308



# Fungal Communities of the Pine Wilt Disease Complex: Studying the Interaction of Ophiostomatales With *Bursaphelenchus xylophilus*

**Cláudia S. L. Vicente<sup>1,2</sup>, Miguel Soares<sup>3</sup>, Jorge M. S. Faria<sup>2</sup>, Margarida Espada<sup>1</sup>, Manuel Mota<sup>4</sup>, Filomena Nóbrega<sup>2</sup>, Ana P. Ramos<sup>3</sup> and Maria L. Inácio<sup>2,5\*</sup>**

<sup>1</sup> MED - Mediterranean Institute for Agriculture, Environment and Development & CHANGE - Global Change and Sustainability Institute, Institute for Advanced Studies and Research, Universidade de Évora - Pólo da Mitra, Évora, Portugal

<sup>2</sup> Instituto Nacional de Investigação Agrária e Veterinária (INIAV, I.P.), Quinta do Marquês, Oeiras, Portugal

<sup>3</sup> Laboratório de Patologia Vegetal “Veríssimo de Almeida” (LPVVA), Instituto Superior de Agronomia (ISA), University of Lisbon, Lisboa, Portugal

<sup>4</sup> MED - Mediterranean Institute for Agriculture, Environment and Development & CHANGE - Global Change and Sustainability Institute, Department of Biology, Universidade de Évora - Pólo da Mitra, Évora, Portugal

<sup>5</sup> GREEN-IT Bioresources for Sustainability, ITQB NOVA, Oeiras, Portugal

**Edited by:**

Xiangming Xu, National Institute of Agricultural Botany (NIAB), United Kingdom

**Reviewed by:**

Noritoshi Maehara, Forestry and Forest Products Research Institute, Japan

Pablo Castillo, Spanish National Research Council (CSIC), Spain

**\*Correspondence:** Maria L. Inácio, lurdes.inacio@iniav.pt

**Specialty section:** This article was submitted to Plant Pathogen Interactions, a section of the journal *Frontiers in Plant Science*

**Received:** 30 March 2022

**Accepted:** 02 May 2022

**Published:** 14 June 2022

**Citation:** Vicente CSL, Soares M, Faria JMS, Espada M, Mota M, Nóbrega F, Ramos AP and Inácio ML (2022) Fungal Communities of the Pine Wilt Disease Complex: Studying the Interaction of Ophiostomatales With *Bursaphelenchus xylophilus*. *Front. Plant Sci.* 13:908308. doi: 10.3389/fpls.2022.908308

Considered one of the most devastating plant-parasitic nematodes worldwide, *Bursaphelenchus xylophilus* (commonly known as pinewood nematode, PWN) is the causal agent of the pine wilt disease in the Eurasian coniferous forests. This migratory parasitic nematode is carried by an insect vector (*Monochamus* spp.) into the host tree (*Pinus* species), where it can feed on parenchymal cells and reproduce massively, resulting in the tree wilting. In declining trees, PWN populations are strongly dependent on fungal communities colonizing the host (predominantly ophiostomatoid fungi known to cause sapwood blue-staining, the blue-stain fungi), which not only influence their development and life cycle but also the number of individuals carried by the insect vector into a new host. Our main aim is to understand if PWN-associated mycobiota plays a key role in the development of PWD, in interaction with the PWN and the insect vector, and to what extent it can be targeted to disrupt the disease cycle. For this purpose, we characterized the fungal communities of *Pinus pinaster* trees infected and non-infected with PWN in three collection sites in Continental Portugal with different PWD temporal incidences. Our results showed that non-infected *P. pinaster* mycoflora is more diverse (in terms of abundance and fungal richness) than PWN-infected pine trees in the most recent PWD foci, as opposed to the fungal communities of long-term PWD history sites. Then, due to their ecological importance for PWN survival, representatives of the main ophiostomatoid fungi isolated (*Ophiostoma*, *Leptographium*, and *Graphilbum*) were characterized for their adaptative response to temperature, competition in-between taxa, and as food source for PWN. Under the conditions studied, *Leptographium* isolates showed promising results for PWN control. They could outcompete the other species, especially *O. ips*, and significantly reduce the development of PWN populations when compared to *Botrytis cinerea* (routinely used for PWN lab culturing), suggesting this to be a natural antagonist not only for the other blue-stain species but also for the PWN.

**Keywords: biocontrol, blue-stain fungi, diversity, ecological interactions, mycoflora, pine wood nematode**

## INTRODUCTION

Pine wilt disease (PWD) is a devastating disease that affects mainly coniferous trees of the *Pinus* genus. The plant parasitic nematode *Bursaphelenchus xylophilus* (Steiner & Buhrer) Nickle, commonly known as the pinewood nematode (PWN), is responsible for the onset of PWD symptoms, namely, the characteristic needle yellowing and wilting as a result of shoot desiccation and chlorosis, that can lead to tree death in under 2 months (Futai, 2013). The PWN was first identified in North America, where it is believed to be an endemic. In its native range, the PWN only seldom causes host disease, generally in weakened native species or on exotic introduced pine species (Dwinell, 1997). There, the disease has a low expression because of the co-evolution of the PWN with native pines. In the beginning of the 20th century, in the Japanese islands, extensive ranges of pine forest began developing PWD symptoms, and the PWN was identified soon after (Mamiya, 1983). Since then, PWD has spread throughout the Asian continent causing strong ecological and economic impacts in Japan, China, Korea, and Taiwan (Vicente et al., 2012). In 1999, Portugal became its entry point into the European continent leading to the enforcement of strong containment strategies by national authorities and the EU and was set under quarantine (Mota et al., 1999). However, by 2008, the Portuguese continental area and Madeira Island (Fonseca et al., 2012) were considered affected and even more restringing measures were applied (Rodrigues et al., 2015). Several outbreaks have been reported in border Spanish forests (Abelleira et al., 2011). The PWN is now considered an A2 quarantine pest in the EU and a strong yearly investment is made in its containment and eradication for fear of a European pandemic in its susceptible pine forests (Robertson et al., 2011; Fonseca et al., 2012; de la Fuente and Saura, 2021).

The development of PWD and the intensity of its symptomatology are highly dependent on environmental and biological factors (Liu et al., 2021). Besides its causal agent, the PWN, other organisms are known to influence the development of PWD. Fungi are of great importance for the PWN. For dispersal, the PWN depends on an insect vector, the *Monochamus* genus, that

carries and transmits the parasite to the new susceptible healthy host pines. Once inside the new host, the PWN enters the resin canals, attacks the epithelial cells, and causes extensive damage as it moves through the canal system and rapidly reproduces. During this reproductive phase on dead or decaying wood, the PWN depends necessarily on local fungal flora as a source of food for rapid multiplication (Futai, 2013). A weakened pine tree is more easily attacked by the fungi transmitted by bark beetles (Coleoptera: Scolytidae) that further increase the symptomatology of wilting and function as a necessary food source for the PWN. Thus, these fungi are essential for nematode survival and reproduction (Vicente et al., 2021). Generally called blue-stain fungi, referring to the damage they cause, namely blue or even black discoloration of the sapwood of trees, mostly on conifers (Harrington, 1993; Kim et al., 2003; Zhou et al., 2006; Six, 2012), these bark beetle vectored fungi are also known as “ophiostomatoid fungi” (Kirisits, 2007). Within this group, Ophiostomatales, comprising six genera, *Ophiostoma* sensu stricto (s. str.), *Raffaelea* s. str., *Ceratocystiopsis*, *Fragspaeria*, *Graphilbum*, and *Leptographium* senso lato (s. l.) are clearly separated from fungi of the Microascales order, namely *Ceratocystis* sp. (de Beer et al., 2013). *Ceratocystis*, *Ceratocystiopsis*, and *Ophiostoma* fungi and their related anamorphs could be distinguished based on the chemical composition of their cell walls. Besides chitin, cell walls of *Ophiostoma* also contain cellulose and rhamnose, which is quite unusual for ascomycete fungi. In contrast, the cell walls of *Ceratocystis* and *Ceratocystiopsis* spp. consist mainly of chitin. The cell walls of *Ophiostoma* fungi make them highly tolerant to cycloheximide that inhibits the protein synthesis of most eukaryotic organisms (Harrington, 1981), while species of *Ceratocystis* and *Ceratocystiopsis* are very sensitive to even low concentrations of this antibiotic (Kirisits et al., 2002; Plattner et al., 2009; Reid et al., 2010).

The hypothesis of PWN nutritional dependency in relation to some species of ophiostomatoid fungi inhabiting pine trees is supported by significant observations: (1) PWN propagates at higher rates in fungus-inoculated wood than in uninoculated wood (Maehara and Futai, 2000); and the number of PWN individuals transferred to a beetle is much higher in fungus-colonized wood than in fungal-free wood (Maehara and Futai, 1996). Maehara and Futai (1996, 1997) showed that *O. minus*-inoculated wood-blocks of *P. densiflora* presented a higher percentage of PWN transferred by beetles than when inoculated with *Trichoderma* spp. or in uninoculated

blocks. Beetles emerging from pupal chambers having an intense colonization by blue-stain fungi vectored higher numbers of dauer juveniles (J<sub>IV</sub>), highlighting the relation between the PWN population and the fungal species present in the infected tree (Maehara and Futai, 2005). These results and further work (to Maehara et al., 2006; Maehara, 2008; Niu et al., 2012; Futai, 2013; Pimentel et al., 2021) undoubtedly suggest a mutualistic symbiosis between the nematode and certain fungi, possibly because of a long-term co-evolution. This effect is not surprising considering the mycetophagous status of *Bursaphelenchus* nematodes and might represent the trace of an evolutionary transition from this fungal-feeding behavior to the plant parasitic activity of *B. xylophilus* (Kanzaki et al., 2014).

Although there is strong evidence of fungal involvement in the expression of PWD, this subject is controversial, and to understand the complex dynamics of PWD it is crucial to identify the fungal community in declining trees, ascertaining which species have a role in PWN feeding, reproduction, and dispersal. The comprehensive scenario of the fungal community in the PWN life cycle, through a spatio-temporal analysis of the mycobiota associated with the nematode and the susceptible host tree, constitutes a pioneering approach in Portuguese maritime pine stands with a high prevalence of PWD. The present study characterizes the: (i) fungal communities in non-infected and PWN-infected *P. pinaster* trees from three contrasting PWD focus on Continental Portugal and (ii) adaptative responses of ophiostomatoid fungi (genus *Ophiostoma*, *Leptographium* and *Graphilbum*) inhabiting Portuguese pine stands to temperature, antagonism, and PWN interaction due to their well-recognized history with PWN.

## MATERIALS AND METHODS

### Wood Sampling and Processing, and Nematode Collection

Three surveys were conducted in mainland Portugal during the period of October 2019 in Seia (Guarda District, Central Portugal) in January 2020 in Companhia das Lezírias (Santarém, Central Portugal) and June 2020 in Tróia (Setúbal District, Coast of Portugal) (Table 1). The first location (Seia) is considered a transitional PWD focus, where the disease was identified in 2018–2019. The other two locations, Companhia das Lezírias and Tróia, are

known as long-term PWD foci, nearby the first PWN detection site in Portugal (Mota et al., 1999). At each site, 10 PWD-symptomatic trees and 10 non-symptomatic trees were randomly selected according to the wilting/defoliation classification: 0, no symptoms; 1, first branch with yellow needles; 2, yellow tree canopy; 3, yellow to reddish tree canopy; and 4, brown canopy to dead tree (Cadahia et al., 1991). Wood disk were collected and stored in plastic bags for transportation to INIAV I.P. laboratories (Oeiras, Portugal). Concerning wood processing, cutting was conducted thoroughly with disinfection of the mechanical woodworking band saw with 70% (v/v) ethanol in-between cuttings and beginning with non-symptomatic trees. Approximately 100 g of wood pieces were used for nematode extraction by the modified tray method (Whitehead and Hemming, 1965). The rest of the material was stored at 4°C. After 48 h of incubation, samples were observed under a stereoscopic microscope (Olympus SZX12, Tokyo, Japan) to detect PWN. The following classes were considered to score nematode abundance in 100 g of wood: class 0, no nematodes recovered; class I, <50 nematodes; class II, between 51 and 200 nematodes; class III, between 201 and 1,000 nematodes; class IV, with 1,001 to 5,000 nematodes; and class V, more than 5,000 nematodes. The suspension of PWN was collected and stored in sterile 50 mL Falcon tubes. All material (wood pieces, and nematode suspensions) were stored at 4°C until further processing. The selection of *P. pinaster* trees for fungal isolation was based on: PWD symptomology and presence of PWN in higher proportion to other tree-inhabiting nematodes.

**Table 1.** Characterization of geographic and climate conditions for each collection site (Seia, Tróia, Companhia das Lezírias).

Location	Collection Sites				Pinus pinaster samples			
	GPS	Tmax (°C) <sup>a</sup>	Tmin (°C) <sup>a</sup>	Precipitation (mm) <sup>a</sup>	PWD symptoms	Tree ID	PWD symptoms <sup>b</sup>	PWN class <sup>c</sup>
Seia (S)	40°15'57.0"N 7°42'47.6"W	18	0.5	50–100	No	S1	0	0
						S2	0	0
						S13	0	0
						S19	0	0
						S32	0	0
	38°49'17.6"N 8°52'20.5"W	10	1.5	50–100	Yes	S35	3	IV
						S36	3	IV
						S38	3	IV
						S39	3	III
						S40	3	III
Companhia das Lezírias (L)	38°28'07"N 8°52'18"W	20	0.5	1–5	No	L7	0	0
						L8	0	0
						L9	0	0
						L10	0	0
						L11	0	0
					Yes	L2	4	III
	38°28'07"N 8°52'18"W	20	0.5	1–5		L3	3	III
						L4	3	IV
						L5	3	III
						L6	4	IV
						T8	0	0
						T9	0	0
Tróia (T)	38°28'07"N 8°52'18"W	20	0.5	1–5	No	T10	0	0
						T11	0	0
						T12	0	0
					Yes	T1	4	IV
						T2	4	III
	38°28'07"N 8°52'18"W	20	0.5	1–5		T3	4	II
						T4	4	III
						T7	4	IV

Classification of *Pinus pinaster* trees sampled (disease symptoms and nematode class).

<sup>a</sup>Average values at collection time obtained from IPMA Bulletins (Portugal) (Instituto Português do Mar e da Atmosfera (IPMA), 2019, 2020); <sup>b</sup>Symptoms Class: 0, no symptoms; 1, one yellow branch; 2, yellow canopy; 3, yellowish to reddish canopy; 4, brown canopy—dead tree. <sup>c</sup>Nematode Class (per 100 grams of wood): 0, no nematodes; I, < 50 nematodes; II, 51–200 nematodes; III, 201–1000 nematodes; IV, 1001–5000 nematodes; V, > 5001 nematodes.

## Isolation of Ophiostomatales and Other Wood-Inhabiting Fungi

Under aseptic conditions, wood pieces from the selected trees were firstly cut into small fragments, surface sterilized with 70% ethanol (v/v) for 15 s, followed by serial washes with sterile distilled water, and dried in a sterilized filter paper. Following, surface-sterilized fragments were transferred to 2% (w/v) malt extract agar (MEA, Difco) supplemented with 200 mg/l of cycloheximide and 100 mg/l streptomycin. Plates were incubated at 25°C in the dark and monitored daily for fungal growth for at least 1 week. Hyphal tips of emerging colonies were transferred to fresh MEA plates. Pure cultures of the fungal isolates were grouped according to culture morphology. Representatives from each group were selected for further identification and

characterization and deposited in the culture collection of INIAV institute (Micoteca da Estação Agronómica Nacional (MEAN).

## **DNA Extraction, Amplification, and Phylogenetic Analysis**

For each fungal representative, fresh mycelium was grown in 2% MEA and incubated for 7 days at 25°C. Total DNA was extracted using the DNeasy Plant mini kit (Qiagen GmbH, Hilden, Germany) following the protocol provided by the manufacturer. Partial gene sequences were determined for the internal transcribed spacer region (ITS),  $\beta$ -tubulin (TUB), elongation factor 1- $\alpha$  (TEF), and calmodulin (CAL) using primers listed in Supplementary Table 1 (White et al., 1990; Gardes and Brunts, 1993; Glass and Donaldson, 1995; Carbone and Kohn, 1999; Duong et al., 2012; Marincowitz et al., 2015). For a final volume of 25  $\mu$ l, the PCR reaction mixture consisted of 2.5  $\mu$ l of 10x reaction Buffer, 0.5U Supreme NZYtaq II (NZYTECH, Portugal), 1.0  $\mu$ l dNTP mix (10 mM), 1.25  $\mu$ l of each primer (10  $\mu$ M), 1.25  $\mu$ l Mg<sup>2+</sup> (50 mM), and 2  $\mu$ l template DNA. The PCR conditions were: (i) initial denaturation at 95°C for 5 min; (ii) 34 cycles of denaturation at 94°C for 30 s, annealing at 48–52°C (depending on the marker gene), and extension at 72°C for 15–30 s; and (iii) final extension at 72°C for 10 min. PCR products were cleaned using EXO-SAP (Exonuclease I and FastAP™ Thermosensitive Alkaline Phosphatase, ThermoScientific, CA, USA) following the manufacturer's recommendations. The amplified PCR products were sequenced at Stabvida (Costa da Caparica, Portugal) using the same primers used for their amplification. All sequences from selected fungal isolates were deposited in NCBI GenBank.

Sequences were used as the query at NCBI GenBank for preliminary identification using BLAST tool (<https://blast.ncbi.nlm.nih.gov/>). Published sequences from closely related species were retrieved from the database (Supplementary Table 2). Different datasets of ITS, TUB, and CAL gene sequences were compiled based on the species complex or genera. Multiple sequence alignment was conducted using MAFFT v7.0 (Katoh and Standley, 2013) and trimmed with trimAl v.1.4.1 (Capella-Gutiérrez et al., 2009). Phylogenetic trees were reconstructed for each dataset using Maximum likelihood (ML) method, and the best fitting substitution model selected using the Akaike Information Criterion (AIC) estimated in the Model Testing plugin from CLC Main Workbench 21.0.5 software (QIAGEN, Aarhus A/S). Final adjustments were made in iTOL (<https://itol.embl.de>) (Letunic and Bork,

2021). Phylogenetic trees were supported by 1,000 bootstrap to assess node support and overall robustness of the tree topology.

### **Growth Studies and Direct Inhibition Antagonistic Trials**

Representatives of the ophiostomatoid isolates were selected for growth studies and antagonistic trials. For the growth studies, mycelium of each fungal representative was cultured on three 9-cm (Ø) Petri dishes containing 2% MEA (Difco®). Plates were inoculated with a 7 mm diameter mycelial plug taken from the margin of 5 days actively growing cultures and incubated in the dark at seven different temperatures: 5, 10, 20, 25, 30, 35, and 40°C. The radial growth of each plate was measured every 24 h, until the colonies reached 7 cm in diameter.

To assess the direct inhibition antagonism between ophiostomatoid-like isolates, different combinations were tested by dual culture assay (Royse and Ries, 1977; Almeida et al., 2020). A mycelium plug from pure cultures of the selected fungal isolates were placed on opposite sides of a 9-cm potato dextrose agar (PDA, Difco) plate, ~1 cm to the edge of the plate. Each combination was repeated three times and incubated at 25°C in dark conditions for 5 days. Measurements of the radial growth (from the edge of the plug until the end of the colony) were taken daily. The inhibition percentage was calculated by  $I (\%) = [(R1-R2)/R1] \times 100$ , where R1 was the radial growth of the potential antagonist and R2 was the radial growth of the test organism.

### **PWN Feeding Trials in the Different Ophiostomatoid Fungi**

The reference culture *B. xylophilus* BX013.003 (N 39°43'338", W 9°01'557") from INIAV Nematology collection (INIAV I.P., Oeiras) was used in this study. Nematodes were routinely cultured in the non-sporulating strain *Botrytis cinerea* grown on autoclaved barley seeds at 25°C. Prior to the experiments, the nematodes were extracted using the modified Baermann funnel technique (Whitehead and Hemming, 1965) and counted under an Olympus SZX12 (Tokyo, Japan) stereomicroscope for concentration adjustment.

The selected ophiostomatoid isolates were tested on feeding trials with PWN. Cultures of *B. cinerea* were used as a positive control for PWN population growth. For each isolate and control tested, six PDA plates were previously prepared and grown for 7 days at 25°C. Freshly extracted

nematodes, mixed life-stages, were adjusted for a concentration of 1,000 nematodes per ml of distilled water, and 500  $\mu$ l (ca. 500 nematodes) was inoculated into PDA plates containing the chosen isolates. Seven days after PWN inoculation, the nematodes were extracted by the modified Baermann method for 24 h and counted under an Olympus SZX12 stereomicroscope. The approximate total number of PWN was calculated for the total volume of the nematode suspension (final volume adjusted to 20 mL). Six replicates were conducted for each isolate. Each counting was repeated three times to correctly access the number of nematodes of each sample according to Aikawa and Kikuchi (2007).

## **Data Analysis**

The relative frequency of isolation (%) was estimated as the number of isolates of each order divided by the total number of species isolated and multiplied by 100 (Chang et al., 2017). To characterize the species diversity and richness of fungal communities from the different sites, the following indexes were calculated in PAST 4.02 software (Hammer et al., 2001): Simpson diversity index (S1-D), Shannon diversity index (H), dominance (D), evenness (E), and Sørensen index. Statistical analyses were performed using R in jamovi software 1.6.23 (R Core Team, 2020; The jamovi project, 2021). Kruskal–Wallis test (non-parametric one-way analysis of variance, ANOVA) was used to infer differences in the total number of PWN grown in the different ophiostomatoid isolates; the data was also analyzed using DSCF pairwise comparison ( $p < 0.05$ ) for multiple mean comparisons.

# **RESULTS**

## **Fungal Isolation and Diversity Analysis**

Three surveys were conducted before the maturation feeding phase of the insect vector, when the insect vector is not yet flying (and carrying PWN) for new host trees. The three locations were sorted by long-term PWD foci (Tróia; and Companhia das Lezírias) and transitional or recent PWD focus (Seia), aiming the description of shifts in the fungal communities as the result of disease history in these locations. In each survey (Table 1), a total of 10 *P. pinaster* trees were considered for fungal isolation, namely, 5 non-

symptomatic trees with symptoms and nematode class 0; and 5 PWD symptomatic trees with symptoms between class 3 and 4, and nematode concentration ranging from class III (201–1,000 nematodes per 100 g of wood) and class IV (1001–5000 nematodes per 100 g of wood). The presence of PWN was only detected and identified in symptomatic *P. pinaster* trees. Hereafter, symptomatic trees will be designated as PWN-infected, and non-symptomatic trees will be referred to as non-infected.

In terms of the total number of fungal isolations, 242 isolates were obtained from *P. pinaster* trees (45 from Companhia das Lezírias; 94 from Tróia; and 103 from Seia). Culture morphology and color supported by molecular marker sequencing were used for the taxonomic identification of each fungal isolate. Overall, the most abundant orders were Ophiostomatales (58% in Tróia, 60% in Companhia das Lezírias, and 90% in Seia) mostly detected in PWN-infected *P. pinaster*, followed by orders Pleosporales (2% in Companhia das Lezírias and 33% in Seia) and Eurotiales (64% in Companhia das Lezírias and 66% in Tróia) only in non-infected trees (Figure 1). The representative genera of Ophiostomatales were *Ophiostoma* with 34% (17 isolates in non-infected trees in Seia; and 65 isolates in all PWN-infected trees), *Leptographium* with 10% (24 isolates only in PWN-infected *P. pinaster*), *Graphilbum* with 2.1% (5 isolates in PWN-infected *P. pinaster*), and *Sporothrix* with 0.1% (one isolate detected in PWN-infected trees). In the orders Pleosporales and Eurotiales, the most predominant genera were *Alternaria* with 6.2% (15 isolates in non-infected trees) and *Penicillium* with 23.1% (56 isolates in non-infected trees). Only 2.5% of the fungal isolates were not identified as being classified as unidentified. Based on this general identification, and since the number of isolates was uneven between collection sites (Supplementary Figure 1), diversity indexes (Simpson 1-D and Shannon-H) varied widely among locations (Table 2). The fungal communities in the non-infected *P. pinaster* were more diverse (S1-D = 0.71; SH = 1.43) than in PWN-infected *P. pinaster* (S1-D = 0.46; SH = 0.87) in Seia. However, for the case of Companhia das Lezírias and Tróia, the results were different being PWN-infected more diverse in what concerns fungal composition than non-infected *P. pinaster*. For each site, similarity Sørensen index indicated that fungal communities from non-infected and PWN-infected trees were dissimilar, this observation being clearer in Tróia (S = 0.182) and Companhia das Lezírias (S = 0.2) than in Seia (S = 0.6). The PCoA analysis clearly separated PWN-infected fungal

communities from non-infected *P. pinaster* fungal communities in Seia and Tróia (Supplementary Figure 2). Fungal communities from both PWN-infected and non-infected *P. pinaster* in Companhias das Lezírias clustered together, denoting no separation.

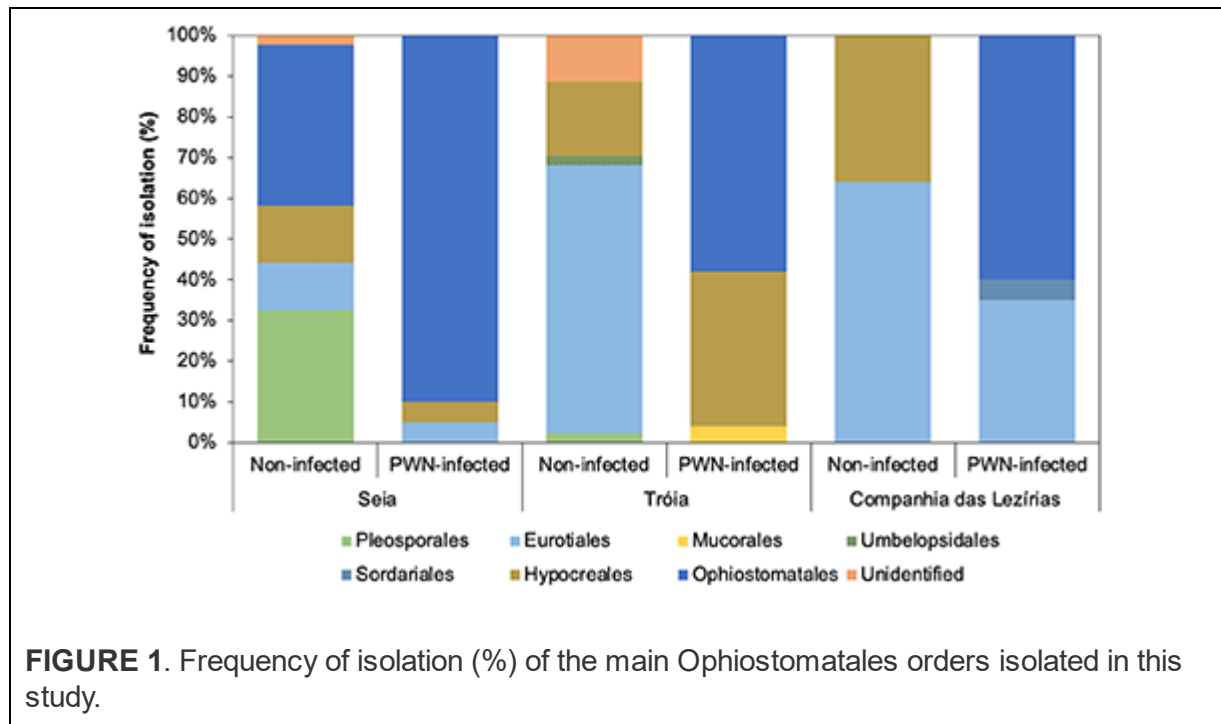


**Table 2.** Ecological diversity indexes (taxa = order) of fungal communities from non-infected and PWN-infected *Pinus pinaster* trees sampled.

Diversity indexes	Seia		Companhia das Lezírias		Tróia	
	Non-infected	PWN-infected	Non-infected	PWN-infected	Non-infected	PWN-infected
Taxa S	6	4	4	6	6	5
Individuals	43	60	25	20	44	50
Dominance D	0.2872	0.535	0.36	0.255	0.469	0.3096
Simpson 1-D	0.7128	0.465	0.64	0.745	0.531	0.6904
Shannon H	1.434	0.8711	1.139	1.51	1.106	1.276
Evenness e <sup>h</sup> /S	0.6989	0.5974	0.7808	0.7544	0.5038	0.7162
Sørensen index	0.60		0.2		0.182	

## Phylogenetic Analyses of Ophiostomatoid Isolates

A total of 366 DNA sequences (126 ITS; 84 TUB; 89 TEF; 67 CAL) were obtained to fully describe fungal communities in the non-infected and PWN-infected *P. pinaster* trees. All representative sequences for the four loci were BLAST against the NCBI GenBank database to retrieve the closest accessions (Supplementary Tables 2–5). From these sequences, only

Ophiostomatales were considered for further phylogenetic analyses due to their close relation with *B. xylophilus* (Futai, 2013) (Table 3). Two datasets were considered based on preliminary BLAST results from ITS data: *Ophiostoma* s. l. and *Leptographium* s. l. as defined by de Beer et al. (2013). The amplification of ITS sequences for *Leptographium* s. l. species is often problematic (de Beer et al., 2013; Chang et al., 2017), and for some isolates were not obtained. In these cases, their taxonomic identification was supported by the other molecular markers. Additionally, the presence and absence of introns for TUB, TEF, and CAL sequences in both complexes, forced their separate analyses. Reference sequences for complexes within each dataset (*Ophiostoma* s. l. and *Leptographium* s. l.) were retrieved from GenBank (Supplementary Table 3).

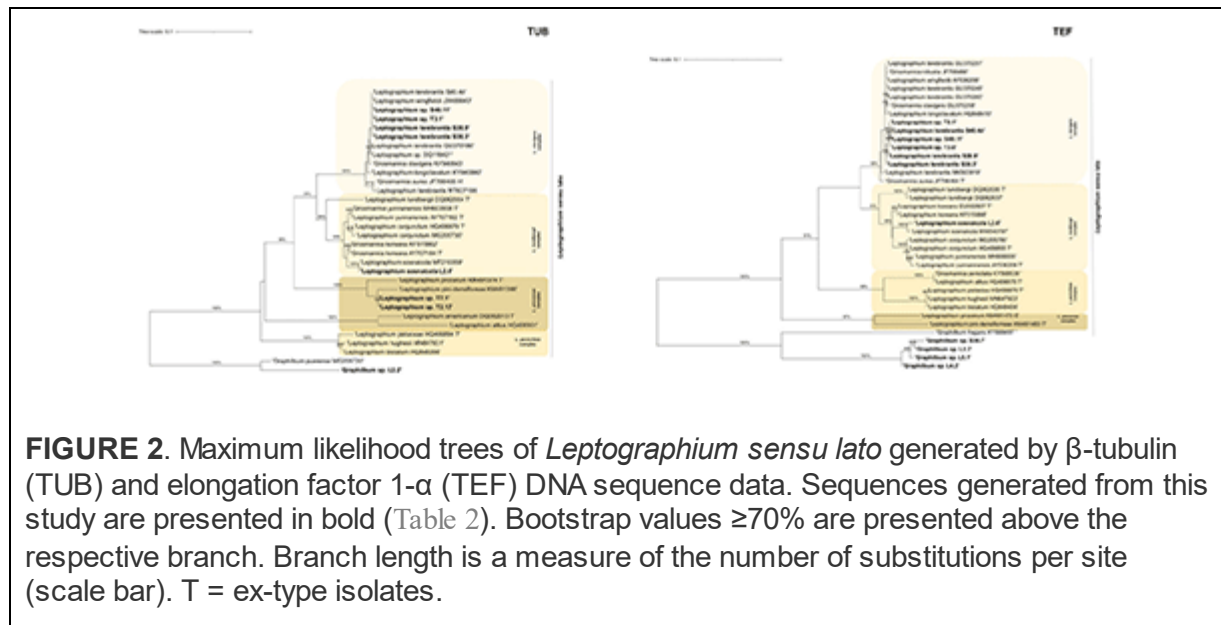
**Table 3.** Fungal isolates representative of the main Ophiostomatales genus isolated in this study.

Group taxon	Species	Isolate no.	PWD	Origin	GenBank Accession no.			
					ITS	TUB	TEF	CAL
1	<i>Graphilbum</i> sp. 1	L2.2	PWD-symptomatic	Companhia das Lezírias	OM468578	–	–	–
	<i>Graphilbum</i> sp. 2	L4.2	PWD-symptomatic	Companhia das Lezírias	OK559549	–	OM616860	–
	<i>Graphilbum</i> sp. 3	L5.1	PWD-symptomatic	Companhia das Lezírias	OK559550	–	OM616861	–
	<i>Graphilbum</i> sp. 4	S38.7	PWD-symptomatic	Seia	–	–	–	–
2	<i>Leptographium terebrantis</i>	S38.3	PWD-symptomatic	Seia	OM468594	OM514986	–	–
	<i>Leptographium terebrantis</i>	S38.9	PWD-symptomatic	Seia	OM468595	ON333628	ON333659	ON333660
	<i>Leptographium terebrantis</i>	S40.4b	PWD-symptomatic	Seia	OK559544	OM514987	OM616854	–
3	<i>Leptographium sosnaicola</i>	L2.6	PWD-symptomatic	Companhia das Lezírias	OK559548	OM514991	OM616859	OM616866
4	<i>Leptographium</i> sp. 1	T2.13	PWD-symptomatic	Tróia	OK559547	OM514990	–	–
	<i>Leptographium</i> sp. 2	T7.1	PWD-symptomatic	Tróia	OM468585	ON333629	–	ON333661
	<i>Leptographium</i> sp. 3	S40.11	PWD-symptomatic	Seia	–	OM513989	OM616856	–
	<i>Leptographium</i> sp. 4	T3.1	PWD-symptomatic	Tróia	OK559545	OM514988	OM616857	OM616865
	<i>Leptographium</i> sp. 5	T3.6	PWD-symptomatic	Tróia	–	–	OM616858	–
5	<i>Ophiostoma ips</i>	L3.1	PWD-symptomatic	Companhia das Lezírias	OM468579	ON333612	ON333630	ON333647
	<i>Ophiostoma ips</i>	L4.1	PWD-symptomatic	Companhia das Lezírias	OM468580	ON333613	ON333631	–
	<i>Ophiostoma ips</i>	L5.2	PWD-symptomatic	Companhia das Lezírias	OM468581	ON333614	ON333632	–
	<i>Ophiostoma ips</i>	T1.4	PWD-symptomatic	Tróia	OM468583	ON333615	ON333633	ON333648
	<i>Ophiostoma ips</i>	T2.3	PWD-symptomatic	Tróia	OM468584	ON333616	ON333634	ON333649
	<i>Ophiostoma ips</i>	T7.4	PWD-symptomatic	Tróia	OM468586	ON333617	ON333635	ON333650
	<i>Ophiostoma ips</i>	S13.1	Non-symptomatic	Seia	OM468587	ON333618	ON333636	ON333651
	<i>Ophiostoma ips</i>	S19.2	Non-symptomatic	Seia	OM468588	ON333619	ON333637	ON333652
	<i>Ophiostoma ips</i>	S19.17	Non-symptomatic	Seia	OM468589	ON333620	ON333638	–
	<i>Ophiostoma ips</i>	S32.10	Non-symptomatic	Seia	OM468590	ON333621	ON333639	ON333653
	<i>Ophiostoma ips</i>	S35.1	PWD-symptomatic	Seia	OM468591	ON333622	ON333640	ON333654
	<i>Ophiostoma ips</i>	S35.3	PWD-symptomatic	Seia	OM468592	ON333623	ON333641	ON333655
	<i>Ophiostoma ips</i>	S36.1	PWD-symptomatic	Seia	OK559539	OM616846	OM616850	–
	<i>Ophiostoma ips</i>	S36.9	PWD-symptomatic	Seia	OM468593	ON333624	ON333642	ON333656
	<i>Ophiostoma ips</i>	S38.16	PWD-symptomatic	Seia	OK559541	OM616848	OM616853	OM616862
	<i>Ophiostoma ips</i>	S39.1	PWD-symptomatic	Seia	OK559540	OM616847	OM616851	–
	<i>Ophiostoma ips</i>	S39.6	PWD-symptomatic	Seia	OM468596	–	ON333643	–
	<i>Ophiostoma ips</i>	S40.10	PWD-symptomatic	Seia	OK559542	OM616849	OM616855	OM616863
	<i>Ophiostoma ips</i>	S40.1a	PWD-symptomatic	Seia	OM468597	ON333625	ON333644	ON333657
	<i>Ophiostoma ips</i>	S40.7	PWD-symptomatic	Seia	OM468598	ON333626	ON333645	ON333658
6	<i>Sporothrix</i> sp. 1	L5.3	PWD-symptomatic	Companhia das Lezírias	OM468583	ON333627	ON333646	–

## Leptographium Sensu Lato

Within *Leptographium* s. l., four taxa were described: taxon 1, *Graphilbum* sp. 1-4; taxon 2, *Leptographium terebrantis*; taxon 3, *Leptographium* sp. 1-4; and taxon 4, *Leptographium sosnaicola* (Table 3). Multiple sequence alignment contained for each marker, respectively: 39 sequences with 665 bp, with gaps, for ITS; 31 sequences with 414 characters (with gaps) for TUB; 37 sequences with 528 bp (with gaps) for TEF; and 13 sequences with 597 bp (with gaps) for CAL (Figure 2, Supplementary Figures 3, 5). The best evolutionary substitution models for both trees were general time reversible (GTR) +G (rate variation) + T (topology variation). The *Leptographium* s. l.

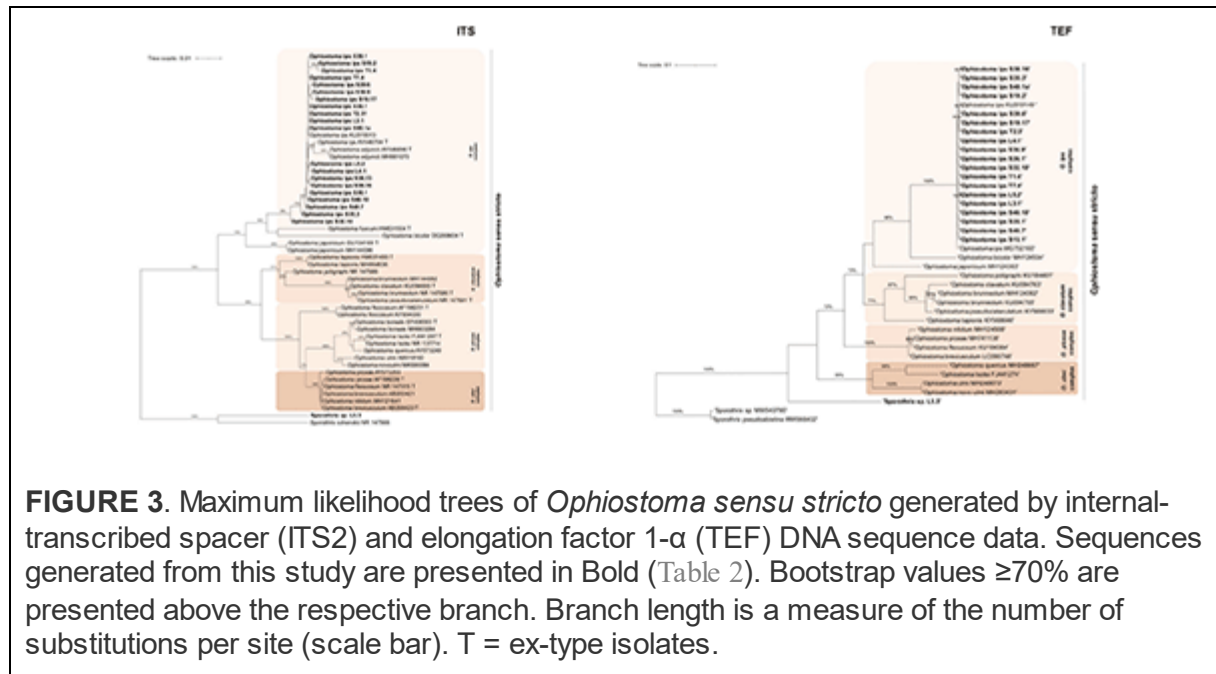
is well-represented by *L. clavigera*, *L. lundbergii*, *L. penicillate*, and the *L. procerum* complexes (Figure 2). The group taxon 1, *Graphilbum* sp., was considered the outgroup of all trees of *Leptographium* s. l. Within this group, *Graphilbum* sp. L 2.2 (TUB, TEF), *Graphilbum* sp. L4.2, L5.1, and S38.7 (TEF) clustered together with other *Graphilbum* species; however, their percentage of identity was lower than 98% (Supplementary Table 2), not allowing their species-level assignment. Taxon 2 and Taxon 3 belonged to *L. clavigera* complex (in both markers) and were grouped in-between *L. wingfieldii* and *L. terebrantis* with high support. In fact, isolates S38.3/S38.9 (isolated from the same tree) and S40.4b shared 100% similarity with *L. terebrantis*, while the other isolates (T3.1, T3.6, S40.11) were 100% identical in TUB but 99% in TEF (Supplementary Table 2). In CAL sequences, these isolates were identified as *Grosmannia clavigera* (100%) by the lack of *Leptographium* sequences in the database (Supplementary Table 2). Taxon 4 *L. sosnaicola* L2.6 formed a monophyletic group with *L. sosnaicola* MT210359 (TUB) and *L. sosnaicola* MW540787 (TEF), with good support, and clustering in between *L. koreana* and *L. conjunctum* within the *L. lundbergii* complex.



## Ophiostoma Sensu Lato

Within this lineage, only two taxa were described: taxon 5, *Ophiostoma ips* and taxon 6, *Sporothrix* sp.1 (Table 3). The alignment matrixes contained, respectively, 48 sequences (Table 2, Supplementary Table 3) with 648

characters, including gaps, for ITS marker; 43 sequences with 220 bp for TUB marker; 40 sequences with 379 bp for TEF; and 29 sequences with 339 bp for CAL (Figure 3, Supplementary Figures 4, 5). The best evolutionary substitution models for ITS and TEF phylogenograms were, respectively, Hasegawa-Kishino-Yano (HKY) +G+T and GTR+G+T. The well-defined phylogenetic complexes with *Ophiostoma* s. str. (*O. ips* complex, *O. piceae* complex, *O. ulmi* complex, and *O. clavatum* complex) were maintained, when possible, for all phylogenetic trees of *Ophiostoma* s. l. Fungal isolates from all locations and tree status, previously identified as *O. ips*, clustered together with good support with the type strain *O. ips* AY546704 and *O. ips* KU319013 (described in *P. sylvestris* in Poland) within the *O. ips* complex (Figure 3). Similar topologies were obtained in ML phylogenetic trees with the other molecular markers (BT, TEF and CAL; Figure 3, Supplementary Figures 4, 5), which sustained the identification of *O. ips* fungal isolates. Belonging to *Ophiostoma* s. l., the isolate L5.3 was identified as *Sporothrix* sp. 1 (99% similarity with *Sporothrix* sp. MW540762.1 with ITS; 100% *S. pseudoabietina* MH583598 with TUB; and 99.39% *Sporothrix* sp. KY568667 with TEF; Supplementary Table 2). In Figure 3, this isolate clustered with good support with *S. schenckii* NR\_147566, being considered as the outgroup of this phylogenetic tree. Its position is also corroborated in Supplementary Figures 4, 5.



## Adaptative Responses of Ophiostomatoid Isolates to Temperature, Antagonism, and PWN Interaction

To characterize the adaptative response (in terms of growth and antagonistic performance and PWN food source) of the main Ophiostomatales taxon (genus *Ophiostoma*, *Leptographium*, and *Graphilbum*) isolated from PWN-infected *P. pinaster*, ten ophiostomatoid fungal isolates (S36.1; S39.1; S38.16; S40.4b; S40.10; T2.13; T3.1; T3.6; L4.2; and L5.1) were selected as representatives. Only one isolate of *Sporothrix* was obtained and therefore was not included in these trials. Since the collection sites presented different geographic and climate conditions (in terms of average temperature and precipitation; Table 1), the selected fungal isolates were tested in a wide amplitude of temperatures between 5 and 40°C during 15 days of incubation (Figure 4). Overall, almost all fungal isolates could grow between 20 and 35°C; however with different optimal temperatures. All taxa failed to grow at 40°C. For *Ophiostoma* group (Figure 4A), the optimal growth temperature varied between 20°C (for S40.10) and 30°C (for S36.1, S39.1, S38.16). At lower temperatures (5–10°C), only S40.10 exhibited discrete growth but failed to grow at 35°C. For *Leptographium* group (Figure 4B), the optimal growth temperature ranged between 25°C (S40.4b, T3.1, and T3.6) and 30°C (T2.13). For *Graphilbum* sp. L4.2 and L5.1, the optimal growth temperature was 35°C (Figure 4C), yet these isolates were unable to grow at 5 or 10°C.

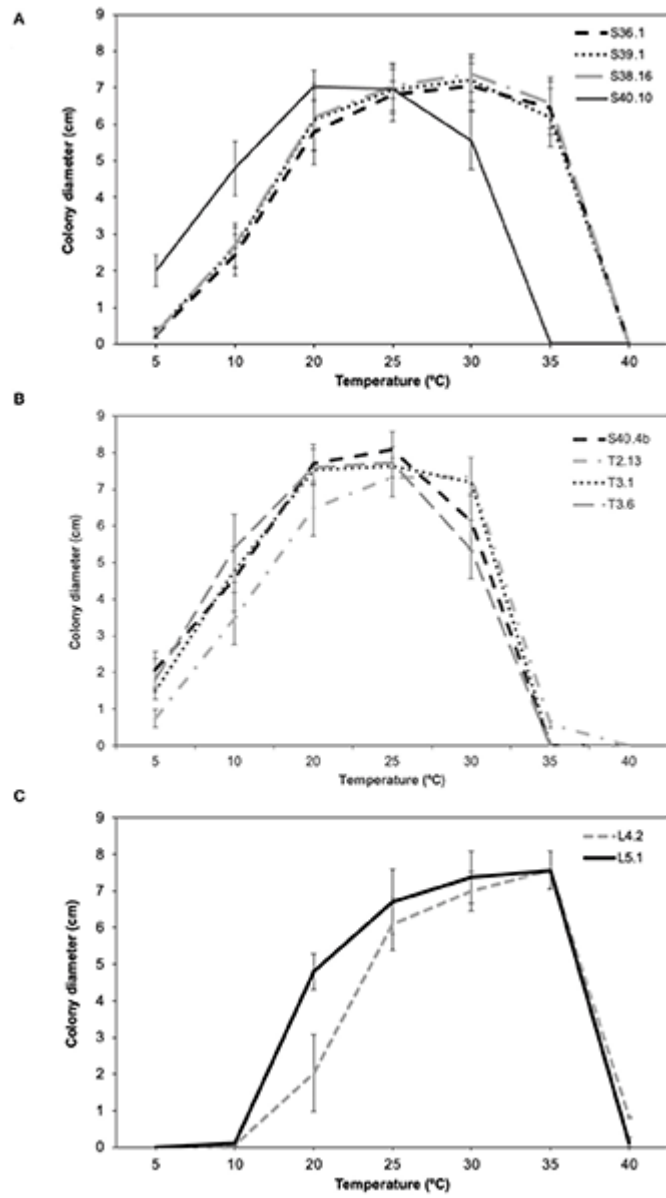


**FIGURE 4.** Comparison of mean growth per day ( $\pm$  standard error) of (A) *Ophiostoma ips* (S36.1, S39.1, S38.16, S40.10), (B) *Leptographium* sp. (S40.4b, T2.13, T3.1, T3.6), and (C) *Graphilbum* sp. (L4.2, L5.1).

For antagonistic performance of ophiostomatoid isolates, different combinations between representatives of the main taxa were tested considering a potential antagonist (R1) and a test organism (R2) (Supplementary Figure 6). Overall, the fungal isolate *Leptographium* sp. T3.6 inhibited the growth of the other 3 isolates [*O. ips* S36.1; *Graphilbum* sp. L4.2; *L. terebrantis* S40.4b (Figure 5)]. The percentage of inhibition of

*Leptographium* sp. T3.6 and *Ophiostoma ips* S36.1 was 75%, while for *Graphilbum* sp. L4.2 and *L. terebrantis* S40.4b, they were 44 and 46%, respectively. No differences were seen between *Leptographium* sp. T3.6 and *L. terebrantis* S40.4b or *Graphilbum* sp. L4.2. The dual culture of *Graphilbum* sp. L4.2 x *O. ips* S36.1 and *O. ips* S36.1 x *L. terebrantis* S40.4b recorded the lowest inhibition, respectively, 33 and 15%.

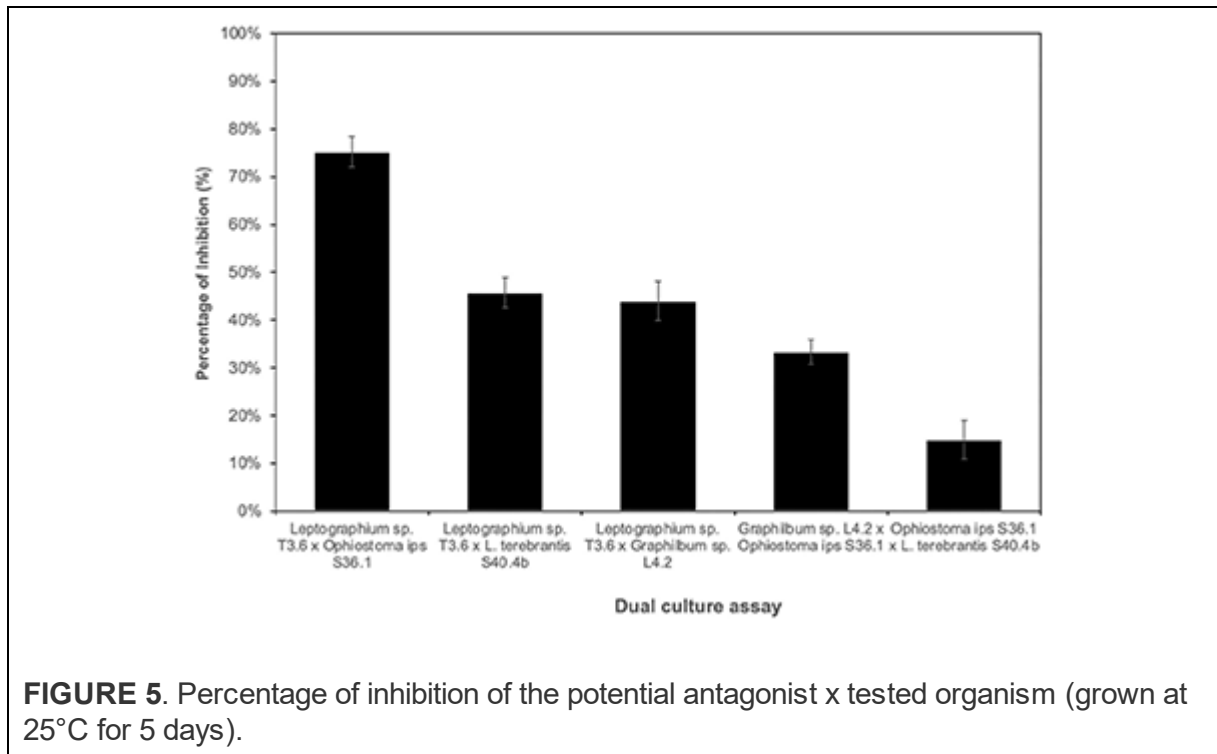


**FIGURE 5.** Percentage of inhibition of the potential antagonist x tested organism (grown at 25°C for 5 days).

Not all Ophiostomatales could support PWN growth. Except for *O. ips* S38.16 and S39.1, all fungal isolates tested were unsuitable for PWN as the food source ( $p < 0.001$ ), when comparing with *B. cinerea* (total number of PWN after 7 days was  $11,733 \pm 546$ ) (Figure 6). Within the group of *O. ips*, isolate S40.10 recorded a population increase of 27.4% when compared with the control, while S36.1 and S39.1 were, respectively, 54.8 and 80%. *Ophiostoma ips* S38.16 showed a close result with *B. cinerea*, with 94.6% of PWN growth ( $p > 0.001$ ). For the *Leptographium* group, PWN growth was relatively low (<13%). In fact, PWN could not grow completely in S40.4b. The total number of PWN recovered from *Leptographium* sp. T2.13 and T3.1 were, respectively,  $649 \pm 160$  and  $636 \pm 251$  nematodes (~5.5% in comparison with *B. cinerea*). The two isolates of *Graphilbum* tested, L4.2

and L5.1, were also not suitable for PWN, with 12 and 4.5%, respectively, of PWN growth in comparison with the control fungus.

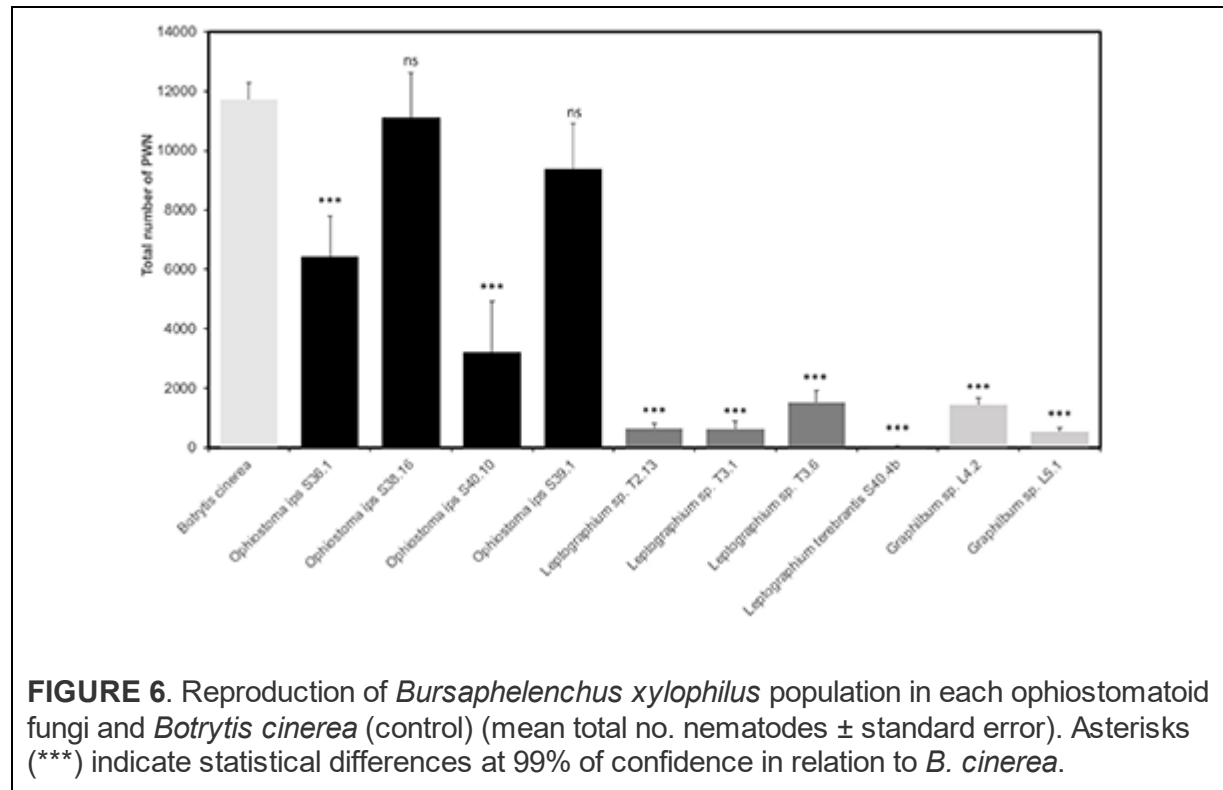


**FIGURE 6.** Reproduction of *Bursaphelenchus xylophilus* population in each ophiostomatoid fungi and *Botrytis cinerea* (control) (mean total no. nematodes ± standard error). Asterisks (\*\*\* or ns) indicate statistical differences at 99% of confidence in relation to *B. cinerea*.

## DISCUSSION

Fungal communities seem to dominate different ecological niches in forest tree habitats due to their easy adaptation to wood colonization (de Boer et al., 2005). In this sense, these communities are more likely to undergo more severe shifts in abundance and composition due to biotic and abiotic stresses (Baldrian, 2017). The study of the fungal communities in the PWD complex, and their intermediates, are still underrated (Zhao et al., 2014; Nascimento et al., 2015) in spite of their strong influence on PWN populations (Vicente et al., 2021). In this study, we present a detailed characterization of fungal communities from non-infected and PWN-infected *P. pinaster* trees from three contrasting PWD foci (long-term PWN presence, Companhia das Lezírias and Tróia, and transitional/recent PWN detection, Seia). This is the first study focused exclusively on the fungal diversity in PWD affected areas, in Europe. In addition, we also characterized the adaptative response of a

specific group of Ophiostomatales fungi (genus *Ophiostoma*, *Leptographium*, *Graphilbum*) due to their well-recognized history with PWN (Vicente et al., 2021), as means to uncover their resilience in the disease complex.

## Mycoflora Communities in the PWD

The surveys were conducted during early winter 2019 and spring 2020 before the maturation feeding of the insect-vector, which could justify the high PWN numbers extracted from the sampled wood. Despite the discrepancy in the total number of fungal isolates between sampling locations, overall, we observed clear differences in the fungal communities between collection sites, being long-term PWD loci (Companhia das Lezírias and Tróia) closest between themselves than each with the most recent PWD area (Seia). Several factors may influence this result, e.g., their PWD history or biogeographical conditions of the locations, which are completely distinct in terms of temperature/precipitation/altitude, as well as seasonality. In Seia, the fungal communities of non-infected and PWN-infected *P. pinaster* showed substantial differences in terms of composition and species richness, the non-infected pine trees being more biodiverse than PWN-infected trees. This observation suggests that the presence of the nematode could explain the community shifts which is corroborated by recent works with other *Pinus* species (Liu et al., 2021; Zhang et al., 2021). Still, this result is not evident for fungal communities in Companhia das Lezírias or Tróia, according to the diversity indexes. The fact that these locations have a long-term history of PWN presence could be an indication of communities' stability in the presence of the nematode invader. Kuroda and Ito (1992) also reported similar species in healthy and wilted *P. thunbergii*, which varied vaguely among seasons. Zhao et al. (2013) also suggested a link between disease history and microbial communities' diversity; however only infected trees were used in this study. In our work, most of the taxa observed were already reported for other *Pinus* species, as well as PWN and insect-vector *Monochamus* sp. (Hyun et al., 2007; Zhao et al., 2013, 2018). However, with the exception of two *P. pinaster* trees from Seia, only PWN-infected *P. pinaster* trees were colonized by Ophiostomatales, the causal agents of blue-stain (Six, 2012) commonly present in pine trees infected by the PWN (Futai, 2013). The most dominant ophiostomatoid species was *O. ips*. This species was firstly reported in association with the infection of bark beetles in south-

eastern North America (Rumbold, 1931), and nowadays is distributed worldwide. In PWD complex, *O. ips* was described as associated with PWN-infected *P. thunbergii*, PWN, and *M. alternatus* in Korea (Hyun et al., 2007) in *P. massoniana* and *P. thunbergii* in China (Zhao et al., 2013, 2018; Wang et al., 2018), and *M. galloprovincialis* and *P. pinaster* in Portugal (Inácio et al., 2015; Trindade, 2019). As suggested by Wang et al. (2018), the dominance of *O. ips* can have either an indigenous origin or be an effective adaptation to local pine forests. In fact, the presence of *O. ips* in non-infected trees in Seia could be explained by natural infection with various species of bark beetles as is common in European pine forests (Chang et al., 2017; Jankowiak et al., 2021). The other ophiostomatoid isolates were *Leptographium* sp., *Graphilbum* sp., and *Sporothrix* sp., which were also described in other studies (Zhao et al., 2013, 2018; Wang et al., 2018). For the first time, we report *Leptographium* species associated with PWN-infected *P. pinaster* trees in Portugal, namely *L. sosnaicola* and *L. terebrantis*. *Leptographium sosnaicola* was described in logs of *P. sylvestris* in Poland and probably vectored by *Ips sexdentatus* (Jankowiak et al., 2021). The authors showed that *L. sosnaicola* formed a monophyletic line within other members of *Leptographium*, and its morphology did not resemble any known *Leptographium* species. Our results also show *L. sosnaicola* L2.6 within *L. lundburgii* complex and totally separated from the other sister species, corroborating the previous observations (Jankowiak et al., 2021). The other *Leptographium* species identified *L. terebrantis*, firstly described as associated with the black turpentine beetle *Dendroctonus terebrans* (Barras and Perry, 1971), was reported as pathogen of woody roots and recently related to crown symptoms and tree mortality in *P. taeda* (Mensah et al., 2021). Hausner et al. (2005) showed that ex-type culture of *L. terebrantis* is very similar morphologically to *L. wingfieldii*, which explains their clustering and non-resolved placement in the phylogenetic trees of this study. Although only a few isolates were recovered from PWN-infected *P. pinaster*, *Graphilbum* and *Sporothrix* genus are common in pine trees infected with the nematode. Zhao et al. (2013) showed that *Sporothrix* sp. 1 could sustain PWN growth with female-biased sex ratio offspring and suggested that the prevalence of this species was correlated with higher tree mortality that possibly influenced the nematode and insect-vector populations in the area studied. This ophiostomatoid fungi was also isolated in South Korea (Hyun et al., 2007) and other regions of China (Wang et al., 2018). As

for other *Leptographium* isolates in this study, neither morphological characterization nor molecular identification was resolved enough to assign it into species level, which will be explored in future studies for the description of new species.

## **Ophiostomatales Adaptation and Interaction With PWN**

The presence of the PWN induces a disturbance in microbial (bacteria and fungi) community stability, which has been already analyzed using metagenomics approaches (Alves et al., 2016; Liu et al., 2021). Ecologically, this is often related with community insensitivity (resistance) or the rate at which community returns to a pre-disturbance condition, intrinsically related to their functional role in the ecosystem (Shade et al., 2012). In this study, the isolates of *Ophiostoma*, *Leptographium*, and *Graphilbum* groups showed differences in temperature adaptation, which may reflect the environmental conditions of their collection sites. The *O. ips* group grew in lower temperatures such as 5–10°C, which is characteristic of the Northern areas. *Leptographium* sp. isolates and *Graphilbum* sp. isolates showed a preference for higher temperatures, with an optimal growth at 25 and 35°C, respectively. Zhao et al. (2018) surveyed distinct regions of China forests and detected *O. ips* mainly in the Southern sites, with higher annual temperatures (16°C) and rainfall (1,020–1,408 mm). Cobian et al. (2019) demonstrated that plant-microbe specificity varies with different abiotic parameters such as temperature or elevation. They also showed a strong interaction between host and fungal endophyte, and that the environment plays a secondary role in fungal communities, mostly by modulating host specialization (Cobian et al., 2019). Overall, it seems that associations between ophiostomatoid fungi and the pine species in the context of PWD may be variable, suggesting a co-evolution history, however further studies are needed to address this issue.

Competitive interactions among different fungal symbionts of bark-beetles (such as *O. minus*, *C. ranaculosis*, and *Entomocorticium* sp.) have been reported in artificial and natural conditions (Klepzig and Hofstetter, 2011). Klepzig (1998) showed that on an artificial medium the biological control fungus *O. piliferum* outcompete all three fungi (*O. minus*, *C. ranaculosis*, and *Entomocorticium* sp.); however, in inoculations of natural substrate, *O. piliferum* compete successfully with the two mutualistic fungi *C. ranaculosis* and *Entomocorticium* sp., but not with *O. minus*. Here, we

evaluated pairwise competition between the three main taxa and found that *Leptographium* sp. could outcompete neither with *Ophiostoma* nor with *Graphilbum*, suggesting potential antagonism between Ophiostomatales. Considering our sampled trees, this result could also explain why only few *O. ips* were collected in the trees mainly dominated with *Leptographium*. So far, we could not find any other study suggesting this kind of ecological interactions between ophiostomatoid fungi in the context of PWD.

Fukushige (1991a,b) showed that *B. xylophilus* propagation on fungus could differ in agar media and pine wood. The colonization of *O. minus* in pine-branch segments of *P. densiflora* resulted in a quick increase of PWN population (Maehara and Futai, 2000). Zhao et al. (2018) showed that *L. pini-densiflorae* could promote the highest population density, followed by *Sporothrix* sp. 1, while *O. ips* or *O. minus* resulted in significantly lower PWN populations. Pimentel et al. (2021) evaluated nematode propagation in 10 different species of Ascomycota fungi, including different Ophiostomatales species (*O. ips*, *O. piliferum*, *O. minus*) and *Leptographium* (*L. procerum*, *L. terebrantis*). After 20 days of incubation, the nematode propagation in these fungal isolates was unexceptioned, since all were unsuitable for PWN growth (Pimentel et al., 2021). In this sense, not all ophiostomatoid fungi have been considered suitable for PWN growth in declining trees (Zhao et al., 2014). In this study, the highest PWN multiplication in comparison with their *B. cinerea* culture fungi was obtained in the *O. ips* group, while *Leptographium* and *Graphilbum* group resulted in significantly lower PWN numbers in the conditions tested. Intraspecific variability within the *O. ips* group was also seen. With the exception of *O. ips* S40.10, all the other isolates had a positive impact on the PWN population, which seems to be in line with other studies (Maehara and Futai, 1997; Maehara, 2008). Indeed, this pattern seemed to be sustained by the initial quantification of PWN-infected trees. In Seia site, where *O. ips* was the most prevalent ophiostomatoid fungi (almost 70% of community composition, 3 out of the 5 pine trees presented a population of PWN between 1,001 and 5,000 nematodes per 100 g of wood (class IV). The Tróia site evidenced low to medium levels of PWN infection. In the specific case of one tree (T3), classified as class II (51-200 nematodes per 100 g of wood), the low concentration of PWN could be explained by the mycoflora present, given that all isolated fungi belonged to the *Leptographium* genus, which could not support PWN multiplication in the feeding trials. As for the two *Graphilbum*

sp. isolates, the defoliation class of the trees sampled were class III and IV, not supporting the previous observations. Still, this seemingly relation between the host defoliation class and the impact of their isolated fungi in PWN multiplication is worth pursuing, especially confirming their effect in the native host *P. pinaster*. The present research constitutes a milestone in the study of the functional role of fungal communities inhabiting wilted trees, their ecological interactions, and their suitability for PWN growth, as well as their impact on PWD expression. This knowledge can lead to the identification of key points in PWN life cycle that can be targeted to disrupt the disease cycle using more natural alternatives.

## DATA AVAILABILITY STATEMENT

The datasets presented in this study can be found in online repositories. The names of the repository/repositories and accession number(s) can be found in the article/Supplementary Material.

## AUTHOR CONTRIBUTIONS

CV and MI: conceptualization. CV, MS, AR, and ME: research and data analysis. CV and JF: writing—original draft preparation. ME, AR, MM, FN, and MI: writing—review and editing. AR, MM, and MI: resources. All authors contributed to the article and approved the submitted version.

## FUNDING

This research was funded by the Fundação para a Ciência e Tecnologia (FCT) and Fundo Europeu de Desenvolvimento Regional (FEDER) within the Programa Operacional Regional de Lisboa and Programa Operacional Regional do Alentejo through the national project LISBOA-01-0145-FEDER028724 - PTDC/ASP-PLA/28724/2017 (ALT20-03-0145-FEDER-028724) PineENEMY, Exploring the NEmatode-MYcobiota interactions in Pine Wilt Disease, through the R&D Unit, UIB/04551/2020 (GREEN-IT - Bioresources for Sustainability), and the CEECIND/00040/2018 (to CV).

# ACKNOWLEDGMENTS

The authors would like to thank the team of PineENEMY project (Laboratory of Nematology, Mycology and Entomology of INIAV). A special thanks to Helena Bragança (Mycology Lab) for supporting this work, to Luis Bonifácio (Entomology Lab, INIAV) for his dedication and expertise given in the selection of the collection sites.

# SUPPLEMENTARY MATERIAL

The Supplementary Material for this article can be found online at: <https://www.frontiersin.org/articles/10.3389/fpls.2022.908308/full#supplementary-material>

# REFERENCES

Abelleira, A., Picoaga, A., Mansilla, J. P., and Aguin, O. (2011). Detection of *Bursaphelenchus xylophilus*, causal agent of pine wilt disease on *Pinus pinaster* in northwestern Spain. *Plant Dis.* 95, 776. doi: 10.1094/PDIS-12-10-0902

Aikawa, T., and Kikuchi, T. K. (2007). Estimation of virulence of *Bursaphelenchus xylophilus* (Nematoda: Aphelenchoididae) based on its reproductive ability. *Nematology* 9, 371–377. doi: 10.1163/156854107781352007

Almeida, A. B., Concas, J., Campos, M. D., Materatski, P., Varanda, C., Patanita, M., et al. (2020). Endophytic fungi as potential biological control agents against grapevine trunk diseases in Alentejo region. *Biology* 9,1–23. doi: 10.3390/biology9120420

Alves, M., Pereira, A., Matos, P., Henriques, J., Vicente, C., Aikawa, T., et al. (2016). Bacterial community associated to the pine wilt disease insect vectors *Monochamus galloprovincialis* and *Monochamus alternatus*. *Sci. Rep.* 6, 23908. doi: 10.1038/srep23908

Baldrian, P. (2017). Forest microbiome: diversity, complexity, and dynamics. *FEMS Microbiol. Rev.* 41, 109–130. doi: 10.1093/femsre/fuw040

Barras, S. J., and Perry, T. (1971). *Leptographium terebrantis* sp. nov. associated with *Dendroctonus terebrans* in loblolly pine. *Mycopathol. Mycol. Appl.* 43, 1–10 doi: 10.1007/BF02051496

Cadahia, D., Cobos, J. M., Soria, S., Clouser, F., Gellini, R., Grossoni, P., et al. (1991). “Observation of damaged to Mediterranean forest species. ministry of agriculture, fisheries and food,” in *Commission of the European Communities* (Madrid), 96.

Capella-Gutiérrez, S., Silla-Martínez, J. M., and Gabaldón, T. (2009). trimAl: a tool for automated alignment trimming in large-scale phylogenetic analyses. *Bioinformatics* 25, 1972–1973. doi: 10.1093/bioinformatics/btp348

Carbone, I., and Kohn, L. M. (1999). A method for designing primer sets for speciation studies in filamentous ascomycetes. *Mycologia* 91, 553–556. doi: 10.1080/00275514.1999.12061051

Chang, R., Duong, T. A., Taerum, S. J., Wingfield, M. J., Zhou, X., and de Beer, Z. W. (2017). Ophiostomatoid fungi associated with conifer-infesting beetles and their phoretic mites in Yunnan, China. *MycoKeys* 28, 19–64. doi: 10.3897/mycokeys.28.21758

Cobian, G., CP, E., and Amend, A. (2019). Plant-microbe specificity varies as a function of elevation. *ISME J.* 13, 2778–2788. doi: 10.1038/s41396-019-0470-4

de Beer, Z. W., Seifert, K. A., and Wingfield, M. J. (2013). A nomenclator for ophiostomatoid genera and species in the Ophiostomatales and Microascales. *Biodiversity Series* 12, 245–322.

de Boer, W., Folman, L. B., Summerbell, R. C., and Boddy, L. (2005). Living in a fungal world: impact of fungi on soil bacterial niche development. *FEMS Microbiol. Rev.* 29, 795–811. doi: 10.1016/j.femsre.2004.11.005

de la Fuente, B., and Saura, S. (2021). Long-term projections of the natural expansion of the pine wood nematode in the Iberian Peninsula. *Forests* 12, 849. doi: 10.3390/f12070849

Duong, T. A., de Beer, Z. W., Wingfield, B. D., and Wingfield, M. J. (2012). Phylogeny and taxonomy of species in the Grosmannia serpens complex. *Mycologia* 104, 715–732. doi: 10.3852/11-109

Dwinell, L. D. (1997). The Pinewood Nematode: regulation and mitigation. *Annu. Rev. Phytopathol.* 35, 153–166. doi: 10.1146/annurev.phyto.35.1.153

Fonseca, L., Cardoso, J. M. S., Lopes, A., Pestana, M., Abreu, F., Nunes, N., et al. (2012). The pinewood nematode, *Bursaphelenchus xylophilus*, in Madeira Island. *Helminthologia* 49, 96–103. doi: 10.2478/s11687-012-0020-3

Fukushige (1991a). Propagation of *Bursaphelenchus xylophilus* (Nematoda: Aphelenchoididae) on fungi growing in pine-shoot segments. *Appl. Entomol. Zool.* 371–376. doi: 10.1303/aez.26.371

Fukushige (1991b). Effects of fungi coexisting with *Ceratocystis* sp. on propagation of *Bursaphelenchus xylophilus* (Nematoda: Aphelenchoididae). *Appl. Entomol. Zool.* 377–380. doi: 10.1303/aez.26.377

Futai, K. (2013). Pine wood nematode, *Bursaphelenchus xylophilus*. *Ann. Rev. Phytopathol.* 51, 61–83. doi: 10.1146/annurev-phyto-081211-172910

Gardes, M., and Brunts, T. D. (1993). ITS primers with enhanced specificity for basidiomycetes – application to the identification of mycorrhizae and rusts. *Mol. Ecol.* 2, 113–118. doi: 10.1111/j.1365-294X.1993.tb00005.x

Glass, N. L., and Donaldson, G. C. (1995). Development of primer sets designed for use with the PCR to amplify conserved genes from filamentous ascomycetes. *Appl. Environ. Microbiol.* 61, 1323–1330. doi: 10.1128/aem.61.4.1323-1330.1995

Hammer, Ø, Harper, D. A. T., and Ryan, P. D. (2001). PAST: paleontological statistics software package for education and data analysis. *Palaeontol. Electron.* 4, 1–9.

Harrington, T. (1993). “Diseases of conifers caused by species of *Ophiostoma* and *Leptographium*,” in *Ceratocystis and Ophiostoma: Taxonomy, ecology and pathogenicity*, eds M. J. Wingfield, K. A. Siefert, and J. F. Webber (The American Phytopathological Society Press), 161–172.

Harrington, T. C. (1981). Cycloheximide sensitivity as a taxonomic character in *Ceratocystis*. *Mycologia* 73, 1123–1129. doi: 10.1080/00275514.1981.12021447

Hausner, G., Iranpour, M., Kim, J., Breuil, C., Davis, C., Gibb, E. A., et al. (2005). Fungi vectored by the introduced bark beetle *Tomicus piniperda* in Ontario, Canada, and comments on the taxonomy of *Leptographium lundbergii*, *Leptographium terebrantis*, *Leptographium truncatum*, and *Leptographium wingfieldii*. *Canad. J. Bot.* 83, 1222–1237. doi: 10.1139/b05-095

Hyun, M., Kim, J., Suh, D., Lee, S., and Kim, S. (2007). Fungi isolated from pine wood nematode, its vector Japanese pine sawyer, and the nematode-infected Japanese black pine wood in Korea. *Mycobiology* 35, 159. doi: 10.4489/MYCO.2007.35.3.159

Inácio, M. L., Nóbrega, F., Trindade, J., Bonifácio, L., Naves, P., Sousa, E., et al. (2015). “Fungi associated with the vector of the pinewood nematode and their influence on Pine Wilt Disease,” in *XVII Congress of European Mycologists* (Madeira, Portugal), 21–25.

Instituto Português do Mar e da Atmosfera (IPMA) (2019). ISSN 2183-1076.

Instituto Português do Mar e da Atmosfera (IPMA) (2020). ISSN 2183-1076.

Jankowiak, R., Szewczyk, G., Bilański, P., Jazłowiecka, D., Harabin, B., and Linnakoski, R. (2021). Blue-stain fungi isolated from freshly felled Scots pine logs in Poland, including *Leptographium sosnaicola* sp. nov. *For. Pathol.* 51, 1–16. doi: 10.1111/efp.12672

Kanzaki, N., Tanaka, R., Giblin-Davis, R. M., and Davies, K. (2014). New plant-parasitic nematode from the mostly mycophagous genus *Bursaphelenchus* discovered inside figs in Japan. *PLoS ONE* 9, e99241. doi: 10.1371/journal.pone.0099241

Katoh, K., and Standley, D. (2013). MAFFT multiple sequence alignment software version 7: improvements in performance and usability. *Mol. Biol. Evol.* 30, 772–780. doi: 10.1093/molbev/mst010

Kim, J. J., Kim, S. H., Lee, S., and Breuil, C. (2003). Distinguishing *Ophiostoma ips* and *Ophiostoma montium*, two bark beetle-associated sapstain fungi. *FEMS Microbiol. Lett.* 222, 187–192. doi: 10.1016/S0378-1097(03)00304-5

Kirisits, T. (2007). “Fungal associates of European bark beetles with special emphasis on the ophiostomatoid fungi,” in *Bark and Wood Boring Insects in Living Trees in Europe, a Synthesis*, eds F. Lieutier, K. R. Day, A. Battisti, J. C. Grégoire, and H. F. Evans (Dordrecht: Springer), 181–235. doi: 10.1007/978-1-4020-2241-8\_10

Kirisits, T., Wingfield, M. J., and Chhetri, D. B. (2002). *Studies on the Association of Blue-Stain Fungi With the Eastern Hymalayan Spruce Bark Beetle (*Ips schmutzenhoferi*) and With Other Bark Beetles in Bhutan. Yusipang Report* (Vienna), 55.

Klepzig, K. (1998). Competition between a biological control fungus, *Ophiostoma piliferum*, and symbionts of the southern pine beetle. *Mycologia* 90, 69–75. doi: 10.1080/00275514.1998.12026880

Klepzig, K. D., and Hofstetter, R. W. (2011). “From attack to emergence: interactions between southern pine beetle, mites, microbes, and trees,” in *2011 Southern Pine Beetle II. Gen. Tech. Rep. SRS-140*, eds R. N. Coulson, and K. D. Klepzig (Asheville, NC: U.S. Department of Agriculture Forest Service, Southern Research Station), 141–152.

Kuroda, K., and Ito, S. (1992). Migration speed of pine wood nematodes and activities of other microbes during the development of pine wilt disease in *Pinus thunbergii*. *Kansai Res. Center Prod. Res. Inst.* 74, 383–389.

Letunic, I., and Bork, P. (2021). Interactive Tree Of Life (iTOL) v5: an online tool for phylogenetic tree display and annotation. *Nucleic Acids Res.* 49, W293–W296, doi: 10.1093/nar/gkab301

Liu, Y., Qu, Z. L., Liu, B., Ma, Y., Xu, J., Shen, W. X., et al. (2021). The impact of pine wood nematode infection on the host fungal community. *Microorganisms* 9, 1–17. doi: 10.3390/microorganisms9050896

Maehara, N. (2008). Reduction of *Bursaphelenchus xylophilus* (Nematoda: Parasitaphelenchidae) population by inoculating *Trichoderma* spp. into pine wilt-killed trees. *Biol. Control* 44, 61–66. doi: 10.1016/j.biocontrol.2007.09.005

Maehara, N., and Futai, K. (1996). Factors affecting both the numbers of the pinewood nematode, *Bursaphelenchus xylophilus* (Nematoda: Aphelenchoididae), carried by the Japanese Pine Sawyer,

*Monochamus alternatus* (Coleoptera: Cerambycidae), and the Nematode's Life History. *Appl. Entomol. Zool.* 31, 443–452. doi: 10.1303/aez.31.443

Maehara, N., and Futai, K. (1997). Effect of fungal interactions on the numbers of the pinewood nematode, *Bursaphelenchus xylophilus* (Nematoda: Aphelenchoididae), carried by the Japanese pine sawyer, *Monochamus alternatus* (Coleoptera: Cerambycidae). *Fundam. Appl. Nematol.* 20, 611–617.

Maehara, N., and Futai, K. (2000). Population changes of the pinewood nematode, *Bursaphelenchus xylophilus* (Nematoda: Aphelenchoididae), on fungi growing in pine-branch segments. *Appl. Entomol. Zool.* 35, 413–417. doi: 10.1303/aez.2000.413

Maehara, N., and Futai, K. (2005). Effect of blue-stain fungi on the number of *Bursaphelenchus xylophilus* (Nematoda: Aphelenchoididae) carried by *Monochamus alternatus* (Coleoptera: Cerambycidae). *Nematology* 7: 161–167. doi: 10.1163/1568541054879557

Maehara, N., Tsuda, K., Yamasaki, M., Shirakikawa, S., and Futai, K. (2006). Effect of fungus inoculation on the number of *Bursaphelenchus xylophilus* (Nematoda: Aphelenchoididae) carried by *Monochamus alternatus* (Coleoptera: Cerambycidae). *Nematology* 8, 59–67. doi: 10.1163/156854106776179944

Mamiya, Y. (1983). Pathology of the pine wilt disease caused by *Bursaphelenchus xylophilus*. *Ann. Rev. Phytopathol.* 21, 201–220. doi: 10.1146/annurev.py.21.090183.001221

Marincowitz, S., Duong, T., Wilhelm de Beer, Z., and Wingfield, M. (2015). Cornuvesica: a little known mycophilic genus with a unique biology and unexpected new species. *Fungal Biol.* 119, 615–630. doi: 10.1016/j.funbio.2015.03.007

Mensah, J. K., Sayer, M. A. S., Nadel, R. L., Matusick, G., Fan, Z., Carter, E. A., et al. (2021). Leptographium terebrantis inoculation and associated crown symptoms and tree mortality in *Pinus taeda*. *Fungal Ecol.* 51, 101057. doi: 10.1016/j.funeco.2021.101057

Mota, M. M., Braasch, H., Bravo, M. A., Penas, A. C., Burgermeister, W., Metge, K., et al. (1999). First report of *Bursaphelenchus xylophilus* in Portugal and in Europe. *Nematology* 1, 727–734. doi: 10.1163/156854199508757

Nascimento, F. X., Hasegawa, K., Mota, M., and Vicente, C. S. L. (2015). Bacterial role in pine wilt disease development - review and future perspectives. *Environ. Microbiol. Rep.* 7, 51–63. doi: 10.1111/1758-2229.12202

Niu, H. T., Zhao, L. L., Lu, M., Zhang, S., and Sun, J. H. (2012). The ratio and concentration of two monoterpenes mediate fecundity of the pinewood nematode and growth of its associated fungi. *PLoS ONE* 7, e31716. doi: 10.1371/journal.pone.0031716

Pimentel, C. S., Firmino, P. N., and Ayres, M. P. (2021). Interactions between pinewood nematodes and the fungal community of pine trees. *Fungal Ecol.* 51, 101046. doi: 10.1016/j.funeco.2021.101046

Plattner, A., Kim, J.-J., Reid, J., Hausner, G., Lim, Y. W., Yamaoka, Y., and Breuil, C. (2009). Resolving taxonomic and phylogenetic incongruence within species *Ceratocystiopsis minuta*. *Mycologia* 101, 878–887. doi: 10.3852/08-132

R Core Team (2020). *R: A Language and Environment for Statistical Computing*. R Foundation for Statistical Computing. Available online at: <https://www.R-project.org/> (accessed March 29, 2022).

Reid, J., Iranpour, M., Rudski, S. M., Loewen, P. C., and Hausner, G. (2010). A new conifer-inhabiting species of *Ceratocystis* from Norway. *Botany* 88, 971–983. doi: 10.1139/B10-069

Robertson, L., Arcos, S. C., Escuer, M., Merino, R. S., Esparrago, G., Abelleira, A., et al. (2011). Incidence of the pinewood nematode *Bursaphelenchus xylophilus* (Steiner & Buhrer, 1934) Nickle, 1970 in Spain. *Nematology* 13, 755–757. doi: 10.1163/138855411X578888

Rodrigues, J. M., Sousa, E., and Abrantes, I. (2015). "Pine Wilt Disease historical overview," in *Pine Wilt Disease in Europe – Biological Interactions and Integrated Management*. 1st ed, E. Sousa, F. Vale, and I. Abrantes (Lisbon: Federação Nacional das Associações de Proprietários Florestais), 13–32

Royse, D. J., and Ries, S. M. (1977). The influence of fungi isolated from peach twigs on the pathogenicity of *Cytospora cincta*. *Ecol. Epidemiol.* 68, 603–607. doi: 10.1094/Phyto-68-603

Rumbold, C. T. (1931). Two blue-staining fungi associated with bark beetle infestation of pines. *J. Agric. Res.* 43, 847–873.

Shade, A., Peter, H., Allison, S. D., Baho, D. L., Berga, M., Bürgmann, H., et al. (2012). Fundamentals of microbial community resistance and resilience. *Front. Microbiol.* 3, 1–19. doi: 10.3389/fmicb.2012.00417

Six, D. L. (2012). Ecological and evolutionary determinants of bark beetle —fungus symbioses. *Insects* 3, 339–366. doi: 10.3390/insects3010339

The jamovi project (2021). *jamovi (Version 1.6) [Computer Software]*. Retrieved from: <https://www.jamovi.org> (accessed March 29, 2022)

Trindade, M. J. F. (2019). *Estudo da população de fungos em Pinus pinaster em Portugal*. Master Thesis, Instituto Superior de Agronomia, Lisbon.

Vicente, C., Espada, M., Vieira, P., and Mota, M. (2012). Pine Wilt Disease: a threat to European forestry. *Eur. J. Plant Pathol.* 133, 89–99. doi: 10.1007/s10658-011-9924-x

Vicente, C. S. L., Soares, M., Faria, J. M. S., Ramos, A. P., and Inácio, M. L. (2021). Insights into the role of fungi in pine wilt disease. *J. Fungi* 7, 1–16. doi: 10.3390/jof7090780

Wang, H. M., Lun, Y. Y., Lu, Q., Liu, H. X., Decock, C., and Zhang, X. Y. (2018). Ophiostomatoid fungi associated with pines infected by *Bursaphelenchus xylophilus* and *Monochamus alternatus* in China, including three new species. *MycoKeys* 39, 1–27. doi: 10.3897/mycokes.39.27014

White, T., Bruns, T., Lee, S., and Taylor, J. (1990). "Amplification and direct sequencing of fungal ribosomal RNA genes for phylogenetics," in *PCR protocols: A Guide to Methods and Applications*, eds M. A. Innis, D. H. Gelfand, J. J. Sninsky, and T. J. White (Academic Press), 315–322. doi: 10.1016/B978-0-12-372180-8.50042-1

Whitehead, A. G., and Hemming, J. R. (1965). A comparison of some quantitative methods of extracting small vermiform nematodes from soil. *Ann. Appl. Biol.* 55, 25–38. doi: 10.1111/j.1744-7348.1965.tb07864.x

Zhang, W., Wang, X., Li, Y., Wei, P., Sun, N., Wen, X., et al. (2021). Differences between microbial communities of pine species having differing level of resistance to the pinewood nematode. *Microl. Ecol.* doi: 10.1007/s00248-021-01907-4

Zhao, L., Lu, M., Niu, H., Fang, G., Zhang, S., and Sun, J. (2013). A native fungal symbiont facilitates the prevalence and development of an invasive pathogen–native vector symbiosis. *Ecology* 94, 2817–2826. doi: 10.1890/12-2229.1

Zhao, L., Mota, M., Vieira, P., Butcher, R. A., and Sun, J. (2014). Interspecific communication between pinewood nematode, its insect vector, and associated microbes. *Trends Parasitol.* 30, 299–308. doi: 10.1016/j.pt.2014.04.007

Zhao, L.; Ahmad, F., Lu, M., Zhang, W., Wickham, J. D., Sun, J., et al. (2018). Ascarosides promote the prevalence of ophiostomatoid fungi and an invasive pathogenic nematode, *Bursaphelenchus xylophilus*. *J. Chem.* 44, 701–710. doi: 10.1007/s10886-018-0996-3

Zhou, X., de Beer, Z. W., and Wingfield, M. J. (2006). DNA sequence comparisons of Ophiostoma spp., including *Ophiostoma aurorae* sp. nov., associated with pine bark beetles in South Africa. *Stud Mycol.* 55, 269–277. doi: 10.3114/sim.55.1.269

**Conflict of Interest:** The authors declare that the research was conducted in the absence of any commercial or financial relationships that could be construed as a potential conflict of interest.

**Publisher's Note:** All claims expressed in this article are solely those of the authors and do not necessarily represent those of their affiliated organizations, or those of the publisher, the editors and the reviewers. Any product that may be evaluated in this article, or claim that may be made by its manufacturer, is not guaranteed or endorsed by the publisher.

*Copyright © 2022 Vicente, Soares, Faria, Espada, Mota, Nóbrega, Ramos and Inácio. This is an open-access article distributed under the terms of the Creative Commons Attribution License (CC BY). The use, distribution or reproduction in other forums is permitted, provided the original author(s) and the copyright owner(s) are credited and that the original publication in this journal is cited, in accordance with accepted academic practice. No use, distribution or reproduction is permitted which does not comply with these terms.*

# Advantages of publishing in Frontiers

<p><b>Frontiers</b> Avenue du Tribunal-Fédéral 34 1005 Lausanne   Switzerland</p> <p>Visit us: <a href="http://www.frontiersin.org">www.frontiersin.org</a> Contact us: <a href="http://frontiersin.org/about/contact">frontiersin.org/about/contact</a></p>	 <p><b>OPEN ACCESS</b> Articles are free to read for greatest visibility and readership</p>	 <p><b>FAST PUBLICATION</b> Around 90 days from submission to decision</p>	
	 <p><b>HIGH QUALITY PEER-REVIEW</b> Rigorous, collaborative, and constructive peer-review</p>	 <p><b>TRANSPARENT PEER-REVIEW</b> Editors and reviewers acknowledged by name on published articles</p>	
	 <p><b>REPRODUCIBILITY OF RESEARCH</b> Support open data and methods to enhance research reproducibility</p>	 <p><b>DIGITAL PUBLISHING</b> Articles designed for optimal readership across devices</p>	
 <p><b>FOLLOW US</b> <a href="https://twitter.com/frontiersin">@frontiersin</a></p>	 <p><b>IMPACT METRICS</b> Advanced article metrics track visibility across digital media</p>	 <p><b>EXTENSIVE PROMOTION</b> Marketing and promotion of impactful research</p>	 <p><b>LOOP RESEARCH NETWORK</b> Our network increases your article's readership</p>